frontiers | Research Topics

Tumour microenvironment in cancer research and drug discovery

Edited by
Syed Mahmood, Nur Akmarina Mohd Said and Kenneth K. W. To

Published in
Frontiers in Pharmacology
Frontiers in Oncology

ISSN 1664-8714
ISBN 978-2-8325-4885-1
DOI 10.3389/978-2-8325-4885-1

About Frontiers

Frontiers is more than just an open access publisher of scholarly articles: it is a pioneering approach to the world of academia, radically improving the way scholarly research is managed. The grand vision of Frontiers is a world where all people have an equal opportunity to seek, share and generate knowledge. Frontiers provides immediate and permanent online open access to all its publications, but this alone is not enough to realize our grand goals.

Frontiers journal series

The Frontiers journal series is a multi-tier and interdisciplinary set of open-access, online journals, promising a paradigm shift from the current review, selection and dissemination processes in academic publishing. All Frontiers journals are driven by researchers for researchers; therefore, they constitute a service to the scholarly community. At the same time, the *Frontiers journal series* operates on a revolutionary invention, the tiered publishing system, initially addressing specific communities of scholars, and gradually climbing up to broader public understanding, thus serving the interests of the lay society, too.

Dedication to quality

Each Frontiers article is a landmark of the highest quality, thanks to genuinely collaborative interactions between authors and review editors, who include some of the world's best academicians. Research must be certified by peers before entering a stream of knowledge that may eventually reach the public - and shape society; therefore, Frontiers only applies the most rigorous and unbiased reviews. Frontiers revolutionizes research publishing by freely delivering the most outstanding research, evaluated with no bias from both the academic and social point of view. By applying the most advanced information technologies, Frontiers is catapulting scholarly publishing into a new generation.

What are Frontiers Research Topics?

Frontiers Research Topics are very popular trademarks of the *Frontiers journals series*: they are collections of at least ten articles, all centered on a particular subject. With their unique mix of varied contributions from Original Research to Review Articles, Frontiers Research Topics unify the most influential researchers, the latest key findings and historical advances in a hot research area.

Find out more on how to host your own Frontiers Research Topic or contribute to one as an author by contacting the Frontiers editorial office: frontiersin.org/about/contact

Tumour microenvironment in cancer research and drug discovery

Topic editors

Syed Mahmood — University of Malaya, Malaysia

Nur Akmarina Mohd Said — University of Malaya, Malaysia

Kenneth K. W. To — The Chinese University of Hong Kong, China

Citation

Mahmood, S., Said, N. A. M., To, K. K. W., eds. (2024). *Tumour microenvironment in cancer research and drug discovery*. Lausanne: Frontiers Media SA.

doi: 10.3389/978-2-8325-4885-1

Table of contents

frontiers | Frontiers in Pharmacology

TYPE Editorial
PUBLISHED 03 May 2024
DOI 10.3389/fphar.2024.1403176

OPEN ACCESS

EDITED AND REVIEWED BY
Olivier Feron,
Université catholique de Louvain, Belgium

*CORRESPONDENCE
Nur Akmarina B. M. Said,
nur_akmarina@um.edu.my

RECEIVED 19 March 2024
ACCEPTED 04 April 2024
PUBLISHED 03 May 2024

CITATION
Said NABM, Mahmood S and To KKW (2024), Editorial: Tumour microenvironment in cancer research and drug discovery.
Front. Pharmacol. 15:1403176.
doi: 10.3389/fphar.2024.1403176

Editorial: Tumour microenvironment in cancer research and drug discovery

Nur Akmarina B. M. Said*, Syed Mahmood[2] and Kenneth K. W. To[3]

[1]Department of Pharmaceutical Life Sciences, Faculty of Pharmacy, University of Malaya, Kuala Lumpur, Malaysia, [2]Department of Pharmaceutical Technology, Faculty of Pharmacy, University of Malaya, Kuala Lumpur, Malaysia, [3]School of Pharmacy, Faculty of Medicine, The Chinese University of Hong Kong, Hong Kong, Hong Kong SAR, China

KEYWORDS

cancer, tumor microenvironment (TME), drug repurposing, immunotherapy, immune cells

Editorial on the Research Topic
Tumour microenvironment in cancer research and drug discovery

It has been long accepted that tumours do not exist or function in silos; indeed tumour progression is the orchestrated consequence of paracrine networking between tumours and their surrounding factors. Considering the tumour microenvironment (TME) in cancer research has profoundly shifted the paradigms in molecular investigation and translational drug discovery.

The TME components, including immune-inflammatory cells, cancer-associated fibroblasts, and endothelial and adipose cells, are correlated with cancer signatures, which carry diagnostic, therapeutic, and predictive values. There has been evidence to suggest changes in these microenvironmental cell types play an important role in even from somatic clonal expansions (Munugula et al.) and potentially the initial stages of cancer progression in normal tissues. In this Research Topic, we highlighted the significant impact of the TME component on cancer research, with a special focus on immune cells and drug repurposing targeting this component.

Immune cells surrounding tumours can be regulated by the metabolic microenvironment, which further reshapes the immune landscape. A myriad of key molecular regulators involved in lipid metabolism and glucose homeostasis have been implicated in reshaping the TME as well as assisting immune infiltration towards tumour progression and treatment resistance. In this edition, proliferator-activated receptor gamma (PPARγ) (Ran et al.) is comprehensively analysed.

Cancer metabolism takes place from the level of cellular metabolism down to nucleotide/amino acid metabolism. In glioma with active tryptophan catabolism and less tryptophan in the tumour, their high tryptophan metabolism-related genes signature (TrMRS) (Zhang et al.) was correlated with more immune cell infiltration and a "hot" immunological phenotype. Interestingly, this immuno-metabolic correlation holds the predictive value towards patients' response to immune checkpoint inhibitors.

Indeed, the involvement of immune cells in cancer progression has guided many treatment choices. Intensive lymphocyte infiltration has been shown to occur in higher-grade or recurrent gastric tumours (Zheng et al.). Immune cell infiltration has also been linked to m7G RNA methylation (Chen et al.) in renal clear cell carcinoma, with the

proposed m7G score being used to predict the cancer prognosis. In glioma too, the necroptosis index (NI) (Ma et al.) has been shown to influence sensitivity to immunotherapy, particularly anti-PD1 therapy. The prediction of the immunotherapy response has become the center of attention in studies evolving around TME. While this is not surprising given immune cells are the predominant gatekeeper cells that are often compromised in cancer, questions remain about whether the myriad of predictive data could be supported with strong mechanistic studies, both *in vitro* and *in vivo*.

Drug repurposing in targeting the TME is another Research Topic of interest in this area. It is very interesting to see how non-cancer-targeting substances/drugs could influence the immune landscape to the extent that they affect the response towards immunotherapy. This category includes aspirin and statins, which have been demonstrated to target the metabolic and immunomodulatory landscape of TME in preclinical models (Yu et al., 2022; Jing et al., 2023). It is more intriguing to see that most of the drugs being researched are 'accessory' drugs that are often being used by cancer patients in one way or another.

In this special edition, an antidepressant is shown to not only alleviate the depressant condition of cancer patients but also strengthen antitumour immunity. When using the antidepressant drug ansofaxine hydrochloride (Jing et al.), it is demonstrated this is achieved by the exhaustion of CD8+T, which also enhances the antitumour effects of anti-TNFR2.

Another drug—propofol anaesthesia usually administered during surgical resection of solid tumours—has been clinically shown to contribute to a better postoperative outcome in some malignant tumour surgeries, and it participates in reshaping the TME. Specifically, anti-angiogenesis was observed along with regulation of immunity, reduction of inflammation, and remodelling of the extracellular matrix. In this special edition, propofol (Zhou et al.) is extensively and mechanistically reviewed to provide a better understanding of its role in modulating TME with a theoretical guide for the selection of anaesthetics used in malignant tumour surgery.

A combination treatment using cordycepin (the vital bioactive compound of *Cordyseps* (Feng et al.) that has been used for its therapeutic potential) and the anti-CD47 antibody has been demonstrated to significantly enhance tumour suppression. This is in parallel with the increase in the proportion of M1 macrophages and the decrease in the M2 macrophages proportion. M1 and M2 are the two distinctive phenotypes of tumour-associated macrophages (TAMs), where M1 is known to inhibit tumour progression by inducing inflammatory responses and M2 supports tumour progression by suppressing immune responses.

Despite the concerted effort in the development of drugs targeting TME, such as BLZ945 (a colony-stimulating factor-1 receptor inhibitor) (Wei et al., 2020), there is a gap in the market for clinically satisfactory drugs that target this intricate factor. Among the highly researched is Focal adhesion kinase (FAK) (Hu et al.)—a non-receptor tyrosine kinase reviewed in this special edition. Numerous FAK inhibitors, including IN10018, defactinib, GSK2256098, conteltinib, and APG-2449, have demonstrated positive antitumour effects in preclinical studies and are undergoing clinical trials for their tumour scaffold function in sustaining TME.

siRNA and miRNA nanotherapeutics targeting TME molecular components is another tool being employed owing to their powerful gene-silencing properties, although formulation for effective delivery remains a challenge. In this context, it has been demonstrated that T7 peptide-decorated exosomes were able to package and protect cholesterol-modified Cy3-siYY1 (siRNA for Yin Yang transcription factor) (Liu et al.) to be released in the cytoplasmic reductive environment that is often observed in the tumourigenesis of glioblastoma.

The translational impact of the manipulation of the TME components is yet to be ascertained, but the landscape shows promise. The combination of a new treatment targeting TME with standard chemotherapy/immunotherapy also consistently demonstrates synergistic effects, and it will be very interesting to see this extended to targeting cell types other than immune cells within the TME in this regard.

Author contributions

NS: Conceptualization, Writing–original draft, Writing–review and editing. SM: Writing–review and editing. KT: Writing–review and editing.

Funding

The author(s) declare that no financial support was received for the research, authorship, and/or publication of this article.

Conflict of interest

The authors declare that the research was conducted in the absence of any commercial or financial relationships that could be construed as a potential conflict of interest.

The author(s) declared that they were an editorial board member of Frontiers, at the time of submission. This had no impact on the peer review process and the final decision.

Publisher's note

References

Jing, P., Luo, Y., Chen, Y., Tan, J., Liao, C., and Zhang, S. (2023). Aspirin-loaded cross-linked lipoic acid nanodrug prevents postoperative tumor recurrence by residual cancer cell killing and inflammatory microenvironment improvement. *Bioconjug Chem.* 34 (2), 366–376. doi:10.1021/acs.bioconjchem.2c00548

Wei, Q., Shen, N., Yu, H., Wang, Y., Tang, Z., and Chen, X. (2020). FXIIIa substrate peptide decorated BLZ945 nanoparticles for specifically remodeling tumor immunity. *Biomater. Sci.* 8 (20), 5666–5676. doi:10.1039/d0bm00713g

Yu, Z., Guo, J., Liu, Y., Wang, M., Liu, Z., Gao, Y., et al. (2022). Nano delivery of simvastatin targets liver sinusoidal endothelial cells to remodel tumor microenvironment for hepatocellular carcinoma. *J. Nanobiotechnology* 20 (1), 9. doi:10.1186/s12951-021-01205-8

frontiers | Frontiers in Pharmacology

TYPE Original Research
PUBLISHED 19 August 2022
DOI 10.3389/fphar.2022.975291

OPEN ACCESS

EDITED BY
Zhi Sheng,
Virginia Tech, United States

REVIEWED BY
Hernando Lopez-Bertoni,
Johns Hopkins Medicine, United States
Andrey A. Rosenkranz,
Lomonosov Moscow State University, Russia

*CORRESPONDENCE
Qunxing An,
1690896699@qq.com
Qingdong Guo,
guoqd1991@sina.cn
Jintao Gu,
gujintao@fmmu.edu.cn

†These authors have contributed equally to this work

SPECIALTY SECTION
This article was submitted to Pharmacology of Anti-Cancer Drugs, a section of the journal Frontiers in Pharmacology

RECEIVED 22 June 2022
ACCEPTED 21 July 2022
PUBLISHED 19 August 2022

CITATION
Liu X, Cao Z, Liu N, Gao G, Du M, Wang Y, Cheng B, Zhu M, Jia B, Pan L, Zhang W, Jiang Y, He W, Xu L, Zhang W, An Q, Guo Q and Gu J (2022), Kill two birds with one stone: Engineered exosome-mediated delivery of cholesterol modified YY1-siRNA enhances chemoradiotherapy sensitivity of glioblastoma.
Front. Pharmacol. 13:975291.
doi: 10.3389/fphar.2022.975291

Kill two birds with one stone: Engineered exosome-mediated delivery of cholesterol modified YY1-siRNA enhances chemoradiotherapy sensitivity of glioblastoma

Xiao Liu[1,2†], Zhengcong Cao[1†], Nannan Liu[3†], Guangxun Gao[2], Mingrui Du[4], Yingwen Wang[1], Boyang Cheng[1], Maorong Zhu[1], Bo Jia[2], Luxiang Pan[1], Wangqian Zhang[1], Yuran Jiang[5], Wei He[1], Linlin Xu[2], Wei Zhang[1], Qunxing An[2]*, Qingdong Guo[2]* and Jintao Gu[1]*

[1]State Key Laboratory of Cancer Biology, Biotechnology Center, School of Pharmacy, The Fourth Military Medical University, Xi'an, China, [2]The First Affiliated Hospital, The Fourth Military Medical University, Xi'an, China, [3]Experimental Teaching Center of Basic Medicine, The Fourth Military Medical University, Xi'an, China, [4]The Second Affiliated Hospital, The Fourth Military Medical University, Xi'an, China, [5]The Third Affiliated Hospital, The Forth Military Medical University, Xi'an, China

Glioblastoma (GBM) is the most malignant tumor of the central nervous system in adults. Irradiation (IR) and temozolomide (TMZ) play an extremely important role in the treatment of GBM. However, major impediments to effective treatment are postoperative tumor recurrence and acquired resistance to chemoradiotherapy. Our previous studies confirm that Yin Yang 1 (YY1) is highly expressed in GBM, whereby it is associated with cell dedifferentiation, survival, and therapeutic resistance. Targeted delivery of small interfering RNA (siRNA) without blood-brain barrier (BBB) restriction for eradication of GBM represents a promising approach for therapeutic interventions. In this study, we utilize the engineering technology to generate T7 peptide-decorated exosome (T7-exo). T7 is a peptide specifically binding to the transferrin receptor. T7-exo shows excellent packaging and protection of cholesterol-modified Cy3-siYY1 while quickly releasing payloads in a cytoplasmic reductive environment. The engineered exosomes T7-siYY1-exo could deliver more effciently to GBM cells both *in vitro* and *in vivo*. Notably, *in vitro* experiments demonstrate that T7-siYY1-exo can enhance chemoradiotherapy sensitivity and reverse therapeutic resistance. Moreover, T7-siYY1-exo and TMZ/IR exert synergistic anti-GBM effect and significantly improves the survival time of GBM bearing mice. Our findings indicate that T7-siYY1-exo may be a potential approach to reverse the chemoradiotherapy resistance in GBM.

KEYWORDS

glioblastoma, Yin Yang 1, T7, exosome, chemoradiotherapy sensitization

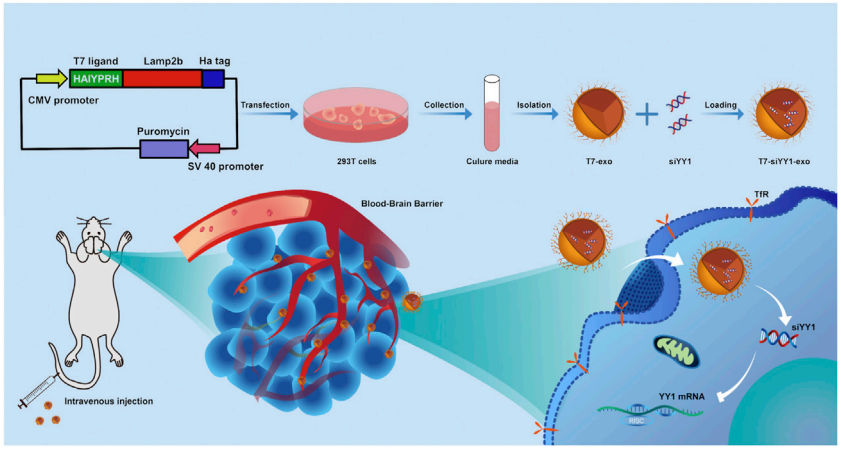

Graphical Abstract

Introduction

Glioblastoma (GBM) is a primary brain cancer with the highest mortality (Movahedpour et al., 2021). The average lifespan of patients with GBM is less than 1 year, and only 5% of them live for more than 5 years. The standard treatment for glioblastoma is surgical resection, followed by radiotherapy and chemotherapy with temozolomide (TMZ) (Kim et al., 2020). Nevertheless, surgical treatment is limited because of the high invasiveness of GBM and may not suitable for some patients depending on their condition. In addition, most drugs including TMZ are very toxic with severe side-effects (Yasaswi et al., 2021). Despite the maximal surgical resection followed by adjuvant chemoradiotherapy, the median time to tumor recurrence is approximately 8 months (Adamus et al., 2022). To overcome this problem, new strategies are necessary to counteract both TMZ and radiation resistance.

Yin Yang 1 (YY1), a transcription factor overexpressed in GBM, has been identified in our research as well as in previous research. As reported, it can help to regulate cell dedifferentiation, cell survival, and therapeutic resistance (Gu et al., 2021). Moreover, according to previous studies, knockdown of YY1 can significantly block the tumor malignance and reverse the resistance (Sarvagalla et al., 2019). Considering that YY1 overexpression is observed in many cancers and has various biological functions with respect to the hallmarks of cancer, it is an attractive approach to utilize YY1 as a novel target for therapeutic interventions. However, cancer-promoting transcription factors cannot be easily targeted due to their nuclear localization, YY1 is predominantly present in nuclei and not easily targeted (Verheul et al., 2020).

Gene therapy is a new clinical strategy for GBM treatment and has attracted extensive attention recently. Compared with other existing techniques for gene regulation, RNA interference is a methodology able to silence cancer-promoting genes as reported (Cui et al., 2018). Small interfering RNA (siRNA) combined with chemotherapy is considered as one promising strategy against cancer, and many studies demonstrated the outcomes of such co-treatment are significantly better than those using the siRNA or chemotherapeutic drug alone (Xiao et al., 2018). However, siRNA is unstable in systemic circulation and bio-membrane permeability. Thus it is necessary to find suitable carriers for the effective delivery of siRNA *in vivo* (Ruan et al., 2018). Examinations confirmed the effectiveness of liposomal, viral vectors and nanoparticles for RNA transfection, while they are immunogenic, toxic and degrade slowly (Kase et al., 2021).

Exosomes are small membrane vesicles of endocytic origin, which can be released into the extracellular environment during the fusion of multivesicular bodies with the cytomembrane (Yu et al., 2022). Because of their low immunogenicity and toxicity, biodegradability, and strong ability to protect endogenous biologically active ingredients, exosomes have become a new therapeutic strategy in drug delivery (Fu et al., 2021). However, natural exosomes lack targetability and present a rapid accumulate in peripheral organs like the spleen and liver following the systemic treatment, instead of targeting specific tissues (Jiang et al., 2018). According to recent studies, specific ligands can be expressed on the exosome membrane surface via gene modification, achieving the targeted exosome delivery (Huang et al., 2022). In brain tumor, the TfRs are highly expressed in brain microvascular endothelial cells (BMVECs) and GBM cell line for regulation of brain uptake of iron (Tortorella and Karagiannis, 2014; Choudhury et al., 2018; Mojarad-Jabali et al., 2022). T7 is a transferrin receptor (TfR)-binding peptide with the sequence HAIYPRH. On that account, it is possible that T7 is an ultrahigh-efficiency targeting strategy for GBM-targeted delivery.

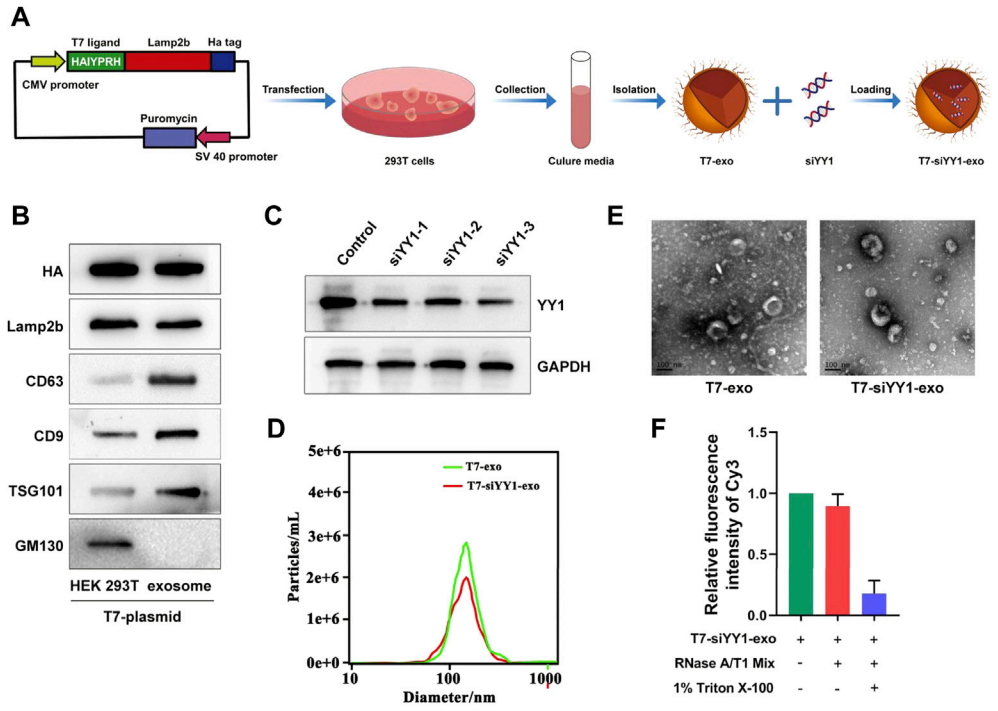

FIGURE 1
Preparation and characterization of T7-siYY1-exo. **(A)** Schematic diagram of preparation and isolation of T7-siYY1-exo. **(B)** Detection of CD9, CD63, TSG101, Lamp2b, HA, and GM130 expression by Western blot. **(C)** Detection of YY1 knockdown efficiency. **(D)** Size distribution of T7-exo and T7-siYY1-exo measured by NANO SIGHT. **(E)**Transmission electron micrograph of T7-exo and T7-siYY1-exo. **(F)** qRT-PCR analysis of siYY1-Cy3 after treatments with RNase A/T1 Mix and 1% Triton X-100 for 30 min.

Herein, a TfR-targeting exosome was produced by creating a fusion protein of T7 peptide and Lamp2b. After systemic administration, the T7 ligand-decorated exosome (T7-exo) could bind to GBM in the brain and enhance the efficiency of cholesterol-modified siYY1 delivery. Therefore, T7-exo was evaluated as a GBM-targeting carrier of siYY1. In the orthotopic GBM mice model, combined with temozolomide or radiotherapy, targeting knockdown of YY1 via cholesterol-modified siYY1 delivered by engineered exosomes synergistically inhibited the growth of GBM. Overall, T7-siYY1-exo has the potential to overcome chemoradiotherapy resistance in GBM by multiple mechanisms.

Results

Characterization of T7-decorated exosomes and siYY1-loaded exosomes

To generate T7-exo, stable cell lines were prepared by transfection of plasmids encoding T7-Lamp2b into 293T cells (Figure 1A). Ligand-decorated exosomes were then isolated and confirmed by western blotting with an anti-HA-tag antibody which could be expressed as a fusion protein regarding ligand-Lamp2b. Moreover, exosome membrane proteins CD9, CD63, TSG101, and GM130 assisted in further identifying the T7-exo (Figure 1B). These data confirmed that T7-exo had characteristics of exosomes and targeting ligands. To screen out a cholesterol-modified Cy3-siYY1 sequence of which gene knockdown efficiency is best, three siRNA sequences for YY1 were designed and transfected into LN229 cells. The results showed that the third siRNA sequence exhibited a gene knockdown efficiency of more than 80%, significantly higher than the other two (Figure 1C), and the third siRNA YY1 was used for subsequent experiments. Then, T7-siYY1-exo was prepared and characterized. The isolated exosomes had a homogenous size, and a single peak was shown in distribution graphs. The dimensions of exosomes were measured at about 120 nm, and there was no significant effect on the size of exosomes encapsulated with siYY1 (Figure 1D). TEM images assisted in evaluating the morphology of exosomes and siYY1-loaded exosomes. The morphology of unmodified exosomes was not obviously different from that of ligand-decorated T7-siYY1-exo (Figure 1E). Additionally, when treated with RNase A/T1 mix, it was found that the Cy3 fluorescence intensity was not reduced, which proved that siYY1 was protected,

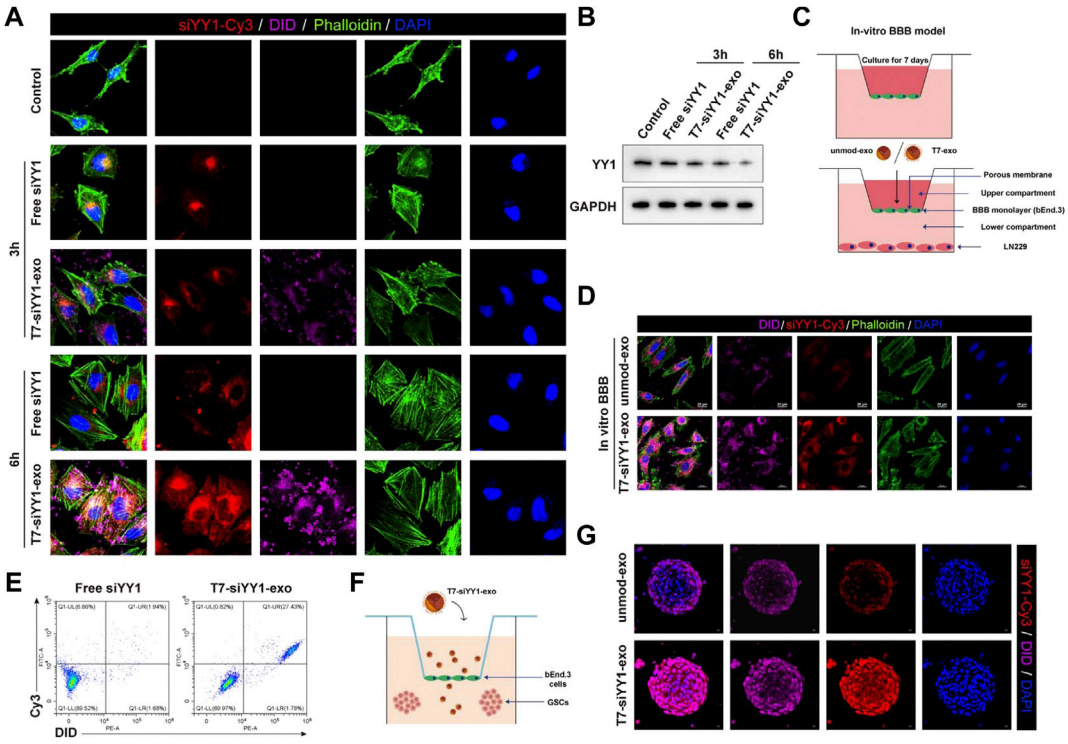

FIGURE 2
Cellular uptake of T7-siYY1-exo in vitro and BBB/BBTB model. **(A)** The delivery efficiency of Free siYY1 and T7-siYY1-exo in LN229 cells. Cy3-labeled siYY1 and loaded DID-labeled exosomes (5 μg/ml) were used to treat LN229 cells. After 24h incubation, the cytoskeleton was stained with phalloidin and the cell nuclei were stained with DAPI. The fluorescent was photographed under a confocal laser scanning microscope using Nikon NIS-Elements software (Nikon, Tokyo, Japan). **(B)** The knockdown efficiency of YY1 was detected by Western blot. **(C)** Schematic diagram of the BBB model *in-vitro*. **(D)** Representative immunofluorescence images showing T7-siYY1-exo uptake into LN229 cells after passing through a bEnd.3 monolayer. Unmod-exo/T7-siYY1-exo (5 μg/ml) was added to upper compartment. The fluorescent was photographed under a confocal laser scanning microscope using Nikon NIS-Elements software (Nikon, Tokyo, Japan). **(E)** The positive rates of DiD and Cy3 were detected by flow cytometry. **(F,G)** The penetrating and tumor targeting efficacy of T7-siYY1-exo evaluated through BBTB/LN229 tumor spheroids co-culture model. The treatment concentration of unmod-exo/T7-siYY1-exo was 5 μg/ml. The fluorescent was photographed under a confocal laser scanning microscope using Nikon NIS-Elements software (Nikon, Tokyo, Japan).

unless 1% Triton X-100 was co-applied to the treatment, which resulted in the degradation of exosome membranes (Figure 1F). These findings revealed that the engineered exosomes were successfully isolated and prepared.

In vitro BBB/BBTB penetrating ability of T7-siYY1-exo

To evaluate the siYY1 delivery efficiency of T7-exo, electroporation was applied to loading the cholesterol-modified cy3-siYY1 into exosomes to form complexes. Fluorescence microscope results showed that cholesterol-modified cy3-siYY1 could be more efficiently integrated into cells via T7-exo than transfection alone to facilitate gene knockdown (Figure 2A). The T7-siYY1-exo group showed a lower YY1 expression than the Free-siYY1 group. Both Free-siYY1 and T7-siYY1-exo could silence YY1 *in vitro*, with the latter exhibiting a more substantial effect (Figure 2B).

An *in vitro* BBB model which has a transwell system was first used for assessing the ability of T7-siYY1-exo to penetrate the BBB. Under this system, bEnd.3 cells were cultured in the upper compartment and used T7-siYY1-exo and Free siYY1 for treatment, respectively, together with culturing LN229 cells in the lower room (Figure 2C). As shown in Figure 2D, only T7-siYY1-exo could pass through the BBB monolayer and reach the LN229 cells cultured in the lower compartment. Flow cytometry assisted in examining the DiD and Cy3 signal intensity, finding T7-exo significantly enhanced Cy3 signal in LN229 cells compared to Free siYY1 (Figure 2E). It can be concluded that T7-exo can penetrate the *in vitro* BBB model meanwhile accumulating in the cytoplasm of LN229 cells.

To evaluate the transcytosis efficiency of T7-siYY1-exo, we established the bEnd.3/LN229 tumor spheroids co-culture model for imitating the blood–brain tumor barrier (BBTB) *in vitro*

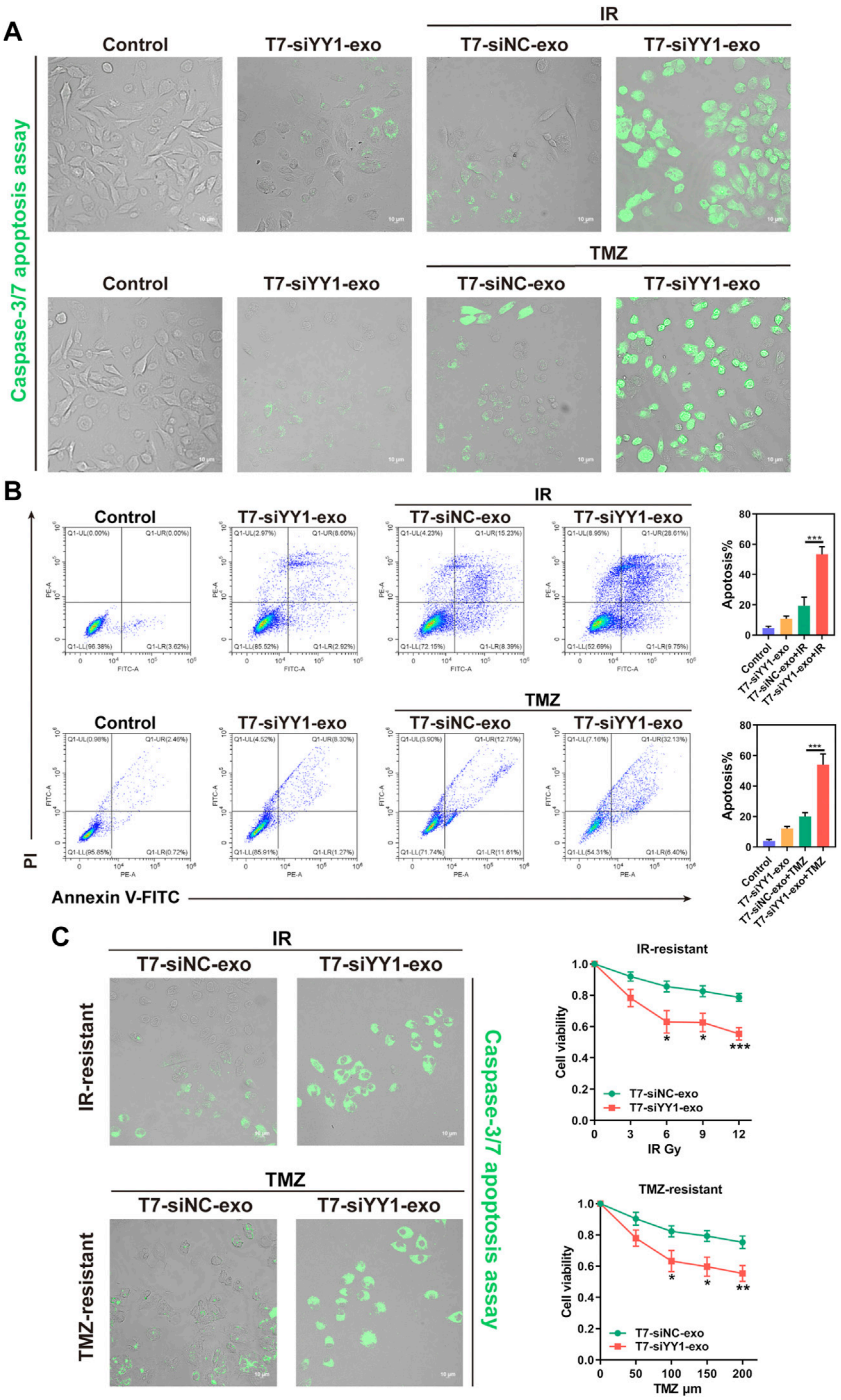

FIGURE 3
The therapeutic effect of T7-siYY1-exo in vitro. **(A)** LN229 cells were cultured in the presence of T7-siNC-exo/T7-siYY1-exo (5 μg/ml) and TMZ (50 μM)/IR (6Gy) for 2 days and apoptotic cells were visualized by caspase-3/7 apoptosis assay. The fluorescent was photographed under a confocal laser scanning microscope using Nikon NIS-Elements software (Nikon, Tokyo, Japan). Data in a are representative of three independent biological experiments. **(B)** LN229 cells administrated with T7-siNC-exo/T7-siYY1-exo (5 μg/ml) and TMZ (50 μM)/IR (6Gy) were subjected to FACS to detect apoptosis. *p* values are displayed as $*p \leq 0.05$, $**p \leq 0.01$, $***p \leq 0.001$. **(C)** The effect of T7-siYY1-exo on LN229-IR-resistant and LN229-TMZ-resistant cells. The concentration of TMZ was 200 μM and the dose of IR was 12Gy. *p* values are displayed as $*p \leq 0.05$, $**p \leq 0.01$, $***p \leq 0.001$.

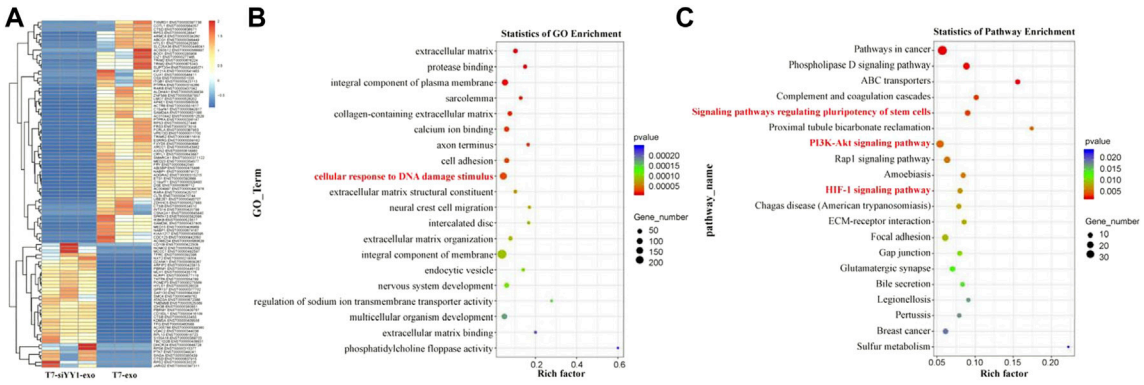

FIGURE 4
Molecular mechanism of T7-siYY1-exo. **(A)** RNA sequencing was performed on T7-siYY1-exo treated cells. **(B)** Gene ontology (GO) enrichment analysis enrichment of differential genes after T7-siYY1-exo treatment. **(C)** KEGG bioinformatics analysis of differential genes after T7-siYY1-exo treatment.

(Figure 2F). Interestingly, the Cy3 and DiD fluorescence were powerful inside the tumor spheroids receiving the treatment with T7-siYY1-exo, supporting T7-siYY1-exo effectively penetrated into GBM. In contrast, tumor spheroid receiving the treatment of unmod-exo displayed weak Cy3 and DiD fluorescence only in the superficial area (Figure 2G). The above findings confirmed that the functionalization of the exosome with T7 peptide is capable of remarkably enhancing the BBTB penetration ability and the GBM targeting ability.

T7-siYY1-exo enhanced TMZ and radiation sensitivity of GBM cells *in vitro*

The above findings revealed the effective taking up of engineered exosomes by recipient cells. We then determined whether T7-siYY1-exo was sufficient to enhance the chemoradiotherapy sensitivity of GBM cells. Apoptotic cells were visualized by caspase-3/7 apoptosis assay. The single delivery of siYY1 could not bring perfect and effective treatment, indicating that single siYY1 lacked strong therapeutic function. Besides, T7-siYY1-exo together with TMZ or IR led to a substantial enhancement of apoptosis compared with that of the cells treated with T7-Negative Control of siRNA-exo (T7-siNC-exo) together with TMZ or IR (Figure 3A). Flow cytometry analysis of LN229 cells undergoing apoptosis found that T7-siYY1-exo caused a noticeable increase in TMZ and radiation sensitivity. That is to say, T7-siYY1-exo exhibited an enhanced synergistic effect on inducing apoptosis in the target cells (Figure 3B).

In order to further observe the sensitizing effect of T7-siYY1-exo on chemoradiotherapy resistant cells, a TMZ-resistant derivative of the LN229 GBM cell line (LN229-TMZ-resistant) was produced via the serial passage of these cells in the presence of increasing TMZ concentrations. Moreover, LN229-IR-resistant cells were generated by parental cells after 6 times of 2Gy irradiation. Surprisingly, T7-siYY1-exo enhanced the sensitivity of LN229-TMZ-resistant and LN229-IR-resistant cells to chemotherapy and radiotherapy, reversed the therapeutic resistance of cells (Figure 3C). Thus, the results suggested that T7-siYY1-exo can simultaneously enhance the sensitivity of GBM cells to chemotherapy and radiotherapy.

To gain insights into the mechanism of T7-siYY1-exo, transcriptomic sequencing was performed on T7-siYY1-exo and T7-exo treated cells (Figure 4A). Gene ontology (GO) analysis showed that gene sets for cellular response to DNA damage stimulus were enriched in T7-siYY1-exo treatment cells (Figure 4B). Additionally, KEGG bioinformatics analysis revealed the enrichment of signaling pathways that regulated the pluripotency of stem cells, PI3K-Akt signaling pathway and HIF-1 signaling pathway in T7-siYY1-exo treatment cells (Figure 4C). Indeed, previous studies revealed the close association of these gene sets with TMZ and radiotherapy resistance (Persano et al., 2012; Tomar et al., 2020; Nie et al., 2021).

Efficiency of *in vivo* systemic delivery of T7-exo to the brain tumor

The uptake and the function of T7-exo were identified in GBM cells *in vitro*, followed by the determination of the biodistribution of T7-exo *in vivo*. We injected 200 μg of DiD-labeled unmod-exo or T7-exo loaded with 0.5OD Cy3 labeled siYY1 into mice via the tail vein, and detect fluorescence signal through *in vivo* imaging system (IVIS). As shown in Figure 5A, the intensity and distribution of

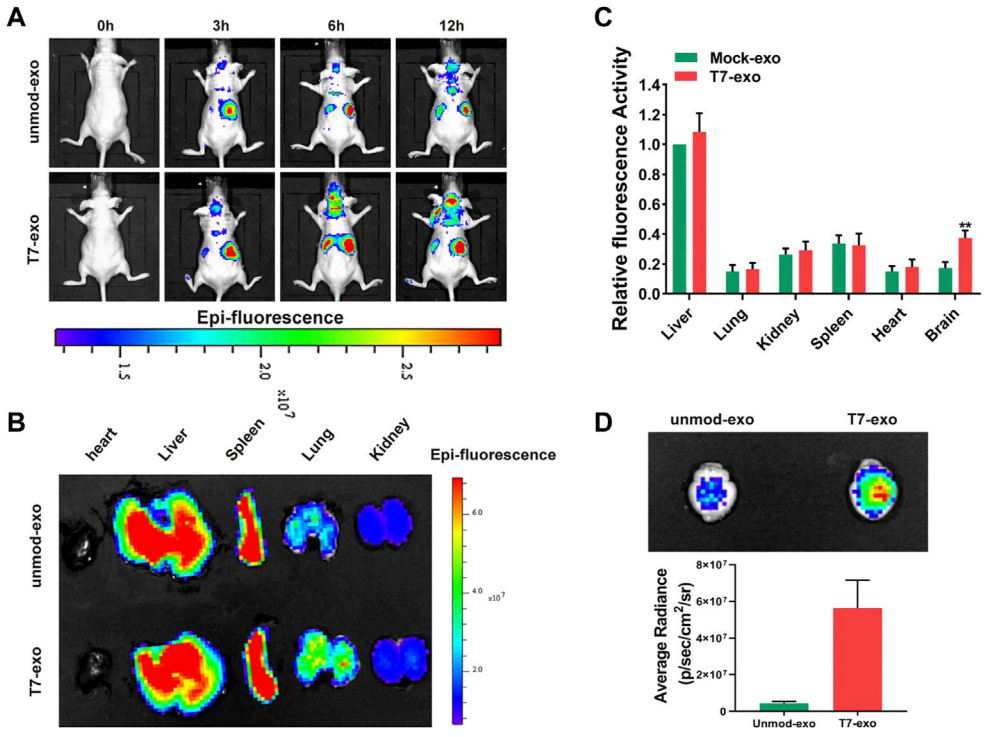

FIGURE 5
Tumor targeting ability of T7-siYY1-exo in orthotopic GBM xenograft model using LN229 cells. **(A)** *In vivo* florescence imaging of Orthotopic GBM xenograft mice at 0, 3, 6 and 12 h time point after intravenous administration of unmod-exo/T7-siYY1-exo (200 ug). **(B)** *Ex vivo* fluorescence images of Liver, Spleen, Lung, Heart and Kidney from mice sacrificed at 12 h post-injection. **(C)** Fluorescence quantitative analysis of *ex vivo* organs of LN229 tumor-bearing mice after intravenous injection. *p* values are displayed as $*p \leq 0.05$, $**p \leq 0.01$, $***p \leq 0.001$. **(D)** *Ex vivo* images and quantitative analysis of the GBM-bearing brains.

fluorescence were recorded at different time points (0, 3, 6, 12 h) after mock unmod-exo or T7-exo injection. According to the fluorescence quantification of different organs (brain, heart, liver, spleen, lung, and kidney), we found that the fluorescence intensity exhibited an obvious concentration in the peripheral organs at 12 h following the injection with unmod-exo or T7-exo. Then, the assessment on the ability of T7-exo to deliver cholesterol-modified siYY1 *in vivo* was conducted via Cy3 fluorescence intensity, detecting the relative fluorescence intensity of siYY1-Cy3 in various organs of mice after unmod-exo or T7-exo injection. As shown in Figure 5B, siYY1-Cy3 exhibited enrichment in a variety of organs at different time points of post-injection. Unsurprisingly, fluorescent images of the other organs show that T7-siYY1-exo was mainly metabolized in the liver (Figure 5C). Notably, based on the *ex vivo* imaging regarding brains at 12 h together with the fluorescence quantitative analysis, the T7-siYY1-exo showed an obvious accumulation in GBM tissue instead of normal brain tissue (Figure 5D). These results revealed that T7-modified exosomes possessed a better ability to overcome BBB and target GBM than did unmodified exosomes.

T7-siYY1-exo enhance the *in vivo* efficacy of chemotherapy and radiotherapy for GBM

To investigate the *in vivo* effects of T7-siYY1-exo for GBM, we established Orthotopic GBM xenograft model as described. Tumors were allowed for a 14 days growth followed by treatment daily with saline, T7-siYY1-exo, IR, TMZ, IR + T7-siYY1-exo or TMZ + T7-siYY1-exo for 7 days, and tumor signals were evaluated using luciferase bioluminescence. Based on the tumor bioluminescence quantification, T7-siYY1-exo combined with TMZ or IR could hinder the tumor growth to a much larger extent than TMZ or IR alone (Figure 6A). It should further be noted that T7-siYY1-exo monotherapy had a slightly treatment effect on GBM. The tumor volume as a reflection of tumor burden, Hematoxylin-eosin (HE) staining showed that T7-siYY1-exo combined with TMZ or IR regimens showed significantly increased antitumor activity, relative to monotherapy (Figures 6B,C). For further examining the efficacy of T7-siYY1-exo against GBM *in vivo*, we plotted as well as monitored Kaplan-Meier survival curves regarding the model mice, finding that relative to mice in the control group,

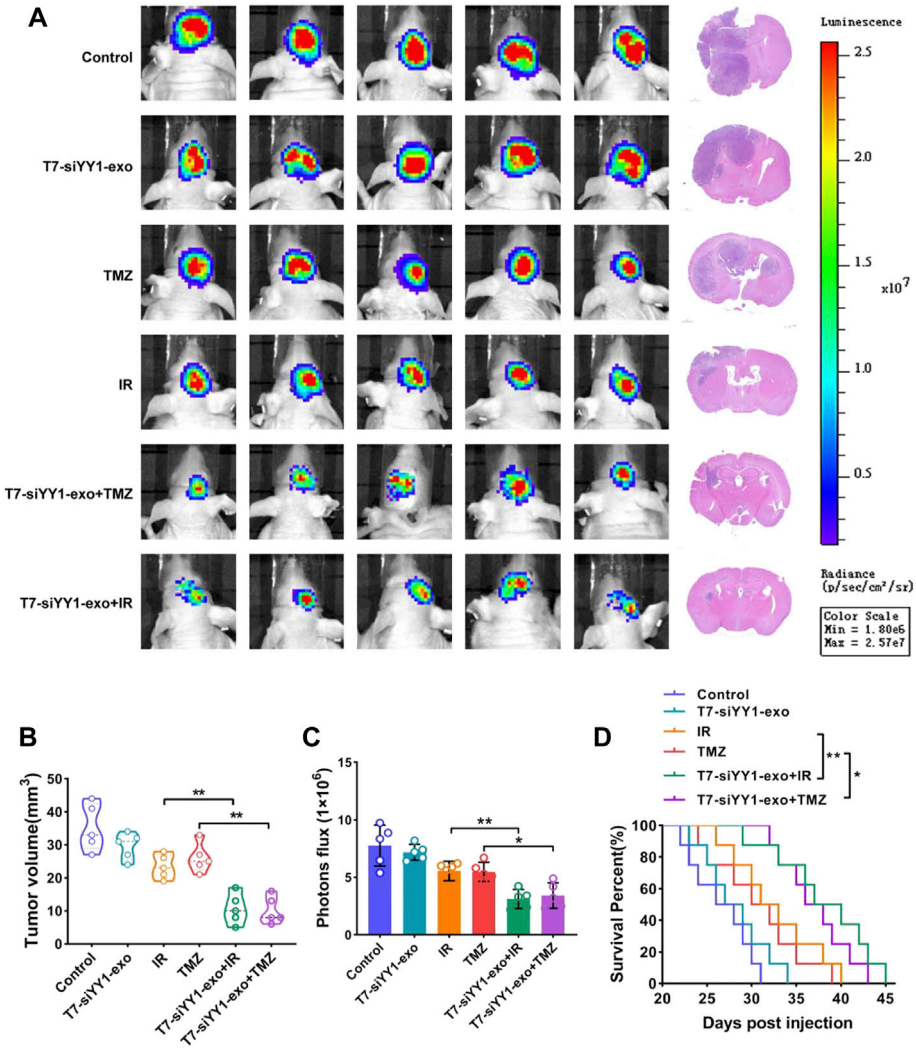

FIGURE 6
Anti-tumor efficiency of T7-siYY1-exo in vivo. **(A)** Left, representative images of *in vivo* orthotopic GBM bioluminescence. Right, Representative images of H&E staining. Bioluminescence images were captured by IVIS on day 21 in all groups. After mice sacrifice, brain tissue samples were obtained for HE staining. **(B)** The tumor volume was calculated using a modified ellipsoid formula. Brain tissue samples were obtained after mice sacrifice. *p* values are displayed as $*p \leq 0.05$, $**p \leq 0.01$, $***p \leq 0.001$. **(C)** Quantification of the bioluminescence of xenografts derived from the luciferase-labeled LN229 cells in each group. Bioluminescence images were captured by IVIS on day 21 in all groups. *p* values are displayed as $*p \leq 0.05$, $**p \leq 0.01$, $***p \leq 0.001$. **(D)** Kaplan–Meier survival plot was graphed to evaluate mice lifespan in each group, mice were collected at end stage. *p* values are displayed as $*p \leq 0.05$, $**p \leq 0.01$, $***p \leq 0.001$.

treatment with IR and TMZ helped to extend a little the survival of GBM mice. Importantly, mice administrated with T7-siYY1-exo and TMZ/IR had an obvious loner survival time compared to mice receiving IR and TMZ alone (Figure 6D).

In vivo safety evaluation

Toxicity is considered to be another significant parameter of a suitable delivery vehicle besides the delivery efficiency. In the *in vivo* safety experiment, in order to eliminate the influence of immune deficiency, we carried out relevant experiments in BALB/c mice. We intravenously injected 15 mg/kg T7-exo into healthy BALB/c mice for 12 days for evaluating the systematic toxicity exhibited by T7-exo. Obviously, the mononuclear phagocyte system absorbed as well as cleared the majority of exosomes after intravenous injection. Hence, we conducted an investigation on the T7-exo-induced potential pathological damage on such organs. In the group receiving T7-exo treatment, major tissues, including the heart, liver, spleen, lung, and kidney, did not exhibit any distinct histopathological abnormalities or damage (Figure 7A). Blood biochemistry

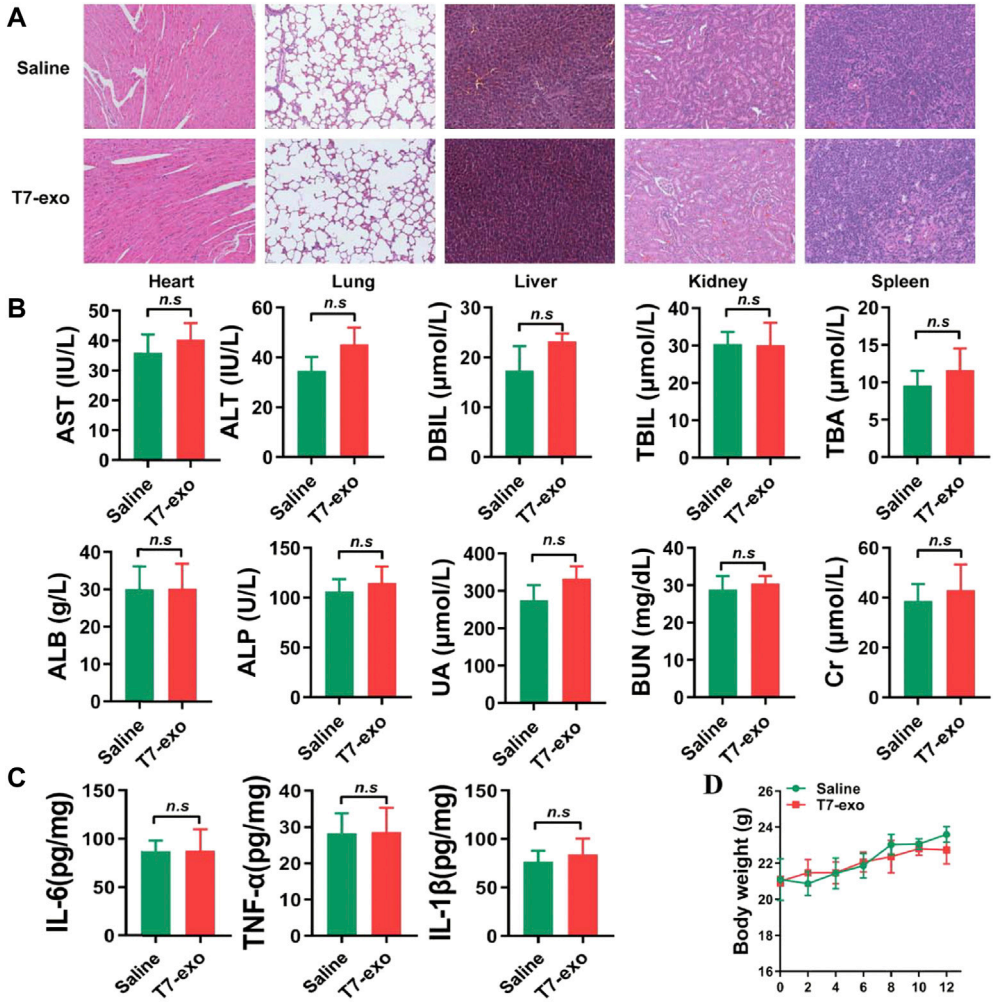

FIGURE 7
The systematic toxicity assessment of T7-siYY1-exo. **(A)** Histological analyses of liver, heart, kidney, lung and spleen sections stained with H&E of BALB/c mice post-intravenous injection of T7-siYY1-exo (200 μg) or Saline for 12 days (one dose every other day). **(B)** Clinical chemistry and hematology parameters for T7-siYY1-exo treated mice. *p* values are displayed as not significant (ns) for $p > 0.05$. **(C)** The expression level of serum inflammatory cytokines TNF-α, IL-1β and IL-6. **(D)** Body weight changes in T7-siYY1-exo treated mice.

together with the hematology analysis assisted in revealing the potential toxic action exerted by exosomes over treated mice. Measurement of the key biomarkers of liver and kidney injury, including alanine aminotransferase (ALT), aspartate aminotransferase (AST), alkaline phosphatase (ALP), direct bilirubin (DBIL), total bilirubin (TBIL), total bile acid (TBA), serum albumin (ALB), creatinine (CR), uric acid (UA) and blood urea nitrogen (BUN) was performed before the completion of the experiment. As shown in Figure 7B, all the above indicators were the same as animals treated with saline, indicating that T7-exo had no significant hepatorenal toxicity within the dosing regimen. No obvious immune response was elicited in T7-exo and saline, as serum inflammatory cytokines like IL-1β, TNF-α and IL-6 exhibited similar levels to the saline control group (Figure 7C), suggesting that T7-exo did not lead to an inflammatory response. During the study period, the experimental group presented no deaths or serious weight loss (Figure 7D). These results showed that T7-exo did not cause acute toxicity to the hematological system and major organs in mice.

Materials and methods

Cell culture and treatment

Human GBM cell lines LN229 were obtained from American Type Culture Collection (ATCC). The cell line bEnd.3 was

TABLE 1 The siRNA sequence of YY1.

siRNA constructs	Target sequence in mRNA (5′-3′)
YY1 siRNA-1 sense	CGACGACUACAUUGAACAATT
YY1 siRNA-1 antisense	UUGUUCAAUGUAGUCGUCGTT
YY1 siRNA-2 sense	CGACGACGACUACAUUGAATT
YY1 siRNA-2 antisense	UUCAAUGUAGUCGUCGUCGTT
YY1 siRNA-3 sense	GAUGAUGCUCCAAGAACAATT
YY1 siRNA-3 antisense	UUGUUCUUGGAGCAUCAUCTT

acquired from Beina Chuanglian Biology Research Institute (Beijing, China). All cells were cultured in Dulbecco's modified Eagle's medium (DMEM) supplemented with 10% FBS (Gibco, Australia origin), 1% penicillin/streptomycin (NCM biotech, Suzhou, China) at 37°C with 5% CO_2.

Establishment of the TMZ-resistant cell line

The LN229 cells were inducted of drug resistance by TMZ (TOPSCIENCE, Shanghai, China) with increasing concentration gradient as following concentrations: 20, 50, 100, 200, 400 μM. Each dose was maintained for 15 days, and finally a stable TMZ-resistant cell line was obtained. Simultaneously, intermittent high-concentration stimulation (800 μM TMZ for 48 h) and maintenance was conducted as necessary.

pcDNA3.1 (+)-T7 ligand-LAMP2B-HA construction, preparation

For construction of a T7-Lamp2b plasmid (pT7-Lamp2b), the cDNA fragments encoding the T7 (HAIYPRH) peptide and Lamp2b were inserted downstream of the CMV promoter in the pcDNA3.1 vector. The Human influenza hemagglutinin (HA) tag was added at the end of the Lamp2b sequence.

Preparation of ligand-decorated exosomes

To prepare stable cell lines for generation of ligand-decorated exosomes, 293T cells were cultured in DMEM supplemented with 10% FBS. T7-Lamp2b were transfected into the cells using Lipo 3,000 according to the manufacturer's manual. After 4 h of transfection, the medium was replaced with fresh medium containing puromycin at 2 μg/ml concentration. Stable 293T cell lines containing T7-Lamp2b were cultured for 3 days in DMEM supplemented with 10% FBS. Then, the medium was harvested, the cell medium containing exosomes was harvested by centrifugation at 300 *g* for 5 min to eliminate cells and subsequently centrifuged at 10,000×g for 30 min to remove dead cells and cell debris. Finally, the clear supernatant was centrifuged for 90 min at 120,000×g to pellet exosomes using ultracentrifuge (Beckman, United States). At last, exosomes were resuspended into 100 μL of 1× PBS and stored immediately at -80°C. All the centrifugation steps were carried out at 4°C.

Nanoparticle tracking analysis

The NTA was performed as described previously (Mao et al., 2017). In brief, the size distribution of the exosomes was analyzed using a Nano Sight LM10 instrument (Marvern instruments, UK). The particle suspensions were diluted with PBS to a concentration of 10^8 particles/mL for analysis.

Screening of siRNA sequences

To screen the effective cholesterol-modified siYY1 sequence that silenced YY1 protein, we designed three different siRNA sequences and transfected into LN229 (Table 1). The YY1 protein was collected and examined by Western Blot to screen the sequence with the highest silence efficiency.

Loading of siYY1 oligonucleotide into exosomes

The cholesterol-modified siYY1 sequence of YY1 is 5′- GAU GAUGCUCCAAGAACAATT-3′; 5′-UUGUUCUUGGAGCAU CAUCTT-3′. To encapsulate siYY1 into exosomes, exosomes at a total protein concentration of 20 μg were mixed with 20 μg of siYY1 in 400 μL of PBS. The mixture was electroporated at 400 V in a 4 mm cuvette. Unloaded siYY1 were removed by ultracentrifugation at 120,000 g. The supernatants were removed and the pellets were resuspended.

In vitro BBB model

An *in-vitro* BBB model was established using LN229 and bEnd.3 cells as described previously (Yang et al., 2021). In brief, bEnd.3 cells were seeded into the upper chamber of Transwell inserts coated with 2% gelatin solution and cultured for 7 days in DMEM supplemented with 10% FBS. LN229 cells were seeded in the lower Transwell compartment. Cy3-labeled siYY1 and T7-siYY1-exo were added to the upper chamber to assess the penetration efficiency of free siYY1 and T7-siYY1-exo across the BBB.

Exosomes labeling

The fuorescent dye DiD was purchased from Lumiprobe (United States) and used to label exosomes. Purified exosomes were incubated in the presence of 5 mM DiD for 15 min at 37°C then ultracentrifuged at 120,000×g, 90 min to remove the unbounded dye. After being washed twice in PBS with 120,000×g centrifugation, the labeled exosomes were resuspended in PBS prior to use.

RNA protection assay

T7-siYY1-exo were incubated with 20 μL RNase A/T1 mix with or without 1% Triton X-100 at 37°C for 30 min. The fluorescence intensity of Cy3 was detected by confocal microscope.

Cell viability assay

For the cell viability assay, 5×10^3 cells were plated in 96-well plates and treated in triplicate for 3 days with TMZ. Cell proliferation was estimated using the Cell Counting Kit-8 (CCK-8) following the protocol, the absorbance was measured at 450 nm using a Microplate Reader (Biotek, United States).

Orthotopic mouse xenografts

Male, 6-week-old BAL B/c nude mice (~18 g) were obtained from Gempharmatech Co., Ltd. (Nanjing, China). GBM cells expressing luciferase were intracranially transplanted into immunocompromised mice. In brief, a burr hole was made 2.5 mm left of the sagittal suture and 0.5 mm anterior to the bregma using a dental drill with a diameter of 0.7 mm, and the injection depth is 2.5 mm. To examine the tumor growth, animals were administrated intraperitoneally with 3.0 mg/100 uL solution of D-Luciferin potassium salt (Abcam, United States) and anesthetized with isoflurane for the imaging analysis. The tumor luciferase images were captured by using an IVIS 100 imaging system (PerkinElmer, United States).

Animal studies

For *in vivo* evaluating delivery of engineered T7-exos, unmod-exos and T7-exos (about 200 ug) were labeled with the DID and injected into the tumor-bearing mice via the tail vein to analyze the distribution of exosomes. Fluorescence signals were detected by IVIS at 0, 3, 6 and 12 h after injection. Afterwards, the mice were sacrificed by cervical dislocation, then the organs and tumors were taken out, and the distribution of fluorescently labeled exosomes in various organs was observed using IVIS.

To evaluate *in vivo* effect of T7 exos, orthotopic mice xenografts with Luc-LN229 cells were divided into six groups. Saline, T7-siYY1-exo, TMZ, IR, T7-siYY1-exo + TMZ and T7-siYY1-exo + IR. The treatment was started after tumor formation on day 14. All animal studies were performed in accordance with protocols approved by the Ethical Committee and Institutional Review Board of Fourth Military Medical University.

In vivo safety evaluation

Eight female BALB/c mice were randomly divided into two groups. One group received an intravenous injection of T7-siYY1-exo (20 mg/kg) at one dose for 12 days and the other group was treated with Saline as control. Blood samples and major organ tissues were collected at 24 h after the last administration, for hematologic and histochemistry analysis. The serum alanine aminotransferase (ALT), aspartate aminotransferase (AST), alkaline phosphatase (ALP), direct bilirubin (DBIL), total bilirubin (TBIL), total bile acid (TBA), serum albumin (ALB), creatinine (CR), uric acid (UA) and blood ureanitrogen (BUN) levels were analyzed by Hitachi 7,080 Chemistry Analyzer. Major organs such as brain, heart, lung, liver, spleen, and kidney were fixed with paraformaldehyde for 48 h and embedded in paraffin. All animal procedures were conducted in accordance with the care and use of laboratory animals' protocol approved by the institutional animal care committee of FMMU.

RNA preparation and qRT-PCR

Cells were harvested in Trizol (Thermo Fisher Scientific), and the total RNA was extracted using chloroform extraction and isopropanol precipitation. After spectrophotometric quantification, RNA (500 ng) was reverse transcribed into cDNA following the protocol of the PrimeScript RT Master Mix (Takara, China). The real-time PCR analyses were performed using SYBR Premix Ex Taq II on the 7,500 fast Real-Time PCR System (Applied Biosystems, United States) and Ct thresholds were determined by the matched software. Target gene expression was calculated using the $2^{-\Delta\Delta CT}$ method. Each quantitative PCR assay was performed in triplicate and independently repeated three times.

Western blot

Proteins were extracted from treated GBM cells with RIPA buffer containing proteinase inhibitor (NCM). Protein

concentrations were determined by BSA protein assay kit (Thermo Fisher Scientific). Equivalent amounts of protein were separated by SDS-PAGE and transferred onto polyvinylidene fluoride membranes (PVDF). After blocking with 5% non-fat milk, membranes were successively incubated with primary (anti-HA, anti-CD63, anti-CD9, anti-GM130, anti-YY1, anti-TSG101, anti-Lamp2b anti-GAPDH) and HRP-conjugated secondary antibodies before visualizing bands using chemiluminescence (Tanon Science & Technology, Shanghai, China). The results were visualized on Tanon-5200 Chemiluminescent Imaging System (Tanon Science & Technology).

Apoptosis assay

A FACSCalibur Flow Cytometer (BD Biosciences, United States) was used for the apoptosis assay followed the product manual. Cells were seeded in 6-well plates, harvesting in centrifuge tube after different treatment for 24h. Then washing, resuspension and staining were in accordance with the BD Pharmingen™ FITC Annexin V Apoptosis Detection Kit I (BD) protocol. The data were then analyzed with Flow Jo 10.0 software (Tree Star, San Francisco, CA, United States). Each assay was independently repeated three times.

Statistical analysis

Data are presented as the mean ± standard deviation. One-way analysis of variance was used to determine significance among groups. Kaplan-Meier analysis was used to determine the survival curve, in which the log-rank (Mantel-Cox) test was applied to confirm significance between different groups. A value of $p < 0.05$ was considered to be significant.

Discussion

Glioblastoma (GBM) exhibits heterogeneity, vigorous motility and large enormous ability, which is highly resistant to the existing conventional treatments, making it a kind of brain tumor with the heaviest invasiveness and fatality (Shi et al., 2018). Bevacizumab, a humanised monoclonal antibody against VEGF, received accelerated approval from the FDA for treatment of recurrent GBM, which is also used for adjuvant treatment (Tamura et al., 2019). Nevertheless, the therapeutic effect of bevacizumab combined with chemotherapy and radiotherapy or not cannot last a long time and tumors will recur 3–5 months later (Bao et al., 2021). One way to further improve the efficacy of routine treatments might be to identify genes responsible for tumor resistance. Recently, we and others demonstrated the role of YY1 on GBM cells and glioma stem cells. YY1 activates the expression of many oncogenes that affect different cellular functions, like the proliferation, the redox homeostasis, the DNA damage response, the apoptosis, the angiogenesis, the metastasis, as well as the immunosuppression (Li et al., 2020). YY1 is an attractive drug target due to its central role in tumor progression. However, it is not easy to target YY1 considering the nuclear localization.

The delivery of RNA molecules, like small interfering RNA (siRNA), microRNA (miRNA), short hairpin RNA (shRNA), as well as long non-coding RNA (lncRNA) for silencing aberrant gene expression in a cell can effectively assist in treating various transcription factors (Yang et al., 2022). Nevertheless, plenty of evidence finds that the efficacy and specificity exhibited by these therapies are not acceptable. Accumulating evidence reported that exosomes released from somatic cells might serve as proper nanocarriers of therapeutic agents specific to clinical therapeutic drugs (Shi et al., 2019). However, the way to enable exosomes to be capable of specifically delivering therapeutic molecules to target cells remains unclear. Murine pancreatic cancer cells saw the functional modification of exosomes that carry a specific siRNA for targeting oncogenic KRAS, explaining the potential of these exosomes for treating the malignant tumors with identified molecular targets (Xie et al., 2020). Our previous also found that TfR was rarely expressed in normal human astrocytes cells but significantly increased in radioresistant cells and glioma stem cells (Gu et al., 2021). Besides, a mass of TfRs is also expressed in brain capillary endothelial cells, assisting exosomes in penetrating the BBB more efficiently (Zhao et al., 2016). Kim et al. (2020) designed exosomes containing antisense microRNA oligonucleotides and decorated them with the T7-peptide. The authors aimed to selectively deliver antisense oligonucleotide against miR-21 that is commonly upregulated in GBM and involved in the inhibition of tumor cell death and consequent tumor progression.

The study of the *in vitro* and *in vivo* uptake was consistent with the proposed hypothesis that T7 functionalization promoted exosome uptake by both cerebral vascular endothelial cells and glioblastoma cells. Despite the enhanced brain targeting due to T7-modified exosomes, our study found that exosomes were remarkably enriched in peripheral organs, especially in the liver, which is consistent with previous studies. In our study, T7-siYY1-exo was used in combination with TMZ and radiotherapy, which played a better anticancer and apoptotic role in comparison with a single therapeutic strategy.

Notably, according to the histological analyses regarding major organs, the tissues of experimental mice were not damaged obviously, which indicated the favorable biocompatibility of the modified exosome. Based on these advantages, exosomes have shown great value in nucleic acid delivery, and can protect therapeutic substances from degradation and clearance by the host immune system. We believe that this modified exosome may emerge as a promising strategy for synergistic and targeted

chemoradiotherapy to eradicate glioblastoma. However, it is important to emphasize that the clinical therapeutic potential of engineered exosomes is limited by the large-scale production of exosomes for clinical trials. Furthermore, the low loading efficiency of current exosome-nucleic acid-loading strategies, including electroporation, incubation, and transfection, limits their application.

Data availability statement

The original contributions presented in the study are included in the article/supplementary materials, further inquiries can be directed to the corresponding authors.

Ethics statement

The animal study was reviewed and approved by Fourth Military Medical University Animal Experimental Ethics.

Author contributions

XL, ZC, and NL carried a majority of experiments and analyzed data and prepared figures. XL and ZC wrote the manuscript. MD and GG engineered and constructed the exosome. MZ, YW, and BC provided support for animal experiment. BJ, WZ, and LP analyzed the bioinformatic data. WZ, YJ, and WH performed the statistical analysis. JG, QG, and QA conceived the study, designed the study, evaluated data and revised the manuscript. All authors read and approved the final manuscript.

Funding

This work was supported by the National Natural Science Foundation of China (82003220, 81803053 and 81872049).

Conflict of interest

The authors declare that the research was conducted in the absence of any commercial or financial relationships that could be construed as a potential conflict of interest.

Publisher's note

All claims expressed in this article are solely those of the authors and do not necessarily represent those of their affiliated organizations, or those of the publisher, the editors and the reviewers. Any product that may be evaluated in this article, or claim that may be made by its manufacturer, is not guaranteed or endorsed by the publisher.

References

Adamus, T., Hung, C-Y., Yu, C., Kang, E., Hammad, M., Flores, L., et al. (2022). Glioma-targeted delivery of exosome-encapsulated antisense oligonucleotides using neural stem cells. *Mol. Ther. Nucleic Acids* 27, 611–620. doi:10.1016/j.omtn.2021.12.029

Bao, Z., Wang, Y., Wang, Q., Fang, S., Shan, X., Wang, J., et al. (2021). Intratumor heterogeneity, microenvironment, and mechanisms of drug resistance in glioma recurrence and evolution. *Front. Med.* 15 (4), 551–561. doi:10.1007/s11684-020-0760-2

Choudhury, H., Pandey, M., Chin, P. X., Phang, Y. L., Cheah, J. Y., Ooi, S. C., et al. (2018). Transferrin receptors-targeting nanocarriers for efficient targeted delivery and transcytosis of drugs into the brain tumors: A review of recent advancements and emerging trends. *Drug Deliv. Transl. Res.* 8 (5), 1545–1563. doi:10.1007/s13346-018-0552-2

Cui, X., Sun, Y., Shen, M., Song, K., Yin, X., Di, W., et al. (2018). Enhanced chemotherapeutic efficacy of paclitaxel nanoparticles Co-delivered with MicroRNA-7 by inhibiting paclitaxel-induced EGFR/ERK pathway activation for ovarian cancer therapy. *ACS Appl. Mat. Interfaces* 10 (9), 7821–7831. doi:10.1021/acsami.7b19183

Fu, Z., Zhang, X., Zhou, X., Ur-Rehman, U., Yu, M., Liang, H., et al. (2021). *In vivo* self-assembled small RNAs as a new generation of RNAi therapeutics. *Cell Res.* 31 (6), 631–648. doi:10.1038/s41422-021-00491-z

Gu, J., Mu, N., Jia, B., Guo, Q., Pan, L., Zhu, M., et al. (2021). Targeting radiation-tolerant persister cells as a strategy for inhibiting radioresistance and recurrence in glioblastoma. *Neuro. Oncol.* 24, 1056–1070. doi:10.1093/neuonc/noab288

Huang, X., Wu, W., Jing, D., Yang, L., Guo, H., Wang, L., et al. (2022). Engineered exosome as targeted lncRNA MEG3 delivery vehicles for osteosarcoma therapy. *J. Control. Release* 343, 107–117. doi:10.1016/j.jconrel.2022.01.026

Jiang, Y., Zhang, J., Meng, F., and Zhong, Z. (2018). Apolipoprotein E peptide-directed chimeric polymersomes mediate an ultrahigh-efficiency targeted protein therapy for glioblastoma. *ACS Nano* 12 (11), 11070–11079. doi:10.1021/acsnano.8b05265

Kase, Y., Uzawa, K., Wagai, S., Yoshimura, S., Yamamoto, J. I., Toeda, Y., et al. (2021). Engineered exosomes delivering specific tumor-suppressive RNAi attenuate oral cancer progression. *Sci. Rep.* 11 (1), 5897. doi:10.1038/s41598-021-85242-1

Kim, G., Kim, M., Lee, Y., Byun, J. W., Hwang, D. W., and Lee, M. (2020). Systemic delivery of microRNA-21 antisense oligonucleotides to the brain using T7-peptide decorated exosomes. *J. Control. Release* 317, 273–281. doi:10.1016/j.jconrel.2019.11.009

Li, H., Li, T., Huang, D., and Zhang, P. (2020). Long noncoding RNA SNHG17 induced by YY1 facilitates the glioma progression through targeting miR-506-3p/CTNNB1 axis to activate Wnt/β-catenin signaling pathway. *Cancer Cell Int.* 20 (1), 29. doi:10.1186/s12935-019-1088-3

Mao, J., Ran, D., Xie, C., Shen, Q., Wang, S., and Lu, W. (2017). EGFR/EGFRvIII dual-targeting peptide-mediated drug delivery for enhanced glioma therapy. *ACS Appl. Mat. Interfaces* 9 (29), 24462–24475. doi:10.1021/acsami.7b05617

Mojarad-Jabali, S., Mahdinloo, S., Farshbaf, M., Sarfraz, M., Fatahi, Y., Atyabi, F., et al. (2022). Transferrin receptor-mediated liposomal drug delivery: Recent trends in targeted therapy of cancer. *Expert Opin. Drug Deliv.* 19 (6), 685–705. doi:10.1080/17425247.2022.2083106

Movahedpour, A., Khatami, S. H., Khorsand, M., Salehi, M., Savardashtaki, A., Mirmajidi, S. H., et al. (2021). Exosomal noncoding RNAs: Key players in glioblastoma drug resistance. *Mol. Cell. Biochem.* 476 (11), 4081–4092. doi:10.1007/s11010-021-04221-2

Nie, E., Jin, X., Miao, F., Yu, T., Zhi, T., Shi, Z., et al. (2021). TGF-β1 modulates temozolomide resistance in glioblastoma via altered microRNA processing and elevated MGMT. *Neuro. Oncol.* 23 (3), 435–446. doi:10.1093/neuonc/noaa198

Persano, L., Pistollato, F., Rampazzo, E., DellA PuppA, A., Abbadi, S., Frasson, C., et al. (2012). BMP2 sensitizes glioblastoma stem-like cells to Temozolomide by affecting HIF-1α stability and MGMT expression. *Cell Death Dis.* 3, e412. doi:10.1038/cddis.2012.153

Ruan, H., Chai, Z., Shen, Q., Chen, X., Su, B., Xie, C., et al. (2018). A novel peptide ligand RAP12 of LRP1 for glioma targeted drug delivery. *J. Control. Release* 279, 306–315. doi:10.1016/j.jconrel.2018.04.035

Sarvagalla, S., Kolapalli, S. P., and Vallabhapurapu, S. (2019). The two sides of YY1 in cancer: A friend and a foe. *Front. Oncol.* 9, 1230. doi:10.3389/fonc.2019.01230

Shi, S., Fu, W., Lin, S., Tian, T., Li, S., Shao, X., et al. (2019). Targeted and effective glioblastoma therapy via aptamer-modified tetrahedral framework nucleic acid-paclitaxel nanoconjugates that can pass the blood brain barrier. *Nanomedicine* 21, 102061. doi:10.1016/j.nano.2019.102061

Shi, Y., Jiang, Y., Cao, J., Yang, W., Zhang, J., Meng, F., et al. (2018). Boosting RNAi therapy for orthotopic glioblastoma with nontoxic brain-targeting chimaeric polymersomes. *J. Control. Release* 292, 163–171. doi:10.1016/j.jconrel.2018.10.034

Tamura, R., Miyoshi, H., Yoshida, K., Okano, H., and Toda, M. (2019). Recent progress in the research of suicide gene therapy for malignant glioma. *Neurosurg. Rev.* 44 (1), 29–49. doi:10.1007/s10143-019-01203-3

Tomar, V. S., Patil, V., and Somasundaram, K. (2020). Temozolomide induces activation of wnt/β-catenin signaling in glioma cells via PI3K/akt pathway: Implications in glioma therapy. *Cell Biol. Toxicol.* 36 (3), 273–278. doi:10.1007/s10565-019-09502-7

Tortorella, S., and Karagiannis, T. C. (2014). Transferrin receptor-mediated endocytosis: A useful target for cancer therapy. *J. Membr. Biol.* 247 (4), 291–307. doi:10.1007/s00232-014-9637-0

Verheul, T. C. J., van Hijfte, L., Perenthaler, E., and Barakat, T. S. (2020). The why of YY1: Mechanisms of transcriptional regulation by Yin Yang 1. *Front. Cell Dev. Biol.* 8, 592164. doi:10.3389/fcell.2020.592164

Xiao, B., Viennois, E., Chen, Q., Wang, L., Han, M. K., Zhang, Y., et al. (2018). Silencing of intestinal glycoprotein CD98 by orally targeted nanoparticles enhances chemosensitization of colon cancer. *ACS Nano* 12 (6), 5253–5265. doi:10.1021/acsnano.7b08499

Xie, Y., Hang, Y., Wang, Y., Sleightholm, R., Prajapati, D. R., Bader, J., et al. (2020). Stromal modulation and treatment of metastatic pancreatic cancer with local intraperitoneal triple miRNA/siRNA nanotherapy. *ACS Nano* 14 (1), 255–271. doi:10.1021/acsnano.9b03978

Yang, J., Luo, S., Zhang, J., Yu, T., Fu, Z., Zheng, Y., et al. (2021). Exosome-mediated delivery of antisense oligonucleotides targeting α-synuclein ameliorates the pathology in a mouse model of Parkinson's disease. *Neurobiol. Dis.* 148, 105218. doi:10.1016/j.nbd.2020.105218

Yang, K., Wu, Z., Zhang, H., Zhang, N., Wu, W., Wang, Z., et al. (2022). Glioma targeted therapy: Insight into future of molecular approaches. *Mol. Cancer* 21 (1), 39. doi:10.1186/s12943-022-01513-z

Yasaswi, P. S., Shetty, K., and Yadav, K. S. (2021). Temozolomide nano enabled medicine: Promises made by the nanocarriers in glioblastoma therapy. *J. Control. Release* 336, 549–571. doi:10.1016/j.jconrel.2021.07.003

Yu, X., Bai, Y., Han, B., Ju, M., Tang, T., Shen, L., et al. (2022). Extracellular vesicle-mediated delivery of circDYM alleviates CUS-induced depressive-like behaviours. *J. Extracell. Vesicles* 11 (1), e12185. doi:10.1002/jev2.12185

Zhao, Y., Jiang, Y., Lv, W., Wang, Z., Lv, L., Wang, B., et al. (2016). Dual targeted nanocarrier for brain ischemic stroke treatment. *J. Control. Release* 233, 64–71. doi:10.1016/j.jconrel.2016.04.038

frontiers | Frontiers in Pharmacology

TYPE Original Research
PUBLISHED 06 September 2022
DOI 10.3389/fphar.2022.900006

OPEN ACCESS

EDITED BY
Nan Liu,
Shenzhen University, China

REVIEWED BY
Jianye Xu,
Tianjin Medical University General Hospital, China
Kunqi Chen,
Fujian Medical University, China

*CORRESPONDENCE
Shufang Zhang,
zsf66189665@126.com

SPECIALTY SECTION
This article was submitted to Pharmacology of Anti-Cancer Drugs, a section of the journal Frontiers in Pharmacology

RECEIVED 19 March 2022
ACCEPTED 15 August 2022
PUBLISHED 06 September 2022

CITATION
Chen M, Nie Z, Gao Y, Cao H, Zheng L, Guo N, Peng Y and Zhang S (2022), m7G regulator-mediated molecular subtypes and tumor microenvironment in kidney renal clear cell carcinoma.
Front. Pharmacol. 13:900006.
doi: 10.3389/fphar.2022.900006

m7G regulator-mediated molecular subtypes and tumor microenvironment in kidney renal clear cell carcinoma

Mei Chen, Zhenyu Nie, Yuanhui Gao, Hui Cao, Linlin Zheng, Na Guo, Yanling Peng and Shufang Zhang*

Central Laboratory, Affiliated Haikou Hospital of Xiangya Medical College, Central South University, Haikou, China

Background: RNA methylation modification plays an important role in immune regulation. m7G RNA methylation is an emerging research hotspot in the RNA methylation field. However, its role in the tumor immune microenvironment of kidney renal clear cell carcinoma (KIRC) is still unclear.

Methods: We analyzed the expression profiles of 29 m7G regulators in KIRC, integrated multiple datasets to identify a novel m7G regulator-mediated molecular subtype, and developed the m7G score. We evaluated the immune tumor microenvironments in m7G clusters and analyzed the correlation of the m7G score with immune cells and drug sensitivity. We tested the predictive power of the m7G score for prognosis of patients with KIRC and verified the predictive accuracy of the m7G score by using the GSE40912 and E-MTAB-1980 datasets. The genes used to develop the m7G score were verified by qRT-PCR. Finally, we experimentally analyzed the effects of WDR4 knockdown on KIRC proliferation, migration, invasion, and drug sensitivity.

Results: We identified three m7G clusters. The expression of m7G regulators was higher in cluster C than in other clusters. m7G cluster C was related to immune activation, low tumor purity, good prognosis, and low m7G score. Cluster B was related to drug metabolism, high tumor purity, poor survival, and high m7G score. Cluster A was related to purine metabolism. The m7G score can well-predict the prognosis of patients with KIRC, and its prediction accuracy based on the m7G score nomogram was very high. Patients with high m7G scores were more sensitive to rapamycin, gefitinib, sunitinib, and vinblastine than other patients. Knocking down WDR4 can inhibit the proliferation, migration, and invasion of 786-0 and Caki-1 cells and increase sensitivity to sorafenib and sunitinib.

Conclusion: We proposed a novel molecular subtype related to m7G modification and revealed the immune cell infiltration characteristics of different subtypes. The developed m7G score can well-predict the prognosis of patients with KIRC, and our research provides a basis for personalized treatment of patients with KIRC.

KEYWORDS

m7G, kidney renal clear cell carcinoma, molecular subtype, tumor microenvironment, prognosis, drug sensitivity

Introduction

m7G RNA methylation is catalyzed by the Trm8–Trm82 complex in yeast and by the METTL1–WDR4 complex in humans under the action of methyltransferases (A Alexandrov et al., 2002). m7G RNA methylation can regulate mRNA transcription, miRNA biological function, tRNA stability, nuclear processing, and 18S rRNA maturation. m7G regulators are prognostic markers of a variety of cancers. METTL1 and WDR4 are highly expressed in a variety of tumors, such as liver cancer (Chen D et al., 2021), intrahepatic cholangiocarcinoma (Dai S et al., 2021), and lung cancer (Ma et al., 2021), which is related to poor prognosis of patients. High expression of NSUN2 is associated with poor prognosis of gastric cancer (Hu J et al., 2021) and esophageal squamous cell carcinoma (Su et al., 2021). NUDT10 is a reliable prognostic marker of gastric cancer (Chen Z et al., 2021). GEMIN5, EIF4E3, and GEMIN5 can specifically bind to the m7G cap (Bradrick and Gromeier, 2009; Osborne et al., 2013; Xu et al., 2016). Meanwhile, NUDT16 can remove the m7G cap (Lu et al., 2011). AGO2 inhibits mRNA translation by binding to the m7G cap (Kiriakidou et al., 2007). EIF4E binds to the m7G cap to mediate mRNA translation and can increase the capping efficiency of coding and noncoding RNAs (Culjkovic-Kraljacic et al., 2020). EIF4E overexpression can promote cell proliferation and invasion of renal cell carcinoma (RCC) (Li et al., 2017). The knockdown of EIF3D can inhibit the progression of RCC by inducing G2/M arrest (Pan et al., 2016). Current studies only focused on the role of a single m7G regulator. However, multiple genes are involved in tumor occurrence, and the prognostic role of multiple m7G regulators has not been clarified.

Kidney renal clear cell carcinoma (KIRC), the most common histological subtype of RCC, is characterized by high heterogeneity and poor prognosis (Hsieh et al., 2017). Immunotherapy has led to significant progress in the treatment of patients with KIRC, and immune checkpoint inhibitors have been used as the first-line treatment of advanced KIRC (Bedke et al., 2021; Braun et al., 2021). However, some patients still experience spontaneous regression due to tumor immune escape, and the effect of immunotherapy still greatly varies across different patients. KIRC has a high degree of immune infiltration, with T-cell infiltration being the highest (şenbabaoğlu et al., 2016). $CD8^+$ T-cell infiltration is associated with poor prognosis of KIRC (Dai Z et al., 2021; Li et al., 2020). The tumor microenvironment plays an important role in tumor biology and treatment. Understanding the characteristics of the tumor microenvironment under the mediation of m7G is of great importance for predicting the immunotherapy of patients with KIRC.

In this study, first, we performed consistent cluster analysis on 702 patients with KIRC, identified three m7G clusters, and studied the characteristics of immune cell infiltration, function, and survival among different subtypes. We classified the patients into three gene clusters in accordance with the differentially expressed genes (DEGs) among the three m7G clusters. We developed the m7G score to predict the prognosis of patients and analyzed its correlation with the tumor microenvironment, mutation, tumor mutation burden (TMB), and stemness indices. Finally, we verified the genes used for developing the m7G score by utilizing clinical samples.

Materials and methods

Data collection and processing

RNA-seq data [fragments per kilobase million (FPKM)] and KIRC clinical and mutation data were downloaded from the TCGA database (https://portal.gdc.cancer.gov/). FPKM was converted into transcripts per kilobase million (TPM). The GSE29609 (Edeline et al., 2012), GSE40912 (Fachel et al., 2013), and GSE172165 datasets were downloaded from the GEO database (https://www.ncbi.nlm.nih.gov/geo/). The E-MTAB-1980 (Sato et al., 2013) dataset was downloaded from the ArrayExpress database (https://www.ebi.ac.uk/arrayexpress/). The details of these cohorts are provided in Supplementary Data Sheet S1. A total of 702 samples were obtained through batch correction with the "sva" package. In the molecular signature database (http://www.gsea-msigdb.org/gsea), "7-methylguanosine" was used as the search term to obtain three m7G-related gene sets (GOMF_M7G_5_PPPN_DIPHOSPHATASE_ACTIVITY, GOMF_RNA_7_METHYLGUANOSINE_CAP_BINDING, and GOMF_RNA_CAP_BINDING), and 26 m7G regulators were acquired from these gene sets. Three m7G regulators were sourced from previous literature (Tomikawa, 2018). A total of 29 m7G regulators were used for analysis in this research (Supplementary Table S1). The m7GHub (http://180.208.58.19/m7g/index.html) contains m7G sites, a sequence-based high accuracy predictor, evaluation of the effects of m7G status mutations, and gene mutations regulated by m7G methylation (Song et al., 2020). Immune checkpoints with m7G methylation were screened from the m7GHub database.

Identification of m7G subtypes

The unsupervised clustering analysis of 702 samples was conducted with the "ConsensusClusterPlus" package. The correlation between the groups was the lowest, and the correlation within the groups was the highest. The optimal K value was selected to obtain different subtypes.

Enrichment analysis of DEGs

The DEGs among m7G subtypes were analyzed using the "limma" package. |Fold change| > 1 and adjusted *p*-value < 0.01 were set as the thresholds to identify DEGs. The DEGs were enriched and analyzed by using Gene Ontology (GO) and Kyoto Encyclopedia of Genes and Genomes (KEGG) with the "clusterProfiler" package.

Development of the m7G score

Univariate Cox analysis was performed on the DEGs to obtain prognostic genes. The prognostic genes were analyzed through unsupervised clustering with the "ConsensusClusterPlus" package, and the patients were divided into different gene subtypes. The m7G score was developed after LASSO regression analysis. Its calculation formula is as follows:

$$\text{m7G score} = \sum \text{Expi} \times \text{coefi}$$

Here, Expi and coefi represent the gene expression values and correlation coefficients, respectively. The score of each patient was calculated in accordance with the formula, and the patients were divided into the training and testing groups at the ratio of 1: 1. The patients were divided into the high- and low-risk groups in accordance with the median value of the training group. Kaplan–Meier (K–M) analysis was performed on the high- and low-risk groups with the "survival" and "survminer" packages. Receiver operator curves (ROC) were drawn with the "timeROC" package to evaluate the accuracy of the m7G score in predicting prognosis. A nomogram was constructed with the "rms" package in combination with clinicopathological variables.

Pathway enrichment analysis

The "c2.cp.kegg.v7.4.symbols" gene set was selected, and the "GSVA" package was used to calculate the differential gene set among different subtypes. Molecular subtypes were visualized with the "ggplot2" package. "C2.cp.kegg.v7.5.symbols.gmt" in GSEA4.1.0 software was selected for analysis, and the other operation steps in this work were consistent with those in previous studies (Chen M et al., 2021).

Immune cell infiltration in KIRC

The "estimate" package was used to run the ESTIMATE algorithm (Yoshihara et al., 2013), which was utilized to evaluate the presence of stromal cells and infiltration of immune cells in tumor samples and infer tumor purity. ssGSEA (Hänzelmann et al., 2013), CIBERSORT (Newman et al., 2015), and MCP counter algorithm (Becht et al., 2016) were applied to analyze the differences of immune cells between different subtypes, and Spearman's correlation analysis was performed between the m7G score and immune cells.

Correlation analysis between the m7G score and therapeutic drugs

The expression profiles of immune checkpoints in the high- and low-risk groups were analyzed with the "limma" package, and the IC_{50} of chemotherapeutic drugs (rapamycin, gefitinib, sunitinib, vinblastine, gemcitabine, lapatinib, and sorafenib) in KIRC was calculated with the "pRRophetic" package. The association between WDR4 and drug IC_{50} was analyzed using data from the GDSC database (https://www.cancerrxgene.org/).

The DEGs between high- and low-risk groups were divided into upregulated and downregulated genes and entered into the cAMP database (https://clue.io/) to obtain potential therapeutic drugs. The 2D and 3D structures of the drugs were obtained from the PubChem database (https://pubchem.ncbi.nlm.nih.gov/). A negative score indicates that the drug can be beneficial for treatment of patients in the high-risk group. Scores < −90 were used to identify associated small molecules.

Clinical sample validation

Paired cancer and adjacent tissues were collected from 13 patients with KIRC in our hospital. The informed consent of the patients and the approval of the ethics committee of Haikou Hospital, affiliated to Xiangya Medical College of Central South University were obtained before specimen collection. The operation steps and calculation methods of quantitative real-time polymerase chain reaction (qRT-PCR) are shown in our previous research (Chen et al., 2020). cDNA was amplified with an Applied Biosystems QuantStudio 5 Real-Time PCR instrument. Primer sequences are provided in Supplementary Table S2.

Cell culture and small interfering RNA transfection

786-0 and Caki-1 cell lines were purchased from the China Centre for Type Culture Collection (Wuhan, China) and cultured in an atmosphere of 5% CO_2 and 95% air at 37°C. siWDR4 was designed and synthesized by RiboBio (Guangzhou, China) and transfected with Lipofectamine 3000 (Thermo Fisher, NY, United States). At 48 h after transfection, the cells were collected for functional experiments. Interference efficiency was detected through qRT-PCR.

Cell viability assay

A total of 2000 cells were plated in 96-well plates, and 10 μL of CCK-8 was added to each well. The cells were incubated in an incubator for 1 h. The wavelength was set at 450 nm. The IC_{50} values of sunitinib and sorafenib were detected at 24, 48, and 72 h. Drugs were purchased from MedChemExpress (Monmouth Junction, NJ, United States).

Colony formation assay

Cells at the logarithmic growth stage were collected, and 1000 cells were plated in six-well plates. The cells were cultured for 10 days, fixed with methanol for 20 min, and stained with 0.1% crystal violet for 15 min. The number of clones that formed in each well was counted and photographed.

Transwell assay

A total of 600 μL of medium containing 10% serum was added into the lower chamber of a 24-well plate. Cells were added into the upper chamber and incubated in the incubator for 24 h. The liquid in the upper chamber was aspirated dry, and the cells were fixed with formaldehyde for 20 min and stained with 0.1% crystal violet for 15 min. After air drying, a microscope was used for observation and photography. Invasion experiments required a layer of Matrigel in the upper chamber.

Statistical analysis

Survival analysis was performed through the K–M method. The Wilcoxon signed-rank test was used to analyze DEGs, and paired *t*-test was conducted to analyze gene expression in the clinical samples. Statistical analysis was performed by using R4.0.2 and GraphPad Prism 8.0.2. $p < 0.05$ was considered a significant difference.

Result

Genetic variations and expression levels of m7G regulators in KIRC

Among the 29 m7G regulators analyzed in this study, LARP1 had the highest mutation frequency (Supplementary Figure S1). We found a significant correlation among 23 genes. METTL1 was negatively correlated with DCPS, NUDT3, NUDT4, and EIF4E3 and positively correlated with other genes. Most genes were favorable factors for patients with KIRC, whereas NUDT11, NUDT10, NSUN2, WDR4, METTL1, LSM1, and EIF4A1 were risk factors (Figure 1A). We found significant differences in 24 genes between cancer and normal tissues in the TCGA–KIRC cohort (Figure 1B). These results suggested that m7G may play an important role in KIRC.

Expression levels of m7G regulators in KIRC

We combined the TCGA–KIRC, GSE29609, GSE49012, and E-MTAB-1980 cohorts to obtain a total of 702 samples to further understand the possible role of m7G in KIRC. Through unsupervised clustering, the samples were divided into three subtypes for analysis (Figure 1C). A total of 291, 104, and 307 cases were included in clusters A, B, and C, respectively. PCA revealed that the m7G regulator can well-distinguish the samples of each cluster (Figure 1D). Significant differences were found in overall survival (OS) and disease-free survival (DFS) among the three subtypes. The survival of cluster C was longer than that of clusters A and B (Figures 1E,F). m7G regulator expression was higher in cluster C than in other clusters (Supplementary Figure S2A).

Pathways between different subtypes

GSVA enrichment analysis showed that immune-related pathways, such as the RIG-I-like receptor signaling pathway, the chemokine signaling pathway, the T-cell receptor signaling pathway, and apoptosis, were significantly active in the m7G cluster C (Figure 2A). Drug metabolism-related pathways were significantly active in m7G cluster B, and purine metabolism was significantly active in m7G cluster A (Figures 2B,C). In addition, RCC was significantly active in m7G cluster C. GSEA also demonstrated that immune-related pathways and apoptosis were enriched in the m7G cluster C. Autophagy was also significantly enriched in m7G cluster C (Figures 2D–F). These results can account for better prognosis of m7G cluster C than that of m7G clusters A and B.

Differences in the immune microenvironments of the m7G clusters

After scoring the tumor microenvironment by using the ESTIMATE algorithm, we found differences in stromal scores, ESTIMATE scores, and tumor purity among m7G clusters A, B, and C. m7G cluster C had higher stromal and estimate scores and lower tumor purity than the other groups (Figures 3A–C). We used ssGSEA to evaluate the degree of immune cell infiltration in the three groups. Most immune cells differed among the three subtypes. Activated $CD4^+$ T cells, activated dendritic cells, CD56 dim natural killer cells, eosinophil, gamma delta T cells,

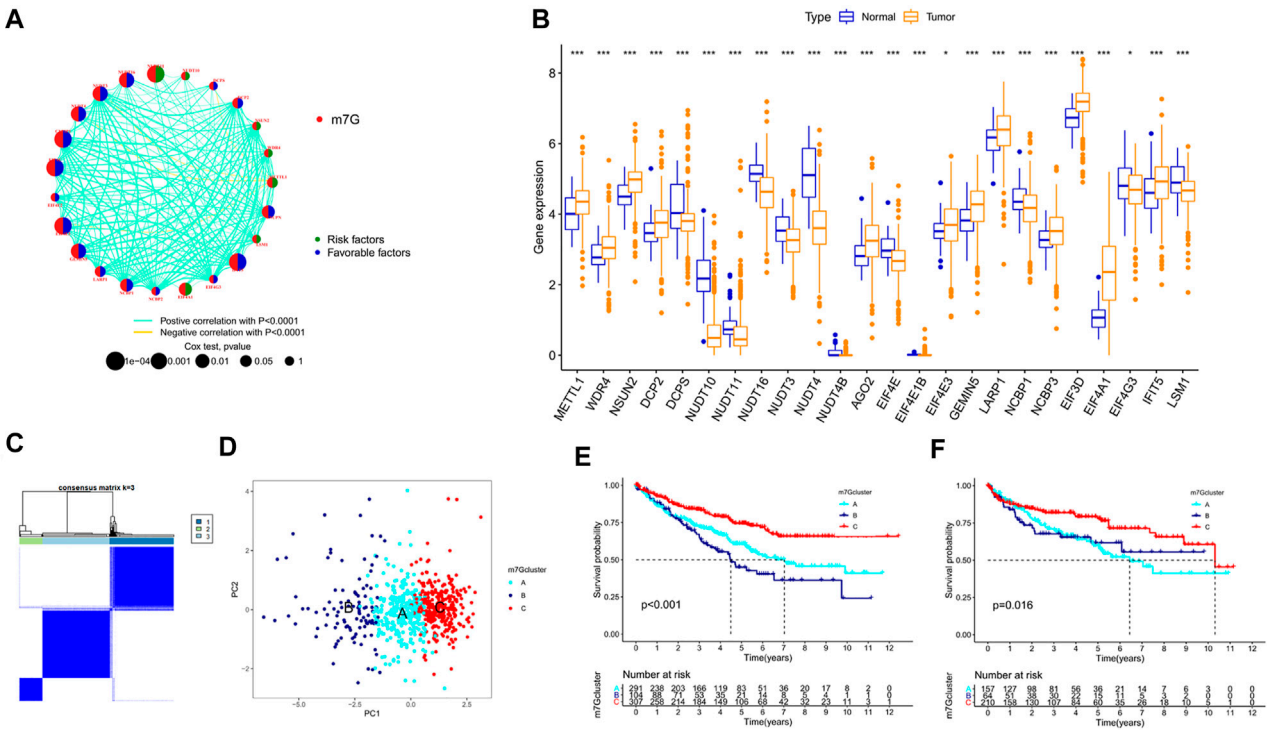

FIGURE 1
Unsupervised clustering analysis of m7G regulators in KIRC. **(A)** Interaction network of m7G regulators. **(B)** Expression levels of m7G regulators in KIRC. **(C)** Heat maps of the consensus clustering matrix. **(D)** PCA distinguishing the three subtypes. **(E–F)** K–M curves of OS and DFS in the three subtypes. KIRC, kidney renal clear cell carcinoma; OS, overall survival; DFS, disease-free survival; K–M, Kaplan–Meier.

mast cells, monocytes, natural killer T cells, natural killer cells, regulatory T cells, and type 2 T helper cells had higher distributions in m7G cluster C than in the other clusters, whereas activated $CD8^+$ T cells, CD56 bright natural killer cells, immature dendritic cells, and neutrophils had lower distributions in m7G cluster C than in other clusters (Figure 3D). In addition, higher expression levels of immune checkpoints (Figure 3E) and chemokines (Supplementary Figure S2B) were found in m7G cluster C than in other clusters. Interestingly, in the m7GHub database, we found that 15 immune checkpoints have m7G methylation modification (Supplementary Table S3).

Development and validation of the m7G score

We obtained 80 DEGs among m7G subtypes to explore their potential biological functions in different subtypes. GO and KEGG analyses revealed that the DEGs were enriched in cancer-related pathways, such as the positive regulation of cell adhesion, the positive regulation of vasculature development, cell molecules, the PI3K–Akt signaling pathway, and the JAK–STAT signaling pathway (Supplementary Figures S3A,B). m7G modification may play a key role in carcinogenesis in KIRC. A total of 75 prognostic genes were identified through univariate Cox analysis (Supplementary Table S4). We performed unsupervised clustering of prognostic genes to obtain three gene subtypes (Supplementary Figure S3C). Significant differences in OS and PFS existed among gene clusters A, B, and C (Figures 4A,B). A total of 702 samples were divided into the training group (n = 351) and the testing group (n = 351), and the formula used to develop the m7G score was obtained after LASSO regression analysis as follows: m7G score = (−0.222 × G3BP2) + (0.195 × THBS1) + (−0.224 × BCL2) + (−0.509 × PTPRB) + (0.284 × CD36) + (−0.124 × PDK4) + (−0.187 × TMEM125). The patients were divided into high- and low-risk groups in accordance with the median value of the training group. The prognosis of the patients in the high-risk group was poorer than that of the low-risk group (Figures 4C–E). The area under the curve (AUC) showed that the m7G score has good prediction accuracy (Figures 4F–H). A Sanggi diagram was used to depict the interrelationships between the m7G cluster, gene cluster, risk, and patient survival status (Supplementary Figure S4). Significant differences in m7G scores were found between gene and m7G subtypes, and the scores of m7G cluster C and

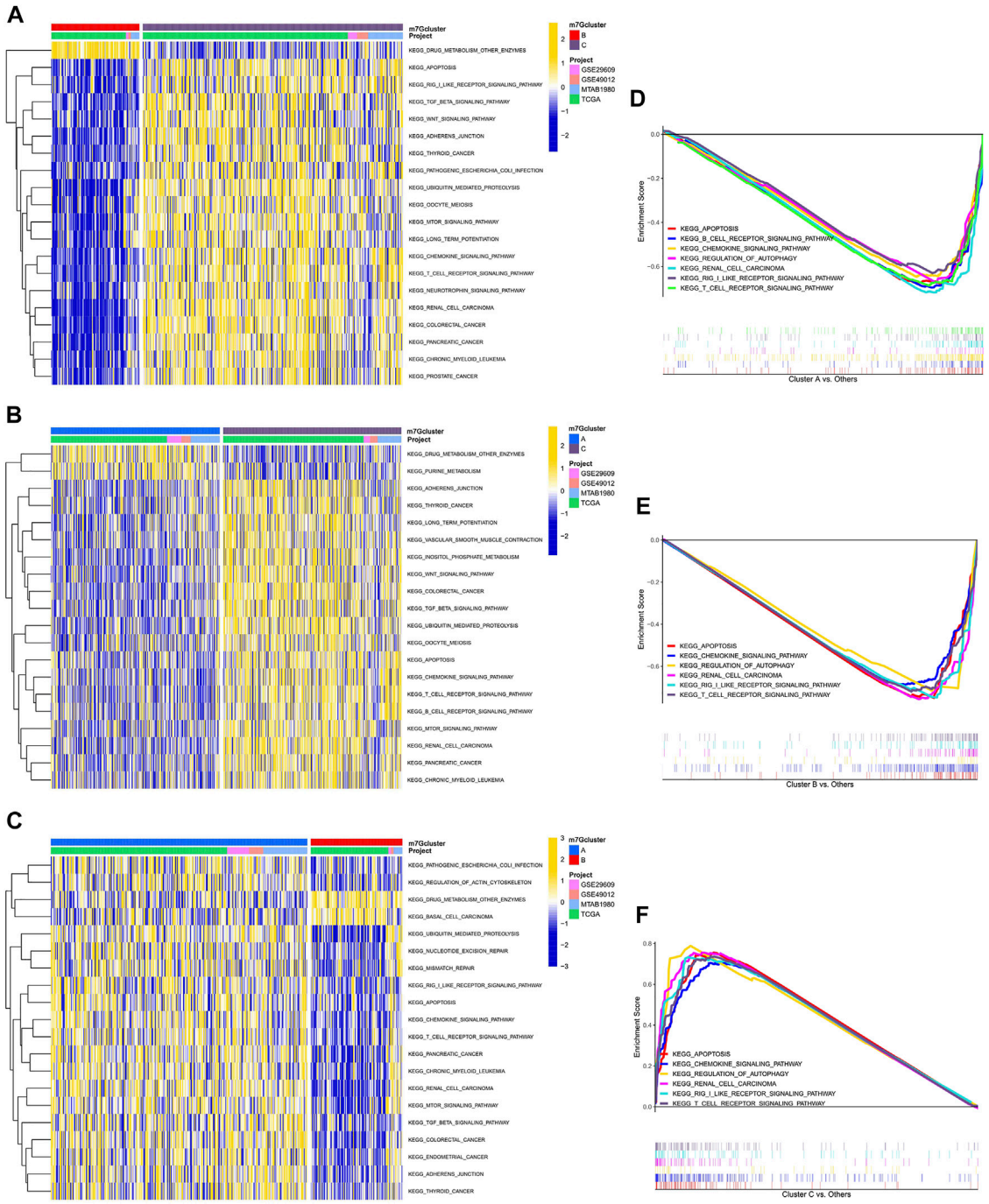

FIGURE 2
Enrichment analysis among different subtypes. **(A)** Pathway enrichment analysis between m7G clusters B and C. **(B)** Pathway enrichment analysis between m7G clusters A and C. **(C)** Pathway enrichment analysis between m7G clusters A and B. **(D–F)** Gene enrichment analysis among different subtypes.

gene cluster C were lower than those of other clusters (Figures 4I,J).

We conducted external validation to prove the applicability of the m7G score. The m7G score still had good prediction performance on the GSE40912 and E-MTAB-1980 datasets. The prognosis of the patients in the low-risk group was better than that of the patients in the high-risk group. AUC analysis showed that the m7G score

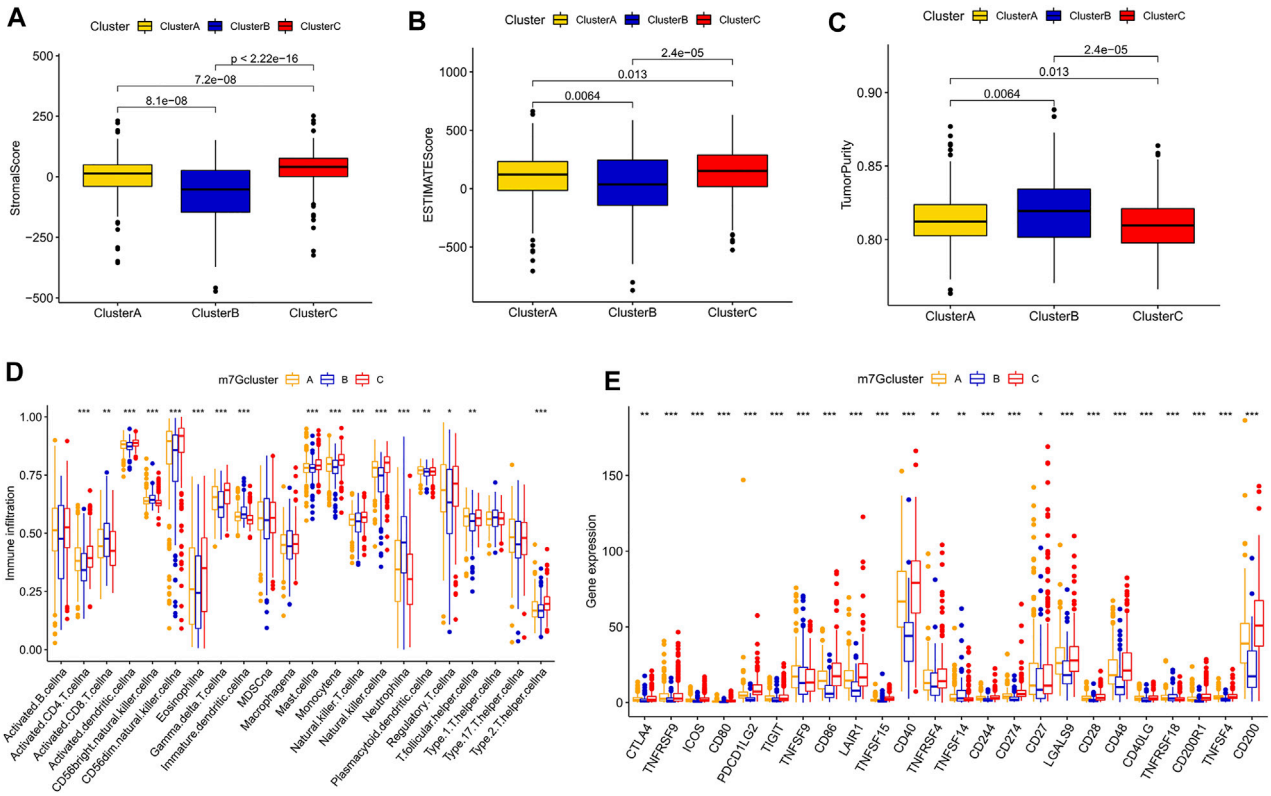

FIGURE 3
Differences in the immune microenvironment among different subtypes. **(A–C)** Differences in stromal and ESTIMATE scores and tumor purity among different subtypes. **(D)** Differences in immune cell infiltration among different subtypes based on ssGSEA. **(E)** Differences in immune checkpoint expression among different subtypes.

has a high prediction accuracy (Figures 5A,B). In addition, the m7G score had good predictive performance for DFS in the TCGA–KIRC cohort. A significant difference was found between high- and low-risk groups, and the survival of the patients in the low-risk group was better than that of the patients in the high-risk group (Figure 5C). The nomogram that was constructed in combination with clinicopathological variables can well-predict the survival of patients. The 1-, 3-, and 5-year AUCs reached 0.887, 0.883, and 0.857, respectively, with high prediction accuracy (Figures 5D,E).

TME characteristics in the high- and low-risk groups

By using the CIBERSORT algorithm, we found that the m7G score was negatively correlated with resting dendritic cells, M1 macrophages, and gamma delta T cells (Supplementary Figure S5A) and positively correlated with M0 macrophages, M2 macrophages, and neutrophils (Supplementary Figure S5B). The ssGSEA algorithm showed that aDCs, $CD8^+$ T cells, macrophages, Tfh, Th1 cells, and Th2 cells had higher scores in the high-risk group than in the low-risk group. Moreover, iDCs, mast cells, and neutrophils had higher scores in the low-risk group than in the high-risk group (Figure 6A). The scores of APC co-stimulation, CCR, check-point, cytolytic activity, inflammation promotion, para-inflammation, and T cell co-stimulation were higher in the high-risk group than in the low-risk group, whereas the scores of MHC-class I and type-II IFN response were higher in the low-risk group than in the high-risk group (Figure 6B). We used the ESTIMATE algorithm to score the tumor microenvironment and found differences among stromal, immune, and estimate scores. The estimate score of the high-risk group was higher than that of the low-risk group (Figure 6C). The MCP counter algorithm showed that the m7G score was positively correlated with B lineage and fibroblasts and negatively correlated with NK cells, monocytic lineage, myeloid dendritic cells, neutrophils, and endothelial cells (Figure 6D).

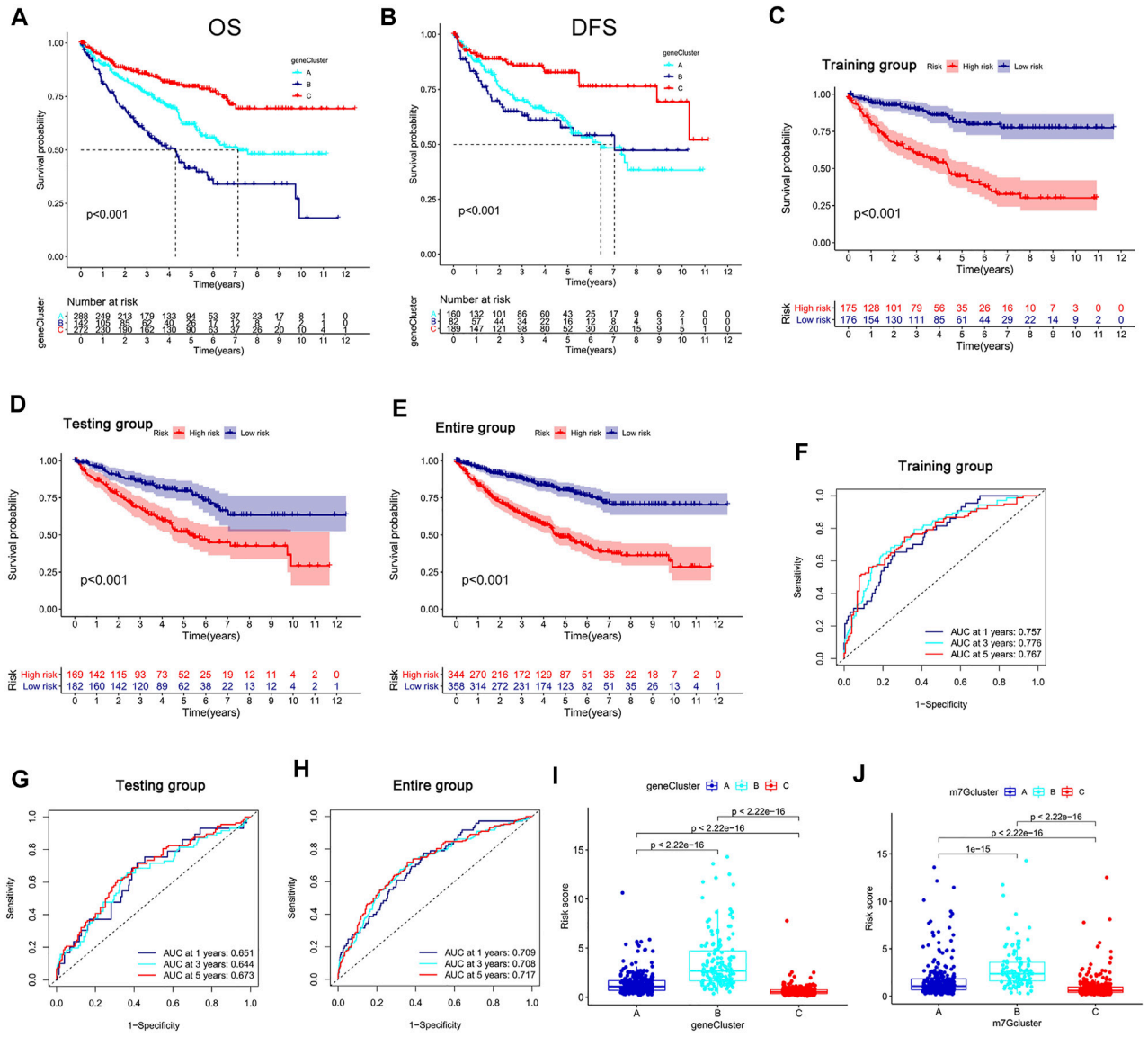

FIGURE 4
Development and validation of the m7G score. **(A,B)** K–M analysis of OS and DFS among different gene subtypes. **(C–E)** K–M survival analysis between high- and low-risk groups in the training and testing groups and the entire group. **(F–H)** ROC curve evaluating the prediction accuracy of the m7G score in the training and testing groups and the entire group. **(I,J)** Risk scores of different genes and m7G clusters. K–M, Kaplan–Meier; OS, overall survival; DFS, disease-free survival; ROC, receiver operator curve.

Correlation analysis of the m7G score with mutation, TMB and stem cell index

The mutation frequency of VHL was highest in the two groups, and the mutation frequency of mTOR was higher in the high-risk group (Figures 6E,F). The m7G score was positively correlated with stemness indices and TMB (Figures 6G,H). The higher TMB of the high-risk group than that of the low-risk group (Figure 6I) suggested that immunotherapy was more effective in high-risk patients than in low-risk patients.

Functional mechanism analysis of high- and low-risk groups

GSEA revealed that immune- and metabolism-related pathways were significantly enriched in the low-risk groups, such as the B-cell receptor signaling pathway, the T-cell receptor signaling pathway, the chemokine signaling pathway, endocytosis, fatty acid metabolism, fructose and mannose metabolism, glycolysis, gluconeogenesis, histidine metabolism, and pyruvate metabolism (Supplementary Figure S6A).

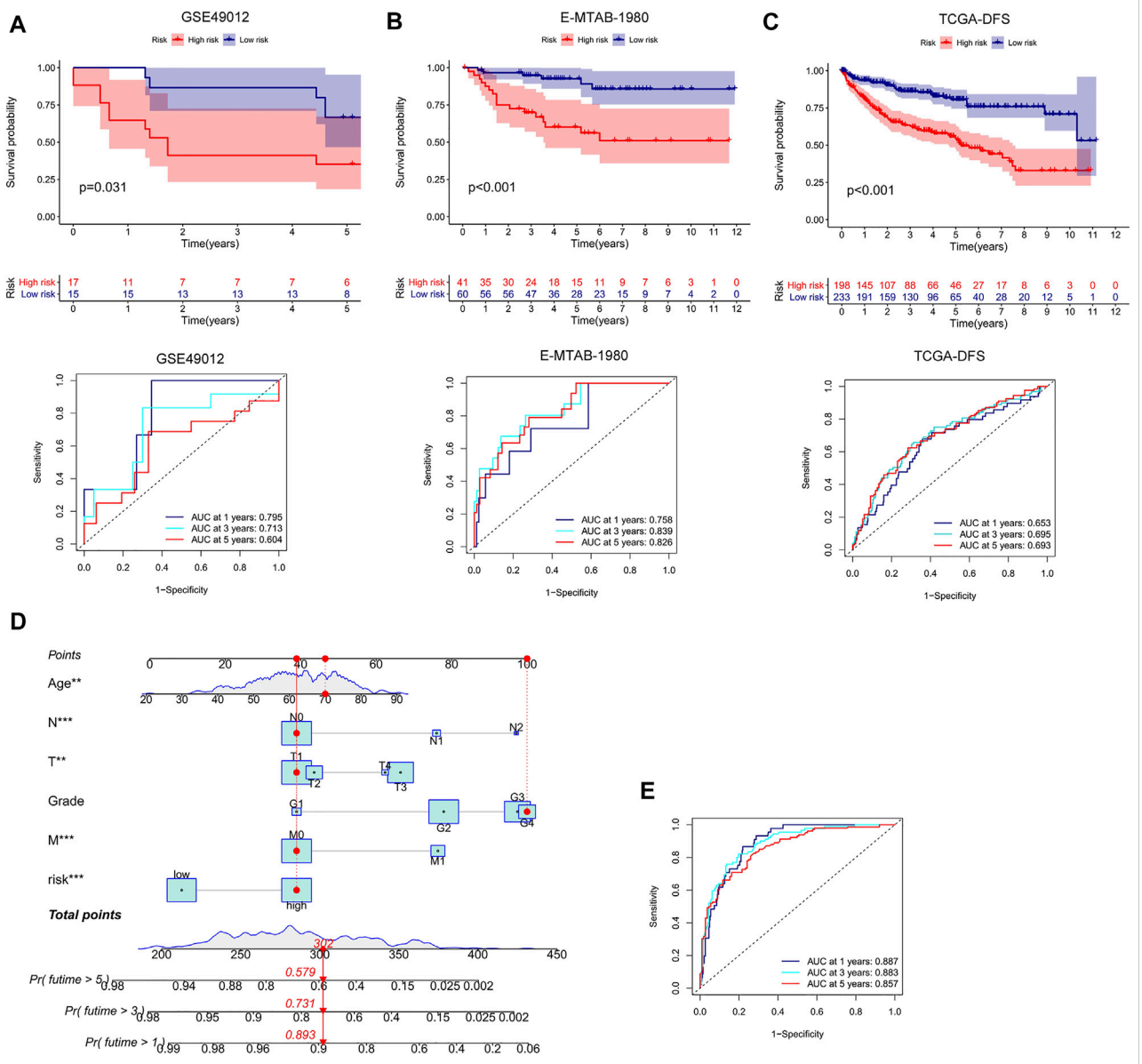

FIGURE 5
External validation and nomogram construction of the m7G score. **(A,B)** K–M analysis and ROC curve of the m7G score for the GSE40912 and E-MTAB-1980 datasets. **(C)** K–M analysis of the DFS of the TCGA–KIRC cohort. **(D)** Nomogram combining clinicopathological variables and risk score. **(E)** ROC curve was used to evaluate the accuracy of the normogram in predicting survival. K–M, Kaplan–Meier; DFS, disease-free survival; ROC, receiver operator curve; KIRC, kidney renal clear cell carcinoma.

Correlation analysis between the m7G score and therapeutic drugs

We found that checkpoints significantly differed between the high- and low-risk groups, and the expression of PDCD1 was higher in the high-risk group than in the low-risk group (Figure 7A). The two groups also had significantly different chemokine and chemokine receptor expression profiles (Supplementary Figure S6B). Rapamycin, gefitinib, sunitinib, and vinblastine had lower IC_{50} values in the high-risk group than in the low-risk group (Figures 7B–E), and gemcitabine, lapatinib, and sorafenib had higher IC_{50} values in the high-risk group than in the low-risk group (Figures 7F–H).

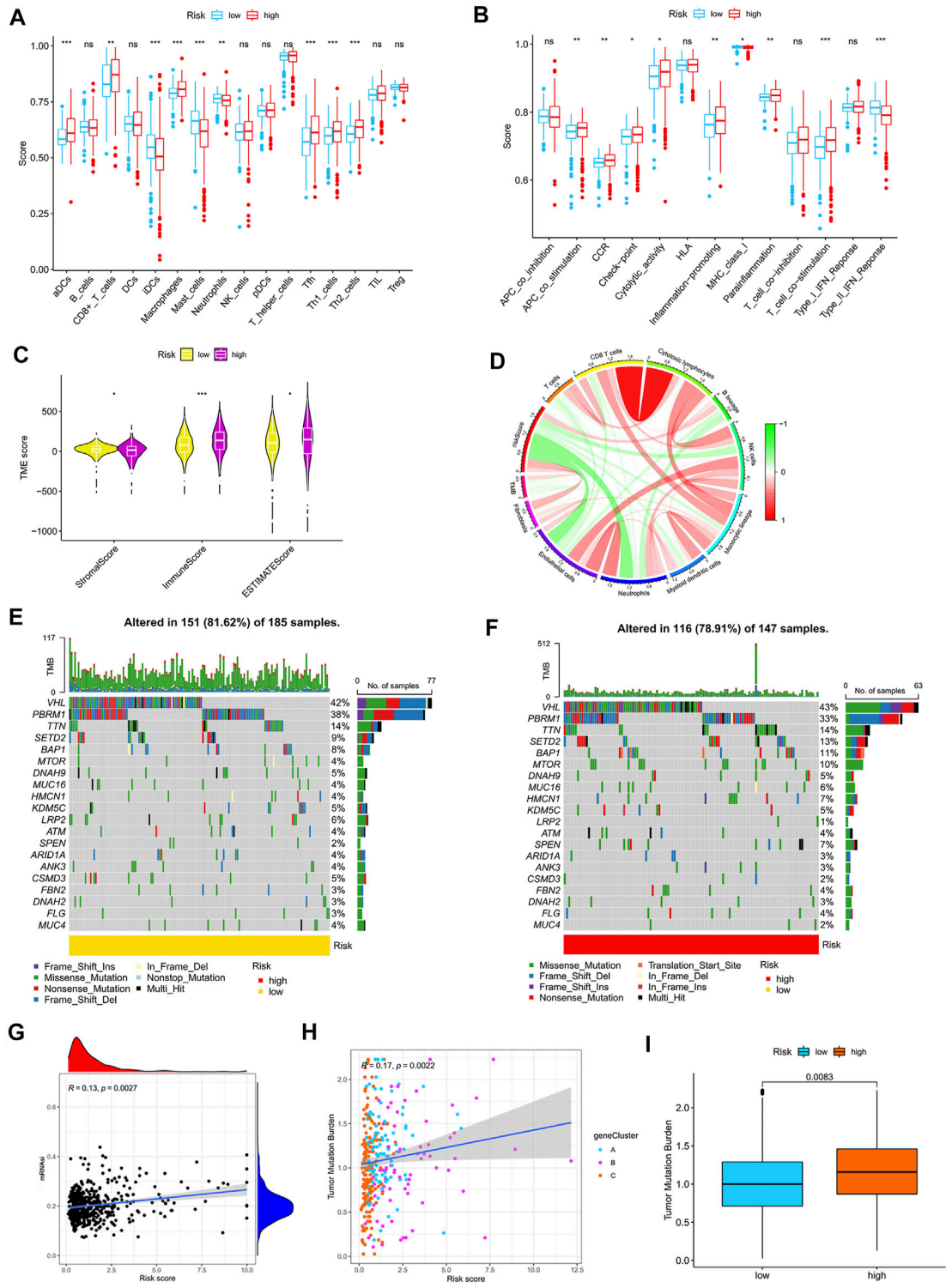

FIGURE 6
Relationship between the m7G score and tumor immune microenvironment. **(A,B)** ssGSEA of the correlation of the m7G score with immune cells and immune function. **(C)** ESTIMATE algorithm analysis of the correlation of the m7G score with immune cells and immune function. **(D)** MCP counter algorithm analysis of the correlation between the m7G score and immune cells. **(E,F)** Mutation characteristics of the high- and low-risk groups. **(G)** Correlation analysis between the m7G score and stemness indices. **(H,I)** Correlation analysis between the m7G score and TMB. TMB, tumor mutation burden.

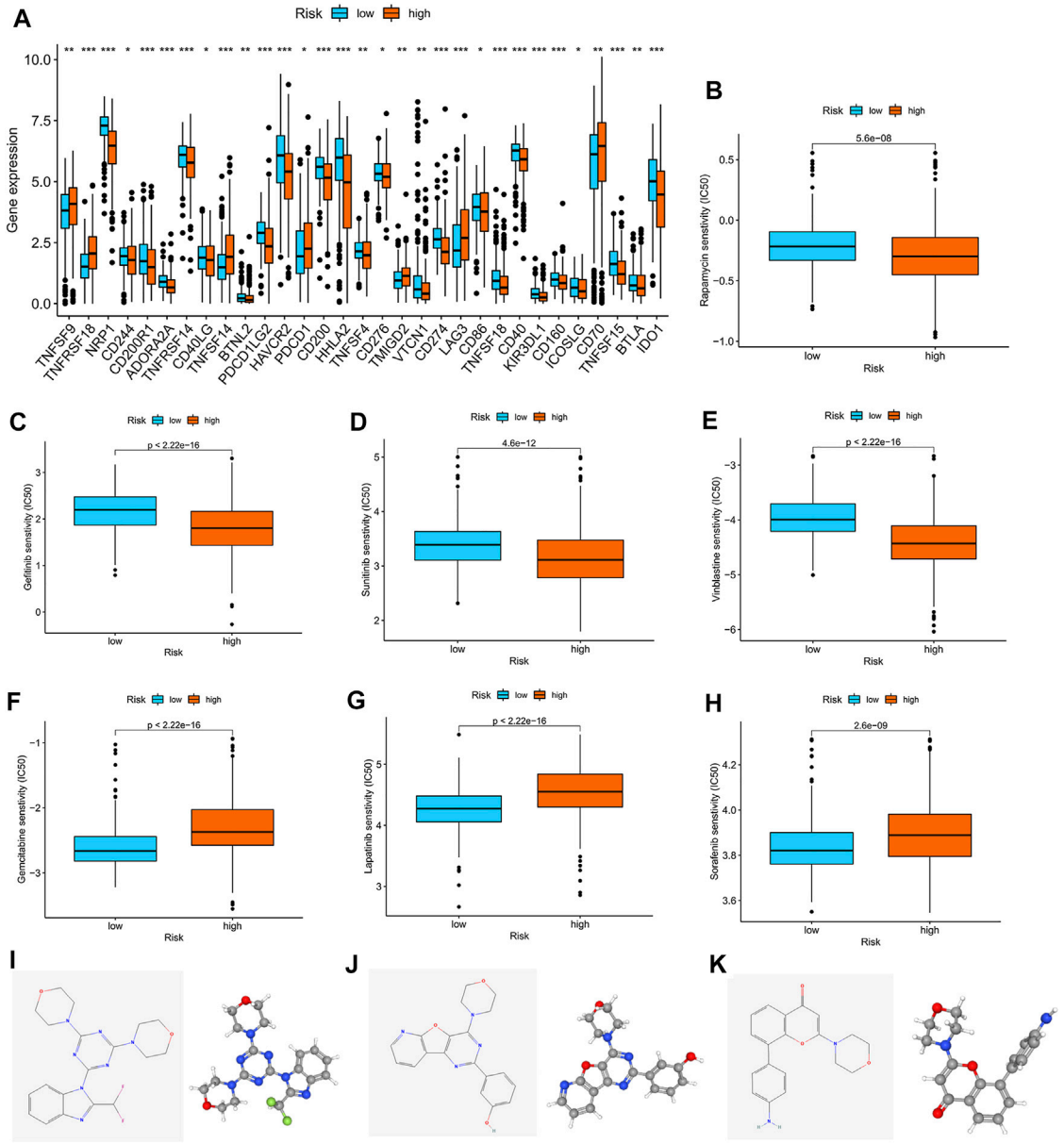

FIGURE 7
Correlation analysis between the m7G score and therapeutic drugs. **(A)** Expression profiles of checkpoints in the high- and low-risk groups. **(B–H)** Correlation analysis between the m7G score and IC_{50} of rapamycin, gefitinib, sunitinib, vinblastine, gemcitabine, lapatinib, and sorafenib. The 2D and 3D structures of **(I)** ZSTK-474, **(J)** PI-103, and **(K)** PI-828.

Furthermore, we used the cAMP database to explore potential small-molecule drugs for the therapy of patients with KIRC. The top 10 compounds with the strongest negative correlation with the patients in the high-risk group are shown in Table 1. Among these compounds, ZSTK-474, PI-103, and PI-828 are PI3K inhibitors. The 2D and 3D structures of the three compounds are shown in Figures 7I–K.

Validation in clinical samples

We validated the expression profiles of the genes that were used to develop the m7G score in paired cancer and normal tissues. CD36, THBS1, and PDK4 were highly expressed in cancer tissues, whereas PTPRB, G3BP2, and TMEM125 were lowly expressed in cancer tissues (Figures 8A–F). However, we found no difference in the expression of BCL2 between cancer and normal tissues (Figure 8G).

TABLE 1 Ten most negatively correlated small-molecule compounds screened from the CMap database.

Score	CMap name	Target	MOA
−96.37	Calyculin	PPP1CA, PPP1CC, and PPP2CA	Protein phosphatase inhibitor
−96.48	TG-101348	JAK2, FLT3, BRD4, JAK1, JAK3, RET, TYK2	FLT3 inhibitor, JAK inhibitor
−96.93	AZD-7762	CHEK1, and CHEK2	CHK inhibitor
−97.18	CS-110266	SLC6A3	Dopamine receptor agonist
−97.42	PI-828		PI3K inhibitor
−97.6	PI-103	PIK3CA, PIK3CG, MTOR, PIK3CB, PIK3CD, and PRKDC	MTOR inhibitor, PI3K inhibitor
−97.71	RO-90-7501	APP	Beta amyloid inhibitor
−97.77	Naftopidil	ADRA1A and ADRA1D	Adrenergic receptor antagonist
−97.8	PJ-34	EEF2, PARP1, PARP15, and PARP3	PARP inhibitor
−98.41	ZSTK-474	PIK3CG, PIK3CA, PIK3CB, and PIK3CD	PI3K inhibitor

MOA: Mechanisms of action.

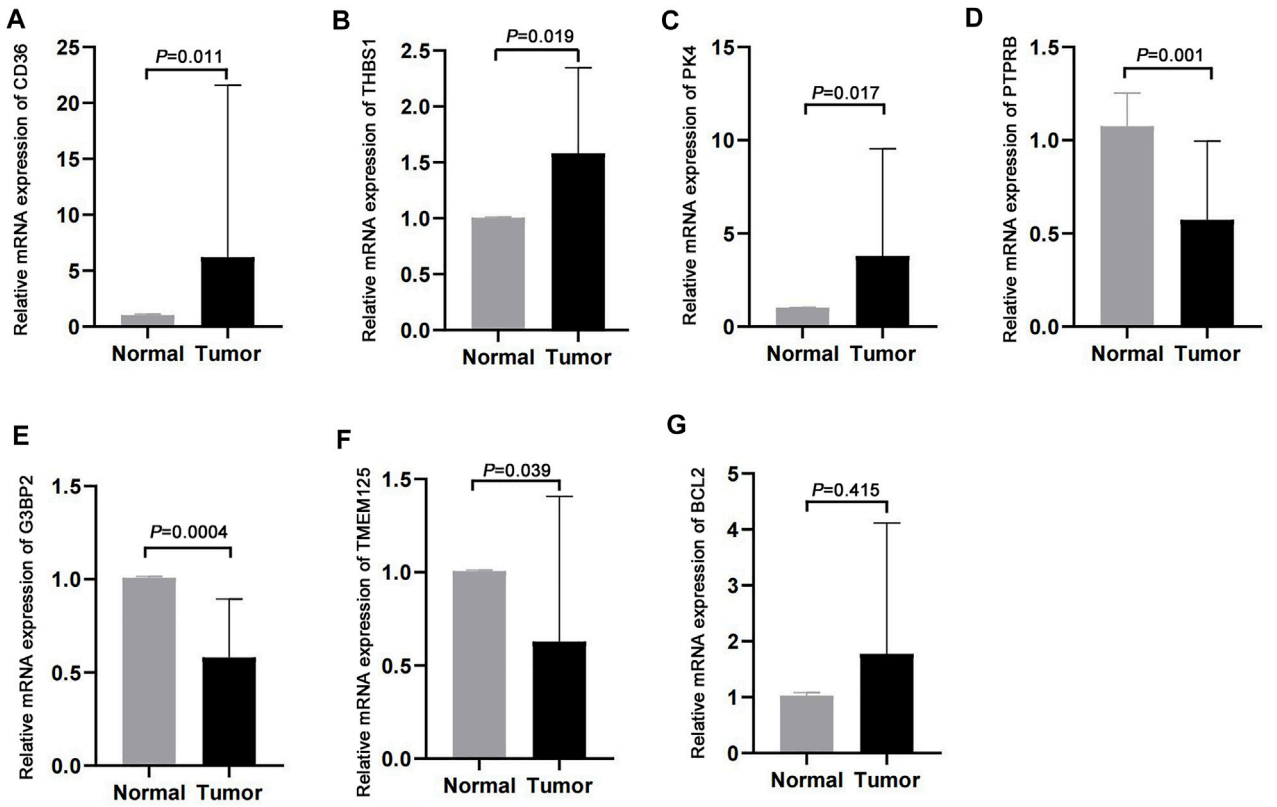

FIGURE 8
Validation in clinical samples. **(A–G)** Expression of CD36, THBS1, PDK4, PTPRB, G3BP2, TMEM125, and BCL2 in cancer and normal tissues.

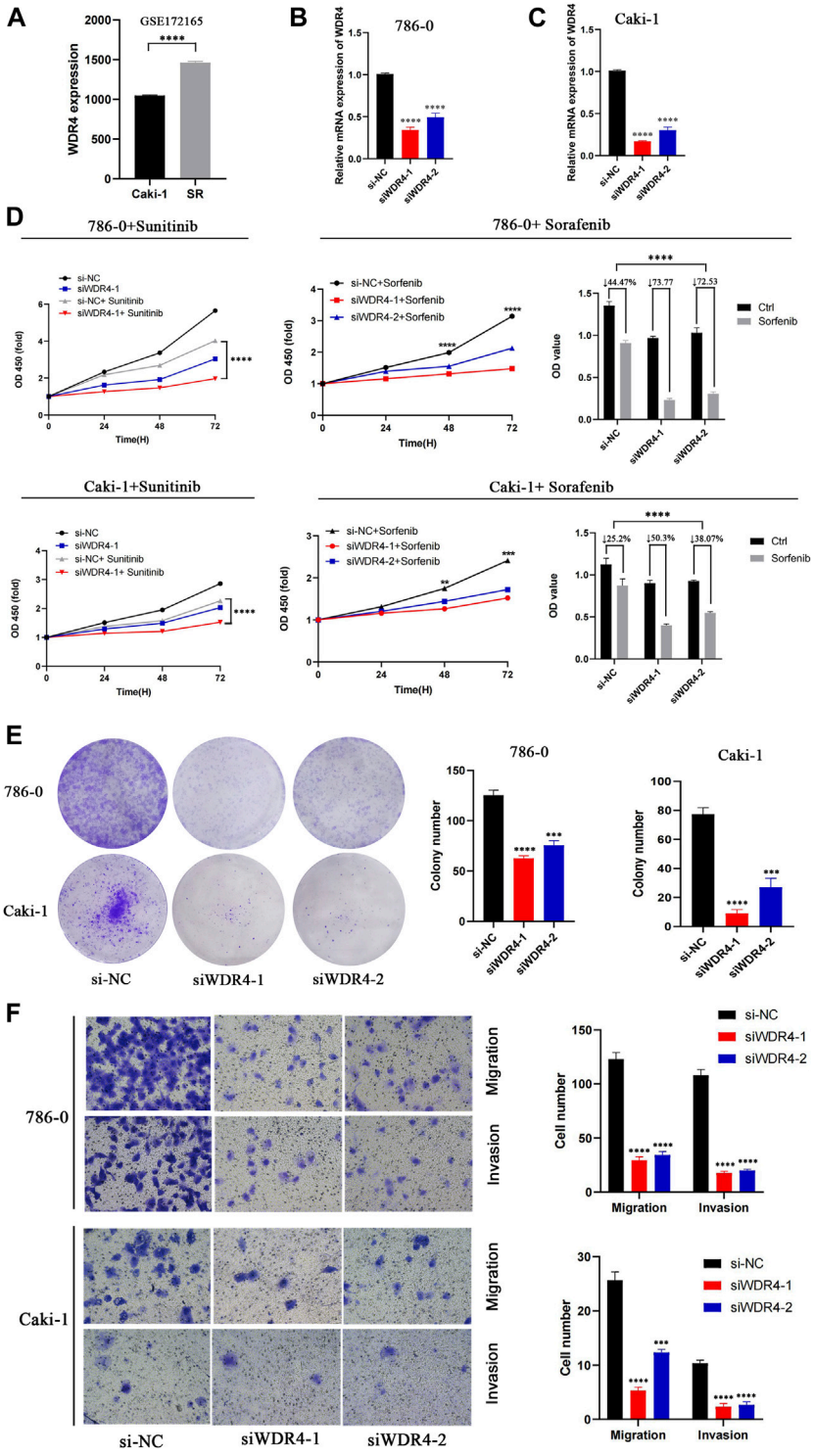

FIGURE 9
Effects of WDR4 on the biological function and drug resistance of KIRC cells. **(A)** Expression of WDR4 in sunitinib-resistant cell lines. **(B–C)** Detection of WDR4 knockdown efficiency. **(D)** Effects of WDR4 knockdown on KIRC cell proliferation and drug sensitivity. **(E)** Effect of WDR4 knockdown on the colony formation ability of KIRC cells. **(F)** Effects of knockdown of WDR4 on the migration and invasion of KIRC cells. SR: sunitinib-resistant.

TABLE 2 Four most correlated anticancer drugs screened from the GDSC database.

Gene	Drug	Cor	Label	*p* Value
WDR4	Lapatinib	0.587	Positive	0.000336
WDR4	Erlotinib	0.545	Positive	0.000863
WDR4	Entinostat	0.531	Positive	0.001175
WDR4	Sorafenib	0.526	Positive	0.001310

GDSC: Genomics of drug sensitivity in cancer.

Effects of WDR4 on the biological function and drug resistance of KIRC cells

In the GSE172165 dataset, WDR4 was significantly upregulated in the sunitinib-resistant Caki-1 cell line (Figure 9A). The anticancer drugs with the highest correlation with WDR4 in the GDSC database are shown in Table 2. WDR4 was positively correlated with the IC_{50} values of lapatinib, erlotinib, entinostat, and sorafenib. We further experimentally verified the effect of WDR4 on sensitivity to sunitinib and sorafenib, which are common chemotherapeutic drugs for KIRC. We used siRNA to knock down WDR4 in 786-0 and Caki-1 cells. The qRT-PCR results showed that interference with WDR4 significantly reduced the expression of WDR4 (Figures 9B,C). The knockdown of WDR4 decreased the cell viability and the IC_{50} values of sunitinib and sorafenib in 786-0 and Caki-1 cells (Figure 9D). Colony-formation assays demonstrated that the knockdown of WDR4 significantly inhibited the proliferation of 786-0 and Caki-1 cells (Figure 9E). The Transwell assay illustrated that knocking down WDR4 could significantly inhibit the migration and invasion of 786-0 and Caki-1 cells (Figure 9F). These results suggested that WDR4 may be a potential therapeutic target in patients with KIRC and sunitinib and sorafenib resistance.

Discussion

KIRC is highly heterogeneous, and the evaluation of its prognosis is dependent on TNM staging (Pichler et al., 2013). Reliable biomarkers for predicting the prognosis of KIRC are lacking. Molecular subtype predictors can be used to predict prognosis and response to immunotherapy and provide a basis for the precise treatment of patients with cancer. Exploring the molecular regulatory mechanisms of different subtypes has become a research hotspot in the field of cancer. m6A is the most common RNA methylation modification, and the molecular subtype based on m6A regulators can well-predict the efficacy of immunotherapy and evaluate the prognosis of patients (Shen et al., 2020; Zhang et al., 2020; Zhong et al., 2021). 5mC, another type of methylation modification, can also well-predict the prognosis of patients (Hu Y et al., 2021).

In our research, we found that most m7G regulators were favorable factors for KIRC, whereas NUDT11, NUDT10, NSUN2, WDR4, METTL1, LSM1, and EIF4A1 were risk factors. These genes all play an oncogenic role in cancer (Chen Z et al., 2021; Grisanzio et al., 2012; Hu J et al., 2021; Little et al., 2016; Wang et al., 2021; Xia et al., 2021; Ying et al., 2021; Zhao et al., 2021). Pan-cancer analysis showed that WDR4 and METTL1 were closely related to cancer immune infiltration and were immunotherapy targets in patients, and the high expression of KIRC was associated with poor prognosis of patients (Gao et al., 2022; Zeng et al., 2021). On the basis of the 29 m7G regulators, we divided the 702 patients with KIRC into three subtypes. We found significant differences in the OS and DFS between subtypes and that the prognosis of m7G cluster C was better than that of other clusters. m7G cluster C is related to immune activation pathways, such as RIG-I-like receptor, chemokine, and T-cell receptor signaling pathways. Cluster B is related to drug metabolism-related pathways, and cluster A is related to purine metabolism. Tumor purity and $CD8^+$ T cell infiltration were lower in the m7G cluster C than in other clusters. In RCC, $CD8^+$ T cells were mostly disabled and promoted immune escape. Studies have shown that in contrast to that in most solid tumors, the high infiltration of $CD8^+$ T cells in RCC predicts poor survival outcomes (Fridman et al., 2017). These results can explain why m7G cluster C had better prognosis than other clusters. Checkpoint inhibitors have been approved for the first-line treatment of KIRC. In our study, most checkpoints were more highly expressed in m7G cluster C than in other clusters, thereby suggesting that m7G cluster C may benefit more from checkpoint inhibitor therapy than other clusters. DEGs among different m7G subtypes were enriched in cancer-related pathways, such as the positive regulation of cell adhesion, the positive regulation of vasculature development, cell molecule adhesion, the PI3K–Akt signaling pathway, and the AKT–STAT signaling pathway. PI3K–Akt signaling pathway activation can promote the metastasis and progression of RCC (Du et al., 2021; Lin et al., 2021; Zhu et al., 2020). We divided the patients into three gene types in accordance with the three m7G subtypes and found significant differences in OS and PFS among the subtypes. We developed a new m7G score and validated the genes in clinical samples. CD36, PDK4, and THBS1 were highly expressed in cancer tissues, and G3BP2, PTPRB, and TMEM125 were lowly expressed in cancer tissues. However, we found no difference in the expression of BCL2 between cancer and normal tissues, likely due to our small sample size. The high expression of CD36, THBS1, and PDK4 in cancer is related to poor prognosis and promotes tumor progression (Guda et al., 2018; Huang et al., 2017; Kim et al., 2019; Liu et al., 2021; Liu et al., 2020; Xu et al., 2019; Zhou et al., 2009). G3BP2 and PTPRB are lowly expressed in cancer and are reliable markers for prognosis of patients (Qi et al., 2016; Wei et al., 2015). In addition, single-cell transcriptomes showed that PTPRB was expressed in the endothelial cells of normal kidney tissue (Young et al., 2018).

A total of 702 patients were divided into training and testing groups. The m7G score can well-predict the prognosis of the patients in the training and testing groups and the entire group with high prediction accuracy. The m7G score was externally validated with the GSE40912 and E-MTAB-1980 datasets and still had a good predictive performance. Therefore, the m7G score can be used as an effective biomarker for prediction of the prognosis of patients with KIRC and is helpful in clinical treatment decision-making. In addition, for improving the prediction of the prognosis of patients, we combined the TNM stage, grade, and age to construct a nomogram. This approach improved the predictive performance of the m7G score. At the same time, we found that cluster C of the immune activation subtype had a low m7G score. The tumor microenvironment plays an important role in the development of cancer. The main function of M1 macrophages is to promote antigen presentation, secrete immune-activating factors, and play an antitumor role (Chanmee et al., 2014; Hu et al., 2016). M2-like macrophage polarization can promote the formation of an immunosuppressive microenvironment in glioma (Xu et al., 2021). NELF in $CD8^+$ T cells acts on the enhancers and promoters of TCF1 target genes to exert antitumor immunity (Wu et al., 2022). The absence of a role of $CD8^+$ T cells in KIRC is related to poor prognosis (Dai S et al., 2021). Fibroblasts can inhibit cancer immunity, promote cancer progression, and make patients resistant to immunotherapy, which is related to poor prognosis (Peltier et al., 2022). Our results were consistent with these findings. The m7G score was negatively correlated with M1 macrophages. M2 macrophages, $CD8^+$ T cells, and fibroblasts were more abundant in the high-risk group than in the low-risk group. These immune cells were associated with the poor prognosis of patients with KIRC (Davidsson et al., 2020; Komohara et al., 2011; Li et al., 2020; Nakayama et al., 2018; Xie et al., 2021; You et al., 2021).

TMB is a reliable prognostic marker in patients with cancer, and high TMB predicts a poor prognosis (Song et al., 2022; Yang et al., 2022). High stemness indices suggest a poor prognosis and a high degree of malignancy in cancer (Zheng et al., 2021). The m7G score was positively correlated with TMB and stemness indices. The low-risk group was closely related to the immune activation pathway, which plays a role in inhibiting cancer. These results can be used to explain why the prognosis of patients with high scores is poorer than that of patients in the low-risk group. Studies have shown that the VHL mutation is the most common mutation in KIRC (Au et al., 2021). Consistent with our results, the frequency of the VHL mutation was highest in the high- and low-risk groups. Sunitinib is the first-line treatment for patients with metastatic KIRC. We found that high-risk patients were sensitive to rapamycin, gefitinib, sunitinib, and vinblastine but resistant to gemcitabine, lapatinib, and sorafenib. These findings provide a basis for personalized treatment of patients with KIRC. In addition, we found that the knockdown of WDR4 could inhibit the proliferation, migration, and invasion of 786-0 and Caki-1 cells and increase the drug sensitivity of sunitinib and sorafenib. WDR4 is a potential therapeutic target in patients with KIRC.

Our study has limitations. First, we only validated the m7G score with a small sample. Therefore, we need to validate this index with a large clinical cohort. Second, there is a lack of validation of the immunotherapy cohort, and the prediction of the m7G score for KIRC immunotherapy is limited.

Conclusion

This study proposed a new m7G modification-related molecular subtype and illustrated the immune cell infiltration characteristics of different subtypes. The developed m7G score can well-predict the prognosis of patients with KIRC and provide a basis for their personalized treatment.

Data availability statement

The datasets presented in this study can be found in online repositories. The names of the repository/repositories and accession number(s) can be found in the article/ Supplementary Material.

Ethics statement

The studies involving human participants were reviewed and approved by the ethics committee of Haikou Hospital affiliated to Xiangya Medical College of Central South University. The patients/participants provided their written informed consent to participate in this study.

Author contributions

MC designed the research. ZN, YG, and HC carried out the analyses. LZ, NG, and YP performed the experiments. SZ wrote the manuscript. All authors contributed to the article and approved the submitted version.

Funding

The research is supported with fund from Hainan Provincial Natural Science Foundation of China (2017CXTD010), Finance science and technology project of Hainan province (ZDYF2019163 and ZDYF2021SHFZ249), the National Science Foundation of China (82160531 and 81760465), and the health department of Hainan province (19A200184).

Conflict of interest

The authors declare that the research was conducted in the absence of any commercial or financial relationships that could be construed as a potential conflict of interest.

Publisher's note

All claims expressed in this article are solely those of the authors and do not necessarily represent those of their affiliated organizations, or those of the publisher, the editors, and the reviewers. Any product that may be evaluated in this article, or claim that may be made by its manufacturer, is not guaranteed or endorsed by the publisher.

Supplementary material

The Supplementary Material for this article can be found online at: https://www.frontiersin.org/articles/10.3389/fphar.2022.900006/full#supplementary-material

References

Alexandrov, A., Martzen, M. R., and Phizicky, andE. M. (2002). Two proteins that form a complex are required for 7-methylguanosine modification of yeast tRNA. *RNA* 8 (10), 1253–1266. doi:10.1017/s1355838202024019

Au, L., Hatipoglu, E., Robert de Massy, M., Litchfield, K., Beattie, G., Rowan, A., et al. (2021). Determinants of anti-PD-1 response and resistance in clear cell renal cell carcinoma. *Cancer Cell.* 39 (11), 1497–1518.e11. doi:10.1016/j.ccell.2021.10.001

Becht, E., Giraldo, N. A., Lacroix, L., Buttard, B., Elarouci, N., Petitprez, F., et al. (2016). Estimating the population abundance of tissue-infiltrating immune and stromal cell populations using gene expression. *Genome Biol.* 17 (1), 218. doi:10.1186/s13059-016-1070-5

Bedke, J., Albiges, L., Capitanio, U., Giles, R. H., Hora, M., Lam, T. B., et al. (2021). Updated european association of urology guidelines on renal cell carcinoma: Nivolumab plus cabozantinib joins immune checkpoint inhibition combination therapies for treatment-naïve metastatic Clear-Cell renal cell carcinoma. *Eur. Urol.* 79 (3), 339–342. doi:10.1016/j.eururo.2020.12.005

Bradrick, S. S., and Gromeier, M. (2009). Identification of gemin5 as a novel 7-methylguanosine cap-binding protein. *PLoS One* 4 (9), e7030. doi:10.1371/journal.pone.0007030

Braun, D. A., Bakouny, Z., Hirsch, L., Flippot, R., Van Allen, E. M., Wu, C. J., et al. (2021). Beyond conventional immune-checkpoint inhibition - novel immunotherapies for renal cell carcinoma. *Nat. Rev. Clin. Oncol.* 18 (4), 199–214. doi:10.1038/s41571-020-00455-z

Chanmee, T., Ontong, P., Konno, K., and andItano, N. (2014). Tumor-associated macrophages as major players in the tumor microenvironment. *Cancers* 6 (3), 1670–1690. doi:10.3390/cancers6031670

Chen, D., Zhang, R., Xie, A., Yuan, J., Zhang, J., Huang, Y., et al. (2021). Clinical correlations and prognostic value of Nudix hydroxylase 10 in patients with gastric cancer. *Bioengineered* 12 (2), 9779–9789. doi:10.1080/21655979.2021.1995104

Chen, M., Nie, Z., Cao, H., Gao, Y., Wen, X., Zhang, C., et al. (2021). Rac3 expression and its clinicopathological significance in patients with bladder cancer. *Pathol. Oncol. Res.* 27, 598460. doi:10.3389/pore.2021.598460

Chen, M., Zhang, S., Wen, X., Cao, H., and andGao, Y. (2020). Prognostic value of CLIC3 mRNA overexpression in bladder cancer. *PeerJ* 8, e8348. doi:10.7717/peerj.8348

ChenZ, ., Zhu, W., Zhu, S., Sun, K., Liao, J., Liu, H., et al. (2021). METTL1 promotes hepatocarcinogenesis via m G tRNA modification-dependent translation control. *Clin. Transl. Med.* 11 (12), e661. doi:10.1002/ctm2.661

Culjkovic-Kraljacic, B., Skrabanek, L., Revuelta, M. V., Gasiorek, J., Cowling, V. H., Cerchietti, L., et al. (2020). The eukaryotic translation initiation factor eIF4E elevates steady-state mG capping of coding and noncoding transcripts. *P. Natl. Acad. Sci. Usa.* 117 (43), 26773–26783. doi:10.1073/pnas.2002360117

Dai, S., Zeng, H., Liu, Z., Jin, K., Jiang, W., Wang, Z., et al. (2021). Intratumoral CXCL13^{+}CD8^{+}T cell infiltration determines poor clinical outcomes and immunoevasive contexture in patients with clear cell renal cell carcinoma. *J. Immunother. Cancer* 9 (2), e001823. doi:10.1136/jitc-2020-001823

Dai, Z., Liu, H., Liao, J., Huang, C., Ren, X., Zhu, W., et al. (2021). N^{7}-Methylguanosine tRNA modification enhances oncogenic mRNA translation and promotes intrahepatic cholangiocarcinoma progression. *Mol. Cell.* 81 (16), 3339–3355.e8. doi:10.1016/j.molcel.2021.07.003

Davidsson, S., Fiorentino, M., Giunchi, F., Eriksson, M., Erlandsson, A., Sundqvist, P., et al. (2020). Infiltration of m2 macrophages and regulatory t cells plays a role in recurrence of renal cell carcinoma. *Eur. Urol. Open Sci.* 20, 62–71. doi:10.1016/j.euros.2020.06.003

Du, X., Li, H., Xie, X., Shi, L., Wu, F., Li, G., et al. (2021). PiRNA-31115 promotes cell proliferation and invasion via PI3K/AKT pathway in clear cell renal carcinoma. *Dis. Markers* 2021, 6915329. doi:10.1155/2021/6915329

Edeline, J., Mottier, S., Vigneau, C., Jouan, F., Perrin, C., Zerrouki, S., et al. (2012). Description of 2 angiogenic phenotypes in clear cell renal cell carcinoma. *Hum. Pathol.* 43 (11), 1982–1990. doi:10.1016/j.humpath.2012.01.023

Fachel, A. A., Tahira, A. C., Vilella-Arias, S. A., Maracaja-Coutinho, V., Gimba, E. R., Vignal, G. M., et al. (2013). Expression analysis and *in silico* characterization of intronic long noncoding RNAs in renal cell carcinoma: Emerging functional associations. *Mol. Cancer* 12 (1), 140. doi:10.1186/1476-4598-12-140

Fridman, W. H., Zitvogel, L., Sautès-Fridman, C., and andKroemer, G. (2017). The immune contexture in cancer prognosis and treatment. *Nat. Rev. Clin. Oncol.* 14 (12), 717–734. doi:10.1038/nrclinonc.2017.101

Gao, Z., Xu, J., Zhang, Z., Fan, Y., Xue, H., Guo, X., et al. (2022). A comprehensive analysis of METTL1 to immunity and stemness in Pan-Cancer. *Front. Immunol.* 13, 795240. doi:10.3389/fimmu.2022.795240

Grisanzio, C., Werner, L., Takeda, D., Awoyemi, B. C., Pomerantz, M. M., Yamada, H., et al. (2012). Genetic and functional analyses implicate the NUDT11, HNF1B, and SLC22A3 genes in prostate cancer pathogenesis. *Proc. Natl. Acad. Sci. U. S. A.* 109 (28), 11252–11257. doi:10.1073/pnas.1200853109

Guda, M. R., Asuthkar, S., Labak, C. M., Tsung, A. J., Alexandrov, I., Mackenzie, M. J., et al. (2018). Targeting PDK4 inhibits breast cancer metabolism. *Am. J. Cancer Res.* 8 (9), 1725–1738.

Hänzelmann, S., Castelo, R., and andGuinney, J. (2013). Gsva: Gene set variation analysis for microarray and RNA-seq data. *BMC Bioinforma.* 14, 7. doi:10.1186/1471-2105-14-7

Hsieh, J. J., Purdue, M. P., Signoretti, S., Swanton, C., Albiges, L., Schmidinger, M., et al. (2017). Renal cell carcinoma. *Nat. Rev. Dis. Prim.* 3, 17009. doi:10.1038/nrdp.2017.9

Hu, J., Othmane, B., Yu, A., Li, H., Cai, Z., Chen, X., et al. (2021). 5MC regulator-mediated molecular subtypes depict the hallmarks of the tumor microenvironment and guide precision medicine in bladder cancer. *BMC Med.* 19 (1), 289. doi:10.1186/s12916-021-02163-6

Hu, W., Li, X., Zhang, C., Yang., Y., Jiang, J., and Wu, C. (2016). Tumor-associated macrophages in cancers. *Clin. Transl. Oncol.* 18 (3), 251–258. doi:10.1007/s12094-015-1373-0

Hu, Y., Chen, C., Tong, X., Chen, S., Hu, X., Pan, B., et al. (2021). NSUN2 modified by SUMO-2/3 promotes gastric cancer progression and regulates mRNA m5C methylation. *Cell. Death Dis.* 12 (9), 842. doi:10.1038/s41419-021-04127-3

Huang, T., Wang, L., Liu, D., Li, P., Xiong, H., Zhuang, L., et al. (2017). FGF7/FGFR2 signal promotes invasion and migration in human gastric cancer through upregulation of thrombospondin-1. *Int. J. Oncol.* 50 (5), 1501–1512. doi:10.3892/ijo.2017.3927

Kim, Y. S., Jung, J., Jeong, H., Lee, J. H., Oh, H. E., Lee, E. S., et al. (2019). High membranous expression of fatty acid transport protein 4 is associated with tumorigenesis and tumor progression in clear cell renal cell carcinoma. *Dis. Markers* 2019, 5702026. doi:10.1155/2019/5702026

Kiriakidou, M., Tan, G. S., Lamprinaki, S., De Planell-Saguer, M., Nelson, P. T., and Mourelatos, Z. (2007). An mRNA m7G cap binding-like motif within human Ago2 represses translation. *Cell.* 129 (6), 1141–1151. doi:10.1016/j.cell.2007.05.016

Komohara, Y., Hasita, H., Ohnishi, K., Fujiwara, Y., Suzu, S., Eto, M., et al. (2011). Macrophage infiltration and its prognostic relevance in clear cell renal cell carcinoma. *Cancer Sci.* 102 (7), 1424–1431. doi:10.1111/j.1349-7006.2011.01945.x

Li, G., Chong, T., Xiang, X., Yang, J., and andLi, H. (2017). Downregulation of microRNA-15a suppresses the proliferation and invasion of renal cell carcinoma via direct targeting of eIF4E. *Oncol. Rep.* 38 (4), 1995–2002. doi:10.3892/or.2017.5901

Li, Y., Wang, Z., Jiang, W., Zeng, H., Liu, Z., Lin, Z., et al. (2020). Tumor-infiltrating TNFRSF9^{+} CD8^{+} T cells define different subsets of clear cell renal cell carcinoma with prognosis and immunotherapeutic response. *Oncoimmunology* 9 (1), 1838141. doi:10.1080/2162402X.2020.1838141

Lin, H., Zeng, W., Lei, Y., Chen, D., and andNie, Z. (2021). Tuftelin 1 (TUFT1) promotes the proliferation and migration of renal cell carcinoma *via* PI3K/AKT signaling pathway. *Pathol. Oncol. Res.* 27, 640936. doi:10.3389/pore.2021.640936

Little, E. C., Camp, E. R., Wang, C., Watson, P. M., Watson, D. K., and Cole, D. J. (2016). The CaSm (LSm1) oncogene promotes transformation, chemoresistance and metastasis of pancreatic cancer cells. *Oncogenesis* 5, e182. doi:10.1038/oncsis.2015.45

Liu, B., Zhang, Y., and andSuo, J. (2021). Increased expression of PDK4 was displayed in gastric cancer and exhibited an association with glucose metabolism. *Front. Genet.* 12, 689585. doi:10.3389/fgene.2021.689585

Liu, X., Xu, D., Liu, Z., Li, Y., Zhang, C., Gong, Y., et al. (2020). THBS1 facilitates colorectal liver metastasis through enhancing epithelial-mesenchymal transition. *Clin. Transl. Oncol.* 22 (10), 1730–1740. doi:10.1007/s12094-020-02308-8

Lu, G., Zhang, J., Li, Y., Li, Z., Zhang, N., Xu, X., et al. (2011). HNUDT16: A universal decapping enzyme for small nucleolar RNA and cytoplasmic mRNA. *Protein Cell.* 2 (1), 64–73. doi:10.1007/s13238-011-1009-2

Ma, J., Han, H., Huang, Y., Yang, C., Zheng, S., Cai, T., et al. (2021). METTL1/WDR4-mediated m^{7}G tRNA modifications and m^{7}G codon usage promote mRNA translation and lung cancer progression. *Mol. Ther.* 29 (12), 3422–3435. doi:10.1016/j.ymthe.2021.08.005

Nakayama, T., Saito, K., Kumagai, J., Nakajima, Y., Kijima, T., Yoshida, S., et al. (2018). Higher serum c-reactive protein level represents the immunosuppressive tumor microenvironment in patients with clear cell renal cell carcinoma. *Clin. Genitourin. Cancer* 16 (6), e1151–e1158. doi:10.1016/j.clgc.2018.07.027

Newman, A. M., Liu, C. L., Green, M. R., Gentles, A. J., Feng, W., Xu, Y., et al. (2015). Robust enumeration of cell subsets from tissue expression profiles. *Nat. Methods* 12 (5), 453–457. doi:10.1038/nmeth.3337

Osborne, M. J., Volpon, L., Kornblatt, J. A., Culjkovic-Kraljacic, B., Baguet, A., and Borden, K. L. (2013). EIF4E3 acts as a tumor suppressor by utilizing an atypical mode of methyl-7-guanosine cap recognition. *Proc. Natl. Acad. Sci. U. S. A.* 110 (10), 3877–3882. doi:10.1073/pnas.1216862110

Pan, X. W., Chen, L., Hong, Y., Xu, D. F., Liu, X., Li, L., et al. (2016). EIF3D silencing suppresses renal cell carcinoma tumorigenesis via inducing G2/M arrest through downregulation of Cyclin B1/CDK1 signaling. *Int. J. Oncol.* 48 (6), 2580–2590. doi:10.3892/ijo.2016.3459

Peltier, A., Seban, R. D., Buvat, I., Bidard, F. C., and andMechta-Grigoriou, F. (2022). Fibroblast heterogeneity in solid tumors: From single cell analysis to whole-body imaging. *Semin. Cancer Biol.* doi:10.1016/j.semcancer.2022.04.008

Pichler, M., Hutterer, G. C., Chromecki, T. F., Jesche, J., Kampel-Kettner, K., Groselj-Strele, A., et al. (2013). Predictive ability of the 2002 and 2010 versions of the Tumour-Node-Metastasis classification system regarding metastasis-free, cancer-specific and overall survival in a European renal cell carcinoma single-centre series. *BJU Int.* 111, E191–E195. doi:10.1111/j.1464-410X.2012.11584.x

Qi, Y., Dai, Y., and andGui, S. (2016). Protein tyrosine phosphatase PTPRB regulates Src phosphorylation and tumour progression in NSCLC. *Clin. Exp. Pharmacol. Physiol.* 43 (10), 1004–1012. doi:10.1111/1440-1681.12610

Sato., Y., Yoshizato, T., Shiraishi, Y., Maekawa, S., Okuno, Y., Kamura, T., et al. (2013). Integrated molecular analysis of clear-cell renal cell carcinoma. *Nat. Genet.* 45 (8), 860–867. doi:10.1038/ng.2699

Şenbabaoğlu, Y., Gejman, R. S., Winer, A. G., Liu, M., Van Allen, E. M., de Velasco, G., et al. (2016). Tumor immune microenvironment characterization in clear cell renal cell carcinoma identifies prognostic and immunotherapeutically relevant messenger RNA signatures. *Genome Biol.* 17 (1), 231. doi:10.1186/s13059-016-1092-z

Shen, X., Hu, B., Xu, J., Qin, W., Fu, Y., Wang, S., et al. (2020). The m6A methylation landscape stratifies hepatocellular carcinoma into 3 subtypes with distinct metabolic characteristics. *Cancer Biol. Med.* 17 (4), 937–952. doi:10.20892/j.issn.2095-3941.2020.0402

Song, B., Tang, Y., Chen, K., Wei, Z., Rong, R., Lu, Z., et al. (2020). M7GHub: Deciphering the location, regulation and pathogenesis of internal mRNA N7-methylguanosine (m7G) sites in human. *Bioinforma. Oxf. Engl.* 36 (11), 3528–3536. doi:10.1093/bioinformatics/btaa178

Song, J. P., Liu, X. Z., Chen, Q., and andLiu, Y. F. (2022). High tumor mutation burden indicates a poor prognosis in patients with intrahepatic cholangiocarcinoma. *World J. Clin. Cases* 10 (3), 790–801. doi:10.12998/wjcc.v10.i3.790

Su, J., Wu, G., Ye, Y., Zhang, J., Zeng, L., Huang, X., et al. (2021). NSUN2-mediated RNA 5-methylcytosine promotes esophageal squamous cell carcinoma progression via LIN28B-dependent GRB2 mRNA stabilization. *Oncogene* 40 (39), 5814–5828. doi:10.1038/s41388-021-01978-0

Tomikawa, C. (2018). 7-Methylguanosine modifications in transfer RNA (tRNA). *Int. J. Mol. Sci.* 19 (12), E4080. doi:10.3390/ijms19124080

Wang, C., Wang, W., Han, X., Du, L., Li, A., and Huang, G. (2021). Methyltransferase-like 1 regulates lung adenocarcinoma A549 cell proliferation and autophagy via the AKT/mTORC1 signaling pathway. *Oncol. Lett.* 21 (4), 330. doi:10.3892/ol.2021.12591

Wei, S. C., Fattet, L., Tsai, J. H., Guo, Y., Pai, V. H., Majeski, H. E., et al. (2015). Matrix stiffness drives epithelial-mesenchymal transition and tumour metastasis through a TWIST1-G3BP2 mechanotransduction pathway. *Nat. Cell. Biol.* 17 (5), 678–688. doi:10.1038/ncb3157

Wu, B., Zhang, X., Chiang, H. C., Pan, H., Yuan, B., Mitra, P., et al. (2022). RNA polymerase II pausing factor NELF in CD8^{+} T cells promotes antitumor immunity. *Nat. Commun.* 13 (1), 2155. doi:10.1038/s41467-022-29869-2

Xia, P., Zhang, H., Xu, K., Jiang, X., Gao, M., Wang, G., et al. (2021). MYC-targeted WDR4 promotes proliferation, metastasis, and sorafenib resistance by inducing CCNB1 translation in hepatocellular carcinoma. *Cell. Death Dis.* 12 (7), 691. doi:10.1038/s41419-021-03973-5

Xie, Y., Chen, Z., Zhong, Q., Zheng, Z., Chen, Y., Shangguan, W., et al. (2021). M2 macrophages secrete CXCL13 to promote renal cell carcinoma migration, invasion, and EMT. *Cancer Cell. Int.* 21 (1), 677. doi:10.1186/s12935-021-02381-1

Xu, C., Ishikawa, H., Izumikawa, K., Li, L., He, H., Nobe, Y., et al. (2016). Structural insights into Gemin5-guided selection of pre-snRNAs for snRNP assembly. *Genes. Dev.* 30 (21), 2376–2390. doi:10.1101/gad.288340.116

Xu, J., Zhang, J., Zhang, Z., Gao, Z., Qi, Y., Qiu, W., et al. (2021). Hypoxic glioma-derived exosomes promote M2-like macrophage polarization by enhancing autophagy induction. *Cell. Death Dis.* 12 (4), 373. doi:10.1038/s41419-021-03664-1

Xu, W. H., Qu, Y. Y., Wang, J., Wang, H. K., Wan, F. N., Zhao, J. Y., et al. (2019). Elevated CD36 expression correlates with increased visceral adipose tissue and predicts poor prognosis in ccRCC patients. *J. Cancer* 10 (19), 4522–4531. doi:10.7150/jca.30989

Yang, H., Yu, M., Zhong, S., You, Y., and andFeng, F. (2022). Neoantigens and the tumor microenvironment play important roles in the prognosis of high-grade serous ovarian cancer. *J. Ovarian Res.* 15 (1), 18. doi:10.1186/s13048-022-00955-9

Ying, X., Liu, B., Yuan, Z., Huang, Y., Chen, C., Jiang, X., et al. (2021). METTL1-m^{7} G-EGFR/EFEMP1 axis promotes the bladder cancer development. *Clin. Transl. Med.* 11 (12), e675. doi:10.1002/ctm2.675

Yoshihara, K., Shahmoradgoli, M., Martínez, E., Vegesna, R., Kim, H., Torres-Garcia, W., et al. (2013). Inferring tumour purity and stromal and immune cell admixture from expression data. *Nat. Commun.* 4, 2612. doi:10.1038/ncomms3612

You, Y., Ren, Y., Liu, J., and andQu, J. (2021). Promising epigenetic biomarkers associated with Cancer-Associated-Fibroblasts for progression of kidney renal clear cell carcinoma. *Front. Genet.* 12, 736156. doi:10.3389/fgene.2021.736156

Young, M. D., Mitchell., T. J., Braga, F. A. Vieira., Tran., M. G. B., Stewart, B. J., Ferdinand, J. R., et al. (2018). Single-cell transcriptomes from human kidneys reveal the cellular identity of renal tumors. *Science* 361 (6402), 594–599. doi:10.1126/science.aat1699

Zeng, H., Xu, S., Xia, E., Hirachan, S., Bhandari, A., and Shen, Y. (2021). Aberrant expression of WDR4 affects the clinical significance of cancer immunity in pan-cancer. *Aging* 13 (14), 18360–18375. doi:10.18632/aging.203284

Zhang, B., Wu, Q., Li, B., Wang, D., Wang, L., and Zhou, Y. L. (2020). m^{6}A regulator-mediated methylation modification patterns and tumor microenvironment infiltration characterization in gastric cancer. *Mol. Cancer* 19 (1), 53. doi:10.1186/s12943-020-01170-0

Zhao, Y., Wang, Y., Chen, W., Bai, S., Peng, W., Zheng, M., et al. (2021). Targeted intervention of eIF4A1 inhibits EMT and metastasis of pancreatic cancer cells via c-MYC/miR-9 signaling. *Cancer Cell. Int.* 21 (1), 670. doi:10.1186/s12935-021-02390-0

Zheng, H., Song, K., Fu, Y., You, T., Yang, J., Guo, W., et al. (2021). An absolute human stemness index associated with oncogenic dedifferentiation. *Brief. Bioinform.* 22 (2), 2151–2160. doi:10.1093/bib/bbz174

Zhong, J., Liu, Z., Cai, C., Duan, X., Deng, T., and Zeng, G. (2021). m^{6}A modification patterns and tumor immune landscape in clear cell renal carcinoma. *J. Immunother. Cancer* 9 (2), e001646. doi:10.1136/jitc-2020-001646

Zhou, Z. Q., Cao, W. H., Xie, J. J., Lin, J., Shen, Z. Y., Zhang, Q. Y., et al. (2009). Expression and prognostic significance of THBS1, Cyr61 and CTGF in esophageal squamous cell carcinoma. *BMC Cancer* 9, 291. doi:10.1186/1471-2407-9-291

Zhu, Q., Zhong, A. L., Hu, H., Zhao, J. J., Weng, D. S., Tang, Y., et al. (2020). Acylglycerol kinase promotes tumour growth and metastasis via activating the PI3K/AKT/GSK3β signalling pathway in renal cell carcinoma. *J. Hematol. Oncol.* 13 (1), 2. doi:10.1186/s13045-019-0840-4

frontiers | Frontiers in Pharmacology

TYPE Original Research
PUBLISHED 01 November 2022
DOI 10.3389/fphar.2022.1061597

OPEN ACCESS

EDITED BY
Kenneth K. W. To,
The Chinese University of Hong Kong, China

REVIEWED BY
Tao Jiang,
Zhejiang Chinese Medical University, China
Ravindra Deshpande,
Wake Forest University, United States

*CORRESPONDENCE
Yanhui Liu,
liuyh@scu.edu.cn
Mina Chen,
chenmina2010@scu.edu.cn

†These authors have contributed equally to this work

SPECIALTY SECTION
This article was submitted to Pharmacology of Anti-Cancer Drugs, a section of the journal Frontiers in Pharmacology

RECEIVED 04 October 2022
ACCEPTED 21 October 2022
PUBLISHED 01 November 2022

CITATION
Zhang S, Chen S, Wang Z, Li J, Yuan Y, Feng W, Li W, Chen M and Liu Y (2022), Prognosis prediction and tumor immune microenvironment characterization based on tryptophan metabolism-related genes signature in brain glioma.
Front. Pharmacol. 13:1061597.
doi: 10.3389/fphar.2022.1061597

Prognosis prediction and tumor immune microenvironment characterization based on tryptophan metabolism-related genes signature in brain glioma

Shuxin Zhang[1,2†], Siliang Chen[1†], Zhihao Wang[1], Junhong Li[3], Yunbo Yuan[1], Wentao Feng[1], Wenhao Li[1], Mina Chen[4*] and Yanhui Liu[1*]

[1]Department of Neurosurgery, West China Hospital of Sichuan University, Chengdu, Sichuan, China, [2]Department of Head and Neck Surgery, Sichuan Cancer Hospital and Institute, School of Medicine, University of Electronic Science and Technology of China, Chengdu, China, [3]Department of Neurosurgery, Chengdu Second People's Hospital, Chengdu, Sichuan, China, [4]State Key Laboratory of Biotherapy, Neuroscience and Metabolism Research, West China Hospital, Sichuan University, Chengdu, China

Glioma is the most common malignant tumor in the central nervous system with no significant therapeutic breakthrough in recent years. Most attempts to apply immunotherapy in glioma have failed. Tryptophan and its metabolism can regulate malignant features of cancers and reshape immune microenvironment of tumors. However, the role of tryptophan metabolism in glioma remains unclear. In current study, we explored the relationships between the expression pattern of tryptophan metabolism-related genes (TrMGs) and tumor characteristics, including prognosis and tumor microenvironment of gliomas through analyzing 1,523 patients' samples from multiple public databases and our own cohort. Based on expression of TrMGs, K-means clustering analysis stratified all glioma patients into two clusters with significantly different TrMG expression patterns, clinicopathological features and immune microenvironment. Furthermore, we constructed a tryptophan metabolism-related genes signature (TrMRS) based on seven essential TrMGs to classify the patients into TrMRS low- and high-risk groups and validated the prognostic value of the TrMRS in multiple cohorts. Higher TrMRS represented for potentially more active tryptophan catabolism, which could subsequently lead to less tryptophan in tumor. The TrMRS high-risk group presented with shorter overall survival, and further analysis confirmed TrMRS as an independent prognostic factor in gliomas. The nomograms uniting TrMRS with other prognostic factors manifested with satisfactory efficacy in predicting the prognosis of glioma patients. Additionally, analyses of tumor immune landscapes demonstrated that higher TrMRS was correlated with more immune cell infiltration and "hot" immunological phenotype. TrMRS was also demonstrated to be positively correlated with the expression of multiple immunotherapy targets, including PD1 and PD-L1. Finally, the TrMRS high-risk group manifested better predicted response to immune checkpoint inhibitors. In conclusion, our study illustrated the relationships between expression pattern of TrMGs and characteristics of gliomas, and presented a novel model based on TrMRS for prognosis prediction in glioma

patients. The association between TrMRS and tumor immune microenvironment of gliomas indicated an important role of tryptophan and its metabolism in reshaping immune landscape and the potential ability to guide the application of immunotherapy for gliomas.

KEYWORDS

tryptophan, glioma, metabolism, prognosis, immune infiltration, immune checkpoint inhibitor, tumor microenvironment

Introduction

Glioma, a type of malignant tumor arising from glial cells, is responsible for approximately 80% of all malignant tumors in the central nervous system (Ostrom et al., 2021). Current standard treatment regime for glioma consists of surgery, radiotherapy, and chemotherapy (Stupp et al., 2005; Weller et al., 2021). However, even with entire process of standard treatment, the prognosis of glioma patients remains unsatisfactory, especially for glioblastoma, which manifests with highly malignant features and only achieved a median overall survival of fewer than 2 years (Chinot et al., 2014; Gilbert et al., 2014; Stupp et al., 2015). Hence, plenty studies devoted to exploring novel therapies to improve prognosis of glioma patients, one of which was immunotherapy. Immunotherapy, aiming to restrict the immune escape phenomenon of tumors and enhance the anti-tumor immunity executed by immune cells, has been proved with ability to improve patients' overall survival in numerous cancers, including melanoma (Larkin et al., 2015), cervical cancer (Tewari et al., 2022), gastric cancer (Janjigian et al., 2021), and lung cancer (Reck et al., 2016). However, almost all trials of immune checkpoint inhibitors (ICIs) did not endorse improvement of overall survival in glioblastoma patients (Reardon et al., 2020; Lim et al., 2022; Omuro et al., 2022). One of the potential reasons of these failures is immunologically quiescent environment of the central nervous system. But the metastatic brain tumor patients could benefit from ICIs therapy (Tawbi et al., 2018; Hendriks et al., 2019), suggesting that ICIs could deliver robust anti-tumor effects into CNS and the distinctive immune landscape of gliomas may be a potential reason for failures of ICIs. Besides, the application of neoadjuvant ICIs in glioblastoma was proved could enhance the immune response and reshape the immune landscape (Cloughesy et al., 2019; Schalper et al., 2019). Furthermore, multiple factors, including lifestyle, metabolic disorders, and social behaviors, could also influence the expression of checkpoint inhibitors and responses to immunotherapy (Deshpande et al., 2020). For example, obesity could upregulate the production of leptin and consequently promoted PD-1 expression on T-cells, leading to high response rate to immunotherapy in overweighted individuals (Wang et al., 2019). Besides, the responses to immunotherapy were observed more effective in smokers compare to never smoking individuals in lung cancer, which might result from high mutation rate in smokers (Abdel-Rahman, 2018). Hence, exploring possible pathways to reshape the immune landscape and enhance the response to immunotherapy can contribute to reinforcing the effects of immunotherapy and improving prognosis of glioma patients.

Tryptophan, an essential amino acid for human, is gained exclusively from diary intake. Tryptophan, together with its metabolites, is proved to play critical roles in multiple physiological processes, including cell maintenance and growth (Platten et al., 2019). Furthermore, tryptophan and its metabolites could also function as neurotransmitter and signalling molecules (Cervenka et al., 2017). Furthermore, shortage of tryptophan would activate the General control nonderepressible 2 (GCN2) pathway and lead to dysfunction of antigen-presenting cells and T-cells (Munn et al., 2005). Reduced tryptophan level was detected in multiple cancers (Huang et al., 2002; Schroecksnadel et al., 2005; Weinlich et al., 2007; Suzuki et al., 2010), suggesting potential role of tryptophan in cancers. In the tryptophan metabolism, over 95% of free tryptophan is degraded by the kynurenine pathway (Le Floc'h et al., 2011; van der Goot and Nollen, 2013). Indoleamine-2,3-dioxygenase (IDO) and tryptophan-2,3-dioxygenase (TDO), which catalyzes the same reaction, are rate-limiting enzymes in the kynurenine pathway (Grohmann et al., 2017). IDO was confirmed with immunosuppressive effect (Munn et al., 1998), and silencing the expression of IDO could enhance the antitumor immunity (Yen et al., 2009). TDO was also proved with similar immunosuppressive effects by inhibiting proliferation of T-cells and blocking infiltration of immune cells (Opitz et al., 2011; Pilotte et al., 2012). These studies revealed that tryptophan plays a critical role in tumor progression and process of antitumor immunity, and the metabolism of tryptophan has a significant impact on immunological feature of tumors. However, the role of tryptophan metabolism in the progression and immune landscape of glioma was not well elucidated.

In our current study, we utilized multiple glioma patients' cohort, including TCGA, CGGA, REMBRANDT, and our own cohort, to explore relationship between the expression pattern of tryptophan metabolism-related genes (TrMGs) and the characteristics of gliomas. Besides, we constructed a tryptophan metabolism-related gene signature (TrMRS) to assess the clinical significance of TrMG expression profile. Furthermore, we performed multiple analyses to elucidated relationship between the expression of tryptophan metabolism-related genes and the landscape of tumor immune microenvironment of gliomas. Based on these analyses, we look forward to exploring the potential applications of tryptophan metabolism in improving responses to immune checkpoint inhibitors and guiding selection of immunotherapy in glioma patients.

TABLE 1 Clinicopathological characteristics of patients in TCGA, CGGA, REMBRANDT, and WCH cohort.

Characteristics	TCGA (N = 662)	CGGA (N = 415)	REMBRANDT (N = 369)	WCH (N = 77)
Age: mean (range)	46 (18–89)	43 (19–76)	52 (22–87)	46 (19–77)
Gender				
Female	282 (42.6%)	176 (42.4%)	118 (32.0%)	30 (39.0%)
Male	380 (57.4%)	239 (57.6%)	196 (53.1%)	47 (77.0%)
NA	0	0	55 (14.9%)	0
Histology				
Astrocytoma	341 (51.5%)	182 (43.9%)	133 (36.0%)	22 (28.6%)
Oligodendroglioma	167 (25.2%)	94 (22.7%)	59 (16.0%)	21 (27.3%)
Glioblastoma	154 (23.3%)	139 (33.5%)	177 (48.0%)	34 (44.2%)
Grade				
G2	214 (32.3%)	134 (32.3%)	88 (23.8%)	29 (37.7%)
G3	237 (35.8%)	142 (34.2%)	66 (17.9%)	14 (18.2%)
G4	154 (23.3%)	139 (33.5%)	177 (48.0%)	34 (44.2%)
NA	57 (8.6%)	0	38 (10.3%)	0
IDH status				
WT	236 (35.6%)	169 (40.7%)	NA	42 (54.5%)
Mutant	421 (63.6%)	207 (49.9%)	NA	35 (45.5%)
NA	5 (0.8%)	39 (9.4%)	NA	0
1p/19q codeletion				
Non-codel	488 (73.7%)	267 (64.3%)	148 (40.1%)	43 (55.8%)
Codel	167 (25.2%)	88 (21.2%)	24 (6.5%)	19 (24.7%)
NA	7 (1.1%)	60 (14.5%)	197 (53.4%)	15 (19.5%)
TERT promoter status				
Mutant	340 (51.4%)	NA	NA	23 (29.9%)
WT	156 (23.6%)	NA	NA	30 (39.0%)
NA	166 (25.1%)	NA	NA	24 (31.2%)
MGMT promoter status				
Unmethylated	157 (23.7%)	141 (34.0%)	NA	13 (16.9%)
Methylated	472 (71.3%)	195 (47.0%)	NA	35 (45.5%)
NA	33 (5.0%)	79 (19.0%)	NA	29 (37.7%)
ATRX status				
Mutant	192 (29.0%)	NA	NA	53 (68.8%)
WT	459 (69.3%)	NA	NA	22 (28.6%)
NA	11 (1.7%)	NA	NA	2 (2.6%)

TCGA, the cancer genome atlas; CGGA, chinese glioma genome atlas; WCH, west china hospital; IDH, isocitrate dehydrogenase; TERT, telomerase reverse transcriptase; MGMT, O6-methylguanine-DNA, methyltransferase; ATRX, alpha-thalassemia x-linked intellectual disability syndrome; WT, wild type; NA, not available.

Materials and methods

RNA-sequencing and clinicopathological data collection and preprocessing

The RNA-sequencing and clinicopathological data enrolled in this study were acquired from three public databases and an own cohort. Patients with primary gliomas included in this study. Here, the notion of gliomas is restricted to astrocytomas, oligodendrogliomas, and glioblastomas. Those with recurrent gliomas or age < 18 were excluded from this study. In total, 662 primary gliomas from the Cancer Genome Atlas (TCGA, of which 655 had survival data) were included in our study, and the fragments per kilobase million (FPKM) and survival data of them were downloaded from the TCGA website (https://portal.gdc.cancer.gov/). Another 415 primary gliomas were from the Chinese Glioma Genome Atlas (CGGA) 693 cohort, and the REMBRANDT cohort which consists of 369 primary gliomas. FPKM data of the CGGA cohort and array data of REMBRANDT cohort were obtained from the CGGA website (http://www.cgga.org.cn/). For data preprocessing, the genes with too low expression levels

(FPKM maximum < 0.1 or standard deviation < 0.01) were excluded from subsequent analyses.

Our own cohort included 77 primary glioma patients from West China Hospital (WCH). We obtained their tumor tissues during craniotomy and sequenced mRNA of these tumor tissues. Subsequently, we used STAR to quantify the mRNA sequencing data and normalized them to FPKM. Survival data of these patients were acquired by regular follow-up, and the overall survival (OS) was defined as the period from surgery to death or the time of last follow-up (censored value). Additionally, the patients younger than 18 years old were excluded from analyses in all four cohorts. The detailed clinicopathological information of these patients is given in Table 1.

K-means clustering analysis based on expression pattern of tryptophan metabolism-related genes

By searching the Molecular Signature Database (MSigDB) with the keyword "tryptophan metabolism" or "tryptophan metabolic process," we identified 56 tryptophan metabolism-related genes (TrMGs), and 44 of which were kept after excluding the genes with low expression level. Subsequently, we performed unsupervised K-means clustering analysis to illuminate the distinctive tryptophan metabolism patterns in gliomas based on the expression patterns of tryptophan metabolism-related genes. We utilized the R package "factoextra" to determine the optimal number of clusters, which corresponded to the maximum average silhouette width (average distances of points to the centroids of clusters that it does not belong to minus the distance of points to the centroid of the cluster that it belongs to). To visualize the different expression patterns of TrMGs in each cluster, we conducted the t-Distributed Stochastic Neighbor Embedding (tSNE) analysis. Additionally, we utilized the TrMGs expression and cluster labels based on the TCGA cohort to construct a naïve Bayes classifier, and then stratified the patients of the other cohort into different clusters using this classifer.

Construction and validation of the risk signature based on tryptophan metabolism-related genes

Based on the expression of TrMGs, we constructed a risk signature system to elucidate the relationship between TrMGs and gliomas. First, we split the patients of TCGA cohort into training and validation tests with a ratio of 6:4. All the other three cohorts were utilized as validation sets. In the training set, we selected the TrMGs using the Least Absolute Shrinkage And Selection Operator (LASSO) Cox regression analysis. The TrMGs were determined as essential TrMGs in glioma if their coefficient was not zero at the lambdas corresponding to maximum C-index in over 80 random repetitions of LASSO Cox regression out of 100. Furthermore, a final multivariate Cox regression model was fitted to the training set with essential TrMGs. The tryptophan metabolism-related genes risk signature (TrMRS) was calculated using the following formula:

$$TrMRS\ Risk\ Signature = \sum_{i=1}\left(\beta_i * Exp_i\right)$$

In this calculating formula, β stand for the coefficient of each essential TrMG as fitted by the final multivariate Cox regression model, and Exp represented for the expression level of each essential TrMG. Subsequently, we determined the optimal TrMRS cut-off value by "surv_cutpoint" in the R package "survminer" with group proportion ≥ 0.3 for each dataset. Based on the optimal cut-off value, we allocated all patients into TrMRS low-risk or high-risk group. Additionally, we depicted the receiver operating characteristic (ROC) curve in validation sets of 1, 2, and 3-years survival and computed the area under the ROC curve (AUC) using the R package "timeROC."

Analyses of gene alternations and copy number variation

For the analyses of gene alternations and copy number variations (CNVs), we obtain the data of gene alterations and CNVs from the cBioPortal database (https://www.cbioportal.org/) for the TCGA cohort. The R package "maftools" was utilized to illustrate the different patterns of gene alterations and tumor mutation burdens (TMB) between different K-means clusters and TrMRS risk groups. Furthermore, the Genomic Identification of Significant Targets in Cancer (GISTIC) score was used to assess the different CNV levels in different clusters and risk groups.

Gene set enrichment analysis and comprehensive analysis of tumor immune microenvironment landscape

To interpret the biological functions of the differential transcriptomes between clusters and TrMRS risk groups, we utilized the over-representation and gene set enrichment analysis (GSEA) to evaluate the differentially expressed genes (DEGs) with the R package "clusterProfiler". R package "limma" was used to identify the DEGs between different clusters and risk groups. In the process of DEGs identification for GSEA, we stratified the patients into TrMRS high- and low-risk groups based on cut-off values of each cohort. Those genes with adjusted p-value < 0.05 and $|\log_2 FC| > 0.5$ were identified as DEGs. Furthermore, we used the R package "GSVA" to convert the logFPKM matrix of genes to pathway expression matrix. We identified the differentially expressed pathways between different clusters and risk groups with the "limma" package. To calculate the infiltration fraction of immune cells in glioma, we utilized the CIBERSORTx (https://cibersortx.stanford.edu/) and TIMER 2.0 [http://timer.comp-genomics.org/,

which is based on signature genes correlated with estimated tumor purity and immune cell fractions (Li et al., 2016)]. Additionally, the Estimation of Stromal and Immune Cells in Malignant Tumor tissues using Expression data (ESTIMATE) was used to evaluate the infiltration of stromal and immune cells in tumor microenvironment and calculate the stromal, immune and ESTIMATE scores (Yoshihara et al., 2013). In this algorithm, the stromal-related genes were selected from the non-hematopoiesis-related genes that were differentially expressed between tumor cell fraction and match stromal cells fraction separated by laser capture microdissection in multiple cancers. Furthermore, the tumor purity data published by Aran et al. (2015) which included ESTIMATE score-based tumor purity and consensus purity estimation (CPE), were used to represent the tumor purity in gliomas. Another previously published algorithm was utilized to compute the tumor immunological phenotype (TIP) gene signature (Wang et al., 2021). Based on TIP signature, we identified immunological phenotypes of gliomas and distinguish relatively "hot" tumors from "cold" tumors. Furthermore, we also utilized the Tumor Immune Dysfunction and Exclusion (TIDE) suite (http://tide.dfci.harvard.edu/) to predict response to immune checkpoint inhibitors therapy in gliomas.

Construction of nomogram based on tryptophan metabolism-related genes and other prognostic factors

To determine prognostic factors in glioma, we used univariate and multivariate Cox regression analyses. We firstly enrolled TrMRS and other potential prognostic factors, including tumor grade, age, chemotherapy, radiotherapy, KPS, gender, 1p/19q codeletion, and IDH mutation, into the univariate Cox regression analysis. Subsequently, those factors with a p-value < 0.05 in univariate analysis were enrolled into multivariate Cox regression analysis to identify independent prognostic factors. Those factors with a p-value < 0.1 in multivariate Cox regression analysis were identified as independent factors and enrolled into construction of nomograms. The R package "rms" was utilized to construct the nomograms. The calibration curves were used to evaluate the efficacy of nomograms for prognosis prediction in glioma patients.

Statistical Analysis

In all proceedings of bioinformatic analyses, we used the R software (version 4.2.1). To assess the differences between clusters or risk groups for continuous variables, we used the Wilcoxon rank sum test. To assess the differences for categorical variables, we used the chi-square test. The R package "survminer" was used to deliver survival analysis and generate Kaplan-Meier (K-M) curves, which were tested for differences by log-rank test. The "coxph" function in the R package "survival" was applied to conduct Cox regression analyses. The R package "glmnet" was utilized to perform the LASSO Cox regression analysis. T Iterative Grubbs tests were applied to expel the outliers in liner regression analysis.

Ethical approval, consent to participate, and data availability

Tumor samples and clinical data collection and use were performed strictly with ethics regulations and approved by the institutional review board of West China Hospital (No. 2018.569) based on local ethics regulations and the 1964 Helsinki declaration and its later amendments. In addition, the patients signed written consent for tumor tissue collection and processing. The sequencing data of West China Hospital generated in this study are available at the Genome Sequence Archive for Humans: accession code HRA002839 (access link: https://ngdc.cncb.ac.cn/gsa-human/s/JQssVoV1).

Results

K-means clustering analysis based on tryptophan metabolism-related genes

Based on 44 identified tryptophan metabolism-related genes, we conducted an unsupervised K-means clustering analysis in the TCGA cohort. Then the gliomas in the TCGA cohort were stratified into two clusters according to the average silhouette widths as described in the Material and Method section (Supplementary Figure S1A). Distinctions in TrMGs expression profile between two clusters were illustrated by tSNE analysis (Figure 1A). The expression levels of TrMGs in each glioma was given out in heatmap ordered by clusters (Supplementary Figure S1B). The critical metabolites and enzymes in two branches of tryptophan metabolism, kynurenine pathway and serotonin pathway, were interpreted in a schematic diagram (Figure 1B). The differences in the expression levels of ten important TrMGs involved in the tryptophan metabolism were also illustrated (Figure 1C). The cluster 2 was demonstrated with higher expression of IDO1, TDO2, KYNU, KMO, and HAAO, which were critical enzymes in the kynurenine pathway for tryptophan metabolism. Besides, KAT2, HADHA, GCDH, DDC, and ALDH2 were highly expressed in cluster 1, suggesting more consumption of metabolites of kynurenine pathway and more active serotonin pathway. The differences in the expression levels of each TrMG were shown in Supplementary Figure S1C.

Survival analysis revealed that the prognosis of cluster 1 was significantly better than cluster 2 (median OS, 63.8 vs. 17.7 months) (Figure 1D). The patients in the CGGA, REMBRANDT, and WCH cohorts were also stratified into

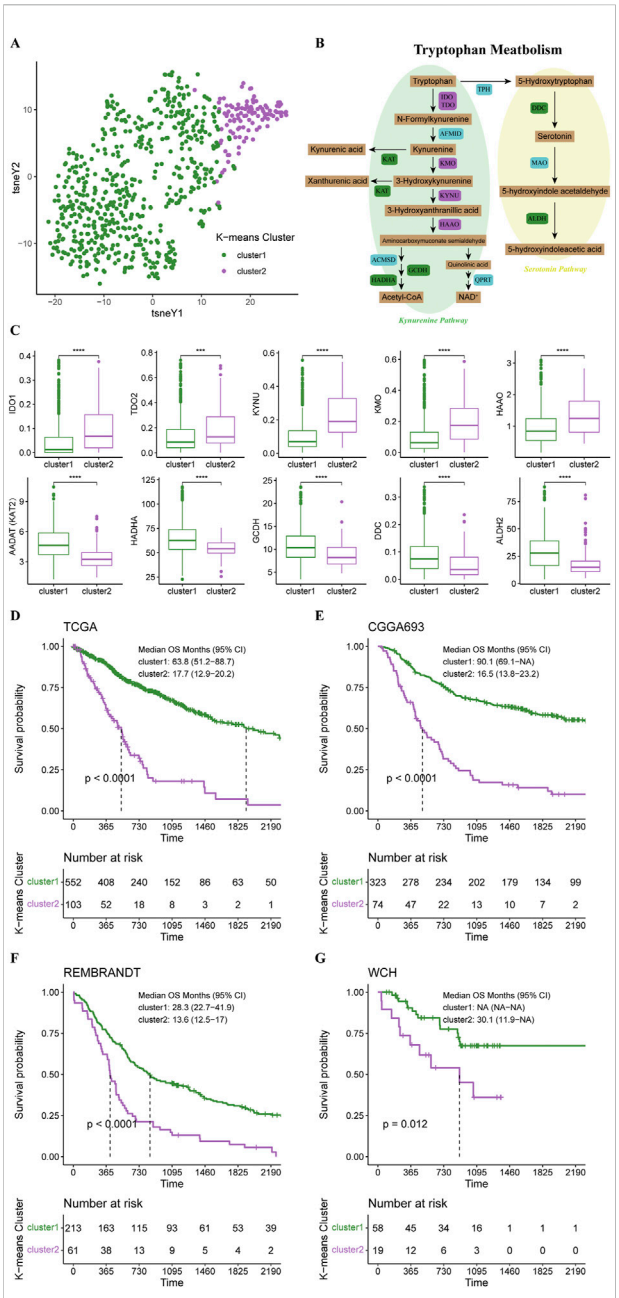

FIGURE 1
K-means clustering of gliomas based on expression of TrMGs. **(A)** TrMGs expression t-SNE. **(B)** Schematic diagram for tryptophan metabolism **(C)** The expression levels of ten important TrMGs between two K-means clusters (cluster 1: *N* = 556, cluster 2: *N* = 106). **(D)** Kaplan-Meier Curve based on K-means clusters in TCGA, **(E)** CGGA, **(F)** REMBRANDT, and **(G)** WCH cohorts. IDO, indoleamine 2,3-dioxygenase; TDO, tryptophan 2,3-dioxygenase; AFMID, arylformamidase; KMO, kynurenine 3-monooxygenase; KYNU, kynureninase; KAT, kynurenine aminotransferase; HAAO, 3-hydroxyanthranilic acid oxygenase; ACMSD, aminocarboxymuconate semialdehyde decarboxylase; GCDH, glutaryl-CoA dehydrogenase; HADHA, hydroxyacyl-CoA dehydrogenase trifunctional multienzyme complex subunit alpha; QPRT, quinolinic acid phosphoribosyltransferase; TPH, tryptophan hydroxylase; DDC, dopa decarboxylase; MAO, monoamine oxidase; ALDH, aldehyde dehydrogenase.

two clusters based on the naïve Bayes clustering classifier train with the TCGA data. Survival analyses in these three cohorts also revealed significantly better prognosis in cluster 1 (Figures 1E–G), suggesting that the TrMG expression patterns were robust among different glioma cohorts.

The functional enrichment analyses based on two clusters depicted distinctive pathway alterations. The ECM receptor interaction, cell adhesion molecules, other pathways were identified as key pathway associated with differentially expressed genes (DEGs) between clusters in the KEGG gene sets (Figure 2A). In REACTOME gene sets, extracellular matrix organization and interferon gamma signaling pathways were found to be over-represented in the cluster DEGs (Figure 2B).

The gene alteration analyses revealed a different gene alteration landscape between two clusters. Cluster 1 gliomas were characterized by IDH1 mutations with co-occurring TP53 and ATRX mutations or CIC, FUBP1 and NOTCH1 mutations (Figures 2C,D). Higher proportion of EGFR could be found in cluster2, which were mutually exclusive with IDH1 mutations but co-occurrent with PTEN mutations (Figures 2C,E). The analysis of CNVs demonstrated that 1p/19q co-deletion, which was recognized as an essential diagnostic marker for oligodendroglioma, mainly occurred in the cluster 1 (Figure 2F). The gain of chromosome 7 and loss of chromosome 10 (+7/-10), which was a novel diagnostic marker for glioblastoma and indicated worse prognosis, occurred more frequently in cluster 2 compared to cluster 1, in line with the worse prognosis of cluster 2 in survival analysis. Analysis of clinicopathological features of these two clusters also demonstrated that cluster 2 had higher tumor grade, lower incidence of IDH mutation, and lower incidence of 1p/19q codeletion (Figure 2G). The differences in other clinicopathological features between two clusters were given in Supplementary Figure S2.

Analyses of immunological features in tumor microenvironment based on K-means clusters

Based on these two K-means clusters, we conducted multiple analyses of immunological features to elucidate the differences in tumor immune landscape. The results of the TIMER score of TCGA cohort revealed that the tumor microenvironment of cluster 2 carried more macrophages, neutrophils, and CD8$^+$ T-cells (Figure 3A). This conclusion could also be verified in the CGGA cohort (Figure 3B), suggesting a more complex tumor microenvironment in cluster 2. Furthermore, the results of the ESTIMATE revealed that the stromal score, immune score, and ESTIMATE score of the cluster 2 were significantly higher

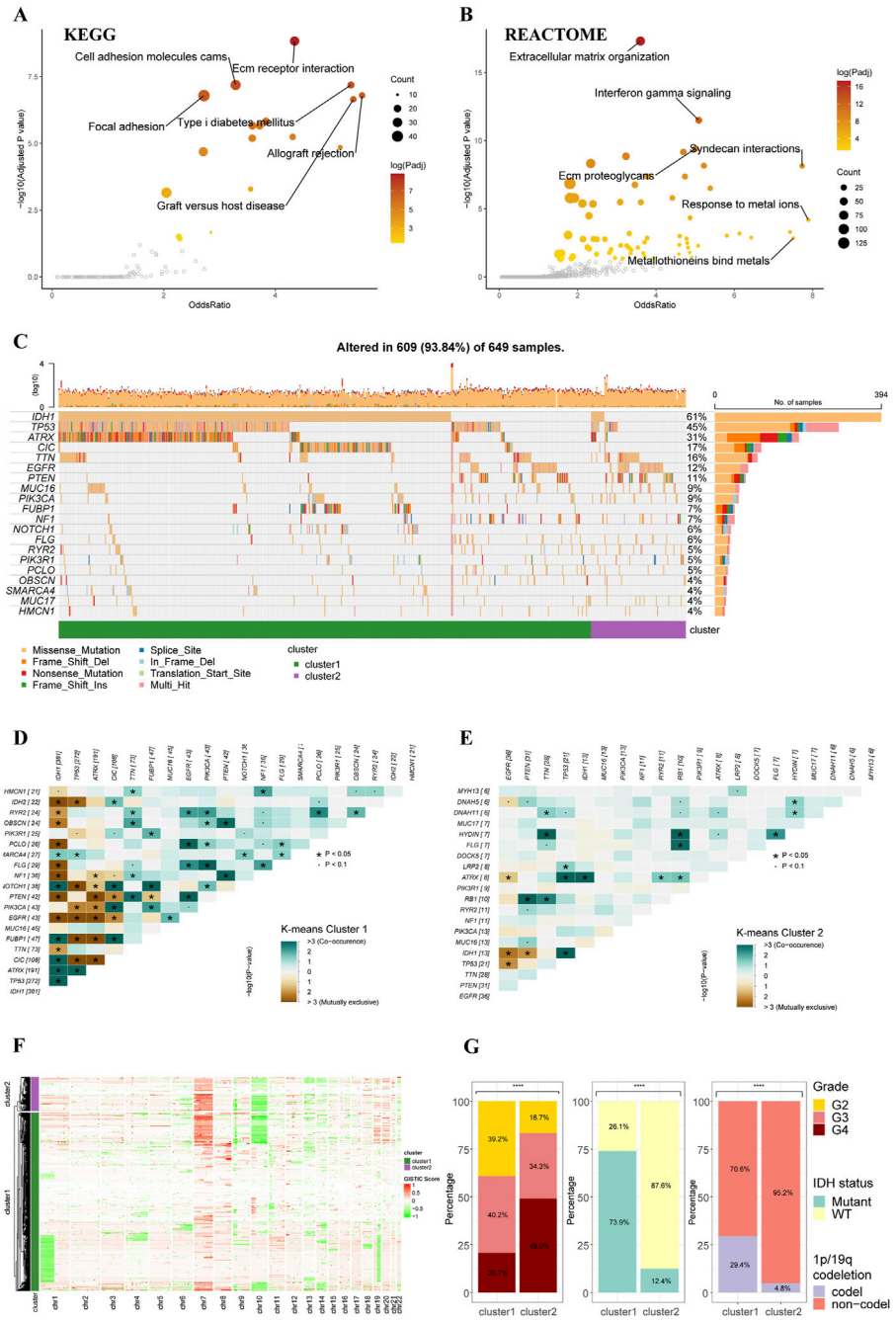

FIGURE 2
Functional enrichment and clinicopathological features of the K-means clusters. **(A)** Pathways with high odds ratio and confidence in the KEGG gene sets. **(B)** Pathways with high odds ratio and confidence in the REACTOME gene sets. **(C)** Top 20 mutated genes of the K-means clusters. **(D,E)** Co-occurrence and mutually exclusive of the gene mutations in cluster 1 **(D)** and cluster 2 **(E)**. **(F)** Heatmap of copy number variations of the two clusters. **(G)** The difference in tumor grade, IDH mutation, and 1p/19q codeletion between two K-means clusters (cluster 1: *N* = 556, cluster 2: *N* = 106).

than cluster 1 in all four cohorts (Figure 3C). The tumor purity of cluster 2 was significantly lower than cluster 1 in all four cohorts (Figure 3C), indicating purer tumor cell microenvironment in gliomas of cluster 1. Through the calculation of TIP score, we were able to demonstrate that most gliomas of cluster 2 were more likely to be "hot" tumor

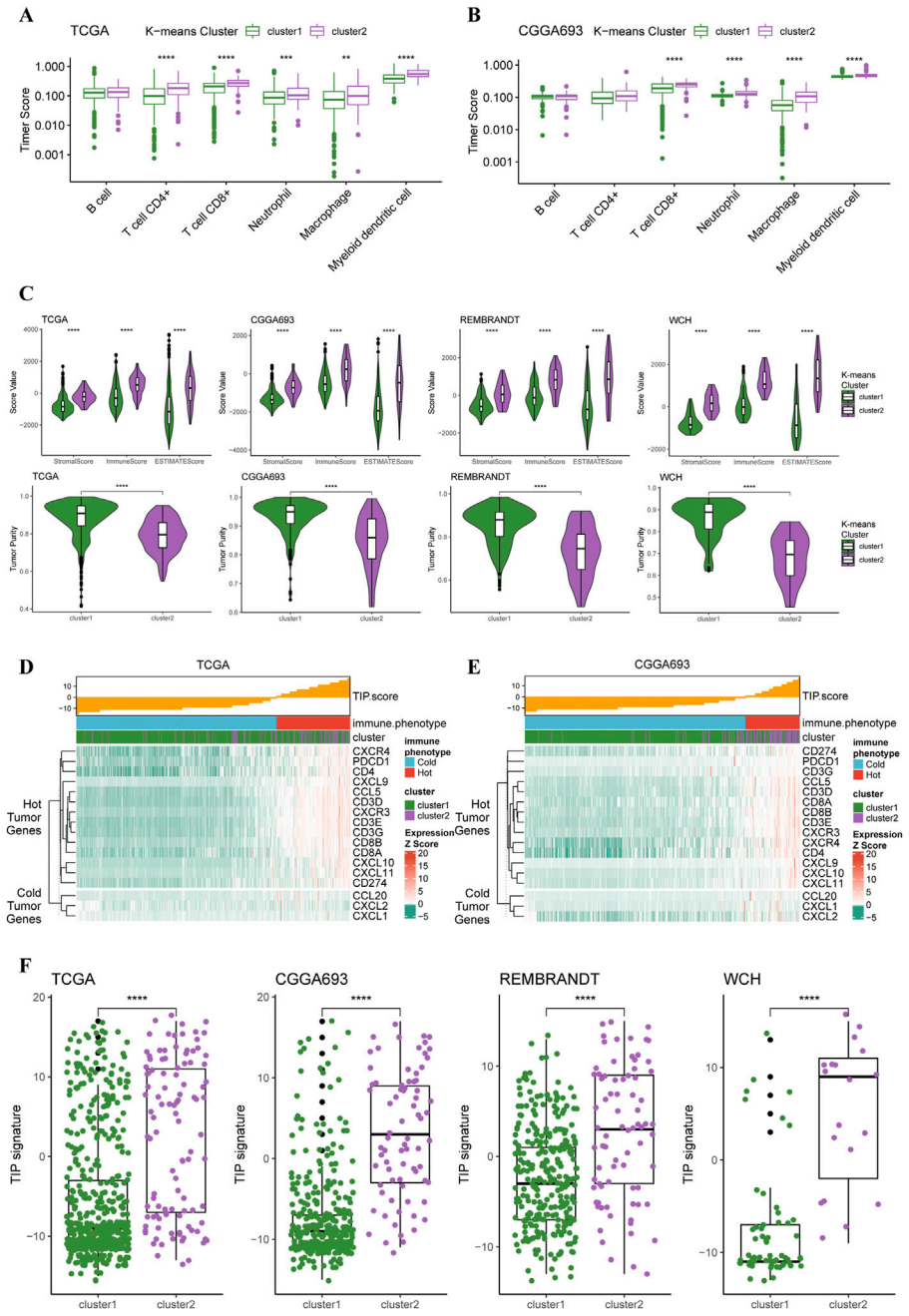

FIGURE 3
Different immunological features of tumor microenvironment between two clusters. **(A)** Boxplots of infiltration of six types of immune cells in glioma based on TIMER score in TCGA cohort (cluster 1: *N* = 556, cluster 2: *N* = 106) and **(B)** CGGA cohort (cluster 1: *N* = 339, cluster 2: *N* = 76). **(C)** Differences in stromal, immune, and ESTIMATE scores between two clusters in all four cohorts. **(D)** TIP score and related gene expression levels between two clusters in TCGA and **(E)** CGGA cohort. **(F)** Boxplots with every point on the differences in TIP score between two clusters in all four cohorts.

immunological phenotype and expressed higher levels of gene markers for 'hot' tumors compared to gliomas in cluster 2 (Figure 3D). The analysis of TIP score in the CGGA cohort reached similar results (Figure 3E). Additionally, the TIP scores for the gliomas of cluster 2 were significantly higher than cluster 1 in all four cohorts (Figure 3F). All these results supported that

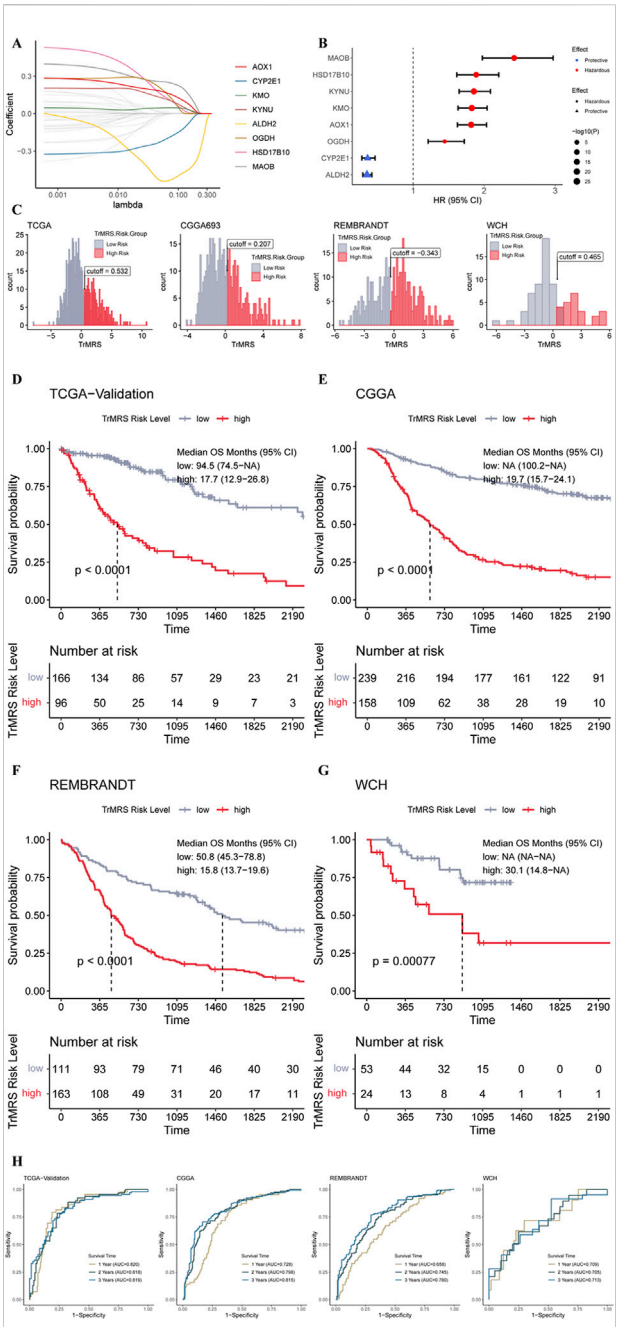

FIGURE 4
Expression signature of TrMGs and its relationship with prognosis of glioma. **(A)** Average of coefficients of eight essential TrMGs in the LASSO Cox regression at each lambda value. **(B)** The effect of each essential TrMG on the prognosis of glioma. **(C)** Histogram and optimal cut-off values of TrMRS in four cohorts (TCGA: *N* = 655 with survival data out of 662 in total, CGGA: *N* = 415, REMBRANDT: *N* = 369, WCH: *N* = 77). **(D)** K-M curve of the TCGA validation set, cut off = 0.532, **(E)** CGGA cohort, cut off = 0.207, **(F)** REMBRANDT cohort, cut off = −0.343, and **(G)** WCH cohort, cut off = 0.465. **(H)** ROC curves and matched AUC of 1-, 2-, and 3-years survival in all four cohorts.

the gliomas of cluster 2 had more complex tumor microenvironment, more immune cell infiltration, and presented with features of immunologically 'hotter' tumors.

Construction and validation of the tryptophan metabolism-related genes risk signature and its relationship with clinicopathological features

To determine essential genes for the construction of TrMRS, we filtered the 44 TrMGs using the LASSO Cox regression in the training dataset. Subsequently, eight genes, including AOX1, CYP2E1, KMO, KYNU, ALDH2, OGDH, HSD17B10, and MAOB, were identified as essential TrMGs for the construction of TrMRS (Figure 4A). The formula to compute the TrMRS was as follows: 1.216*KYNU+0.254*KMO+0.231*AOX1+0.034*OGDH+0.006*HSD17B10 + 0.001*MAOB-0.066*ALDH2-1.064*CYP2E1.

Six genes of these essential TrMGs, including MAOB, HSD17B10, KYNU, AOX1, and OGDH, were determined as hazardous factors for glioma patients, and other two genes (CYP2E1 and ALDH2) were identified as protective factors (Figure 4B). Besides, representative immunohistochemical (IHC) staining for KYNU and ALDH2 from the Human Protein Atlas (Ponten et al., 2008) (https://www.proteinatlas.org/) was utilized to validate these results. The results of IHC demonstrated that the expression level of KYNU was higher in high-grade glioma compared to low-grade glioma (Supplementary Figure S3A), and the expression level of ALDH2 was higher in low-grade glioma (Supplementary Figure S3B), confirming the results from sequencing that KYNU was hazardous factor and ALDH2 was protective factor. Furthermore, we utilized the "surv_cutpoint" algorithm to calculate the optimal TrMRS cut-off for every cohort and allocated all the patients into TrMRS low- or high-risk groups according to this cut-off (Figure 4C). Survival analyses revealed that the overall survival of the patients in TrMRS high-risk groups was significantly poorer than TrMRS low-risk group in all four validation cohorts (Figures 4D–G), suggesting that TrMRS potentially functioned as factor for prognosis prediction. To test the efficacy of TrMRS in predicting prognosis of glioma patients, we performed ROC analyses to evaluate the performance of TrMRS alone in survival rate prediction at 1, 2, and 3 years. In the TCGA test set, the AUCs of TrMRS at 1, 2, and 3 years were 0.820, 0.818, and 0.819, respectively (Figure 4H). In other three validation cohorts, similar performances were also achieved (Figure 4H).

The expression pattern of eight essential TrMGs was exhibited with a heatmap ordered by TrMRS (Figure 5A). The relationship of other clinicopathological features, including tumor grade, histological diagnosis, IDH mutation status, 1p/19q codeletion, TERT promoter status, ATRX status, and MGMT promoter status, with the TrMRS were also given out (Figure 5A). Further analysis of gene mutations discovered that IDH1, TP53, and ATRX were top 3 most frequently mutated genes in TrMRS low-risk group (Figure 5B). TP53, PTEN, and EGFR were top 3 most frequently mutated genes in TrMRS high-risk group (Figure 5C). Additionally,

analyses of tumor mutation burden (TMB) revealed that TrMRS high-risk group harbored higher TMB than low-risk group, and the correlation analysis demonstrated that TMB was positively correlated with the TrMRS (Figure 5D). Further analysis manifested the incidence of gene amplification, including EGFR, SEC61G, and LANCL2, was significantly higher in high-risk group than low-risk group (Figure 5E). Besides, the incidence of gene homozygous deletion, including CDKN2A and CDKN2B, was also higher in high-risk group (Figure 5F).

To explore the impact of TrMRS in terms of pathway, we utilized KEGG and REACTOME pathway gene sets in enrichment analyses of the DEGs between the TrMRS risk groups. The patient samples were stratified into TrMRS high- and low-risk groups. The analyses of GSEA were based on the differentially expressed genes (DEGs) between TrMRS high- and low-risk groups. The complement and coagulation cascades pathway (normalized enrichment score (NES) = 3.085, adjusted *p*-value < 0.001) and graft *versus* host disease

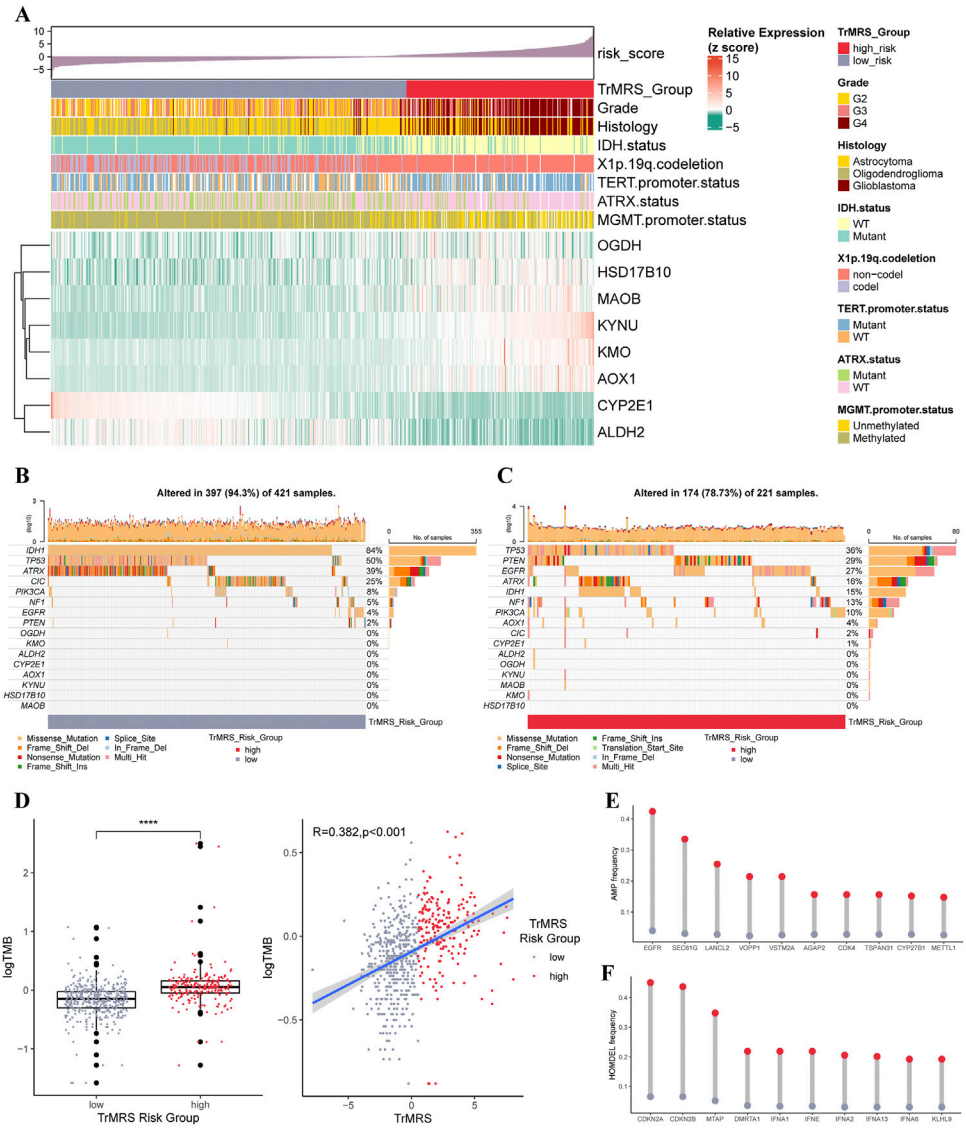

FIGURE 5
Gene mutations and copy number variations of the two risk groups. **(A)** Expression level of eight essential TrMGs and its relationship with clinicopathological features. **(B)** Gene mutations of eight essential TrMGs and top eight frequently mutated genes in TrMRS low-risk group (*N* = 429) and **(C)** high-risk group (*N* = 226). **(D)** Difference in tumor mutation burden between two TrMRS risk groups and its correlation with TrMRS. **(E)** Difference in top 10 frequent gene amplification between two risk groups. **(F)** Difference in top 10 frequent gene homozygous deletion between two risk group. *$p < 0.05$; **$p < 0.01$; ***$p < 0.001$; ****$p < 0.0001$.

pathway (NES = 2.855, adjusted p-value < 0.001) were ranked in the top five gene sets of the KEGG in the comparison between two risk groups (Figure 6A) using GSEA. Besides, the cytokine signaling in immune system pathway (NES = 2.950, adjusted p-value <0.001) and innate immune system pathway (NES = 3.248, adjusted p-value < 0.001) of REACTOME gene sets were ranked in the top five (Figure 6B). Furthermore, over-representation of the extracellular matrix receptor interaction of KEGG gene sets and the extracellular matrix organization of REACTOME gene sets were identified in the biological functions of DEGs between the two TrMRS risk groups (Figures 6C,D). Finally, the GSVA result demonstrating the top differentially expressed pathways in KEGG and REACTOME gene sets were also illustrated through heatmaps (Figures 6E,F).

Construction of nomograms based on TrMRS and prognosis prediction

To construct nomograms for the prediction of glioma patients' prognosis, we first conducted univariate followed by multivariate Cox analyses to identify potential independent prognostic factors. Result demonstrated that the tumor grade, age, radiotherapy, TrMRS, chemotherapy, 1p/19q codeletion, and IDH mutation were significant univariate prognostic factor (Figure 7A). Subsequently, these factors were enrolled in multivariate Cox regression analysis and the result revealed that TrMRS, tumor grade, 1p/19q codeletion, and IDH mutation were independent prognostic factors in glioma (Figure 7B). Eventually, these factors were combined in the construction of a nomogram for personalized survival prediction (Figure 7C). The four factors were also used to construct a nomogram for the CGGA cohort (Figure 7D). The corrected C-indexes of the nomograms based on TCGA and CGGA cohort were 0.851 and 0.779, respectively. Additionally, the 1-, 2-, and 3-years calibration curves of the nomograms also validated their efficacy in predicting survival time of glioma patients (Figures 7E,F).

Relationship between the tryptophan metabolism-related genes and immune landscape of tumor microenvironment in glioma

To elucidate the relationship between the TrMRS and tumor immune microenvironment in glioma, we conducted bundles of analyses on immunological features based on TrMRS. Firstly, the CIBERSORTx estimation of immune cell fractions depicted distinctive patterns of immune cell infiltration between two TrMRS risk groups. The TrMRS high-risk group manifested with more infiltration of resting NK cells, Macrophages (M0, M1, and M2), and neutrophils in its tumor microenvironment (Figure 8A). The low-risk group, on the other hand, had higher infiltration of activated NK cells and plasma cells. Further correlation analyses demonstrated that the infiltration of plasma cells and activated NK cells was negatively correlated with the TrMRS, and the infiltration of M2 macrophage and neutrophils was positively correlated with the TrMRS (Figure 8B). Besides, analyses of immune scores demonstrated that the TrMRS high-risk group presented with significantly higher stromal score, immune score, and ESTIMATE score (Figure 8C). The tumor purity of TrMRS high-risk group was remarkably lower than low-risk group (Figure 8D), suggesting more complicated tumor microenvironment in gliomas of TrMRS high-risk group with more immune cell infiltration. Correlation analyses revealed that the stromal score, immune score, ESTIMATE score, and tumor purity were strongly correlated with the TrMRS (R = 0.82, 0.762, 0.805, and 0.808) (Figure 8E).

To predict potential response to immunotherapy response, we also performed analysis on the expression of immunity-related genes. Gliomas of TrMRS high-risk group presented with significantly higher expression level of CD274 (PD-L1), CD276 (B7H3), HAVCR2 (TIM3), PD1 (CD279, PDCD1), and CD44 (Figure 9A). Correlation analysis also confirmed that the expression levels of these immunotherapy-related markers were positively correlated with the value of TrMRS (Figure 9B), suggesting potential ability of TrMRS to guide the choice of immunotherapy. Furthermore, immune phenotype analysis of high- and low-risk gliomas revealed that most gliomas of TrMRS high-risk group were identified as more likely to be immunological "hot" tumors, and most tumors of low-risk group were presumed "cold" tumors (Figure 9C). A strong positive correlation between TrMRS and TIP score was also confirmed by the correlation analysis (Figure 9D). The analyses of TIP score based on the CGGA cohort also manifested with similar results (Figures 9E,F). Additionally, we utilized TIDE algorithm to predict response to immune checkpoint inhibitors. The result revealed that the glioma patients of TrMRS high-risk group were more likely to benefit from therapy of immune checkpoint inhibitors in the TCGA and CGGA cohorts (Figures 9G,H). Most above findings can be validated in the other cohorts (Supplementary Figure S4).

Discussion

Based on the estimation in the global cancer statistics of 2020, 251 thousand death were caused by CNS malignant tumors every year (Siegel et al., 2021). Among these cases, glioma accounted for approximately 80%. Despite countless attempts worldwide to improve the clinical outcomes of glioma patients, almost no satisfactory breakthrough was achieved in recent years. For instance, the median overall survival of glioblastoma, which accounted for about 50% of all gliomas, was only 22 months

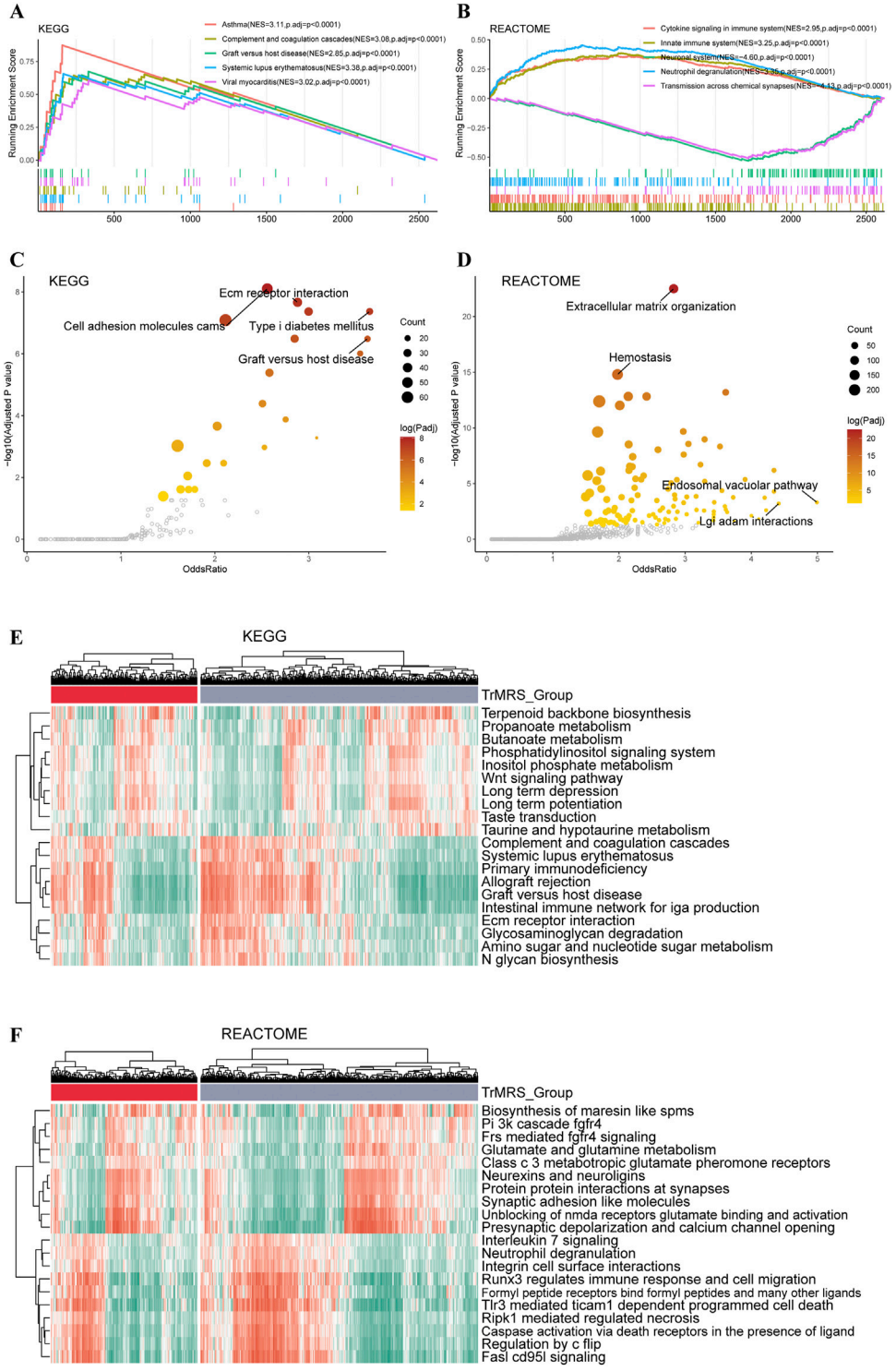

FIGURE 6
Functional enrichment analyses of the transcriptome of TrMRS risk groups. **(A)** The top five pathways with the highest normalized enrichment score in the KEGG gene sets between two risk groups. **(B)** The top five pathways with the highest normalized enrichment score in the REACTOME gene sets between two risk groups. **(C)** Pathways with high odds ratio and confidence in the KEGG and **(D)** REACTOME gene sets. **(E)** Top 20 differentially expressed KEGG gene sets (*N* = 655, low-risk group: *N* = 429, high-risk group: *N* = 226). **(F)** Top 20 differentially expressed REACTOME gene sets.

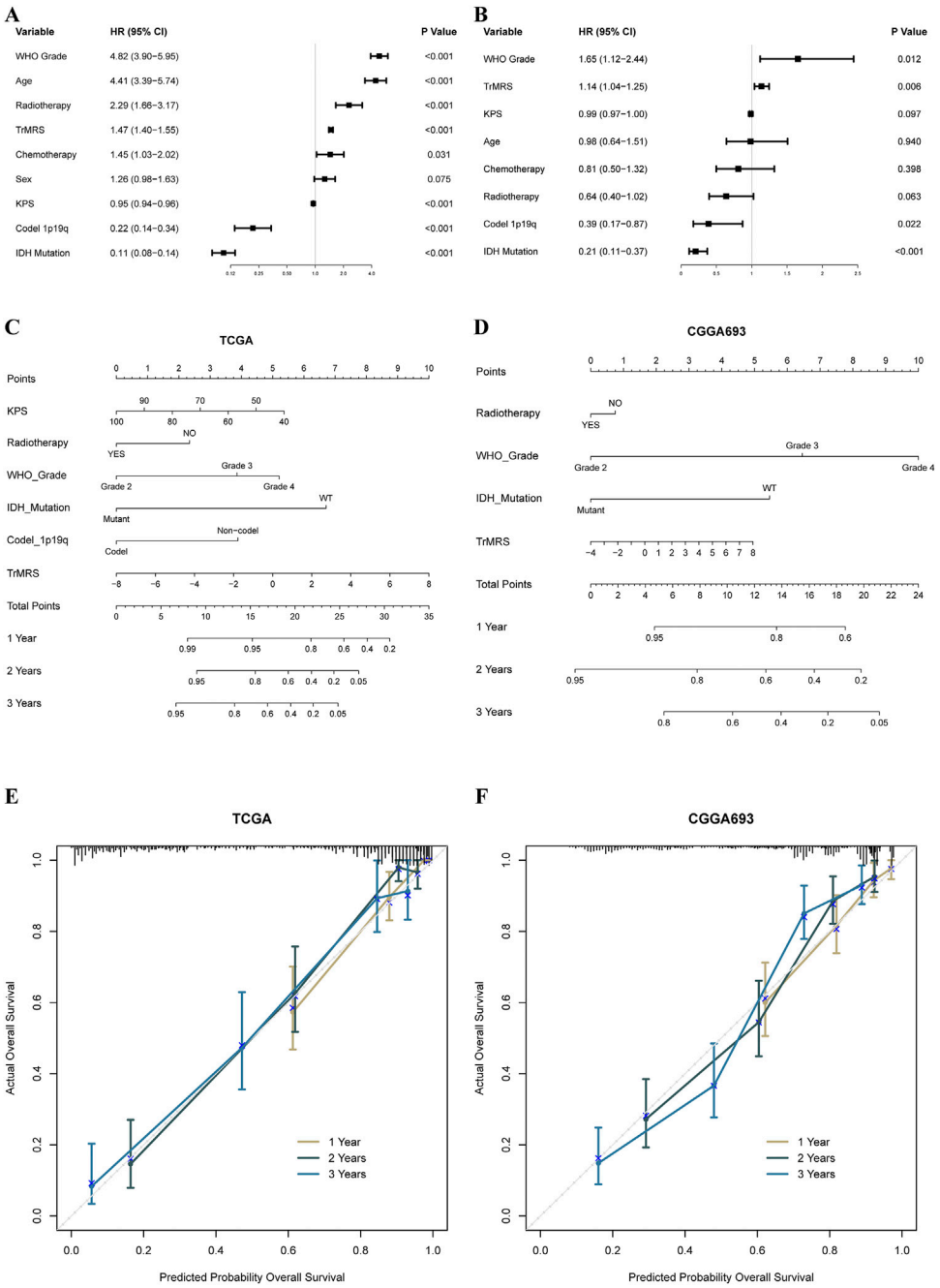

FIGURE 7
Prognostic value of TrMRS and construction of TrMRS-based nomograms. **(A)** Univariate and **(B)** Multivariate Cox regression analyses of potential prognostic factors in overall survival of gliomas. Nomogram of 1-, 2-, and 3-years survival of glioma patients based on **(C)** TCGA cohort (*N* = 655), **(D)** CGGA cohort (*N* = 415). Calibration plots of the nomogram based on **(E)** TCGA cohort and **(F)** CGGA cohort.

after thorough treatment regime, including surgery, chemotherapy, radiotherapy, and even tumor treating field (Stupp et al., 2005; Stupp et al., 2017). Immunotherapy has proved its value in many cancers (Eggermont et al., 2018; Gandhi et al., 2018; Choueiri et al., 2021; Cortes et al., 2022). However, the application of immunotherapy in glioma faced unprecedented challenges, and all these attempts eventually failed to improve overall survival (Weller et al., 2017; Wakabayashi et al., 2018; Reardon et al., 2020; Lim et al., 2022; Omuro et al., 2022). Among all reasons, the blood-brain

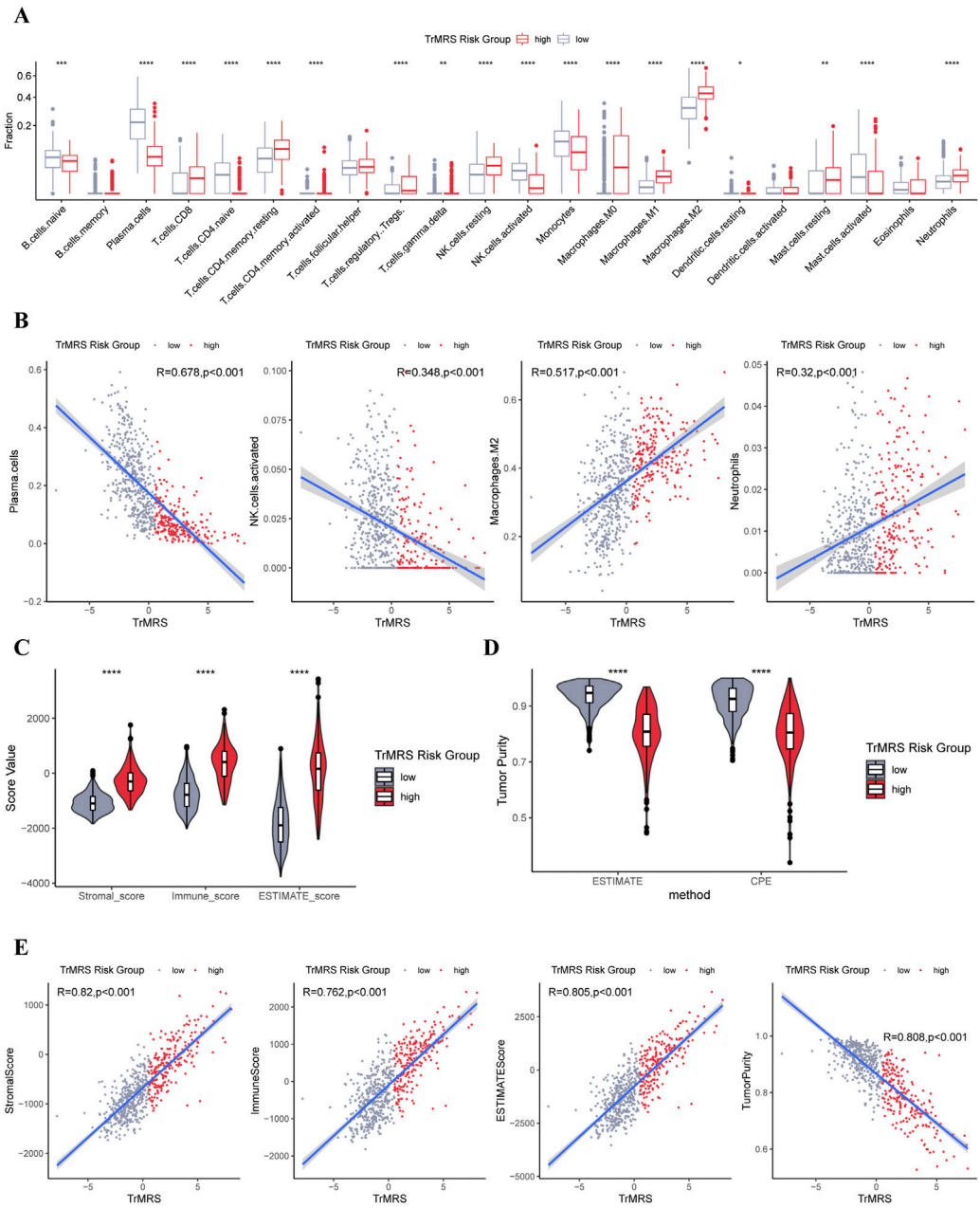

FIGURE 8
Differences in immune features of tumor microenvironment between two TrMRS risk groups. **(A)** Boxplot of the estimated fraction of 22 immune cells in tumors (low-risk group: *N* = 429, high-risk group: *N* = 226). **(B)** Analyses of correlations of TrMRS with the infiltration of plasma cells, activated NK cells, M2 macrophages, and neutrophils (*N* = 655). **(C)** Differences in the stromal, immune, and ESTIMATE scores of the two risk groups. **(D)** Tumor purity of the two risk groups based on the ESTIMATE and CPE algorithms. **(E)** Analyses of correlations of TrMRS with the stromal, immune, ESTIMATE score, and tumor purity. *$p < 0.05$; **$p < 0.01$; ***$p < 0.001$; ****$p < 0.0001$.

barrier (BBB), which could preclude most peripheral immune cells from entering central nervous system and consequently create an immunological quiescent environment, was considered important. However, an inspiring study introduced a brand-new lymphatic pathway, which permitted antigen-presenting cells to egress from brain (Louveau et al., 2015). After that, the T and B lymphocytes outside brain could be primed and then infiltrated to brain and delivered immune responses (Lim et al., 2018). These studies indicated that CNS was not a forbidden zone for immunotherapy. If we could further explore and elucidate the details of immune landscape, there were plenty of opportunities for applications of immunotherapy in gliomas.

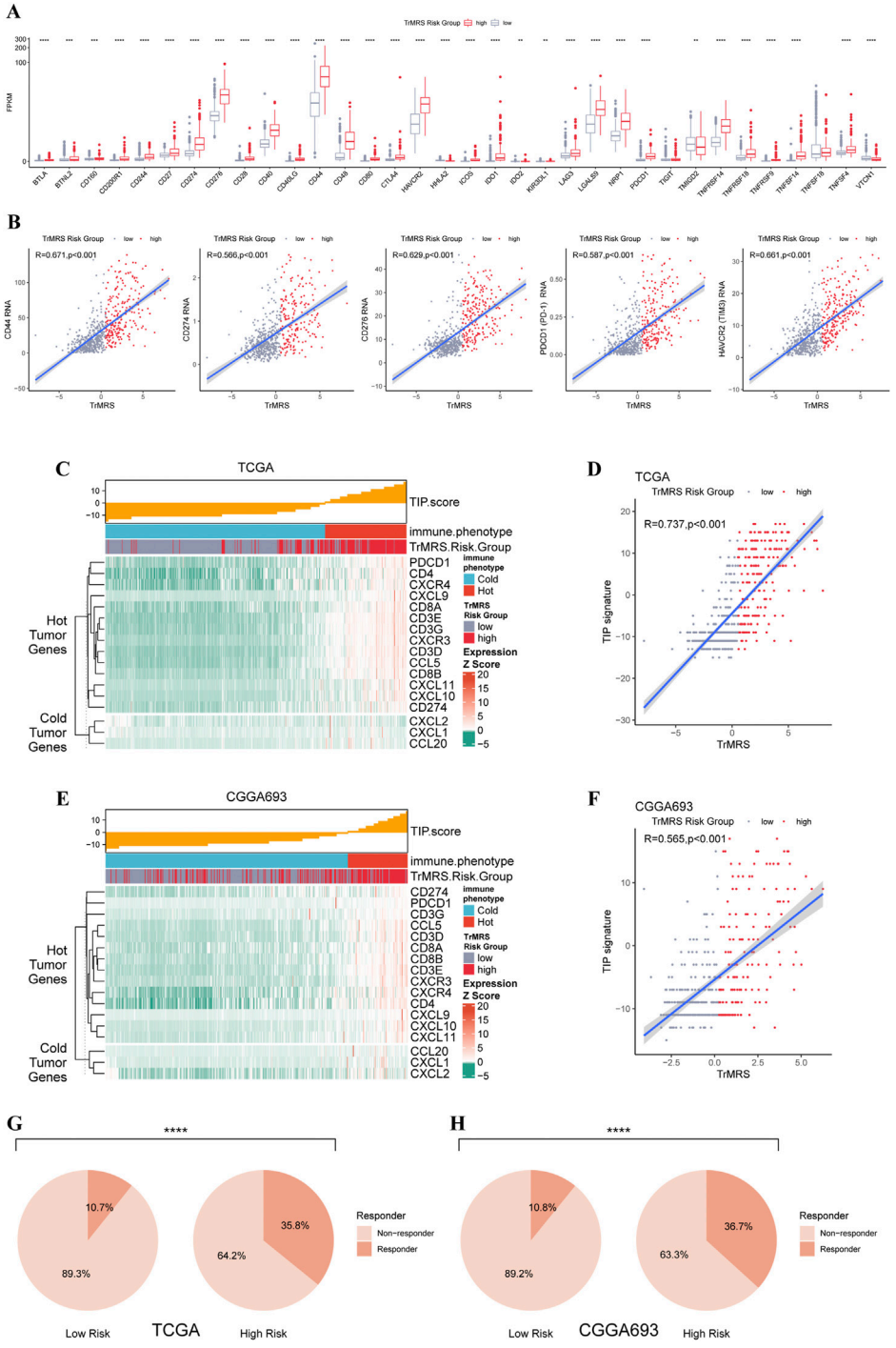

FIGURE 9
Differences in expression of immunotherapy targets and response to ICIs between two TrMRS risk groups. **(A)** The expression level of 34 immunotherapy-related genes in two risk groups (low-risk group: *N* = 429, high-risk group: *N* = 226). **(B)** Analyses of correlations of TrMRS with the expression of CD44, CD274, CD276, and PDCD1 (*N* = 655). **(C)** TIP scores and related gene expression levels between two risk groups in TCGA dataset. **(D)** Analyses of correlations of TrMRS with the TIP score in TCGA dataset. **(E)** TIP scores and related gene expression levels between two risk groups in CGGA dataset (*N* = 415, low-risk group: *N* = 249, high-risk group: *N* = 166). **(F)** Analyses of correlations of TrMRS with the TIP score in CGGA dataset. **(G)** Percentage of predicted responders to immune checkpoint inhibitors therapy in each risk group based on TCGA dataset and **(H)** CGGA dataset.

The relationship between reshaped metabolic model of tumors and immunological landscapes has attracted surging attention (Xia et al., 2021). Several evidence have suggested that tryptophan metabolism plays a critical role in cancer (Uyttenhove et al., 2003; Muller et al., 2005). Reduced concentration has been observed in multiple cancers (Giusti et al., 1996; Huang et al., 2002), including glioma (Zhai et al., 2015). Besides, the tryptophan metabolism can regulate the T-cells and immune cell infiltration in cancer (Nakamura et al., 2007). The expression of IDO1 was also proved correlated with the immune infiltration in multiple cancers (Brandacher et al., 2006; Ino et al., 2008; Inaba et al., 2009). Therefore, to investigate whether tryptophan metabolism was correlated with malignant features and immune landscape of glioma, we analyzed the expression pattern of tryptophan metabolism-related genes in gliomas and evaluated the relationship of the TrMRS with clinicopathological features and immune landscape of gliomas.

Based on the different expression patterns of TrMGs, we allocated all patients into two K-means clusters. Subsequently, we depicted the distinctive patterns of clinicopathological features and prognosis between two clusters. The cluster 2, which presented with poorer prognosis, had a significantly higher expression level of multiple enzymes in the kynurenine pathway, including IDO1, TDO2, KYNU, and KMO, and lower expression level of KAT2, DDC, and ALDH2. IDO and TDO, which function to initiate the kynurenine pathway by converting tryptophan to N-formylkynurenine, were proved to contribute to the malignancy of glioma (Du et al., 2020), indicating that activation of kynurenine pathway was a hazardous factor for glioma, in line with our findings. Moreover, kynurenine aminotransferase 2 (KAT2), which convert kynurenine into kynurenic acid (KYNA), was manifested with higher expression level in cluster 1, suggesting protective effects of KYNA in glioma. KYNA was initially recognized with neuroprotective and anticonvulsant functions (Stone, 1993; Carpenedo et al., 2001; Erhardt et al., 2001). Besides, it has been proved that low grade gliomas synthesized more KYNA than glioblastoma (Vezzani et al., 1990). A previous study demonstrated that the concentration of KYNA was lower in the blood of glioblastoma patients compared to healthy volunteers (Adams et al., 2014). Another index for the activation of kynurenine pathway, kynurenine/tryptophan ratio, was higher in glioblastoma patients than in healthy volunteers (Adams et al., 2014). These findings were accordance with our study and suggested that activation of kynurenine pathway and inhibition of production of neuroprotective KYNA may contribute to the malignancy of gliomas. Furthermore, upregulated expression levels of DDC and ALDH, two critical enzymes in the serotonin pathway, were also confirmed in cluster 1. This phenomenon suggested that activation of serotonin pathway, which can consume tryptophan and consequently compete with kynurenine pathway for tryptophan, was related to better prognosis in glioma patients, supporting that downregulating the kynurenine pathway may reduce the malignancy of gliomas.

The incidence of gene alterations differed in these clusters. For example, IDH mutation, which has been defined as an essential marker for classification of gliomas and would result in aberrant metabolism (Yan et al., 2009; Pirozzi and Yan, 2021), mostly occurred in one of these two clusters. Because both TCA cycle and tryptophan metabolism are nicotinamide adenine dinucleotide (NAD^+)-related pathways (Pang et al., 2021), as an essential enzyme in TCA cycle, IDH might also interact with tryptophan metabolism. Despite these potential interaction between IDH and tryptophan metabolism, the TrMRS was still identified as independent prognostic factor in multivariate analysis, which simultaneously enrolled IDH and TrMRS, suggesting that TrMRS was a strong prognostic factor in gliomas.

After monitoring TrMGs, eight TrMGs were determined as essential genes for glioma prognosis. For example, kynureninase (KYNU) is a critical enzyme in kynurenine pathway and functioned to converted kynurenine to anthranilic acid (Schwarcz and Stone, 2017). Silencing expression of KYNU could inhibit the growth of tumor cells in cutaneous squamous cells carcinoma (Ci et al., 2020). The overexpression of KYNU was also confirmed correlated with poor prognosis in gastric cancer (Zheng et al., 2020). In our study, KYNU was also confirmed as a hazardous factor in gliomas. Kynurenine monooxygenase (KMO) was a rate-limiting enzyme in kynurenine pathway and functioned to control the conversion from kynurenine to neuroactive and neurotoxic metabolites (Platten et al., 2019). Numerous studies demonstrated that KMO played a key role in tumorigenesis and tumor progression (Huang et al., 2020; Liu et al., 2021). Cytochrome P450 family two subfamily E member 1 (CYP2E1) was a critical enzyme for the metabolism of indole, which was converted from tryptophan by bacterial tryptophanases and could suppress the immune response in central nervous system (Devlin et al., 2016; Rothhammer et al., 2016). Previous study has revealed that downregulation of CYP2E1 would promote tumor progression in gliomas (Ye et al., 2021), in line with our results. Among these essential TrMGs, KYNU, and KMO are critical enzymes of tryptophan catabolism. Upregulation expression of these enzymes would subsequently increase the catabolism of tryptophan and decrease the concentration of tryptophan. KYNU and KMO were recognized as hazardous factors in previous and our studies, indicating that upregulated tryptophan catabolism and low concentration of tryptophan would lead to worse prognosis in gliomas. On the contrary, CYP2E1 was recognized as protective factor in our study, suggesting that eradication of indole, an immunosuppressive metabolites of tryptophan, would improve the prognosis of gliomas.

Further analyses of immune landscapes illustrated the relationship between tryptophan metabolism and the immune

microenvironment of glioma. The CIBERSORTx analyses depicted that the infiltration of multiple immune cells, including macrophages and NK cells was correlated with the TrMRS. For example, the infiltration of M2 macrophage was positively correlated with TrMRS. M2 macrophage played a critical role in tumor promotion and immunosuppressive effects (Noy and Pollard, 2014). This result indicates that higher TrMRS value, which represents for higher tryptophan catabolism and lower level of tryptophan, is a marker for more M2 macrophage infiltration, and subsequently leads to immunosuppression. Tumors can recruit circulating monocytes and neighboring resident macrophages to their microenvironment and then polarized them from M1 to M2 macrophages, composing tumor-associated macrophages (TAMs) (Anderson et al., 2021). TAMs can produce cytokines to inhibit T-cells' function and upregulate immunosuppressive surface proteins (Curiel et al., 2004; Colombo and Piconese, 2007; Yang and Zhang, 2017). These immunosuppressive effects of TAMs lead to immune escape in glioma and result in worse prognosis for gliomas with high TrMRS. The ESTIMATE analyses revealed that the complexity of glioma was strongly positively correlated with the TrMRS, indicating that more tryptophan catabolism and less tryptophan might help reconstruct a more complex tumor microenvironment in glioma. The expression levels of targets for ICIs, PD-1 and PD-L1, were also strongly positively correlated with the TrMRS, endorsing the potential ability of TrMRS to predict the response to ICIs. Furthermore, T-cell immunoglobulin and mucin domain-containing protein 3 (TIM3) was part of a module that contained several checkpoint receptors (Wolf et al., 2020). TIM3 frequently co-expressed with PD-1 (Sakuishi et al., 2010; Fourcade et al., 2014), which made it attractive for immunotherapy. Co-blockade of TIM3 and PD-1 can achieve greater enhancement of T-cell responses than blockade of PD-1 alone (Ngiow et al., 2011; Zhou et al., 2011). Our study demonstrated that the expression of TIM3 was strongly positively correlated with TrMRS, which also endorsed the potential ability of TrMRS to guide the application of co-blockade of TIM3 and PD-1. Hence, the correlation between TrMRS and expression of immunotherapy targets suggested that gliomas with high TrMRS would express more immunotherapy targets and have better response to immunotherapy, such as PD-1/PD-L1 inhibitors and TIM3 inhibitors. Higher TrMRS correlated with more expression of "hot tumor" features and more potential responders to ICIs. These findings demonstrated that high TrMRS would predict worse prognosis and more immunosuppressive effects. But it also predicted more expression of immunotherapy targets, which endorsed the potential ability of TrMRS to guide the application of immunotherapy.

Despite multiple analyses endorsed same results in our current study, there are still several limitations. First, protocol of sequencing and data preprocessing differed among these four independent cohorts. Second, the REMBRANDT cohort lacks some important markers, including IDH mutation status. Third, these findings of our current study still require future validation by basic experiments. Besides, due to the limitations of bulk RNA-sequencing, the potential interaction between the aberrant tryptophan metabolism in gliomas and neurons remains uncovered. However, neurons typically consist a small fraction of gliomas (Couturier et al., 2020), and is unlikely to produce significant influence on the findings of the present study. Finally, the mechanism of how tryptophan metabolism influenced immune landscape of gliomas remains unclear and requires further exploration.

Conclusion

In conclusion, we revealed that the expression pattern of TrMGs was closely correlated with clinicopathological and immunological features in glioma. The novel tryptophan metabolism evaluation score system, TrMRS, showed for strong ability to predict prognosis of glioma patients. Moreover, higher TrMRS, representing for more active tryptophan catabolism and less tryptophan, predicts more immune infiltration, immunosuppression and, more targets for immunotherapy, endorsing the usages of TrMRS in guiding immunotherapy in gliomas.

Data availability statement

The datasets presented in this study can be found in online repositories. The names of the repository/repositories and accession number(s) can be found in the article/ Supplementary Material.

Ethics statement

The studies involving human participants were reviewed and approved by the institutional review board of West China Hospital (No. 2018569). The patients/participants provided their written informed consent to participate in this study.

Author contributions

Study design: SZ, SC, YL, and MC. Data retrieve: SZ and ZW. Statistical Analysis: SZ and YY. Result interpretation: SC, SZ, WF, and WL. Writing-original draft: All authors. Writing-revise: YL, SZ, SC, and JL.

Funding

This work was supported by a grant from Sichuan Province Science and Technology Support Program

(2017SZ0006 to YL), Science and technology project, technology innovation research and development project, Chengdu (2022-YF05-01456-SN to MC) and Post-Doctor Research Project, West China Hospital, Sichuan University (Grant No. 20HXBH035 to SZ).

Conflict of interest

The authors declare that the research was conducted in the absence of any commercial or financial relationships that could be construed as a potential conflict of interest.

Publisher's note

All claims expressed in this article are solely those of the authors and do not necessarily represent those of their affiliated organizations, or those of the publisher, the editors and the reviewers. Any product that may be evaluated in this article, or claim that may be made by its manufacturer, is not guaranteed or endorsed by the publisher.

Supplementary material

The Supplementary Material for this article can be found online at: https://www.frontiersin.org/articles/10.3389/fphar.2022.1061597/full#supplementary-material

SUPPLEMENTARY FIGURE S1
(A) Average silhouette width corresponding to each cluster number (k) in K-means clustering of the gliomas based on TrMG expression. **(B)** Heatmap of expression of 44 TrMGs based on two clusters. **(C)** Differences in the expression of 44 TrMGs between two K-means clusters. *$p < 0.05$; **$p < 0.01$; ***$p < 0.001$; ****$p < 0.0001$.

SUPPLEMENTARY FIGURE S2
Differences in the clinicopathological features between two K-means clusters. *$p < 0.05$; **$p < 0.01$; ***$p < 0.001$; ****$p < 0.0001$.

SUPPLEMENTARY FIGURE S3
Representative immunohistochemical staining for KYNU and ALDH2 from the Human Protein Atlas. **(A)**Representative staining for KYNU in high- and low-grade glioma (https://www.proteinatlas.org/ENSG00000115919-KYNU/, antibody: HPA031686). **(B)** Representative staining for ALDH2 in high- and low-grade glioma (https://www.proteinatlas.org/ENSG00000111275-ALDH2/, antibody: HPA051065).

SUPPLEMENTARY FIGURE S4
Differences in immunological characteristics of tumor microenvironment between two TrMRS risk groups in CGGA, REMBRANDT, and WCH cohorts. *$p < 0.05$; **$p < 0.01$; ***$p < 0.001$; ****$p < 0.0001$.

References

Abdel-Rahman, O. (2018). Smoking and EGFR status may predict outcomes of advanced nsclc treated with PD-(l)1 inhibitors beyond first line: A meta-analysis. *Clin. Respir. J.* 12 (5), 1809–1819. doi:10.1111/crj.12742

Adams, S., Teo, C., McDonald, K. L., Zinger, A., Bustamante, S., Lim, C. K., et al. (2014). Involvement of the kynurenine pathway in human glioma pathophysiology. *PLoS One* 9 (11), e112945. doi:10.1371/journal.pone.0112945

Anderson, N. R., Minutolo, N. G., Gill, S., and Klichinsky, M. (2021). Macrophage-based approaches for cancer immunotherapy. *Cancer Res.* 81 (5), 1201–1208. doi:10.1158/0008-5472.Can-20-2990

Aran, D., Sirota, M., and Butte, A. J. (2015). Systematic pan-cancer analysis of tumour purity. *Nat. Commun.* 6, 8971. doi:10.1038/ncomms9971

Brandacher, G., Perathoner, A., Ladurner, R., Schneeberger, S., Obrist, P., Winkler, C., et al. (2006). Prognostic value of indoleamine 2, 3-dioxygenase expression in colorectal cancer: Effect on tumor-infiltrating T cells. *Clin. Cancer Res.* 12 (4), 1144–1151. doi:10.1158/1078-0432.Ccr-05-1966

Carpenedo, R., Pittaluga, A., Cozzi, A., Attucci, S., Galli, A., Raiteri, M., et al. (2001). Presynaptic kynurenate-sensitive receptors inhibit glutamate release. *Eur. J. Neurosci.* 13 (11), 2141–2147. doi:10.1046/j.0953-816x.2001.01592.x

Cervenka, I., Agudelo, L. Z., and Ruas, J. L. (2017). Kynurenines: Tryptophan's metabolites in exercise, inflammation, and mental health. *Science* 357 (6349), eaaf9794. doi:10.1126/science.aaf9794

Chinot, O. L., Wick, W., Mason, W., Henriksson, R., Saran, F., Nishikawa, R., et al. (2014). Bevacizumab plus radiotherapy-temozolomide for newly diagnosed glioblastoma. *N. Engl. J. Med.* 370 (8), 709–722. doi:10.1056/NEJMoa1308345

Choueiri, T. K., Tomczak, P., Park, S. H., Venugopal, B., Ferguson, T., Chang, Y. H., et al. (2021). Adjuvant pembrolizumab after nephrectomy in renal-cell carcinoma. *N. Engl. J. Med.* 385 (8), 683–694. doi:10.1056/NEJMoa2106391

Ci, C., Wu, C., Lyu, D., Chang, X., He, C., Liu, W., et al. (2020). Downregulation of kynureninase restrains cutaneous squamous cell carcinoma proliferation and represses the PI3K/AKT pathway. *Clin. Exp. Dermatol.* 45 (2), 194–201. doi:10.1111/ced.14072

Cloughesy, T. F., Mochizuki, A. Y., Orpilla, J. R., Hugo, W., Lee, A. H., Davidson, T. B., et al. (2019). Neoadjuvant anti-PD-1 immunotherapy promotes a survival benefit with intratumoral and systemic immune responses in recurrent glioblastoma. *Nat. Med.* 25 (3), 477–486. doi:10.1038/s41591-018-0337-7

Colombo, M. P., and Piconese, S. (2007). Regulatory-T-cell inhibition versus depletion: The right choice in cancer immunotherapy. *Nat. Rev. Cancer* 7 (11), 880–887. doi:10.1038/nrc2250

Cortes, J., Rugo, H. S., Cescon, D. W., Im, S. A., Yusof, M. M., Gallardo, C., et al. (2022). Pembrolizumab plus chemotherapy in advanced triple-negative breast cancer. *N. Engl. J. Med.* 387 (3), 217–226. doi:10.1056/NEJMoa2202809

Couturier, C. P., Ayyadhury, S., Le, P. U., Nadaf, J., Monlong, J., Riva, G., et al. (2020). Single-cell RNA-seq reveals that glioblastoma recapitulates a normal neurodevelopmental hierarchy. *Nat. Commun.* 11 (1), 3406. doi:10.1038/s41467-020-17186-5

Curiel, T. J., Coukos, G., Zou, L., Alvarez, X., Cheng, P., Mottram, P., et al. (2004). Specific recruitment of regulatory T cells in ovarian carcinoma fosters immune privilege and predicts reduced survival. *Nat. Med.* 10 (9), 942–949. doi:10.1038/nm1093

Deshpande, R. P., Sharma, S., and Watabe, K. (2020). The confounders of cancer immunotherapy: Roles of lifestyle, metabolic disorders and sociological factors. *Cancers (Basel)* 12 (10), E2983. doi:10.3390/cancers12102983

Devlin, A. S., Marcobal, A., Dodd, D., Nayfach, S., Plummer, N., Meyer, T., et al. (2016). Modulation of a circulating uremic solute via rational genetic manipulation of the gut microbiota. *Cell. Host Microbe* 20 (6), 709–715. doi:10.1016/j.chom.2016.10.021

Du, L., Xing, Z., Tao, B., Li, T., Yang, D., Li, W., et al. (2020). Both Ido1 and TDO contribute to the malignancy of gliomas via the Kyn-AhR-AQP4 signaling pathway. *Signal Transduct. Target. Ther.* 5 (1), 10. doi:10.1038/s41392-019-0103-4

Eggermont, A. M. M., Blank, C. U., Mandala, M., Long, G. V., Atkinson, V., Dalle, S., et al. (2018). Adjuvant pembrolizumab versus placebo in resected stage III melanoma. *N. Engl. J. Med.* 378 (19), 1789–1801. doi:10.1056/NEJMoa1802357

Erhardt, S., Oberg, H., and Engberg, G. (2001). Pharmacologically elevated levels of endogenous kynurenic acid prevent nicotine-induced activation of nigral dopamine neurons. *Naunyn. Schmiedeb. Arch. Pharmacol.* 363 (1), 21–27. doi:10.1007/s002100000325

Fourcade, J., Sun, Z., Pagliano, O., Chauvin, J. M., Sander, C., Janjic, B., et al. (2014). PD-1 and Tim-3 regulate the expansion of tumor antigen-specific CD8$^+$ T cells induced by melanoma vaccines. *Cancer Res.* 74 (4), 1045–1055. doi:10.1158/0008-5472.Can-13-2908

Gandhi, L., Rodríguez-Abreu, D., Gadgeel, S., Esteban, E., Felip, E., De Angelis, F., et al. (2018). Pembrolizumab plus chemotherapy in metastatic non-small-cell lung cancer. *N. Engl. J. Med.* 378 (22), 2078–2092. doi:10.1056/NEJMoa1801005

Gilbert, M. R., Dignam, J. J., Armstrong, T. S., Wefel, J. S., Blumenthal, D. T., Vogelbaum, M. A., et al. (2014). A randomized trial of bevacizumab for newly diagnosed glioblastoma. *N. Engl. J. Med.* 370 (8), 699–708. doi:10.1056/NEJMoa1308573

Giusti, R. M., Maloney, E. M., Hanchard, B., Morgan, O. S., Steinberg, S. M., Wachter, H., et al. (1996). Differential patterns of serum biomarkers of immune activation in human T-cell lymphotropic virus type I-associated myelopathy/tropical spastic paraparesis, and adult T-cell leukemia/lymphoma. *Cancer Epidemiol. Biomarkers Prev.* 5 (9), 699–704.

Grohmann, U., Mondanelli, G., Belladonna, M. L., Orabona, C., Pallotta, M. T., Iacono, A., et al. (2017). Amino-acid sensing and degrading pathways in immune regulation. *Cytokine Growth Factor Rev.* 35, 37–45. doi:10.1016/j.cytogfr.2017.05.004

Hendriks, L. E. L., Henon, C., Auclin, E., Mezquita, L., Ferrara, R., Audigier-Valette, C., et al. (2019). Outcome of patients with non-small cell lung cancer and brain metastases treated with checkpoint inhibitors. *J. Thorac. Oncol.* 14 (7), 1244–1254. doi:10.1016/j.jtho.2019.02.009

Huang, A., Fuchs, D., Widner, B., Glover, C., Henderson, D. C., and Allen-Mersh, T. G. (2002). Serum tryptophan decrease correlates with immune activation and impaired quality of life in colorectal cancer. *Br. J. Cancer* 86 (11), 1691–1696. doi:10.1038/sj.bjc.6600336

Huang, T. T., Tseng, L. M., Chen, J. L., Chu, P. Y., Lee, C. H., Huang, C. T., et al. (2020). Kynurenine 3-monooxygenase upregulates pluripotent genes through β-catenin and promotes triple-negative breast cancer progression. *EBioMedicine* 54, 102717. doi:10.1016/j.ebiom.2020.102717

Inaba, T., Ino, K., Kajiyama, H., Yamamoto, E., Shibata, K., Nawa, A., et al. (2009). Role of the immunosuppressive enzyme indoleamine 2, 3-dioxygenase in the progression of ovarian carcinoma. *Gynecol. Oncol.* 115 (2), 185–192. doi:10.1016/j.ygyno.2009.07.015

Ino, K., Yamamoto, E., Shibata, K., Kajiyama, H., Yoshida, N., Terauchi, M., et al. (2008). Inverse correlation between tumoral indoleamine 2, 3-dioxygenase expression and tumor-infiltrating lymphocytes in endometrial cancer: Its association with disease progression and survival. *Clin. Cancer Res.* 14 (8), 2310–2317. doi:10.1158/1078-0432.Ccr-07-4144

Janjigian, Y. Y., Shitara, K., Moehler, M., Garrido, M., Salman, P., Shen, L., et al. (2021). First-line nivolumab plus chemotherapy versus chemotherapy alone for advanced gastric, gastro-oesophageal junction, and oesophageal adenocarcinoma (CheckMate 649): A randomised, open-label, phase 3 trial. *Lancet* 398 (10294), 27–40. doi:10.1016/s0140-6736(21)00797-2

Larkin, J., Chiarion-Sileni, V., Gonzalez, R., Grob, J. J., Cowey, C. L., Lao, C. D., et al. (2015). Combined nivolumab and ipilimumab or monotherapy in untreated melanoma. *N. Engl. J. Med.* 373 (1), 23–34. doi:10.1056/NEJMoa1504030

Le Floc'h, N., Otten, W., and Merlot, E. (2011). Tryptophan metabolism, from nutrition to potential therapeutic applications. *Amino Acids* 41 (5), 1195–1205. doi:10.1007/s00726-010-0752-7

Li, B., Severson, E., Pignon, J. C., Zhao, H., Li, T., Novak, J., et al. (2016). Comprehensive analyses of tumor immunity: Implications for cancer immunotherapy. *Genome Biol.* 17 (1), 174. doi:10.1186/s13059-016-1028-7

Lim, M., Weller, M., Idbaih, A., Steinbach, J., Finocchiaro, G., Raval, R. R., et al. (2022). Phase III trial of chemoradiotherapy with temozolomide plus nivolumab or placebo for newly diagnosed glioblastoma with methylated *MGMT* promoter. *Neuro. Oncol.* 2022, noac116. doi:10.1093/neuonc/noac116

Lim, M., Xia, Y., Bettegowda, C., and Weller, M. (2018). Current state of immunotherapy for glioblastoma. *Nat. Rev. Clin. Oncol.* 15 (7), 422–442. doi:10.1038/s41571-018-0003-5

Liu, C. Y., Huang, T. T., Chen, J. L., Chu, P. Y., Lee, C. H., Lee, H. C., et al. (2021). Significance of kynurenine 3-monooxygenase expression in colorectal cancer. *Front. Oncol.* 11, 620361. doi:10.3389/fonc.2021.620361

Louveau, A., Smirnov, I., Keyes, T. J., Eccles, J. D., Rouhani, S. J., Peske, J. D., et al. (2015). Structural and functional features of central nervous system lymphatic vessels. *Nature* 523 (7560), 337–341. doi:10.1038/nature14432

Muller, A. J., DuHadaway, J. B., Donover, P. S., Sutanto-Ward, E., and Prendergast, G. C. (2005). Inhibition of indoleamine 2, 3-dioxygenase, an immunoregulatory target of the cancer suppression gene Bin1, potentiates cancer chemotherapy. *Nat. Med.* 11 (3), 312–319. doi:10.1038/nm1196

Munn, D. H., Sharma, M. D., Baban, B., Harding, H. P., Zhang, Y., Ron, D., et al. (2005). GCN2 kinase in T cells mediates proliferative arrest and anergy induction in response to indoleamine 2, 3-dioxygenase. *Immunity* 22 (5), 633–642. doi:10.1016/j.immuni.2005.03.013

Munn, D. H., Zhou, M., Attwood, J. T., Bondarev, I., Conway, S. J., Marshall, B., et al. (1998). Prevention of allogeneic fetal rejection by tryptophan catabolism. *Science* 281 (5380), 1191–1193. doi:10.1126/science.281.5380.1191

Nakamura, T., Shima, T., Saeki, A., Hidaka, T., Nakashima, A., Takikawa, O., et al. (2007). Expression of indoleamine 2, 3-dioxygenase and the recruitment of Foxp3-expressing regulatory T cells in the development and progression of uterine cervical cancer. *Cancer Sci.* 98 (6), 874–881. doi:10.1111/j.1349-7006.2007.00470.x

Ngiow, S. F., von Scheidt, B., Akiba, H., Yagita, H., Teng, M. W., and Smyth, M. J. (2011). Anti-TIM3 antibody promotes T cell IFN-γ-mediated antitumor immunity and suppresses established tumors. *Cancer Res.* 71 (10), 3540–3551. doi:10.1158/0008-5472.Can-11-0096

Noy, R., and Pollard, J. W. (2014). Tumor-associated macrophages: From mechanisms to therapy. *Immunity* 41 (1), 49–61. doi:10.1016/j.immuni.2014.06.010

Omuro, A., Brandes, A. A., Carpentier, A. F., Idbaih, A., Reardon, D. A., Cloughesy, T., et al. (2022). Radiotherapy combined with nivolumab or temozolomide for newly diagnosed glioblastoma with unmethylated *MGMT* promoter: An international randomized phase III trial. *Neuro. Oncol.* 2022, noac099. doi:10.1093/neuonc/noac099

Opitz, C. A., Litzenburger, U. M., Sahm, F., Ott, M., Tritschler, I., Trump, S., et al. (2011). An endogenous tumour-promoting ligand of the human aryl hydrocarbon receptor. *Nature* 478 (7368), 197–203. doi:10.1038/nature10491

Ostrom, Q. T., Cioffi, G., Waite, K., Kruchko, C., and Barnholtz-Sloan, J. S. (2021). CBTRUS statistical report: Primary brain and other central nervous system tumors diagnosed in the United States in 2014-2018. *Neuro. Oncol.* 23 (12), iii1–iii105. doi:10.1093/neuonc/noab200

Pang, H., Jiang, Y., Li, J., Wang, Y., Nie, M., Xiao, N., et al. (2021). Aberrant NAD(+) metabolism underlies Zika virus-induced microcephaly. *Nat. Metab.* 3 (8), 1109–1124. doi:10.1038/s42255-021-00437-0

Pilotte, L., Larrieu, P., Stroobant, V., Colau, D., Dolusic, E., Frédérick, R., et al. (2012). Reversal of tumoral immune resistance by inhibition of tryptophan 2, 3-dioxygenase. *Proc. Natl. Acad. Sci. U. S. A.* 109 (7), 2497–2502. doi:10.1073/pnas.1113873109

Pirozzi, C. J., and Yan, H. (2021). The implications of IDH mutations for cancer development and therapy. *Nat. Rev. Clin. Oncol.* 18 (10), 645–661. doi:10.1038/s41571-021-00521-0

Platten, M., Nollen, E. A. A., Röhrig, U. F., Fallarino, F., and Opitz, C. A. (2019). Tryptophan metabolism as a common therapeutic target in cancer, neurodegeneration and beyond. *Nat. Rev. Drug Discov.* 18 (5), 379–401. doi:10.1038/s41573-019-0016-5

Pontén, F., Jirström, K., and Uhlen, M. (2008). The human protein atlas--a tool for pathology. *J. Pathol.* 216 (4), 387–393. doi:10.1002/path.2440

Reardon, D. A., Brandes, A. A., Omuro, A., Mulholland, P., Lim, M., Wick, A., et al. (2020). Effect of nivolumab vs bevacizumab in patients with recurrent glioblastoma: The CheckMate 143 phase 3 randomized clinical trial. *JAMA Oncol.* 6 (7), 1003–1010. doi:10.1001/jamaoncol.2020.1024

Reck, M., Rodríguez-Abreu, D., Robinson, A. G., Hui, R., Csőszi, T., Fülöp, A., et al. (2016). Pembrolizumab versus chemotherapy for PD-L1-positive non-small-cell lung cancer. *N. Engl. J. Med.* 375 (19), 1823–1833. doi:10.1056/NEJMoa1606774

Rothhammer, V., Mascanfroni, I. D., Bunse, L., Takenaka, M. C., Kenison, J. E., Mayo, L., et al. (2016). Type I interferons and microbial metabolites of tryptophan modulate astrocyte activity and central nervous system inflammation via the aryl hydrocarbon receptor. *Nat. Med.* 22 (6), 586–597. doi:10.1038/nm.4106

Sakuishi, K., Apetoh, L., Sullivan, J. M., Blazar, B. R., Kuchroo, V. K., and Anderson, A. C. (2010). Targeting Tim-3 and PD-1 pathways to reverse T cell exhaustion and restore anti-tumor immunity. *J. Exp. Med.* 207 (10), 2187–2194. doi:10.1084/jem.20100643

Schalper, K. A., Rodriguez-Ruiz, M. E., Diez-Valle, R., López-Janeiro, A., Porciuncula, A., Idoate, M. A., et al. (2019). Neoadjuvant nivolumab modifies the tumor immune microenvironment in resectable glioblastoma. *Nat. Med.* 25 (3), 470–476. doi:10.1038/s41591-018-0339-5

Schroecksnadel, K., Winkler, C., Fuith, L. C., and Fuchs, D. (2005). Tryptophan degradation in patients with gynecological cancer correlates with immune activation. *Cancer Lett.* 223 (2), 323–329. doi:10.1016/j.canlet.2004.10.033

Schwarcz, R., and Stone, T. W. (2017). The kynurenine pathway and the brain: Challenges, controversies and promises. *Neuropharmacology* 112, 237–247. doi:10.1016/j.neuropharm.2016.08.003

Siegel, R. L., Miller, K. D., Fuchs, H. E., and Jemal, A. (2021). Cancer statistics, 2017. *Ca. Cancer J. Clin.* 71 (1), 7–30. doi:10.3322/caac.21387

Stone, T. W. (1993). Neuropharmacology of quinolinic and kynurenic acids. *Pharmacol. Rev.* 45 (3), 309–379.

Stupp, R., Mason, W. P., van den Bent, M. J., Weller, M., Fisher, B., Taphoorn, M. J., et al. (2005). Radiotherapy plus concomitant and adjuvant temozolomide for glioblastoma. *N. Engl. J. Med.* 352 (10), 987–996. doi:10.1056/NEJMoa043330

Stupp, R., Taillibert, S., Kanner, A. A., Kesari, S., Steinberg, D. M., Toms, S. A., et al. (2015). Maintenance therapy with tumor-treating fields plus temozolomide vs

temozolomide alone for glioblastoma: A randomized clinical trial. *Jama* 314 (23), 2535–2543. doi:10.1001/jama.2015.16669

Stupp, R., Taillibert, S., Kanner, A., Read, W., Steinberg, D., Lhermitte, B., et al. (2017). Effect of tumor-treating fields plus maintenance temozolomide vs maintenance temozolomide alone on survival in patients with glioblastoma: A randomized clinical trial. *Jama* 318 (23), 2306–2316. doi:10.1001/jama.2017.18718

Suzuki, Y., Suda, T., Furuhashi, K., Suzuki, M., Fujie, M., Hahimoto, D., et al. (2010). Increased serum kynurenine/tryptophan ratio correlates with disease progression in lung cancer. *Lung Cancer* 67 (3), 361–365. doi:10.1016/j.lungcan.2009.05.001

Tawbi, H. A., Forsyth, P. A., Algazi, A., Hamid, O., Hodi, F. S., Moschos, S. J., et al. (2018). Combined nivolumab and ipilimumab in melanoma metastatic to the brain. *N. Engl. J. Med.* 379 (8), 722–730. doi:10.1056/NEJMoa1805453

Tewari, K. S., Monk, B. J., Vergote, I., Miller, A., de Melo, A. C., Kim, H. S., et al. (2022). Survival with cemiplimab in recurrent cervical cancer. *N. Engl. J. Med.* 386 (6), 544–555. doi:10.1056/NEJMoa2112187

Uyttenhove, C., Pilotte, L., Théate, I., Stroobant, V., Colau, D., Parmentier, N., et al. (2003). Evidence for a tumoral immune resistance mechanism based on tryptophan degradation by indoleamine 2, 3-dioxygenase. *Nat. Med.* 9 (10), 1269–1274. doi:10.1038/nm934

van der Goot, A. T., and Nollen, E. A. (2013). Tryptophan metabolism: Entering the field of aging and age-related pathologies. *Trends Mol. Med.* 19 (6), 336–344. doi:10.1016/j.molmed.2013.02.007

Vezzani, A., Gramsbergen, J. B., Versari, P., Stasi, M. A., Procaccio, F., and Schwarcz, R. (1990). Kynurenic acid synthesis by human glioma. *J. Neurol. Sci.* 99 (1), 51–57. doi:10.1016/0022-510x(90)90198-v

Wakabayashi, T., Natsume, A., Mizusawa, J., Katayama, H., Fukuda, H., Sumi, M., et al. (2018). JCOG0911 INTEGRA study: A randomized screening phase II trial of interferonβ plus temozolomide in comparison with temozolomide alone for newly diagnosed glioblastoma. *J. Neurooncol.* 138 (3), 627–636. doi:10.1007/s11060-018-2831-7

Wang, H., Li, S., Wang, Q., Jin, Z., Shao, W., Gao, Y., et al. (2021). Tumor immunological phenotype signature-based high-throughput screening for the discovery of combination immunotherapy compounds. *Sci. Adv.* 7 (4), eabd7851. doi:10.1126/sciadv.abd7851

Wang, Z., Aguilar, E. G., Luna, J. I., Dunai, C., Khuat, L. T., Le, C. T., et al. (2019). Paradoxical effects of obesity on T cell function during tumor progression and PD-1 checkpoint blockade. *Nat. Med.* 25 (1), 141–151. doi:10.1038/s41591-018-0221-5

Weinlich, G., Murr, C., Richardsen, L., Winkler, C., and Fuchs, D. (2007). Decreased serum tryptophan concentration predicts poor prognosis in malignant melanoma patients. *Dermatology* 214 (1), 8–14. doi:10.1159/000096906

Weller, M., Butowski, N., Tran, D. D., Recht, L. D., Lim, M., Hirte, H., et al. (2017). Rindopepimut with temozolomide for patients with newly diagnosed, EGFRvIII-expressing glioblastoma (ACT IV): A randomised, double-blind, international phase 3 trial. *Lancet. Oncol.* 18 (10), 1373–1385. doi:10.1016/s1470-2045(17)30517-x

Weller, M., van den Bent, M., Preusser, M., Le Rhun, E., Tonn, J. C., Minniti, G., et al. (2021). EANO guidelines on the diagnosis and treatment of diffuse gliomas of adulthood. *Nat. Rev. Clin. Oncol.* 18 (3), 170–186. doi:10.1038/s41571-020-00447-z

Wolf, Y., Anderson, A. C., and Kuchroo, V. K. (2020). TIM3 comes of age as an inhibitory receptor. *Nat. Rev. Immunol.* 20 (3), 173–185. doi:10.1038/s41577-019-0224-6

Xia, L., Oyang, L., Lin, J., Tan, S., Han, Y., Wu, N., et al. (2021). The cancer metabolic reprogramming and immune response. *Mol. Cancer* 20 (1), 28. doi:10.1186/s12943-021-01316-8

Yan, H., Parsons, D. W., Jin, G., McLendon, R., Rasheed, B. A., Yuan, W., et al. (2009). IDH1 and IDH2 mutations in gliomas. *N. Engl. J. Med.* 360 (8), 765–773. doi:10.1056/NEJMoa0808710

Yang, L., and Zhang, Y. (2017). Tumor-associated macrophages: From basic research to clinical application. *J. Hematol. Oncol.* 10 (1), 58. doi:10.1186/s13045-017-0430-2

Ye, L., Xu, Y., Wang, L., Zhang, C., Hu, P., Tong, S., et al. (2021). Downregulation of CYP2E1 is associated with poor prognosis and tumor progression of gliomas. *Cancer Med.* 10 (22), 8100–8113. doi:10.1002/cam4.4320

Yen, M. C., Lin, C. C., Chen, Y. L., Huang, S. S., Yang, H. J., Chang, C. P., et al. (2009). A novel cancer therapy by skin delivery of indoleamine 2, 3-dioxygenase siRNA. *Clin. Cancer Res.* 15 (2), 641–649. doi:10.1158/1078-0432.Ccr-08-1988

Yoshihara, K., Shahmoradgoli, M., Martínez, E., Vegesna, R., Kim, H., Torres-Garcia, W., et al. (2013). Inferring tumour purity and stromal and immune cell admixture from expression data. *Nat. Commun.* 4, 2612. doi:10.1038/ncomms3612

Zhai, L., Dey, M., Lauing, K. L., Gritsina, G., Kaur, R., Lukas, R. V., et al. (2015). The kynurenine to tryptophan ratio as a prognostic tool for glioblastoma patients enrolling in immunotherapy. *J. Clin. Neurosci.* 22 (12), 1964–1968. doi:10.1016/j.jocn.2015.06.018

Zheng, X., Wang, X., Zheng, L., Zhao, H., Li, W., Wang, B., et al. (2020). Construction and analysis of the tumor-specific mRNA-miRNA-lncRNA network in gastric cancer. *Front. Pharmacol.* 11, 1112. doi:10.3389/fphar.2020.01112

Zhou, Q., Munger, M. E., Veenstra, R. G., Weigel, B. J., Hirashima, M., Munn, D. H., et al. (2011). Coexpression of Tim-3 and PD-1 identifies a CD8+ T-cell exhaustion phenotype in mice with disseminated acute myelogenous leukemia. *Blood* 117 (17), 4501–4510. doi:10.1182/blood-2010-10-310425

frontiers | Frontiers in Pharmacology

TYPE Review
PUBLISHED 25 November 2022
DOI 10.3389/fphar.2022.1057571

OPEN ACCESS

EDITED BY
Marie-Odile Parat,
The University of Queensland, Australia

REVIEWED BY
Thiên-Nga Chamaraux-Tran,
Groupe Hospitalier Saint Vincent, France
Weiguang Li,
Hong Kong Polytechnic University, Hong Kong SAR, China

*CORRESPONDENCE
Jing Sun,
sj11788@rjh.com.cn
Lei Zhuang,
leileihead@hotmail.com

SPECIALTY SECTION
This article was submitted to Pharmacology of Anti-Cancer Drugs, a section of the journal Frontiers in Pharmacology

RECEIVED 29 September 2022
ACCEPTED 15 November 2022
PUBLISHED 25 November 2022

CITATION
Zhou X, Shao Y, Li S, Zhang S, Ding C, Zhuang L and Sun J (2022), An intravenous anesthetic drug-propofol, influences the biological characteristics of malignant tumors and reshapes the tumor microenvironment: A narrative literature review.
Front. Pharmacol. 13:1057571.
doi: 10.3389/fphar.2022.1057571

An intravenous anesthetic drug-propofol, influences the biological characteristics of malignant tumors and reshapes the tumor microenvironment: A narrative literature review

Xueliang Zhou[1,2,3], Yanfei Shao[1,2,3], Shuchun Li[1,2], Sen Zhang[1,2,3], Chengsheng Ding[1,2,3], Lei Zhuang[4]* and Jing Sun[1,2]*

[1]Department of General Surgery, Ruijin Hospital, Shanghai Jiao Tong University School of Medicine, Shanghai, China, [2]Shanghai Minimally Invasive Surgery Center, Ruijin Hospital, Shanghai Jiao Tong University School of Medicine, Shanghai, China, [3]Shanghai Institute of Digestive Surgery, Ruijin Hospital, Shanghai Jiao Tong University School of Medicine, Shanghai, China/, [4]Department of Anesthesiology, Ruijin Hospital, Shanghai Jiaotong University School of Medicine, Shanghai, China

Malignant tumors are the second leading cause of death worldwide. This is a public health concern that negatively impacts human health and poses a threat to the safety of life. Although there are several treatment approaches for malignant tumors, surgical resection remains the primary and direct treatment for malignant solid tumors. Anesthesia is an integral part of the operation process. Different anesthesia techniques and drugs have different effects on the operation and the postoperative prognosis. Propofol is an intravenous anesthetic that is commonly used in surgery. A substantial number of studies have shown that propofol participates in the pathophysiological process related to malignant tumors and affects the occurrence and development of malignant tumors, including anti-tumor effect, pro-tumor effect, and regulation of drug resistance. Propofol can also reshape the tumor microenvironment, including anti-angiogenesis, regulation of immunity, reduction of inflammation and remodeling of the extracellular matrix. Furthermore, most clinical studies have also indicated that propofol may contribute to a better postoperative outcome in some malignant tumor surgeries. Therefore, the author reviewed the chemical properties, pharmacokinetics, clinical application and limitations, mechanism of influencing the biological characteristics of malignant tumors and reshaping the tumor microenvironment, studies of propofol in animal tumor models and its relationship with postoperative prognosis of propofol in combination with the relevant literature in recent years, to lay a foundation for further study on the correlation between propofol and malignant tumor and provide theoretical guidance for the selection of anesthetics in malignant tumor surgery.

KEYWORDS

malignant tumor, anesthetic drug, propofol, chemical properties, pharmacokinetic, biological characteristics, tumor microenvironment, postoperative prognosis

1 Introduction

Malignant tumor is one of the diseases that seriously affect the human quality of life (Siegel et al., 2020). According to GLOBOCAN 2020 global cancer statistics, there were 9,958,133 deaths worldwide from malignant tumors in 2020 (Sung et al., 2021). Therefore, in-depth research into the pathogenesis of malignant tumors and the factors influencing their development has become a major scientific research direction for global health strategies. Currently, radiation therapy, chemotherapy, targeted therapy, and immunotherapy have improved the clinical outcome and extended the life of more patients with advanced malignant tumors, but surgical resection remains the most useful and effective treatment for solid malignant tumors. As a matter of fact, different surgical techniques and perioperative risk factors can influence the prognosis of tumor patients (Cuk et al., 2021).

The influence of perioperative anesthesia management on the postoperative prognosis of malignant tumors has increasingly come to light in the recent years. Studies have found that different anesthesia techniques and drugs can affect tumor recurrence and metastasis, resulting in different postoperative prognoses. Propofol exerts sedative-hypnotic effects by the means of chloride transport and γ-aminobutyric acid (GABA) receptors and is commonly used in terms of the induction and maintenance of general anesthesia, with the characteristics of rapid induction, rapid recovery, and few adverse effects (Feng et al., 2021). It is worth noting that many studies have demonstrated that propofol not only induces anesthesia and sedation but also alters the biological characteristics of the malignant tumors. It can suppress the malignant biological characteristics of tumor cells and promote apoptosis of tumor cells with anti-cancer activity (Eden et al., 2018). Interestingly, propofol has also been found to promote proliferation, invasion and metastasis of tumor cells in certain specific tumor types or conditions. In terms of therapeutic response, propofol modulates resistance to a number of chemotherapeutic agents and promotes drug sensitivity in tumor cells (Jiang et al., 2018). In addition, propofol can reshape the tumor microenvironment, reducing the degree of immunosuppression in the tumor microenvironment and inhibiting the signaling pathways that are involved in the development of inflammation and the production of inflammatory mediators, which has immune-activating and anti-inflammatory activity (Xu et al., 2020). Neoangiogenesis, hypoxia, and degradation of the extracellular matrix are important features of the tumor microenvironment that is also modulated by propofol. Clinical studies have shown that propofol is closely associated with postoperative prognosis for tumor patients, with the most extensive studies focusing on breast cancer (Wang et al., 2018). According to most studies, tumor patients receiving propofol-based anesthesia have a better prognosis than those receiving inhalation anesthesia. However, some retrospective studies have showed no significant difference between the prognosis of tumor patients undergoing propofol *versus* inhalation anesthesia, highlighting the need for large, multi-center, and prospective randomized controlled trials in the future.

Here we conducted a narrative literature review on propofol regarding its chemical properties, pharmacokinetics, clinical application and limitations, studies in animal tumor models as well as effects on the biological characteristics of malignant tumors, reshaping of the tumor microenvironment and postoperative prognosis, intending to lay a theoretical foundation for future large-scale prospective multi-center clinical trials and provide potential guidance for the precise selection of surgical anesthetics (Figure 1).

2 Chemical properties of propofol

Originally known as 2,6-diisopropyl phenol, propofol was discovered by Scottish chemist John B. Glen and used as an anesthetic. The 2D and 3D chemical structure of propofol is presented in Figure 2 (Cited from the PubChem database). Currently, propofol is currently the most widely used anesthetic drug in clinical practice, with the advantages of rapid onset of action, rapid recovery, rapid metabolic clearance and few adverse effects. In clinical practice, propofol fat emulsion is commonly used because it is a colorless or light-yellow liquid, almost insoluble in water but soluble in many organic solvents (Dinis-Oliveira, 2018). At present, it is widely believed that propofol has antioxidant effects. Studies have shown that the chemical structure of propofol contains phenolic hydrocarbon groups, which are similar to the known antioxidants 2, 6-di-tert-butylp-cresol and the endogenous antioxidant vitamin E. Propofol can directly react with oxygen free radicals to generate stable 2, 6-diisopropyl phenoxy group, which is to replace the highly active free radical with the low active free radical and reduce the lipid peroxidation cascade reaction triggered by the latter (Tsuchiya et al., 2010). Murphy et al. used electron rotational resonance spectroscopy to demonstrate that propofol acts as an antioxidant by reacting with free radicals to form phenoxy (Stratford and Murphy, 1997). Naohiro et al. (Kokita and Hara, 1996) found that small amounts of propofol in plasma could protect cell membranes by acting as an antioxidant, even when bound to plasma proteins. Several *in vivo* and *in vitro* studies have also shown that propofol can act as an antioxidant by rapidly and stably scavenging free radicals and inhibiting the process of lipid peroxidation (Li et al., 2012; Rosenfeldt et al., 2013).

It has been found that chemotherapeutic drugs such as formyl benzamide and chlorobenzene butyric acid have benzene ring or aromatic structures that contribute to their antitumor pharmacological effects (Wu et al., 2022). Propofol also exhibits antitumor effects and possesses a benzene ring

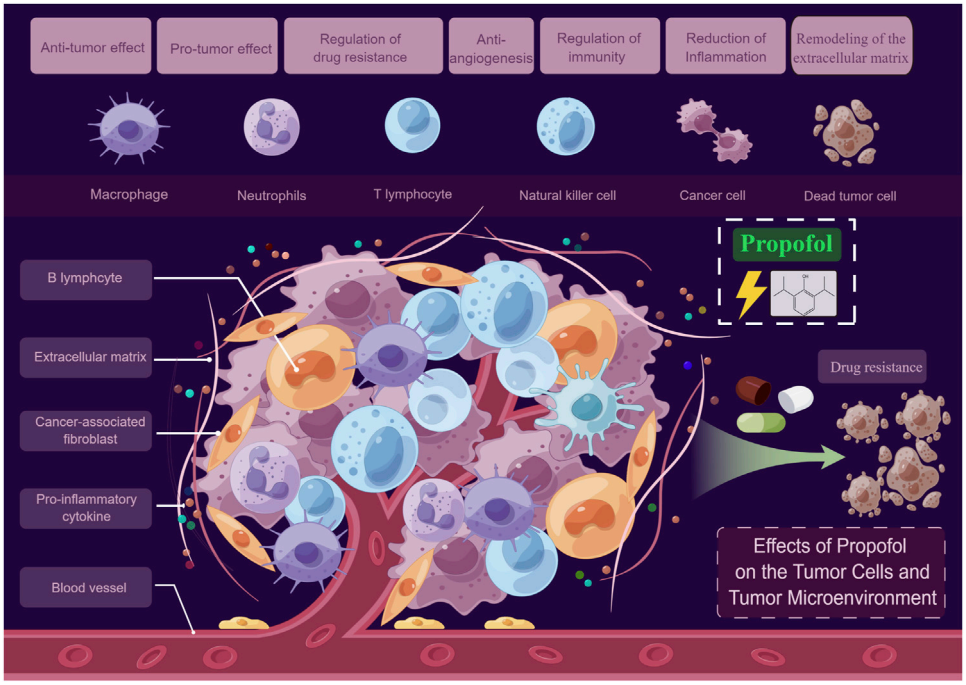

FIGURE 1
Effects of propofol on the tumor cells and tumor microenvironment. On one hand, propofol may directly act on tumor cells, exerting anti-tumor and pro-tumor effects, and regulating drug resistance. On the other hand, propofol may act indirectly on the tumor microenvironment by anti-angiogenesis, regulating immunity, reducing inflammation, and remodeling the extracellular matrix (By Figdraw).

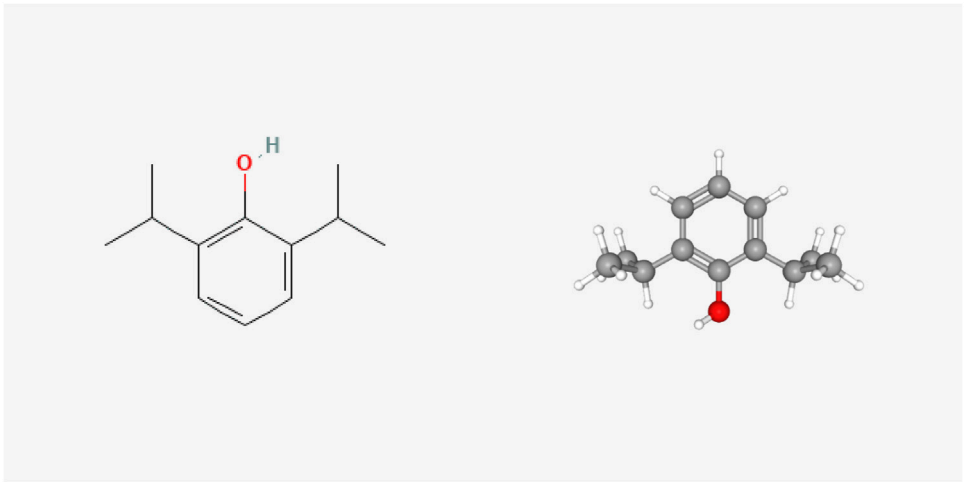

FIGURE 2
2D and 3D chemical structure of propofol.

structure, whereas other anesthetic drugs that do not exhibit antitumor effects, such as desflurane and sevoflurane, do not possess this ring structure. As a result, it has been speculated that the anti-tumor activities of propofol may be correlated with the benzene ring structure, but further research is needed to determine the exact relationship.

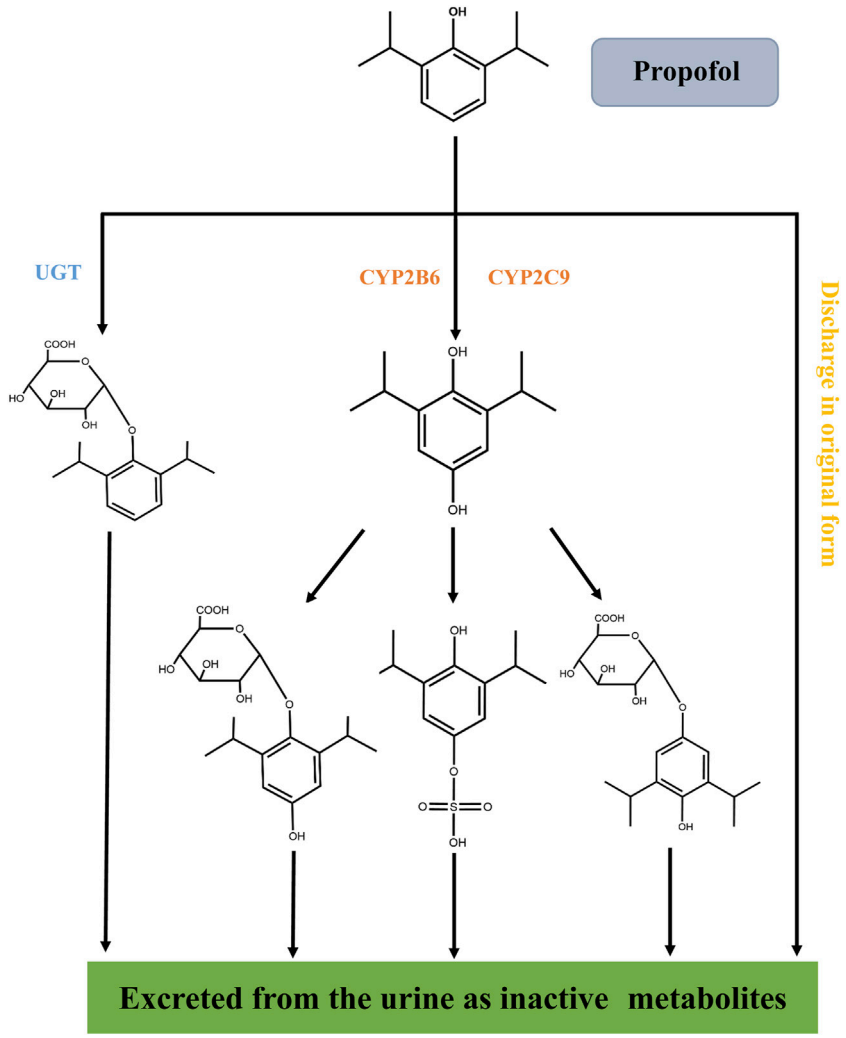

FIGURE 3
Metabolic process of propofol *in vivo*. Propofol is rapidly metabolized into inactive compounds in the liver through the hydroxylation of cytochrome P450 (CYP2B6 and CYP2C9) isomers and the UDP-glucuronosyhransferase (UGT) pathway and excreted by the kidney. Less than 1% of propofol is excreted in urine and 2% in feces.

3 Pharmacokinetics of propofol

The pharmacokinetics of propofol is characterized by a three-compartment linear model. The three-compartment model refers to plasma, fast equilibrium tissue, and slow equilibrium tissue, characterized by rapid distribution and rapid elimination. Propofol is rapidly distributed in the whole body after intravenous injection. Within 40 s (single-arm cerebral circulation time), propofol can rapidly produce a slightly hypnotic effect. It is estimated that the half-life of blood-brain balance is about one to 3 min, which is probably the reason for the rapid induction of anesthesia (Wan Hassan et al., 2018). Propofol is highly lipophilic and is widely distributed in the brain and liver, followed by the heart, kidney, gastrointestinal tract, and fat tissue. The tissue concentration rapidly decreases 2 h after administration, indicating there is no apparent accumulation of propofol in tissue (Hüppe et al., 2020). However, a longer infusion of propofol resulted in a significant tissue accumulation, slowing down the decrease of circulating propofol, which subsequently increased the awakening time. Three phases are involved in the elimination of propofol. Phase I represents the rapid distribution of propofol with a half-life of 2–10 min; Phase II represents the elimination of propofol from the blood through metabolism with a half-life of 21–56 min; Phase III represents the return of propofol from poorly perfused tissue to the blood with the half-life of termination 200–300 min (Ji et al., 2020).

Propofol is mainly metabolized in the liver (Figure 3). It is rapidly metabolized to inactive compounds through the hydroxylation of cytochrome P450 (CYP2B6 and CYP2C9) isomers and UDP-glucuronosyhransferase (UGT) pathway and eliminated by the kidney (Kodama et al., 2020). Less than 1% of propofol is excreted in urine and 2% in feces (Sandra et al., 2021).

Through the in-depth study of the pharmacokinetics of propofol, we can understand the absorption, distribution, and elimination process of propofol in the human body and the target organs where it exerts its pharmacological effects, which will further indicate the target organs and directions for the study of propofol. Propofol is highly lipophilic and protein-binding and is widely distributed in the liver, brain, gastrointestinal tract, and adipose tissue, so propofol tends to act in these organs. From a review of the literature, we found that propofol exerted a greater effect on liver cancer, gastric cancer, colorectal cancer and breast cancer, which is more consistent with the pharmacokinetic characteristics of propofol. Therefore, an in-depth understanding of the pharmacokinetics of propofol in the human body is of great significance for the rational use of drugs, the prediction of efficacy and toxicity, and the study of pharmacological effects.

4 Clinical application and limitations of propofol

4.1 Clinical application

Propofol is a short-acting intravenous anesthetic with the advantages of rapid onset, short duration of action, rapid elimination and low incidence of post-operative nausea and vomiting. It can depress the central nervous system and produce sedative and hypnotic effects, and is commonly used for induction and maintenance of anesthesia as well as sedation and analgesia. It is now commonly used for the induction and maintenance of general anesthesia (GA) and total intravenous anesthesia (TIVA), as well as for sedation during anesthesia, after surgery and in the intensive care unit (ICU).

4.1.1 Total intravenous anesthesia

The most common types of general anesthesia are propofol-based total intravenous anesthesia (TIVA) and volatile drug-based inhalation anesthesia. Of course, in many cases a combination of intravenous and inhalation anaesthesia is also used. Total intravenous anesthesia is a method of administering anesthesia to patients using intravenous anesthetics and its auxiliary agents with the advantages of rapid induction, smooth anesthesia, no contamination and quicker awakening (Ramirez and Cata, 2021). Propofol has been the basis of TIVA, with the development of target-controlled infusion (TCI) system, TCI has the advantages of fast adjustment speed, strong controllability and stable anesthesia depth, which is conducive to the personalized and refined administration of propofol, and can effectively avoid the sedation or anesthesia of too deep or too shallow due to individual differences and changes in surgical stimulation intensity (Anderson and Bagshaw, 2019).

4.1.2 Sedation in ICU

At present, sedation and analgesia has become one of the important treatment methods in ICU, which can reduce stress, reduce the body oxygen consumption, make the patient in a comfortable state, reduce the accident of extubation and is conducive to prevent accidents and the recovery of the patients. Propofol is a fast-acting, short-acting, fast-recovery intravenous anesthetic. It can achieve good sedative effect under the premise of analgesia and is suitable for short-term sedation in ICU (Garcia et al., 2021).

4.1.3 Application in outpatient endoscopic surgery

In recent years, with the continuous development of endoscopic techniques and the increased demand for painless endoscopy, propofol is also being used for various outpatient endoscopic surgeries such as painless gastrointestinal endoscopy and tracheoscopy. Propofol is becoming increasingly popular in sedation for gastrointestinal endoscopy due to its unique pharmacokinetic properties, predictable recovery process and rapid recovery (Goudra et al., 2021).

4.2 Limitations in clinical practice

Currently, propofol is commonly used clinically as a fat emulsion formulation, and a number of problems remain in its clinical application. Apart from producing pharmacological adverse effects such as dose-related blood pressure drop, heart rate decreases and apnea, others are mainly associated with propofol in fat emulsion formulations, such as injection site pain, thrombophlebitis, hypertriglyceridemia, potentially fatal bacterial infections, rupture and blockage of the infusion line during prolonged infusion, propofol infusion syndrome (PRIS) and allergic reactions, *etc.*

4.2.1 Decreased blood pressure and respiratory depression

Propofol has a cardiovascular depressant effect and causes hypotension associated with reduced peripheral vascular resistance, reduced cardiac preload, reduced sympathetic activity and myocardial contractility (Doğanay et al., 2018). Studies have confirmed that propofol-induced hypotension is related to the rate of injection, the dose injected and the effect on the central nervous system. The drop in blood pressure induced by propofol usually lasts for a short period of time and its cause of persistent hypotension is most often seen in elderly, female, poor general condition or in patients on concomitant morphine-like drugs.

In clinical use, propofol is highly likely to cause respiratory depression. Even the induced dose of propofol can cause slower

respiration, reduced tidal volume and even greater degree and frequency of apnea than other intravenous anesthetics of the same type (Jiang et al., 2021).

4.2.2 Injection site pain

Injection site pain can occur in both adults and children, this pain can be immediate or delayed. This pain is due to the activation of the plasma pancreatic Vaso peptide system by propofol and the subsequent production of bradykinin, which is not the only factor causing the pain (Miniksar, 2022). Pain caused by intravenous propofol is not a very serious complication, but pain can be an important source of excessive stress in patients during surgery and an important limiting factor for ideal anaesthesia.

4.2.3 Hypertriglyceridemia

Propofol is mainly given as an emulsion, and prolonged infusion is accompanied by elevated lipid levels. The long-chain triglycerides in the emulsion are the main factor causing elevated lipid levels (Corrado et al., 2020). In addition. The ability to metabolize and remove fat is reduced by changes in the enzymatic systems involved in lipid clearance and metabolism, which may result in hypertriglyceridemia due to the increased fat load and metabolic disturbances associated with the administration of propofol in stressful situations.

4.2.4 Propofol infusion syndrome

PRIS is a dangerous adverse reaction in the use of propofol and its treatment success rate is low. It was found that when propofol dose > 4 mg/(kg h) and infusion time >48 h may lead to PRIS. The main manifestations are unexplained cardiac arrhythmias, metabolic acidosis, hyperkalemia and cardiomyocyte lysis, which eventually develop into severe heart failure and even lead to the death (Hemphill et al., 2019). Triggers of PRIS include low age, severe central nervous system disease, excessive intake of glucocorticoids or exogenous catecholamines and inadequate carbohydrate intake.

5 Effect of propofol on biological characteristics of malignant tumor cells

Surgical resection is the primary treatment for solid malignancies. Numerous studies have demonstrated that the choice of anesthetic is closely associated with the postoperative prognosis of tumor patients. As a commonly used anesthetic, propofol not only has an anesthetic effect but also may act on tumor cells directly, which affects the biological characteristics of tumor cells, including anti-tumor effect, pro-tumor effect, and regulation of drug resistance.

5.1 Anti-tumor effect

The progression of malignant tumors is regulated by a variety of key factors both *in vitro* and *in vivo*. It has been shown that the anti-tumor effects of propofol are mainly through the regulation of microRNAs (miRNAs) and long non-coding RNAs (lncRNAs) expression to target multiple signaling pathways, oncogenes and functional proteins (Figure 4). Interestingly, in recent studies, propofol can also inhibit the progression of tumors by attenuating the function of tumor stem cells and regulating metabolic reprogramming.

5.1.1 Propofol and miRNAs

MiRNAs are a large family with distinctive structural and functional characteristics and are small non-coding single-stranded RNAs. Mature miRNAs are about 20–24 bases in length and are formed from a segment of single-stranded RNA precursor of 70–90 bases in length with a hairpin loop structure processed by an RNA enzyme called Dicer (Budakoti et al., 2021). Mature miRNAs inhibit translation or induce degradation of target gene mRNA molecules mainly by forming RNA-induced silencing complexes (RISCs) through complementary matching with their 3′-UTRs (Slack and Chinnaiyan, 2019). Numerous studies have demonstrated that miRNAs are closely related to tumorigenesis and development, affecting tumor differentiation, proliferation, invasion, metastasis, and drug resistance through controlling the expression of target genes, as well as their cell cycle and apoptosis process, thus serving as anti-oncogenes. (He et al., 2020). Therefore, miRNAs can be used as biological markers for diagnosis and prognosis prediction, as well as valuable therapeutic targets for tumors.

Some miRNAs, as proto-oncogenes, can negatively regulate anti-oncogenes, promote malignant transformation of normal cells, enhance proliferation, and differentiation and inhibit apoptosis of tumor cells. Propofol can suppress tumor cell proliferation, migration and invasion by downregulating proto-oncogenic miRNAs (Table 1). In bladder cancer, Qi et al. (2019a) found that propofol downregulated the miR-10b expression and increased the expression of its target gene HOXD10, exerting tumor-suppressive effects. Propofol suppresses the malignant biology of lung cancer cells through down-regulation of miRNAs. Wu et al. (2020) have showed that propofol inhibited NSCLC cell viability by downregulating the miR-21-5p/MAPK10 axis. Sun and Gao (2018) demonstrated that propofol suppressed the proliferation and migration of lung cancer A549 cells, partly due to downregulation of miR-372. In breast cancer, propofol could promote apoptosis of tumor cells by upregulating P27 and cleaved caspase-3 expression *via* downregulating miR-24 (Yu et al., 2018). Du et al. (2019) also found that propofol inhibited the activation of PI3K/AKT and Wnt/β-catenin signaling pathways through down-regulation of

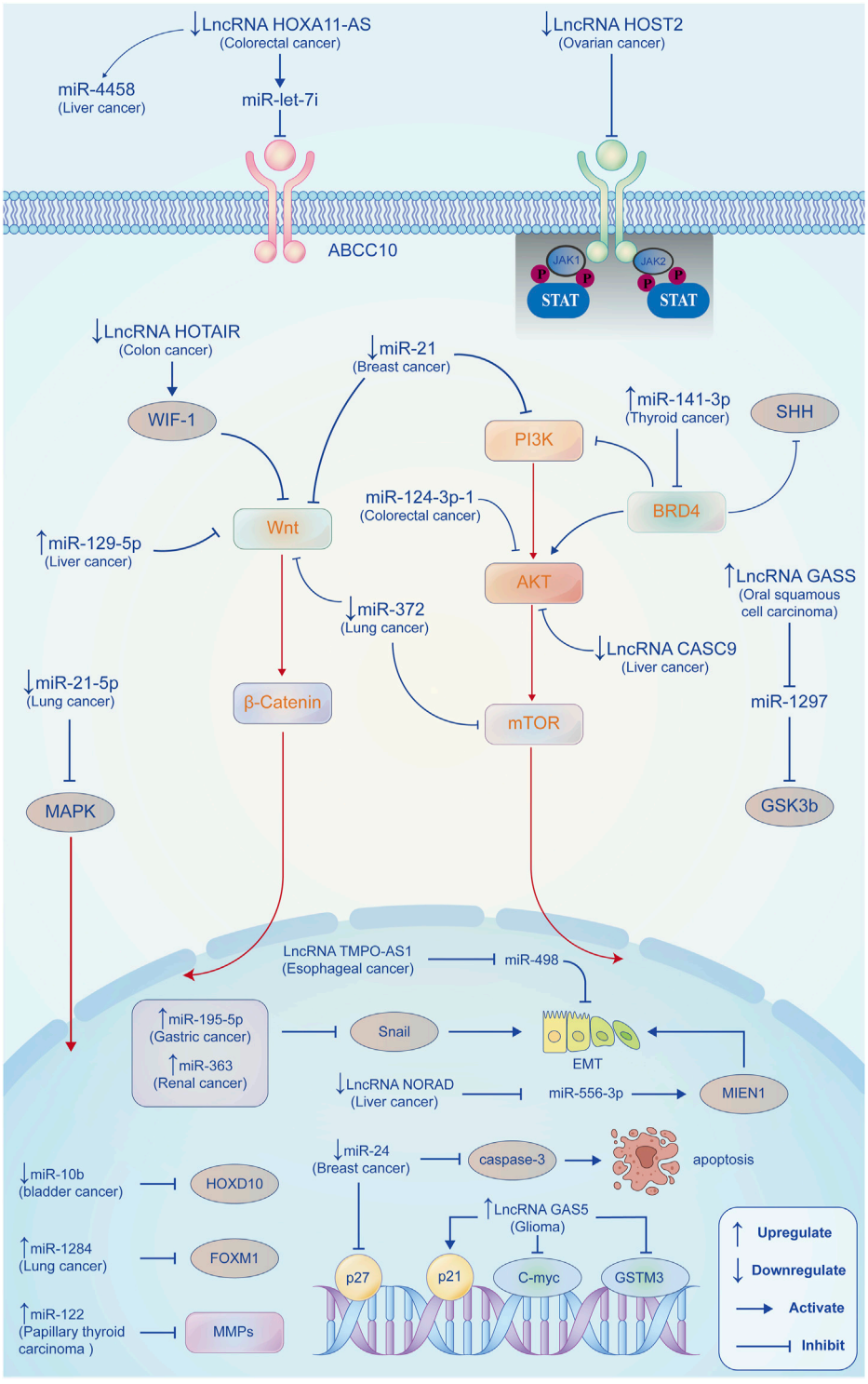

FIGURE 4
Propofol exerts anti-tumor effects by regulating miRNAs/lncRNAs. In different tumor types, propofol regulates the expression of miRNAs (proto and anti-oncogenes) and lncRNAs to regulate different tumorigenesis and development-related signaling pathways, genes, and proteins expressions, such as PI3K/AKT, Wnt/β-catenin, MMPs, P27, and P21, thus inhibiting the proliferation, invasion, and metastasis of tumor cells, reducing EMT process and promoting apoptosis.

TABLE 1 Propofol inhibits tumors by regulating miRNAs/lncRNAs.

MiRNA/ LncRNA	Regulation	Cancer types	Targets	Mechanism	Ref
MiRNA	**Downregulation**	Bladder cancer	miR-10b	miR-10b/HOXD10	Qi et al. (2019a)
		Lung cancer	miR-21-5p	miR-21-5p/MAPK10	Wu et al. (2020)
		Lung cancer	miR-372	Suppressed Wnt/β-catenin and mTOR signaling pathways	Sun and Gao, (2018)
		Breast cancer	miR-24	Upregulating p27 and cleaved caspase-3 expression	Yu et al. (2018)
		Breast cancer	miR-21	Suppressed Wnt/β-catenin and PI3K/AKT signaling pathways	Du et al. (2019)
	Upregulation	Gastric cancer	miR-195-5p	miR-195-5p/snail	Liu et al. (2020)
		Renal cancer	miR-363	Reduced the expression of Snail1	Shi et al. (2021)
		Lung cancer	miR-1284	Reduced the expression of FOXM1	Liu and Liu, (2018)
		Papillary thyroid carcinoma	miR-122	Reduced the expression of MMP2 and MMP9	Li et al. (2020a)
		Colorectal cancer	miR-124-3p	Reduced the expression of AKT3	Li et al. (2020b)
		Liver cancer	miR-219-5p	Suppression of GPC3-mediated Wnt/β-catenin signaling activation	Gong et al. (2019)
		Thyroid cancer	miR-141-3p	Suppressing SHH and PI3K/AKT signaling pathways *via* the miR-141-3p/BRD4 axis	Zhang et al. (2021a)
LncRNA		Ovarian cancer	lncRNA HOST2	Suppressing JAK2/STAT3 signaling pathway	Shen et al. (2021)
		Liver cancer	lncRNA CASC9	Suppressing Akt/mTOR signaling pathway	Chang et al. (2022)
		Colon cancer	lncRNA HOTAIR	Activating WIF-1 and Suppressing Wnt pathway	Zhang et al. (2020a)
		Glioma	lncRNA GAS5	Increasing the expression of P21, decreasing the expression of c-myc and GSTM3	Cheng et al. (2022)
		Oral squamous cell carcinoma	lncRNA GAS5	FoxO1-GAS5-miR-1297-GSK3b axis	Gao et al. (2019)
	Interactions between lncRNA and miRNA	Colorectal cancer	lncRNA HOXA11-AS	lncRNA HOXA11-AS/miR-let-7i/ABCC10	Ren and Zhang, (2020)
		Liver cancer	lncRNA HOXA11-AS	lncRNA HOXA11-AS/miR-4458	Song et al. (2020)
		Liver cancer	LncRNA NORAD	lncRNA NORAD/miR-556-3p/MIEN1	Liu et al. (2021a)
		Esophageal cancer	lncRNA TMPO-AS1	lncRNA TMPO-AS1/miR-498	Gao et al. (2020)

miR-21 expression, thereby reducing cell proliferation of breast cancer.

Some other miRNAs can also act as anti-oncogenes, antagonizing proto-oncogenes, inhibiting proliferation, differentiation, migration, and invasion, as well as promoting apoptosis of tumor cells. Studies show that propofol can inhibit tumor progression and improve prognosis by up-regulating anti-oncogenic miRNAs (Table 1). The epithelial-mesenchymal transition (EMT) is the conversion of polar epithelial cells into mesenchymal cells with the capacity for invasive metastasis, which is closely related to tumor development. Propofol can inhibit the EMT process by regulating miRNA. Liu et al. (2020) reported that propofol could inhibit snail expression by promoting the activity of miR-195-5p, thereby reducing EMT, migration and invasion of gastric cancer cells. Shi et al. (2021) revealed that propofol could upregulate the expression of miR-363 and decrease the expression of Snail1 to inhibit the EMT process of kidney cancer cells. In lung cancer (Liu and Liu, 2018), propofol inhibits the proliferation and EMT process of lung cancer cells by upregulating the expression of miR-1284. In papillary thyroid cancer, Li et al. (2020a) reported that propofol upregulated miR-122 expression to suppress the invasion and the EMT process of tumor cells. Similarly, Propofol can target several important signaling pathways in tumors through upregulation of tumor suppression-related miRNAs. In colorectal cancer (Li et al., 2020b), propofol suppressed the malignant properties of colorectal cancer cells by upregulating miR-124-3p expression

and downregulating AKT3 expression. Gong et al. (2019) found that miR-219-5p induced by propofol inhibited hepatocellular carcinoma proliferation and invasion by suppressing the Wnt/β-catenin signaling pathway mediated by GPC3. In thyroid cancer, propofol inhibited tumor cell proliferation, migration, and invasion by suppressing SHH and PI3K/AKT signaling pathways *via* the miR-141-3p/BRD4 axis (Zhang et al., 2021a). These studies indicate that miRNAs are pivotal therapeutic targets for tumors, and propofol can exert anti-tumor effects by regulating miRNAs expression, which further enriches the anti-tumor mechanism of propofol.

5.1.2 Propofol and lncRNAs

Long non-coding RNA (lncRNA) is a kind of functional RNA molecule that cannot be translated into protein. They have mRNA-like structures and complex mechanisms of action. Numerous studies have demonstrated that lncRNAs play an important role in tumorigenesis and development by regulating epigenetic transmission, cell cycle and cell differentiation. Propofol can target various signaling pathways by regulating lncRNA expressions in tumor cells, such as the Wnt pathway, JAK2/STAT3 pathway, and Akt/mTOR pathway (Table 1). Shen et al. (2021) showed that propofol could inhibit the proliferation, invasion and apoptosis of ovarian cancer cells through the lncRNA HOST2/JAK2/STAT3 axis. Chang et al. (2022) reported that propofol exerted an anti-tumor effect by down-regulating lncRNA CAS9, thereby inhibiting the Akt/mTOR signaling pathway in hepatocellular carcinoma. In colon cancer, propofol promoted cell apoptosis and inhibited distant metastasis through the activation of WIF-1 and inhibition of Wnt signaling pathway by negatively regulating the expression of lncRNA HOTAIR (Zhang et al., 2020a). GAS5 is a FoxO1-activated long noncoding RNA that can be regulated by propofol. In glioma, Cheng et al. (2022) showed that propofol inhibited the growth and migration of glioma cells through upregulation of the lncRNA GAS5. Gao et al. (2019) found that lncRNA GAS5 promoted the apoptosis of propofol-induced oral squamous cell carcinoma by regulating the miR-1297-GSK3β axis.

It is worth noting that both lncRNAs and miRNAs are non-coding functional RNAs with epigenetic regulation, which are closely related to the malignant biological characteristics of tumor cells. LncRNAs can bind to miRNAs and affect their functions, while miRNAs can regulate the stability of LncRNAs. Numerous studies have indicated that propofol could exert its anti-tumor activity by modulating the interaction between lncRNAs and miRNAs. Among which, lncRNA HOXA11-AS is currently more widely reported. Ren and Zhang (2020) reported that propofol could promote apoptosis in colorectal cancer cells by reducing the inhibitory effect of HOXA11-AS on miR-let-7i. In hepatocellular carcinoma, Song et al. (2020) revealed that propofol downregulated the expression of lncRNA HOXA11-AS to enhance the expression of miR-4458 and inhibit the malignant biological behavior of tumor cells. In addition, propofol can also regulate the interaction between other lncRNAs and miRNAs, such as lncRNA NORAD/miR-556-3p/Migration and Invasion Enhancer 1 (MIEN1) axis (Liu et al., 2021a) and lncRNA TMPO-AS1/miR-498 axis (Gao et al., 2020). Therefore, an in-depth study of the interaction between lncRNAs and miRNAs is essential to understanding the mechanism of the anti-tumor effects of propofol.

5.1.3 Attenuating the function of tumor stem cells

Tumor stem cells are cells in tumors that have the ability to self-renew and generate heterogeneous tumor cells, which play an important role in tumor survival, proliferation, metastasis and recurrence, and are also a cause of drug resistance (Richard et al., 2021). Recent studies have suggested that propofol could attenuate the function of tumor stem cells. Li et al. (2021) reported that propofol could inhibit the ability of bladder cancer stem cells to self-renew by targeting the hedgehog pathway, thereby inhibiting bladder tumor development and recurrence. In breast cancer, Zhang et al. (2019) found that propofol could reduce mammosphere formation in tumor stem cells *in vitro via* the PD-L1/Nanog pathway, thereby inhibiting cancer cell recurrence and metastasis. Another study showed that propofol inhibited the expression of circNOLC1 to attenuate tumor stem cell function *via* miR-365a-3p/STAT3 signaling pathway in breast cancer.

5.1.4 Regulation of metabolic reprogramming

Metabolic reprogramming is an important feature of tumors. To adapt to the rapid and continuous proliferation of tumor cells, various metabolic pathways such as aerobic glycolysis, lipid biosynthesis, and glutamine metabolism will be reprogrammed in tumor cells, the most prominent of which is aerobic glycolysis, namely the Warburg effect (Gao et al., 2021a). The Warburg effect refers to the fact that under aerobic conditions, glucose in normal cells is oxidized in the mitochondria, whereas in cancer cells glucose does not enter the mitochondria but remains converted to lactate (Lebelo et al., 2019). Several studies have indicated that propofol can influence the metabolic reprogramming of tumor cells, with inhibition of glycolysis being the most commonly reported. Hu et al. (2019) reported that propofol could downregulated GLUT1 and MPC expression by downregulating HIF-1α and upregulating PEDF, thereby interfering with cancer cell glucose metabolism and inhibiting tumor progression. N-methyl-D-aspartate receptor (NMDAR), which controls Ca^{2+} flux, has recently been found to be associated with propofol-induced inhibition of glycolysis. Qi et al. found that (Qi et al., 2019b) propofol reduced intracellular Ca^{2+} concentration, CaMKII, AKT phosphorylation, and HIF-1α expression by inhibiting NMDA receptors, which in turn inhibited tumor and endothelial cell glycolysis levels and ultimately reduced tumor cell adhesion and metastasis. Chen

et al. (2018) found that propofol inhibited aerobic glycolysis by inactivating the NMDAR-CAMKII-ERK signaling pathway in colorectal cancer. Circular RNAs (circRNAs) are a class of conserved non-coding RNAs with a closed-loop structure that is widely found in a variety of eukaryotes and are produced in higher eukaryotes by reverse splicing of multiple protein-coding genes through exons, which play an important modulatory role in tumorigenesis and progression. Propofol could inhibit glycolysis in tumor cells *via* the regulation of the circRNAs expression. Qu et al. (2022) found that propofol inhibited glycolysis in ovarian tumors by inhibiting the circular RNA-zinc finger RNA binding protein (circ-ZFR)/mir-212-5p/superoxide dismutase 2 (SOD2) axis. In lung cancer, propofol disrupted cell carcinogenesis and aerobic glycolysis by regulating circRNA transcriptional adaptor 2A (circTADA2A)/miR-455-3p/forkhead box M1 (FOXM1) axis (Zhao et al., 2020).

The presence of lipid-metabolism-related molecules and signaling cascades may contribute to tumor progression. However, no systematic studies have been published showing the specific mechanisms by which propofol regulates the reprogramming of lipid metabolism in tumor cells, but some basic and clinical researches reveal that propofol indeed affects lipid metabolic processes *in vivo*. Zhang et al. (2022a) found that propofol could promote glucagon-regulated gluconeogenesis and accelerate fatty acid beta-oxidation *via* the CREB/PGC-1α signaling pathway. A metabolomics study found that propofol significantly increased the ratio of saturated fatty acids to total fatty acids (SFA_FA), very large VLDL free cholesterol content (XL_VLDL_FC), and very large HDL triglyceride content, and slightly increased serum total triglyceride levels (Nummela et al., 2022). The above studies provide a new strategy for propofol to exert anti-tumor effects by regulating metabolic reprogramming.

5.2 Pro-tumor effect

Currently, numerous studies have found that propofol could inhibit the proliferation, differentiation, migration and invasion of tumor cells, mainly exerting anti-tumor effects. However, some studies have also confirmed that propofol can also promote tumor cell proliferation and migration in certain tumor types under certain conditions. In oral squamous carcinoma, propofol (Li et al., 2020c) promoted the migration of tumor cells *via* the upregulation of the SNAI1 expression. Another study in breast cancer also confirmed that propofol could induce the proliferation of breast cancer cells *via* downregulation of p53 protein and promote the invasion and migration of tumor cells *via* the activation of the Nrf2 signaling pathway (Meng et al., 2017). The adhesion of circulating tumor cells to vascular endothelial cells is a crucial factor in the development of solid tumor metastasis. Liu et al. (2021b) found that propofol could activate the GABA receptor in tumor cells and reduce TRIM21, thereby increasing the expression of the cell adhesion-related protein Src and enhancing the adhesion and extension of tumor cells to vascular endothelial cells, thus promoting tumor metastasis in the lung of mouse models. Therefore, an in-depth investigation into the mechanism of propofol-promoting tumor cell proliferation and migration will further enrich the pharmacological effects and the scope of application of propofol, and also raises more attention to the selection of propofol in clinical practice.

5.3 Regulation of drug resistance

Due to the loss of the best surgical opportunity, chemotherapy often becomes the main treatment method to prolong the survival and improve the life quality of patients with unresectable distant metastases. In recent years, the diversity of chemotherapeutic drugs and treatment options has improved the survival rate of patients with advanced-stage cancer. However, the emergence of chemo-resistance is still a great challenge in the process of chemotherapy (Sadri Nahand et al., 2021). Studies have found that the use of propofol can regulate the chemo-resistance of tumors and improve the therapeutic effect of a variety of chemotherapy drugs. Several platinum-based chemotherapeutic agents, such as cisplatin (DDP) and oxaliplatin, have become the first-line chemotherapeutic agents for many malignant tumors based on the abilities to block DNA replication and inhibit mitosis. Huang et al. (2020a) found that propofol could enhance the DDP sensitivity of lung cancer cells *via* inhibition of the Wnt/β-catenin signaling pathway. According to Zhang et al. (2020b), propofol inhibited autophagy, promoted cisplatin sensitivity, and suppressed tumor progression *via* modulating the lncRNA MALAT1/miR-30e/ATG5 axis in gastric cancer. Sun et al. (2020) indicated that propofol restrained DDP resistance by downregulating miR-374a and upregulating FOXO1. In liver cancer, it is shown that propofol enhanced the lethality of cisplatin on tumor cells by up-regulating miR-195-5p (Gao and Zhang, 2022). Paclitaxel (PTX) and docetaxel, which are taxane-based chemotherapy drugs, boost the polymerization of microtubule proteins and prevent their depolymerization in order to block the mitotic process and induce apoptosis, which are used together with other anti-cancer drugs in the treatment of a variety of tumors. Yang et al. (2021) showed that propofol enhanced the sensitivity of prostate cancer cells to PTX by reducing the expression of HOTAIR, which promoted apoptosis of cancer cells. In prostate cancer, propofol also reversed hypoxia-induced docetaxel resistance by inhibiting HIF-1α to prevent epithelial-mesenchymal transition (Qian et al., 2018). 5-Fluorouracil (5-FU) is an anti-metabolic chemotherapeutic agent that inhibits the synthesis of DNA and RNA. Yang et al. (2022) found that propofol-induced apoptosis ameliorated 5-FU resistance in oral squamous cell carcinoma cells by the reduction of amphiregulin expression and secretion. Considering that propofol can modulate glucose

and lipid metabolism in tumor cells, we speculate that it may modulate resistance to anti-metabolic chemotherapeutic drugs *via* metabolic pathways.

In recent years, the emergence of new therapeutic agents such as targeted therapy and immunotherapy has provided new strategies for the treatment of malignant tumors. Trastuzumab, a monoclonal antibody against Her-2, is a valuable targeted therapeutic agent. Tian et al. (2020) found that propofol could epigenetically regulate trastuzumab resistance *via* the IL-6/miR-149-5p axis in breast cancer. However, no studies have been reported on whether propofol modulates the sensitivity of immunotherapy drugs, and this deserves further investigation. The above studies suggest that propofol plays an important role in modulating systemic treatment resistance, which will provide new therapeutic strategies for the clinical reversal of drug resistance in cancer treatment.

6 Effect of propofol on tumor microenvironment

The tumor microenvironment (TME) can be described as a highly complex system, which is composed of tumor cells, interstitial cells around tumor cells (such as immune cells, fibroblasts, adipocytes, and endothelial cells), extracellular matrix (ECM), and signal molecules (such as cytokines and chemokines). The two-way interaction between tumor cells and TME affects the tumorigenesis and progression at multiple levels. Tumor cells can change TME to produce a suitable living environment, and TME can in turn affect the behavior of tumor cells (Deepak et al., 2020). With the increasing understanding of the interaction between tumor cells and TME, TME may become the target of novel drugs (Xiao and Yu, 2021). Studies have shown that propofol can play a role in reshaping the tumor microenvironment, including anti-angiogenesis, regulation of immunity, reduction of inflammation and remodeling of the ECM, indirectly affecting the biological characteristics of tumor cells (Figure 5).

6.1 Anti-angiogenesis

Tumor growth and metastasis are inseparable from the formation of neovascularization. When the tumor volume continues to increase and the center of tumor necrosis occurs as a result of hypoxia, tumor cells will release pro-angiogenic factors to stimulate peripheral neovascularization (Dzhalilova and Makarova, 2021). Blood circulation not only provides the necessary oxygen and nutrients for tumor growth but also acts as an important way for tumor cells to metastasize (Wang et al., 2021a). Currently, anti-angiogenesis has become an important targeted therapy strategy for maximum disease control of unresectable metastatic solid tumors. More and more studies have indicated that propofol can suppress angiogenesis and play an anti-tumor role. A clinical trial found that total intravenous anesthesia with propofol during radical lung cancer surgery significantly reduced serum concentrations of VEGF and other angiogenesis-related factors in patients, favoring the anti-angiogenesis effect (Sen et al., 2019). Wang et al. (2021b) found that propofol could inhibit tumor angiogenesis by targeting VEGF/VEGFR and mTOR/eIF4E signaling, thus exerting anti-cancer activity. In human esophageal cancer EC-1 cells. Guo et al. (2015) demonstrated that propofol downregulated S100A4 expression levels to inhibit proliferation, invasion, and angiogenesis, as well as promote apoptosis. Chen et al. (2017) found that propofol could inhibit the expression of VEGF in pancreatic cancer cells *in vitro* and *in vivo*, possibly by inhibiting the NMDA receptor. Hypoxia is an important feature of the tumor microenvironment and is an important cause of tumor neovascularization. When the oxygen partial pressure of the tumor microenvironment is reduced, hypoxia-inducible factors (HIF) are activated to regulate primary transcriptional adaptation to the hypoxic microenvironment (Li et al., 2020d). Yang et al. (2017) found that HIF-1α was upregulated at both the gene and protein levels in LPS-treated NSCLC tumor cells compared to normal tissue. Propofol could inhibit the upregulation of HIF-1α expression and reactive oxygen species (ROS) production in NSCLC tumor cells induced by LPS, suppressing the expression of VEGF, promoting tumor cell apoptosis as well as inhibiting invasion and metastasis. The above studies give strong support for the anti-angiogenic effect of propofol and its anti-cancer activity, providing new ideas on the effects and mechanisms of propofol on tumor neovascularization, as well as providing more options for the use of propofol and targeted tumor angiogenesis therapy.

6.2 Regulation of immunity

The development of the tumor is closely related to the immune microenvironment, which is often in an immunosuppressive status providing a favorable environmental basis for tumor growth and proliferation, immune escape, and acquired drug resistance (Pansy et al., 2021). Some studies have shown that propofol increases immune cell infiltration in the immune microenvironment and is closely associated with NK cell activity. Zhou et al. (2018) found that the use of propofol in esophageal cancer surgery can significantly enhance the toxicity of NK cells to cancer cells and enhance the killing activity of NK cells. Liu et al. (2018) collected 20 colorectal patients and isolated NK cells by screening and found that the expression of NK cell killing effector molecules was significantly increased in colorectal patients after treatment with propofol, indicating that propofol has the effect of

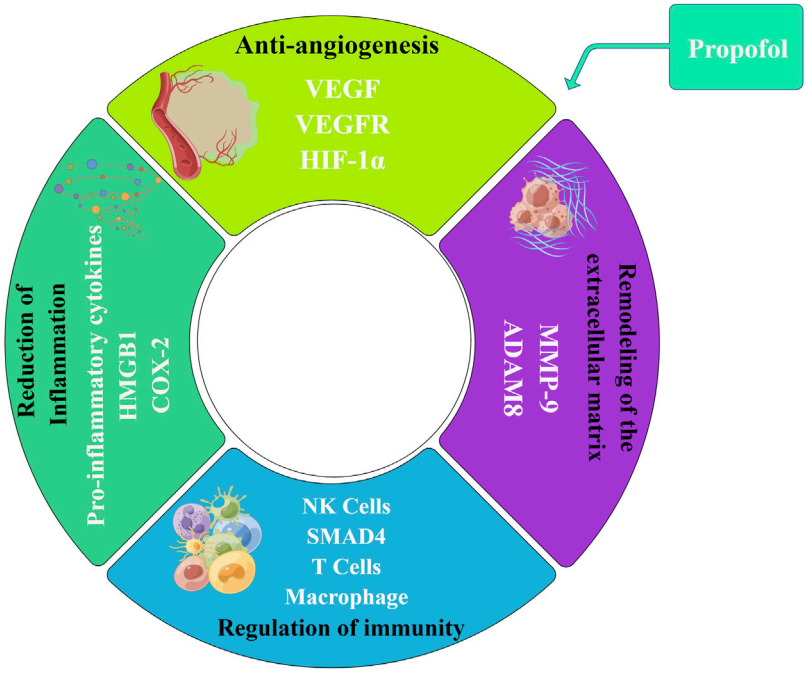

FIGURE 5
Effect of propofol on the tumor microenvironment. Propofol can play a role in reshaping the tumor microenvironment, including anti-angiogenesis, regulation of immunity, reduction of inflammation, and remodeling of the extracellular matrix, indirectly affecting the biological characteristics of tumor cells. Propofol can inhibit the expression of VEGF/VEGFR and play an anti-angiogenesis role. Propofol regulates immunity by affecting the infiltration and activity of a variety of immune cells, such as T cells, NK cells, and macrophages. Propofol can reduce inflammation via inhibiting the release of pro-inflammatory cytokines and targeting the expression of HMGB1 and COX-2 inflammatory proteins. In addition, propofol can target the expression of MMP-9 and ADAM8 to remodel the tumor extracellular matrix.

enhancing NK cell killing activity. Another study compared propofol with sevoflurane anesthesia and showed that propofol could enhance the cytotoxicity of NK cells by up-regulating SMAD4 in gastric cancer surgery (Ai and Wang, 2020). However, there is no consensus on whether propofol can improve or reverse microenvironmental immunosuppression. By performing an immunoassay on 201 patients who randomly received propofol or sevoflurane anesthesia, Oh et al. (2018) found no significant differences in the infiltration levels of natural killer cells, cytotoxic T cells, cytokines, neutrophils, and lymphocytes between the two groups, indicating that propofol has few effects on the tumor immune microenvironment. Subsequently, the team conducted a prospective randomized trial of propofol on immune cell expression profiles in colorectal cancer patients. The results showed that propofol was not superior to sevoflurane in the alleviation of the suppression of immune cells in colorectal cancer surgery (Oh et al., 2022). Another randomized controlled trial on the effect of volatile anesthesia (sevoflurane) *versus* intravenous anesthesia (propofol) on immunosuppression in renal cancer also showed that propofol was not effective in improving the immunosuppressive state of the tumor microenvironment (Efremov et al., 2020). Therefore, the regulatory effects of propofol on the immune system, including immune cell infiltration and expression of immune checkpoints, are still unclear and need to be further investigated, which will enrich the immunomodulatory role of propofol and provide a new direction for tumor immunotherapy.

6.3 Reduction of inflammation

Inflammatory infiltrating cells interact with tumor cells through the release of mediators such as pro-inflammatory cytokines, constituting a complex tumor inflammatory microenvironment (McLaughlin et al., 2020). A variety of signaling pathways are activated by inflammatory stimulation, leading to an increase in oxidative enzyme activity, resulting in DNA and mitochondrial damage, and, ultimately, causing tumorigenesis (Atretkhany et al., 2016).

Studies have confirmed that propofol inhibits the release of pro-inflammatory cytokines and reduces inflammation in microenvironment. In the non-tumor tissue microenvironment, Liu et al. (2017a) showed that propofol attenuates the upregulation of pro-inflammatory cytokines in

microglia by suppressing the NF-κB/p38 MAPK pathway activation. Ma et al. (2018) found that propofol increased ABCA1 expression and inhibited the production of pro-inflammatory cytokines in a LncRNA LOC286367-dependent manner. In the colorectal cancer microenvironment, Gao et al. (2021b) found that propofol might reduce the secretion of inflammatory cytokines by suppressing the activation of the NF-κB pathway *via* downregulating miR-155. The above study suggests that propofol might be used as a novel therapeutic strategy to alleviate the chronic inflammatory stimulation state of the tumor microenvironment.

The high mobility group protein B1 (HMGB1) is a well-conserved, highly adhesive nuclear protein involved in maintaining the nucleosome integrity and facilitating gene transcription, which is now considered to be an important late-stage inflammatory factor and is of greater clinical importance than early-onset rapid inflammatory factors such as TNF and IL-1 (Kim and Lee, 2020). Targeting HMGB1 is an effective strategy to improve the tumor inflammatory microenvironment. Li et al. (2020e) found that in papillary thyroid cancer, propofol decreased HMGB1 expression and inhibited tumor progression through downregulation of ANRIL. Jia et al. (2017) found that propofol could down-regulate LPS-stimulated HMGB1 expression in RAW 264.7 cell supernatants and reduce the releasing of LPS-stimulated IL-6, IL-8, and TNF-α.

Cyclooxygenase (COX), also known as prostaglandin endooxygenase reductase, is the key enzyme that catalyzes the conversion of arachidonic acid to prostaglandins (Timur et al., 2020). It consists of two isozymes, COX-1 and COX-2. Among them, COX-2 is inducible, which is the key to triggering the inflammatory response. Li et al. (2018) reported that propofol downregulates COX-2 expression to suppress proliferation and invasion of MCF-7 cells.

In conclusion, propofol can reduce inflammation in the tissue microenvironment by inhibiting the production and release of pro-inflammatory cytokines and targeting multiple inflammation-related proteins, which will lay a theoretical foundation for propofol to inhibit tumorigenesis by improving the tumor inflammatory microenvironment.

6.4 Remodeling of the extracellular matrix

The extracellular matrix (ECM) is a macromolecular substance that is synthesized and secreted by cells and distributed on the surface of cells or between cells, consisting of the basement membrane (BM) and the intercellular matrix. The ECM is linked to the inside and outside of the cell by membrane integrins, which involve cell survival, cell shape determination, cell differentiation modulation and cell migration control (Winkler et al., 2020).

Metalloproteinases (MMPs) are zinc-dependent endopeptidases that degrade almost all protein components of the extracellular matrix and disrupt the histological barrier. They are closely associated with tumor invasion and metastasis, and are an important biological marker for tumor invasion and metastasis (Dofara et al., 2020). Xu et al. (2013) found that propofol significantly downregulated the expression level of MMP-9 in esophageal cancer Eca-109 cells and inhibited invasion and metastasis.

The disintegrin and metalloprotease (ADAM) family are multifunctional proteins, consisting of eight structural domains including the metalloproteinase domain and deintegrin domain, which can be divided into membrane-anchored and secreted types (Camodeca et al., 2019). ADAM is closely related to tumor progression and is engaged in critical pathophysiological processes such as extracellular matrix degradation, cell signaling, and regulation of cell adhesion (Jones et al., 2016). In pancreatic cancer (Yu et al., 2020), propofol was found to downregulate the expression of ADAM8 and suppress tumor cells proliferation, invasion and migration. Yu et al. (2019) found that propofol could restrain the invasive and metastasis of tumor cells by upregulating miR-328 expression and suppressing the expression level of its target ADAM8 in pancreatic cancer.

7 Studies of propofol in animal tumor models

Advances in biomedical research often rely on the use of animal models as the basis for both experimental and clinical hypotheses. Animal studies can fill the gap between *in vivo* and clinical research. Propofol can not only affect the biological characteristics of tumor cells *in vitro*, but also play a role in animal tumor models. In hepatocellular carcinoma, Liu et al. (2017b) found that propofol could inhibit tumor growth and protein expression of MMP-2 and VEGF in xenograft model in a dose-dependent manner. Propofol can also activate AMPK to induce autophagy and thereby inhibit hepatocarcinogenesis and tumor volume in a xenograft mouse tumor model (Wang et al., 2020). Li et al. (2020f) conducted a study about the effect of propofol and sevoflurane on lung metastases in both syngeneic murine 4T1 and xenograft human MDA-MB-231 breast cancer models. For a long time, there is a lack of validated preclinical models for anesthesia studies, most of which do not use anesthesia itself as the primary endpoint to explore the effects of anesthesia on the tumor itself, the microenvironment and the postoperative prognosis. It is worth mentioning that Dubowitz et al. (2021) have successfully replicated key steps in clinical drug administration using propofol-TIVA anesthesia in a mouse model of mastectomy for breast cancer. The successful construction of this model will be of great help in studying

TABLE 2 The effects of propofol on postoperative prognosis of tumors.

Study type	Cancer type	Research design	Outcomes	Ref
Retrospective	Gastric cancer	Propofol vs. Sevoflurane	Improved survival	Zheng et al. (2018)
Retrospective	Gastric cancer	Propofol vs. Desflurane	Improved survival and reduced the risk of recurrence	Huang et al. (2020b)
Retrospective	Hepatocellular carcinoma	Propofol vs. Inhalation anesthetics	Decreased 2-year recurrence	Koo et al. (2020)
Retrospective	Hepatocellular carcinoma	Propofol vs. Desflurane	Better survival	Lai et al. (2019a)
Retrospective	Hepatocellular carcinoma	Propofol vs. Sevoflurane	Reduced mortality and recurrence	Meng et al. (2020)
Retrospective	Intrahepatic cholangiocarcinoma	Propofol vs. Desflurane	Improved survival and reduced the recurrence	Lai et al. (2019b)
Retrospective	Colon cancer	Propofol vs. Desflurane	Better survival	Wu et al. (2018)
Retrospective	Esophageal cancer	Propofol vs. Inhalation anesthetics	Better overall and recurrence-free survival	Jun et al. (2017)
Retrospective	Pancreatic cancer	Propofol vs. Desflurane	Improved survival	Lai et al. (2020a)
Prospective	Bladder cancer	Propofol vs. Sevoflurane	Improved disease-free Survival	Guerrero Orriach et al. (2020)
Retrospective	Prostate cancer	Propofol vs. Desflurane	Improved overall survival	Lai et al. (2020b)
Retrospective	Lung cancer	Propofol vs. Inhalation anesthetics	Better prognosis	Hayasaka et al. (2021)
Retrospective	Glioblastoma	Propofol vs. Desflurane	Better survival	Huang et al. (2021)
Retrospective	Breast cancer	Propofol vs. Sevoflurane	Better survival	Enlund et al. (2020)
Retrospective	Breast cancer	Propofol vs. Sevoflurane	Reduced local regional recurrence	(Zhang et al., 2021b), (Zhang et al., 2022b)
Retrospective	Breast cancer	Propofol vs. Desflurane	No difference	Huang et al. (2019)
Retrospective	Breast cancer	Propofol vs. Inhalation anesthetics	No difference	Yoo et al. (2019)
Retrospective	Breast cancer	Propofol vs. Sevoflurane	No difference	Shiono et al. (2020)
Prospective	Breast cancer	Propofol vs. Sevoflurane	No difference	Yan et al. (2018)
Retrospective	Gastric cancer	Propofol vs. Inhalation anesthetics	No difference	Oh et al. (2019)
Retrospective	Digestive tract tumor	Propofol vs. Inhalation anesthetics	No difference	Makito et al. (2020)
Retrospective	Glioblastoma	Propofol vs. Sevoflurane	No difference	Schmoch et al. (2021)
Retrospective	Glioma	Propofol vs. Sevoflurane	No difference	Dong et al. (2020)

the prognosis and mechanisms of action of anesthesia on patients with different cancer types.

8 Effect of propofol on postoperative prognosis

Perioperative factors such as inflammatory stimulation and metabolic changes can affect the prognosis of a tumor patient. In recent years, more and more attention has been paid to intraoperative anesthesia management, indicating that the different methods of anesthesia and drugs used have a significant impact on the prognosis of the tumor after surgery. Studies have shown that the use of propofol during operation is closely related to the disease-free survival rate and overall survival rate of various types of tumor patients. Therefore, the author combs and summarizes the clinical studies in the recent 5 years, hoping to lay a foundation for further study on the effect of propofol on postoperative prognosis (Table 2).

Several retrospective clinical researches have shown that the use of propofol in anesthesia in tumor surgery can significantly improve the prognosis of patients. Propofol may improve the survival rate and reduce the recurrence and metastasis of patients with digestive tumors. In gastric cancer, Zheng et al. (2018) found that propofol-based anesthesia was correlated with better prognosis of patients undergoing gastrectomy. Huang et al. (2020b) found that propofol significantly improved the survival rate and reduced the risk of recurrence and metastasis in gastric cancer patients after a 5-year follow-up. In liver cancer, Koo et al. (2020) found that propofol can reduce the 2-year recurrence rate of early hepatocellular carcinoma, and significantly improve the prognosis of patients. Through a retrospective study on propofol and desflurane anesthesia in hepatectomy, Lai et al. (2019a) proved that propofol anesthesia is associated with a better prognosis. Meng et al. (2020) proved that propofol could significantly reduce

the postoperative mortality and recurrence rate of hepatocellular carcinoma. Another study found that propofol could improve the postoperative survival rate and reduce the recurrence of intrahepatic cholangiocarcinoma (Lai et al., 2019b). Consistent with the above conclusion, the survival rate of propofol total intravenous anesthesia is higher than that of desflurane anesthesia in colon cancer surgery (Wu et al., 2018). Similarly, Jun et al. (2017) found that a better postoperative prognosis of esophageal cancer is closely related to propofol-based intravenous anesthesia. In pancreatic cancer, a retrospective analysis shows that propofol anesthesia can improve the postoperative survival rate of pancreatic cancer compared with desflurane anesthesia (Lai et al., 2020a). Propofol can also improve the prognosis of urinary tumors. Guerrero Orriach et al. (2020) found that compared with inhaled anesthetics and opioid analgesia, propofol intravenous anesthesia can improve the disease-free survival rate of patients with bladder cancer undergoing radical cystectomy. In radical prostatectomy for prostate cancer, propofol-based anesthesia also had a better survival rate than desflurane anesthesia (Lai et al., 2020b). Recently, Hayasaka et al. (2021) found that the use of propofol in early lung cancer surgery is correlated with a improved survival rate. Huang et al. (2021) found that propofol anesthesia was associated with better survival than desflurane anesthesia in glioblastoma surgery. In breast cancer, a multicenter retrospective analysis of 6,305 Swedish patients performed by Enlund et al. (2020) demonstrated that propofol improved the postoperative prognosis of patients better compared to sevoflurane. Zhang et al. (2021b); Zhang et al. (2022b) compared local-regional recurrence (LRR) in patients with invasive ductal carcinoma (IDC) under propofol-based paravertebral block-regional anesthesia (PB-RA) with LRR in patients undergoing inhalational general anesthesia (INHA-GA) with sevoflurane. The results suggested that propofol may be beneficial in reducing LRR in breast IDC patients compared to sevoflurane. The above studies suggest that propofol-based total intravenous anesthesia may contribute to better postoperative prognosis in many types of tumors.

However, some studies have found that intravenous anesthesia with propofol does not improve the postoperative prognosis of tumor patients compared with other volatile anesthesia. In breast cancer, Huang et al. (2019), Yoo et al. (2019), and Shiono et al. (2020) found that propofol anesthesia did not affect postoperative prognosis and survival of patients by retrospective analysis. A prospective, randomized and controlled study found that propofol/remifentanil total intravenous anesthesia was effective in inhibiting surgically induced VEGF-C release from breast cancer but did not appear to have a beneficial effect on short-term recurrence rates compared to sevoflurane inhalation anesthesia (Yan et al., 2018). In gastric cancer, Oh et al. (2019) found that propofol-based total intravenous anesthesia did not reduce overall or cancer-related mortality 1 year after surgery compared with inhalation anesthesia. In addition, Makito et al. (2020) found that propofol could not significantly improve the overall survival rate and recurrence-free survival rate of patients undergoing digestive tract tumor surgery (selective esophagectomy, gastrectomy, hepatectomy, cholecystectomy, pancreatectomy, colectomy, and rectal cancer surgery). Similarly, propofol-based intravenous anesthesia has no significant effect on the postoperative prognosis of glioblastoma (Schmoch et al., 2021) and glioma [139] in patients with nervous system tumors.

At present, the clinical research on the effect of propofol on the postoperative prognosis of tumors is mainly focused on retrospective analysis, which covers a wide range of tumor types, especially breast cancer. However, due to the limited sample size, the defects of retrospective study analysis, and the heterogeneity of clinical samples, the view that propofol can improve the postoperative prognosis and reduce recurrence and metastasis is worth further exploration and research. The conclusion is not yet consistent. We hope that in the future there will be more multi-center, large-scale prospective clinical trials with large samples to provide more theoretical evidence on whether propofol affects the postoperative prognosis of tumor patients and more precise guidance on the choice of anesthetic drugs in clinical practice.

9 Conclusion and prospect

Propofol is a commonly used clinical agent for total intravenous anesthesia. In this review, the chemical properties, pharmacokinetics, clinical application and limitations and studies in animal tumor models of propofol were summarized, as well as the effects on the biological characteristics of tumors and the reshaping of the tumor microenvironment were discussed in detail. *In vitro* and *in vivo* studies have shown that propofol exerts anti-tumor effects through mechanisms of action such as regulation of microRNA, lncRNA, stem cell function, and metabolic reprogramming. For some specific types of tumors or conditions, propofol can promote malignant biological behavior of tumors through a variety of mechanisms. Chemotherapy is an important treatment for malignant tumors, and chemo-resistance is one of the difficulties in oncology research and poor prognosis. Propofol regulates resistance to many common chemotherapeutic agents such as cisplatin, paclitaxel, and 5-fluorouracil, which provides a new strategy for reversing drug resistance. For the reshaping of the tumor microenvironment, propofol can act through anti-angiogenesis, regulation of immunity, reduction of inflammation, and remodeling of the ECM.

However, at present, the interaction between propofol and tumors is contradictory, and the conclusion is not yet consistent. Most studies found that propofol could suppress tumor proliferation, differentiation, metastases and promote apoptosis, and it is related to good postoperative prognosis. Nevertheless, some studies have demonstrated that propofol could promote the proliferation and migration of certain types of tumor cells, and it does not significantly improve the postoperative prognosis. Therefore, it is very important to clarify the mechanism of propofol on the occurrence and development of a malignant

tumor and the relationship between propofol and postoperative prognosis. Meanwhile, we hope that there will be more large-scale prospective clinical trials with the multi-center, multi-sample, and multi-level to further explore the internal relationship between propofol and malignant tumors and guide more accurate intraoperative anesthesia management. Finally, it is worth emphasizing that this is a narrative review and the studies listed are not exhaustive, such as miRNA and lncRNA studies.

Author contributions

Conceptualization:JS and XZ; Funding acquisition:JS and LZ; Investigation and Literature collection: XZ, YS, and SL;Supervision: JS and LZ; Visualization: XZ and CD; Writing—original draft: XZ; Writing—review and editing:SZ, LZ and JS.

Funding

This work was supported by the National Nature Science Foundation of China (NSFC) (Grant No. 81871984), the National Nature Science Foundation of China(NSFC)(GrantNo.82273344) and Research Physician Project of Shanghai Jiao Tong University School of Medicine (Grant No. 826304).

Conflict of interest

The authors declare that the research was conducted in the absence of any commercial or financial relationships that could be construed as a potential conflict of interest.

Publisher's note

All claims expressed in this article are solely those of the authors and do not necessarily represent those of their affiliated organizations, or those of the publisher, the editors and the reviewers. Any product that may be evaluated in this article, or claim that may be made by its manufacturer, is not guaranteed or endorsed by the publisher.

References

Ai, L., and Wang, H. (2020). Effects of propofol and sevoflurane on tumor killing activity of peripheral blood natural killer cells in patients with gastric cancer. *J. Int. Med. Res.* 48 (3), 300060520904861. doi:10.1177/0300060520904861

Anderson, B. J., and Bagshaw, O. (2019). Practicalities of total intravenous anesthesia and target-controlled infusion in children. *Anesthesiology* 131 (1), 164–185. doi:10.1097/ALN.0000000000002657

Atretkhany, K. N., Drutskaya, M. S., Nedospasov, S. A., Grivennikov, S. I., and Kuprash, D. V. (2016). Chemokines, cytokines and exosomes help tumors to shape inflammatory microenvironment. *Pharmacol. Ther.* 168, 98–112. doi:10.1016/j.pharmthera.2016.09.011

Budakoti, M., Panwar, A. S., Molpa, D., Singh, R. K., Büsselberg, D., Mishra, A. P., et al. (2021). Micro-RNA: The darkhorse of cancer. *Cell. Signal.* 83, 109995. doi:10.1016/j.cellsig.2021.109995

Camodeca, C., Cuffaro, D., Nuti, E., and Rossello, A. (2019). ADAM metalloproteinases as potential drug targets. *Curr. Med. Chem.* 26 (15), 2661–2689. doi:10.2174/0929867325666180326164104

Chang, Q., Wu, J., An, Y., Liu, H., and Sun, Y. (2022). Propofol suppresses proliferation, migration, invasion, and tumor growth of liver cancer cells via suppressing cancer susceptibility candidate 9/phosphatase and tensin homolog/AKT serine/threonine kinase/mechanistic target of rapamycin kinase axis. *Hum. Exp. Toxicol.* 41, 9603271211065972. doi:10.1177/09603271211065972

Chen, X., Wu, Q., Sun, P., Zhao, Y., Zhu, M., and Miao, C. (2018). Propofol disrupts aerobic glycolysis in colorectal cancer cells via inactivation of the NMDAR-CAMKII-ERK pathway. *Cell. Physiol. biochem.* 46 (2), 492–504. doi:10.1159/000488617

Chen, X., Wu, Q., You, L., Chen, S., Zhu, M., and Miao, C. (2017). Propofol attenuates pancreatic cancer malignant potential via inhibition of NMDA receptor. *Eur. J. Pharmacol.* 795, 150–159. doi:10.1016/j.ejphar.2016.12.017

Cheng, Y., Zheng, L., Yang, C., Zhang, W., and Wang, H. (2022). Propofol inhibits proliferation and migration of glioma cells by up-regulating lncRNA GAS5. *Toxicol. Vitro.* 80, 105321. doi:10.1016/j.tiv.2022.105321

Corrado, M. J., Kovacevic, M. P., Dube, K. M., Lupi, K. E., Szumita, P. M., and DeGrado, J. R. (2020). The incidence of propofol-induced hypertriglyceridemia and identification of associated risk factors. *Crit. Care Explor.* 2 (12), e0282. doi:10.1097/CCE.0000000000000282

Cuk, P., Simonsen, R. M., Komljen, M., Nielsen, M. F., Helligsø, P., Pedersen, A. K., et al. (2021). Improved perioperative outcomes and reduced inflammatory stress response in malignant robot-assisted colorectal resections: A retrospective cohort study of 298 patients. *World J. Surg. Oncol.* 19 (1), 155. doi:10.1186/s12957-021-02263-w

Deepak, K., Vempati, R., Nagaraju, G. P., Dasari, V. R., S, N., Rao, D. N., et al. (2020). Tumor microenvironment: Challenges and opportunities in targeting metastasis of triple negative breast cancer. *Pharmacol. Res.* 153, 104683. doi:10.1016/j.phrs.2020.104683

Dinis-Oliveira, R. J. (2018). Metabolic profiles of propofol and fospropofol: Clinical and forensic interpretative aspects. *Biomed. Res. Int.* 2018, 6852857. doi:10.1155/2018/6852857

Dofara, S. G., Chang, S. L., and Diorio, C. (2020). Gene polymorphisms and circulating levels of MMP-2 and MMP-9: A review of their role in breast cancer risk. *Anticancer Res.* 40 (7), 3619–3631. doi:10.21873/anticanres.14351

Doğanay, F., Ak, R., Alışkan, H., Abut, S., Sümer, E., and Onur, Ö. (2018). The effects of intravenous lipid emulsion therapy in the prevention of depressive effects of propofol on cardiovascular and respiratory systems: An experimental animal study. *Med. Kaunas. Lith.* 55 (1), 1. doi:10.3390/medicina55010001

Dong, J., Zeng, M., Ji, N., Hao, S., Zhou, Y., Gao, Z., et al. (2020). Impact of anesthesia on long-term outcomes in patients with supratentorial high-grade glioma undergoing tumor resection: A retrospective cohort study. *J. Neurosurg. Anesthesiol.* 32 (3), 227–233. doi:10.1097/ANA.0000000000000588

Du, Q., Zhang, X., Zhang, X., Wei, M., Xu, H., and Wang, S. (2019). Propofol inhibits proliferation and epithelial-mesenchymal transition of MCF-7 cells by suppressing miR-21 expression. *Artif. Cells Nanomed. Biotechnol.* 47 (1), 1265–1271. doi:10.1080/21691401.2019.1594000

Dubowitz, J. A., Jost-Brinkmann, F., Ziegler, A. I., Gillis, R. D., Riedel, B., and Sloan, E. K. (2021). An *in vivo* mouse model of total intravenous anesthesia during cancer resection surgery. *J. Vis. Exp.* 2021 (172), 62747. doi:10.3791/62747

Dzhalilova, D. S., and Makarova, O. V. (2021). HIF-dependent mechanisms of relationship between hypoxia tolerance and tumor development. *Biochemistry.* 86 (10), 1163–1180. doi:10.1134/S0006297921100011

Eden, C., Esses, G., Katz, D., and DeMaria, S., Jr (2018). Effects of anesthetic interventions on breast cancer behavior, cancer-related patient outcomes, and postoperative recovery. *Surg. Oncol.* 27 (2), 266–274. doi:10.1016/j.suronc.2018.05.001

Efremov, S. M., Kozireva, V. S., Moroz, G. B., Abubakirov, M. N., Shkoda, O. S., Shilova, A. N., et al. (2020). The immunosuppressive effects of volatile versus intravenous anesthesia combined with epidural analgesia on kidney cancer: A pilot randomized controlled trial. *Korean J. Anesthesiol.* 73 (6), 525–533. doi:10.4097/kja.19461

Enlund, M., Berglund, A., Ahlstrand, R., Walldén, J., Lundberg, J., Wärnberg, F., et al. (2020). Survival after primary breast cancer surgery following propofol or sevoflurane

general anesthesia-A retrospective, multicenter, database analysis of 6305 Swedish patients. *Acta Anaesthesiol. Scand.* 64 (8), 1048–1054. doi:10.1111/aas.13644

Feng, C., Qian, D., and Chen, C. (2021). A meta-analysis and systematic review of propofol on liver ischemia-reperfusion injury protection during hepatocellular carcinoma anesthesia surgery. *Ann. Palliat. Med.* 10 (6), 6726–6735. doi:10.21037/apm-21-1242

Gao, C., Ren, C., Liu, Z., Zhang, L., Tang, R., and Li, X. (2019). GAS5, a FoxO1-actived long noncoding RNA, promotes propofol-induced oral squamous cell carcinoma apoptosis by regulating the miR-1297-GSK3β axis. *Artif. Cells Nanomed. Biotechnol.* 47 (1), 3985–3993. doi:10.1080/21691401.2019.1670189

Gao, F., Zhang, X., Wang, S., Zheng, L., Sun, Y., Wang, G., et al. (2021). TSP50 promotes the Warburg effect and hepatocyte proliferation via regulating PKM2 acetylation. *Cell Death Dis.* 12 (6), 517. doi:10.1038/s41419-021-03782-w

Gao, L., and Zhang, X. (2022). Propofol enhances the lethality of cisplatin on liver cancer cells by up-regulating miR-195-5p. *Tissue Cell* 74, 101680. doi:10.1016/j.tice.2021.101680

Gao, M., Guo, R., Lu, X., Xu, G., and Luo, S. (2020). Propofol suppresses hypoxia-induced esophageal cancer cell migration, invasion, and EMT through regulating lncRNA TMPO-AS1/miR-498 axis. *Thorac. Cancer* 11 (9), 2398–2405. doi:10.1111/1759-7714.13534

Gao, Y., Han, T., Han, C., Sun, H., Yang, X., Zhang, D., and Ni, X. (2021). Propofol regulates the TLR4/NF-κB pathway through miRNA-155 to protect colorectal cancer intestinal barrier. *Inflammation* 44 (5), 2078–2090. doi:10.1007/s10753-021-01485-0

Garcia, R., Salluh, J., Andrade, T. R., Farah, D., da Silva, P., Bastos, D. F., et al. (2021). A systematic review and meta-analysis of propofol versus midazolam sedation in adult intensive care (ICU) patients. *J. Crit. Care* 64, 91–99. doi:10.1016/j.jcrc.2021.04.001

Gong, T., Ning, X., Deng, Z., Liu, M., Zhou, B., Chen, X., et al. (2019). Propofol-induced miR-219-5p inhibits growth and invasion of hepatocellular carcinoma through suppression of GPC3-mediated Wnt/β-catenin signalling activation. *J. Cell. Biochem.* 120 (10), 16934–16945. doi:10.1002/jcb.28952

Goudra, B., Gouda, G., and Singh, P. M. (2021). Recent developments in devices used for gastrointestinal endoscopy sedation. *Clin. Endosc.* 54 (2), 182–192. doi:10.5946/ce.2020.057

Guerrero Orriach, J. L., Raigon Ponferrada, A., Malo Manso, A., Herrera Imbroda, B., Escalona Belmonte, J. J., Ramirez Aliaga, M., et al. (2020). Anesthesia in combination with propofol increases disease-free survival in bladder cancer patients who undergo radical tumor cystectomy as compared to inhalational anesthetics and opiate-based analgesia. *Oncology* 98 (3), 161–167. doi:10.1159/000504807

Guo, X. G., Wang, S., Xu, Y. B., and Zhuang, J. (2015). Propofol suppresses invasion, angiogenesis and survival of EC-1 cells *in vitro* by regulation of S100A4 expression. *Eur. Rev. Med. Pharmacol. Sci.* 19 (24), 4858–4865.

Hayasaka, K., Shiono, S., Miyata, S., Takaoka, S., Endoh, M., and Okada, Y. (2021). Prognostic significance of propofol-based intravenous anesthesia in early-stage lung cancer surgery. *Surg. Today* 51 (8), 1300–1308. doi:10.1007/s00595-020-02216-y

He, B., Zhao, Z., Cai, Q., Zhang, Y., Zhang, P., Shi, S., et al. (2020). miRNA-based biomarkers, therapies, and resistance in Cancer. *Int. J. Biol. Sci.* 16 (14), 2628–2647. doi:10.7150/ijbs.47203

Hemphill, S., McMenamin, L., Bellamy, M. C., and Hopkins, P. M. (2019). Propofol infusion syndrome: A structured literature review and analysis of published case reports. *Br. J. Anaesth.* 122 (4), 448–459. doi:10.1016/j.bja.2018.12.025

Hu, C., Liu, Z., Iwasaki, M., Lian, Q., and Ma, D. (2019). Propofol inhibits cancer malignancy by disturbing glucose metabolism through hypoxia-inducible factor-1α and pigment epithelium-derived factor modulation. *Br. J. Anaesth.* 123 (4), e499–e500. doi:10.1016/j.bja.2019.04.018

Huang, N. C., Lee, M. S., Lai, H. C., Lin, H. T., Huang, Y. H., Lu, C. H., et al. (2020). Propofol-based total intravenous anesthesia improves survival compared to desflurane anesthesia in gastric cancer surgery: A retrospective analysis. *Medicine* 99 (25), e20714. doi:10.1097/MD.0000000000020714

Huang, Y. H., Lee, M. S., Lou, Y. S., Lai, H. C., Yu, J. C., Lu, C. H., et al. (2019). Propofol-based total intravenous anesthesia did not improve survival compared to desflurane anesthesia in breast cancer surgery. *PloS one* 14 (11), e0224728. doi:10.1371/journal.pone.0224728

Huang, Y. H., Wu, Z. F., Lee, M. S., Lou, Y. S., Wu, K. L., Cheng, K. I., et al. (2021). Propofol-based total intravenous anesthesia did not improve survival compared to desflurane anesthesia in breast cancer surgery. *PloS one* 16 (8), e0224728. doi:10.1371/journal.pone.0224728

Huang, Y., Lei, L., and Liu, Y. (2020). Propofol improves sensitivity of lung cancer cells to cisplatin and its mechanism. *Med. Sci. Monit.* 26, e919786. doi:10.12659/MSM.919786

Hüppe, T., Maurer, F., Sessler, D. I., Volk, T., and Kreuer, S. (2020). Retrospective comparison of Eleveld, Marsh, and Schnider propofol pharmacokinetic models in 50 patients. *Br. J. Anaesth.* 124 (2), e22–e24. doi:10.1016/j.bja.2019.10.019

Ji, S. H., Lee, J. H., Cho, J. Y., Kim, H. S., Jang, Y. E., Kim, E. H., et al. (2020). External validation of a pharmacokinetic model of propofol for target-controlled infusion in children under two years old. *J. Korean Med. Sci.* 35 (11), e70. doi:10.3346/jkms.2020.35.e70

Jia, J., Sun, Y., Hu, Z., Li, Y., and Ruan, X. (2017). Propofol inhibits the release of interleukin-6, 8 and tumor necrosis factor-α correlating with high-mobility group box 1 expression in lipopolysaccharides-stimulated RAW 264.7 cells. *BMC Anesthesiol.* 17 (1), 148. doi:10.1186/s12871-017-0441-0

Jiang, J., Jiao, Y., Gao, P., Yin, W., Zhou, W., Zhang, Y., et al. (2021). Propofol differentially induces unconsciousness and respiratory depression through distinct interactions between GABAA receptor and GABAergic neuron in corresponding nuclei. *Acta Biochim. Biophys. Sin.* 53 (8), 1076–1087. doi:10.1093/abbs/gmab084

Jiang, S., Liu, Y., Huang, L., Zhang, F., and Kang, R. (2018). Effects of propofol on cancer development and chemotherapy: Potential mechanisms. *Eur. J. Pharmacol.* 831, 46–51. doi:10.1016/j.ejphar.2018.04.009

Jones, J. C., Rustagi, S., and Dempsey, P. J. (2016). ADAM proteases and gastrointestinal function. *Annu. Rev. Physiol.* 78, 243–276. doi:10.1146/annurev-physiol-021014-071720

Jun, I. J., Jo, J. Y., Kim, J. I., Chin, J. H., Kim, W. J., Kim, H. R., et al. (2017). Impact of anesthetic agents on overall and recurrence-free survival in patients undergoing esophageal cancer surgery: A retrospective observational study. *Sci. Rep.* 7 (1), 14020. doi:10.1038/s41598-017-14147-9

Kim, S. W., and Lee, J. K. (2020). Role of HMGB1 in the interplay between NETosis and thrombosis in ischemic stroke: A review. *Cells* 9 (8), 1794. doi:10.3390/cells9081794

Kodama, M., Higuchi, H., Ishii-Maruhama, M., Nakano, M., Honda-Wakasugi, Y., Maeda, S., et al. (2020). Multi-drug therapy for epilepsy influenced bispectral index after a bolus propofol administration without affecting propofol's pharmacokinetics: A prospective cohort study. *Sci. Rep.* 10 (1), 1578. doi:10.1038/s41598-020-58460-2

Kokita, N., and Hara, A. (1996). Propofol attenuates hydrogen peroxide-induced mechanical and metabolic derangements in the isolated rat heart. *Anesthesiology* 84 (1), 117–127. doi:10.1097/00000542-199601000-00014

Koo, B. W., Lim, D. J., Oh, A. Y., and Na, H. S. (2020). Retrospective comparison between the effects of propofol and inhalation anesthetics on postoperative recurrence of early- and intermediate-stage hepatocellular carcinoma. *Med. Princ. Pract.* 29 (5), 422–428. doi:10.1159/000506637

Lai, H. C., Lee, M. S., Lin, C., Lin, K. T., Huang, Y. H., Wong, C. S., et al. (2019). Propofol-based total intravenous anaesthesia is associated with better survival than desflurane anaesthesia in hepatectomy for hepatocellular carcinoma: A retrospective cohort study. *Br. J. Anaesth.* 123 (2), 151–160. doi:10.1016/j.bja.2019.04.057

Lai, H. C., Lee, M. S., Lin, K. T., Chan, S. M., Chen, J. Y., Lin, Y. T., et al. (2019). Propofol-based total intravenous anesthesia is associated with better survival than desflurane anesthesia in intrahepatic cholangiocarcinoma surgery. *Medicine* 98 (51), e18472. doi:10.1097/MD.0000000000018472

Lai, H. C., Lee, M. S., Lin, K. T., Huang, Y. H., Chen, J. Y., Lin, Y. T., et al. (2020). Propofol-based total intravenous anesthesia is associated with better survival than desflurane anesthesia in robot-assisted radical prostatectomy. *PloS one* 15 (3), e0230290. doi:10.1371/journal.pone.0230290

Lai, H. C., Lee, M. S., Liu, Y. T., Lin, K. T., Hung, K. C., Chen, J. Y., et al. (2020). Propofol-based intravenous anesthesia is associated with better survival than desflurane anesthesia in pancreatic cancer surgery. *PloS one* 15 (5), e0233598. doi:10.1371/journal.pone.0233598

Lebelo, M. T., Joubert, A. M., and Visagie, M. H. (2019). Warburg effect and its role in tumourigenesis. *Arch. Pharm. Res.* 42 (10), 833–847. doi:10.1007/s12272-019-01185-2

Li, C., Xia, M., Wang, H., Li, W., Peng, J., and Jiang, H. (2020). Propofol facilitates migration and invasion of oral squamous cell carcinoma cells by upregulating SNAI1 expression. *Life Sci.* 241, 117143. doi:10.1016/j.lfs.2019.117143

Li, G., Zhang, X., Guo, X., Li, Y., and Li, C. (2021). Propofol inhibits the proliferation, migration, and stem-like properties of bladder cancer mainly by suppressing the hedgehog pathway. *Cell Transpl.* 30, 963689720985113. doi:10.1177/0963689720985113

Li, M., Qu, L., Chen, F., and Zhu, X. (2020). Propofol upregulates miR-320a and reduces HMGB1 by downregulating ANRIL to inhibit PTC cell malignant behaviors. *Pathol. Res. Pract.* 216 (4), 152856. doi:10.1016/j.prp.2020.152856

Li, R., Huang, Y., and Lin, J. (2020). Distinct effects of general anesthetics on lung metastasis mediated by IL-6/JAK/STAT3 pathway in mouse models. *Nat. Commun.* 11 (1), 642. doi:10.1038/s41467-019-14065-6

Li, T., Mao, C., Wang, X., Shi, Y., and Tao, Y. (2020). Epigenetic crosstalk between hypoxia and tumor driven by HIF regulation. *J. Exp. Clin. Cancer Res.* 39 (1), 224. doi:10.1186/s13046-020-01733-5

Li, W., Zhang, Y., Liu, Y., Yue, F., Lu, Y., Qiu, H., et al. (2012). *In vitro* kinetic evaluation of the free radical scavenging ability of propofol. *Anesthesiology* 116 (6), 1258–1266. doi:10.1097/ALN.0b013e3182567dcc

Li, X., Li, L., Liang, F., Liu, G., and Zhao, G. (2018). Anesthetic drug propofol inhibits the expression of interleukin-6, interleukin-8 and cyclooxygenase-2, a potential mechanism for propofol in suppressing tumor development and metastasis. *Oncol. Lett.* 15 (6), 9523–9528. doi:10.3892/ol.2018.8515

Li, Y., Dong, W., Yang, H., and Xiao, G. (2020). Propofol suppresses proliferation and metastasis of colorectal cancer cells by regulating miR-124-3p.1/AKT3. *Biotechnol. Lett.* 42 (3), 493–504. doi:10.1007/s10529-019-02787-y

Li, Y., Zeng, Q. G., Qiu, J. L., Pang, T., Wang, H., and Zhang, X. X. (2020). Propofol suppresses migration, invasion, and epithelial-mesenchymal transition in papillary thyroid carcinoma cells by regulating miR-122 expression. *Eur. Rev. Med. Pharmacol. Sci.* 24 (9), 5101–5110. doi:10.26355/eurrev_202005_21203

Liu, D., Sun, X., Du, Y., and Kong, M. (2018). Propofol promotes activity and tumor-killing ability of natural killer cells in peripheral blood of patients with colon cancer. *Med. Sci. Monit.* 24, 6119–6128. doi:10.12659/MSM.911218

Liu, F., Qiu, F., Fu, M., Chen, H., and Wang, H. (2020). Propofol reduces epithelial to mesenchymal transition, invasion and migration of gastric cancer cells through the MicroRNA-195-5p/snail Axis. *Med. Sci. Monit.* 26, e920981. doi:10.12659/MSM.920981

Liu, Q., Sheng, Z., Cheng, C., Zheng, H., Lanuti, M., Liu, R., et al. (2021). Anesthetic propofol promotes tumor metastasis in lungs via GABAA R-dependent TRIM21 modulation of Src expression. *Adv. Sci.* 8 (18), e2102079. doi:10.1002/advs.202102079

Liu, S., Sun, J. Y., Ren, L. P., Chen, K., and Xu, B. (2017). Propofol attenuates intermittent hypoxia induced up-regulation of proinflammatory cytokines in microglia through inhibiting the activation of NF-Bκ/p38 MAPK signalling. *Folia Neuropathol.* 55 (2), 124–131. doi:10.5114/fn.2017.68579

Liu, W. Z., and Liu, N. (2018). Propofol inhibits lung cancer A549 cell growth and epithelial-mesenchymal transition process by upregulation of MicroRNA-1284. *Oncol. Res.* 27 (1), 1–8. doi:10.3727/096504018X15172738893959

Liu, Y., Wang, X., Li, H., Guan, E., and Luo, K. (2021). Propofol ameliorates the proliferation and epithelial-mesenchymal transition of hepatoma carcinoma cells via non-coding RNA activated by DNA damage (NORAD)/microRNA (miR)-556-3p/Migration and invasion enhancer 1 (MIEN1) Axis. *J. Environ. Pathol. Toxicol. Oncol.* 40 (4), 87–97. doi:10.1615/JEnvironPatholToxicolOncol.2021039471

Liu, Y., Zhang, N., Cao, Q., Cui, X., Zhou, Q., and Yang, C. (2017). The effects of propofol on the growth behavior of hepatoma xenografts in Balb/c mice. *Biomed. Pharmacother. = Biomedecine Pharmacother.* 90, 47–52. doi:10.1016/j.biopha.2017.03.041

Ma, X., Wang, T., Zhao, Z. L., Jiang, Y., and Ye, S. (2018). Propofol suppresses proinflammatory cytokine production by increasing ABCA1 expression via mediation by the long noncoding RNA LOC286367. *Mediat. Inflamm.* 2018, 8907143. doi:10.1155/2018/8907143

Makito, K., Matsui, H., Fushimi, K., and Yasunaga, H. (2020). Volatile versus total intravenous anesthesia for cancer prognosis in patients having digestive cancer surgery. *Anesthesiology* 133 (4), 764–773. doi:10.1097/ALN.0000000000003440

McLaughlin, M., Patin, E. C., Pedersen, M., Wilkins, A., Dillon, M. T., Melcher, A. A., et al. (2020). Inflammatory microenvironment remodelling by tumour cells after radiotherapy. *Nat. Rev. Cancer* 20 (4), 203–217. doi:10.1038/s41568-020-0246-1

Meng, C., Song, L., Wang, J., Li, D., Liu, Y., and Cui, X. (2017). Propofol induces proliferation partially via downregulation of p53 protein and promotes migration via activation of the Nrf2 pathway in human breast cancer cell line MDA-MB-231. *Oncol. Rep.* 37 (2), 841–848. doi:10.3892/or.2016.5332

Meng, X. Y., Zhang, X. P., Sun, Z., Wang, H. Q., and Yu, W. F. (2020). Distant survival for patients undergoing surgery using volatile versus IV anesthesia for hepatocellular carcinoma with portal vein tumor thrombus: A retrospective study. *BMC Anesthesiol.* 20 (1), 233. doi:10.1186/s12871-020-01111-w

Miniksar, Ö. H. (2022). Effectiveness of different doses of tenoxicam in preventing propofol injection pain. *Turk. J. Anaesthesiol. Reanim.* 50 (1), 31–36. doi:10.5152/TJAR.2021.1422

Nummela, A. J., Laaksonen, L. T., Laitio, T. T., Kallionpää, R. E., Långsjö, J. W., Scheinin, J. M., et al. (2022). Effects of dexmedetomidine, propofol, sevoflurane and S-ketamine on the human metabolome: A randomised trial using nuclear magnetic resonance spectroscopy. *Eur. J. Anaesthesiol.* 39 (6), 521–532. doi:10.1097/EJA.0000000000001591

Oh, C. S., Lee, J., Yoon, T. G., Seo, E. H., Park, H. J., Piao, L., et al. (2018). Effect of equipotent doses of propofol versus sevoflurane anesthesia on regulatory T cells after breast cancer surgery. *Anesthesiology* 129 (5), 921–931. doi:10.1097/ALN.0000000000002382

Oh, C. S., Park, H. J., Piao, L., Sohn, K. M., Koh, S. E., Hwang, D. Y., et al. (2022). Expression profiles of immune cells after propofol or sevoflurane anesthesia for colorectal cancer surgery: A prospective double-blind randomized trial. *Anesthesiology* 136 (3), 448–458. doi:10.1097/ALN.0000000000004119

Oh, T. K., Kim, H. H., and Jeon, Y. T. (2019). Retrospective analysis of 1-year mortality after gastric cancer surgery: Total intravenous anesthesia versus volatile anesthesia. *Acta Anaesthesiol. Scand.* 63 (9), 1169–1177. doi:10.1111/aas.13414

Pansy, K., Uhl, B., Krstic, J., Szmyra, M., Fechter, K., Santiso, A., et al. (2021). Immune regulatory processes of the tumor microenvironment under malignant conditions. *Int. J. Mol. Sci.* 22 (24), 13311. doi:10.3390/ijms222413311

Qi, J., Wu, Q., Zhu, X., Zhang, S., Chen, X., Chen, W., et al. (2019). Propofol attenuates the adhesion of tumor and endothelial cells through inhibiting glycolysis in human umbilical vein endothelial cells. *Acta Biochim. Biophys. Sin.* 51 (11), 1114–1122. doi:10.1093/abbs/gmz105

Qi, Z., Yuan, L., and Sun, N. (2019). Propofol exhibits a tumor-suppressive effect and regulates cell viability, migration and invasion in bladder carcinoma by targeting the microRNA-10b/HOXD10 signaling pathway. *Oncol. Lett.* 18 (6), 6228–6236. doi:10.3892/ol.2019.10968

Qian, J., Shen, S., Chen, W., and Chen, N. (2018). Propofol reversed hypoxia-induced docetaxel resistance in prostate cancer cells by preventing epithelial-mesenchymal transition by inhibiting hypoxia-inducible factor 1α. *Biomed. Res. Int.* 2018, 4174232. doi:10.1155/2018/4174232

Qu, D., Zou, X., and Liu, Z. (2022). Propofol modulates glycolysis reprogramming of ovarian tumor via restraining circular RNA-zinc finger RNA-binding protein/microRNA-212-5p/superoxide dismutase 2 axis. *Bioengineered* 13 (5), 11881–11892. doi:10.1080/21655979.2022.2063649

Ramirez, M. F., and Cata, J. P. (2021). Anesthesia techniques and long-term oncological outcomes. *Front. Oncol.* 11, 788918. doi:10.3389/fonc.2021.788918

Ren, Y. L., and Zhang, W. (2020). Propofol promotes apoptosis of colorectal cancer cells via alleviating the suppression of lncRNA HOXA11-AS on miRNA let-7i. *Biochem. Cell Biol. = Biochimie Biol. Cell.* 98 (2), 90–98. doi:10.1139/bcb-2018-0235

Richard, V., Kumar, T., and Pillai, R. M. (2021). Transitional dynamics of cancer stem cells in invasion and metastasis. *Transl. Oncol.* 14 (1), 100909. doi:10.1016/j.tranon.2020.100909

Rosenfeldt, F., Wilson, M., Lee, G., Kure, C., Ou, R., Braun, L., et al. (2013). Oxidative stress in surgery in an ageing population: Pathophysiology and therapy. *Exp. Gerontol.* 48 (1), 45–54. doi:10.1016/j.exger.2012.03.010

Sadri Nahand, J., Rabiei, N., Fathazam, R., Taghizadieh, M., Ebrahimi, M. S., Mahjoubin-Tehran, M., et al. (2021). Oncogenic viruses and chemoresistance: What do we know? *Pharmacol. Res.* 170, 105730. doi:10.1016/j.phrs.2021.105730

Sandra, L., Smits, A., Allegaert, K., Nicolaï, J., Annaert, P., and Bouillon, T. (2021). Population pharmacokinetics of propofol in neonates and infants: Gestational and postnatal age to determine clearance maturation. *Br. J. Clin. Pharmacol.* 87 (4), 2089–2097. doi:10.1111/bcp.14620

Schmoch, T., Jungk, C., Bruckner, T., Haag, S., Zweckberger, K., von Deimling, A., et al. (2021). The anesthetist's choice of inhalational vs. intravenous anesthetics has no impact on survival of glioblastoma patients. *Neurosurg. Rev.* 44 (5), 2707–2715. doi:10.1007/s10143-020-01452-7

Sen, Y., Xiyang, H., and Yu, H. (2019). Effect of thoracic paraspinal block-propofol intravenous general anesthesia on VEGF and TGF-β in patients receiving radical resection of lung cancer. *Medicine* 98 (47), e18088. doi:10.1097/MD.0000000000018088

Shen, X., Wang, D., Chen, X., and Peng, J. (2021). Propofol inhibits proliferation, migration, invasion and promotes apoptosis by regulating HOST2/JAK2/STAT3 signaling pathway in ovarian cancer cells. *Cytotechnology* 73 (2), 243–252. doi:10.1007/s10616-021-00462-7

Shi, H., Yan, C., Chen, Y., Wang, Z., Guo, J., and Pei, H. (2021). Propofol inhibits the proliferation, migration, invasion and epithelial to mesenchymal transition of renal cell carcinoma cells by regulating microRNA-363/Snail1. *Am. J. Transl. Res.* 13 (4), 2256–2269.

Shiono, S., Shibata, S. C., Kabata, D., Shintani, A., Ikeda, T., and Fujino, Y. (2020). Comparison of 1-year recurrence-free survival between sevoflurane and propofol

use for general anesthesia management in primary breast cancer surgery. *J. Anesth.* 34 (5), 694–701. doi:10.1007/s00540-020-02806-7

Siegel, R. L., Miller, K. D., and Jemal, A. (2020). Cancer statistics, 2020. *Ca. Cancer J. Clin.* 70 (1), 7–30. doi:10.3322/caac.21590

Slack, F. J., and Chinnaiyan, A. M. (2019). The role of non-coding RNAs in oncology. *Cell* 179 (5), 1033–1055. doi:10.1016/j.cell.2019.10.017

Song, F., Liu, J., Feng, Y., and Jin, Y. (2020). Propofol-induced HOXA11-AS promotes proliferation, migration and invasion, but inhibits apoptosis in hepatocellular carcinoma cells by targeting miR-4458. *Int. J. Mol. Med.* 46 (3), 1135–1145. doi:10.3892/ijmm.2020.4667

Stratford, N., and Murphy, P. (1997). Effect of lipid and propofol on oxidation of haemoglobin by reactive oxygen species. *Br. J. Anaesth.* 78 (3), 320–322. doi:10.1093/bja/78.3.320

Sun, H., and Gao, D. (2018). Propofol suppresses growth, migration and invasion of A549 cells by down-regulation of miR-372. *BMC cancer* 18 (1), 1252. doi:10.1186/s12885-018-5175-y

Sun, Y., Peng, Y. B., Ye, L. L., Ma, L. X., Zou, M. Y., and Cheng, Z. G. (2020). Propofol inhibits proliferation and cisplatin resistance in ovarian cancer cells through regulating the microRNA-374a/forkhead box O1 signaling axis. *Mol. Med. Rep.* 21 (3), 1471–1480. doi:10.3892/mmr.2020.10943

Sung, H., Ferlay, J., Siegel, R. L., Laversanne, M., Soerjomataram, I., Jemal, A., et al. (2021). Global cancer statistics 2020: GLOBOCAN estimates of incidence and mortality worldwide for 36 cancers in 185 countries. *Ca. Cancer J. Clin.* 71 (3), 209–249. doi:10.3322/caac.21660

Tian, D., Tian, M., Ma, Z. M., Zhang, L. L., Cui, Y. F., and Li, J. L. (2020). Anesthetic propofol epigenetically regulates breast cancer trastuzumab resistance through IL-6/miR-149-5p axis. *Sci. Rep.* 10 (1), 8858. doi:10.1038/s41598-020-65649-y

Timur, U. T., Caron, M., Jeuken, R. M., Bastiaansen-Jenniskens, Y. M., Welting, T., van Rhijn, L. W., et al. (2020). Chondroprotective actions of selective COX-2 inhibitors *in vivo*: A systematic review. *Int. J. Mol. Sci.* 21 (18), 6962. doi:10.3390/ijms21186962

Tsuchiya, H., Ueno, T., Tanaka, T., Matsuura, N., and Mizogami, M. (2010). Comparative study on determination of antioxidant and membrane activities of propofol and its related compounds. *Eur. J. Pharm. Sci.* 39 (1-3), 97–102. doi:10.1016/j.ejps.2009.11.001

Wan Hassan, W., Tan, H. S., and Mohamed Zaini, R. H. (2018). Comparison of the effects of dexmedetomidine on the induction of anaesthesia using marsh and schnider pharmacokinetic models of propofol target-controlled infusion. *Malays. J. Med. Sci.* 25 (1), 24–31. doi:10.21315/mjms2018.25.1.4

Wang, J., Cheng, C. S., Lu, Y., Ding, X., Zhu, M., Miao, C., et al. (2018). Novel findings of anti-cancer property of propofol. *Anticancer. Agents Med. Chem.* 18 (2), 156–165. doi:10.2174/1871520617666170912120327

Wang, K., Chen, Q., Liu, N., Zhang, J., and Pan, X. (2021). Recent advances in, and challenges of, anti-angiogenesis agents for tumor chemotherapy based on vascular normalization. *Drug Discov. Today* 26 (11), 2743–2753. doi:10.1016/j.drudis.2021.07.024

Wang, Y., Xu, B., Zhou, J., and Wu, X. (2020). Propofol activates AMPK to inhibit the growth of HepG2 cells *in vitro* and hepatocarcinogenesis in xenograft mouse tumor models by inducing autophagy. *J. Gastrointest. Oncol.* 11 (6), 1322–1332. doi:10.21037/jgo-20-472

Wang, Z., Cao, B., Ji, P., and Yao, F. (2021). Propofol inhibits tumor angiogenesis through targeting VEGF/VEGFR and mTOR/eIF4E signaling. *Biochem. Biophys. Res. Commun.* 555, 13–18. doi:10.1016/j.bbrc.2021.03.094

Winkler, J., Abisoye-Ogunniyan, A., Metcalf, K. J., and Werb, Z. (2020). Concepts of extracellular matrix remodelling in tumour progression and metastasis. *Nat. Commun.* 11 (1), 5120. doi:10.1038/s41467-020-18794-x

Wu, K., Peng, X., Chen, M., Li, Y., Tang, G., Peng, J., et al. (2022). Recent progress of research on anti-tumor agents using benzimidazole as the structure unit. *Chem. Biol. Drug Des.* 99 (5), 736–757. doi:10.1111/cbdd.14022

Wu, X., Li, X., and Xu, G. (2020). Propofol suppresses the progression of non-small cell lung cancer via downregulation of the miR-21-5p/MAPK10 axis. *Oncol. Rep.* 44 (2), 487–498. doi:10.3892/or.2020.7619

Wu, Z. F., Lee, M. S., Wong, C. S., Lu, C. H., Huang, Y. S., Lin, K. T., et al. (2018). Propofol-based total intravenous anesthesia is associated with better survival than desflurane anesthesia in colon cancer surgery. *Anesthesiology* 129 (5), 932–941. doi:10.1097/ALN.0000000000002357

Xiao, Y., and Yu, D. (2021). Tumor microenvironment as a therapeutic target in cancer. *Pharmacol. Ther.* 221, 107753. doi:10.1016/j.pharmthera.2020.107753

Xu, Y. B., Du, Q. H., Zhang, M. Y., Yun, P., and He, C. Y. (2013). Propofol suppresses proliferation, invasion and angiogenesis by down-regulating ERK-VEGF/MMP-9 signaling in Eca-109 esophageal squamous cell carcinoma cells. *Eur. Rev. Med. Pharmacol. Sci.* 17 (18), 2486–2494.

Xu, Y., Jiang, W., Xie, S., Xue, F., and Zhu, X. (2020). The role of inhaled anesthetics in tumorigenesis and tumor immunity. *Cancer Manag. Res.* 12, 1601–1609. doi:10.2147/CMAR.S244280

Yan, T., Zhang, G. H., Wang, B. N., Sun, L., and Zheng, H. (2018). Effects of propofol/remifentanil-based total intravenous anesthesia versus sevoflurane-based inhalational anesthesia on the release of VEGF-C and TGF-β and prognosis after breast cancer surgery: A prospective, randomized and controlled study. *BMC Anesthesiol.* 18 (1), 131. doi:10.1186/s12871-018-0588-3

Yang, K. S., Che, P. C., Hsieh, M. J., Lee, I. N., Wu, Y. P., Chen, M. S., et al. (2022). Propofol induces apoptosis and ameliorates 5-fluorouracil resistance in OSCC cells by reducing the expression and secretion of amphiregulin. *Mol. Med. Rep.* 25 (1), 36. doi:10.3892/mmr.2021.12552

Yang, N., Liang, Y., Yang, P., and Ji, F. (2017). Propofol suppresses LPS-induced nuclear accumulation of HIF-1α and tumor aggressiveness in non-small cell lung cancer. *Oncol. Rep.* 37 (5), 2611–2619. doi:10.3892/or.2017.5514

Yang, X., Qin, J., Gong, C., and Yang, J. (2021). Propofol enhanced the cell sensitivity to paclitaxel (PTX) in prostatic cancer (PC) through modulation of HOTAIR. *Genes Genomics* 43 (7), 807–814. doi:10.1007/s13258-021-01093-0

Yoo, S., Lee, H. B., Han, W., Noh, D. Y., Park, S. K., Kim, W. H., et al. (2019). Total intravenous anesthesia versus inhalation anesthesia for breast cancer surgery: A retrospective cohort study. *Anesthesiology* 130 (1), 31–40. doi:10.1097/ALN.0000000000002491

Yu, B., Gao, W., Zhou, H., Miao, X., Chang, Y., Wang, L., et al. (2018). Propofol induces apoptosis of breast cancer cells by downregulation of miR-24 signal pathway. *Cancer Biomark.* 21 (3), 513–519. doi:10.3233/CBM-170234

Yu, X., Gao, Y., and Zhang, F. (2019). Propofol inhibits pancreatic cancer proliferation and metastasis by up-regulating miR-328 and down-regulating ADAM8. *Basic Clin. Pharmacol. Toxicol.* 125 (3), 271–278. doi:10.1111/bcpt.13224

Yu, X., Shi, J., Wang, X., and Zhang, F. (2020). Propofol affects the growth and metastasis of pancreatic cancer via ADAM8. *Pharmacol. Rep.* 72 (2), 418–426. doi:10.1007/s43440-019-00015-y

Zhang, H., Tan, M., Zhang, J., Han, X., and Ma, Y. (2021). Propofol inhibits thyroid cancer cell proliferation, migration, and invasion by suppressing SHH and PI3K/AKT signaling pathways via the miR-141-3p/BRD4 Axis. *J. Healthc. Eng.* 2021, 2704753. doi:10.1155/2021/2704753

Zhang, J., Chang, C. L., Lu, C. Y., Chen, H. M., and Wu, S. Y. (2022). Anesthesia with propofol sedation reduces locoregional recurrence in patients with breast cancer receiving total mastectomy compared with non-propofol anesthesia. *Front. Oncol.* 12, 708632. doi:10.3389/fonc.2022.708632

Zhang, J., Chang, C. L., Lu, C. Y., Chen, H. M., and Wu, S. Y. (2021). Paravertebral block in regional anesthesia with propofol sedation reduces locoregional recurrence in patients with breast cancer receiving breast conservative surgery compared with volatile inhalational without propofol in general anesthesia. *Biomed. Pharmacother. = Biomedecine Pharmacother.* 142, 111991. doi:10.1016/j.biopha.2021.111991

Zhang, W. W., Xue, R., Mi, T. Y., Shen, X. M., Li, J. C., Li, S., et al. (2022). Propofol ameliorates acute postoperative fatigue and promotes glucagon-regulated hepatic gluconeogenesis by activating CREB/PGC-1α and accelerating fatty acids beta-oxidation. *Biochem. Biophys. Res. Commun.* 586, 121–128. doi:10.1016/j.bbrc.2021.11.073

Zhang, X., Li, F., Zheng, Y., Wang, X., Wang, K., Yu, Y., et al. (2019). Propofol reduced mammosphere formation of breast cancer stem cells via PD-L1/nanog *in vitro*. *Oxid. Med. Cell. Longev.* 2019, 9078209. doi:10.1155/2019/9078209

Zhang, Y. F., Li, C. S., Zhou, Y., and Lu, X. H. (2020). Effects of propofol on colon cancer metastasis through STAT3/HOTAIR axis by activating WIF-1 and suppressing Wnt pathway. *Cancer Med.* 9 (5), 1842–1854. doi:10.1002/cam4.2840

Zhang, Y. F., Li, C. S., Zhou, Y., and Lu, X. H. (2020). Propofol facilitates cisplatin sensitivity via lncRNA MALAT1/miR-30e/ATG5 axis through suppressing autophagy in gastric cancer. *Life Sci.* 244, 117280. doi:10.1016/j.lfs.2020.117280

Zhao, H., Wei, H., He, J., Wang, D., Li, W., Wang, Y., et al. (2020). Propofol disrupts cell carcinogenesis and aerobic glycolysis by regulating circTADA2A/miR-455-3p/FOXM1 axis in lung cancer. *Cell cycleGeorget. Tex.)* 19 (19), 2538–2552. doi:10.1080/15384101.2020.1810393

Zheng, X., Wang, Y., Dong, L., Zhao, S., Wang, L., Chen, H., et al. (2018). Effects of propofol-based total intravenous anesthesia on gastric cancer: A retrospective study. *Onco. Targets. Ther.* 11, 1141–1148. doi:10.2147/OTT.S156792

Zhou, M., Dai, J., Zhou, Y., Wu, J., Xu, T., Zhou, D., et al. (2018). Propofol improves the function of natural killer cells from the peripheral blood of patients with esophageal squamous cell carcinoma. *Exp. Ther. Med.* 16 (1), 83–92. doi:10.3892/etm.2018.6140

Glossary

GABA γ-aminobutyric acid
UGT UDP-glucuronosyhransferase
miRNA micro-RNA
lncRNA long non-coding RNA
RISC RNA-induced silencing complex
EMT epithelial-mesenchymal transition
MIEN1 migration and Invasion Enhancer 1
NMDAR N-methyl-D-aspartate receptor
circRNA circular RNA
SOD2 superoxide dismutase 2
FOXM1 forkhead box M1
SFA_FA saturated fatty acids to total fatty acids
DDP cisplatin
PTX Paclitaxel
5-FU 5-Fluorouracil
TME The tumor microenvironment
ECM extracellular matrix
HIF hypoxia-inducible factor
ROS reactive oxygen species
HMGB1 The high mobility group protein B1
COX cyclooxygenase
BM basement membrane
MMP metalloproteinase
ADAM disintegrin and metalloprotease
LRR local-regional recurrence
IDC invasive ductal carcinoma
TM total mastectomy
BCS breast conservative surgery
PB-RA paravertebral block-regional anesthesia
INHA-GA inhalational general anesthesia.

frontiers | Frontiers in Oncology

TYPE Brief Research Report
PUBLISHED 01 December 2022
DOI 10.3389/fonc.2022.1021940

OPEN ACCESS

EDITED BY
Syed Mahmood,
University of Malaya, Malaysia

REVIEWED BY
Luis Zapata,
Institute of Cancer Research (ICR), United Kingdom
Jean-Pascal Capp,
Institut National des Sciences Appliquées de Toulouse (INSA), France

*CORRESPONDENCE
V. Yellapantula
vyellapantula@chla.usc.edu

SPECIALTY SECTION
This article was submitted to Pharmacology of Anti-Cancer Drugs, a section of the journal Frontiers in Oncology

RECEIVED 17 August 2022
ACCEPTED 15 November 2022
PUBLISHED 01 December 2022

CITATION
Munugula C, Hu J, Christodoulou E and Yellapantula V (2022) Microenvironmental changes co-occur with mosaic somatic clonal expansions in normal skin and esophagus tissues. *Front. Oncol.* 12:1021940. doi: 10.3389/fonc.2022.1021940

Microenvironmental changes co-occur with mosaic somatic clonal expansions in normal skin and esophagus tissues

C. Munugula[1], J. Hu[1], E. Christodoulou[1] and V. Yellapantula[1,2]*

[1]Center for Personalized Medicine, Children's Hospital Los Angeles, Los Angeles, CA, United States, [2]Keck School of Medicine, University of Southern California, Los Angeles, CA, United States

The presence of somatic mutations, previously identified in cancers, are being increasingly recognized in normal tissues. While the role of microenvironment (ME) in tumor progression is well understood, the changes that occur in the microenvironment of normal tissues that harbor somatic mutations has not been systematically studied. Here, using normal RNA-Seq data accrued from 6544 samples across 27 tissue types from Genotype-Tissue Expression (GTEx) project, we studied the association of microenvironmental changes in the presence of somatic clonal expansions of previously implicated cancer genes. We focused our analysis on skin and esophagus since they have the highest number of samples and mutation burden together. We observed changes in microenvironmental cell-types previously implicated in tumor progression including endothelial cells, epithelial cells, pericytes, fibroblasts, chondrocytes, among others. The Epithelial-Mesenchymal-Transition (EMT) pathway is dysregulated in both skin and esophagus, along with increased hypoxia scores in samples with clonal expansions. These results suggest that microenvironmental changes play an important role in clonal expansions and potentially the initiating stages of cancer progression. Studying these changes may provide new avenues for early intervention of cancer, for targeted therapies, or enhance activities of conventional therapies.

KEYWORDS

ageing and cancer, microenvironment, genomics, computation biology, bioinforamtics

Introduction

Cancers arise due to the sequential accrual of mutations that confer a selective advantage to the cells harboring them. Clonal hematopoiesis mutations, ie. mutations that cause clonally expanded hematopoietic stem cells in normal individuals, present an increased risk for developing myeloid malignancies. However, additional changes are

necessary for cancer progression (1, 2). The recent discovery of clonal expansions of mutant cells in skin and esophagus suggests the pervasiveness of this process across tissue types (3, 4).

Evading immune destruction, epigenetic reprogramming of the microenvironment, and angiogenesis (5), are hallmarks of cancer, all of which rely on the microenvironment (ME). For example, to provide nutrients and oxygen to the proliferating cells, new endothelial cells are assembled into tubes; additionally sprouting of new vessels from existing blood vessels occurs (6). This process is akin to processes in embryogenesis, however, unlike in embryogenesis, this "angiogenic-switch" is always left "on" during tumorigenesis. Tumor-associated inflammatory responses, which were earlier thought to work to eradicate tumors, also function as tumor-promoting by providing bioactive molecules conducive to a proliferative microenvironment milieu (7). Inflammation anecdotally is observed in the earliest stages of cancer progression. The Pre-Cancer Atlas (PCA) underscores the importance of understanding the ME changes in pre-malignant samples as an important step for effective risk stratification and intervention strategies (8). Others have also observed pro-inflammatory signaling in adjacent normal tissues of tumors (9). Yet, the changes in the ME that occur during clonal expansions have not been systematically studied.

Bioinformatics methods also make it possible to identify somatic mutations from RNA-Seq data (10–12). The application of this approach to normal sequencing data from GTEx showed a pervasive presence of clonal expansions in normal tissues. Of note, hotspot, mutations in *TP53, PIK3CA*, *KRAS, GNAS*, among others, were previously identified in normal tissues (10). The dN/dS ratios of the identified somatic mutations were indicative of a selective advantage of the clones harboring them, suggesting an ideal resource to observe the earliest changes in the ME that occur with such clonal expansions. Recent developments in computational methods, allow the deconvolution of microenvironment composition, including immune and stromal cells, from bulk RNA-seq data (13, 14). Here, using GTEx RNA-Seq data from 27 normal tissue types and 6544 samples, we identified esophagus and skin to have the highest mutation rate and number of samples. We report changes in the microenvironment that occur in these tissues that have somatic mutation-related clonal expansions.

Methods

Microenvironment content enumeration and classification

Previously reported methods have performed an extensive analysis of commonly used microenvironment deconvolution methods: 1) XCell 2) CIBERSORTx (15, 16). Despite the differences in the deconvolution approaches, earlier studies show a high correlation of the immune and stromal scores (15). GTEx Version v8, normalized TPM values were downloaded from GTEx. Samples were limited to those which had somatic mutations previously called by Yizhak et al (10). Deconvolution was performed using CIBERSORTx-Relative, CIBERSORTx-Absolute and XCell. CIBERSORTx significance scores were generated using 1000 permutations and quantile normalization disabled. For XCell, as previously suggested (15), samples were separated by tissue, and deconvolution was performed using the XCell R script using the default settings.

Classifying samples by mutations status

Mutations previously called by Yizhak et al. were downloaded through dpGAP (Study Accession: phs000424.v8.p2) (10). Mutations were limited to non-synonymous mutations namely, missense, nonsense, nonstop, splice site and start codon mutations. Subsequently, cancer gene census (CGC) genes defined by COSMIC v94 were downloaded. Each sample was then classified into one of the following three categories 1) non-synonymous mutation in a cancer gene present (CGC-m) 2) non-synonymous mutation in a non-cancer gene present (non-CGC) 3) no non-synonymous mutation present (non-m) (Figure 1). Additionally, we classified samples by their presence of a non-synonymous mutation in Significantly Mutated Genes (SMG-m) previously identified in esophageal and cutaneous melanoma (17, 18).

Linear model

A linear regression was fit for each cell type and tissue type by regressing cell type abundance scores from XCell or CIBERSORTx on mutation status (CGC-m or non-m), along with age and sex as covariates. T-tests of estimated coefficients were performed, and p-values were adjusted to control for false discovery rate using the Benjamini-Hochberg correction. The model was fit in R using the lm function as shown below and p-values were adjusted using the p.adjust() function.

$$model < - lm(Cell\ Type\ Abundance\ Score \sim Group + Sex + Age)$$

DEG and pathway analysis

Raw gene counts from GTEx v8 were downloaded. Within a given tissue type, differential gene expression testing was performed using Deseq2 between CGC-m and non-m samples as defined above. Genes with p-adjusted value > 0.01, base-mean value< 200 and absolute log2 fold-change< 0.2 were excluded for downstream analysis. Orthogonally, a Wilcoxon rank-sum test was run between the CGC-m and non-m groups. Genes significantly differentially expressed (DE) by both approaches was used for downstream analysis.

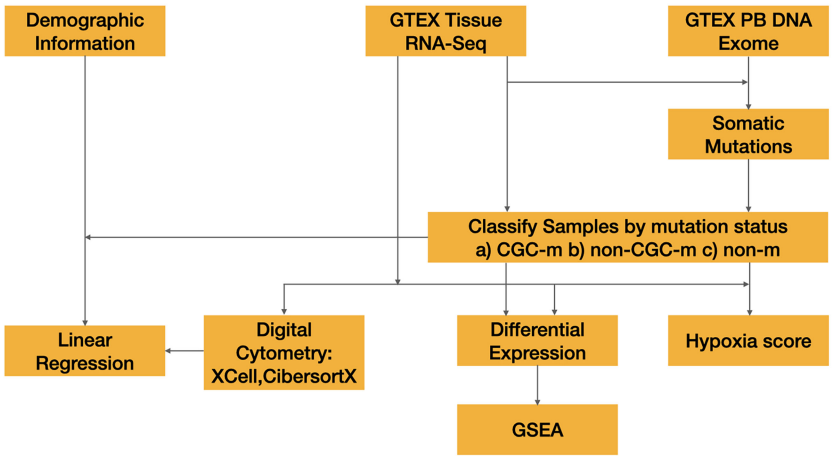

FIGURE 1
Overview of methods workflow used to detect microenvironment changes in normal tissues.

Results

Changes in microenvironment with somatic mutations status

We looked at the effect of how expansion of somatic mutations are associated with changes in the microenvironment. For this analysis, we limited the studied tissue types to skin and esophagus due to presence of the highest non-synonymous mutation burden in cancer genes and the highest number of samples present (Esophagus: N=600, CGC-m rate = 0.13; Skin: N=512, CGC-m rate = 0.3; Supplementary Table S1). Earlier reports have shown that age and especially sex are significantly associated with differences in microenvironment (ME) (15). For example, there is an increased lymphocyte content in breast and thyroid tissues in females when compared to males. Interestingly, women portend a higher prevalence of auto-immune and neoplastic disorders suggesting that such ME differences could play a role in pathology (15). Several age-associated differences such as an increase in lymphocytes and myeloid cells in the artery were associated with age (15). Secondly, it is well known that somatic mutations in healthy individuals is associated with age (15). To account for such associations, we use a linear regression model using age and sex as covariates. Of relevance, for esophagus, we observed the most significant association (p-adjusted< 0.01) of CGC-m status with an increased presence of epithelial cells, keratinocytes, sebocytes and reduced expression of endothelial and lymphatic endothelial cells, pericytes, smooth muscles and fibroblasts (Figure 2A, Supplementary Table S3). Unsupervised hierarchical clustering using significant ME cell-types classified 50/56 (89%) CGC-m cases into cluster same cluster. Interestingly, recent studies in Barret's Esosphagus (BE), which is a precursor to esophageal cancer, show that it is characterized by the occurrence of specialized columnar epithelium (19). Lymphatic endothelial cells and their cross-talk with pericytes were shown to be important for microvasculature for mature and were both reduced in CGC-m samples (20). For skin, we observed a significant association of CGC-m with increased Chondrocytes and Granulocyte-Macrophage Progenitor (GMP) cells (p-adjusted< 0.1) (Figure 2B, Supplementary Table S4). Chondrocytes respond to outside stimuli and tissue damage by proliferating and secreting extracellular matrix that maintains and sustains cartilage (21).GMP cells which are precursors to monoblasts and myeloblasts are also elevated in CGC-m samples.

Differential gene expression and pathway analysis

We looked at genes that are differentially expressed between the CGC-m and non-m cases in skin and esophagus. Interestingly, differential gene expression testing between CGC-mutant and non-mutant esophagus samples identified genes commonly aberrant in carcinomas. *ERBB2, CDH1, SOX2*, and *TP63* were all significantly overexpressed (adjusted p-value< 0.01) in the CGC-mutant samples (Figure 3B). No mutations were identified in these genes suggesting that alternate mechanisms could potentially drive clonal expansions in normal tissues. This is consistent with previous reports that showed copy-number aberrations in normal tissues (4).

Pathway analysis of DEGs revealed a dysregulated Epithelial-Mesenchymal-Transition (EMT) pathway in both Skin and Esophagus tissues (Figures 3A–D). The EMT process is a highly dynamic process that enables interconversion of epithelial cells to mesenchymal-like states which have stem-cell like properties and a variety of intermediate states. In neoplasia, mesenchymal cells are capable of increased resistance to

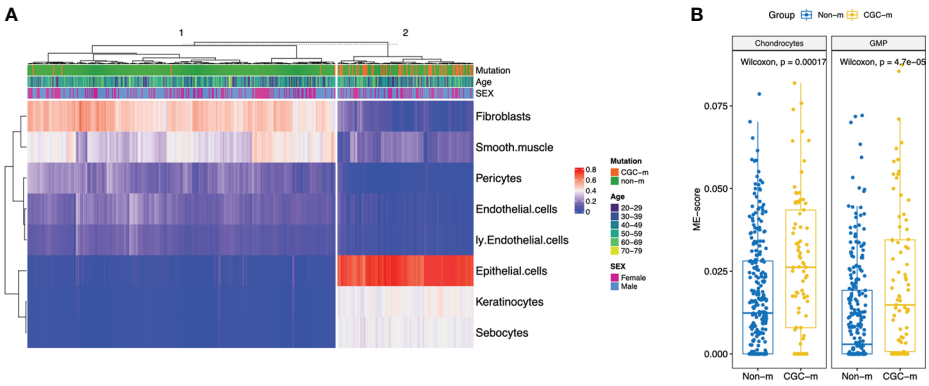

FIGURE 2
XCell scores of significantly different microenvironment cell-types, between CGC-m and non-m groups, identified using linear regression with age and gender as covariates. **(A)** Heatmap of significantly different ME scores in Esophagus previously implicated in cancer progression **(B)** Boxplots of significantly different ME scores in skin.

destruction by the adaptive immune system. An activated EMT pathway also results in degradation of cell-cell adhesive junctions and reorganization of extra-cellular matrix (22). Interestingly, in the esophagus, ECM2 which encodes extra-cellular matrix protein and is implicated in involvement with cell-ECM recognition is downregulated in samples with CGC-m compared to the non-m cohort. EMT transcription factors *ZEB1* represses *CDH1* thereby orchestrating EMT programs (23). *ZEB1* however is under expressed while *CDH1* is over-expressed in CGC-m samples in the esophagus. Other genes previously implicated in the EMT pathway and downregulated in CGC-m esophagus include *CDH2, FGF2, TGFBI, TPM1*, and *VIM* (Figure 3B) (24). These patterns of expression along with increased epithelial cells in CGC-m are suggestive of a repressed EMT program or perhaps a Mesenchymal Epithelial Transition (MET) phenotype. Of relevance, the cell-cycle/G2M pathway in the esophagus is also dysregulated (Supplementary Figure 1). Cyclin D1 which is essential for a cell to enter the G1 phase, transcription factors *E2F1* and *E2F2* required for a cell to progress to the S phase are all overexpressed in CGC-m samples (25). Other dysregulated genes in the cell cycle pathway include *CCNA2, CCND2*, and *MYB* among others (Figure 3B). Between the SMG-m and non-m groups, as seen in CGC-m, we also observed dysregulation of EMT and G2M pathway (Supplementary Figure 2B, C).

ECM2, whose function is known to promote matrix assembly and cell adhesiveness is dysregulated in the esophagus as previously described but also in the skin (26). However, interestingly, unlike in the esophagus, *ECM2* in the skin is upregulated in CGC-m cases. This is consistent with other EMT pathway genes in the skin (24); *COMP, CTHRC1, ECM2, FBN1, LOX*, and *SPARC* were all upregulated in samples with a mutation in a cancer gene. In the skin, the UV response pathway is also altered (Supplementary Figure 1). c-fos whose activation is the hallmark of response to UV is incidentally downregulated in CGC-m cases. Other key genes implicated in UV response *ATF3*, and *FOSB* among others are also downregulated in mutant cases (Figure 3D). In skin, only 7 samples were present in the SMG-m category which did not yield any significant results due to the small number of samples in this group.

Hypoxia associated with clonal expansions

Hypoxia has been shown to play an important role in cancer progression, therapy resistance and metastatic growth. Hypoxia-rich environments were implicated in causing "angiogenic-switch" which dysregulated neovascularization that promotes tumor growth (27). Hypoxic environments were also shown to promote cell mobility and metastatic abilities through acquisition of epithelial-to-mesenchymal phenotype (27). Given that we identified dysregulated EMT-pathways in both Esophagus and Skin, along with the dysregulation of endothelial cells and pericyte in the ME, we hypothesized that hypoxia could play an important role in early clonal expansions. Using hypoxia gene signatures, we generated hypoxia scores for all samples using Ragnum et al. and Buffa et al. hypoxia gene signatures previously described (28). We observed a high correlation of Hypoxia scores identified using both signatures (p-value< 0.01, Pearson's corr. = 0.82, Figure 4A, Supplementary Table S2). Next, we observed differences between the CGC-m group and the non-m group and secondly the SMG-m and the non-m groups. Interestingly, we observed significant enrichment of hypoxia scores in both esophagus and skin (Wilcoxon p-value:

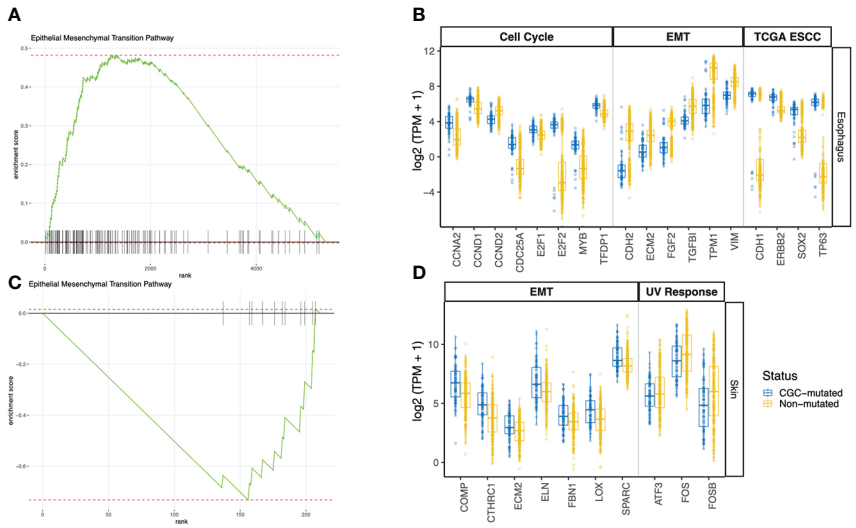

FIGURE 3
GSEA Pathway analysis using differentially expressed genes between CGC-m and non-mutated groups. **(A, C)** Shows GSEA enrichment of EMT pathway in esophagus and skin **(B)** Boxplots of gene expression (log2 TPM +1) between CGC-m and non-m cases for significantly differentially expressed genes (p-adjusted<= 0.01) genes implicated in the EMT pathway, cell cycle pathway and esophageal carcinomas previously reported by TCGA. **(D)** Boxplots of gene expression (log2 TPM +1) between CGC-m and non-m cases for significantly differentially expressed gens (p-adjusted<= 0.01) genes implicated in the EMT and UV response pathways.

esophagus<0.01 and<0.01, skin=0.08, 0.06 for CGC-m and SMG-m respectively) suggesting early initiating roles of hypoxic environments in clonal expansions (Figure 4B, Supplementary Figure 2A).

Discussion

There is a growing body of research investigating genetic aberrations in normal tissues, dysplasia and pre-cancerous lesions with the goal of charting the process of ageing and cancer progression (8). Recent studies in various tissues including skin, colon, esophagus among others predominantly investigated the DNA of the aberrant cells (3, 4, 29). While somatic mutations are age and tissue type-dependent, in skin and esophagus, approximately 30-50% of the cells in middle-aged individuals harbor driver mutations without presentation of cancer (3). Initiatives such as the PreCancer Atlas (PCA) acknowledge the importance of studying the microenvironment in understanding how precancerous lesions evolve into cancers (8).

Herein using RNA-Seq samples from GTEx consortium, we investigated the microenvironmental differences in samples that harbor a non-synonymous mutation in a cancer gene with those without non-synonymous mutations.

Focusing on skin and esophagus tissues, we identified changes in key microenvironment components in both tissues. Clustering samples by the microenvironment score differences classified 89% (50/56) of the CGC-m samples in the same cluster validating our hypothesis that key microenvironment changes occur with clonal expansions. Studying such changes through progress will be critical for our improvement of understanding of cancers. The EMT pathway was dysregulated in both skin and esophagus and its dysregulation could be an essential mechanism for cancer progression. Taken together, these findings, along with elevated hypoxia scores in CGC-mutated samples, suggest that angiogenic-switch could be a mechanism occurring early during cancer progression.

The study has the following limitations. Firstly, previous studies which sequenced normal DNA samples identified somatic copy number changes along with mutations (3, 4, 29). In this study, we were able to classify samples only through their mutation status and it's a technical limitation of the study to not be able to robustly call such changes from RNA-Seq. Secondly, current deconvolution approaches rely on signatures of differentiated cells. However, patterns of de-differentiation are a common mechanism of cancer progression and metastasis. Hence, the approaches used in this study are not able to deconvolute dedifferentiated cell states which might have important implications for cancer progression. Single-cell sequencing of normal cells would aid such discovery. Lastly, the study fails to pinpoint the microenvironment states and mutations that lead to overt presentation of cancer. Studying such changes requires follow up biopsies and various stages of disease progression which are hard to obtain.

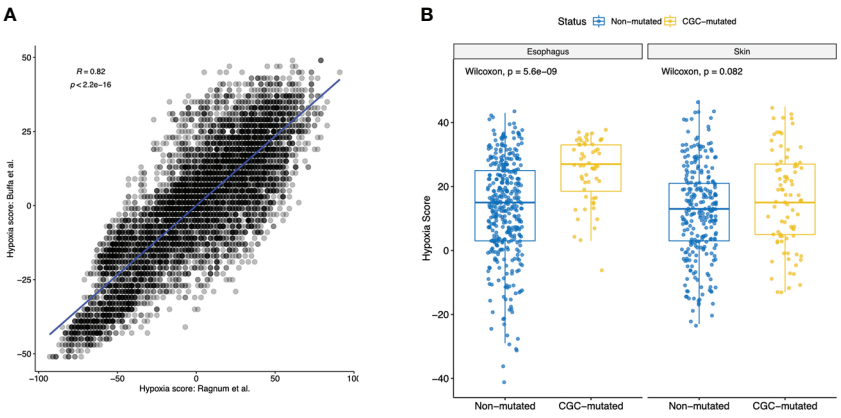

FIGURE 4
Hypoxia scores in all normal tissues using two commonly used gene signatures. **(A)** Shows a high Pearson's correlation of 0.82 between the Hypoxia scores generated using gene signatures described in Ragnum et al. gene and Buffa et al. **(B)** Boxplot showing significant difference (Wilcoxon p-value< 0.1) in hypoxia scores of normal tissues between the CGC-m and non-mutated groups.

Despite these challenges, these results suggest that microenvironmental changes play an important role in the initiating stages of cancer progression and are tissue specific. Studying these changes may provide new avenues for early intervention of cancer, for targeted therapies, or enhance activities of conventional therapies.

Data availability statement

Publicly available datasets were analyzed in this study. This data can be found here: https://gtexportal.org/home/.

Ethics statement

The studies involving human participants were reviewed and approved by GTEX Consortium. Written informed consent to participate in this study was provided by the participants' legal guardian/next of kin. The animal study was reviewed and approved by GTEX Consortium.

Author contributions

VY designed the study, collected, and analyzed the data. CM and JH collected data and analyzed the data. CM, EC, and VY wrote the paper. All authors contributed to the article and approved the submitted version.

Funding

We thank Childrens Hospital Los Angeles, Pathology and Lab Medicine Fund (8231000-TUA010247) for supporting Chetan Munugula.

Conflict of interest

The authors declare that the research was conducted in the absence of any commercial or financial relationships that could be construed as a potential conflict of interest.

Publisher's note

All claims expressed in this article are solely those of the authors and do not necessarily represent those of their affiliated organizations, or those of the publisher, the editors and the reviewers. Any product that may be evaluated in this article, or claim that may be made by its manufacturer, is not guaranteed or endorsed by the publisher.

Supplementary material

The Supplementary Material for this article can be found online at: https://www.frontiersin.org/articles/10.3389/fonc.2022.1021940/full#supplementary-material

References

1. Xie M, Lu C, Wang J, McLellan MD, Johnson KJ, Wendl MC, et al. Age-related mutations associated with clonal hematopoietic expansion and malignancies. *Nat Med* (2014) 20:1472–8. doi: 10.1038/nm.3733

2. Jaiswal S, Natarajan P, Silver AJ, Gibson CJ, Bick AG, Shvartz E, et al. Clonal hematopoiesis and risk of atherosclerotic cardiovascular disease. *New Engl J Med* (2017) 377:111–21. doi: 10.1056/NEJMoa1701719

3. Martincorena I, Roshan A, Gerstung M, Ellis P, Van Loo P, McLaren S, et al. High burden and pervasive positive selection of somatic mutations in normal human skin. *Science* (2015) 348:880–6. doi: 10.1126/science.aaa6806

4. Yokoyama A, Kakiuchi N, Yoshizato T, Nannya Y, Suzuki H, Takeuchi Y, et al. Age-related remodelling of oesophageal epithelia by mutated cancer drivers. *Nature* (2019) 565:312–7. doi: 10.1038/s41586-018-0811-x

5. Hanahan D. Hallmarks of cancer: New dimensions. *Cancer Discovery* (2022) 12:31–46. doi: 10.1158/2159-8290.CD-21-1059

6. Eilken HM, Adams RH. Dynamics of endothelial cell behavior in sprouting angiogenesis. *Curr Opin Cell Biol* (2010) 22:617–25. doi: 10.1016/j.ceb.2010.08.010

7. Wang J, Li D, Cang H, Guo B. Crosstalk between cancer and immune cells: Role of tumor-associated macrophages in the tumor microenvironment. *Cancer Med* (2019) 8:4709–21. doi: 10.1002/cam4.2327

8. Srivastava S, Ghosh S, Kagan J, Mazurchuk R, Boja E, Chuaqui R, et al. The making of a PreCancer atlas: promises, challenges, and opportunities. *Trends Cancer* (2018) 4:523–36. doi: 10.1016/j.trecan.2018.06.007

9. Aran D, Camarda R, Odegaard J, Paik H, Oskotsky B, Krings G, et al. Comprehensive analysis of normal adjacent to tumor transcriptomes. *Nat Commun* (2017) 8:1–14. doi: 10.1038/s41467-017-01027-z

10. Yizhak K, Aguet F, Kim J, Hess JM, Kübler K, Grimsby J, et al. RNA Sequence analysis reveals macroscopic somatic clonal expansion across normal tissues. *Science* (2019) 364(6444):eaaw0726. doi: 10.1126/science.aaw0726

11. García-Nieto PE, Morrison AJ, Fraser HB. The somatic mutation landscape of the human body. *Genome Biol* (2019) 20:298. doi: 10.1186/s13059-019-1919-5

12. Muyas F, Zapata L, Guigó R, Ossowski S. The rate and spectrum of mosaic mutations during embryogenesis revealed by RNA sequencing of 49 tissues. *Genome Med* (2020) 12:49. doi: 10.1186/s13073-020-00746-1

13. Aran D, Hu Z, Butte AJ. xCell: digitally portraying the tissue cellular heterogeneity landscape. *Genome Biol* (2017) 18:1–14. doi: 10.1186/s13059-017-1349-1

14. Steen C. B., Liu C. L., Alizadeh A. A., Newman A. M. (2020). Profiling cell type abundance and expression in bulk tissues with CIBERSORTx. In *Stem cell transcriptional networks* (pp. 135–157). Humana, New York, NY.

15. Marderstein AR, Uppal M, Verma A, Bhinder B, Tayyebi Z, Mezey J, et al. Demographic and genetic factors influence the abundance of infiltrating immune cells in human tissues. *Nat Commun* (2020) 11:1–14. doi: 10.1038/s41467-020-16097-9

16. Sturm G, Finotello F, Petitprez F, Zhang JD, Baumbach J, Fridman WH, et al. Comprehensive evaluation of transcriptome-based cell-type quantification methods for immuno-oncology. *Bioinformatics* (2019) 35:i436–45. doi: 10.1093/bioinformatics/btz363

17. Kim J, Bowlby R, Mungall AJ, Robertson AG, Odze RD, Cherniack AD, et al. Integrated genomic characterization of oesophageal carcinoma. *Nature* (2017) 541:169–75. doi: 10.1038/nature20805

18. Akbani R, Akdemir KC, Aksoy BA, Albert M, Ally A, Amin SB, et al. Genomic classification of cutaneous melanoma. *Cell* (2015) 161:1681–96. doi: 10.1016/j.cell.2015.05.044

19. Voutilainen M, Färkkilä M, Juhola M, Nuorva K, Mauranen K, Mäntynen T, et al. Specialized columnar epithelium of the esophagogastric junction: prevalence and associations. *Am J Gastroenterol* (1999) 94:913–8. doi: 10.1111/j.1572-0241.1999.986_i.x

20. Ricard N, Tu L, Le Hiress M, Huertas A, Phan C, Thuillet R, et al. Increased pericyte coverage mediated by endothelial-derived fibroblast growth factor-2 and interleukin-6 is a source of smooth muscle–like cells in pulmonary hypertension. *Circulation* (2014) 129:1586–97. doi: 10.1161/CIRCULATIONAHA.113.007469

21. Akkiraju H, Nohe A. Role of chondrocytes in cartilage formation, progression of osteoarthritis and cartilage regeneration. *J Dev Biol* (2015) 3:177–92. doi: 10.3390/jdb3040177

22. Roche J. (2018) 10:52. MDPI.

23. Dongre A, Weinberg RA. New insights into the mechanisms of epithelial–mesenchymal transition and implications for cancer. *Nat Rev Mol Cell Biol* (2019) 20:69–84. doi: 10.1038/s41580-018-0080-4

24. Deshmukh AP, Vasaikar SV, Tomczak K, Tripathi S, Den Hollander P, Arslan E, et al. Identification of EMT signaling cross-talk and gene regulatory networks by single-cell RNA sequencing. *Proc Natl Acad Sci* (2021) 118: e2102050118. doi: 10.1073/pnas.2102050118

25. Vermeulen K, Van Bockstaele DR, Berneman ZN. The cell cycle: a review of regulation, deregulation and therapeutic targets in cancer. *Cell prolif* (2003) 36:131–49. doi: 10.1046/j.1365-2184.2003.00266.x

26. Geiger B, Yamada KM. Molecular architecture and function of matrix adhesions. *Cold Spring Harb Perspect Biol* (2011) 3(5):a005033. doi: 10.1101/cshperspect.a005033

27. Muz B, de la Puente P, Azab F, Azab AK. The role of hypoxia in cancer progression, angiogenesis, metastasis, and resistance to therapy. *Hypoxia* (2015) 3:83. doi: 10.2147/HP.S93413

28. Bhandari V, Li CH, Bristow RG, Boutros PC. Divergent mutational processes distinguish hypoxic and normoxic tumours. *Nat Commun* (2020) 11:1–10. doi: 10.1038/s41467-019-14052-x

29. Lee-Six H, Olafsson S, Ellis P, Osborne RJ, Sanders MA, Moore L, et al. The landscape of somatic mutation in normal colorectal epithelial cells. *Nature* (2019) 574:532–7. doi: 10.1038/s41586-019-1672-7

frontiers | Frontiers in Pharmacology

TYPE Original Research
PUBLISHED 17 April 2023
DOI 10.3389/fphar.2023.1144330

OPEN ACCESS

EDITED BY
Kenneth K. W. To,
The Chinese University of Hong Kong, China

REVIEWED BY
Shuzhen Wang,
China Pharmaceutical University, China
Yan Li,
Guangdong Pharmaceutical University, China

*CORRESPONDENCE
Jingting Jiang,
jiangjingting@suda.edu.cn
Lujun Chen,
chenlujun@suda.edu.cn

†These authors have contributed equally to this work

SPECIALTY SECTION
This article was submitted to Pharmacology of Anti-Cancer Drugs, a section of the journal Frontiers in Pharmacology

RECEIVED 14 January 2023
ACCEPTED 21 March 2023
PUBLISHED 17 April 2023

CITATION
Feng C, Chen R, Fang W, Gao X, Ying H, Zheng X, Chen L and Jiang J (2023), Synergistic effect of CD47 blockade in combination with cordycepin treatment against cancer.
Front. Pharmacol. 14:1144330.
doi: 10.3389/fphar.2023.1144330

Synergistic effect of CD47 blockade in combination with cordycepin treatment against cancer

Chen Feng[1,2,3†], Rongzhang Chen[1,2,3†], Weiwei Fang[1,2,3], Xinran Gao[1,2,3], Hanjie Ying[4], Xiao Zheng[1,2,3], Lujun Chen[1,2,3*] and Jingting Jiang[1,2,3*]

[1]Department of Tumor Biological Treatment, The Third Affiliated Hospital of Soochow University, Chang Zhou, Jiang Su, China, [2]Jiangsu Engineering Research Center for Tumor Immunotherapy, The Third Affiliated Hospital of Soochow University, Chang Zhou, Jiang Su, China, [3]Institute of Cell Therapy, The Third Affiliated Hospital of Soochow University, Chang Zhou, Jiang Su, China, [4]College of Biotechnology and Pharmaceutical Engineering, Nanjing Tech University, Nanjing, Jiang Su, China

Cordycepin is widely considered a direct tumor-suppressive agent. However, few studies have investigated as the effect of cordycepin therapy on the tumor microenvironment (TME). In our present study, we demonstrated that cordycepin could weaken the function of M1-like macrophages in the TME and also contribute to macrophage polarization toward the M2 phenotype. Herein, we established a combined therapeutic strategy combining cordycepin and an anti-CD47 antibody. By using single-cell RNA sequencing (scRNA-seq), we showed that the combination treatment could significantly enhance the effect of cordycepin, which would reactivate macrophages and reverse macrophage polarization. In addition, the combination treatment could regulate the proportion of $CD8^+$ T cells to prolong the progression-free survival (PFS) of patients with digestive tract malignancies. Finally, flow cytometry validated the changes in the proportions of tumor-associated macrophages (TAMs) and tumor-infiltrating lymphocytes (TILs). Collectively, our findings suggested that the combination treatment of cordycepin and the anti-CD47 antibody could significantly enhance tumor suppression, increase the proportion of M1 macrophages, and decrease the proportion of M2 macrophages. In addition, the PFS in patients with digestive tract malignancies would be prolonged by regulating $CD8^+$ T cells.

KEYWORDS

cordycepin, anti-CD47, macrophage, tumor microenvironment, scRNA-seq

Introduction

Cordycepin (3′-deoxyadenosine) is a critical bioactive component of *Cordyceps militaris*, which has a wide range of biological effects, such as antitumor, anti-inflammatory, and antidiabetic properties. Recent experiments have shown that cordycepin has a direct and safe antitumor efficacy in breast cancer (Liu et al., 2020a), cholangiocarcinoma (CCA) (Wang et al., 2017; Liu et al., 2020b), non-small cell lung cancer (NSCLC) (Wei et al., 2019), and bladder cancer (Kim et al., 2019). Furthermore, accumulating evidence has indicated that cordycepin can attack the DNA, induce the production of reactive oxygen species (ROS), and promote apoptosis by deactivating the PI3K/AKT pathway (Nasser et al., 2017; Zeng et al.,

2017; Kim et al., 2019; Wang et al., 2019). In addition, cordycepin can enhance cisplatin and temozolomide sensitivity by inhibiting the PI3K/AKT pathway (Bi et al., 2018; Gao et al., 2020). Moreover, with regard to breast cancer, multiple studies have shown that cordycepin can suppress epithelial–mesenchymal transition (EMT), invasion, and metastasis by inhibiting the Hedgehog pathway and the generation of ROS (Liu et al., 2020a; Wei et al., 2022). Overall, cordycepin inhibits migration, proliferation, and invasion of tumor cells and EMT *via* promoting apoptosis. In addition, cordycepin can significantly suppress inflammatory responses in chronic kidney disease (Sun et al., 2019), acute pancreatitis (Yang et al., 2020), and acute pneumonia (Kim et al., 2011) by inhibiting both the phosphorylation of MAPKs and the activation of NF-κB.

In recent years, immunotherapy has emerged as an essential treatment for cancer, in addition to surgery, chemotherapy, and radiotherapy. CD47 is a cell surface molecule that is widely expressed in most cancers. It consists of an extracellular domain known as IgSF, five transmembrane domains, and one variable intracellular domain. Accumulating evidence showed a positive connection between high CD47 expression and poor prognoses in various cancers, such as NSCLC (Arrieta et al., 2020) and gastric cancer (GC) (Shi et al., 2021). The SIRP family includes five primary members, namely, SIRPα, SIRPβ1, SIRPβ2, SIRPγ, and SIRPδ. Among them, SIRPα and SIRPγ, when activated by their corresponding CD47 receptors, played an inhibitory role. When CD47 interacts with SIRPα, the immune-receptor tyrosine-based inhibitory motif (ITIM), the intracellular domain of SIRPα is activated and phosphorylated. In addition, the phosphatases SHP-1 and SHP-2 are activated by ITIM (Kharitonenkov et al., 1997; Jiang et al., 1999). The heterogeneity of macrophages has different responses to pathogens and external stimuli. Macrophages have been activated in a kind of continuous mode from classically activated (M1) macrophages (pro-inflammatory/antitumor) to activated (M2) macrophages (anti-inflammatory/pro-tumor) (Goerdt et al., 1999; Mantovani et al., 2002; Sica et al., 2008). Increased tumor-associated macrophage (TAM) infiltration and phagocytic function are found when the interaction between CD47 and SIRPα is blocked (Weiskopf et al., 2016; Li et al., 2018; Schürch et al., 2019). In addition, it has been confirmed that the blockade of the CD47-SIRPα pathway in the treatment of tumors can significantly increase the phagocytic function of M1 macrophages, leading to a converse shift from M2 macrophages to M1 macrophages (Zhang et al., 2016). Two clinical trials (EudraCT numbers: 2016-004372-22 and NCT02641002) were terminated in 2017 and 2018 due to severe anemia that resulted in adverse drug reactions (ADRs). However, in 2019, a clinical trial about the combination treatment of the CD47 antibody and azacytidine for acute myeloid leukemia (AML) and myelodysplastic syndrome (MDS) indicated high treatment efficacy and high ADRs (Sallman et al., 2019).

In this study, we investigated the effectiveness of a combination treatment using an anti-CD47 antibody and cordycepin to enhance tumor inhibition. By using single-cell RNA sequencing (scRNA-seq), we confirmed that this combination treatment increased the proportion of M1-like macrophages and decreased the proportion of M2-like macrophages. Furthermore, the combination treatment was found to prolong progression-free survival (PFS) in patients with colorectal cancer (CRC) by regulating $CD8^+$ T cells. We also used flow cytometry to analyze the reshaping of the tumor microenvironment (TME). In conclusion, this combination treatment proved to be a valuable therapeutic strategy for various types of cancer.

Materials and methods

Cell culture and experimental animals

The mouse colon cancer cell lines MC38 and CT26 were provided by the Chinese Academy of Sciences, Shanghai Institutes for Biological Sciences (Shanghai, China). Briefly, MC38 and CT26 cells were maintained in DMEM (Gibco, Thermo Fisher Scientific, United States) supplemented with 10% (v/v) fetal bovine serum (FBS) and 100 U/mL penicillin. In addition, male C57BL/6J and Balb/c mice (6–8 weeks old) were housed in a specific pathogen-free (SPF) environment in Cavens Laboratory Animals (Jiangsu Changzhou, China). All animal-related procedures were approved by the Ethics Committee of the Third Affiliated Hospital of Soochow University.

Animal models and *in vivo* treatment

Briefly, 1×10^6 MC38 cells were injected under the skin (s.c.) on the right flank of C57BL/6J mice, and $1e^{-6}$ CT26 cells were injected subcutaneously (s.c.) on the right flank of Balb/c mice. Different treatments were given when the maximal diameter of the tumor was greater than 5 mm, including PBS, cordycepin, CD47 antibody (Clone MIAP301, BioXcell, United States), and combination therapy (anti-CD47+ cordycepin) groups. The mice were treated with the CD47 antibody (200 μg/mouse 200 *i. p.*) on days 0, 4, 8, and 12 during the treatment. Extraction and purification of cordycepin were completed by the College of Biotechnology and Pharmaceutical Engineering, Nanjing Tech University. Cordycepin was kept in clean and dried tubes at 4°C. It was dissolved in saline. The mice were treated daily with cordycepin (500 μg/mouse, i. g.). The tumor volume was measured every 2 days and calculated using the formula as follows: $V = \text{Length} \times \text{Width}^2 \times \pi/6$.

Flow cytometry

The tumor tissues were minced into pieces smaller than 1 mm^3. Next, the tumors were digested with DNase I (REF 10104159001, Roche) and Liberase TL (REF 05401020001, Roche). Once the digestion was complete, a serum-containing culture medium was added, followed by grinding and screening through a 200-μm strainer to obtain a single-cell suspension. Antibodies against mouse CD45 (Clone 30-F11, BD Biosciences), Ghost (No. 59863S, Cell Signaling Technology), CD3 (Clone 17A2, BD Biosciences), CD4 (Clone GK1.5, BD Biosciences), CD8 (Clone 53-6.7, BD Biosciences), GR1 (Clone RB6-8C5, BD Biosciences), CD11b (Clone M1/70, BD Biosciences), MHC-II (Clone M5/114.15.2, BD Biosciences), F4/80 (Clone BM8, BD Biosciences), and CD206 (Clone CO68C2, BD Biosciences) were used to stain

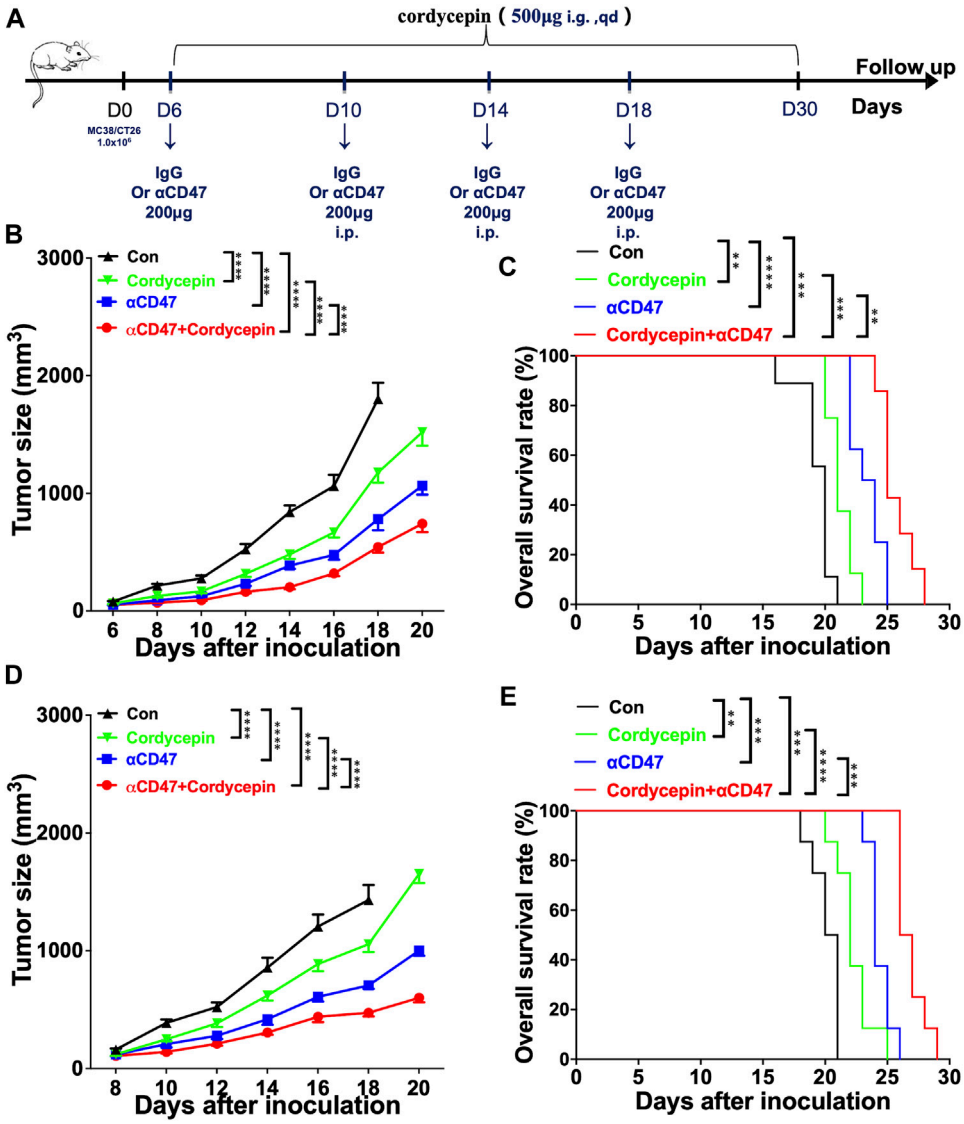

FIGURE 1
Combination treatment shows significant therapeutic effects in animal models **(A)**. Schematic illustration of the experimental design time flow. MC38 tumor-bearing mice or CT26 tumor-bearing mice were treated with anti-CD47 antibodies or IgG (control) on days 6, 10, 14, and 18 after tumor inoculation. The mice were treated with cordycepin *via* daily gavage **(B, D)**. Tumor growth curves of all groups, following the injection of 1×10^6 MC38 or CT26 cells (n > = 6, representative results from three independent experiments) **(C, E)**. KM survival analysis of the mice from **(B, D)** (log-rank (Mantel–Cox) test) (n = 6, representative results from three independent experiments). n. s. (not significant) $p > 0.05$, *$p < 0.05$, **$p < 0.01$, ***$p < 0.001$, and ****$p < 0.0001$.

cells. Data acquisition was conducted using a Beckman Coulter DxFLEX cytometer, followed by data analysis using FlowJo software (version 10.8.1, FlowJo Software, United States).

scRNA-seq

Using the aforementioned method, single-cell suspensions of the tumors were prepared. For FACS sorting, the cells were enriched using the CD45 [tumor-infiltrating lymphocytes (TILs)] Microbead Mouse Kit (Cat. 130-110-618, Miltenyi Biotec, Lerden, Netherlands) and stained with Ghost Dye™ Violet 510 Viability Dye (No. 59863S, Cell Signaling Technology) and Percp-Cy5.5-CD45 (Clone 30-F11, BD Biosciences) antibodies. Each sample contained approximately 1×10^6 $CD45^+$ cells sorted using the BD FACSAria II instrument. FACS analysis was used to sort single cells into flow tubes, and the AOPI was used to determine the viability of the cells. In order to produce single-cell gel beads in the emulsion, the cell suspension, which contained 300–600 living cells per microliter according to CountStar, was loaded onto the chromium single-cell controller (10x Genomics). Using an S1000TM Touch Thermal Cycler (Bio-Rad), single-cell transcriptome amplification was conducted at 53°C for 45 min, followed by incubation at 85°C for 5 min and holding at 4°C for 10 min. An Agilent 4200 instrument was used to assess the

10.3389/fphar.2023.1144330

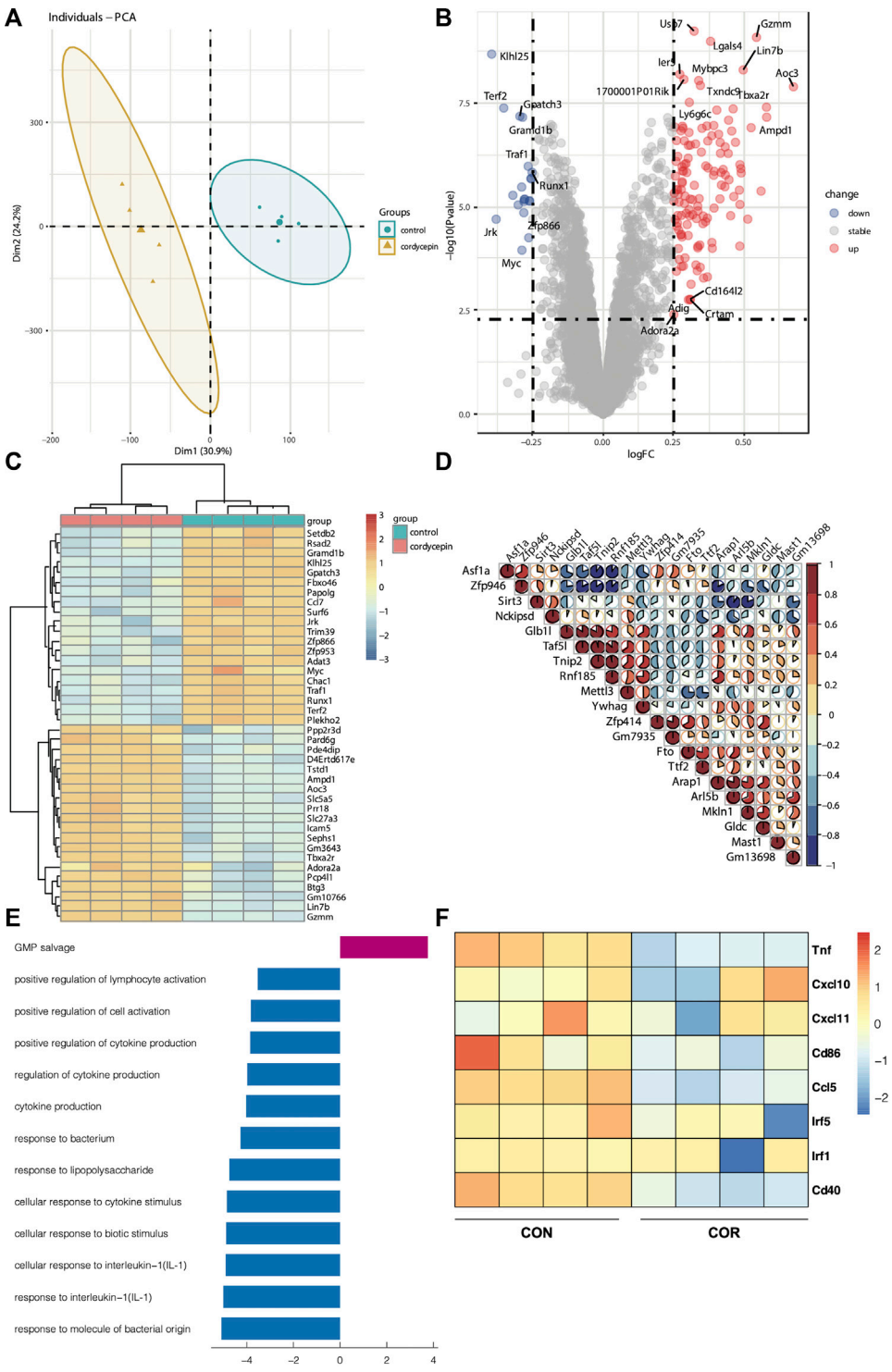

FIGURE 2
Cordycepin decreases the function of macrophage I (M1 macrophages) **(A)**. PCA showed the difference between the two groups **(B)**. DEGs of two groups. The marked genes by tags were those with a *p*-value < 0.005 and a log Fc > 0.25 **(C)**. Heatmap was chosen to show the top 20 up- and downregulated genes **(D)**. Heatmap was chosen to show the correlations of the top 20 genes **(E)**. KEGG pathway enrichment analysis was performed utilizing the KEGG pathway database (http://www.genome.jp/kegg). Based on the function of macrophages, the pathways were selected. The decreasing function is represented by the bar graphs (blue), and the increasing function is represented by the bar graphs (red) **(F)**. Heatmap was chosen to show the differential gene expression of molecular markers of the M1 phenotype. Cordycepin was represented by "COR".

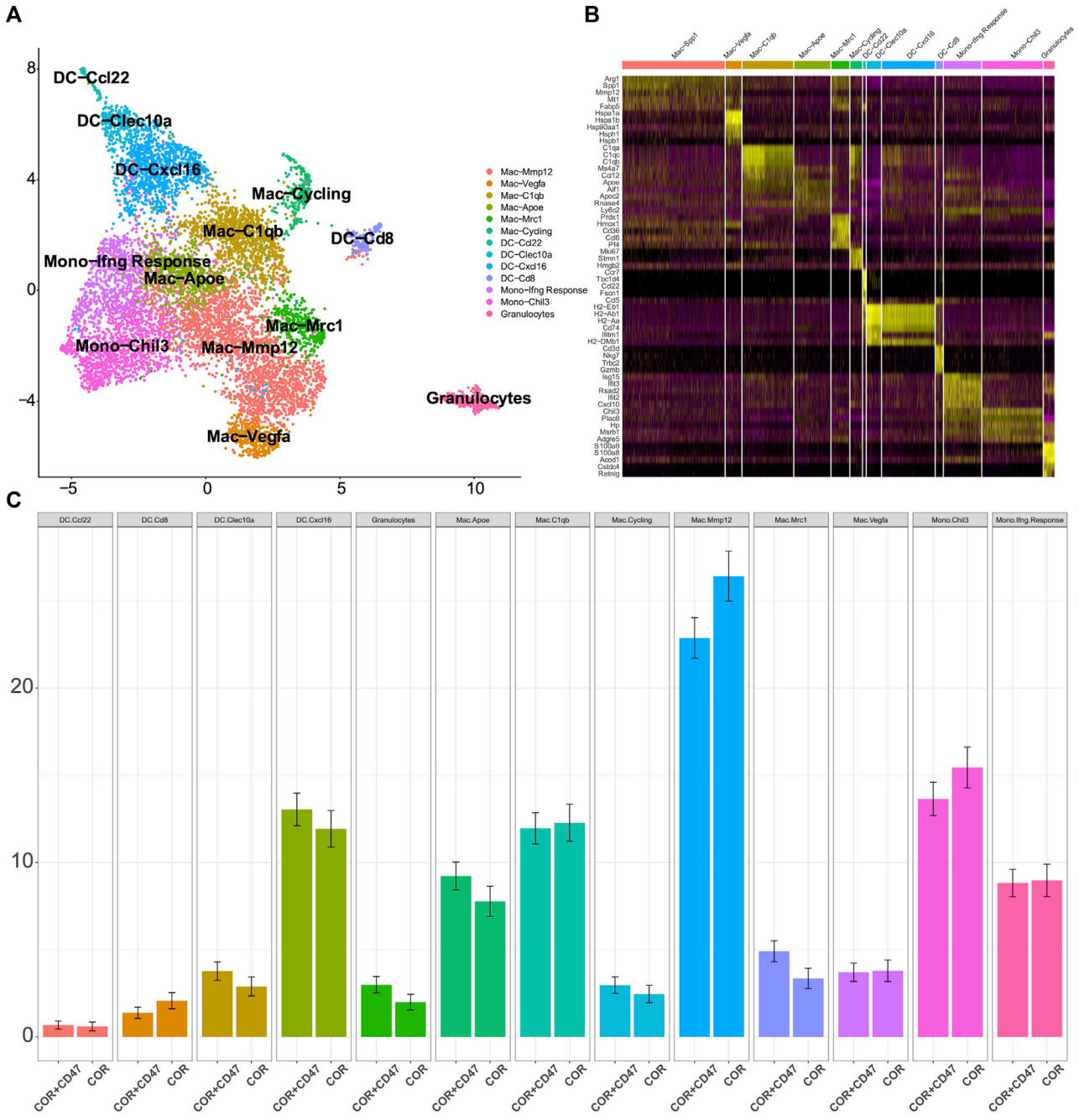

FIGURE 3
scRNA-seq is used to test the changes in myeloid cells **(A)**. Sub-clustering of myeloid cells is shown on the UMAP plots of the scRNA-seq dataset **(B)**. Individual myeloid cell clusters in the scRNA-seq data could be identified phenotypically based on a heatmap of myeloid cell lineage and functional markers **(C)**. MC38 tumors from the combination treatment group or cordycepin group showed the proportions of different subpopulations of myeloid cells. "COR + CD47" represents the combined treatment group; "COR" represents the cordycepin treatment group.

quality of the cDNA templates (performed by CapitalBio Technology, Beijing).

scRNA-seq data processing

Gene-barcode matrices were generated using Cell Ranger (v5.0.0) software by demultiplexing and aligning raw sequencing data to the mm10 mouse reference genome. Filtration, normalization, dimensionality reduction, clustering, and differential expression analysis were performed using the Seurat (v4.1.1) R package. The following criteria were applied to remove low-quality cells: gene number between 200 and 6,000, UMI count >1,000, and mitochondrial content >10%. A total of 12,907 cells were obtained after filtration. The batch effect across different samples was eliminated using the Harmony (v0.1.0) method. The "ElbowPlot" function was

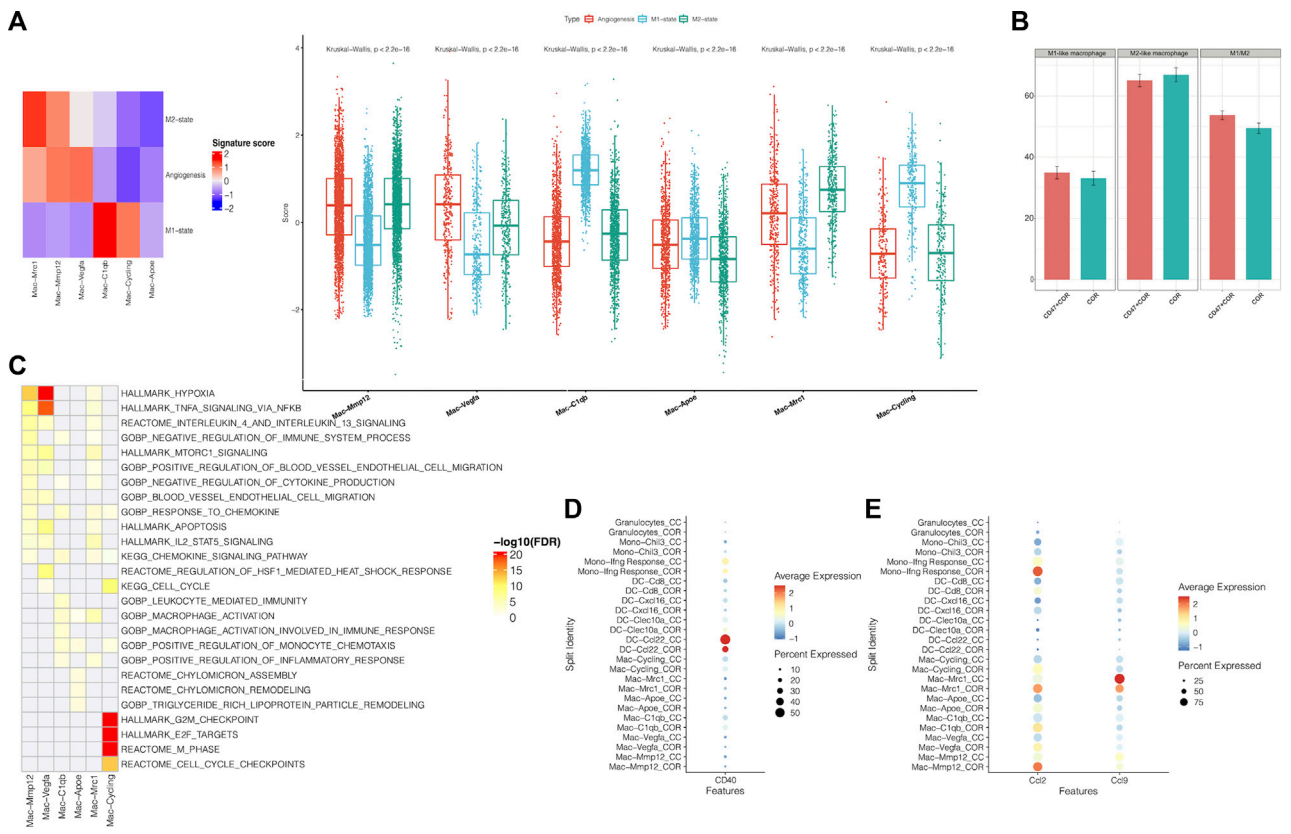

FIGURE 4
Function of sub-clustering in myeloid cells is confirmed by scRNA-seq **(A)**. Using the scRNA-seq data, M1-state, M2-state, and angiogenesis signature scores for each myeloid cell cluster are shown by a heatmap and boxplot **(B)**. This bar graph shows the changes of M1-like macrophages and M2-like macrophages **(C)**. Using the KEGG database, pathways were significantly enriched in the scRNA-seq data for each macrophage cluster **(D)**. A dot plot showed the expression of CD40 on myeloid cells in MC38 tumors from the combination treatment group or cordycepin group **(E)**. Different expressions of chemokines in different subpopulations of myeloid cells are shown by a dot plot in MC38 tumors from the combination treatment group or cordycepin group. "COR + CD47" represents the combined treatment group; "COR" represents the cordycepin treatment group.

adopted to select the top 40 harmony embeddings to perform clustering and visualization. Different clustering results were generated using the "FindClusters" function with resolutions ranging from 0.2 to 1.2. A suitable resolution was determined using the clustree package (v0.5.0) in R. Finally, 24 clusters were obtained (resolution = 1.2). A total of 12,772 cells were retained for further analysis after excluding two clusters (18) that did not express any known markers. The MAST method ("FindAllMarkers") was used for differential gene analysis. Log2-fold changes greater than 0.25 and Bonferroni-adjusted *p*-values less than 0.05 were used to identify differentially expressed genes (DEGs). In the second round of clustering for $CD8^+$ T cells and myeloid cells, the SCTransform method was used to normalize the expression matrix, the Harmony method was used for integration analysis, and the FindNeighbor and FindCluster functions were used for clustering.

Gene Expression Omnibus (GEO) data

The GEO dataset was downloaded from the GEO database (http://www.ncbi.nlm.nih.gov/geo)(GEO accession No. GSE126157). Principal component analysis (PCA) was conducted using the FactoMineR and factoextra R packages. DEGs were identified using the limma R package. Heatmap was constructed using the limma, ggplot2, and pheatmap packages. Finally, KEGG (Kyoto Encyclopedia of Genes and Genomes) pathway analysis was carried out using the org.Mm.eg.db and dplyr R packages.

The Cancer Genome Atlas (TCGA) data and COX survival model

RNA-seq profiles and corresponding clinical information on CRC, CCA, GC, and esophageal carcinoma (ESCC) were downloaded from TCGA database (https://portal.gdc.com). The count data were converted to TPM and normalized, matching with the corresponding clinical information. Log-rank was used to compare differences in survival. The timeROC (version 0.4) analysis was used to compare the predictive accuracy. R package survival was used to build the COX survival model. For Kaplan–Meier (KM) curves, *p*-values and hazard ratios (HRs) with 95% confidence interval (CI) were generated by log-rank tests and univariate cox proportional hazards regression. HOME for researchers (www.home-for-researchers.com) was used to analyze the TCGA data.

10.3389/fphar.2023.1144330

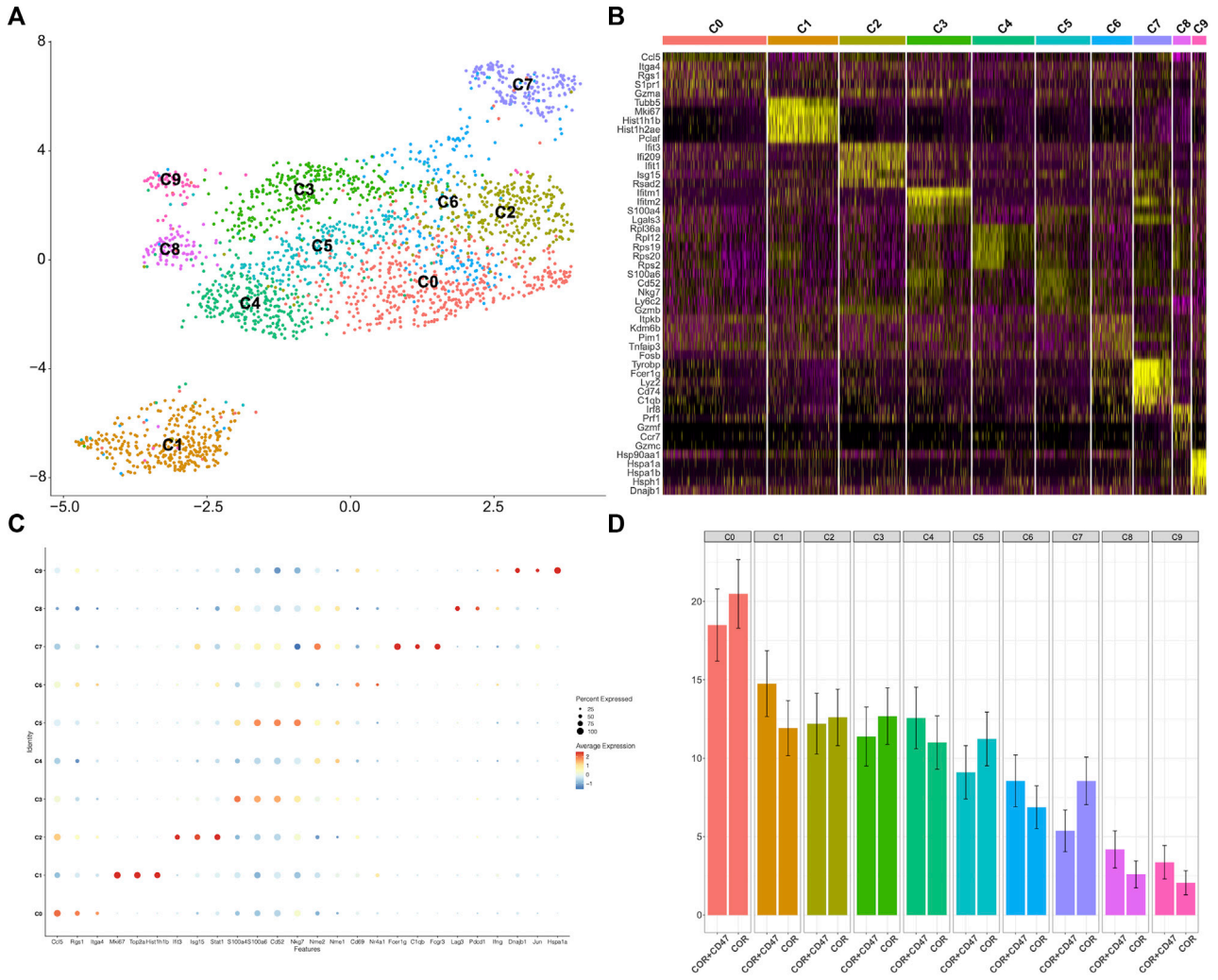

FIGURE 5
scRNA-seq analysis is used to test the changes of CD8⁺ T cells **(A)**. UMAP plots of the scRNA-seq dataset show sub-clustering of CD8⁺ T cells **(B)**. Individual CD8⁺ T-cell clusters in the scRNA-seq data could be identified phenotypically based on a heatmap of CD8⁺ T-cell lineage and functional markers **(C)**. A dot plot showed the expression levels and activity scores of known phenotypic markers in each CD8⁺ T-cell cluster **(D)**. The proportions of different subpopulations of CD8⁺ T cells are shown by bar graphs in MC38 tumors from the combination treatment group or cordycepin group.

Statistical analysis

GraphPad Prism V.10 software was used to perform statistical analyses, and the data were expressed as mean ± SEM. The one-tailed, unpaired Student's t-test was used to compare the two groups. In addition, tumor growth curves were compared by the two-way ANOVA. Finally, the survival of the mice was analyzed using the KM method and the log-rank test. $p < 0.05$ was considered statistically significant.

Results

Anti-CD47 antibody in combination with cordycepin shows a significant therapeutic effect on colon cancer models in mice

We constructed the subcutaneous tumor models to validate the combined therapeutic effect using the murine CRC cell lines MC38 and CT26. Then, the tumor-bearing mice were subjected to anti-CD47, cordycepin, and combination treatments. Cordycepin was administered daily by oral gavage for 30 days. In addition, the anti-CD47 antibody and control IgG were administered every 4 days *via* intraperitoneal injection (Figure 1A). For mouse models of MC38 CRC, combination treatment significantly decreased the proliferation of tumor cells and prolonged survival (Figures 1B, C). Moreover, for mouse models of CT26, the combination treatment showed a significant effect. Taken together, the combination treatment decreased the proliferation of tumor cells and prolonged survival (Figures 1D, E).

Cordycepin inhibits the function of M1 macrophages

Many studies have confirmed that cordycepin exerts its antitumor effects directly by inducing the apoptosis of tumor

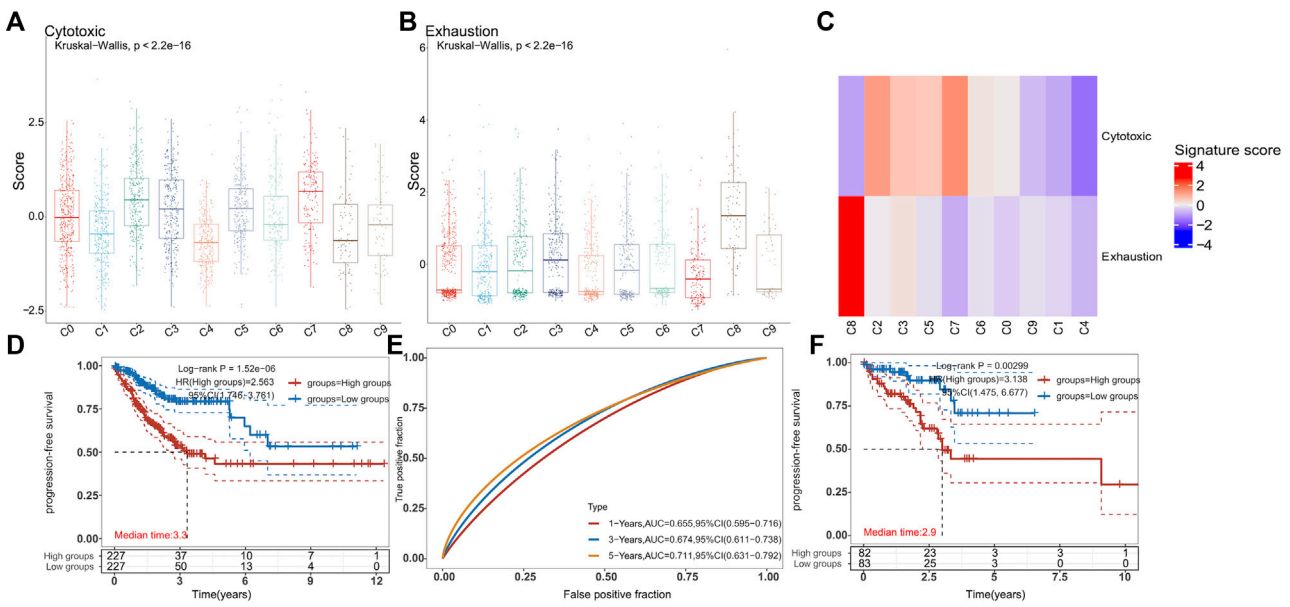

FIGURE 6
Combination treatment is confirmed to increase the PFS of patients with digestive tract malignancy by regulating the CD8$^+$ T-cell sub-cluster **(A–C)**. In the scRNA-seq data, boxplots and heatmaps showed the cytotoxicity and exhaustion signature scores for each CD8$^+$ T-cell cluster. The VISION method was used to calculate signature scores for each cell cluster (two-sided Wilcoxon test) **(D)**. KM survival curves of TCGA-CRC patients (n = 455) grouped by the averaged expression of the COX model (with the median value as the threshold). HR (high expression) represents the hazard ratio of the low-expression sample relative to the high-expression sample. HR (95% CI) represents the median survival time (LT50) for different groups. The blue line represents the low expression of the average expression of the COX model, and the red line represents the high expression **(E)**. The ROC model was used to test the accurate survival prediction for 1 year, 3 years, and 5 years. The higher AUC score corresponded to higher predictive power **(F)**. The rectal cancer data and clinical information were downloaded from TCGA database (n = 165). KM survival curves **(F)** were the same as **(E)**.

cells (Wang et al., 2017; Jin et al., 2018; Liu et al., 2020a). To test the effect of cordycepin on macrophages, we found the matrix used to record the gene expression of macrophages treated by cordycepin (GSE126157) (Ashraf et al., 2019). We selected the LPS-induced macrophage group and LPS-induced macrophages treated with the cordycepin group as a new matrix. This new matrix was then subjected to PCA. Moreover, we found that PCA could discriminate between the control and cordycepin groups (Figure 2A), indicating that cordycepin could significantly influence the function of M1-like macrophages. DEG analysis showed that the expressions of the *Myc* and *Ccl7* genes were decreased in the cordycepin group (Figure 2B), confirming that the *Myc* gene could promote macrophage proliferation in a non-inflammatory manner (Yin et al., 2020; Gerlach et al., 2021). In addition, the *Ccl7* gene could promote macrophage polarization to M1-like macrophages and increase the level of macrophage infiltration (He et al., 2019; Xie et al., 2021). We found that the regulatory genes were enriched in multiple pathways (Figures 2C, D). In addition, enrichment and signaling pathway analysis were performed for DEGs (Figure 2E). We found that cordycepin could dampen the function of M1-like macrophages in the LPS-induced macrophage model (Figure 2E), such as by decreasing the interaction between macrophages and IL-1 and cytokine production. Finally, gene markers of the M1 macrophages were compared in DEGs, and we found that cordycepin would decrease the expression of these molecular markers (Figure 2F).

Anti-CD47 reverses the inhibitory effect of cordycepin on M1-like macrophages

We found that the combination treatment resulted in better effects than the cordycepin treatment alone (Figure 1), and the cordycepin treatment could weaken the function of M1-like macrophages (Figure 2). Therefore, we hypothesized that the anti-CD47 antibody would increase the inhibitory effect. To test this hypothesis, we used scRNA-seq in MC38 tumor-bearing mice. Starting from the second day of the third anti-CD47 mAb treatment cycle, cordycepin was administered daily through gavage. The tumors were dissociated into a single-cell suspension. The dissociated cells were positively selected using CD45 microbeads and sorted by flow cytometry (Supplementary Figures S1A, B). Furthermore, all cells were divided into six clusters, including B cells, CD4$^+$ T cells, CD8$^+$ T cells, γδT, myeloid cells, and natural killer (NK) cells (Supplementary Figure S1C).

The cluster of myeloid cells was chosen to analyze the function of dendritic cells (DCs) and macrophages. First, we used the DEGs to define all clusters (Figures 3A, B). We found that the number of M2 macrophages in the combination treatment group decreased, which accounted for a high proportion of all macrophages. For DCs, *Cxcl16* DCs and *Clex10a* DCs were increased in the combination treatment group (Figure 3C). Moreover, we determined the M1-like macrophage score and the M2-like macrophage score to assess the function of TAMs. Genes associated with M1 macrophages include *C1qc*, *C1qb*, *Il23*, *Tnf*, *Cxcl9*, *Cd86*, *Il1a*, *Il1b*, *Il6*, *Ccl5*, *Irf7*, *Irf1*,

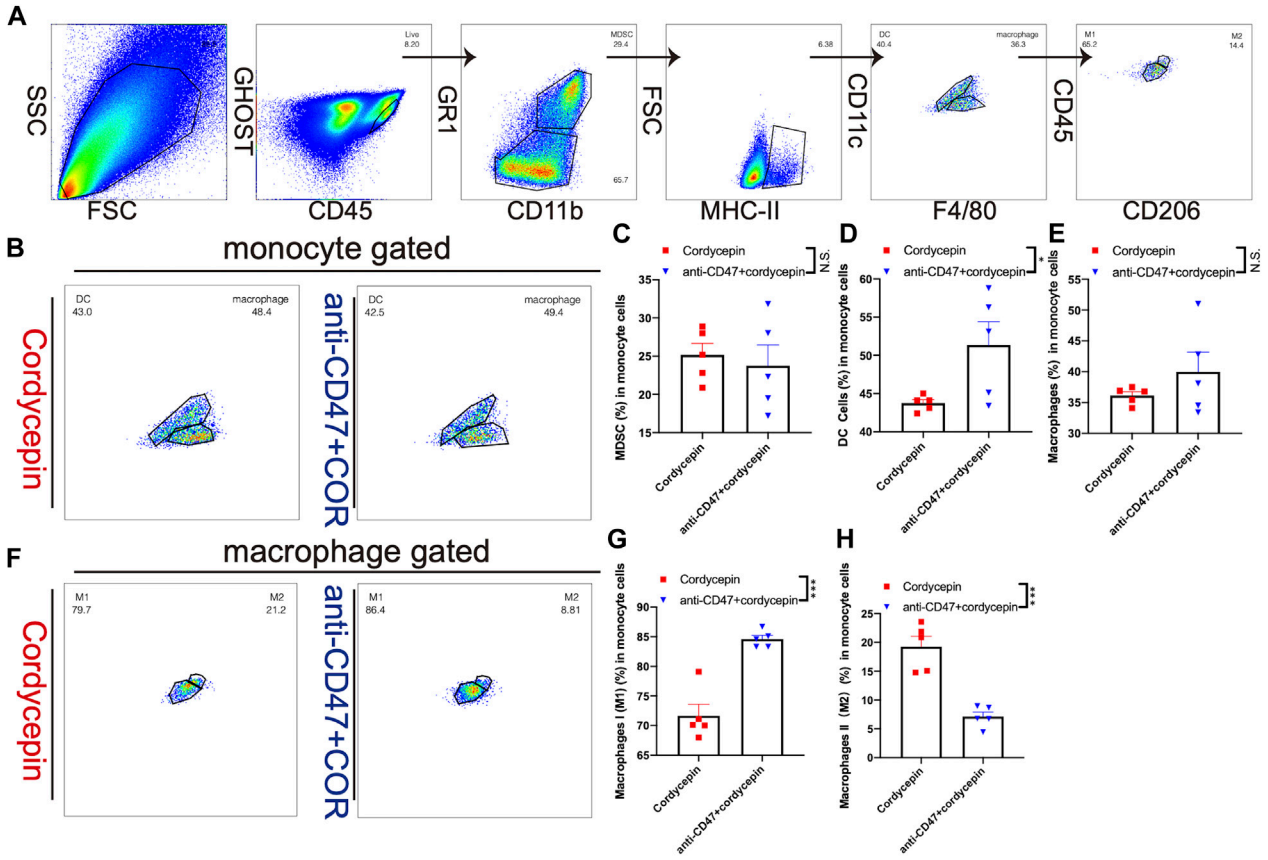

FIGURE 7
Change level of TAMs is shown by flow cytometry **(A)**. Gating strategy for flow cytometric phenotyping was used to identify the proportions of macrophages and DCs **(B)**. Different proportions of macrophages and DCs are shown by a dot plot. (n = 5, representative results from three independent experiments) **(C–E)**. Bar graphs show a difference in the proportions of MDSCs, macrophages, and DCs. The error bars showed SEM representative results from three independent experiments **(F)**. Different proportions of M1-like and M2-like macrophages (n = 5, representative results from three independent experiments) **(G, H)**. Bar graphs show different proportions of M1-like and M2-like macrophages. Error bars show SEM representative results from three independent experiments. n. s. (not significant) $p > 0.05$, *$p < 0.05$, **$p < 0.01$, ***$p < 0.001$, and ****$p < 0.0001$.

Cd40, *Ido1*, *Cx3cr1*, and *Trem2*. In addition, genes associated with M2 macrophages include *Il4r*, *Ccl4*, *Ccl13*, *Ccl20*, *Ccl17*, *Ccl18*, *Ccl24*, *Lyve1*, *Vegfa*, *Vegfb*, *Vegfc*, *Vegfd*, *Egf*, *Ctsa*, *Ctsb*, *Ctsc*, and *Tgfb1*. We observed that M2 macrophages had higher M2-like macrophage scores (Figure 4A). We used the M1-like macrophage score and the M2-like macrophage score to classify cells and identify changes in the number of macrophages. Our findings showed that cordycepin treatment increased M1-like macrophages and decreased M2-like macrophages (Figure 4B). Then, we used the KEGG database to enrich the pathway for each macrophage cluster. In addition, we found that the genes of M2 macrophages were enriched in the hypoxia pathway and TNFα signaling pathway (Figure 4C). In addition, we explored the expression of CD40 in macrophages and DCs. *CCL22*$^{-}$ DCs were found to have a higher expression of CD40 (Figure 4D), which would be a key factor for enhancing antigen presentation capacity (Bullock, 2022). Moreover, the expression of *CCL2* on macrophages and DCs was decreased, and the expression of *CCL9* was increased (Figure 4E). This finding confirmed the correlation between *CCL9* and cytotoxicity (Matloubian et al., 2000; Dangaj et al., 2019; Di Pilato et al., 2021). Furthermore, the expression of *CCL2* has been confirmed to increase tumor cell proliferation through the polarization of TAMs (McClellan et al., 2012).

We found that the combination treatment of the anti-CD47 antibody and cordycepin could decrease M2-like macrophages and increase M1-like macrophages. Furthermore, the combination treatment could enhance the antigen-presenting ability by increasing the expression of CD40. Finally, the combination treatment could regulate *CCL2* and *CCL9* to mediate the functions of macrophages.

Anti-CD47, in combination with cordycepin, regulates CD8^{+} T-cell-mediated antitumor immune response

Because of the increased expression of CD40 in myeloid cells in the combination treatment group, we further explored the proportions of various T-cell subsets. The scRNA-seq data on CD8^{+} T cells were chosen to reduce the dimension of features. Moreover, the DEGs were used to discriminate 10 clusters (Figure 5A). The C0 cluster represented a majority of CD8^{+} T cells, which exhibited high levels of *CCL5*, *Rgs1*, and *Itga4*

(Figures 5B, C). In addition, the combination treatment decreased these clusters (Figure 5D). In contrast, the combination treatment increased the C1 cluster, which showed high expressions of *Mki67*, *Top2a*, and *Hist1h1b*. To explore the function of all clusters, we determined the exhaust score and cytotoxic score for all clusters. We found that the C0 cluster and the C1 cluster had lower exhaustion (Figures 6A, B). In addition, the C8 cluster got the highest exhaust score (Figure 6C). Because the C0 cluster accounted for a significant proportion among all clusters, we used TCGA database to test the function of the C0 cluster for PFS in digestive tract malignancy. We set up a COX survival model using the DEGs of the C0 cluster (Supplementary Figure S2A). The survival data on CRC were chosen to test the COX model. We found that the low-level group showed better PFS (Figure 6D). To evaluate survival prediction, we found that the 5-year AUC of the COX model was 0.711 (Figure 6E), indicating that the COX survival was an accurate prediction model for the 5-year PFS of CRC. Carcinoma data from the TCGA were used to test the COX model. It was confirmed that patients in the low-score group had better PFS (Figure 6F). GC and ESCC data from the TCGA were used to test the COX model. We found that the PFS for GC and ESCC might be prolonged using the combination treatment through regulating $CD8^+$ T-cell subsets (Supplementary Figures S2B, C). Therefore, we confirmed that the combination treatment would regulate $CD8^+$ T-cell subsets, which could decrease the C0 cluster to improve PFS for digestive tract malignancy.

Combination treatment changes the proportion of TAMs

We used flow cytometry to test the changes in TILs and TAMs in MC38 tumor-bearing mice. We explored the effect of the combination treatment on myeloid cells. First, macrophages were gated as MHC-II and F4/80, and DCs were gated as MHC-II and CD11c. Moreover, we used the expression of CD206 to distinguish M1-like and M2-like macrophages (Figure 7A). We found that the proportion of myeloid-derived suppressor cells (MDSCs) was not significantly changed (Figure 7C). Therefore, it was confirmed that the combination treatment increased the proportion of DCs (Figures 7B, D). In addition, the proportion of macrophages was not significantly changed (Figures 7B, E). However, the proportions of macrophage subsets were adjusted: the number of M1-like macrophages was increased, and the number of M2-like macrophages was decreased (Figures 7F–H). In addition, the proportion of TILs was confirmed by flow cytometry, showing that the proportions of $CD3^+$ T cells, $CD4^+$ T cells, and $CD8^+$ T cells were not significantly changed (Supplementary Figures S3A–D). These findings suggested that the combination treatment could regulate $CD8^+$ T-cell subsets rather than increase the proportion of $CD8^+$ T cells.

Discussion

In the present study, we examined the effect and explored the mechanism of the combination treatment of the anti-CD47 antibody and cordycepin. Cordycepin has been well known as an effective tumor inhibitor, while its inhibitory effect on macrophages can also limit its antitumor effect. Our current study aimed to reveal whether the combination treatment had a remarkable effect against MC38 and CT26 tumor-bearing mouse models. Using the scRNA-seq technique, we confirmed that the combination treatment increased the proportion of M1-like macrophages and decreased the proportion of M2-like macrophages. In addition, the combination treatment could increase the $CD8^+$ T subset to improve the survival of patients with digestive tract malignancies. Finally, flow cytometry showed that the combination treatment could increase the proportion of M1 macrophages and decrease the proportion of M2 macrophages.

In Chinese traditional medicine, *Cordyceps militaris* has been confirmed as an essential medicine dealing with fever, hemoptysis, and tumors (Hsu et al., 2008; Das et al., 2020). Cordycepin is the potent, effective constituent of *Cordyceps militaris*. It is widely accepted to be a direct antitumor inhibitor. Cordycepin is improved to decrease the drug resistance of NSCLC by inhibiting the AMPK signaling pathway and inhibit NSCLC with cisplatin resistance by the AMPK signaling pathway and AKT signaling pathway (Wei et al., 2019) (Liao et al., 2020). Moreover, a combination of cordycepin and apatinib can suppress the progression of NSCLC *via* the VEGF/PI3K/AKT signaling pathway (Wei et al., 2019). For breast cancer, cordycepin is confirmed as an essential inhibitor of the Hedgehog pathway, which can regulate angiogenesis, aggressive molecular subtypes, and the metastatic potential of this malignancy (Liu et al., 2020a; Wu et al., 2022) (Di Mauro et al., 2017; Riaz et al., 2018). Because of the high correlation between breast cancer and hormone secretion, cordycepin also serves as a direct inhibitor for ER-independent breast cancer (Choi et al., 2011). Cordycepin has been shown to be a direct inhibitor in many studies of CRC (Lee et al., 2013; Deng et al., 2022). In addition to the direct killing effect of cordycepin, the effect of cordycepin on the TME should be considered. It has been reported that cordycepin is an excellent inhibitor of acute inflammation (Lan et al., 2021; Wei et al., 2021; Chen et al., 2022). Studies have shown that cordycepin can increase the polarization of M2-like macrophages and downregulate M1-like macrophages in sepsis mouse models (Chen et al., 2022). In Alzheimer's disease, cordycepin has been found to enhance the polarization of microglia from M1 to M2 (Wei et al., 2021). Cordycepin has also been observed to decrease macrophage function and increase M2 polarization in multiple models of inflammation. Although cordycepin has a significant effect on suppressing tumor growth, its suppressive effect on macrophages limits its antitumor activity.

Blockade of CD47 signaling is a recently developed regimen targeting macrophages and DCs (Tahk et al., 2021; Cao et al., 2022). Targeting the CD47/SIRP signaling pathway can increase the antibody-dependent cellular phagocytosis (ADCP) of macrophages and regulate macrophage polarization (Kulkarni et al., 2018; Chen et al., 2019). For melanoma, breast cancer, and NSCLC, blocking the CD47/SIRPα pathway is an effective treatment strategy (Zhang et al., 2017; Hu et al., 2020; Rao et al., 2020). Moreover, sorafenib, in combination with anti-CD38 and anti-GD2 antibodies, can significantly increase its effect on inhibiting the tumor (Huang et al., 2021; Müller et al., 2022; Theruvath et al., 2022). However, because of the broad expression of CD47, an essential mechanism of immune regulation is the phagocytosis of old RBCs by macrophages. In clinical trials, anemia is the most common adverse effect of blocking the CD47/SIRPα pathway (Advani et al., 2018; Harrison et al., 2022). Furthermore, it has been confirmed that cordycepin can decrease

the expression of CD47 on tumors in CRC (Deng et al., 2022). However, considering the inhibitory effect of cordycepin on macrophages in the TME, we did not believe that the inhibitory effect of CD47 expression would stimulate the ADCP. Notably, based on Chinese medicine theory, the regulation of cordycepin is bidirectional. Therefore, long-term cordycepin treatment could enhance immune cell function. Generally, we explored the combination treatment of cordycepin and anti-CD47 antibodies in the present study. The combination treatment could decrease the inhibitory effect of ADCP and increase the survival of CRC patients by regulating $CD8^+$ T cells.

Data availability statement

The data presented in the study are deposited in the GEO repository, accession number "GSE224945".

Ethics statement

The animal study was reviewed and approved by the Third Affiliated Hospital of Soochow University's Ethics Committee.

Author contributions

LC and JJ contributed to the conception and design of this study. LC and JJ contributed to administrative support. CF and WF performed the provision of study materials and the collection and assembly of data. RC and XG performed data analysis and interpretation. CF, HY, and XZ wrote sections of the manuscript. All authors approved the manuscript.

Funding

The study was supported by the National Natural Science Foundation Program of PR China (No. 32270955), the Clinical Frontier Technology Project of the Jiangsu Key Research and Development Program (No. BE2022719), the Jiangsu Traditional Chinese Medicine Science and Technology Development Plan Project (No. ZT202115), and the Changzhou Science and Technology Support Projects of Social Development (No. CE20215030).

Conflict of interest

The authors declare that the research was conducted in the absence of any commercial or financial relationships that could be construed as a potential conflict of interest.

Publisher's note

Supplementary material

The Supplementary Material for this article can be found online at: https://www.frontiersin.org/articles/10.3389/fphar.2023.1144330/full#supplementary-material

References

Advani, R., Flinn, I., Popplewell, L., Forero, A., Bartlett, N. L., Ghosh, N., et al. (2018). CD47 blockade by Hu5F9-G4 and rituximab in non-hodgkin's lymphoma. *N. Engl. J. Med.* 379 (18), 1711–1721. doi:10.1056/NEJMoa1807315

Arrieta, O., Aviles-Salas, A., Orozco-Morales, M., Hernández-Pedro, N., Cardona, A. F., Cabrera-Miranda, L., et al. (2020). Association between CD47 expression, clinical characteristics and prognosis in patients with advanced non-small cell lung cancer. *Cancer Med.* 9 (7), 2390–2402. doi:10.1002/cam4.2882

Ashraf, S., Radhi, M., Gowler, P., Burston, J. J., Gandhi, R. D., Thorn, G. J., et al. (2019). The polyadenylation inhibitor cordycepin reduces pain, inflammation and joint pathology in rodent models of osteoarthritis. *Sci. Rep.* 9 (1), 4696. doi:10.1038/s41598-019-41140-1

Bi, Y., Li, H., Yi, D., Sun, Y., Bai, Y., Zhong, S., et al. (2018). Cordycepin augments the chemosensitivity of human glioma cells to temozolomide by activating AMPK and inhibiting the AKT signaling pathway. *Mol. Pharm.* 15 (11), 4912–4925. doi:10.1021/acs.molpharmaceut.8b00551

Bullock, T. N. J. (2022). CD40 stimulation as a molecular adjuvant for cancer vaccines and other immunotherapies. *Cell Mol. Immunol.* 19 (1), 14–22. doi:10.1038/s41423-021-00734-4

Cao, X., Wang, Y., Zhang, W., Zhong, X., Gunes, E. G., Dang, J., et al. (2022). Targeting macrophages for enhancing CD47 blockade-elicited lymphoma clearance and overcoming tumor-induced immunosuppression. *Blood* 139 (22), 3290–3302. doi:10.1182/blood.2021013901

Chen, J., Wang, M., Zhang, P., Li, H., Qu, K., Xu, R., et al. (2022). Cordycepin alleviated metabolic inflammation in Western diet-fed mice by targeting intestinal barrier integrity and intestinal flora. *Pharmacol. Res.* 178, 106191. doi:10.1016/j.phrs.2022.106191

Chen, Q., Wang, C., Zhang, X., Chen, G., Hu, Q., Li, H., et al. (2019). *In situ* sprayed bioresponsive immunotherapeutic gel for post-surgical cancer treatment. *Nat. Nanotechnol.* 14 (1), 89–97. doi:10.1038/s41565-018-0319-4

Choi, S., Lim, M-H., Kim, K. M., Jeon, B. H., Song, W. O., and Kim, T. W. (2011). Cordycepin-induced apoptosis and autophagy in breast cancer cells are independent of the estrogen receptor. *Toxicol. Appl. Pharmacol.* 257 (2), 165–173. doi:10.1016/j.taap.2011.08.030

Dangaj, D., Bruand, M., Grimm, A. J., Ronet, C., Barras, D., Duttagupta, P. A., et al. (2019). Cooperation between constitutive and inducible chemokines enables T cell engraftment and immune attack in solid tumors. *Cancer Cell* 35 (6), 885–900.e10. doi:10.1016/j.ccell.2019.05.004

Das, G., Shin, H-S., Leyva-Gómez, G., Prado-Audelo, M. L. D., Cortes, H., Singh, Y. D., et al. (2020). Cordyceps spp. A review on its immune-stimulatory and other biological potentials. *Front. Pharmacol.* 11, 602364. doi:10.3389/fphar.2020.602364

Deng, Q., Li, X., Fang, C., Li, X., Zhang, J., Xi, Q., et al. (2022). Cordycepin enhances anti-tumor immunity in colon cancer by inhibiting phagocytosis immune checkpoint CD47 expression. *Int. Immunopharmacol.* 107, 108695. doi:10.1016/j.intimp.2022.108695

Di Mauro, C., Rosa, R., D'Amato, V., Ciciola, P., Servetto, A., Marciano, R., et al. (2017). Hedgehog signalling pathway orchestrates angiogenesis in triple-negative breast cancers. *Br. J. Cancer* 116 (11), 1425–1435. doi:10.1038/bjc.2017.116

Di Pilato, M., Kfuri-Rubens, R., Pruessmann, J. N., Ozga, A. J., Messemaker, M., Cadilha, B. L., et al.(2021). CXCR6 positions cytotoxic T cells to receive critical survival signals in the tumor microenvironment. *Cell* 184 (17), 4512–4530.e22. doi:10.1016/j.cell.2021.07.015

Gao, Y., Chen, D-L., Zhou, M., Zheng, Z-S., He, M-F., Huang, S., et al. (2020). Cordycepin enhances the chemosensitivity of esophageal cancer cells to cisplatin by inducing the activation of AMPK and suppressing the AKT signaling pathway. *Cell Death Dis.* 11 (10), 866. doi:10.1038/s41419-020-03079-4

Gerlach, B. D., Ampomah, P. B., Yurdagul, A., Liu, C., Lauring, M. C., Wang, X., et al. (2021). Efferocytosis induces macrophage proliferation to help resolve tissue injury. *Cell Metab.* 33 (12), 2445–2463.e8. doi:10.1016/j.cmet.2021.10.015

Goerdt, S., Politz, O., Schledzewski, K., Birk, R., Gratchev, A., Guillot, P., et al. (1999). Alternative versus classical activation of macrophages. *Pathobiology* 67 (5-6), 222–226. doi:10.1159/000028096

Harrison, C. N., Garcia, J. S., Somervaille, T. C. P., Foran, J. M., Verstovsek, S., Jamieson, C., et al. (2022). Addition of navitoclax to ongoing ruxolitinib therapy for patients with myelofibrosis with progression or suboptimal response: Phase II safety and efficacy. *J. Clin. Oncol.* 40 (15), 1671–1680. doi:10.1200/JCO.21.02188

He, J., Song, Y., Li, G., Xiao, P., Liu, Y., Xue, Y., et al. (2019). Fbxw7 increases CCL2/7 in CX3CR1hi macrophages to promote intestinal inflammation. *J. Clin. Invest.* 129 (9), 3877–3893. doi:10.1172/JCI123374

Hsu, C-H., Sun, H-L., Sheu, J-N., Ku, M-S., Hu, C-M., Chan, Y., et al. (2008). Effects of the immunomodulatory agent Cordyceps militaris on airway inflammation in a mouse asthma model. *Pediatr. Neonatol.* 49 (5), 171–178. doi:10.1016/S1875-9572(09)60004-8

Hu, J., Xiao, Q., Dong, M., Guo, D., Wu, X., and Wang, B. (2020). Glioblastoma immunotherapy targeting the innate immune checkpoint CD47-sirpα Axis. *Front. Immunol.* 11, 593219. doi:10.3389/fimmu.2020.593219

Huang, L., Zhang, Y., Li, Y., Meng, F., Li, H., Zhang, H., et al. (2021). Time-programmed delivery of sorafenib and anti-CD47 antibody via a double-layer-gel matrix for postsurgical treatment of breast cancer. *Nanomicro Lett.* 13 (1), 141. doi:10.1007/s40820-021-00647-x

Jiang, P., Lagenaur, C. F., and Narayanan, V. (1999). Integrin-associated protein is a ligand for the P84 neural adhesion molecule. *J. Biol. Chem.* 274 (2), 559–562. doi:10.1074/jbc.274.2.559

Jin, Y., Meng, X., Qiu, Z., Su, Y., Yu, P., and Qu, P. (2018). Anti-tumor and anti-metastatic roles of cordycepin, one bioactive compound of *Cordyceps militaris*. *Saudi J. Biol. Sci.* 25 (5), 991–995. doi:10.1016/j.sjbs.2018.05.016

Kharitonenkov, A., Chen, Z., Sures, I., Wang, H., Schilling, J., and Ullrich, A. (1997). A family of proteins that inhibit signalling through tyrosine kinase receptors. *Nature* 386 (6621), 181–186. doi:10.1038/386181a0

Kim, H., Naura, A. S., Errami, Y., Ju, J., and Boulares, A. H. (2011). Cordycepin blocks lung injury-associated inflammation and promotes BRCA1-deficient breast cancer cell killing by effectively inhibiting PARP. *Mol. Med.* 17 (9-10), 893–900. doi:10.2119/molmed.2011.00032

Kim, S. O., Cha, H-J., Park, C., Lee, H., Hong, S. H., Jeong, S-J., et al. (2019). Cordycepin induces apoptosis in human bladder cancer T24 cells through ROS-dependent inhibition of the PI3K/Akt signaling pathway. *Biosci. Trends* 13 (4), 324–333. doi:10.5582/bst.2019.01214

Kulkarni, A., Chandrasekar, V., Natarajan, S. K., Ramesh, A., Pandey, P., Nirgud, J., et al. (2018). A designer self-assembled supramolecule amplifies macrophage immune responses against aggressive cancer. *Nat. Biomed. Eng.* 2 (8), 589–599. doi:10.1038/s41551-018-0254-6

Lan, T., Yu, Y., Zhang, J., Li, H., Weng, Q., Jiang, S., et al. (2021). Cordycepin ameliorates nonalcoholic steatohepatitis by activation of the AMP-activated protein kinase signaling pathway. *Hepatol. Baltim. Md)* 74 (2), 686–703. doi:10.1002/hep.31749

Lee, S. Y., Debnath, T., Kim, S-K., and Lim, B. O. (2013). Anti-cancer effect and apoptosis induction of cordycepin through DR3 pathway in the human colonic cancer cell HT-29. *Food Chem. Toxicol.* 60, 439–447. doi:10.1016/j.fct.2013.07.068

Li, F., Lv, B., Liu, Y., Hua, T., Han, J., Sun, C., et al. (2018). Blocking the CD47-SIRPα axis by delivery of anti-CD47 antibody induces antitumor effects in glioma and glioma stem cells. *Oncoimmunology* 7 (2), e1391973. doi:10.1080/2162402X.2017.1391973

Liao, X-Z., Gao, Y., Zhao, H-W., Zhou, M., Chen, D-L., Tao, L-T., et al. (2020). Cordycepin reverses cisplatin resistance in non-small cell lung cancer by activating AMPK and inhibiting AKT signaling pathway. *Front. Cell Dev. Biol.* 8, 609285. doi:10.3389/fcell.2020.609285

Liu, C., Qi, M., Li, L., Yuan, Y., Wu, X., and Fu, J. (2020). Natural cordycepin induces apoptosis and suppresses metastasis in breast cancer cells by inhibiting the Hedgehog pathway. *Food Funct.* 11 (3), 2107–2116. doi:10.1039/c9fo02879j

Liu, T., Zhu, G., Yan, W., Lv, Y., Wang, X., Jin, G., et al. (2020). Cordycepin inhibits cancer cell proliferation and angiogenesis through a DEK interaction via ERK signaling in cholangiocarcinoma. *J. Pharmacol. Exp. Ther.* 373 (2), 279–289. doi:10.1124/jpet.119.263202

Mantovani, A., Sozzani, S., Locati, M., Allavena, P., and Sica, A. (2002). Macrophage polarization: Tumor-associated macrophages as a paradigm for polarized M2 mononuclear phagocytes. *Trends Immunol.* 23 (11), 549–555. doi:10.1016/s1471-4906(02)02302-5

Matloubian, M., David, A., Engel, S., Ryan, J. E., and Cyster, J. G. (2000). A transmembrane CXC chemokine is a ligand for HIV-coreceptor Bonzo. *Nat. Immunol.* 1 (4), 298–304. doi:10.1038/79738

McClellan, J. L., Davis, J. M., Steiner, J. L., Enos, R. T., Jung, S. H., Carson, J. A., et al. (2012). Linking tumor-associated macrophages, inflammation, and intestinal tumorigenesis: Role of MCP-1. *Am. J. Physiol. Gastrointest. Liver Physiol.* 303 (10), G1087–G1095. doi:10.1152/ajpgi.00252.2012

Müller, K., Vogiatzi, F., Winterberg, D., Rösner, T., Lenk, L., Bastian, L., et al. (2022). Combining daratumumab with CD47 blockade prolongs survival in preclinical models of pediatric T-ALL. *Blood* 140 (1), 45–57. doi:10.1182/blood.2021014485

Nasser, M. I., Masood, M., Wei, W., Li, X., Zhou, Y., Liu, B., et al. (2017). Cordycepin induces apoptosis in SGC-7901 cells through mitochondrial extrinsic phosphorylation of PI3K/Akt by generating ROS. *Int. J. Oncol.* 50 (3), 911–919. doi:10.3892/ijo.2017.3862

Rao, L., Zhao, S-K., Wen, C., Tian, R., Lin, L., Cai, B., et al. (2020). Activating macrophage-mediated cancer immunotherapy by genetically edited nanoparticles. *Adv. Mater* 32 (47), e2004853. doi:10.1002/adma.202004853

Riaz, S. K., Khan, J. S., Shah, S. T. A., Wang, F., Ye, L., Jiang, W. G., et al. (2018). Involvement of hedgehog pathway in early onset, aggressive molecular subtypes and metastatic potential of breast cancer. *Cell Commun. Signal* 16 (1), 3. doi:10.1186/s12964-017-0213-y

Sallman, D. A., Donnellan, W. B., Asch, A. S., Lee, D. J., Malki, M. A., Marcucci, G., et al. (2019). The first-in-class anti-CD47 antibody Hu5F9-G4 is active and well tolerated alone or with azacitidine in AML and MDS patients: Initial phase 1b results. *J. Clin. Oncol.* 37 (15), 7009. doi:10.1200/jco.2019.37.15_suppl.7009

Schürch, C. M., Roelli, M. A., Forster, S., Wasmer, M-H., Brühl, F., Maire, R. S., et al. (2019). Targeting CD47 in anaplastic thyroid carcinoma enhances tumor phagocytosis by macrophages and is a promising therapeutic strategy. *Thyroid* 29 (7), 979–992. doi:10.1089/thy.2018.0555

Shi, M., Gu, Y., Jin, K., Fang, H., Chen, Y., Cao, Y., et al. (2021). CD47 expression in gastric cancer clinical correlates and association with macrophage infiltration. *Cancer Immunol. Immunother. CII* 70 (7), 1831–1840. doi:10.1007/s00262-020-02806-2

Sica, A., Allavena, P., and Mantovani, A. (2008). Cancer related inflammation: The macrophage connection. *Cancer Lett.* 267 (2), 204–215. doi:10.1016/j.canlet.2008.03.028

Sun, T., Dong, W., Jiang, G., Yang, J., Liu, J., Zhao, L., et al. (2019). *Cordyceps militaris* improves chronic kidney disease by affecting TLR4/NF-κB redox signaling pathway. *Oxid. Med. Cell Longev.* 2019, 7850863. doi:10.1155/2019/7850863

Tahk, S., Vick, B., Hiller, B., Schmitt, S., Marcinek, A., Perini, E. D., et al. (2021). SIRPα-αCD123 fusion antibodies targeting CD123 in conjunction with CD47 blockade enhance the clearance of AML-initiating cells. *J. Hematol. Oncol.* 14 (1), 155. doi:10.1186/s13045-021-01163-6

Theruvath, J., Menard, M., Smith, B. A. H., Linde, M. H., Coles, G. L., Dalton, G. N., et al. (2022). Anti-GD2 synergizes with CD47 blockade to mediate tumor eradication. *Nat. Med.* 28 (2), 333–344. doi:10.1038/s41591-021-01625-x

Wang, C., Mao, Z. P., Wang, L., Zhang, F. H., Wu, G. H., Wang, D. Y., et al. (2017). Cordycepin inhibits cell growth and induces apoptosis in human cholangiocarcinoma. *Neoplasma* 64 (6), 834–839. doi:10.4149/neo_2017_604

Wang, Y., Lv, Y., Liu, T. S., Yan, W. D., Chen, L. Y., Li, Z. H., et al. (2019). Cordycepin suppresses cell proliferation and migration by targeting CLEC2 in human gastric cancer cells via Akt signaling pathway. *Life Sci.* 223, 110–119. doi:10.1016/j.lfs.2019.03.025

Wei, C., Khan, M. A., Du, J., Cheng, J., Tania, M., Leung, E. L-H., et al. (2022). Cordycepin inhibits triple-negative breast cancer cell migration and invasion by regulating EMT-TFs SLUG, TWIST1, SNAIL1, and ZEB1. *Front. Oncol.* 12, 898583. doi:10.3389/fonc.2022.898583

Wei, C., Yao, X., Jiang, Z., Wang, Y., Zhang, D., Chen, X., et al. (2019). Cordycepin inhibits drug-resistance non-small cell lung cancer progression by activating AMPK signaling pathway. *Pharmacol. Res.* 144, 79–89. doi:10.1016/j.phrs.2019.03.011

Wei, P., Wang, K., Luo, C., Huang, Y., Misilimu, D., Wen, H., et al. (2021). Cordycepin confers long-term neuroprotection via inhibiting neutrophil infiltration and neuroinflammation after traumatic brain injury. *J. Neuroinflammation* 18 (1), 137. doi:10.1186/s12974-021-02188-x

Weiskopf, K., Jahchan, N. S., Schnorr, P. J., Cristea, S., Ring, A. M., Maute, R. L., et al. (2016). CD47-blocking immunotherapies stimulate macrophage-mediated destruction of small-cell lung cancer. *J. Clin. Investigation* 126 (7), 2610–2620. doi:10.1172/JCI81603

Wu, W., Li, X., Qi, M., Hu, X., Cao, F., Wu, X., et al. (2022). Cordycepin inhibits growth and metastasis formation of MDA-MB-231 xenografts in nude mice by modulating the hedgehog pathway. *Int. J. Mol. Sci.* 23 (18), 10362. doi:10.3390/ijms231810362

Xie, C., Ye, F., Zhang, N., Huang, Y., Pan, Y., and Xie, X. (2021). CCL7 contributes to angiotensin II-induced abdominal aortic aneurysm by promoting macrophage infiltration and pro-inflammatory phenotype. *J. Cell Mol. Med.* 25 (15), 7280–7293. doi:10.1111/jcmm.16757

Yang, J., Zhou, Y., and Shi, J. (2020). Cordycepin protects against acute pancreatitis by modulating NF-κB and NLRP3 inflammasome activation via AMPK. *Life Sci.* 251, 117645. doi:10.1016/j.lfs.2020.117645

Yin, M., Guo, Y., Hu, R., Cai, W. L., Li, Y., Pei, S., et al. (2020). Potent BRD4 inhibitor suppresses cancer cell-macrophage interaction. *Nat. Commun.* 11 (1), 1833. doi:10.1038/s41467-020-15290-0

Zeng, Y., Lian, S., Li, D., Lin, X., Chen, B., Wei, H., et al. (2017). Anti-hepatocarcinoma effect of cordycepin against NDEA-induced hepatocellular carcinomas via the PI3K/Akt/mTOR and Nrf2/HO-1/NF-κB pathway in mice. *Biomed. Pharmacother.* 95, 1868–1875. doi:10.1016/j.biopha.2017.09.069

Zhang, M., Hutter, G., Kahn, S. A., Azad, T. D., Gholamin, S., Xu, C. Y., et al. (2016). Anti-CD47 treatment stimulates phagocytosis of glioblastoma by M1 and M2 polarized macrophages and promotes M1 polarized macrophages *in vivo*. *PLoS One* 11 (4), e0153550. doi:10.1371/journal.pone.0153550

Zhang, X., Fan, J., Wang, S., Li, Y., Wang, Y., Li, S., et al. (2017). Targeting CD47 and autophagy elicited enhanced antitumor effects in non-small cell lung cancer. *Cancer Immunol. Res.* 5 (5), 363–375. doi:10.1158/2326-6066.CIR-16-0398

frontiers | Frontiers in Pharmacology

TYPE Original Research
PUBLISHED 07 June 2023
DOI 10.3389/fphar.2023.1170240

OPEN ACCESS

EDITED BY
Syed Mahmood,
University of Malaya, Malaysia

REVIEWED BY
Yutian Zou,
Sun Yat-sen University Cancer Center (SYSUCC), China
Weimin Zhong,
Xiamen Fifth Hospital, China
Jianglong Yan,
Northwestern University, United States

*CORRESPONDENCE
Zhan Liu,
tomliuz@163.com
Shaoshan Hu,
shaoshanhu421@163.com
Shengzhong Tao,
tao2000zz@163.com

†These authors have contributed equally to this work and share first authorship

RECEIVED 20 February 2023
ACCEPTED 22 May 2023
PUBLISHED 07 June 2023

CITATION
Ma S, Wang F, Liu Q, Geng X, Wang Z, Yi M, Jiang F, Zhang D, Cao J, Yan X, Zhang J, Wang N, Zhang H, Peng L, Liu Z, Hu S and Tao S (2023), Systematic analysis of the necroptosis index in pan-cancer and classification in discriminating the prognosis and immunotherapy responses of 1716 glioma patients.
Front. Pharmacol. 14:1170240.
doi: 10.3389/fphar.2023.1170240

Systematic analysis of the necroptosis index in pan-cancer and classification in discriminating the prognosis and immunotherapy responses of 1716 glioma patients

Shuai Ma[1,2,3†], Fang Wang[2†], Qingzhen Liu[4†], Xiaoteng Geng[1], Zaibin Wang[1], Menglei Yi[1], Fan Jiang[1], Dongtao Zhang[1], Junzheng Cao[1], Xiuwei Yan[2], Jiheng Zhang[2], Nan Wang[2], Heng Zhang[1], Lulu Peng[1], Zhan Liu[1*], Shaoshan Hu[2*] and Shengzhong Tao[1*]

[1]Department of Neurosurgery, The Second Affiliated Hospital of Zhengzhou University, Zhengzhou, China, [2]Cancer Center, Department of Neurosurgery, Zhejiang Provincial People's Hospital, Affiliated People's Hospital, Hangzhou Medical College, Hangzhou, Zhejiang, China, [3]Department of Neurosurgery, The Second Affiliated Hospital of Harbin Medical University, Harbin, China, [4]Institute of Psychiatry and Neuroscience, Xinxiang Medical University, Xinxiang, China

Necroptosis is a programmed form of necrotic cell death that serves as a host gatekeeper for defense against invasion by certain pathogens. Previous studies have uncovered the essential role of necroptosis in tumor progression and implied the potential for novel therapies targeting necroptosis. However, no comprehensive analysis of multi-omics data has been conducted to better understand the relationship between necroptosis and tumor. We developed the necroptosis index (NI) to uncover the effect of necroptosis in most cancers. NI not only correlated with clinical characteristics of multiple tumors, but also could influence drug sensitivity in glioma. Based on necroptosis-related differentially expressed genes, the consensus clustering was used to classify glioma patients into two NI subgroups. Then, we revealed NI subgroup I were more sensitive to immunotherapy, particularly anti-PD1 therapy. This new NI-based classification may have prospective predictive factors for prognosis and guide physicians in prioritizing immunotherapy for potential responders.

KEYWORDS

necroptosis index, pancacer, glioma, chemoradiotherapy, immunotherapy

Abbreviations: DEGs, differentially expressed genes; GBM, glioblastoma; LGG, low grade glioma; NI, necroptosis index; ROS, reactive oxygen species; ssGSEA, the single sample gene set enrichment analysis; SCNA, somatic copy number alterations; SNP, single nucleotide polymorphisms; NRGs, necroptosis regulator genes.

Introduction

Glioma is a common primary intracranial tumor that accounts for approximately 40%–50% of all brain tumors. It is one of the leading causes of cancer-related deaths, prone to chemo-resistance, and one of the main reasons for unsatisfactory treatment outcomes (Huang et al., 2019; Han et al., 2020).

Necroptosis, also known as programmed necrosis, is a regulated form of necrotic cell death mediated by RIP1 and RIP3 kinases. It was initially found to be an alternative to apoptosis following the involvement of receptors in the dead region (Degterev et al., 2005). Although necrosis is widely considered to be a compromise strategy adopted by tumors to create a favorable environment for proliferation and metastasis (DARJAKANDUC et al., 2002), its genetically programmed counterpart, i.e., necroptosis, has been found to exert an inhibitory role in most tumors (Lawlor et al., 2015; Newton, 2015). In some tumor cell lines, two-thirds of the RIPK3 protein levels were decreased, indicating that tumor cells tend to escape necroptosis for survival. Furthermore, low expression of RIPK3 suggests a poorer prognosis for tumor patients (Duan-Wu Zhang et al., 2009; Goodall et al., 2016). Drug-induced necroptosis suppresses tumor growth and decreases tumor metastasis using the accumulated reactive oxygen species (ROS) (Fulda, 2013; Marino et al., 2014; Yang et al., 2018); this may be one reason for the observed relationship between the expression of necroptotic-related genes and patient prognosis.

In the present study, we performed the first comprehensive analysis of necroptosis regulator genes (NRGs) and the necroptosis index (NI) in pan-cancer. The results revealed that necroptosis was related to various cancer hallmarks, mutation, the immune system, stemness, and prognosis. Then, we calculated NI in glioma patients using the single sample gene set enrichment analysis (ssGSEA) algorithm. Subsequently, we obtained necroptosis subgroups and explored differences in genomic variants and the tumor microenvironment between the two necroptosis subgroups through integration analysis to determine the differential efficacy of immunotherapy and chemotherapy. These findings discovered the important role of necroptosis in tumors and contributed to further study of necroptosis-related molecular mechanisms. In future, this could assist physicians and glioma patients to individualize survival prediction and provide better treatment choices based on NI classification.

Methods

Data extraction

RNA_seq, copy number alteration data, and clinical characteristic of pan-cancer were gathered from UCSC Xena Browser (https://xenabrowser.net/datapages/). RNA_seq (FPKM) and clinical information for 698 and 1,018 glioma samples were obtained from the TCGA and CGGA databases. Mutation data of low-grade glioma (LGG) and Glioblastoma (GBM) were download from TCGA.

Recognizing necroptosis regulators

In a recent study from 2016, Tania Love Aaes et al. discovered that RIPK1, RIPK3, FADD, and MLKL were the key factors for necroptosis (Aaes et al., 2016). In 2021, Han-Hee Park et al. found that RIPK1, RIPK3, TNF, and MLKL are also proposed to be key molecules in necroptosis (Park et al., 2021). Kim Newton et al. identified TLR3, FASLG, and FAS as key factors in necroptosis in 2016 (Newton and Manning, 2016). Finally, we combined with MSigDB Team (GOBP_NECROPTOTIC_SIGNALING_PATHWAY) (https://www.gsea-msigdb.org/gsea/msigdb/) to obtain these eight Necroptosis-related genes (FADD, TNF, FASLG, MLKL, TLR3, RIPK1, FAS, and RIPK3) (Linkermann and Green, 2014).

Establishing the necroptosis index

The necroptosis index to represent the necroptosis level was established based on the expression data for genes of necroptosis key genes including positive components of FADD, TNF, FASLG, MLKL, TLR3, RIPK1, FAS, and RIPK3. The enrichment score of these genes that regulated necroptosis was calculated using ssGSEA in the R package 'GSVA'.

Gene set enrichment analysis

To identify the pathways associated with necroptosis, the samples of each tumor type were divided into two groups according to the NI, consisting of the top 30% and bottom 30%. Then, the gene set enrichment analysis was performed.

RNA extraction, RT-PCR, and qRT -PCR

Tissue RNA isolation total RNA was extracted from eight Glioblastoma (GBM) and control brain tissue samples. Human specimens were approved by the Ethics Committee of the Second Hospital of Harbin Medical University. TRIzol reagent (Invitrogen) was used to extract total RNA from the cells and tissue specimens. Primers for eight genes were synthesized from Tsingke Biotech (Beijing, China). PrimeScript RT reagent kit with gDNA Eraser (Takara Bio, Inc.) was used to prepare cDNA, and SYBR Green II mixture (Takara Bio, Inc.) was used for RT-qPCR. Calculation of target mRNA levels was based on the CT method and normalization to human ACTB expression. The original PCR data and analysis process of these 16 tissue samples are presented in Supplementary Table S7.

Identification NI subgroups

Consensual clustering uses the k-means algorithm to identify specific NI subgroups associated with the expression of NRGs. Number and stability of clusters were decided by the consensus clustering algorithm using the "ConsensuClusterPlus" package. We

10.3389/fphar.2023.1170240

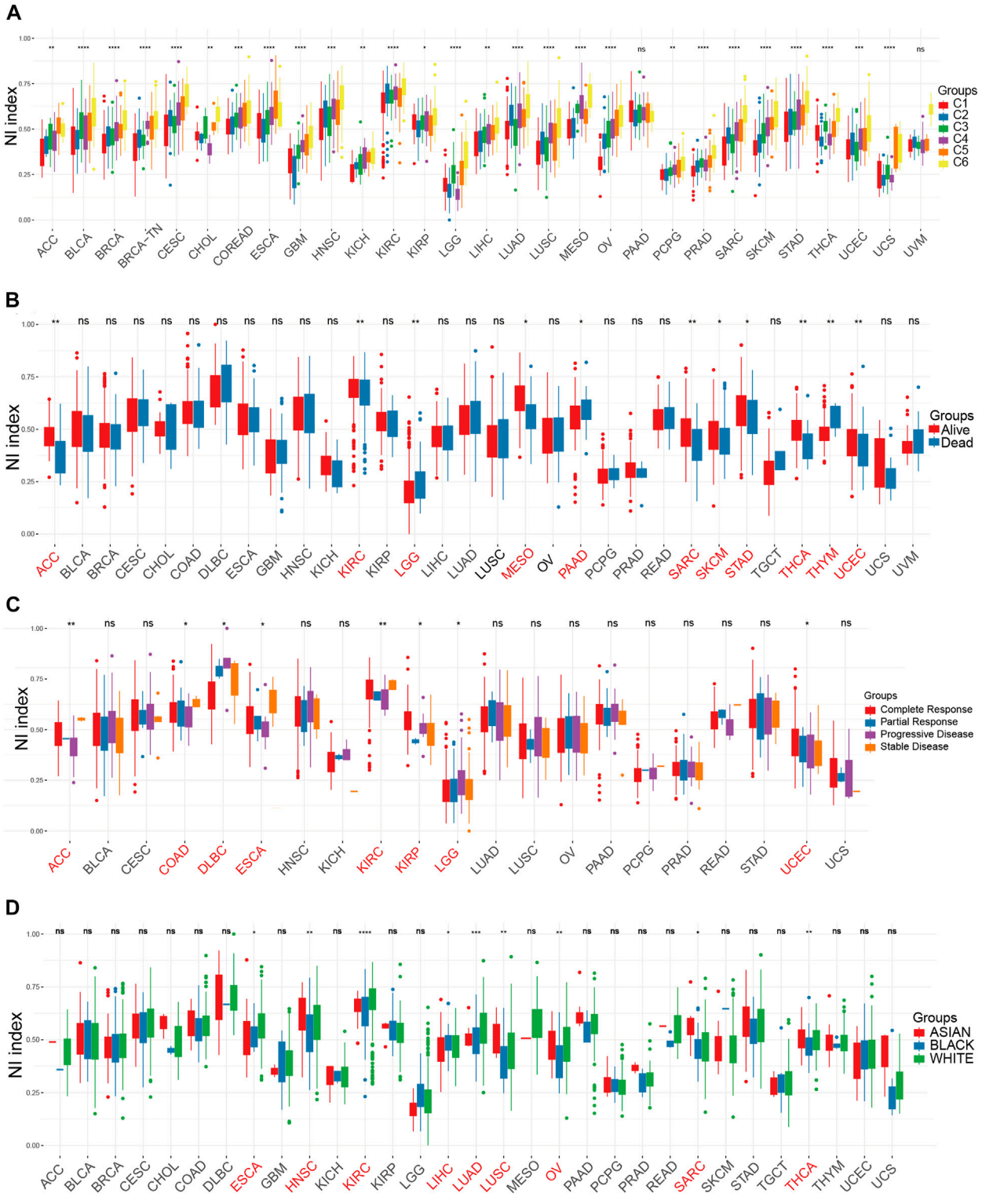

FIGURE 1
The relationship between clinical factors and NI. **(A–D)** The differential expression of NI among Immunophenotype **(A)**, prognostic results **(B)**, treatment response **(C)**, and race **(D)** in pan-cancer.

conducted the experiment with 1,000 iterations to ensure the robustness of our categorizations (Wilkerson and Hayes, 2010; Zhang et al., 2020).

Mutation data in NI subgroups

We detected the SNVs, SNPs, and INDELs using the software VarScan2 (Koboldt et al., 2012a). The co-occurrence and mutually exclusive mutations were identified using theCoMEt algorithm (Leiserson et al., 2015). Mutation data were analyzed in two groups and visualized using the "maftools" R package (Koboldt et al., 2012b).

Differential expression genes analysis of NI subgroups

To test genes differentially expressed between NI subgroups, gene expression data for glioma RNA_seq were downloaded from TCGA. Then, the fold change and adjusted *p*-value were calculated by the limma package (Ritchie et al., 2015). We defined genes with an adjusted *p*-value less than 0.05 and fold change<|2| as the differential expression genes (DEGs).

Clinical features analysis

The R package "survival" was used to assess the prognosis potential of the NRGs and necroptosis index among tumors. For survival analysis, the expression threshold was exhaustively tested and the one with most significant *p*-value was considered the best cut-off.

Immune infiltration

The ssGSEA was applied to detect the infiltrating scores of 28 immune cells. Feature gene panels for each immune cell type were obtained from a recent publication (Charoentong et al., 2017). The relative abundance of each immune cell type was represented by an enrichment score in ssGSEA analysis. The ssGSEA score was normalized to unity distribution, for which zero is the minimal and one is the maximal score for each immune cell type. The bio-similarity of the immune cell filtration was estimated by multi-dimensional scaling (MDS) and a Gaussian fitting model.

WGCNA

The key genes in 4,645 DEGs were identified by applying WGCNA. First, we constructed the adjacency matrix according to the connectivity of the best β values in order to make gene distributions conform to the scale-free network and transformed the adjacency matrix to topology overlap matrix (TOM). Next, we used the heterogeneity among genes to aggregate the genes for the TOM. Finally, the identified TOMs were defined as components and dynamical tree cutting algorithm was used for stratified clustering to identify modules with minimum module size of 25 (Langfelder and Horvath, 2008; Yi et al., 2020).

Significance of the NI subgroups in chemotherapeutic sensitivity

An algorithm developed by Geeleheret et al. (Paul Geeleher and Huang, 2014) and the "pRRophetic" package (Geeleher et al., 2014) were used by the TCGA project to compute the IC50 of commonly used chemotherapeutic agents in order to evaluate the clinical efficacy of NI subgroups. The AJCC guidelines recommend 30 common antineoplastic agents for cancer treatment, such as Imatinib, Adriamycin, Cisplatin, and Vinblastine. The distinction in IC50 of commonly used drugs in two NI subgroups was assessed by the Wilcoxon test.

Statistical analysis

All statistical analyses were executed with R version 4.0.5 (Yoshihara et al., 2013). Adjustment for multiple testing was used to compare differences in immune and mutation status between NI subgroups. $p < 0.05$ was regarded as statistically significant.

Results

Aberrant expression of necroptosis index in cancers

In the present study, the eight genes extracted from MSigDB that play crucial roles in the regulation of necroptosis were identified as NRGs, and included FADD, TNF, FASLG, MLKL, TLR3, RIPK1, FAS, and RIPK3. In order to further understand the importance of necroptosis in tumor progression and explore the factors or biological mechanisms relevant to necroptosis, NI was modeled based on the positive core group component enrichment fraction minus the negative core group component enrichment fraction calculated by ssGSEA (Supplementary Table S1). First, we studied the relationship between NI and molecular features. NI were clearly distinguished in all tumor types according to immunophenotype from a previous article (Figure 1A). We found that the NI of C4, C5, and C6 were significantly higher than those of C1, C2, and C3. We know C3 had the best prognosis, while C2 and C1 had less favorable outcomes. In our study, C4 and C6 had poor clinical outcomes. Thus, the NI in most tumors could respond to the immune status and prognosis of patients. Of all the tumors, NI in 11 tumors showed remarkable distinctions in survival status (Figure 1B), these were ACC, KIRC, LGG, MESO, PAAD, SARC, SKCM, STAD, THCA, THYM, and UCEC. NI in eight tumors revealed markedly different between-treatment results (Figure 1C): ACC, COAD, DLBC, ESCA, KIRC, KIRP, LGG, and UCEC. NI in nine tumors indicated a significant difference in race, which were ESCA, HNSC, KIRC, LIHC, LUAD, LUSC, OV, SARC, and THCA (Figure 1D). The NI of women was higher than men in HNSC, LUAD, and STAD but lower in LIHC (Supplementary Figure S1G). Finally, we performed cox model of NI in pan-cancer. The result showed that ACC, GBM, LGG, LIHC, MESO, PAAD, SARC, SKCM, STAD, THCA, and THYM were obviously meaningful and had prognostic value (Supplementary Figure S1F).

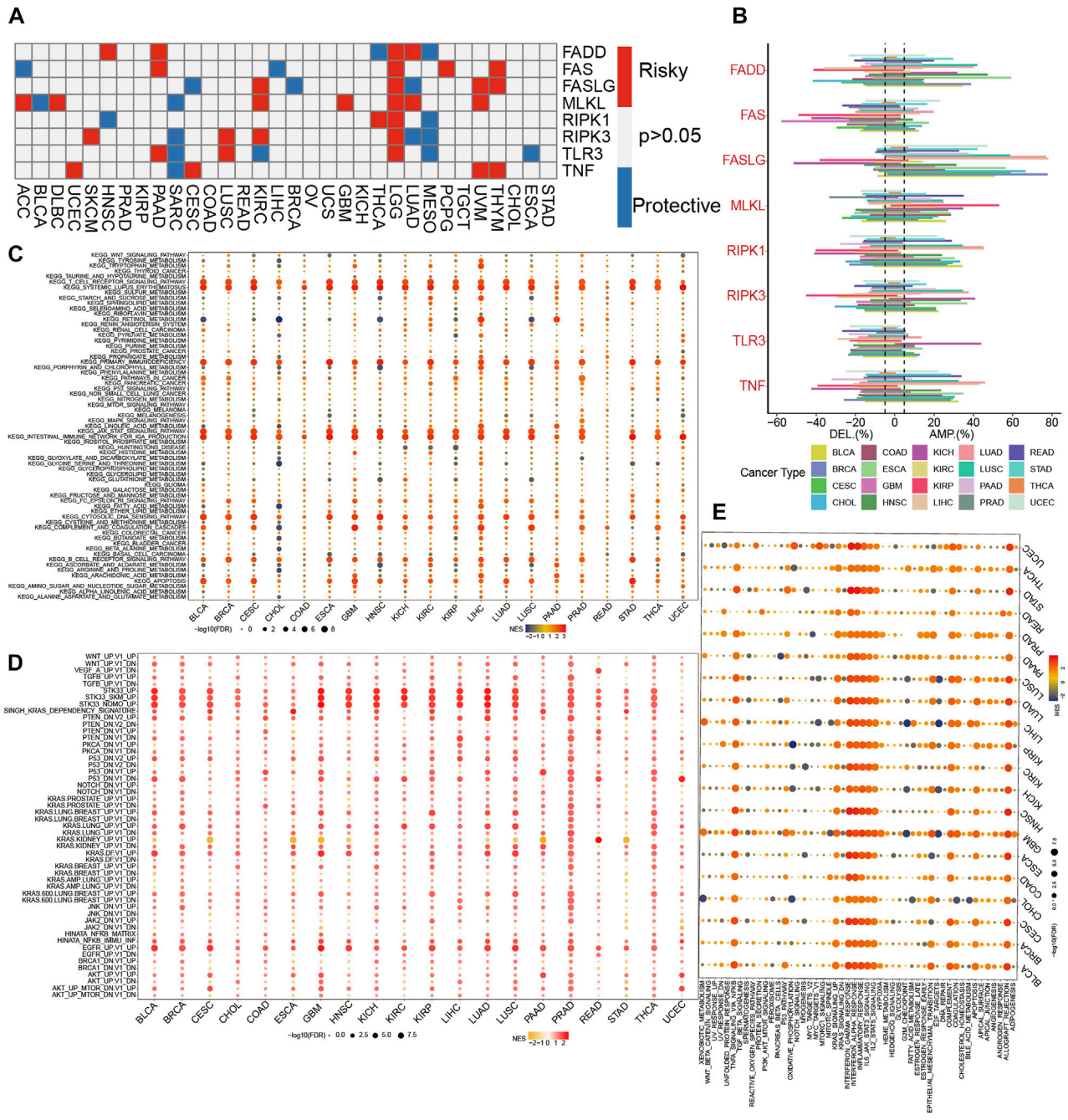

FIGURE 2
The dysregulation of necroptosis regulators. **(A)**The correlation between expression of necroptosis regulators and patient survival in pan-cancer. **(B)** Histogram displays the rate of somatic copy number alterations for NRGs in pan-cancer. **(C–E)** Enrichment analysis for metabolism pathway **(C)**, cancer signaling **(D)**, and hallmark gene sets **(E)** between high- and low-NI tumor tissues.

Association between necroptosis and genetic alterations and pathways in tumors

We found that all of the NRGs were related to the prognosis of patients in most tumor types, except PRAD, KIRP, READ, OV, UCS, KICH, TGCT, and STAD (Figure 2A). This finding revealed that NRGs were associated with the prognosis of most tumor patients. To further explore the mutation profile of NRGs in tumors, the proportion of somatic copy number alterations (SCNA) was detected, and the results demonstrated that SCNA possess a high rate (more than 5%) in most cancers (Figure 2B), but the SCNA frequencies of NRGs were low in THCA. Furthermore, NRGs displayed different SCNA profiles. For instance, FADD, FASLG, RIPK1, RIPK3, and TNF were more prone to copy number gain than

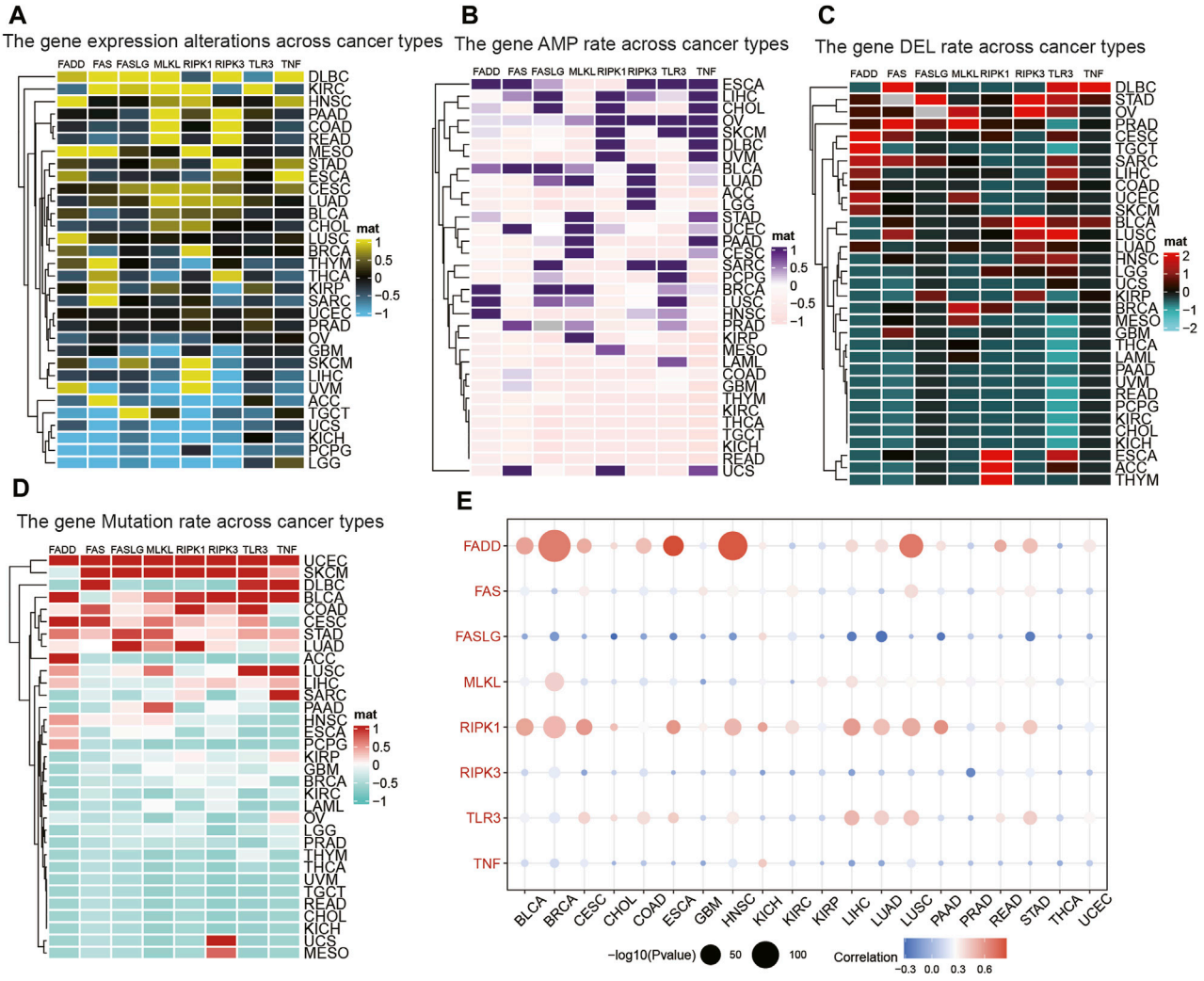

FIGURE 3
The relationship between AMP, DEL, mutation rate, and their expression values of NRGs. **(A)** The expression of NRGs in pan-cancer. **(B)** The AMP of NRGs in pan-cancer. **(C)** The DEL of NRGs in pan-cancer. **(D)** The mutation rate of NRGs in pan-cancer. **(E)** The correlation between the expression and CNV in NRGs.

loss in pan-cancer, but FAS and TLR3 displayed the reverse tendency. To further clarify the association between the NI and pathways, we applied GSEA to investigate the related cellular signaling of necroptosis in tumors based on the RNA_seq of tumors with the top and bottom 30% of NI. It was observed that metabolism-related pathways in KEGG were usually enriched in tumors with lower NI; pathways frequently enriched (>7 cancers) are presented in Figure 2C. For example, T_cell_receptor_signaling_pathway, Systemic lupus erythematosus, Primary_immunodeficiency, JAK_STAT_SIGNALING_pathway, and Intestinal_immune_network_for_iga_production were enriched in the high-NI group in most cancers. Purine_metabolism, Mtor_signaling_pathway, and Galactose_metabolism were also significantly correlated with low-NI in all these cancer types, which indicated that necroptosis was negatively related to these metabolism-related pathways (Figure 2C). Furthermore, the relationship between NI and cancer hallmarks were also analyzed, and the results showed that 12 hallmarks were frequently significantly correlated with NI (Figure 2E). For example, INTERFERON_GAMMA_RESPONSE, INTERFERON_ALPHA_RESPONSE, INTERFERON_ALPHA_RESPONSE, and IL6_JAK_STAT3_SIGNALING were enriched in the high-NI group. This indicated that necroptosis was positively related to these cancer hallmarks. Finally, most oncogenic signatures were also significantly negative with low-NI in pan-cancer. These results are consistent with necroptosis activating tumor immunity and inhibiting tumor growth (Figure 2D). We analyzed the relationship between amplification (AMP), deletion (DEL), mutation rate, and their expression values of these eight genes in Figures 3A–D. Figure 3A showed the expression of eight genes in pan-cancer, Figure 3B displayed the AMP of eight genes in pan-cancer, Figure 3C revealed the DEL of eight genes in pan-cancer, and Figure 3D showed the mutation rate of eight genes in tumor. From the above results, we found that the expression of NRGs with CNV AMP was significantly higher in cancer cells (e.g., FADD, FASLG, RIPK3, and TNF), while the expression of NRGs with CNV DEL was

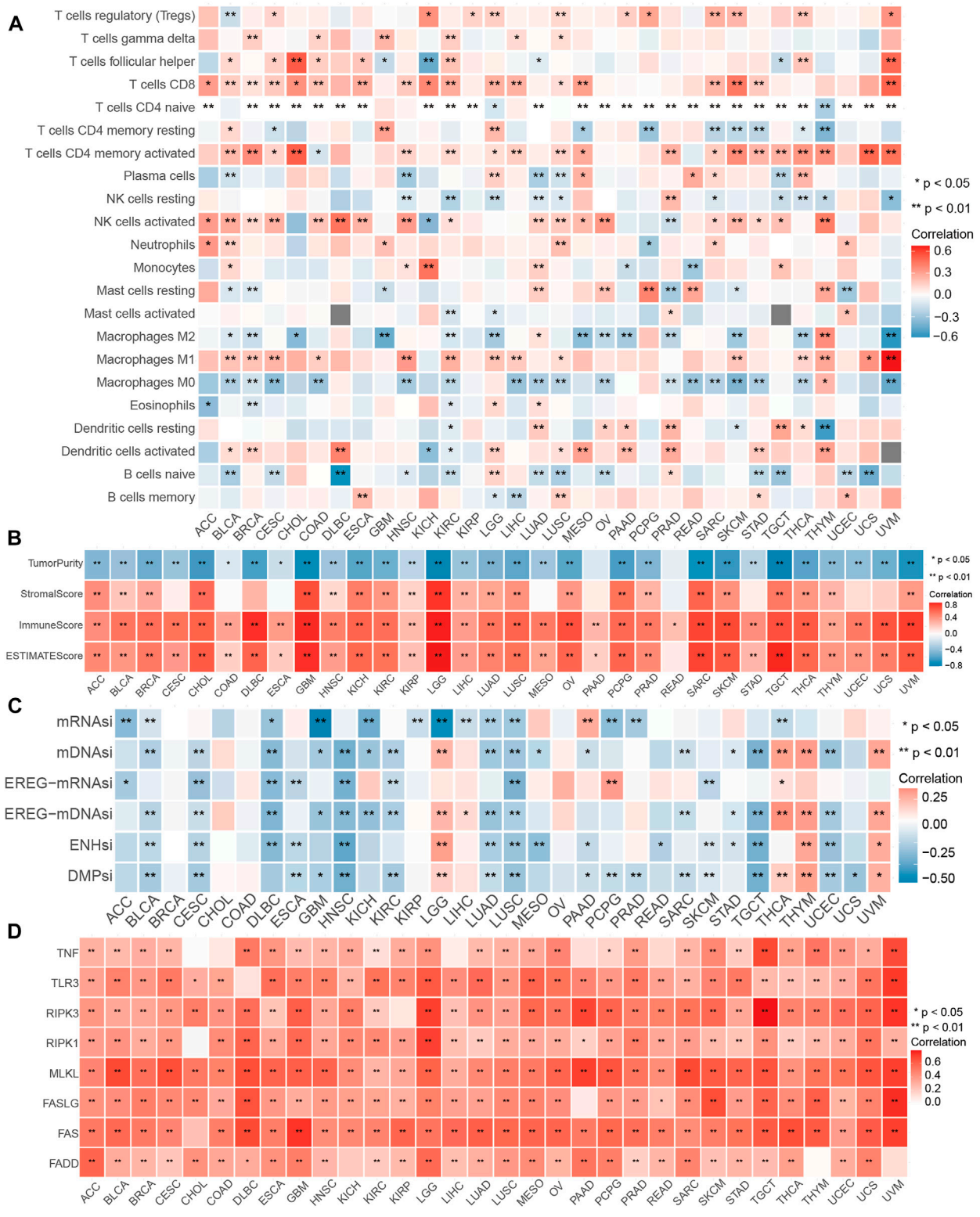

FIGURE 4
Performance of NI in pan-cancers. **(A)** Relationship between the immune cells and NI in pan-cancer. **(B)** Correlations between the NI and ESTIMATE score in pan-cancer. **(C)** Association between the NI and stemness indices in pan-cancer. **(D)** Correlations between the NI and NRG in pan-cancer.

significantly lower (e.g., RIPK1 and TNF). The expression values of FADD, MLKL, RIPK1, and TLR3 were positively correlated with their CNV, while FASLG, RIPK3, and TNF were the opposite (Figure 3E). In conclusion, these findings implied that crosstalk among the NRGs plays a crucial role in the development and progression of most cancer types.

The efficacy of the NI across tumor types

Considering the solid relationship between necroptosis and signaling pathways described above, we further investigated the potency of the NI in different cancer types. We calculated the relationship between the 28 kinds of immune cells and NI and discovered a significant correlation among all tumor types. The percentage of Tregs, T cells follicular helper, T cells CD8, T cells CD4 memory active, NK cells activated, Macrophages M1, and naive B cells were relevant to the NI of most tumor types (Figure 4A; Supplementary Table S2). Interestingly, these cells were antitumor types, suggesting, to some extent, that the NI facilitates tumor immunity. Furthermore, we found a significant correlation between NI and stem cell indices for cancer types, except for BRCA, CHOL, COAD, and OV (Figure 4C; Supplementary Table S3). Meanwhile, we also observed an significant association between the Estimate score and the NI in all tumors (Figure 4B; Supplementary Table S4). We investigated the relationship of NRGs with NI and found that NRGs were significantly positively correlated with NI (Figure 4D; Supplementary Table S5). Finally, we found that NI was significantly correlated with the prognosis of patients in nine tumors: STAD, MESO, GBM, SKCM, LIHC, LGG, ACC, KIRC, and THYM. This result revealed that NI could significantly affect the prognosis of tumor patients (Supplementary Figures S1A–C; Supplementary Table S6). Significant indicators reflecting the reaction to immune checkpoint therapy can be broadly classified into two types: microsatellite instability (MSI) or TMB, and inflammatory infiltrating. The radar plots indicated significant correlation between NI and TMB in 16 tumors (Supplementary Figure S1D). Subsequently, we examined the association between NI and MSI and discovered that COAD displayed the largest positive relevance. These findings may indicate excessive T cell infiltration in DLBC (Supplementary Figure S1E). By analyzing the two immune-related indicators, the correlation between the indicators and reaction was reversed in some tumors. This phenomenon might be related to the heterogeneity of immune infiltration among cancers. For instance, PAAD had a highly positive relevance with TMB and a negative relevance with MSI values, which may be associated with the nontypical immunogenicity of PAAD. The results of these pan-cancer analyses demonstrated the immunological, mutational, and prognostic value of NI in a variety of tumors.

The landscape of NRGs in glioma

In Figure 2A, we found a clear effect of NRGs on the prognosis of glioma. Thus, we further explored the role of NRGs in glioma and found that the alterations of all NRGs were common and mainly focused on copy number amplification (Supplementary Figure S2B). We identified the alterations in CNV characteristics of all the NRGs on the chromosome. These findings revealed that the CNV state of all NRGs is associated with the proliferation and development of glioma. We further investigated the relevance of the NRGs and found that RIPK3 was significantly correlated with other genes, with the highest coefficient of correlation (0.8) between RIPK3 and MLKL (Supplementary Figure S2C). In addition, we studied the correlation between the expression patterns of NRGs and molecular features. Of the NRGs, seven genes showed a significant difference between normal tissues and glioma, while RIPK3 did not (Supplementary Figure S2D). The NRGs were distinct in groups classified according to IDHmut subtypes except RIPK3 (Supplementary Figure S2E). Of the NRGs, seven revealed remarkable distinctions among WHO classification, except TNF (Supplementary Figure S2F). The mutation frequency of NRGs in the 660 samples was 1.52%, and were mostly missense mutations. MLKL exhibited the greatest mutation rate, followed by other NRGs which did not show any mutations in glioma samples (Supplementary Figure S2G). We performed PCR validation of NRGs and found that all genes except RIPK3 were significantly different between tumor and normal tissues (Supplementary Figure S2H; Supplementary Table S7). This result is consistent with the expression of NRGs in the TCGA, indicating the stability of the expression of NRGs. As a result of these findings, we found significant differences in the expression of NRGs, which may play critical roles in glioma development.

Associations between the NI and clinical features

By applying the ssGSEA algorithm, the NI was computed according to the RNA sequence of 698 glioma samples and then ranked from lowest to highest to investigate the association between molecular classification and clinical characteristics (Figures 5A, B). As displayed in Figure 5C, the NI of male patients was significantly higher than female patients, and the NI in dead patients was obviously higher than in alive patients, which suggests that NI could reflect the prognosis of glioma patients. NI was significantly higher in patients older than 80 years than in those younger than 80 years. Patients with 1p19q codes had significantly lower NI than those with non-codes. The patients were significantly higher in IDH-mutant and ATRX-mutant samples than in wild-type samples. As shown in Figure 5D, NI in patients increased significantly with the increase of tumor grade, all of which were statistically significant. Patients aged 60–79 years had significantly higher NI than 40–59 and <40 patients. Meanwhile, there was no significant difference between groups in NI values in the ≥80 group. Among the WHO classification, the GBM had the highest NI, followed by astrocytoma, oligoastrocytoma, and oligodendroglioma. Furthermore, patients with IDHwt subtype demonstrated higher NI than IDHmut-non-codel and IDHmut-codel. These results suggest that NI is positively correlated with the

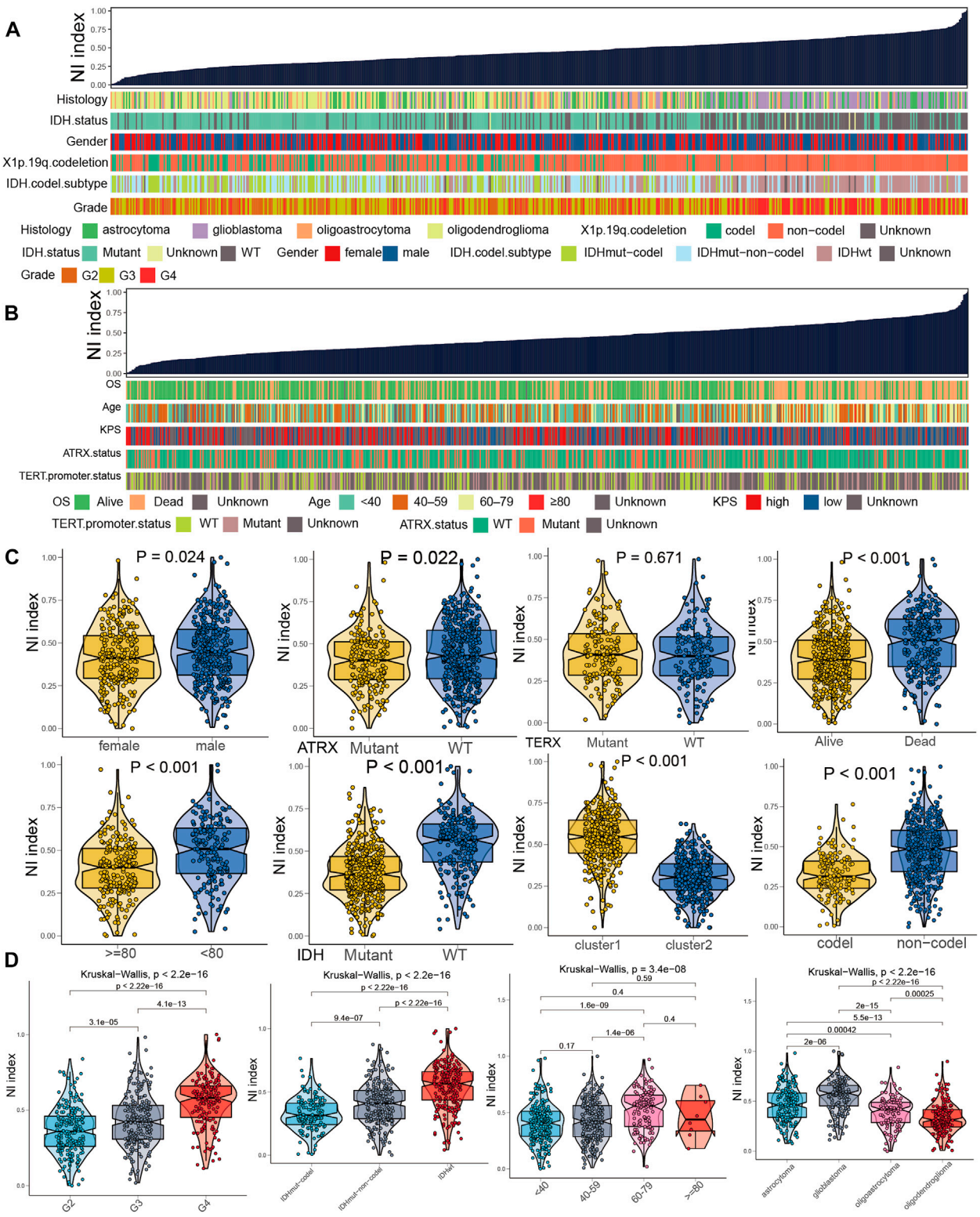

FIGURE 5
Clinical and molecular characteristics of glioma associated with NI. **(A,B)** A comprehensive analysis of the relationship between NI and clinicopathological characteristics of patients. **(C)** Violin plots of NI in glioma patients, stratified by gender, age, ATRX mutation, IDH mutation, TERX mutation, OS status, and 1p19q codel. **(D)** Violin plots of NI in glioma patients, stratified by grades, IDH mutation, ages, and histological classification.

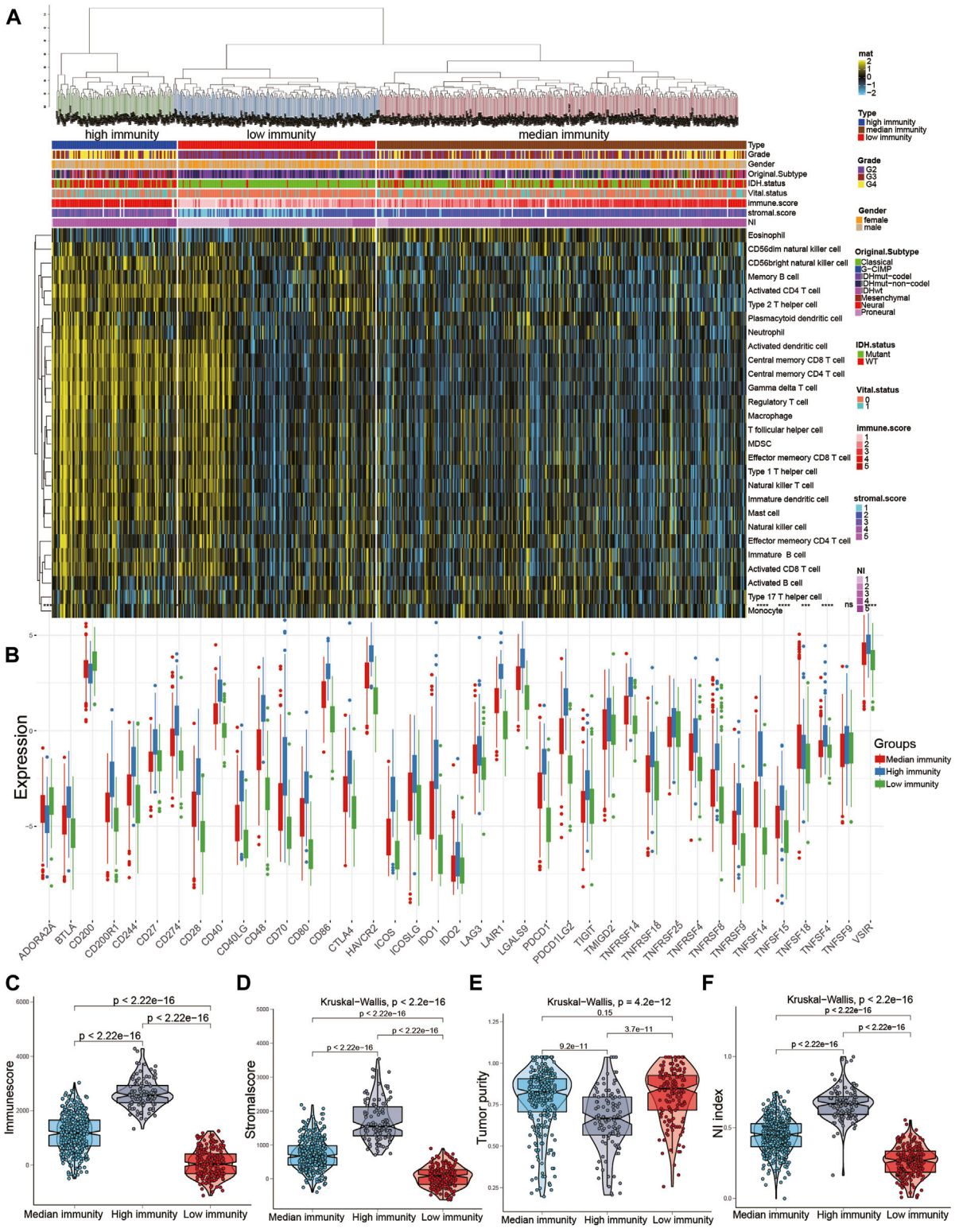

FIGURE 6
Relationship between NI and immune subgroups of gliomas. **(A)** The immune subgroups of glioma were classified based on the overall immune activity of glioma. **(B)** Quantitative analysis of the proportion of immune checkpoint in three immune subtypes. **(C–F)** Quantitative analysis of NI and ESTIMATE score in three immune subtypes.

malignancy and age of glioma and can reflect the condition and prognosis of glioma patients.

Associations between the NI and immune microenvironment

The ssGSEA scores of 29 immune cells were sorted into three immune subgroups using hierarchical clustering. 229 cases (32.8%) had the highest enrichment scores and were considered as high immune group and "hot immune" tumors. 203 cases (29%) had the lowest enrichment scores and were considered as low immune group and "cold immune" tumors. 353 cases (50.5%) had the medium enrichment scores and were considered as medium immune group and "altered immune" tumors, indicating the potential to conversion to cold or hot tumors (Figures 6A,B). The immune checkpoints in high immunity group was higher than other groups. Then, we further investigated the relationship between NI and immunity. The NI was significantly positively correlated with the immune score and stromal score, indicating that, as the NI of glioma increased, the level of infiltration of immune cells and stromal cells increased (Supplementary Figures S3C, E). However, significant negative correlation between NI and tumor purity was observed (Supplementary Figure S3D). Then, the enrichment scores of 22 kinds of immune cells and immune checkpoints were quantified by the ggplot (Supplementary Figures S3A, B). The results revealed the high immune group had the highest scores of immune cells and immune checkpoints, followed by medium and low immune groups. In addition, the immune score and stromal score were both the highest in high immune subgroups, indicating high enrichment scores of stromal cells and immune cells, followed by medium and low immune subgroups (Figures 6C, D). By contrast, tumor purity increases gradually from high to low immune subgroups, and NI gradually decreases. Moreover, the NI in high immunity was higher than other two groups (Figures 6E, F). From the above findings, we suggest the NI has significant association with the immune status of glioma.

Identification of two NI subgroups with different OS and clinical characteristics

We performed DEGs between high and low groups of NI with limma package and obtained 4,645 DEGs and performed univariate and multivariate cox to obtain 125 DEGs. Then, we used consensus clustering to discover a new classification of glioma on the basis of the RNA sequence of 125 necroptosis-related DEGs. Based on the CDF curve, the consensus heatmap, and the PAC algorithm, the best number of clusters was identified as two (k = 2) (Supplementary Figures S4A–C). We also displayed the clusters (k = 2–6) in Supplementary Figures S5A–F. Therefore, glioma patients were classified into two subgroups, which were termed NI subgroup I (359 patients, 51.4%) and NI subgroup II (339 patients, 48.6%). Glioma patients in the NI subgroup II presented superior OS than those in the NI subgroup I in the TCGA and CGGA (Supplementary Figures S4I, J). Then, we found a significantly lower number of high-grade patients in the NI subgroup II than in the NI subgroup I, as well as a higher proportion of deaths, a higher number of patients with IDH mutation, a higher number of patients with 1p19q codel, a higher percentage of MGMT methylation, and a higher percentage of ATRX (Supplementary Figures S3F, S4D–H). For the original subgroup and methylation subgroup, the proportions of idhmuton-codel and IDHmutnon-codel in NI subgroup II were higher than other types, and the proportions of codel and G-CIMP-high in NI subgroup II were higher than other types (Supplementary Figures S3G, H).

Identification of the characteristic of NI subgroups with immunity

In the previous studies, depleted immune and active immune subgroups differed significantly in B cells, cytolytic activity, and M1/M2 macrophages, but not in cytotoxic cells, CD8T cells, and T cells. Immune-active subtypes are strongly associated with immune-active pathways and gene sets, and immune-depleted subgroups are closely related to tumor-promoting signals that restrain host immune response, like activation of the Wnt/TGFβ1 signaling pathway (Chen et al., 2019). To investigate the correlation between NI subgroups and tumor immunity, we investigated the abundance of immune cells' infiltration in NI subgroups and found that activated B cells, activated CD4 T cells, and activated CD8 T cells were significantly higher in NI subgroups I than in NI subgroups II (Figures 7A, B). Immune score and Stromal score in NI subgroup I are significantly higher than NI subgroup II, while tumor purity is the reverse (Figures 7C–E). These results suggest that NI subgroups were closely associated with tumor immunity.

Identification of the characteristic of NI subgroups with mutation

Prior research confirmed the potential role of mutation in regulating tumor immunity (Rooney et al., 2015; Thorsson et al., 2018). Therefore, we performed CNA and somatic mutation profiling to investigate the different mutation status in the two NI subgroups. As displayed in Supplementary Figures S6A, B, NI subgroup I had a higher mutation rate (90.88%) than NI subgroup II (95.02%) (Supplementary Figures S6A, B). The IDH1 mutation rate was higher in NI subgroup II (82%) than NI subgroup I (36%), IDH1 mutation dramatically indicated the outcome of glioma patients, so the distinction in IDH1 mutation between two cluster subgroups may contribute to the prognosis of glioma. Moreover, we examined the landscape of co-occurrence using the top 25 mutation genes with the comet algorithm. Twelve pair cases (EGFR-TP53, MUC16-TP53, PTEN-IDH1, EGFR-IDH1, NF1-IDH1, PTEN-ATRX, EGFR-ATRX, ATRX-CIC, ATRX-FUBP1, ATRX-PIK3CA, TP53-CIC, TP53-FUBP1, TP53-NOTCH1, TP53-ZBTB20, IDH1-IDH2, IDH-EGFR, and IDH1-PTEN) were compared with prevalent mutually exclusive mutations, indicating that they may have a superfluous impact on the common pathway and a selected advantage of retaining the mutation copy between them (Supplementary Figure S6E). After detecting RNA sequence alterations in both subgroups, we further explored genomic-level distinctions between the two NI subgroups. Somatic mutation,

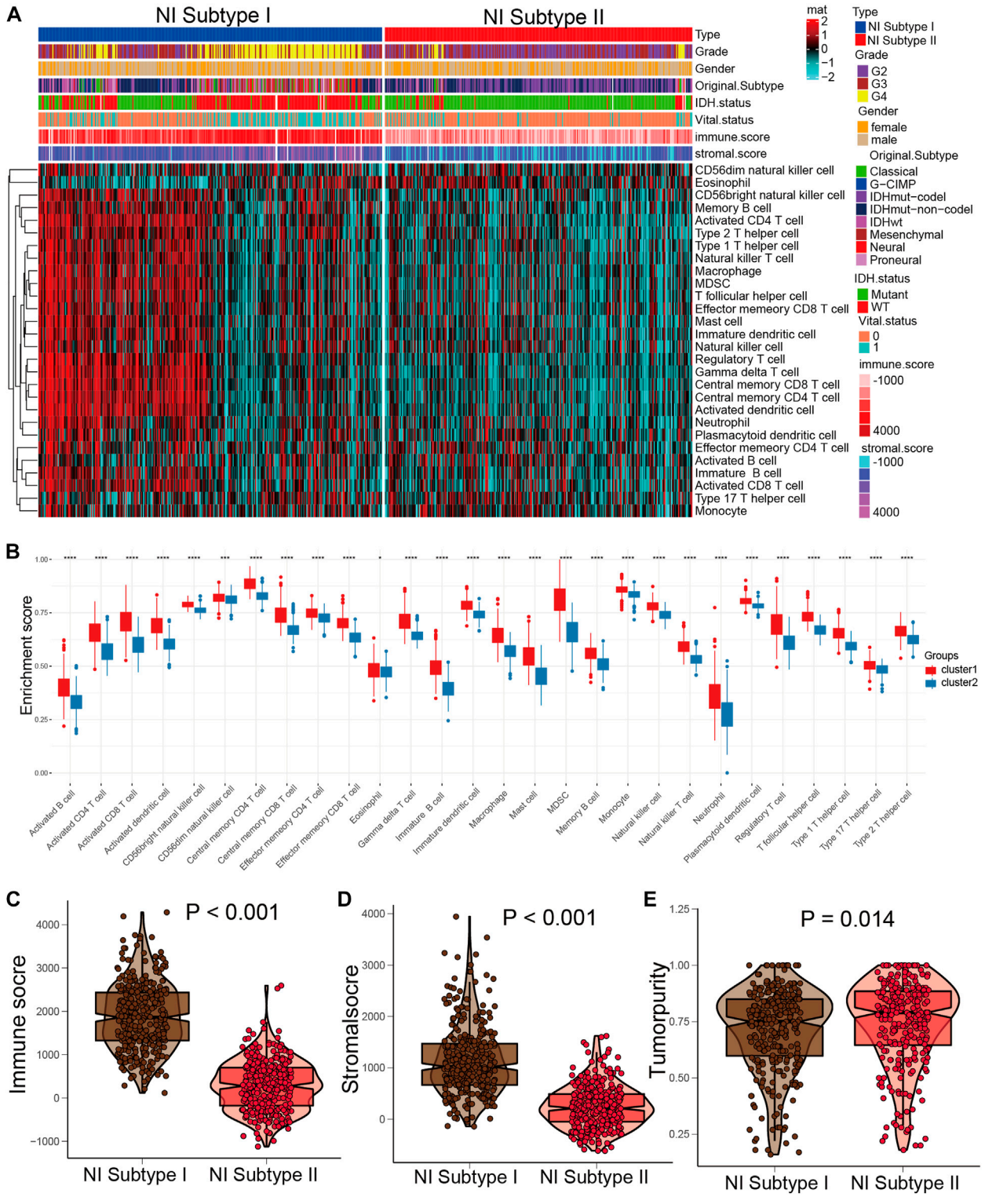

FIGURE 7
Distinct immune patterns of two NI subgroups. **(A)** Quantitative analysis of ESTIMATE score between two NI subgroups. **(B)** Quantitative analysis of the proportion of immune cells in two subgroups. **(C–E)** The expression levels of ESTIMATE score in NI subgroup I and II.

including single nucleotide variants, insertions, single nucleotide polymorphisms (SNP), and deletions, were computed and visualized applying the "maftools" package. The SNPs and Total in NI subgroup I were also exceeded by those in NI subgroup II (Supplementary Figure S6H). More interesting is that several genes had distinct mutation rates between the two cohorts. In terms of outcomes, the top 10 genes were shown in Supplementary Figure S6I. Furthermore, IDH1 is another classic

example demonstrating the distinct mutation sites between two cohorts (Supplementary Figures S6C, D) and the plausible chain reaction of the variance in prognostic effect. Eventually, we evaluated driver genes for the two NI subgroups, and the findings indicated that the dominant driver genes of NI subgroup I were PLCH2 and IDH1, meanwhile, the driver genes of NI subgroup II subgroup were IDH1 and IDH2 (Supplementary Figure S6G). Moreover, the samples in the NI subgroup I have remarkably higher enrichment scores of variant allele fractions than those in the NI subgroup II (Supplementary Figure S6F), which had been thought to be linked to cancer progression and worse prognosis.

Comparison of DEGs in the two NI subgroups

Given the prognostic distinctions between the high and low subgroups, we investigated DEGs between the two subgroups. 4,645 DEGs were identified: 2,219 genes were upregulated and 2,426 genes downregulated in the high NI group. The most upregulated genes were BRSK2, MAST1, CTIF, JPH4, ADGRL1, SCAMP5, SLC25A27, CRIPAP1, USP11, and RUNDC3A, while the most downregulated genes were ARHGDIB, TMEM109, LAT2, HLA-DMA, SPI1, SASH3, LYN, CXCL16, NAGA, and FERMT3 (Supplementary Figure S4K).

Construction and validation of the NI subgroups predictor

The samples were aggregated in a scale-free network using WGCNA algorithm, and 4,645 DEGs co-expression modules were found (Supplementary Figure S7C). The obtained topology matrix was clustered based on the β value to the proximity and topology matrix and based on the differences between genes. The hierarchical clustering method was applied to generate the gene dendrogram. An assignment of modules identified by dynamic cutting tree is shown in the colorful rows at the bottom of the tree diagram (Supplementary Figure S7A). Closed modules were merged into new modules, and the characteristic genes were calculated for each module. As shown in Supplementary Figure S7B, a total of 4,645 DEGs were divided into 24 modules. Since the ME yellow module (GS > 0.5, MM > 0.8) had the highest correlation with NI, we performed a NI subgroups predictor screen for genes in this module. The yellow module obtained 125 genes significantly associated with NI; we then performed multi-cox and lasso regression on 125 genes, and finally obtained 10 hub genes: C3, DOK3, FCER1G, FCGR2A, FCGR3A, GNA15, IL10RA, LRRC25, RGS19, and WAS (Supplementary Figure S7D). We performed model construction based on risk coefficients for these 10 hub genes and found that patients in the low-risk group had significantly higher survival than the high-risk group in the TCGA and CGGA cohorts (Supplementary Figures S7E, F). Finally, timeROC analysis in the TCGA cohort showed that the AUC is greater than 0.79 at 1, 3, 5, and 7 years and greater than 0.74 in the TCGA and CGGA cohorts (Supplementary Figures S6G, H).

Clinical application of NI subgroup

Different NI subgroups should contribute to the clinical treatment of glioma. Therefore, we calculated the sensitivity of the two NI subgroups for 30 anticancer drugs to identify appropriate agents for glioma treatment by using the pRRophetic algorithm. 24 chemotherapeutic drugs had obviously distinct IC50 in the two NI subgroups (Supplementary Figure S8A; Supplementary Table S8). Then, subclass mapping algorithm was employed to forecast the outcome for ICI therapy, containing CTLA4 and PD1 inhibitors. We discovered that the NI subgroup I has a better outcome in anti-PD1 therapy (Supplementary Figure S8B; Supplementary Table S9).

Discussion

Necroptosis is a specific form of cellular necrotic death mediated mainly by MLKL, RIP1, and RIP3 (Gong et al., 2019; Martens et al., 2021). In tumor therapy, necroptosis can be used as a programmed death modality to avoid apoptosis resistance and enhance anti-tumor immunity (Frank and Vince, 2018; Sprooten et al., 2020). Nevertheless, there is an absence of comprehensive studies on necroptosis and NRGs in pan-cancer. In present research, we utilized multiomics and clinical features from TCGA to reveal overall alterations of NRGs at genetic, transcriptional, and epigenetic levels. We also processed expression data using ssGSEA to construct NI to feature necroptosis and determine which genes and non-gene factors are associated with NI. Distinct molecular types affect the NI in most cancers, implying that distinct molecular subgroups responding to therapy may be associated with necroptosis.

It is unclear how necroptosis mediates glioma proliferation, but the association we discovered between NI and cancer features could increase the knowledge on necroptosis. GSEA revealed that the degree of NI is strongly correlated with tumor-associated oncogenic signaling pathway, cancer hallmarks, and metabolism-related pathways in pan-cancer. NRGs can act as both oncogene and tumor suppressor, and the NI plays the role of a protection or risk factor in different tumors. We also discovered that some clinical features affected necroptosis, like therapeutic response, survival status, and immune phenotype. NI also differs between genders in some tumors, including HNSC, LUAD, STAD, and LIHC, and between races in HNSC, LUAD, ESCA, LIHC, LUSC, KIRC, OV, THCA, SARC, and ESCA, implying the need to consider gender and race when considering necroptosis as a treatment strategy. We also observed that superior clinical outcome or status was also associated with higher NI in several cancer types, which further confirmed the double effect of necroptosis. Therefore, a distinct method of modulating the necroptosis of tumor cells may be beneficial to patients and enhance prognosis.

In addition, we found that most NRGs and NI were significantly associated with the prognosis of GBM and LGG in Figure 2A, and we went on to explore the effect played by NRGs in glioma. Then, we thoroughly analyzed the relationship between the necroptosis of glioma and the response of chemotherapy and immunotherapy, and developed the method to differentiate subtypes based on necroptosis. First, we applied the ssGSEA to construct the NI in

1716 glioma samples from a public database. We classified the glioma patients into two subgroups on the basis of their NI and compared their clinical characteristics to identify the relationship between the NI subgroups and clinical characteristics. ICI therapy, especially anti-PD1 therapy, can obtain better treatment results in NI subgroup I, as predicted by the subclass mapping algorithm, while chemotherapeutic agents are effective, as predicted by the pRRophetic algorithm. Furthermore, to distinguish clinical value between these two NI subgroups, we identified the 10 crucial necroptosis subgroup-related DEGs by lasso, univariate, and multivariate cox, and regarded them as predictors of necroptosis subgroup. The 10 genes were C3, DOK3, FCER1G, FCGR2A, FCGR3A, GNA15, IL10RA, LRRC25, RGS19, and WAS.

Although the central nervous system is a relatively specific immune region, immunotherapy has been extensively investigated for glioma in recent years, mainly containing cellular immunotherapy, ICI, and anti-tumor vaccines. Nevertheless, the efficacy of these phase III clinical trials in GBM have been unsatisfactory compared with other tumors (Weller et al., 2017; Reardon et al., 2020). There are numerous parameters that influence the efficacy of GBM immunotherapy. In the case of PD-L1/PD-1 blockade therapy, the expression level of TMB, tumor-infiltrating lymphocytes, PD-L1, and mismatch repair deficiency can all influence ICI therapy (Wang et al., 2019; Touat et al., 2020). But in the current phase III clinical trials, there was no screening of glioma patients for these elements, and this non-distinctive therapy may also account for the failure of these trials, which is a concern for future studies.

In response to the above-mentioned challenges in immunotherapy, this research presented a novel categorization of glioma on the basis of necroptosis. We observed that NI subgroup I presented higher NI and was more responsive to immunotherapy, which offered a novel way of selecting patients who were appropriate for immunotherapy. This study analyzed potential anti-glioma compounds in the "pRRophetic" package. For NI subgroup I, Gemcitabine, Bortezomib, Midostaurin, Lapatinib, Rapamycin, Tipifarnib, Etoposide, Embelin, Roscovitine, Docetaxel, Bexarotene, Pazopanib, and Dasatinib were reconsidered as the targeted drugs. In the case of NI subgroup II, Gefitinib, Axitinib, and Bosutinib were identified as the potential targeted drugs. These are the anti-tumor drugs approved by the FDA for future screening of anti-glioma drugs. Despite the absence of studies on drugs and immunotherapy, our analysis confirmed the validity of drug screening and the clinical translation of drug response to glioma treatment.

Ferroptosis, cuproptosis, and necroptosis are all important cell death modalities that play an important role in the tumor microenvironment (Shen et al., 2022; Xie et al., 2022; Zhang et al., 2023). It was found that ferroptosis could be involved in tumorigenesis, progression, and activation of different regulatory sites in the ferroptosis pathway and could promote tumor cell death. Related studies have shown that cuproptosis is involved in most mechanisms of tumorigenesis and metastasis and complicates tumor immune escape. Tumor cells undergo necrosis as a self-sacrificing strategy to create a favorable environment for their proliferation and metastasis, but necroptosis exerts tumor suppressive effects in most cases. Studying the relationship between cell death and the tumor microenvironment can further contribute to our understanding of how different cell death modalities affect tumor development and provide new ideas to inhibit tumor growth (Zou et al., 2022; Zou et al., 2023).

We reviewed some related literature and found that they all present systematic analysis of necroptosis mainly focusing on low-grade glioma and breast cancer (Xie et al., 2022; Zou et al., 2022), and there is little overall analysis of low-grade and high-grade gliomas. Moreover, previous studies on gliomas have directly performed model construction using key genes, and there is no integration of key genes' enrichment scores to comprehensively evaluate the role of necroptosis-related genes in tumors.

We calculated necroptosis index (NI) using eight necroptosis related genes and found that it significantly responded to the prognosis of patients by NI in most tumors. We also studied its prognosis, immune environment, radiotherapy, and molecular-targeted therapy in glioma patients, and obtained relatively satisfactory results. We performed PCR validation of the expression of eight necroptosis genes in glioma samples, and this cross-corroboration of database and experiment further illustrates the reliability of our experiments.

Our analysis first correlated the role of necroptosis-related genes in pan-cancer and further found that necroptosis was significantly associated with the prognosis of glioma patients, and then further analyzed the close relationship between necroptosis and glioma. Such an analysis is more logical. However, our model has some drawbacks. First, we need to test the expression of these eight key genes in order to evaluate the prognosis of patients, and this associated cost may be high. Second, although the CGGA database has a considerable number of samples to validate the conclusions, we need to develop the sample number of our hospital in the future. Third, due to the very limited number of patients receiving immunotherapy and our study being supported by public databases, the relationship between immunotherapy and NI subgroups needs to be investigated in future immunotherapy cohorts.

Conclusion

In summary, there remains a great potential for immunotherapy in glioma. Screening patients who may be more suitable for immunotherapy is essential. In this research, we classified patients into two distinct subtypes according to NI of glioma, and predicted sensitivity of patients in two subgroups to immunotherapy, offering a method for screening suitable patients for immunotherapy. Our study also identified predictors of NI subgroups, which makes it clinically feasible to translate NI.

Data availability statement

The original contributions presented in the study are included in the article/Supplementary Material, further inquiries can be directed to the corresponding authors.

Ethics statement

The studies involving human participants were reviewed and approved by the Ethics Committee of the Second Hospital of Harbin

Medical University with the reference number KY 2021-172. The patients/participants provided their written informed consent to participate in this study.

Author contributions

SM, FW, ZL, QL, SH, and ST designed the study and drafted the manuscript. XG, ZW, MY, FJ, DZ, JC, XY, JZ, NW, HZ, and LP provided technical support. All authors contributed to the article and approved the submitted version.

Funding

This work was supported by the National Natural Science Foundation of China (No. 61575058).

Acknowledgments

The authors would like to thank ST for his excellent technical support and SH for his critical review of the manuscript.

Conflict of interest

The authors declare that the research was conducted in the absence of any commercial or financial relationships that could be construed as a potential conflict of interest.

Publisher's note

All claims expressed in this article are solely those of the authors and do not necessarily represent those of their affiliated organizations, or those of the publisher, the editors and the reviewers. Any product that may be evaluated in this article, or claim that may be made by its manufacturer, is not guaranteed or endorsed by the publisher.

Supplementary material

The Supplementary Material for this article can be found online at: https://www.frontiersin.org/articles/10.3389/fphar.2023.1170240/full#supplementary-material

References

Aaes, T. L., Kaczmarek, A., Delvaeye, T., De Craene, B., De Koker, S., and Heyndrickx, L. (2016). Vaccination with necroptotic cancer cells induces efficient anti-tumor immunity. *Cell Rep.* 15, 274–287. doi:10.1016/j.celrep.2016.03.037

Charoentong, P., Finotello, F., Angelova, M., Mayer, C., Efremova, M., and Rieder, D. (2017). Pan-cancer immunogenomic analyses reveal genotype-immunophenotype relationships and predictors of response to checkpoint blockade. *Cell Rep.* 18, 248–262. doi:10.1016/j.celrep.2016.12.019

Chen, Y.-Q. W. Y.-P., Lv, J.-W., and Li, Y.-Q. Identification and validation of novel microenvironment-based immune molecular subgroups of head and neck squamous cell carcinoma: Implications for immunotherapy. *Ann. Oncol. (Ann. Oncol.).* 30 2019

Darjakanduc, A. M., Rosario, S. E. R. P. I. C. O., Sinigaglia, E., Sinha, A. A., and Natale, C. (2002). Cell death: Apoptosis versus necrosis (review). *Int. J. Oncol.* 21, 165–170.

Degterev, A., Huang, Z., Boyce, M., Li, Y., Jagtap, P., and Mizushima, N. (2005). Chemical inhibitor of nonapoptotic cell death with therapeutic potential for ischemic brain injury. *Nat. Chem. Biol.* 1, 112–119. doi:10.1038/nchembio711

Duan-Wu Zhang, J. S., Lin, J., Lin, J., Zhang, N., Lu, B. J., and Lin, S. C. (2009). RIP3, an energy metabolism regulator that switches TNF-induced cell death from apoptosis to necrosis. *SCIENCE* 325, 332–336. doi:10.1126/science.1172308

Frank, D., and Vince, J. E. (2018). Pyroptosis versus necroptosis: Similarities, differences, and crosstalk. *Cell Death Differ.* 26, 99–114. doi:10.1038/s41418-018-0212-6

Fulda, S. (2013). The mechanism of necroptosis in normal and cancer cells. *Cancer Biol. Ther.* 14, 999–1004. doi:10.4161/cbt.26428

Geeleher, P., Cox, N., and Huang, R. S. (2014). pRRophetic: an R package for prediction of clinical chemotherapeutic response from tumor gene expression levels. *PLoS One* 9, e107468. doi:10.1371/journal.pone.0107468

Gong, Y., Fan, Z., Luo, G., Yang, C., Huang, Q., and Fan, K. (2019). The role of necroptosis in cancer biology and therapy. *Mol. Cancer* 18, 100. doi:10.1186/s12943-019-1029-8

Goodall, M. L., Fitzwalter, B. E., Zahedi, S., Wu, M., Rodriguez, D., and Mulcahy-Levy, J. M. (2016). The autophagy machinery controls cell death switching between apoptosis and necroptosis. *Dev. Cell* 37, 337–349. doi:10.1016/j.devcel.2016.04.018

Han, B., Meng, X., Wu, P., Li, Z., Li, S., and Zhang, Y. (2020). ATRX/EZH2 complex epigenetically regulates FADD/PARP1 axis, contributing to TMZ resistance in glioma. *Theranostics* 10, 3351–3365. doi:10.7150/thno.41219

Huang, W., Zhong, Z., Luo, C., Xiao, Y., Li, L., and Zhang, X. (2019). The miR-26a/AP-2α/Nanog signaling axis mediates stem cell self-renewal and temozolomide resistance in glioma. *Theranostics* 9, 5497–5516. doi:10.7150/thno.33800

Koboldt, D. C., Zhang, Q., Larson, D. E., Shen, D., McLellan, M. D., and Lin, L. (2012). VarScan 2: Somatic mutation and copy number alteration discovery in cancer by exome sequencing. *Genome Res.* 22, 568–576. doi:10.1101/gr.129684.111

Koboldt, D. C., Zhang, Q., Larson, D. E., Shen, D., McLellan, M. D., and Lin, L. (2012). VarScan 2: Somatic mutation and copy number alteration discovery in cancer by exome sequencing. *Genome Res.* 22, 568–576. doi:10.1101/gr.129684.111

Langfelder, P., and Horvath, S. (2008). Wgcna: an R package for weighted correlation network analysis. *BMC Bioinforma.* 9, 559. doi:10.1186/1471-2105-9-559

Lawlor, K. E., Khan, N., Mildenhall, A., Gerlic, M., Croker, B. A., and D'Cruz, A. A. (2015). RIPK3 promotes cell death and NLRP3 inflammasome activation in the absence of MLKL. *Nat. Commun.* 6, 6282. doi:10.1038/ncomms7282

Leiserson, M. D., Wu, H. T., Vandin, F., and Raphael, B. J. (2015). CoMEt: A statistical approach to identify combinations of mutually exclusive alterations in cancer. *Genome Biol.* 16, 160. doi:10.1186/s13059-015-0700-7

Linkermann, A., and Green, D. R. (2014). *Necroptosis. N. Engl. J. Med.* 370, 455–465. doi:10.1056/NEJMra1310050

Martens, S., Bridelance, J., Roelandt, R., Vandenabeele, P., and Takahashi, N. (2021). MLKL in cancer: More than a necroptosis regulator. *Cell Death Differ.* 28, 1757–1772. doi:10.1038/s41418-021-00785-0

Marino, G., Niso-Santano, M., Baehrecke, E. H., and Kroemer, G. (2014). Self-consumption: The interplay of autophagy and apoptosis. *Nat. Rev. Mol. Cell Biol.* 15, 81–94. doi:10.1038/nrm3735

Newton, K., and Manning, G. (2016). Necroptosis and inflammation. *Annu. Rev. Biochem.* 85, 743–763. doi:10.1146/annurev-biochem-060815-014830

Newton, K. (2015). RIPK1 and RIPK3: Critical regulators of inflammation and cell death. *Trends Cell Biol.* 25, 347–353. doi:10.1016/j.tcb.2015.01.001

Park, H. H., Kim, H. R., Park, S. Y., Hwang, S. M., Hong, S. M., and Park, S. (2021). RIPK3 activation induces TRIM28 derepression in cancer cells and enhances the anti-tumor microenvironment. *Mol. Cancer* 20, 107. doi:10.1186/s12943-021-01399-3

Paul Geeleher, N. J. C., and Huang, R. Stephanie (2014). Clinical drug response can be predicted using baseline gene expression levels and *in vitro* drug sensitivity in cell lines. *Genome Biol.* R47.

Reardon, D. A., Brandes, A. A., Omuro, A., Mulholland, P., Lim, M., and Wick, A. (2020). Effect of nivolumab vs bevacizumab in patients with recurrent glioblastoma: The CheckMate 143 phase 3 randomized clinical trial. *JAMA Oncol.* 6, 1003–1010. doi:10.1001/jamaoncol.2020.1024

Ritchie, M. E., Phipson, B., Wu, D., Hu, Y., Law, C. W., and Shi, W. (2015). Limma powers differential expression analyses for RNA-sequencing and microarray studies. *Nucleic Acids Res.* 43, e47. doi:10.1093/nar/gkv007

Rooney, M. S., Shukla, S. A., Wu, C. J., Getz, G., and Hacohen, N. (2015). Molecular and genetic properties of tumors associated with local immune cytolytic activity. *Cell* 160, 48–61. doi:10.1016/j.cell.2014.12.033

Shen, Y., Li, D., Liang, Q., Yang, M., Pan, Y., and Li, H. (2022). Cross-talk between cuproptosis and ferroptosis regulators defines the tumor microenvironment for the prediction of prognosis and therapies in lung adenocarcinoma. *Front. Immunol.* 13, 1029092. doi:10.3389/fimmu.2022.1029092

Sprooten, J., De Wijngaert, P., Vanmeerbeerk, I., Martin, S., Vangheluwe, P., and Schlenner, S. (2020). Necroptosis in immuno-oncology and cancer immunotherapy. *Cells* 9, 1823. doi:10.3390/cells9081823

Thorsson, V., Gibbs, D. L., Brown, S. D., Wolf, D., Bortone, D. S., and Ou Yang, T. H. (2018). The immune landscape of cancer. *Immunity* 48, 812–830 e14. doi:10.1016/j.immuni.2018.03.023

Touat, M., Li, Y. Y., Boynton, A. N., Spurr, L. F., Iorgulescu, J. B., and Bohrson, C. L. (2020). Mechanisms and therapeutic implications of hypermutation in gliomas. *Nature* 580, 517–523. doi:10.1038/s41586-020-2209-9

Wang, X., Guo, G., Guan, H., Yu, Y., Lu, J., and Yu, J. (2019). Challenges and potential of PD-1/PD-L1 checkpoint blockade immunotherapy for glioblastoma. *J. Exp. Clin. Cancer Res.* 38, 87. doi:10.1186/s13046-019-1085-3

Weller, M., Butowski, N., Tran, D. D., Recht, L. D., Lim, M., and Hirte, H. (2017). Rindopepimut with temozolomide for patients with newly diagnosed, EGFRvIII-expressing glioblastoma (ACT IV): A randomised, double-blind, international phase 3 trial. *Lancet Oncol.* 18, 1373–1385. doi:10.1016/S1470-2045(17)30517-X

Wilkerson, M. D., and Hayes, D. N. (2010). ConsensusClusterPlus: A class discovery tool with confidence assessments and item tracking. *Bioinformatics* 26, 1572–1573. doi:10.1093/bioinformatics/btq170

Xie, J., Tian, W., Tang, Y., Zou, Y., Zheng, S., and Wu, L. (2022). Establishment of a cell necroptosis index to predict prognosis and drug sensitivity for patients with triple-negative breast cancer. *Front. Mol. Biosci.* 9, 834593. doi:10.3389/fmolb.2022.834593

Yang, Z., Wang, Y., Zhang, Y., He, X., Zhong, C. Q., and Ni, H. (2018). RIP3 targets pyruvate dehydrogenase complex to increase aerobic respiration in TNF-induced necroptosis. *Nat. Cell Biol.* 20, 186–197. doi:10.1038/s41556-017-0022-y

Yi, M., Li, T., Qin, S., Yu, S., Chu, Q., and Li, A. (2020). Identifying tumorigenesis and prognosis-related genes of lung adenocarcinoma: Based on weighted gene coexpression network analysis. *Biomed. Res. Int.* 2020, 4169691. doi:10.1155/2020/4169691

Yoshihara, K., Shahmoradgoli, M., Martinez, E., Vegesna, R., Kim, H., and Torres-Garcia, W. (2013). Inferring tumour purity and stromal and immune cell admixture from expression data. *Nat. Commun.* 4, 2612. doi:10.1038/ncomms3612

Zhang, Y., Yang, M., Ng, D. M., Haleem, M., Yi, T., and Hu, S. (2020). Multi-omics data analyses construct TME and identify the immune-related prognosis signatures in human LUAD. *Mol. Ther. Nucleic Acids* 21, 860–873. doi:10.1016/j.omtn.2020.07.024

Zhang, Z., Su, D., Thakur, A., Zhang, K., Xia, F., and Yan, Y. (2023). Immune cell death-related lncRNA signature as a predictive factor of clinical outcomes and immune checkpoints in gastric cancer. *Front. Pharmacol.* 14, 1162995. doi:10.3389/fphar.2023.1162995

Zou, Y., Xie, J., Zheng, S., Liu, W., Tang, Y., and Tian, W. (2022). Leveraging diverse cell-death patterns to predict the prognosis and drug sensitivity of triple-negative breast cancer patients after surgery. *Int. J. Surg.* 107, 106936. doi:10.1016/j.ijsu.2022.106936

Zou, Y., Ye, F., Kong, Y., Hu, X., Deng, X., and Xie, J. (2023). The single-cell landscape of intratumoral heterogeneity and the immunosuppressive microenvironment in liver and brain metastases of breast cancer. *Adv. Sci. (Weinh)* 10, e2203699. doi:10.1002/advs.202203699

frontiers | Frontiers in Pharmacology

TYPE Original Research
PUBLISHED 15 November 2023
DOI 10.3389/fphar.2023.1298341

OPEN ACCESS

EDITED BY
Nur Akmarina Mohd Said,
University of Malaya, Malaysia

REVIEWED BY
Chengliang Zhang,
Huazhong University of Science and Technology, China
Xiaofei Hu,
Army Medical University, China

*CORRESPONDENCE
Lei Tang,
tlei1974@163.com
Jianta Wang,
63402036@163.com
Dan Ma,
md_hust_gmu@163.com

†These authors have contributed equally to this work

RECEIVED 21 September 2023
ACCEPTED 06 November 2023
PUBLISHED 15 November 2023

CITATION
Ran Y, Hu C, Wan J, Kang Q, Zhou R, Liu P, Ma D, Wang J and Tang L (2023), Integrated investigation and experimental validation of PPARG as an oncogenic driver: implications for prognostic assessment and therapeutic targeting in hepatocellular carcinoma.
Front. Pharmacol. 14:1298341.
doi: 10.3389/fphar.2023.1298341

Integrated investigation and experimental validation of PPARG as an oncogenic driver: implications for prognostic assessment and therapeutic targeting in hepatocellular carcinoma

Yunsheng Ran[1,2†], Chujiao Hu[2,3†], Junzhao Wan[1,2], Qian Kang[4], Ruixian Zhou[5], Ping Liu[4], Dan Ma[2,3,4*], Jianta Wang[2,3*] and Lei Tang[2,3,6*]

[1]School of Pharmacy, Guizhou Medical University, Guiyang, China, [2]Guizhou Provincial Engineering Technology Research Center for Chemical Drug R&D, Guizhou Medical University, Guiyang, China, [3]State Key Laboratory of Functions and Applications of Medicinal Plants, Guizhou Medical University, Guiyang, China, [4]Department of Hematology, Affiliated Hospital of Guizhou Medical University, Guiyang, China, [5]Department of Acupuncture and Moxibustion, Affiliated Hospital of Guizhou Medical University, Guiyang, China, [6]Key Laboratory of Endemic and Ethnic Diseases, Ministry of Education and Key Laboratory of Medical Molecular Biology of Guizhou Province, Guizhou Medical University, Guiyang, Guizhou, China

Peroxisome proliferator-activated receptor gamma (PPARG), a key transcription factor involved in lipid metabolism and glucose homeostasis, has been implicated in various types of cancer. However, its precise role in cancer remains unclear. In this study, we conducted a comprehensive pan-cancer analysis of PPARG expression using various types of cancer obtained from public databases. We observed significant heterogeneity in PPARG expression across different types of cancer. The association between PPARG expression and patient prognosis was investigated using Cox proportional hazards regression models and survival analysis. Clinical features and protein expression levels in the cohort showed that PPARG expression was strongly associated, suggesting its potential as a therapeutic target. We also evaluated the prognostic potential of PPARG by analyzing immune infiltration and genomic stability. We experimentally validated the potential of PPARG as a therapeutic target by analyzing drug sensitivity profiles, molecular docking simulations, and *in vitro* cell proliferation assays associated with PPARG expression. We identified common expression patterns of PPARG with other genes involved in key carcinogenic pathways. This provides deeper insights into the molecular mechanisms underlying its carcinogenic role. Additionally, functional enrichment analysis revealed significant enrichment of genes related to drug metabolism, cell proliferation, and immune response pathways associated with PPARG. Our findings highlight the importance of PPARG in the broader biology of cancer and suggest its potential as a diagnostic and therapeutic target for specific types of cancer. The results of

our study provide strong support for the potential role of PPARG as a promising prognostic biomarker and immunotherapeutic target across various types of cancer.

KEYWORDS

PPARG, prognosis, tumor microenvironment, drug sensitivity, immunological function, biomarkers

1 Introduction

Cancer has emerged as the leading cause of global mortality and presents a formidable barrier to enhancing both the quality and quantity of human life in the 21st century (Bray et al., 2018). The prevalence and intricate progression of tumors have presented significant challenges in the fields of cancer prevention, diagnosis, and treatment. Consequently, comprehensive research and exploration of biomarkers related to cancer, along with a deep understanding of their roles in cancer, elucidation of their functional significance, and evaluation of their potential as prognostic and predictive indicators, offer significant potential for advancing our understanding of the disease and enhancing therapeutic strategies (Wild, 2019).

Peroxisome proliferator-activated receptors (PPARs) were initially discovered in 1990 by British scientists Issemann et al. [3] as ligand-activated intranuclear transcription factors. There are three known subtypes of PPAR: PPAR-alpha (α), PPAR-delta (δ), and PPAR-gamma (γ). Among these subtypes, PPARγ, encoded by the *PPARG* gene, acts as a regulator of adipocyte differentiation. Recently, the association between PPAR proteins and cancer has garnered significant attention. PPARγ, a member of the nuclear receptor superfamily, plays a crucial role in controlling various biological processes (BPs), such as cell division, differentiation, and inflammation (Shu et al., 2016; Kesanakurti et al., 2017). Furthermore, PPARG exhibits widespread expression, particularly in the liver, colon, heart, several types of epithelial cells, and skeletal muscle (Verreth et al., 2004; Lewis et al., 2008; Zhang et al., 2012; Yang et al., 2016). As a transcription factor, PPARG is involved in the regulation of lipid anabolism and glycolysis to meet the energy demands of cancer cells. The metabolic reprogramming of glucose, lipids, and amino acid metabolism during tumorigenesis provides essential energy and substrates for sustained tumor cell proliferation and survival (Menezes and Diederich, 2021; Villarroel-Vicente et al., 2021). The activation of PPARG has been associated with beneficial effects on various types of cancer. It has been established that in cancer cells, the activation of PPARG leads to cell cycle arrest, suppression of cell proliferation, and increased apoptosis. (Mal et al., 2021). Additionally, the activation of PPARG has demonstrated anti-inflammatory properties by suppressing the production of pro-inflammatory cytokines and modulating the tumor microenvironment (TME) (Shao et al., 2020). Intriguingly, synthetic compounds known as PPARγ agonists, which activate PPARG, have shown promise as potential therapeutic agents in the treatment of cancer (Ryu et al., 2018; Ballav et al., 2022). Both preclinical and clinical studies have reported the anticancer effects of PPARγ agonists, including inhibition of tumor growth and reduced angiogenesis (Hughes et al., 2014; Joshi et al., 2014). However, the role of PPARG in tumor initiation remains highly intricate and is influenced by environmental factors (Vallee et al., 2018). The significance of PPARG in cancer development and the potential for therapeutic targeting of PPARG remain elusive.

This study aims to comprehensively investigate PPARG expression in human cancers and its impact on prognosis and clinical significance. Additionally, we sought to elucidate the association between PPARG and tumor formation, grading, and metastasis. We examined the expression features of PPARG in cancer, including its effects on genomic stability, the immune microenvironment, and potential molecular mechanisms. Furthermore, cell functional experiments were conducted to confirm the feasibility of targeting PPARG as a potential anticancer therapy. Understanding the intricate interplay between PPARG and tumors holds tremendous potential for the development of novel therapeutic strategies that target this pathway. By exploring the molecular mechanisms underlying the involvement of PPARG in tumorigenesis, we can uncover new avenues for the treatment of cancer and potentially identify biomarkers for patient stratification and personalized therapeutic approaches.

2 Materials and methods

2.1 Data collection and processing

The original raw data were obtained from The Cancer Genome Atlas (TCGA) (accessible at https://cancergenome.nih.gov/) and the Gene Expression Omnibus (GEO) (accessible at https://www.ncbi.nlm.nih.gov/geo/) databases. The obtained data were processed and cleaned separately using the following portals.

2.2 PPARG differential expression analysis in 33 human cancers

To assess the PPARG differential expression in various human cancers, the Tumor IMmune Estimation Resource (TIMER) database (accessible at https://cistrome.shinyapps.io/timer/) and the Gene Expression Profiling Interactive Analysis (GEPIA) database (accessible at http://gepia2.cancer-pku.cn/analysis/)were used. These databases allowed the measurement of PPARG expression in tumor tissues compared to normal tissues across different types of cancer. The differences in mRNA expression levels were analyzed, and the distributions of gene expression levels were visualized using box plots.

2.3 Survival analysis and prognosis in human cancers

The Kaplan-Meier method of survival analysis was used to analyze overall survival (OS), disease-specific survival (DSS),

progression-free interval (PFI), and disease-free interval (DFI). The R software package Survival (version 3.2–7) was used for this analysis. Cox proportional hazards regression models, implemented through the Coxph function, were used to analyze the association between gene expression and prognosis in each type of cancer. The log-rank test was used to perform statistical tests to obtain prognostic significance.

2.4 Genetic alteration analysis

The online platform cBioportal (accessible at https://www.cbioportal.org/) was used to analyze the genetic variation features of PPARG. This analysis involved investigating the query mutation frequency, types of mutation, and post-translational modifications (PTM).

2.5 Estimate of the TME, tumor mutational burden, microsatellite instability, and PPARG expression levels and immunological checkpoint genes in human cancers

Sanger Box, an online tool for TCGA data processing, was used to investigate the association between PPARG expression and immunological checkpoint (ICP) genes, biomarkers, and predicted scores in the TME. The unified and standardized pan-cancer dataset was obtained from the University of California Santa Cruz (UCSC; accessible at https://xenabrowser.net/) database. The dataset used was TCGA TARGET GTEx (PANCAN, N = 19,131, G = 60,499). From this dataset, the gene expression data of PPARG in each sample was extracted. The tumor mutational burden (TMB) of each tumor was calculated using the tmb function from the R package maftools (version 2.8.05). Additionally, the microsatellite instability (MSI) score of each tumor was determined by consulting previous studies.

2.6 Examination of the interaction between PPARG expression and clinical features

RNA-sequencing and clinical data for 31 types of cancer are collected from the UALCAN database (accessible at http://ualcan.path.uab.edu), which provides a reliable platform for examining gene expression in both tumors and healthy tissues. This database was utilized to explore the correlation between specific gene expression levels and clinicopathological features in human tumors.

2.7 Investigating PPARG co-expression networks using a database

The database LinkedOmics (accessible at http://www.linkedomics.org/) provides public access to multi-omics data from all 32 TCGA types of cancer and 10 Clinical Proteomics Tumor Analysis Consortium (CPTAC) cancer cohorts. Pearson's correlation coefficient was used to identify the PPARG co-expressed genes, and the results were visualized through a heat map, volcano plot, and table. Furthermore, gene set enrichment analysis (GSEA) was conducted to explore the association between the Kyoto Encyclopedia of Genes and Genomes (KEGG) pathway and the Gene Ontology (GO) BPs associated with PPARG and its co-expressed genes.

2.8 Sample collection

A total of 20 tissue samples, including 10 pancreatic cancer samples and 10 liver cancer samples, were collected from patients at the Pathology Department of Guizhou Medical University Affiliated Hospital. All tissue wax blocks underwent histological diagnosis following the guidelines of the World Health Organization (WHO). The study was approved by the ethics committee of Guizhou Medical University (Approval No. 538, 2023) and adhered to the principles outlined in the Helsinki Declaration. According to Chinese law, the materials used in this study were collected by the Pathology Department of Guizhou Medical University Affiliated Hospital for the purposes of diagnosis and treatment, and are used in an anonymous form for this research. Therefore, written consent from patients is not required.

2.9 Immunohistochemical staining for PPARG expression in tumor tissue

Immunohistochemical staining was performed using an immunohistochemical kit (Zhongshan Jinqiao, Beijing, China). Paraffin sections were dewaxed at 65°C and subsequently dewaxed using gradient concentrations of xylene and ethanol. Antigen repair was conducted by high-pressure heating with a citric acid solution (Servicebio, Wuhan, China) at pH 9.0 for 5 min. Following the removal of endogenous peroxidase using the peroxidase blocker from the immunohistochemistry kit and blocking non-specific antigen with 10% goat serum (Booster, Wuhan, China), the primary antibody (1:200) was added and incubated overnight at 4°C. The secondary antibody reaction enhancement solution in the kit was incubated for 30 min at 37°C, followed by a 30-min incubation with goat or mouse anti-rabbit immunoglobulin G (IgG) at 37°C. The slides were developed using diaminobenzidine (DAB; Servicebio, Wuhan, China) reagent, counterstained with hematoxylin, fractionated using 1% hydrochloric acid in alcohol for 10 s, and then blued with a saturated lithium carbonate solution. Finally, the slides were sealed with neutral gum and photographed using an ortho-optical microscope (Nikon). Additionally, we obtained immunohistochemistry (IHC) images depicting the protein expression levels of PPARG in LIHC and PAAD from the tissue and pathology modules of the Human Protein Atlas (accessible at https://www.proteinatlas.org/).

2.10 Cell culture

Hepatocellular carcinoma cells (LM3, Huh7, HLF, Hep G2) and normal liver control cells (LO2 and L68) were generously provided by Dr. Chu Jiao Hu from the Guizhou Provincial Engineering

Technology Research Center for Chemical Drug R&D, Guizhou Medical University. The cells were cultured under the following conditions: Dulbecco's modified Eagle medium (Gibco), supplemented with 10% fetal bovine serum (FBS; Cell Box, China). Briefly, the cells were cultured in T25 cell culture flasks at 37°C in a constant temperature incubator with 5% CO_2. When the cell density reached 70%–90%, trypsin digestion with 0.25% ethylenediaminetetraacetic acid (EDTA; Servicebio, Wuhan, China) was used for a 3-min incubation to detach the cells for subsequent experiments.

2.11 Gene expression and drug sensitivity profiling analysis

The analysis involved utilizing the specialist R software OncoPredict, which combines gene expression profiles with drug sensitivity profiles, to assess the drug sensitivity data of relevant cancer cohorts from the TCGA database. Additionally, expression matrices from the GSE14520 and TCGA-LIHC datasets were obtained from the GEO database for the PPARG expression and drug sensitivity analyses.

2.12 Molecular docking

Molecular docking was performed using the AutoDock software, employing specific branches (AutoDock v4.2.6, Autodock Vina, and Autodocktools v1.5.6) for the docking of protein receptors with small-molecule ligands. The three-dimensional (3D) structures of four small molecule compounds (BDP9066, Axitinib, Nilotinib, and Dabrafenib) in SDF format were retrieved from PubChem (accessible at https://pubchem.ncbi.nlm.nih.gov/) and analyzed using SYBYL-X 2.0 for the receptor and small molecule ligand processing, resulting in energy-minimized optimal conformations. Based on previous studies, the three-dimensional spatial locations of the active pocket in the PPARγ protein receptor (PDB: 6K0T) responsible for inhibition of tumor proliferation (Yamamoto et al., 2019), at which were determined using Autodocktools v1.5.6 software with centers of −1.063, 13.081, and 22.373 with sizes of 20 Å, 20 Å, and 20 Å, respectively. The four small-molecule ligands underwent docking analysis using Autodock Vina v1.2.3 software, following the principles of semi-flexible docking. The optimal conformation from the docking results was selected for further analysis and processing using PYMOL v2.1.1 software to generate images.

2.13 Western blot analysis

Western blot analysis was conducted following a previously described protocol (Ma et al., 2023). Protein lysates from whole cells were obtained by using radioimmunoprecipitation assay (RIPA) lysis buffer supplemented with protease inhibitors, and equivalent amounts of protein were loaded onto a 10% sodium dodecyl sulfate-polyacrylamide gel electrophoresis gel. The primary antibodies used in the analysis included rabbit anti-PPARγ (Immunoway, SuZhou, China) and rabbit anti-β-actin (Santa Cruz). The membranes were incubated overnight at 4°C with the primary antibodies, followed by incubation with horseradish peroxidase-conjugated anti-rabbit IgG as the secondary antibody. Chemiluminescence detection was used to visualize the protein bands, and images were captured using a BIO-RAD imager. The greyscale values of the bands were quantified using ImageJ software.

2.14 CCK-8 assay for proliferation and viability of hepatocellular carcinoma cells

After trypsinization and digestion with 0.25% EDTA, the cells were counted and evenly distributed into 96-well plates at a density of 5,000 cells per well. Following a 24-h cell attachment period, the culture medium was replaced with a basal medium containing the appropriate drug concentration. The cells were then incubated under standard cell culture conditions for 24 h. Subsequently, 10 μL of CCK-8 reagent (Abisin, Shanghai, China) was added to each well and incubated for 2 h. The drugs used in the experiment were Axitinib (Aladdin, Shanghai, China), Nilotinib (SelleckChem, Houston, United States), Dabrafenib (Aladdin, Shanghai, China), and BDP9066 (GlpBio, Shanghai, China). The absorbance of each drug concentration was measured at a wavelength of 450 nm using a Microplate reader (Thermo Fisher Scientific Inc., Shanghai, China).

2.15 Statistics analysis

Various investigations, including TBM, MSI, immunological checkpoints, molecular biology, and bioinformatics, were conducted to validate the association between PPAR expression and the research objectives, such as survival prognosis and clinical features. The Pearson test was used to assess the association between PPARG expression and these variables. To compare the expression differences across groups, paired *t*-tests or unpaired *t*-tests were used depending on whether the samples were paired. Statistical significance was defined as $p < 0.05$. R tools were used for data visualization and creating plots, while GraphPad Prism v8.3.0 (San Diego, United States of America) was used for all analyses. For statistical significance analysis involving more than two groups, one-way analysis of variance (ANOVA) was utilized. Two-tailed tests were used to calculate each *p*-value, and a result of $p < 0.05$ was considered statistically significant.

3 Results

3.1 PPARG expression analysis in human cancers

The PPARG mRNA expression levels in tissue samples with cancer and paraneoplasm were evaluated using the TIMER 2.0 and TCGA databases. In various types of cancer, such as breast cancer (BRCA), cervical cancer (CESC), colon adenocarcinoma (COAD), head and neck squamous cell carcinoma (HNSC), lung adenocarcinoma (LUAD), lung squamous cell carcinoma (LUSC), skin cutaneous melanoma (SKCM), prostate adenocarcinoma

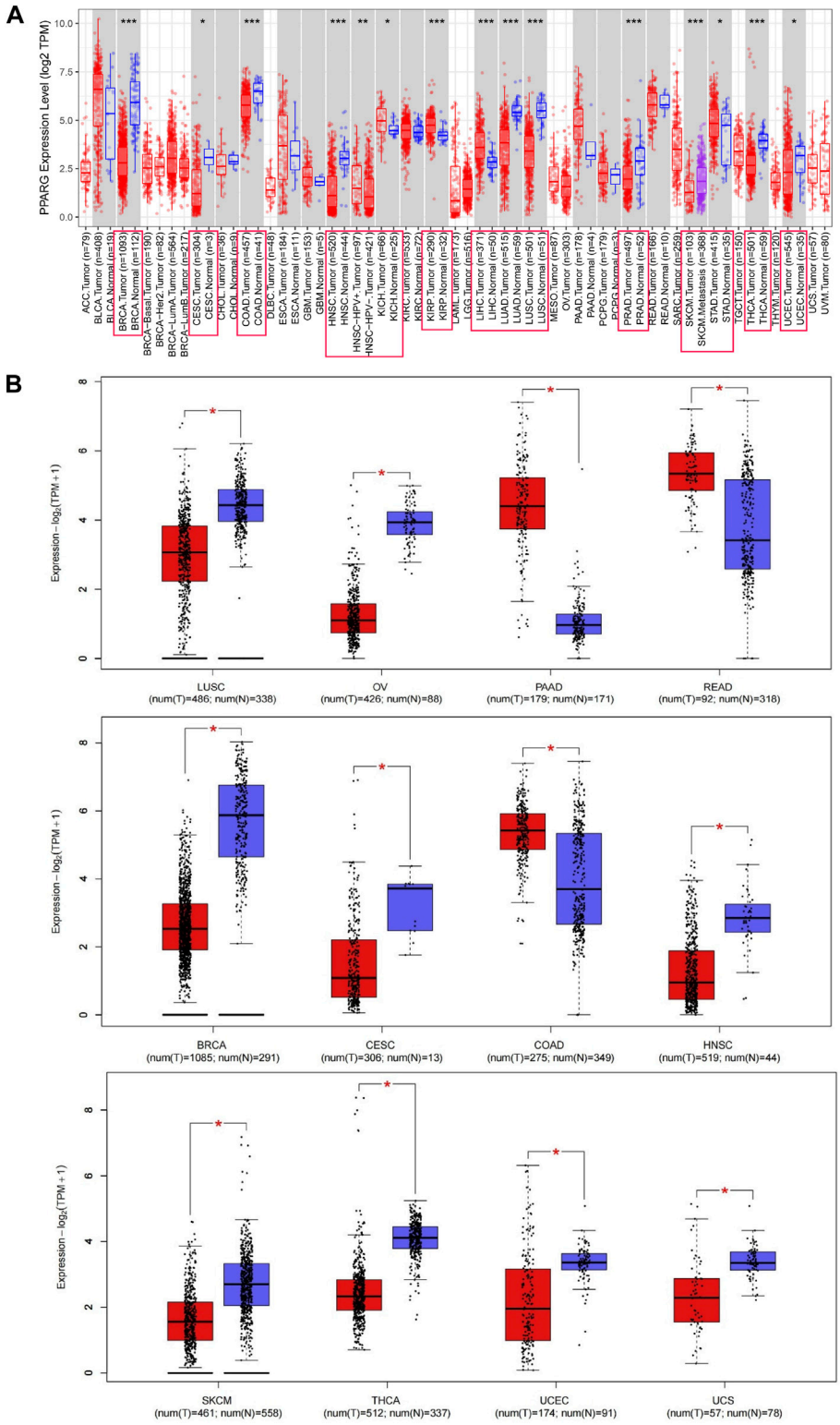

FIGURE 1
Differential gene expression of PPARG in different human tumor types or specific cancer subtypes. **(A)** Analysis of PPARG expression status in 33 subtypes of cancer by TIMER2 database. **(B)** Differential expression of PPARG in various cancers was analysis through the GEPIA2 database in combination with the TCGA dataset and the GTEx dataset. Log2 (TPM+1) was used as a logarithmic scale. (*$p < 0.05$, **$p < 0.01$, and ***$p < 0.001$).

(PRAD), thyroid cancer (THCA), and endometrioid cancer (UCEC), PPARG mRNA expression levels were significantly lower in cancerous tissues compared to paraneoplastic tissues. Conversely, in kidney chromophobe (KICH), kidney renal papillary cell carcinoma (KIRP), stomach cancer (STAD), and liver hepatocellular carcinoma (LIHC), there was a significantly

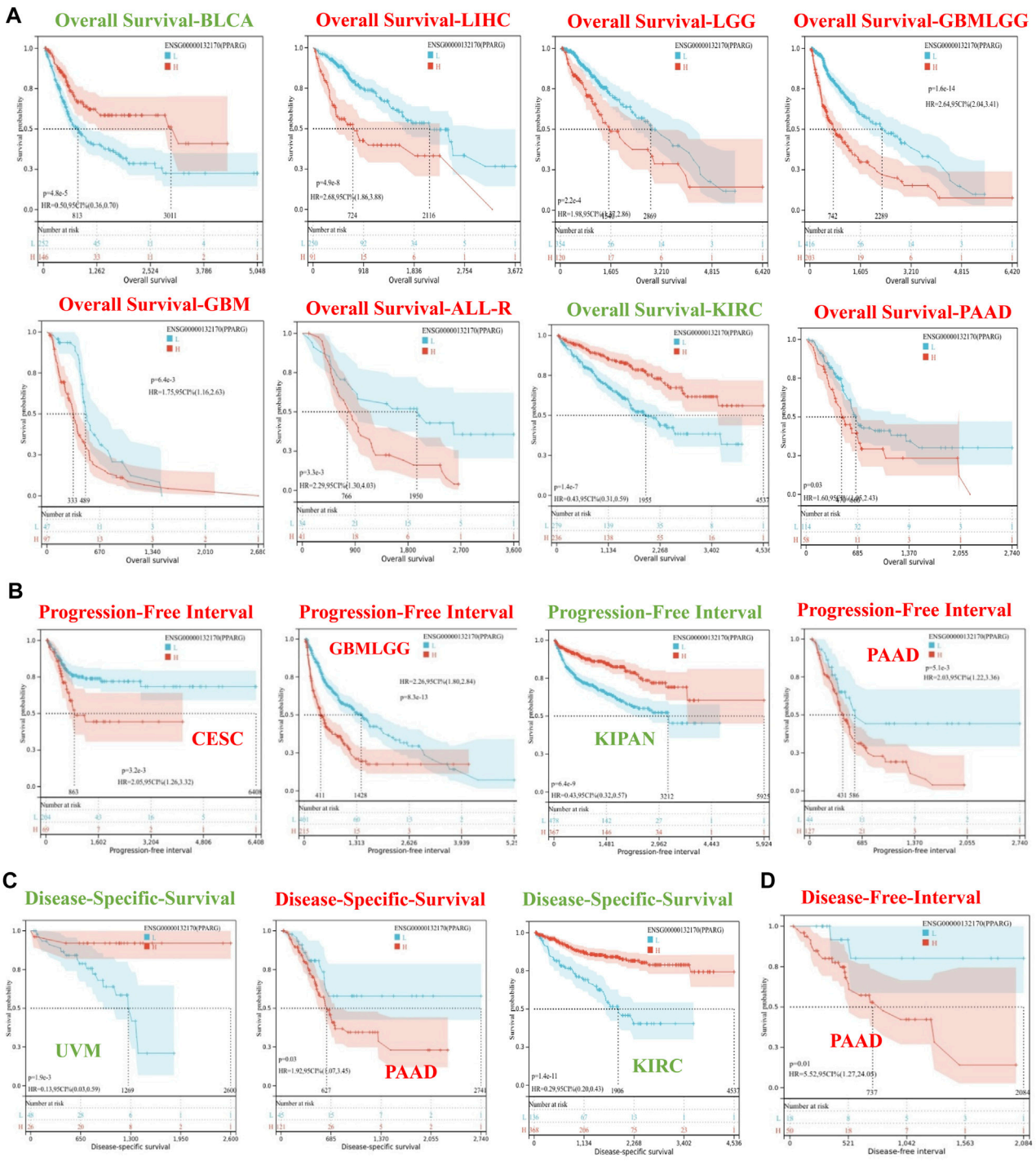

FIGURE 2
Survival curve of human cancers with high and low PPARG expression analyzed by the Kaplan-Meier method. **(A)** High and low PPARG expression was associated with poorer OS in the pan-cancer analysis. **(B)** Kaplan-Meier analysis of the association between PPARG expression and PFI. **(C)** Kaplan-Meier analysis of the association between PPARG expression and DSS. **(D)** Kaplan-Meier analysis of the association between PPARG expression and DFI.

higher PPARG expression level in cancerous tissues compared to paraneoplastic tissues (Figure 1A). However, due to the limited number of normal samples in the TCGA database and potential variations across data center platforms, we combined the normal tissue data from the GTEx database with the tumor tissue data in the GEPIA2 online database. This approach enabled us to analyze the differences in PPARG mRNA expression across 27 types of cancer. As shown in Figure 1B, the results indicated lower PPARG expression levels in nine types of cancer, including LUSC, ovarian serous cystadenocarcinoma (OV), BRCA, CESC, HNSC, SKCM, THCA, UCEC, and uterine carcinosarcoma (UCS). Conversely, PPARG exhibited high expression in pancreatic

cancer (PAAD), rectum adenocarcinoma (READ), and COAD. These findings indicate significant heterogeneity in mRNA PPARG expression levels among different human cancers.

3.2 Risk proportion of PPARG and prognostic survival analysis in cancer

To investigate the association between PPARG expression level and risk, correlation analysis was conducted between PPARG expression level and survival, including OS, DSS, DFI, and PFI. The Cox proportional hazards model analysis was employed to assess the association between gene expression and prognosis in each type of cancer. The OS analysis (Supplementary Figure S1A) revealed that high PPARG expression was associated with poor prognosis in lower-grade glioma and glioblastoma (GBMLGG), lower-grade glioma (LGG), glioblastoma (GBM), LIHC, THCA, PAAD, and ALL-R. Conversely, in five types of cancer, such as pan-kidney cohort (KIPAN), kidney renal clear cell carcinoma (KIRC), bladder urothelial carcinoma (BLCA), READ, and uveal melanoma (UVM), low PPARG expression was associated with a poor prognosis.

The DSS analysis results showed that high PPARG expression was associated with poor prognosis in six types of cancer, including GBMLGG, LGG, CESC, GBM, THCA, and PAAD. Conversely, in KIPAN, KIRC, BLCA, and UVM, low PPARG expression was associated with poor prognosis (Supplementary Figure S1B). In terms of PFI, forest plots (Supplementary Figure S1C) indicated that high PPARG expression was associated with poor prognosis in GBMLGG, LGG, GBM, and PAAD. However, there was no significant correlation observed between PPARG expression and PFI in KIPAN, KIRC, BLCA, or UVM. DFI data analysis revealed a strong association between high PPARG expression and PAAD, unlike in other human cancers where it was not statistically significant (Supplementary Figure S1D).

To determine the appropriate cutoff value for PPARG, we employed the R package maxstat and successfully achieved it. Consequently, the patients were categorized into two groups based on their PPARG expression levels: high and low expression groups. The survfit function in the R software package Survival was used to analyze the prognostic differences between the two groups. The significance of the prognostic difference in OS, PFI, DSS, and DFI among the samples in different groups was evaluated using the log-rank test method (Figure 2). Based on the Kaplan-Meier (KM) survival analysis, patients with LIHC, LGG, GBMLGG, GBM, ALL-R, and PAAD who had high PPARG expression levels had shorter OS compared to those with BLCA and KIRC, who had higher PPARG expression levels and longer OS (Figure 2A). Furthermore, the study revealed that PPARG expression level significantly influenced the survival index of PFI in patients with CESC, GBMLGG, and PAAD (Figure 2B). Additionally, the data indicated that a high PPARG expression level in PAAD was significantly associated with lower DSS and PFI, while high PPARG expression in UVM and KIRC was significantly associated with higher DSS (Figures 2C, D).

3.3 Examination of the association between PPARG expression and clinical features

Our findings highlight the variability of PPARG expression across different types of cancer and its impact on patient survival and prognosis. By investigating the correlation between clinical features and gene expression patterns, we can identify molecular biomarkers associated with cancer development and treatment response (Mun et al., 2018). To further explore the association between PPARG expression and clinical features, we used the UALCAN database for RNA-level analysis (Chandrashekar et al., 2022). We observed significant differences in PPARG expression in PAAD and LIHC tumors concerning lymph node metastasis status, histological subtype, molecular subtype, tumor stage, and *TP53* mutation status (Supplementary Figures S2, S3). However, PPARG expression in CESC and LGG is significantly different only in certain clinical features, such as the race of the patient in CESC and histological subtypes and *TP53* mutation status in LGG. PPARG expression in GBM did not exhibit significant differences with any of the clinical features analyzed (Supplementary Figures S4–S6). Additionally, the UALCAN database does not include datasets for relapsed acute lymphoid leukemia, LGG, or glioblastoma. Therefore, analysis and exploration of the association between PPARG expression and clinical features have not been conducted.

3.4 PPARG protein expression levels in LIHC and PAAD

Using immunohistochemistry analysis, we evaluated the protein expression levels of PPARγ, encoded by the *PPARG* gene, in the pathological tissues of patients with PAAD and LIHC. (Figure 3A). The findings demonstrated significantly higher PPARγ protein expression levels in these malignancies compared to the corresponding paracancerous tissues, consistent with the RNA-level expression pattern. To further investigate the variations in PPARγ protein expression levels in LIHC and PAAD, we used the Human Protein Atlas (HPA) online database (Figures 3B, C). The results from the protein-level analysis aligned with the earlier RNA-level study, revealing significantly elevated PPARγ protein expression levels in PAAD and LIHC compared to their respective paracancerous tissues. Finally, these findings indicate that PPARγ is highly expressed in LIHC and PAAD, and this elevated expression is positively associated with adverse disease outcomes and clinical features. Consequently, PPARγ holds promise as a potential target for evaluating cancer prognosis.

3.5 PPARG gene alterations analysis in cancer

Gene alterations play a critical role in the initiation and progression of various types of cancer. Disruptions in the genome can disturb normal cellular processes, leading to uncontrolled growth and tumor formation, ultimately affecting patient prognosis (Baer et al., 2019; Cagan et al., 2022). Understanding the intricate association between gene mutations

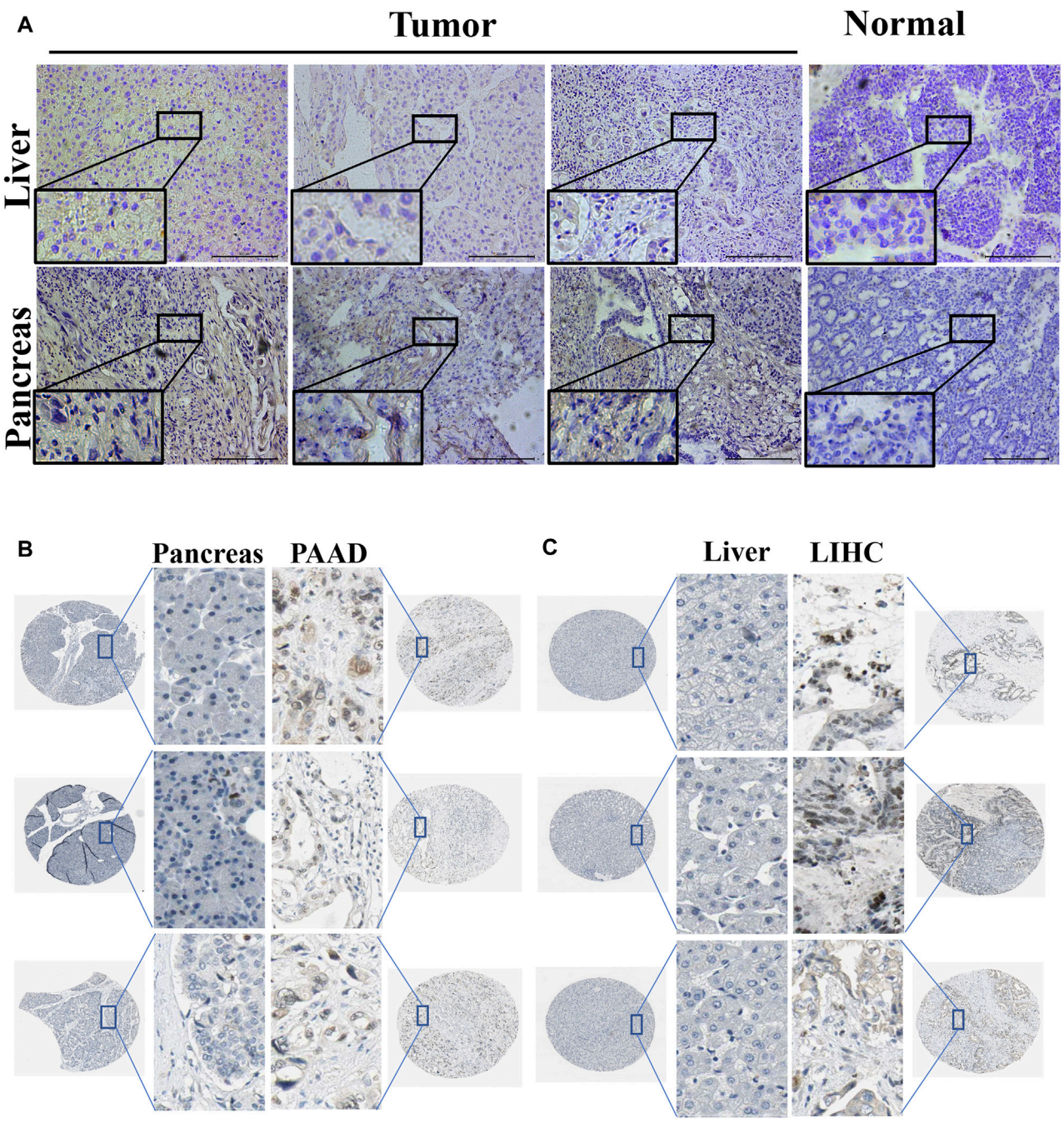

FIGURE 3
Expression of PPARG in tumor and paraneoplastic tissues. **(A)** Detection of PPARG expression levels in hepatocellular carcinoma and pancreatic cancer by immunohistochemical staining. Scale, 200 um. Images are representatives of three independent experiments with similar results. **(B,C)** Immunohistochemical staining images of PPARG in LIHC and PAAD as well as their normal tissues were collected in the HPA database.

and cancer is crucial for unraveling the underlying mechanisms driving tumor occurrence, progression, and response to treatment. To explore the association between PPARG expression and frequent somatic mutations, we analyzed 17 datasets of hepatocellular carcinoma and pancreatic cancer from the cBioprotal database, as well as two datasets of pan-cancer. The findings revealed an overall mutation rate of 0.5% (Figure 4A), including missense mutations, deletion mutations, amplifications, and profound deletions. Amplifications were predominantly observed in LIHC, while profound deletions were more prevalent in PAAD (Figure 4B). Despite the high PPARG expression in human cancers, the total mutation rate at the oncogene level was relatively low (0.5%). This suggests that PPARG expression level as a transcription factor may not directly influence chromatin or DNA structural homeostasis. Furthermore, the post-transcriptional modification analysis revealed multiple amino acid phosphorylation sites of PPARG, including amino acid sites Ser78, Ser95, Ser102, Leu112, Gln269, and Ser273 (Figures 4C, D). This suggests a potential

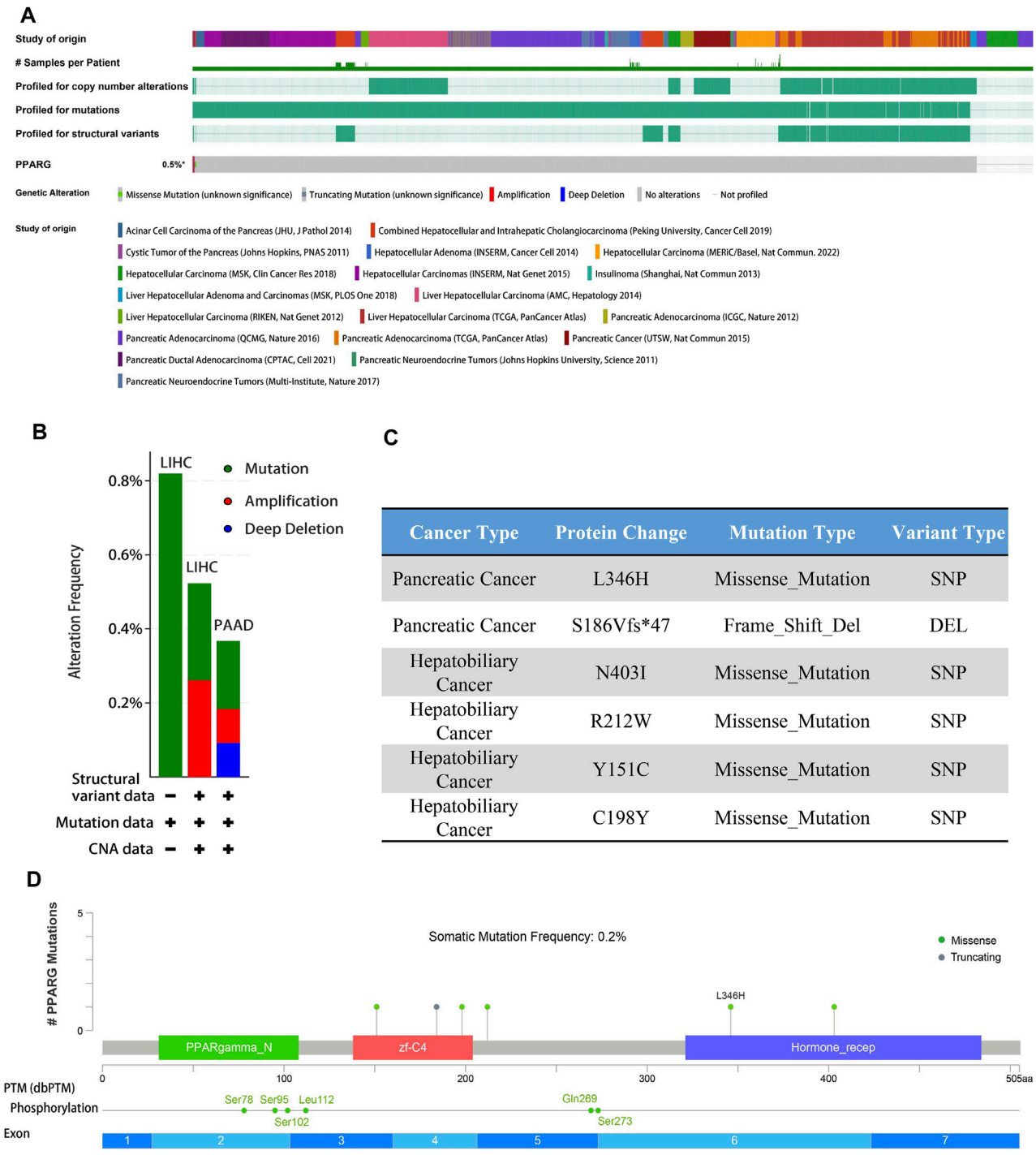

Cancer Type	Protein Change	Mutation Type	Variant Type
Pancreatic Cancer	L346H	Missense_Mutation	SNP
Pancreatic Cancer	S186Vfs*47	Frame_Shift_Del	DEL
Hepatobiliary Cancer	N403I	Missense_Mutation	SNP
Hepatobiliary Cancer	R212W	Missense_Mutation	SNP
Hepatobiliary Cancer	Y151C	Missense_Mutation	SNP
Hepatobiliary Cancer	C198Y	Missense_Mutation	SNP

FIGURE 4
PPARG gene alterations in human cancers analyzed by the cBioPortal database. **(A)** Types of PPARG genetic alterations in different pan-cancer datasets. **(B,C)** Missense mutation, phosphorylation, and acetylation modification of PPARG in the pan-cancer analysis. **(D)** Details of PPARG gene alteration types in the cancer cohort.

role for multisite phosphorylation of PPARG in tumorigenesis. Collectively, these findings indicate the presence of PPARG genetic alterations and differential expression in cancer tissues, particularly in LIHC and PAAD. These observations highlight the potential significance of PPARG in cancer development and progression.

3.6 Correlation of PPARG expression levels with genomic stability in LIHC and PAAD

The higher tumor mutational burden (TMB) signifies increased genetic abnormalities and is linked to elevated microsatellite instability (MSI). These alterations enhance tumor cells'

FIGURE 5
Relationship between PPARG expression and somatic mutation **(A)**, Tumor mutational burden **(B)**, Microsatellite instability **(C)**, and Mismatch repair genes **(D)** in human cancers. (*$p < 0.05$, **$p < 0.01$, and ***$p < 0.001$).

adaptability, potentially leading to treatment evasion and resistance (Petri and Sanz, 2018; Roudko et al., 2020; Fusco et al., 2021). As shown in Figure 5A, the results demonstrate a significant positive correlation between PPARG mRNA expression and TMB in both PAAD and LIHC. This suggests that PPARG is associated with an increased mutational burden in tumors, thereby promoting disease progression. While no statistically significant association was found between the other tumors and MSI, a direct correlation was observed

between MSI and PPARG expression in BRAC, COAD, DLBC, ESCA, KIRC, LUAD, SKCM, and STAD. Among the tumors with high PPARG expression and poor prognosis, only LIHC showed a positive correlation between high PPARG expression and MSI (Figure 5B).

Mismatch repair (MMR) genes are essential for maintaining genomic stability and preventing the accumulation of genetic damage. We evaluated the association between mutations and gene expression in five MMR genes: *MLH1, MSH2, MSH6, PMS2,* and *EPCAM*, using data from the TCGA expression profiling project. In PAAD, there was a significant positive association between PPARG expression and the MMR genes *EPCAM, PMS2,* and *MSH2*. However, in LIHC, except for *EPCAM*, there was no significant correlation between PPARG expression and the other MMR genes, indicating a lack of association (Figure 5C). This suggests that PPARG does not directly affect the MMR family genes, thereby not leading to an increase in genomic instability.

In our previous study, we observed a low mutation rate of PPARG in PAAD and LIHC (0.5%) (Figure 4). However, it may still influence cancer progression by affecting key oncogenes or tumor suppressor genes. To further investigate this, we analyzed co-occurring gene mutations associated with PPARG expression. The mutation landscape plot revealed the presence of prominent genes such as *TP53, KRAS, CTNNB1,* and *SMAD4* in LIHC and PAAD, which are known to promote tumor initiation and development (Figure 5D). Mutations in oncogenes not only lead to a loss of response to targeted anticancer therapies but also activate critical signaling pathways and regulatory mechanisms, thereby conferring advantages in tumor proliferation, migration, and invasion.

3.7 Alterations in the immune microenvironment induced by dysregulated PPARG in LIHC and PAAD

The TCGA dataset analysis reveals a significant correlation between PPARG expression and the occurrence of cancer, as well as a poor prognosis. To further investigate this association, we obtained mRNA expression matrices from the GEO database, specifically for LIHC (GSE14520) and pancreatic cancer (GSE85916). These matrices included both tumor and adjacent non-tumor tissues, accompanied by clinical data associated with the samples. Based on these datasets, we calculated the optimal cutoff value for the PPARG expression using the R software package "maxstat." Subsequently, we categorized patients with tumors from both datasets into two groups: high and low PPARG expression groups. Survival analysis was conducted using the R software package "survival" to assess prognostic differences (Figures 6A, B).

Our findings demonstrate a significant prognostic difference in patients with high PPARG expression levels in both liver and pancreatic cancers (Figures 6C, D). These findings support the notion that higher PPARG expression significantly impacts the prognosis and survival of patients with these malignancies, which aligns with our TCGA database analysis. Furthermore, there is increasing evidence emphasizing the critical role of TME in tumor development. Hence, in this study, we investigated the composition of the TME between the high and low PPARG expression groups. Specifically, using the cell-type identification by estimating relative subsets of RNA transcripts (CIBERSORT) method in conjunction with the LM22 signature matrix, the differential immune cell infiltration was assessed between the high and low PPARG expression groups in the aforementioned GEO datasets.

Our analysis revealed significant differences in immune cell infiltration between the two PPARG expression groups. Specifically, patients with liver cancer with high PPARG expression exhibited a significant increase in the proportions of macrophages M1, macrophages M2, T cells (δ and γ), and T cell regulatory (Tregs). Conversely, the proportions of natural killer (NK) cells activated and mast cells activated were significantly decreased (Figures 6E, F). These findings provide valuable insights into the immune landscape associated with PPARG expression in liver cancer, indicating the potential immunomodulatory effects of PPARG in shaping the TME. Contrastingly, no discernible differences in the immune cell composition were observed between the patients with pancreatic cancer with high and low PPARG expression. Subsequently, we evaluated the association between PPARG gene expression and the statistically significant differences in immune cell populations (Supplementary Figures S7A, 7B). The results revealed a positive correlation between PPARG and macrophages M2, T cell regulatory (Tregs), and T cell (δ and γ), while showing a negative correlation with NK and mast cells activated (Supplementary Figures S7C–7G). These findings suggest that the association between PPARG expression and immune cell infiltration may vary across various types of cancer.

While immune activation and infiltration are crucial for tumor suppression, tumor cells often exploit excessive immune responses and infiltration to establish immune evasion mechanisms. Excessive immune infiltration can lead to immune dysfunction, weakening the anticancer effect and simultaneously promoting tumor progression and dissemination. Elevated ICP expression levels are frequently associated with cancer progression and may contribute to immune evasion, drug resistance, and an unfavorable prognosis in tumor development. In this study, we collected ICP genes and analyzed their correlation with PPARG gene expression. A Pearson correlation analysis was performed to assess the association between PPARG and ICP genes. The results showed a significant positive correlation between PPARG and ICPs in LIHC, in contrast to PAAD. These findings suggest that PPARG effectively regulates ICP expression to evade immune attack (Supplementary Figure S8).

3.8 Correlation between PPARG expression and sensitivity spectrum to anticancer drugs and molecular docking simulation validation

Gene expression plays a crucial role in driving molecular and epigenetic changes within the human body, influencing individual responses to disease treatment drugs, and altering drug sensitivity. In this study, we further investigated the differences in drug

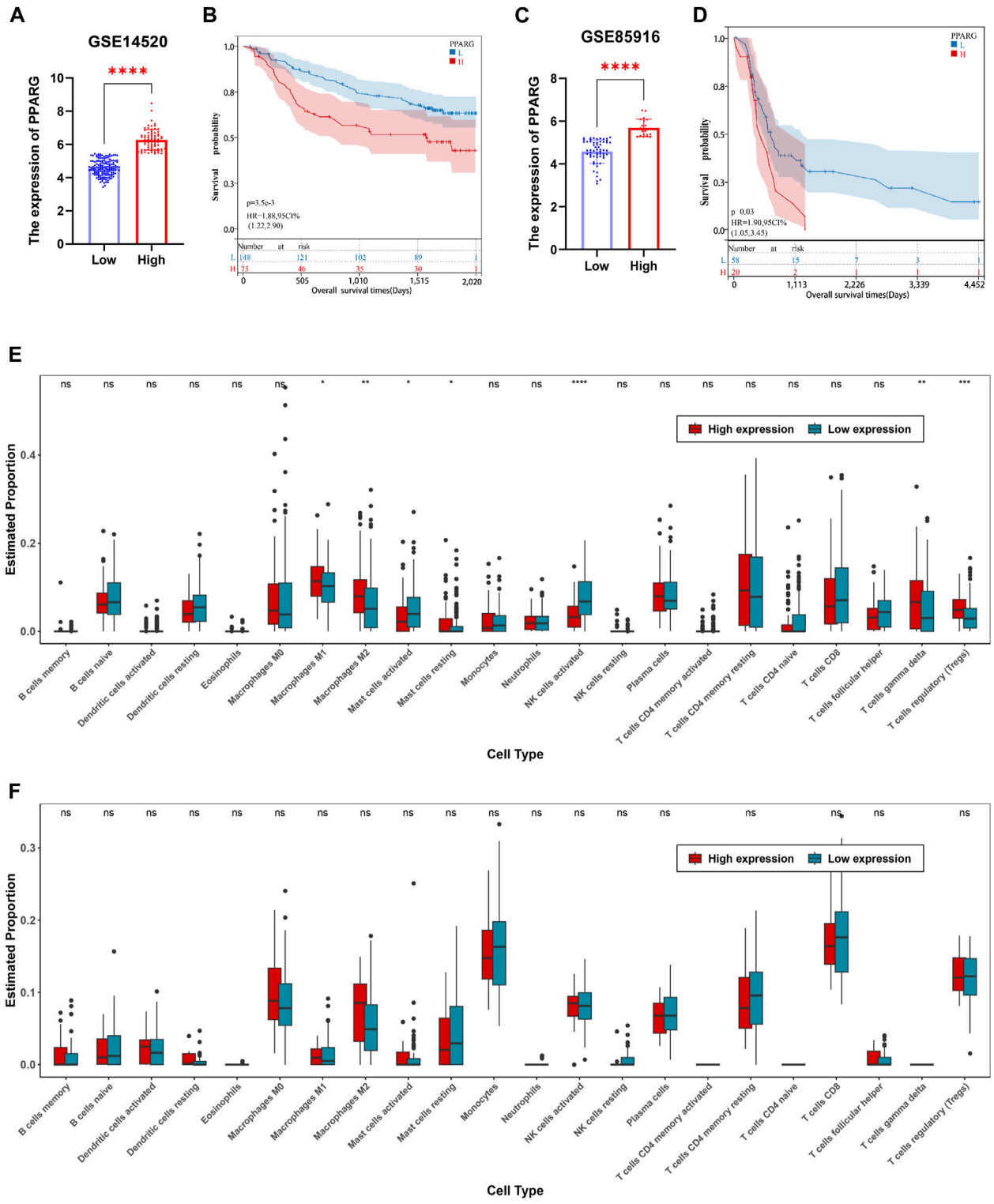

FIGURE 6
Relationship between PPARG expression and tumor microenvironment in human tumors. **(A)** In accordance with the optimal cutoff value determined using the R software package "maxstat", the expression of PPARG in the liver cancer dataset GSE14520 was categorized into high-expression and low-expression groups. **(B)** Prognostic survival analysis based on stratification of high and low expression groups of PPARG. **(C)** Stratification of PPARG expression into high and low expression groups in the pancreatic cancer dataset GSE85916 based on the optimal cutoff value determined using the R software package "maxstat". **(D)** Prognostic survival analysis based on stratification of high and low expression groups of PPARG in the GSE85196 dataset. **(E)** Evaluation of differential immune cell infiltration among high and low expression groups of PPARG using the CIBERSORT algorithm combined with the LM22 signature matrix in the GSE14520 dataset. **(F)** Evaluation of differential immune cell infiltration among high and low expression groups of PPARG using the CIBERSORT algorithm combined with the LM22 signature matrix in the GSE85196 dataset. (*$p < 0.05$, **$p < 0.01$, and ***$p < 0.001$).

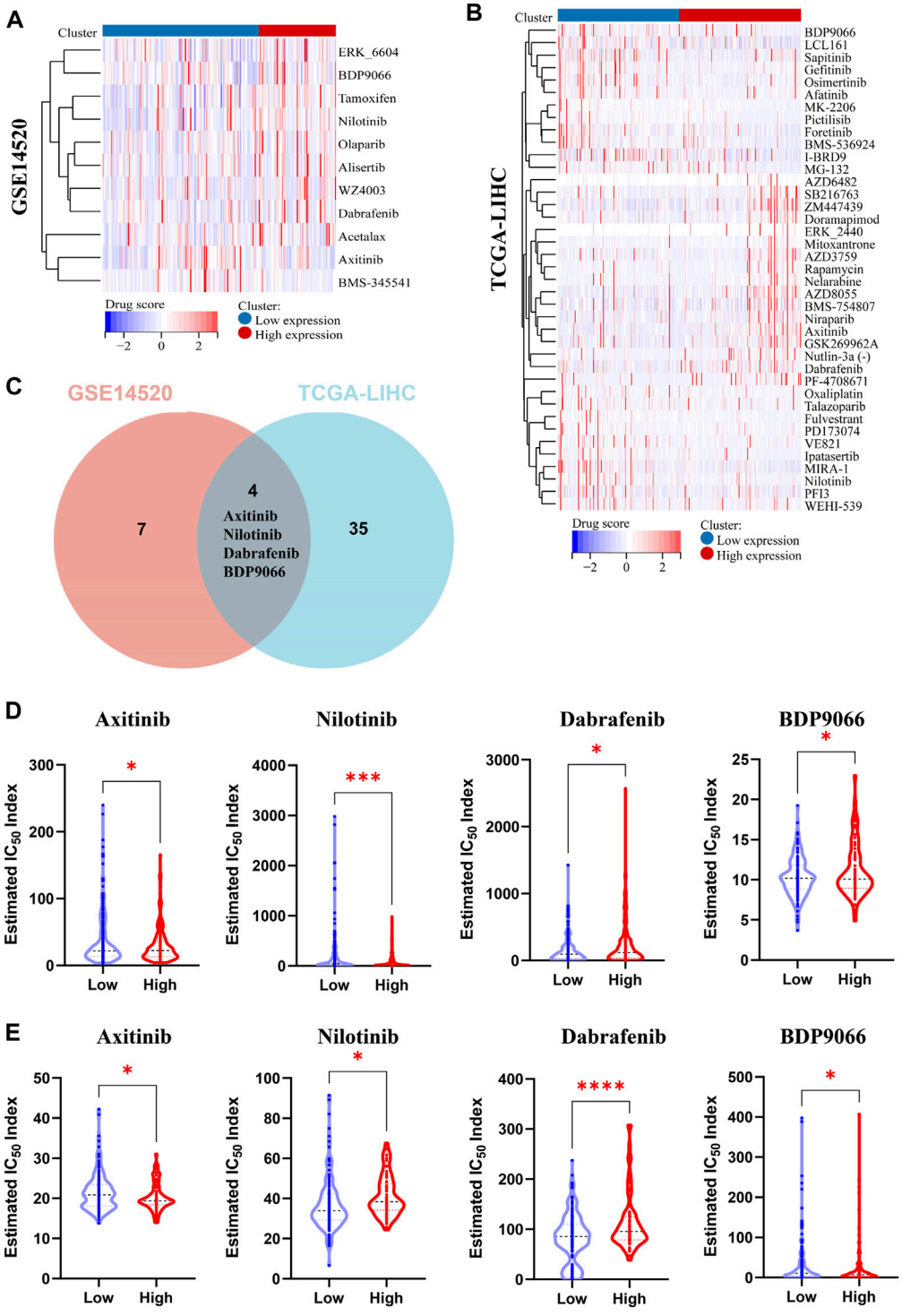

FIGURE 7
Analysis of multiple datasets revealed the relationship between PPARG expression and drug sensitivity profiles. **(A)** The OncoPredict algorithm was used to calculate the drug sensitivity of the liver cancer dataset GSE14520. **(B)** The OncoPredict algorithm was employed to calculate the drug sensitivity of liver cancer datasets from the TCGA-LIHC database. **(C)** The Venn diagram was used to identify the drugs selected by fitting two datasets. **(D)** The relationship between PPARG expression and the sensitivity of four drugs, namely, Axitinib, Nilotinib, Dabrafenib, and BDP9066, in the TCGA-LIHC dataset. **(E)** The association between PPARG expression and drug sensitivity of the same four drugs in the GSE14520 dataset. (*$p < 0.05$, **$p < 0.01$, and ***$p < 0.001$).

sensitivity between patients with high and low PPARG expression levels using RNA-sequencing data. Through genomic stability and immune microenvironment analysis, we identified a significant association between PPARG expression and these factors in LIHC. Subsequently, we evaluated the drug sensitivity profiles in the GSE14520 dataset (LIHC) from the GEO database and the

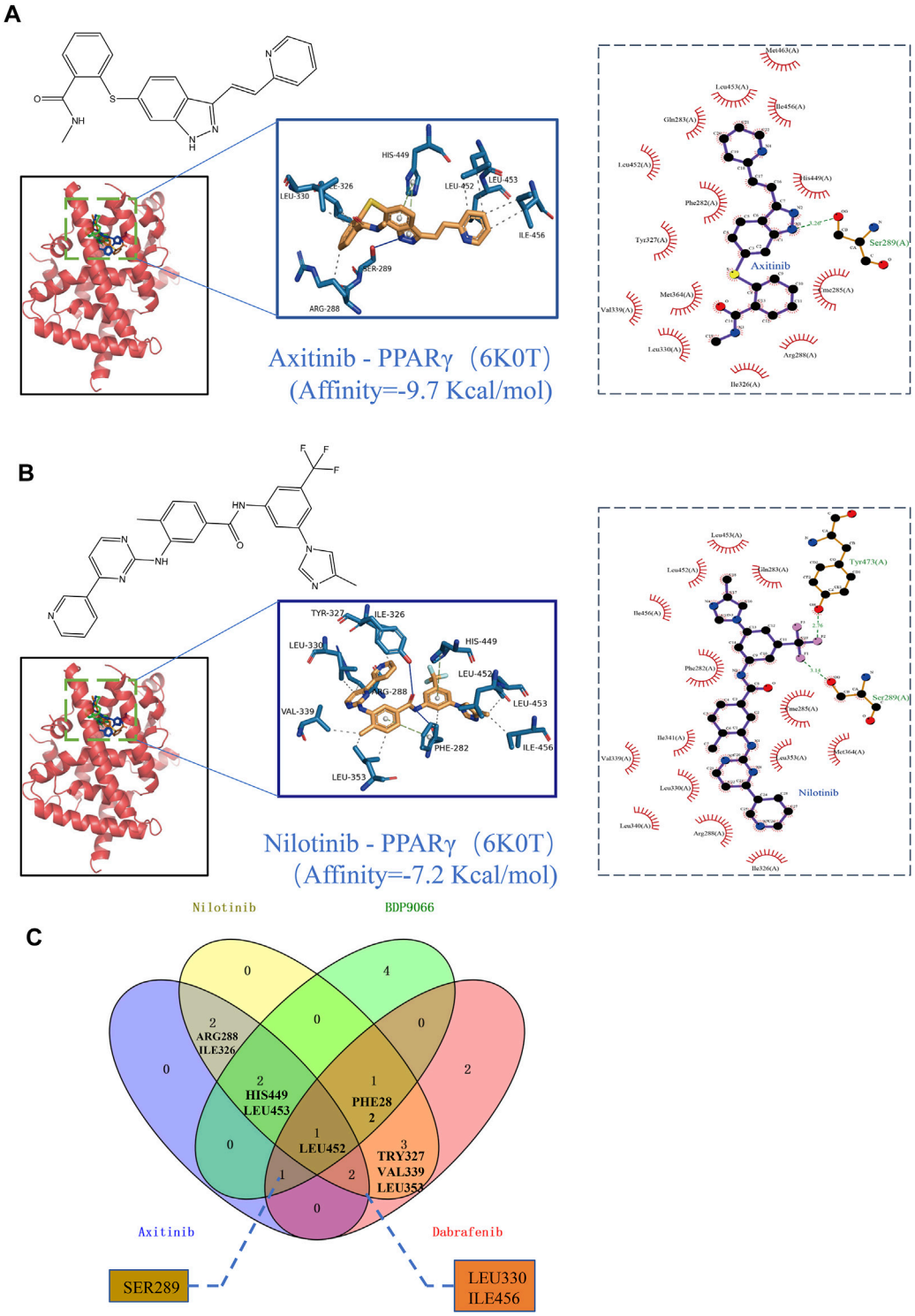

FIGURE 8
Binding scores and binding conformations of potential therapeutic drugs with PPARγ (PDB: 6K0T) simulated using Autodock Vina. **(A)** Analysis of the two-dimensional binding mode of Nilotinib with 6K0T using LigPlot + software (left panel) and the three-dimensional binding conformation using Pymol (right panel), with a binding score of −9.7 kcal/mol. **(B)** Analysis of the two-dimensional binding mode of Axitinib with 6K0T using LigPlot + software (left panel) and analysis of their three-dimensional binding conformation using Pymol (right panel), with a binding score of −7.2 kcal/mol. **(C)** Venn chart analysis of key amino acids in the active pocket for four small molecule anticancer drugs.

TCGA-LIHC patient cohort from the TCGA database using the OncoPredict method (Figures 7A, B). The findings revealed significant differences in drug sensitivity between the groups with high and low PPARG expression. These findings highlight the potential impact of PPARG expression on drug response and emphasize its relevance in personalized medicine for the

10.3389/fphar.2023.1298341

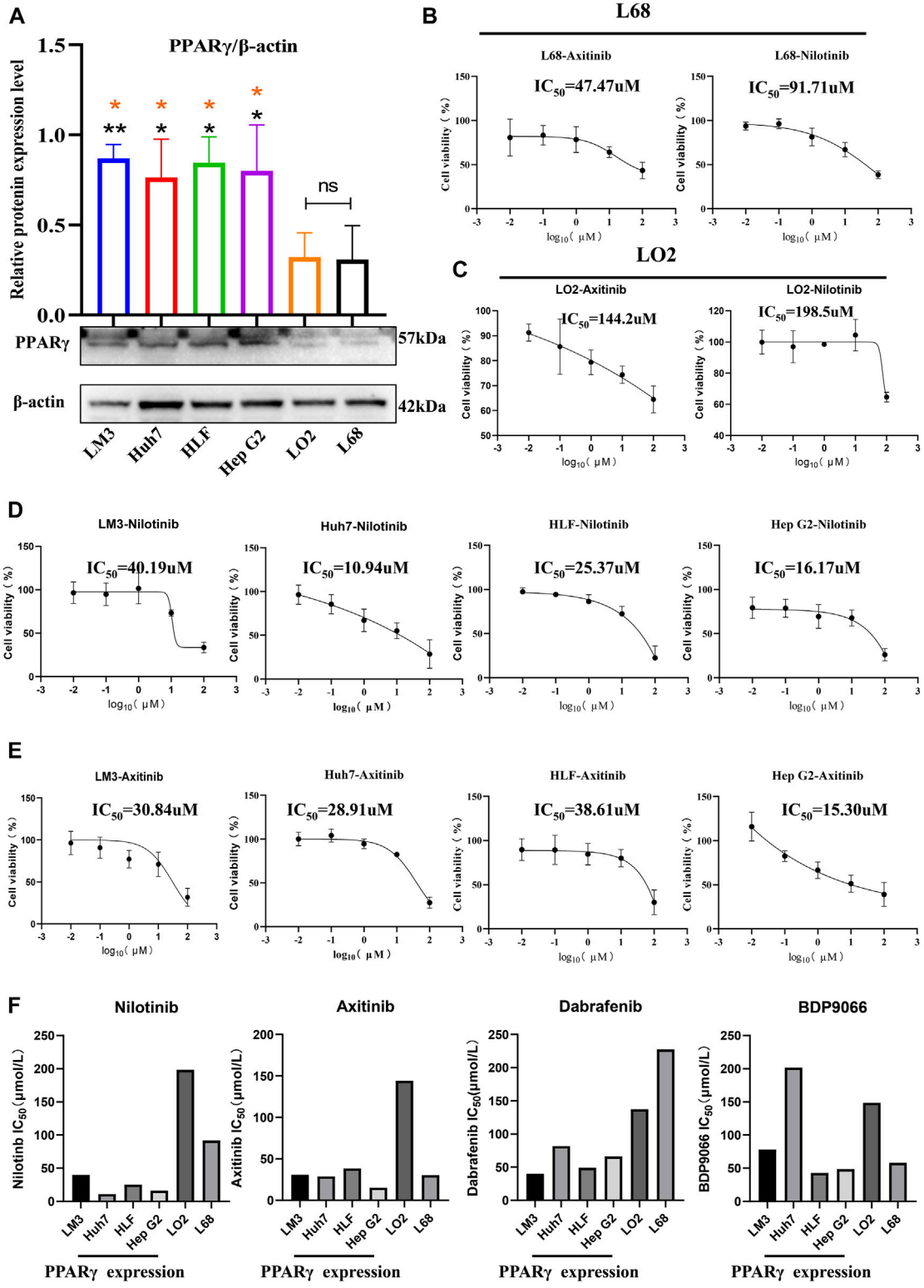

FIGURE 9
Relationship between the expression of PPARγ and drug sensitivity.**(A)** Expression of PPARγ in four hepatocellular carcinoma cell lines (LM3, Huh7, HLF, and Hep G2) and two control liver cell lines (LO2 and L68). **(B,C)** Drug Sensitivity of Nilotinib and Axitinib in control Hepatic Cells LO2 and L68. **(D,E)** Drug sensitivity of Nilotinib and Axitinib in four Hepatocellular Carcinoma Cell Lines LM3, Huh7, HLF, and Hep G2. **(F)** Bar graph of PPARγ expression levels and drug sensitivity of four small molecule compounds.

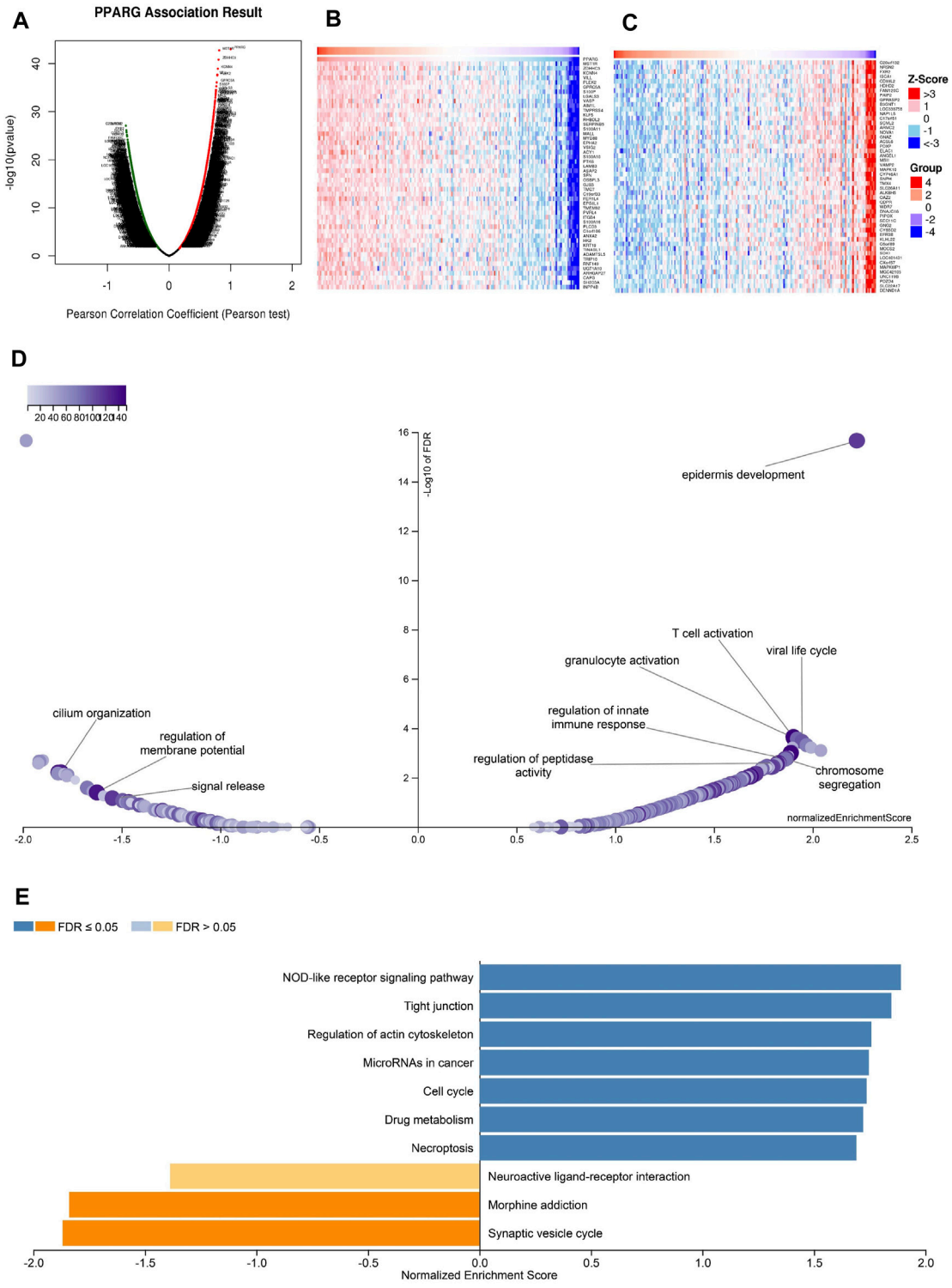

FIGURE 10
PPARG co-expression genes in LIHC analyzed by the LinkedOmics database. **(A)** Highly relevant genes for PPARG expression in the LIHC cohort examined by Pearson's test. Top 50 positive co-expression genes **(B)** and negative co-expression genes **(C)** of in heat map in LIHC. **(D)** Volcano plot of PPARG KEGG pathways in LIHC cohort. **(E)** Directed acyclic graph of PPARG GO analysis (biological process) in LIHC cohort.

treatment of cancer. Furthermore, by integrating drug sensitivity profiles from the TCGA-LIHC and GSE14520 datasets, we identified a common set of drugs, including Nilotinib, BDP9066, Dabrafenib, and Axitinib (Figure 7C). Notably, all four drugs are targeted therapies for the treatment of cancer. The drug sensitivity analysis revealed that patients with high PPARG expression in TCGA-LIHC and GSE14520 may exhibit increased sensitivity to Axitinib and Nilotinib (Figures 7D, E).

The PPARgama molecular pocket formation and its binding with ligands are crucial for the anti-proliferative activity against tumors (Yamamoto et al., 2019). Molecular docking was employed to validate the potential binding of Nilotinib, Axitinib, Dabrafenib, and BDP9066 with the active pocket of PPARG. Our results demonstrated robust binding modes and remarkably low binding energies, indicating stable and favorable interactions between these four anticancer drugs and PPARG (Figures 8A, B). Notably, Axitinib, BDP9066, Dabrafenib, and Nilotinib exhibited notable molecular docking capabilities, with affinity values of −9.7, −6.7, −9.6, and −7.2 kcal/mol, respectively, as determined by the absolute values of their binding energies (Supplementary Figures S9A, 9B). Interactions between four small-molecule anticancer drugs and key amino acid residues within the active pocket were investigated by Venn diagram analysis to examine the molecular interactions and binding affinity of these small molecules with 6K0T (Figure 8C). This analysis illustrates the statistical distribution and frequency of these key amino acids within the active pocket, shedding light on the molecular interactions and binding affinity of the small-molecule drugs. These findings offer potential mechanisms of action for inhibiting tumor growth.

3.9 Inhibition of hepatocellular carcinoma cell proliferation activity through selective targeting of PPARγ

In examining PPARγ expression between cancer cells and healthy control cells, we observed significantly higher PPARγ expression in the four hepatocellular carcinoma cell lines (LM3, HLF, Huh7, and Hep G2) compared to the two normal liver cell lines (LO2 and L68) (Figure 9A). Subsequently, cell proliferation assays were conducted after incubating the 6 cell lines with the four drugs at various concentrations for 24 h. The results revealed increased sensitivity to all four drugs with high PPARγ expression. Particularly, Nilotinib and Axitinib demonstrated significant anti-proliferative activity against liver cancer cells. In Huh7 cells, Nilotinib exhibited an IC_{50} of 10.94 uM, while in Hep G2 cells, the IC_{50} remained around 15 uM. For LM3 cells, both drugs maintained IC_{50} values between 30 and 40 uM. Conversely, Dabrafenib showed weaker inhibitory effects on liver cancer cell proliferation compared to the aforementioned two drugs, with the highest IC_{50} reaching 81.86 uM. However, even in LM3 cells, it reached 40.19 uM (Supplementary Figure S10). Notably, the inhibitory effects of the four drugs on normal liver cells were consistently lower compared to their effects on liver cancer cells (Figures 9D, E). Axitinib exhibited an IC_{50} of 144.2 uM in LO2 cells, while Nilotinib reached concentrations close to 200 uM. Similarly, Dabrafenib demonstrated a similar pattern of activity (Figures 9B, C). Furthermore, we noted a correlation between the four drugs' inhibitory effects on cell proliferation and PPARγ expression. Cells with elevated PPARγ expression in liver cancer displayed increased drug sensitivity (Figure 9F). The results were consistent with the predictions from the Oncopredict algorithm and the protein level validation. Through predictive analysis and experimental testing, we confirmed its potential as a target for cancer treatment.

3.10 The co-expression networks of PPARG demonstrate associations with relevant molecular mechanisms

The above findings further validate the prognostic value of PPARG in pan-cancer and its significant association with the immune response. Elevated PPARG expression in LIHC and PAAD is significantly positively correlated with poor OS, DSS, PFI, and DFI (Figure 2; Supplementary Figure S1). To validate the potential role of the PPARG gene as a biomarker in pan-cancer, its functions and heterogeneity, as well as its potential role in LIHC, were investigated. The LinkOmics database PPARG co-expression network was used for this analysis (Supplementary Figure S11). In LIHC, there was a significant positive correlation between PPARG expression and 4,820 genes (represented by dark red dots) as well as a significant negative correlation between 5,775 genes (represented by dark green dots) [false discovery rate (FDR) <0.01] (Figure 10A). The top 50 genes that exhibited the strongest correlation with PPARG expression are shown in Figure 10B, while Figure 10C shows the top 50 genes with the strongest negative correlation. Furthermore, the positive and negative correlations of the top 50 genes co-expressed with PPARG are shown in Supplementary Tables S1, S2, respectively. Notably, *MST1R, ZDHHC3,* and *KCNN* emerged as the top three genes exhibiting the most significant correlation with PPARG co-expression.

Further investigation of GO BP categories revealed the involvement of PPARG and its co-expressed genes in various functions, including T cell activation, immune response control, and regulation of peptidase activity. This determination was made by using GSEA to identify the major GO terms enriched among PPARG-co-expressed genes (Figure 10D). The co-expressed genes were enriched in the nucleotide oligomerization domain (NOD)-like receptor signaling pathway, tight junction, control of the actin cytoskeleton, cell cycle, and drug metabolism, according to a KEGG pathway analysis (Figure 10E). These findings imply that PPARG expression may influence various human cancers by affecting the immune response within TME.

4 Discussion

PPARG acts as a nuclear receptor that binds peroxisome proliferators, including lipid-lowering drugs and fatty acids. Upon activation by the ligand, the nuclear receptor binds to DNA-specific PPAR response elements (PPRE) and regulates the transcription of its target genes (Park et al., 2010). One such target gene is acyl-coenzyme A oxidase, which controls the peroxisomal β-oxidation pathway of fatty acids. PPARG plays a crucial role as a key regulator of adipocyte differentiation and glucose homeostasis (Mukherjee et al., 1997). While significant progress has been made in understanding the biological activities and functions of various molecules through advancements in molecular biology, there is still a need for further exploration of their roles in human cancer and their potential as therapeutic targets. Previous studies have shown that PPARG gene expression levels are significantly upregulated in bladder cancer, esophageal adenocarcinoma, and prostate cancer. Moreover, they have been associated with treatment resistance and a poor prognosis in cancer (Galbraith et al., 2018; Liu et al., 2019; Ma et al., 2021). In bladder cancer, the potential of PPARG as a biomarker has been confirmed

(Chiu et al., 2017). Furthermore, previous studies have demonstrated a significant association between high PPARG expression and poor prognosis in pancreatic ductal adenocarcinoma, with two key contributing factors being obesity and diabetes (Andersen et al., 2017). These findings align with our current research findings. Concerning lung cancer, miR-130a and miR-130b have been identified to play a regulatory role in macrophage polarization by inhibiting or downregulating PPARG expression (Lin et al., 2015). Moreover, they stimulate vascular endothelial growth factor A (VEGF-A) and anti-apoptotic factor (B-cell lymphoma-2, Bcl-2) expression (Tian et al., 2022), thereby influencing the progression of lung cancer. The PPARG differential expression in human cancers is often associated with tumor growth. However, there remains uncertainty regarding the precise procedures and pathways through which PPARG influences tumor development, leading to a poor prognosis.

Through our investigation, we confirmed the variability of PPARG expression in various types of cancers by analyzing PPARG gene expression levels in human cancers using the TCGA database. Subsequently, we examined the association between PPARG expression heterogeneity and survival outcomes, finding that high PPARG expression in various types of cancer was strongly associated with a poor prognosis. This suggests that the upregulation of PPARG may contribute to human cancer development, particularly in these specific types of cancer. Additionally, our PPARG gene alteration analysis revealed a mutation frequency of 0.5%. Furthermore, we observed higher rates of mutations, including missense mutations, truncating mutations, amplifications, and profound deletions, in PAAD. These findings indicate a potential role in tumorigenesis and cancer progression. The correlation between PPARG and TMB, MSI, and MMRs also demonstrated a close association between PPARG and TME in human cancers.

Furthermore, our findings using immunohistochemical experiments conducted on pathological sections of patients with LIHC and PPAD, where PPARG expression was significantly elevated, validated our previous analysis. These results demonstrated a strong association between PPARG overexpression, tumorigenesis, and cancer progression. Hence, PPARG has the potential to serve as a molecular marker for cancer. Consequently, an *in vitro* screening of anticancer drugs targeting PPARG was performed, which validated our findings. The results revealed a positive correlation between the drug sensitivity of these drug categories and PPARG expression. However, it was observed that BDP9066 exhibited lower selectivity in its anticancer proliferative activity compared to the other three drugs, with an IC_{50} as high as 201.8 μM against Huh7 liver cancer cells. This could be attributed to the binding mode of the small molecule with PPARG and its high binding energy requirement (affinity = −6.7 kcal/mol). To address this issue, further expansion of molecular library screening can be pursued by using ligand- or receptor-based computationally-assisted drug selection. This approach aims to identify small-molecule compounds with enhanced targeting capabilities. Additionally, conducting high-throughput simulations of PPARG ligand efficiency and elucidating key amino acid residues will facilitate precise drug targeting, thereby reducing off-target effects and minimizing the potential for low anticancer activity and high toxic side effects. These advancements will facilitate the clinical application of targeted therapies directed at the potential biomarker PPARG. Furthermore, to understand its potential mode of action, we examined PPARG expression in several immunological and molecular subtypes of human malignancies. The findings revealed significant variations in PPARG expression among different immunological and molecular subgroups in LIHC.

Immune infiltration is typically associated with the suppression of tumor growth and metastasis. However, when immune infiltration becomes excessive, it enables tumor cells to evade immune attacks. Tumor cells establish immune escape mechanisms through various means, including inhibitory factors and ICP molecule expressions such as programmed death-1 (PD-1) and programmed death ligand-1 (PDL-1) (Diesendruck and Benhar, 2017; Sharma et al., 2023). According to this study, increased PPARG expression is associated with a poor prognosis. Notably, PPARG expression is associated with the expression of several ICPs in LIHC. Furthermore, excessive immune infiltration can lead to functional abnormalities within TME.

Recent research has highlighted the involvement of PPARG in regulating lipid degeneration and promoting neutrophil infiltration in the liver during the transition from inflammatory liver disease and fatty liver to hepatocellular carcinoma (Chan et al., 2017; Wang et al., 2017). The attachment of neutrophils to the luminal surface of blood vessels and their subsequent migration to the site of the lesion outside the blood vessels relies on the activation of integrins by chemotactic proteins (Mohs et al., 2017; Wu et al., 2021). Neutrophils play a critical role in the primary defense against infections and tissue damage, and they also exhibit immunoregulatory functions. However, the recruitment of a significant number of neutrophils by chemotactic factors can have detrimental effects. Persistently high expression or upregulation of chemotactic factors, as a part of the active physiological feedback mechanism of the body, can exacerbate the degradation of the extracellular matrix and lead to widespread tissue damage. Consequently, this process directly enhances the survival, invasion, and metastasis capabilities of tumor cells (Hughes and Nibbs, 2018; Petri and Sanz, 2018). Paradoxically, the ultimate outcome can compromise the protective role of immune cells, thus increasing the risk of tissue damage and cancer development.

Moreover, the interaction between PPARG expression and multiple signaling pathways suggests its involvement in modulating the immune microenvironment. These pathways include the NOD-like receptor signaling pathway, T cell activation, cytoskeletal regulation, and drug metabolism. Notably, the NOD-like receptors have been identified as crucial factors in tumorigenesis, angiogenesis, cancer stemness, and chemoresistance. In endometrial cancer (EMC), dysregulation of the NOD-like receptor family protein (NLRP) has been shown to impair the phagocytic function of macrophages and reduce the CD + T cell population, thereby promoting the growth, invasion, and metastasis of EMC cells (Zhu et al., 2023). Furthermore, recent research has revealed that tumor cells can utilize lipids secreted by adipocytes to promote tumor progression and chemoresistance through metabolic reprogramming. In ovarian cancer, adipocytes, as a significant component of the ovarian TME, impact drug distribution and contribute to chemoresistance (Yang et al., 2019). Considering PPARG as a key regulator of adipogenesis and differentiation, it may be one of the underlying contributing factors to tumor progression and chemoresistance. Thus, the manipulation of PPARG expression holds promise as a potential strategy for shaping the immune microenvironment and developing novel therapeutic approaches to combat tumor growth and metastasis.

In summary, the pan-cancer analysis and experimental investigations of PPARG have confirmed its differential expression

across various types of cancers and its association with survival outcomes and poor prognosis, including in PAAD, LIHC, LGG, GBM, and other types of cancer. These associations have been attributed to PPARG gene variants, epigenetic modifications such as acetylation and phosphorylation patterns, and effects on immune infiltration. However, despite the comprehensive research on PPARG, there are certain limitations to this study. Firstly, more direct clinical studies are required to further elucidate the precise function of PPARG in regulating immunological processes. Secondly, the precise significance of PPARG expression in various types of cancer and its precise role in immune regulation within these tumors remain unclear.

5 Conclusion

In this study, we observed heterogeneous PPARG mRNA expression levels across various types of cancer. Moreover, we found a strong correlation between PPARG expression and several important factors, including prognostic value, features related to clinical stages, drug sensitivity profiles, and activation of immune cells. Additionally, we identified PPARG as a key molecule involved in the regulation of key pathways such as the NOD-like receptor signaling pathway, cell cycle, and drug metabolism. These findings highlight the potential utility of PPARG as a valuable cancer biomarker.

Data availability statement

The datasets presented in this study can be found in online repositories. The names of the repository/repositories and accession number(s) can be found below: GSE14520; GSE85916.

Ethics statement

The studies involving humans were approved by the ethics committee of Guizhou Medical University. The studies were conducted in accordance with the local legislation and institutional requirements. Written informed consent for participation was not required from the participants or the participants' legal guardians/next of kin because According to Chinese law, the materials used in this study were collected by the Pathology Department of Guizhou Medical University Affiliated Hospital for the purposes of diagnosis and treatment, and are used in an anonymous form for this research. Therefore, written consent from patients is not required.

Author contributions

YR: Data curation, Methodology, Software, Validation, Visualization, Writing–original draft. CH: Funding acquisition, Project administration, Resources, Writing–review and editing. JuW: Conceptualization, Data curation, Investigation, Methodology, Supervision, Writing–original draft. QK: Data curation, Funding acquisition, Writing–review and editing. RZ: Funding acquisition, Supervision, Validation, Writing–review and editing. PL: Formal Analysis, Funding acquisition, Investigation, Software, Writing–review and editing. DM: Conceptualization, Data curation, Formal Analysis, Funding acquisition, Methodology, Project administration, Resources, Validation, Writing–review and editing, Writing–original draft. JiW: Conceptualization, Funding acquisition, Investigation, Project administration, Resources, Visualization, Writing–review and editing. LT: Conceptualization, Funding acquisition, Investigation, Methodology, Resources, Writing–review and editing.

Funding

The author(s) declare financial support was received for the research, authorship, and/or publication of this article. This study was supported, in part, by the National Natural Science Foundation of China (Nos 82003835, 82160704, 82160665, and 82360732), Basic Research Program of Guizhou Province Technology Bureau [Nos ZK (2021) General-399, ZK (2022) General-412, ZK (2022) General-451, ZK (2021) General-568, and ZK (2023) General-383], Science and Technology Program of Guizhou Province Health Committee (Nos gzwkj 2021-466, gzwkj 2021-468, gzwkj 2021-158, and gzwkj 2021-442), Program of Guizhou Provincial Department of Education (QianJiaoJi 2022-194), National-Local Joint Engineering Research Center for Innovative and Generic Chemical Drug, Guizhou. High-level Innovative Talents Supporting Program (2016-4015), Cultivation Program to National Natural Science Foundation of Affiliated Hospital of Guizhou Medical University (Nos 22NSFCP56 and 22NSFCP58).

Acknowledgments

We would like to express our sincere gratitude to the generous data sharing by research centers such as TCGA (The Cancer Genome Atlas) and GEO (Gene Expression Omnibus).

Conflict of interest

The authors declare that the research was conducted in the absence of any commercial or financial relationships that could be construed as a potential conflict of interest.

The reviewer CZ declared a past co-authorship with the author DM to the handling editor.

Publisher's note

Supplementary material

The Supplementary Material for this article can be found online at: https://www.frontiersin.org/articles/10.3389/fphar.2023.1298341/full#supplementary-material

References

Andersen, D. K., Korc, M., Petersen, G. M., Eibl, G., Li, D., Rickels, M. R., et al. (2017). Diabetes, pancreatogenic diabetes, and pancreatic cancer. *Diabetes* 66, 1103–1110. doi:10.2337/db16-1477

Baer, C., Walter, W., Hutter, S., Twardziok, S., Meggendorfer, M., Kern, W., et al. (2019). Somatic" and "pathogenic" - is the classification strategy applicable in times of large-scale sequencing? *Haematologica* 104, 1515–1520. doi:10.3324/haematol.2019.218917

Ballav, S., Biswas, B., Sahu, V. K., Ranjan, A., and Basu, S. (2022). PPAR-Gamma partial agonists in disease-fate decision with special reference to cancer. *Cells* 11, 3215. doi:10.3390/cells11203215

Bray, F., Ferlay, J., Soerjomataram, I., Siegel, R. L., Torre, L. A., and Jemal, A. (2018). Global cancer statistics 2018: GLOBOCAN estimates of incidence and mortality worldwide for 36 cancers in 185 countries. *CA Cancer J. Clin.* 68, 394–424. doi:10.3322/caac.21492

Cagan, A., Baez-Ortega, A., Brzozowska, N., Abascal, F., Coorens, T. H. H., Sanders, M. A., et al. (2022). Somatic mutation rates scale with lifespan across mammals. *Nature* 604, 517–524. doi:10.1038/s41586-022-04618-z

Chan, A. W., Wong, G. L., Chan, H. Y., Tong, J. H., Yu, Y. H., Choi, P. C., et al. (2017). Concurrent fatty liver increases risk of hepatocellular carcinoma among patients with chronic hepatitis B. *J. Gastroenterol. Hepatol.* 32, 667–676. doi:10.1111/jgh.13536

Chandrashekar, D. S., Karthikeyan, S. K., Korla, P. K., Patel, H., Shovon, A. R., Athar, M., et al. (2022). UALCAN: an update to the integrated cancer data analysis platform. *Neoplasia* 25, 18–27. doi:10.1016/j.neo.2022.01.001

Chiu, M., Mcbeth, L., Sindhwani, P., and Hinds, T. D. (2017). Deciphering the roles of thiazolidinediones and PPARγ in bladder cancer. *PPAR Res.* 2017, 4810672. doi:10.1155/2017/4810672

Diesendruck, Y., and Benhar, I. (2017). Novel immune check point inhibiting antibodies in cancer therapy-Opportunities and challenges. *Drug Resist Updat* 30, 39–47. doi:10.1016/j.drup.2017.02.001

Fusco, M. J., West, H. J., and Walko, C. M. (2021). Tumor mutation burden and cancer treatment. *JAMA Oncol.* 7, 316. doi:10.1001/jamaoncol.2020.6371

Galbraith, L., Leung, H. Y., and Ahmad, I. (2018). Lipid pathway deregulation in advanced prostate cancer. *Pharmacol. Res.* 131, 177–184. doi:10.1016/j.phrs.2018.02.022

Hughes, C. E., and Nibbs, R. J. B. (2018). A guide to chemokines and their receptors. *FEBS J.* 285, 2944–2971. doi:10.1111/febs.14466

Hughes, T. S., Giri, P. K., de Vera, I. M., Marciano, D. P., Kuruvilla, D. S., Shin, Y., et al. (2014). An alternate binding site for PPARγ ligands. *Nat. Commun.* 5, 3571. doi:10.1038/ncomms4571

Joshi, H., Pal, T., and Ramaa, C. S. (2014). A new dawn for the use of thiazolidinediones in cancer therapy. *Expert Opin. Investig. Drugs* 23, 501–510. doi:10.1517/13543784.2014.884708

Kesanakurti, D., Maddirela, D., Banasavadi-Siddegowda, Y. K., Lai, T. H., Qamri, Z., Jacob, N. K., et al. (2017). A novel interaction of PAK4 with PPARγ to regulate Nox1 and radiation-induced epithelial-to-mesenchymal transition in glioma. *Oncogene* 36, 5309–5320. doi:10.1038/onc.2016.261

Lewis, J. D., Lichtenstein, G. R., Deren, J. J., Sands, B. E., Hanauer, S. B., Katz, J. A., et al. (2008). Rosiglitazone for active ulcerative colitis: a randomized placebo-controlled trial. *Gastroenterology* 134, 688–695. doi:10.1053/j.gastro.2007.12.012

Lin, L., Lin, H., Wang, L., Wang, B., Hao, X., and Shi, Y. (2015). miR-130a regulates macrophage polarization and is associated with non-small cell lung cancer. *Oncol. Rep.* 34, 3088–3096. doi:10.3892/or.2015.4301

Liu, C., Tate, T., Batourina, E., Truschel, S. T., Potter, S., Adam, M., et al. (2019). Pparg promotes differentiation and regulates mitochondrial gene expression in bladder epithelial cells. *Nat. Commun.* 10, 4589. doi:10.1038/s41467-019-12332-0

Ma, D., Liu, P., Hu, C., Zhou, Z., Wang, P., Wang, Y., et al. (2023). Intracellular angiopoietin-1 promotes TKI-resistance via activation of JAK/STAT5 pathway in chronic myeloid leukemia. *Oncogene* 42, 124–137. doi:10.1038/s41388-022-02536-y

Mal, S., Dwivedi, A. R., Kumar, V., Kumar, N., Kumar, B., and Kumar, V. (2021). Role of peroxisome proliferator-activated receptor gamma (PPARγ) in different disease states: recent updates. *Curr. Med. Chem.* 28, 3193–3215. doi:10.2174/0929867327666200716113136

Ma, S., Zhou, B., Yang, Q., Pan, Y., Yang, W., Freedland, S. J., et al. (2021). A transcriptional regulatory loop of master regulator transcription factors, PPARG, and fatty acid synthesis promotes esophageal adenocarcinoma. *Cancer Res.* 81, 1216–1229. doi:10.1158/0008-5472.CAN-20-0652

Menezes, J., and Diederich, M. F. (2021). Bioactivity of natural biflavonoids in metabolism-related disease and cancer therapies. *Pharmacol. Res.* 167, 105525. doi:10.1016/j.phrs.2021.105525

Mohs, A., Kuttkat, N., Reissing, J., Zimmermann, H. W., Sonntag, R., Proudfoot, A., et al. (2017). Functional role of CCL5/RANTES for HCC progression during chronic liver disease. *J. Hepatol.* 66, 743–753. doi:10.1016/j.jhep.2016.12.011

Mukherjee, R., Jow, L., Croston, G. E., and Paterniti, J. R., JR. (1997). Identification, characterization, and tissue distribution of human peroxisome proliferator-activated receptor (PPAR) isoforms PPARgamma2 versus PPARgamma1 and activation with retinoid X receptor agonists and antagonists. *J. Biol. Chem.* 272, 8071–8076. doi:10.1074/jbc.272.12.8071

Mun, E. J., Babiker, H. M., Weinberg, U., Kirson, E. D., and von Hoff, D. D. (2018). Tumor-treating fields: a fourth modality in cancer treatment. *Clin. Cancer Res.* 24, 266–275. doi:10.1158/1078-0432.CCR-17-1117

Park, S. H., Choi, H. J., Yang, H., Do, K. H., Kim, J., Lee, D. W., et al. (2010). Endoplasmic reticulum stress-activated C/EBP homologous protein enhances nuclear factor-kappaB signals via repression of peroxisome proliferator-activated receptor gamma. *J. Biol. Chem.* 285, 35330–35339. doi:10.1074/jbc.M110.136259

Petri, B., and Sanz, M. J. (2018). Neutrophil chemotaxis. *Cell Tissue Res.* 371, 425–436. doi:10.1007/s00441-017-2776-8

Roudko, V., Bozkus, C. C., Orfanelli, T., Mcclain, C. B., Carr, C., O'Donnell, T., et al. (2020). Shared immunogenic poly-epitope frameshift mutations in microsatellite unstable tumors. *Cell* 183, 1634–1649. doi:10.1016/j.cell.2020.11.004

Ryu, S., Kim, D. S., Lee, M. W., Lee, J. W., Sung, K. W., Koo, H. H., et al. (2018). Anti-leukemic effects of PPARγ ligands. *Cancer Lett.* 418, 10–19. doi:10.1016/j.canlet.2018.01.020

Shao, W., Kuhn, C., Mayr, D., Ditsch, N., Kailuwait, M., Wolf, V., et al. (2020). Cytoplasmic PPARγ is a marker of poor prognosis in patients with Cox-1 negative primary breast cancers. *J. Transl. Med.* 18, 94. doi:10.1186/s12967-020-02271-6

Sharma, P., Goswami, S., Raychaudhuri, D., Siddiqui, B. A., Singh, P., Nagarajan, A., et al. (2023). Immune checkpoint therapy-current perspectives and future directions. *Cell* 186, 1652–1669. doi:10.1016/j.cell.2023.03.006

Shu, Y., Lu, Y., Pang, X., Zheng, W., Huang, Y., Li, J., et al. (2016). Phosphorylation of PPARγ at Ser84 promotes glycolysis and cell proliferation in hepatocellular carcinoma by targeting PFKFB4. *Oncotarget* 7, 76984–76994. doi:10.18632/oncotarget.12764

Tian, J., Hu, L., Li, X., Geng, J., Dai, M., and Bai, X. (2022). Retraction Note: MicroRNA-130b promotes lung cancer progression via PPARγ/VEGF-A/BCL-2-mediated suppression of apoptosis. *J. Exp. Clin. Cancer Res.* 41, 351. doi:10.1186/s13046-022-02548-2

Vallee, A., Lecarpentier, Y., Guillevin, R., and Vallee, J. N. (2018). Opposite interplay between the canonical WNT/β-catenin pathway and PPAR gamma: a potential therapeutic target in gliomas. *Neurosci. Bull.* 34, 573–588. doi:10.1007/s12264-018-0219-5

Verreth, W., de Keyzer, D., Pelat, M., Verhamme, P., Ganame, J., Bielicki, J. K., et al. (2004). Weight-loss-associated induction of peroxisome proliferator-activated receptor-alpha and peroxisome proliferator-activated receptor-gamma correlate with reduced atherosclerosis and improved cardiovascular function in obese insulin-resistant mice. *Circulation* 110, 3259–3269. doi:10.1161/01.CIR.0000147614.85888.7A

Villarroel-Vicente, C., Gutierrez-Palomo, S., Ferri, J., Cortes, D., and Cabedo, N. (2021). Natural products and analogs as preventive agents for metabolic syndrome via peroxisome proliferator-activated receptors: an overview. *Eur. J. Med. Chem.* 221, 113535. doi:10.1016/j.ejmech.2021.113535

Wang, W., Xu, M. J., Cai, Y., Zhou, Z., Cao, H., Mukhopadhyay, P., et al. (2017). Inflammation is independent of steatosis in a murine model of steatohepatitis. *Hepatology* 66, 108–123. doi:10.1002/hep.29129

Wild, C. P. (2019). The global cancer burden: necessity is the mother of prevention. *Nat. Rev. Cancer* 19, 123–124. doi:10.1038/s41568-019-0110-3

Wu, G., Liu, J., Liu, H., Jin, L., Huang, X., Mo, X., et al. (2021). An applicable inflammation-joined and nutrition-related prognostic indicator in patients with colorectal cancer. *Front. Oncol.* 11, 644670. doi:10.3389/fonc.2021.644670

Yamamoto, K., Tamura, T., Nakamura, R., Hosoe, S., Matsubara, M., Nagata, K., et al. (2019). Development of a novel class of peroxisome proliferator-activated receptor (PPAR) gamma ligands as an anticancer agent with a unique binding mode based on a non-thiazolidinedione scaffold. *Bioorg Med. Chem.* 27, 115122. doi:10.1016/j.bmc.2019.115122

Yang, P. Y., Zou, H., Chao, E., Sherwood, L., Nunez, V., Keeney, M., et al. (2016). Engineering a long-acting, potent GLP-1 analog for microstructure-based transdermal delivery. *Proc. Natl. Acad. Sci. U. S. A.* 113, 4140–4145. doi:10.1073/pnas.1601653113

Yang, J., Zaman, M. M., Vlasakov, I., Roy, R., Huang, L., Martin, C. R., et al. (2019). Adipocytes promote ovarian cancer chemoresistance. *Sci. Rep.* 9, 13316. doi:10.1038/s41598-019-49649-1

Zhang, H., Zhu, S., Chen, J., Tang, Y., Hu, H., Mohan, V., et al. (2012). Peroxisome proliferator-activated receptor gamma polymorphism Pro12Ala Is associated with nephropathy in type 2 diabetes: evidence from meta-analysis of 18 studies. *Diabetes Care* 35, 1388–1393. doi:10.2337/dc11-2142

Zhu, X., Xu, Y., Wang, J., Xue, Z., Qiu, T., and Chen, J. (2023). Loss of NLRP3 reduces oxidative stress and polarizes intratumor macrophages to attenuate immune attack on endometrial cancer. *Front. Immunol.* 14, 1165602. doi:10.3389/fimmu.2023.1165602

frontiers | Frontiers in Pharmacology

TYPE Original Research
PUBLISHED 14 December 2023
DOI 10.3389/fphar.2023.1286061

OPEN ACCESS

EDITED BY
Kenneth KW To,
The Chinese University of Hong Kong, China

REVIEWED BY
Richa Kapoor,
Children's Hospital of Philadelphia, United States
Lenin Pavón,
National Institute of Psychiatry Ramon de la Fuente Muñiz (INPRFM), Mexico

*CORRESPONDENCE
Yingjie Nie,
nienyj@hotmail.com

†These authors share first authorship

RECEIVED 30 August 2023
ACCEPTED 01 December 2023
PUBLISHED 14 December 2023

CITATION
Jing Q, Wan Q, Nie Y, Luo J, Zhang X, Zhu L, Gui H, Li L, Wang C, Chen S, Wang M, Yuan H, Lv H, Pan R, Jing Q and Nie Y (2023), Ansofaxine hydrochloride inhibits tumor growth and enhances Anti-TNFR2 in murine colon cancer model. *Front. Pharmacol.* 14:1286061. doi: 10.3389/fphar.2023.1286061

Ansofaxine hydrochloride inhibits tumor growth and enhances Anti-TNFR2 in murine colon cancer model

Qianyu Jing[1†], Quan Wan[1†], Yujie Nie[2], Junqian Luo[3], Xiangyan Zhang[2], Lan Zhu[4], Huan Gui[4], Linzhao Li[4], Chenglv Wang[4], Shuanghui Chen[4], Mengjiao Wang[4], Haohua Yuan[4], Hang Lv[4], Runsang Pan[5], Qianjun Jing[6] and Yingjie Nie[1,2*]

[1]School of Basic Medical Sciences, Zunyi Medical University, Zunyi, China, [2]NHC Key Laboratory of Pulmonary Immunological Diseases, Guizhou Provincial People's Hospital, Guiyang, China, [3]The First People's Hospital of Jinzhong, Jinzhong, China, [4]School of Medicine, Guizhou University, Guiyang, China, [5]Guizhou Medical University, Guiyang, China, [6]Chongqing Medical University, Chongqing, China

Introduction: As psychoneuroimmunology flourishes, there is compelling evidence that depression suppresses the anti-tumor immune response, promotes the progression of cancer, and inhibits the effectiveness of cancer immunotherapy. Recent studies have reported that antidepressants can not only alleviate the depressant condition of cancer patients, but also strengthen the anti-tumor immunity, thus suppressing tumors. Tumor necrosis factor receptor 2 (TNFR2) antagonistic antibodies (Anti-TNFR2) targeting tumor-infiltrating regulatory T cells (Tregs) has achieved great results in preclinical studies, and with a favorable toxicity profile than existing immunotherapies, and is expected to become a new generation of more effective treatment strategies. Understanding the effects of combination therapy with antidepressants and Anti-TNFR2 may help design new strategies for cancer immunotherapy.

Methods: We treated CT26, HCT116, MCA38 and SW620 colon cancer cells with fluoxetine (0–50 μM), ansofaxine hydrochloride (0–50 μM) and amitifadine hydrochloride (0–150 μM) to examine their effects on cell proliferation and apoptosis. We explored the antitumor effects of ansofaxine hydrochloride in combination with or without Anti-TNFR in subcutaneously transplanted CT26 cells in tumor-bearing mouse model. Antitumor effects were evaluated by tumor volume. NK cell, M1 macrophage cell, $CD4^+$ T cell, $CD8^+$ T cell, exhausted $CD8^+$ T and regulatory T cell (Tregs) subtypes were measured by flow cytometry. 5-hydroxytryptamine, dopamine and norepinephrine levels were measured by ELISA.

Results: Oral antidepression, ansofaxine hydrochloride, enhanced peripheral dopamine levels, promoted $CD8^+$T cell proliferation, promoted intratumoral infiltration of M1 and NK cells, decreased the proportion of tumor-infiltrating exhausted $CD8^+$T cells, and strengthened anti-tumor immunity, thereby inhibiting colon cancer growth. In combination therapy, oral administration of ansofaxine hydrochloride enhanced the efficacy of Anti-TNFR2, and produced long-term

tumor control in with syngeneic colorectal tumor-bearing mice, which was attributable to the reduction in tumor-infiltrating Treg quantity and the recovery of $CD8^+$ T cells function.

Discussion: In summary, our data reveal the role of ansofaxine hydrochloride in modulating the anti-tumor immunity. Our results support that exhausted $CD8^+$T is an important potential mechanism by which ansofaxine hydrochloride activates anti-tumor immunity and enhances anti-tumor effects of anti-TNFR2.

KEYWORDS

ansofaxine hydrochloride, anti-TNFR2, exhausted CD8 + T cells, Tregs, tumor immunotherapy, colon cancer

1 Introduction

Colon cancer (CRC) is the fourth deadliest cancer worldwide, killing hundreds of thousands of people each year (Sung et al., 2021). At the same time, the mental health of patients is also attracting more and more attention, with the occurrence of depression in cancer patients being higher than any other disease patients (Yan et al., 2019; Yang et al., 2021a; Endo et al., 2022). There are convincing evidences that Depression promotes the growth of various cancers by regulating the neuroimmune system, and inhibits the efficacy of cancer treatment (Liu et al., 2015; Sommershof et al., 2017; Zhang et al., 2020). Therefore, research into therapies that can treat both cancer and depression at the same time is clinically valuable.

Currently, colon cancer treatment includes surgery, radiation, chemotherapy, targeted therapy, and immunotherapy. In recent years, immune checkpoint inhibitors such as anti-programmed cell death protein 1 (PD-1) and anti-cytotoxic T lymphocyte–associated protein 4 (CTLA-4) have achieved great results in cancer treatment, however, because to low response rates and immune-related adverse events (irAEs), most patients are unable to benefit (Fritz and Lenardo, 2019). Tumor necrosis factor receptor 2 (TNFR2), one of the two receptors that mediate the biological function of TNF, is involved in cancer cell growth (Vanamee and Faustman, 2017; Torrey et al., 2019; Li et al., 2023), and is high expressed in exhausted CD8T cells and tumor-infiltrating regulatory T cells (Tregs) in a variety of cancers (Liao et al., 2023). Now, there are convincing evidences that TNFR2 can serve as a key mediator involved in the activation and proliferation of Tregs, enhancing immunosuppressive function (Chen et al., 2007; Kawano et al., 2022). In addition, Other types of immunosuppressive cells, such as MDSCs, and some tumor cells also express TNFR2 (Vanamee and Faustman, 2017). Knocking down TNFR2 on cancer cells by CRISPR/Cas9 technology significantly impaired the growth of colon cancer, and increased the number of tumor-infiltrating IFN-γ^+ CD8 cells (Li et al., 2023). TNFR2 antagonistic antibody (anti-TNFR2) inhibit Tregs by targeting TNFR2 *in vitro*, and kill TNFR2-expressing tumor cells and Tregs in advanced Sézary syndrome (Torrey et al., 2019; Moatti et al., 2022). Moreover, in mouse models, anti-TNFR2 was less toxic than anti-CTLA-4 (Tam et al., 2019). Therefore, Anti-TNFR2 is considered a very promising new tumor immunotherapy (Vanamee and Faustman, 2017). Currently, preclinical studies of human anti-TNFR2 antibodies have yielded very encouraging results, justifying their clinical development (Tam et al., 2019).

The combination of antidepressant and immune checkpoint inhibitor has also been reported. Fluoxetine and monoamine oxidase inhibitor (MAOI) were common clinical medications for depression, recent studies have shown that they not only suppress the adverse impact of depression, but also enhance the anti-tumor immunity of the body (Di Rosso et al., 2016; Di Rosso et al., 2018; Marcinkute et al., 2019; Wang et al., 2021a; Yang et al., 2021b; Schneider et al., 2021). Fluoxetine combined with anti-PD1 provides long-term tumor control in mouse models (Schneider et al., 2021). MAOI inhibits macrophage immunosuppressive polarization, and synergistically suppresses tumors in combination with anti-PD-1 therapy (Wang et al., 2021b). However, the effect of fluoxetine is slow and long-term use often induces adverse effects such as loss of appetite or sexual dysfunction, and MAOI was associated with an increased incidence of colorectal cancer (Lee et al., 2017). Triple reuptake inhibitors (TRIs) are believed to enhance neurotransmission in all monoamine systems, and have the advantage of acting quickly, and improving symptoms of sexual disorders and disorientation (Tran et al., 2012; Shao et al., 2014; Sharma et al., 2015). Ansofaxine hydrochloride (LY03005) is a new TRI for the treatment of major depressive disorder in adults, which has completed phase III clinical trials and is well tolerated (Mi et al., 2022). However, the role of ansofaxine hydrochloride in cancer immunotherapy is unclear. Therefore, we took the ansofaxine hydrochloride as a breakthrough point to study its effect on colon cancer.

Here, we found that ansofaxine hydrochloride, like fluoxetine, inhibits colon cancer cell growth *in vitro* by inducing apoptosis. In CT26 colon cancer model, ansofaxine hydrochloride enhanced the proportion of $CD8^+$T cells in spleen, decreased the proportion of tumor infiltration exhausted $CD8^+$T cells, and increased the proportion of natural killer cells (NKs) and M1 macrophages in spleen and tumor, which may be due to the enhancement of peripheral dopamine (DA) and the reduction of peripheral 5-hydroxytryptamine (5-HT), ultimately inhibited tumor growth. In combination therapy, ansofaxine hydrochloride enhanced the efficacy of anti-TNFR2 in colon cancer, enabling eradication of established tumors in 20% of mice, and triggering syngeneic tumor-specific systemic immunity. These results provide a new way of treating colon cancer patients with depression.

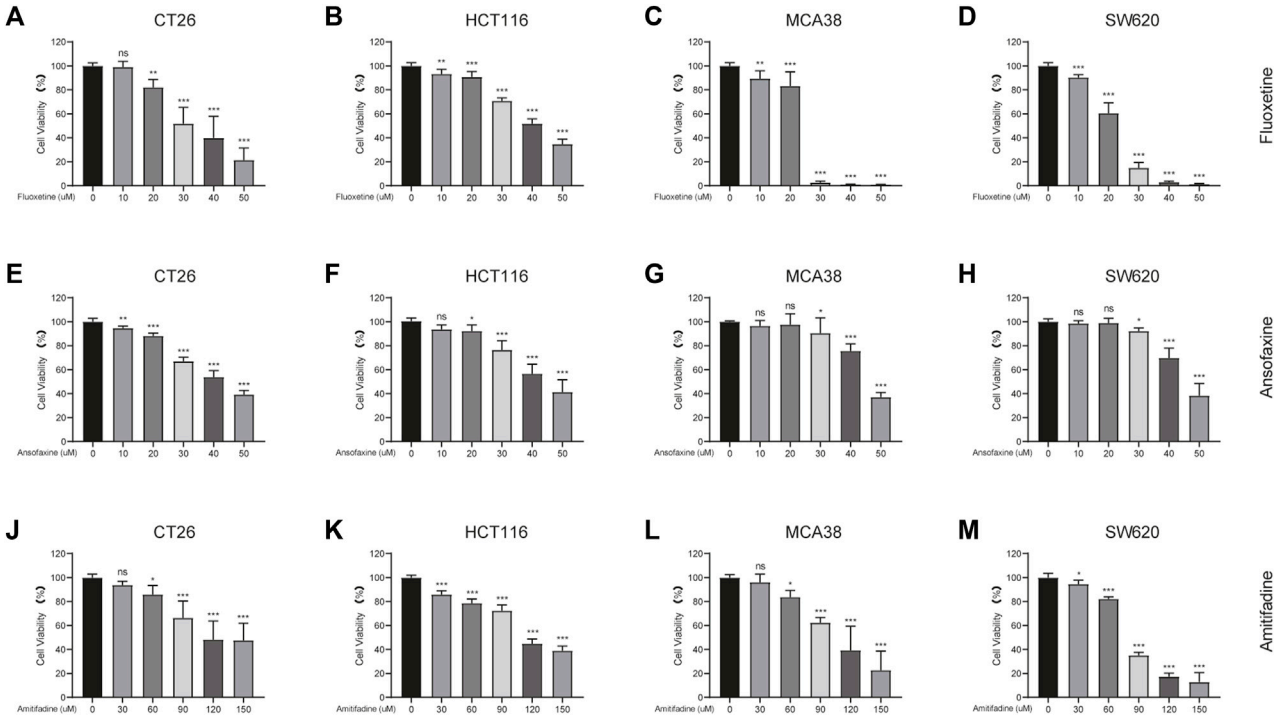

FIGURE 1
Comparison of fluoxetine, ansofaxine hydrochloride and amitifadine hydrochloride for inhibitory effect in various colon cancer cell lines. **(A–D)** CT26, MCA38, HCT116 and SW620 were treated for 24 h with fluoxetine (0, 10, 20, 30, 40, and 50 μM). **(E–H)** CT26, MCA38, HCT116, SW620 were treated for 24 h with Ansofaxine hydrochloride (0, 10, 20, 30, 40, and 50 μM). **(J–M)** CT26, MCA38, HCT116, SW620 cells were treated for 24 h with Amitifadine hydrochloride (0, 30, 60, 90, 120, and 150 μM). CCK8 for measurement of cell viability. Data are expressed as mean ± SD; $*p < 0.05$, $**p < 0.01$, $***p < 0.001$.

2 Methods and materials

2.1 Mice and cell culture

Female wild-type Balb/c mice (6- to 8-week-old) were obtained from Spaefer Biotechnology Co., Ltd. (Beijing, China) (Animal Quality Certificate: SCXK (Beijing) 2019-0008). Mice were housed in a specific pathogen-free (SPF) lab at the Experimental Animal Center of Guizhou University of Traditional Chinese (Animal experiment license: SYXK 2021-0005), and the experiments were started after 7 days of acclimatization to the surrounding environment. This animal experiment was approved by Ethics Committee of Guizhou Provincial People's Hospital, China. The mouse colon cancer cell lines (CT26, MCA38) and mouse breast cancer cell line (4T1) were supplied by Pricella (Wuhan, China). The human colon cancer cell lines (HCT116, SW620) were gifted by Prof. Jie Ding (Guizhou Province People's Hospital, Guizhou, China). The cells were cultured in RPMI-1640 complete medium containing 10% fetal bovine serum (FBS), and supplemented with penicillin (100 units/mL), streptomycin (100 μg/mL) glutamine (2 mM), at 37°C under 5% CO2.

2.2 Chemicals

All chemicals were of analytical grade. Fluoxetine was purchased by Absin (Shanghai, China). Amitifadine hydrochloride (DOV 21947), ansofaxine hydrochloride (LY03005), cell counting kit-8 (CCK-8), and telratolimod (3M-052) were purchased by MedChenExpress (Monmouth Junction, NJ, United States). Anti-mouse TNFR2 (CD120b, clone TR75-54.7) was purchased by BioXCell (W. Lebanon, NH). High mobility group nucleosome binding protein 1 (HMGN1) was purchased by Bio-techne (R&D Systems. United States). ST/5-HT (Serotonin/5-hydroxytryptamine), DA (dopamine), and NA/NE (Noradrenaline/norepinephrine) ELISA Kit, and Annexin-V-FITC/PI were purchased by Elabscience Biotechnology Co., Ltd. (Wuhan, China). Fetal bovine serum (FBS) was purchased by Pricella (Wuhan, China). Penicillin-streptomycin stock solutions was purchased by New Cell and Molecular Biotech Co., Ltd. (Suzhou, China). Trypsin-EDTA (0.25%), EDTA- and phenol red-free trypsin (0.25%) were purchased by Servicebio (Wuhan, China). RPMI-1640 medium was purchased by GIBCO BRL (Grand Island, NY, United States). FITC-anti-mouse CD4 (clone GK1.5) was purchased by Biolegend (California, United States). BV510-anti-mouse CD45 (clone 30-F11), BV605-anti-mouse CD3 (clone 17A2), BV421-anti-mouse CD8 (clone 53-6.7), PerCPcy5.5-anti-mouse CD279 (clone J43), PE-anti-mouse CD223 (clone C9B7W), BV421-anti-mouse CD49b (clone DX5), FITC-anti-mouse CD11b (clone M1/70) and BV650-anti-mouse CD86 (clone GL1) were purchased by BD Biosciences (Franklin Lake, New Jersey, United States). PE-anti-mouse F4/80 (clone BM8) was purchased by eBioscience (California, United States).

10.3389/fphar.2023.1286061

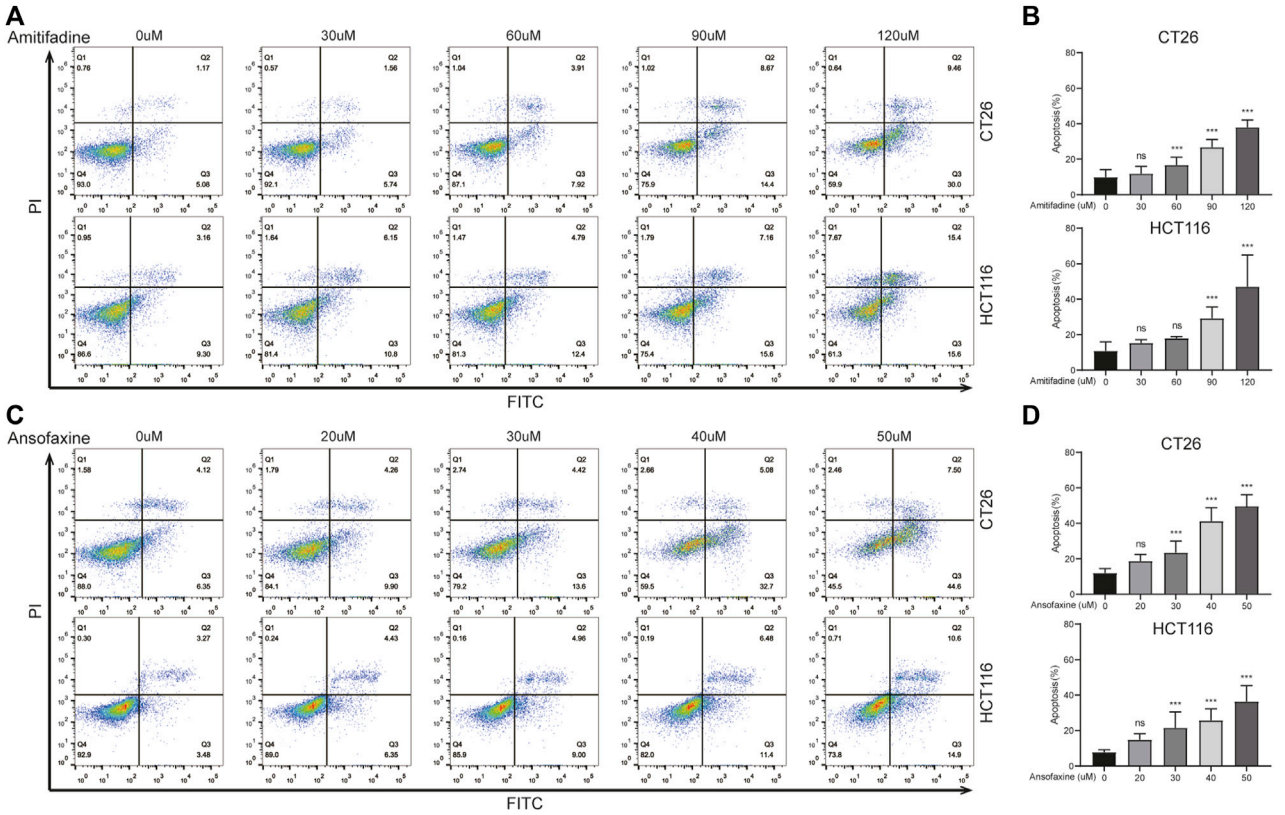

FIGURE 2
(A) CT26 and HCT116 were treated with amitifadine hydrochloride (0–120 μM) for 24 h. **(B)** The proportion of apoptosis cells was analyzed. **(C)** CT26 and HCT116 were treated with ansofaxine hydrochloride (0–50 μM) for 24 h. **(D)** The proportion of apoptosis cells was analyzed.

2.3 Cell counting Kit-8 (CCK-8) assay

The cells (5,000 cells/well) were inoculated in the 96-well plates. After 24 h of incubation, the cells were treated with fluoxetine, amitifadine hydrochloride or ansofaxine hydrochloride for 24 h. The medium was then replaced to FBS-free RPMI-1640 with 10% CCK8 solution in a dark room. The OD values were collected at 450 nm after incubation at 37°C for 1 h.

2.4 Cell apoptosis analysis

Cells (2×10^5 cells/well) were inoculated into 6-well plates. After 24 h of incubation, the cells were treated with amitifadine hydrochloride or ansofaxine hydrochloride at the appropriate concentration. After 24 h, all cells were collected and then incubated with PI-FITC antibody for 15 min. Detection was performed using a flow cytometer (BD FACSCelestaTM).

2.5 Construction and treatment of mouse model of CT26 colon cancer

CT26 colon cancer cells (2×10^5/100 ul/mouse) were injected subcutaneously into the right abdomen of the subject mice. In rechallenge experiments, tumor-free mice surviving for 80 days were inoculated with CT26 cells (2×10^5) in the left abdomen and 4T1 breast cancer cells (2×10^5) in the right abdomen. "Survival" represents the time it takes for the tumor to progress to 2,000 mm^3, which is the humane endpoint for triggering euthanasia. The tumor size was monitored every 3 days, and was calculated as: tumor size = (length × $width^2$)/2.

Treatment was started when tumor volume reached 100 mm^3. Ansofaxine hydrochloride was administered by gavage for 5 or 12 days at 300 μg in 0.1 mL of water. Tumors and spleens were taken from mice the day after the last treatment and studied. In combination treatment, ansofaxine hydrochloride (300 ug/100 ul) was administered by gavage, anti-TNFR2 (200 ug/200 ul) was injected intraperitoneally at days 2 and 7, HMGN1 (0.5 ug/50 ul) and 3M-052 (20 ug/50 ul) was injected intratumoral at days 1, 5 and 9.

2.6 Flow cytometry analysis

To analyze the proportions of $CD8^+$T and exhausted $CD8^+$T cells, cells were stained with BV510-CD45, BV605-CD3, BV421-CD8, PerCPcy5.5-CD279 and PE-CD223 antibodies. To analyze the proportions of $CD4^+$T, Tregs and NK cells, cells were stained with BV510-CD45, BV605-CD3, FITC-CD4, BV421-CD49b and PE-Foxp3 antibodies. To analyze the proportions of M1, cells were stained with BV510-CD45, FITC-CD11b, PE-F4/80, and BV650-CD86 antibodies. All cells were assayed with flow cytometry and data analyzed with Flowjo 10 software.

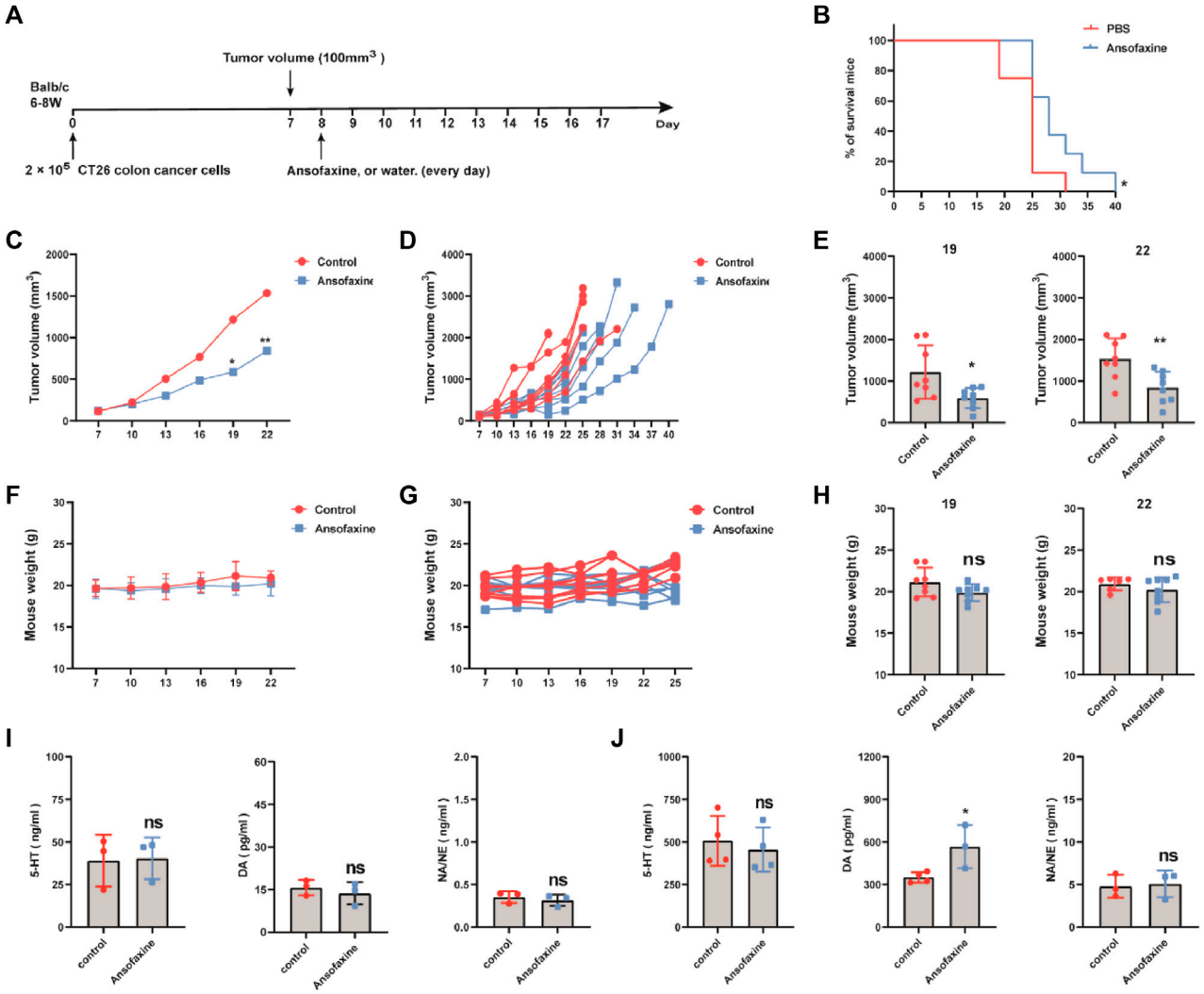

FIGURE 3
(A) Schematic diagram of the experimental program. When tumor volume reached 100 mm^3 (day 7), mice were then treated with water or ansofaxine hydrochloride for 9 days (300 ug/100 ul/mouse). **(B)** Mouse survival curves. **(C)** Average growth curves of the tumors (n = 8). **(D)** Growth curves of tumor in each individual mouse (n = 8). **(E)** Tumor volume in mice on days 19 and 22. **(F–H)** Weights of mice. **(I)** Concentrations of 5-HT, DA, and NA/NE in the supernatant of CT26 colon cancer cells treated with or without ansofaxine hydrochloride for 48 h. **(J)** Concentrations of 5-HT, DA, and NA/NE in the serum of mice with and without ansofaxine hydrochloride treatment for 5 days $^{ns}p > 0.05$, $^{*}p < 0.05$, $^{**}p < 0.01$.

2.7 Detection of neurotransmitters (5-HT, DA and NA/NE)

Cells (2 × 105 cells/well) are inoculated into 6-well plates. After 24 h of incubation, the cells were treated with 40 uM ansofaxine hydrochloride or solvent control. After 48 h, the cell supernatant was collected and then assayed by using ELISA. Mice were executed after ansofaxine hydrochloride treatment for 5 days, peripheral blood was collected, centrifuged at 3,000 rpm for 5 min, and the neurotransmitter levels of serum were measured by ELISA.

2.8 Statistical analysis

Two-tailed Student's t-test, one-way ANOVA and Log-rank test were used to compare statistical differences between groups. p-value < 0.05 was statistically significant.

3 Results

3.1 Comparison of fluoxetine, ansofaxine hydrochloride and amitifadine hydrochloride for inhibitory effect in various colon cancer cell lines

Here, we chose fluoxetine and two TRIs, ansofaxine hydrochloride and amitifadine hydrochloride, as subjects of study. The inhibitory effect of fluoxetine, ansofaxine hydrochloride and amitifadine hydrochloride on different types of colon cancer cells were assayed by CCK8. For human colon cancer cell lines (HCT116, SW620), the dates suggested that ansofaxine hydrochloride and amitifadine hydrochloride inhibited the cell proliferation in a dose-dependent manner such as fluoxetine (Figures 1B, D, F, H, K, M). We then compared the inhibitory effects of the drugs on mouse colon cancer cell lines (CT26, MCA38). The data showed that all drugs inhibited the

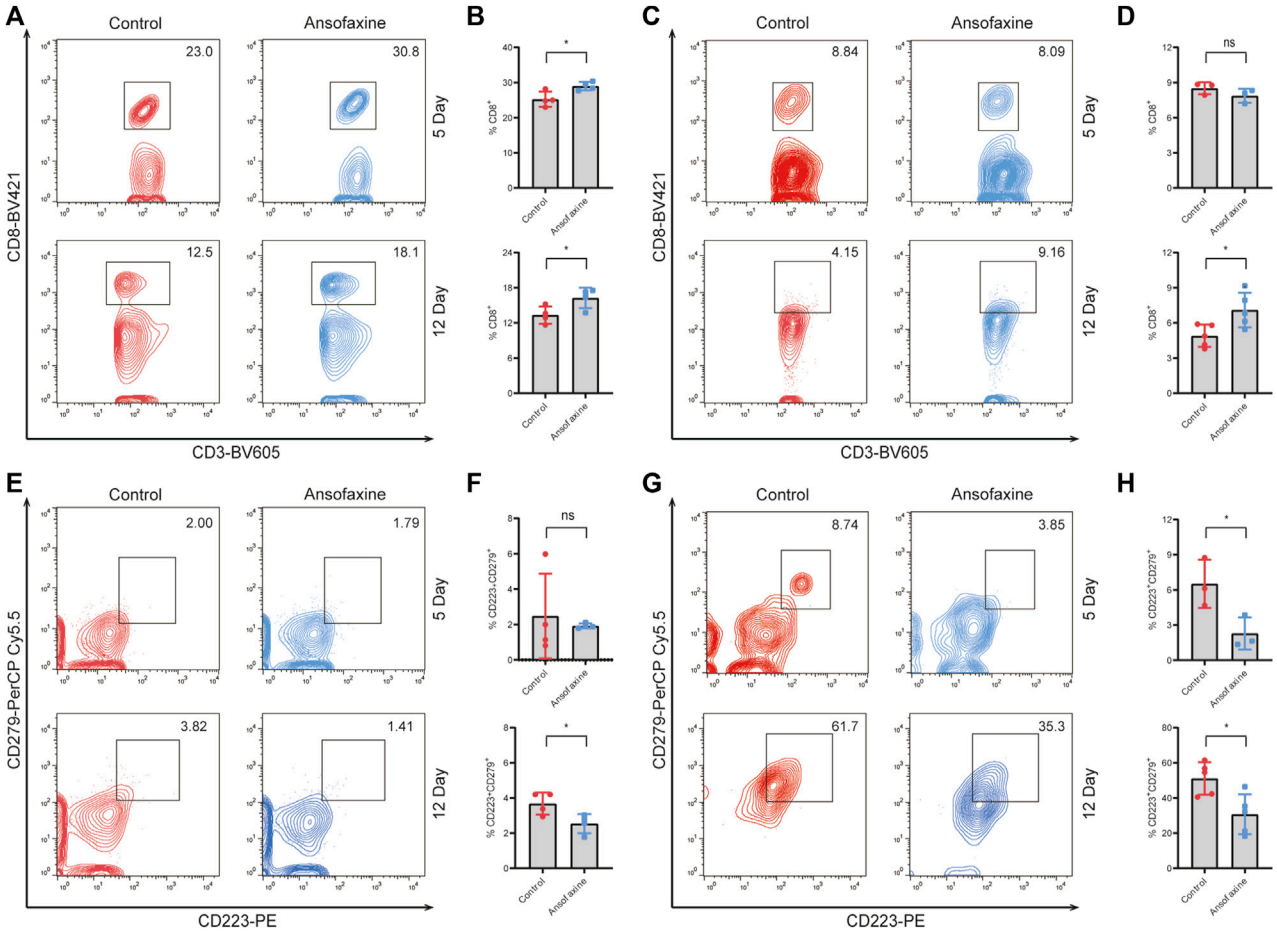

FIGURE 4
Effects of ansofaxine hydrochloride on CD8$^+$ T and exhausted CD8$^+$ T *in Vivo*. **(A, B)** The percentages of CD8$^+$ in CD3$^+$T cells in spleen on days 5 and 12 after ansofaxine hydrochloride administration (n = 4). **(C, D)** The percentages of CD8$^+$ in CD3$^+$T cells in tumor on days 5 (n = 3) and 12 (n = 4) after ansofaxine hydrochloride administration. **(E, F)** The percentages of CD223$^+$CD279$^+$ in CD8$^+$T cells in spleen on days 5 and 12 after ansofaxine hydrochloride administration (n = 4). **(G, H)** The percentages of CD223$^+$CD279$^+$ in CD8$^+$T cells in tumor on days 5 (n = 3) and 12 (n = 5) after ansofaxine hydrochloride administration. Data were expressed as mean ± SD. $^{ns}p > 0.05$, $^*p < 0.05$.

growth of CT26 and MCA38 (Figures 1A, C, E, G, J, L). Therefore, we thought that two TRIs have the antitumor activity *in vitro* such as fluoxetine.

3.2 TRIs induced apoptosis of multiple colon cancer cell lines

To investigate the mechanism by which TRIs inhibit tumor cells, we focused on the cell apoptosis. The proportion of apoptotic cells assessed by flow cytometry. Firstly, we found that ansofaxine hydrochloride and amitifadine hydrochloride could induce apoptosis of CT26 and HCT116 cells in a dose-dependent way (Figures 2A, C), with a significant increase in the proportion of apoptotic cells (Figures 2B, D). In addition, the apoptosis of MCA38 and SW620 cell lines was also induced by ansofaxine hydrochloride and amitifadine hydrochloride in a dose-dependent manner (Supplementary Figure S1). On account of the inhibitory effect of ansofaxine hydrochloride on colon cancer cells was stronger than that of amitifadine hydrochloride, we chose ansofaxine hydrochloride for further study.

3.3 Ansofaxine hydrochloride inhibited tumor growth

Here, we focused on the effects of ansofaxine hydrochloride on the body's immune system, so we choose mouse CT26 colon cancer cells which are more sensitive to it, are selected for further study. Here, we successfully established CT26 colon cancer mouse model (Figure 3A). Treatment was started when the tumor volume reached 100 mm^3. Ansofaxine hydrochloride was administered by gavage. Survival analysis showed that ansofaxine hydrochloride improved survival in the CT26 model (Figure 3B). The tumor volume of control group was significantly larger than that of ansofaxine hydrochloride group (Figures 3C–E), there was no change in mouse weight (Figures 3F–H). These results suggest that ansofaxine hydrochloride has anticancer ability *in vivo*.

Next, we investigated the effects of ansofaxine hydrochloride on neurotransmitter secretion. First, we investigated whether CT26 cells secrete neurotransmitters *in vitro*. The results showed that CT26 cells did not secrete dopamine (Below the lower detection line), secreted small amounts of 5-hydroxytryptamine (5-HT) and

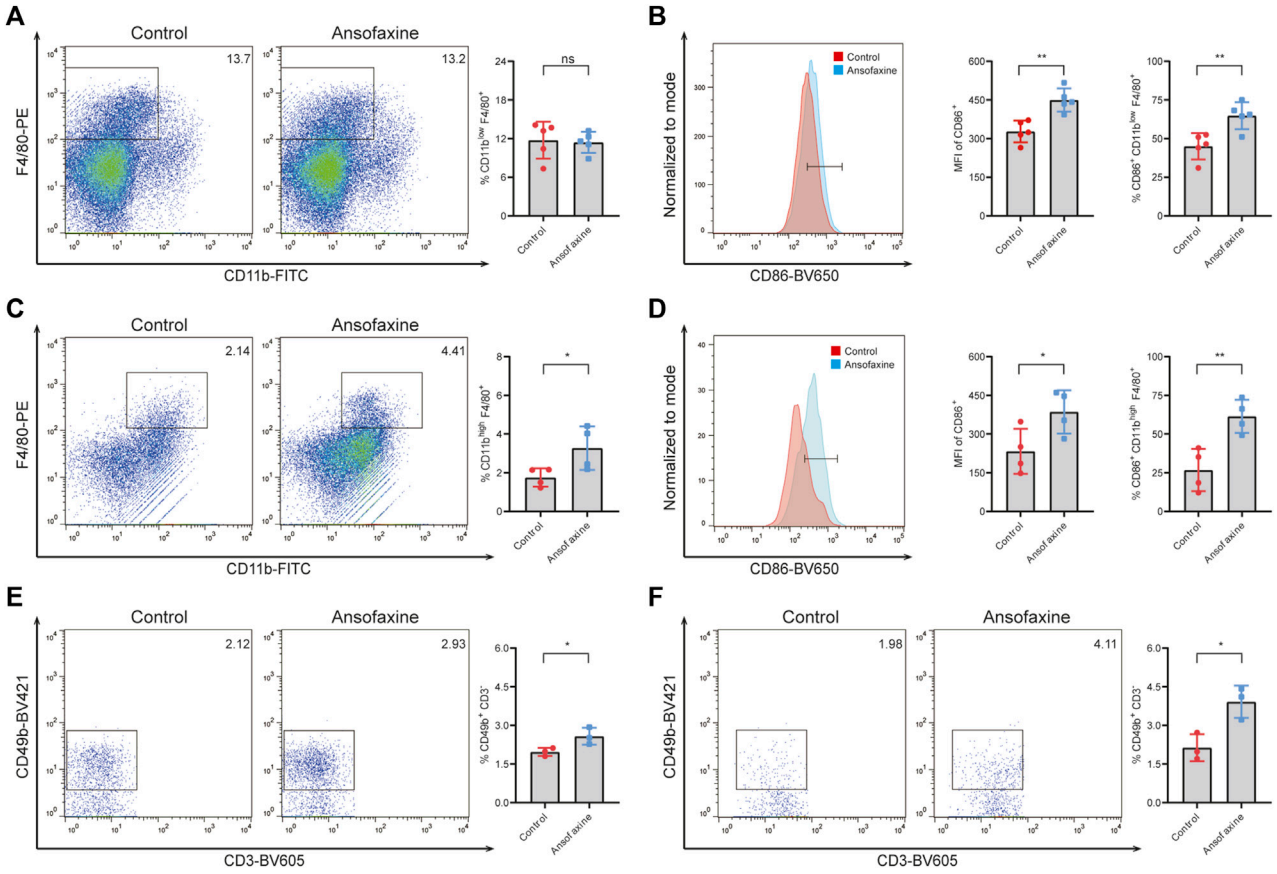

FIGURE 5
Effects of ansofaxine hydrochloride on M1 and NK cells *in Vivo*. **(A)** The percentages of CD11b^{low} F4/80$^+$ M cells in CD45$^+$ cells in the spleens on days 5 after ansofaxine hydrochloride administration (n = 5). **(B)** The percentages and MFI of CD86$^+$ in M cells in the spleens on days 5 after ansofaxine hydrochloride administration (n = 5). **(C)** The percentages of CD11b^{high} F4/80$^+$ M cells in CD45$^+$ cells in the tumor tissues on days 5 after ansofaxine hydrochloride administration (n = 4). **(D)** The percentages and MFI of CD86$^+$ M1 cells in M cells in the tumor tissues on days 5 after ansofaxine hydrochloride administration (n = 4). **(E)** The percentages of CD49b$^+$ CD3$^-$ NK cells in CD45$^+$ cells in spleens on days 5 after ansofaxine hydrochloride administration (n = 3). **(F)** The percentages of CD49b$^+$ CD3$^-$ NK cells in CD45$^+$ cells in tumor on days 5 after ansofaxine hydrochloride administration (n = 3). Data were presented as mean ± SD. $^{ns}p > 0.05$, $^*p < 0.05$, $^{**}p < 0.01$.

norepinephrine (NA/NE), which were not affected by treatment with ansofaxine hydrochloride *in vitro* (Figure 3I). We then investigated the effects of ansofaxine hydrochloride on neurotransmitters *in vivo*. After 5 days of ansofaxine hydrochloride treatment, DA was significantly elevated, 5-HT decreased but did not reach a statistical difference, and there was no significant difference in NA/NE in the serum of the mice.

3.4 Ansofaxine hydrochloride enhanced the levels of CD8$^+$ T cells, inhibited their dysfunction *in vivo*

Next, we explored the influence of ansofaxine hydrochloride therapy on the activity and phenotype of T cells. Mice bearing tumors were executed on days 5 and 12 post treatment initiation, and spleens and tumors were extracted for flow cytometry analysis. The results showed a significant increase in the number of CD8$^+$ T cells in spleens on days 5 and 12 after ansofaxine hydrochloride administration (Figures 4A, B), while intra-tumoral CD8$^+$ T cells no significant change on days 5 after treatment, and significant increased on days 12 after treatment (Figures 4C, D). In addition, the exhausted [programmed death receptor 1 (PD-1)/CD279 and lymphocyte activation gene 3 (LAG3)/CD223] markers showed reduced rates in tumors and spleens in the ansofaxine hydrochloride treatment group (Figures 4E–H).

3.5 Ansofaxine hydrochloride enhanced the levels of M1 and NK cells *in vivo*

Moreover, there was no change in CD11b^{low} F4/80$^+$ macrophages in spleen (Figure 5A), but there was a significant increase in M1 (CD11b^{low} F4/80$^+$ CD86$^+$) (Figure 5B) in spleen on days 5 after ansofaxine hydrochloride treatment. There was significant increase in CD11b^{high} F4/80$^+$ macrophages (Figure 5C) and M1 (CD11b^{high} F4/80$^+$ CD86$^+$) (Figure 5D) in tumor. We also found that the percentages of NK (CD49b$^+$ CD3$^-$) cells in spleen and tumor significant increased on days 5 after ansofaxine hydrochloride treatment (Figures 5E–F).

3.6 Combination therapy with ansofaxine hydrochloride and anti-TNFR2 potently inhibits the growth of CT26 tumors

To investigate the effect of ansofaxine hydrochloride on the efficiency of anti-TNFR2 treatment of colon cancer in mice, we

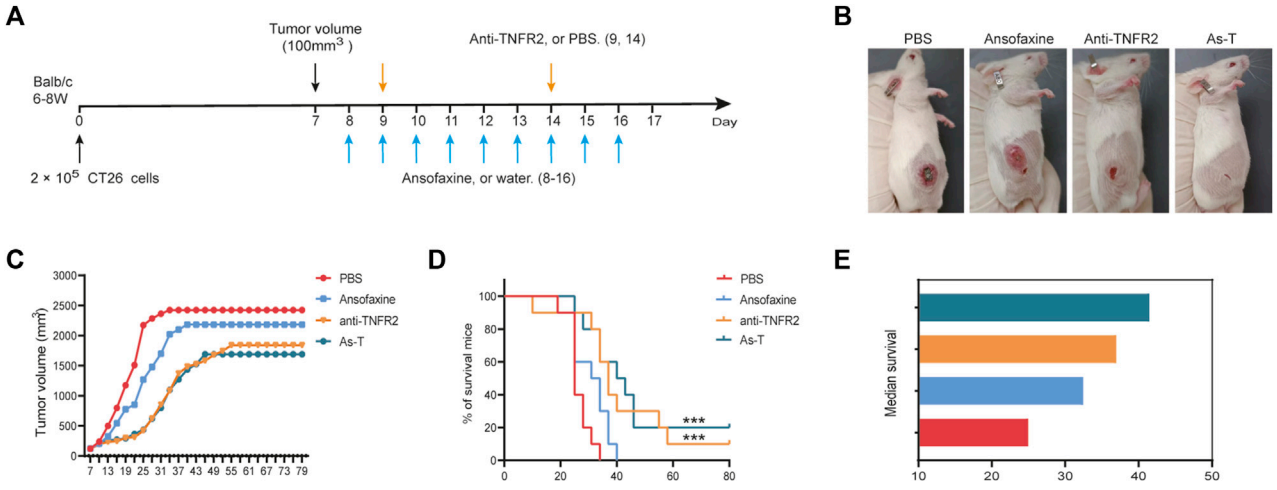

FIGURE 6
Combination therapy with ansofaxine hydrochloride and anti-TNFR2 potently inhibits the growth of CT26 tumors. **(A)** Schematic diagram of the experimental program. When tumor volume reached 100 mm^3 (day 7), mice were then treated with water or ansofaxine hydrochloride (8–16, 300 ug/100 ul/mouse), PBS or anti-TNFR2 (9,14, 200 ug/200 ul/mouse). **(B)** Representative images of mouse on day 19. **(C)** Average growth curves of the tumors (n = 10). **(D)** Mouse survival curves (n = 10). **(E)** Median survival. $^{ns}p > 0.05$, $^{***}p < 0.001$.

treated tumor-bearing mice with anti-TNFR2 and ansofaxine hydrochloride (Figure 6A). Anti-TNFR2 were administered by intraperitoneal injection. The combination of ansofaxine hydrochloride and anti-TNFR2 (As-T) effectively inhibited the growth of colon tumors (Figures 6B, C), 20% of mice were tumor-free and survived for 80 days, which is the end of the experiment (Figure 6D). Although the tumor growth curve of As-T therapy was not significantly different compared with anti-TNFR2 alone, the median survival of tumor-bearing mice was longer after As-T therapy (41.5 days) compared with anti-TNFR2 (37 days) or ansofaxine hydrochloride (32.5 days) monotherapy (Figure 6E).

3.7 Combination therapy with ansofaxine hydrochloride and anti-TNFR2 increases the proportion of $CD8^+$ and $CD4^+$ T cells in spleen, and reduces the proportion of intra-tumoral Tregs and exhausted $CD8^+$ T cells

To investigate the effects of As-T therapy on mice's systemic immunity and tumor immune microenvironment, we studied the distribution of immune cells in mouse spleens, draining lymph nodes (DLN), and tumors by flow cytometry. The proportion of $CD8^+$T and $CD4^+$T cells in spleen were significantly increased by treatment with As-T combination therapy, as compared with Anti-TNFR2 alone (Figures 7A, C). However, there was no significant change in DLN. The proportion of tumor-infiltrating CD8 T cells was no significantly change, and tumor-infiltrating $CD4^+$T cells was significantly decrease by treatment with As-T combination therapy (Figures 7A, C). Furthermore, As-T combination therapy also significantly reduced the amount of $CD223^+$ and $CD279^+$ on intra-tumor $CD8^+$T cells (Figure 7B), and $CD4^+FOXP3^+$ Treg cells (Figure 7D). Thus, our data suggest that As-T combination therapy enhanced mice's systemic immunity, and reduced the ratio of intra-tumor exhausted $CD8^+$T cells and Treg cells, thereby enhanced anti-tumor immune responses.

3.8 Combination therapy with ansofaxine hydrochloride, HMGN1 and 3M-052 potently inhibits the growth of CT26 tumors

In addition, we also evaluated the efficacy of ansofaxine hydrochloride combination with immunotherapy targeting dendritic cells. Our previous studies have shown that HMGN1 [toll-like receptor (TLR) 4 agonist] and 3M-052 (TLR7/8 agonist) can work synergistically to stimulate dendritic cell activation (Zhu et al., 2023). HMGN1 and 3M-052 by intratumoral injection (Figure 6A). The combination of ansofaxine hydrochloride and HMGN1 and 3M-052 (As-NM) effectively inhibited the growth of colon tumors (Figures 8B, C), and one mouse was tumor-free and survived for 80 days (Figure 8D). Survival of As-NM treatment was significantly longer than that of control (Figure 8E).

3.9 Re-challenge experiment in tumor-free mice

To determine whether the tumor-free mice produced long-term tumor-specific systemic immunity, CT26 cells were reinoculated subcutaneously into the left abdomen of tumor-free mice, and 4T1 breast cancer cells were inoculated into their right abdomen. Following the same method, CT26 cells were injected subcutaneously into naïve mice as control. And unsurprisingly, on day 28 after inoculation, all naïve mice developed CT26 tumors, all tumor-free mice developed 4T1 tumors, but none of these mice developed CT26 tumors (Figure 9B). These data show that the tumor-free mice after treatment produced long-term development of tumor antigen-specific immunity.

4 Discussion

In this study, we confirmed that ansofaxine hydrochloride had antitumor effects, possibly by enhancing anti-tumor immune response. Ansofaxine hydrochloride enhanced the effect of

10.3389/fphar.2023.1286061

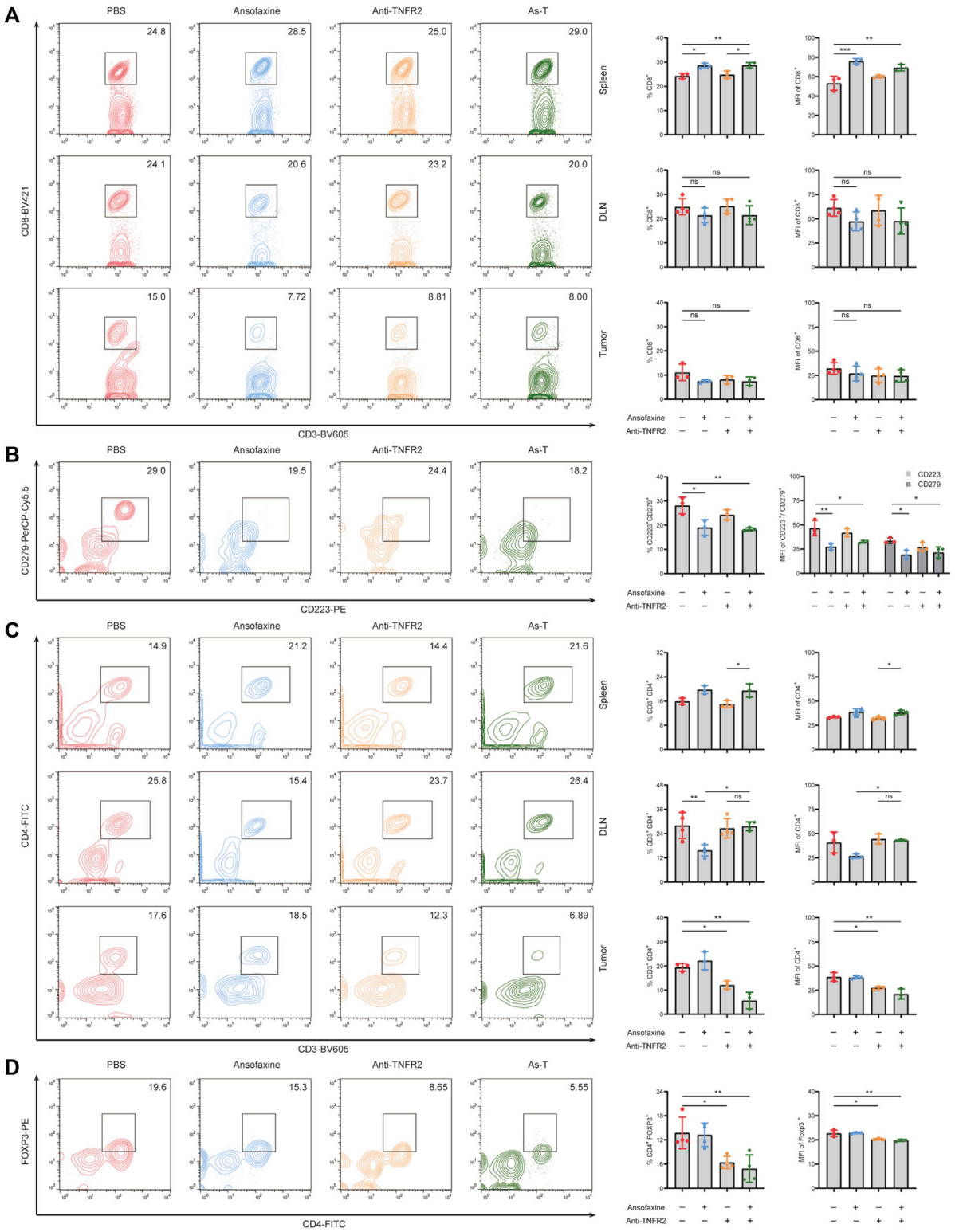

FIGURE 7
Effects of ansofaxine hydrochloride in combination with anti-TNFR2 on $CD8^+$ and $CD4^+$ T cells. **(A)** The percentages and MFI of $CD8^+$ T cells in $CD3^+$ cells in spleen, DLN and tumor (n = 3). **(B)** The percentages and MFI of $CD223^+$ $CD279^+$ cells in $CD8^+$ T cells in tumor (n = 3). **(C)** The percentages and MFI of $CD3^+CD4^+$ in $CD45^+$ cells in spleen, DLN and tumor (n = 3). **(D)** The percentages and MFI of Tregs in $CD3^+$ cells in tumor (n = 3). Data were presented as mean ± SD. $^{ns}p > 0.05$, $^*p < 0.05$, $^{**}p < 0.01$.

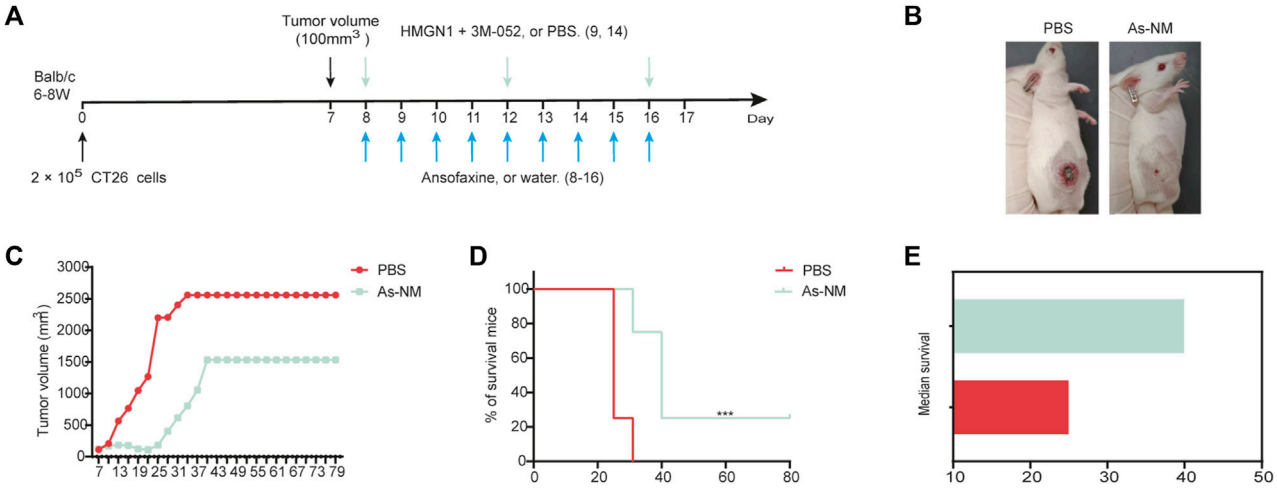

FIGURE 8
(A) Schematic diagram of the experimental program. When tumor volume reached 100 mm^3 (day 7), mice were then treated with water or ansofaxine hydrochloride (8–16, 300 ug/100 ul/mouse), PBS or HMGN1 (8,12,16, 0.5 ug/50 ul/mouse) and 3M-052 (8,12,16, 20 ug/50 ul/mouse). **(B)** Representative images of mouse on day 19. **(C)** Average growth curves of the tumors (n = 4). **(D)** Mouse survival curves (n = 4). **(E)** Median survival. $^{**}p < 0.01$.

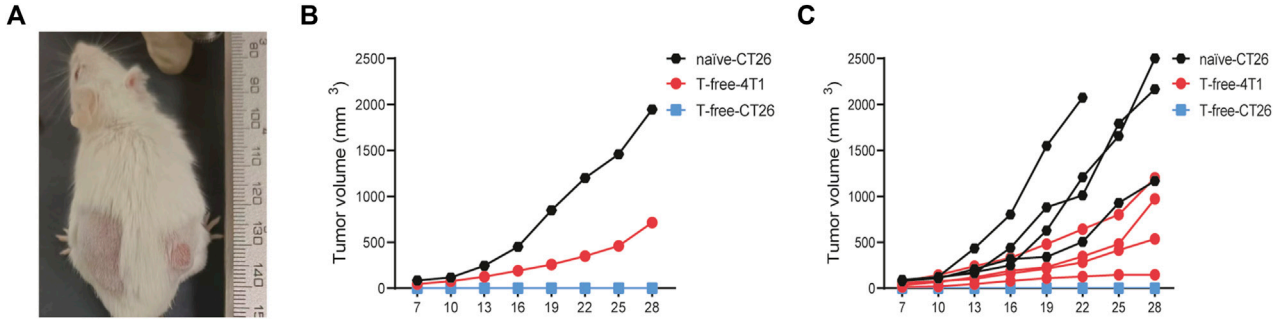

FIGURE 9
(A) Representative images of tumor-free mice rechallenged. **(B, C)** Growth curves of the tumors of tumor-free (T-free) and naïve mice (n = 4).

immunotherapy with Anti-TNFR2 against CT26 tumors, which was attributable to the reduction in Treg quantity and the recovery of intra-tumor $CD8^+$T cells function.

$CD8^+$T cells are key effector cells of anti-tumor immunity, however, immunosuppressive and stromal cells in the tumor microenvironment (TME) may regulate intercellular signaling, and the expression levels of cytokines and receptors, ultimately leading to the development of their "exhausted" state (Dolina et al., 2021). Exhausted $CD8^+$T cells are lowly responsive to tumor cells and may lead to poor response to ICB therapy, characterized by impaired proliferation and viability, and co-expression of various inhibitory receptors (Wherry and Kurachi, 2015). In general, the greater the number of inhibitory receptors, including lymphocyte activation gene 3 (Lag-3), T-cell immunoglobulin domain and mucin domain protein 3 (Tim-3), CD244, CD160, T-cell immunoreceptor with immunoglobulin and ITIM domains (TIGIT), and cytotoxic T-lymphocyte-associated protein 4 (CTLA-4), co-expressed by exhausted $CD8^+$T cells, the more severe the exhaustion. These co-expression patterns are mechanically correlated, and blocking multiple inhibitory receptors simultaneously synergistically inhibits $CD8^+$T-cell exhaustion. Some researchers have suggested that peripheral cells may be active reservoirs of exhausted $CD8^+$T cells functional precursors prior to physical tumor invasion and chronic exposure to tumor-derived antigens (Dolina et al., 2021). Comparing the tumor with normal neighboring tissue and peripheral blood by scTCR-Seq, it was found that the ICB appeared to primarily mobilize effector $CD8^+$T cells from the periphery into the tumor (Wu et al., 2020). In here, we demonstrated that ansofaxine hydrochloride significantly increased the number of peripheral $CD8^+$T cells, and reducing the percentages of intra-tumor exhausted $CD8^+$T cells. Interestingly, the number of $CD8^+$ T cells in the tumor no significantly change after 5 days of ansofaxine hydrochloride treatment, which may be increased consumption of $CD8^+$ T cells due to the restoration of anti-tumor effects. Moreover, we also found a significantly increased ratio of M1 macrophages and NKs in spleen and tumor after ansofaxine hydrochloride treatment. In summary,

we concluded that ansofaxine hydrochloride remodeled the TME and enhanced the anti-tumor immunity in mice. Studies have reported that a variety of neurotransmitters, such as 5-HT, DA and NA/NE, are involved in the regulation of the immune system (Arreola et al., 2015; Arreola et al., 2016; Eduardo et al., 2019). Dopamine expression was positively correlated with $CD8^+$ T-cell infiltration and survival in CRC patients. Dopamine treatment promoted the antitumor activity of $CD8^+$ T cells by the dopamine-DRD5 signaling pathway, and inhibited CRC growth in mice (Chen et al., 2022). 5-HT in peripheral blood impairs the function of effector CD8 T cells in tumors, and 5-HT depletion reduces the growth of pancreatic and colorectal tumors and increases intratumoral infiltration of CD8 T cells in wild-type mice (Schneider et al., 2021). In our study, DA was significantly elevated and 5-HT was decreased in peripheral blood of mice after ansofaxine hydrochloride treatment, which may explain the enhancement of antitumor immunity.

Tregs are a subset of $CD4^+$T cells with significant immunosuppressive effects, characterized by expression of FOXP3(37). A growing body of research suggests that Tregs are key mediators of the tumor immunosuppressive microenvironment (Takeuchi and Nishikawa, 2016). Tregs secrete immunosuppressive cytokines, inhibit the synthesis and secretion of inflammatory factors, downregulate the expression of major histocompatibility complex class II (MHC II) molecules, and inhibit the expression of co-stimulatory molecules (CD80, CD86) on antigen presenting cells (APC), and finally inhibit T-cell response (Zhang et al., 2021). Removal or inactivation of Tregs in TME is considered as a cancer immunotherapy strategy to activate tumor immunity (Govindaraj et al., 2013; Whiteside, 2018). The most inhibitory Tregs express excess TNFR2, which plays a critical role in the activation and expansion of Tregs, on their surfaces in human cancers (Govindaraj et al., 2013; Govindaraj et al., 2014; Liao et al., 2023). Recent studies have demonstrated that anti-TNFR2, as a potential cancer immunotherapy, produces powerful anti-tumor effects and long-lasting protective memory in a variety of mouse tumor models, and that the mechanism of enhancing anti-tumor immunity may be through the disinhibition of Tregs and exhausted $CD8^+$T cells (Torrey et al., 2019; He et al., 2023; Liao et al., 2023). However, other studies have reported that anti-TNFR2 mediates potent co-stimulation of FC-dependent T cells, leading to expansion and improved function of $CD8^+$ T cells, without causing significant depletion of Tregs (Tam et al., 2019). In this study, we found that anti-TNFR2 significantly reduced the abundance of Tregs, while the reduction in exhausted $CD8^+$T was not statistically different compared with control.

In clinical treatment, the combination of anti-cancer drugs has become routine, and an important consideration is that one treatment may regulate the efficacy of the other. Therefore, we further investigated the animal experimental study of ansofaxine hydrochlorid combined with anti-TNFR2 to confirm whether ansofaxine hydrochlorid has a synergistic anti-tumor effect. Our data showed that ansofaxine hydrochloride not only did not impair the inhibition of Tregs by anti-TNFR2, but also enhanced the reduction of intratumoral exhausted $CD8^+$T. In addition, the combination therapy As-T enhanced the number of peripheral $CD8^+$T and $CD4^+$T cells, compared with anti-TNFR2 therapy alone. This provides new theories and therapeutic amplification for cancer treatment. In addition, we explored the effects of a combination therapy of ansofaxine hydrochlorid and dendritic cell-targeting immunotherapy (As-NM), which resulted in complete tumor elimination in one in four mice, and produced long-term development of tumor antigen-specific immunity. Overall, our work suggests that combined ansofaxine hydrochloride may be a promising approach to cancer treatment.

5 Conclusion

In summary, our data reveal the role of ansofaxine hydrochloride in modulating the anti-tumor immunity. Our results support that exhausted $CD8^+$T is an important potential mechanism by which ansofaxine hydrochloride activates anti-tumor immunity and enhances anti-tumor effects of anti-TNFR2. In addition, the study presented here suggests that strategic combination with ansofaxine hydrochloride may enhance the efficacy of tumor immunotherapy in colon cancer.

Data availability statement

The original contributions presented in the study are included in the article/Supplementary Material, further inquiries can be directed to the corresponding author.

Ethics statement

The animal study was approved by Ethics Committee of Guizhou Provincial People's Hospital. The study was conducted in accordance with the local legislation and institutional requirements.

Author contributions

QJ: Conceptualization, Data curation, Formal Analysis, Investigation, Methodology, Project administration, Validation, Writing–original draft. QW: Data curation, Formal Analysis, Investigation, Methodology, Software, Visualization, Writing–original draft. YuN: Conceptualization, Investigation, Project administration, Software, Supervision, Writing–original draft, Writing–review and editing. JL: Investigation, Methodology, Project administration, Supervision, Visualization, Writing–review and editing. XZ: Conceptualization, Formal Analysis, Funding acquisition, Project administration, Supervision, Writing–review and editing. LZ: Investigation, Software, Validation, Writing–review and editing. HG: Methodology, Project administration, Supervision, Writing–review and editing. LL: Conceptualization, Methodology, Project administration, Supervision, Writing–review and editing. CW: Conceptualization, Methodology, Software, Writing–review and editing. SC: Methodology, Visualization, Writing–review and editing. MW: Methodology, Visualization, Writing–review and editing. HY: Methodology, Visualization, Writing–review and editing. HL: Methodology, Software, Visualization, Writing–review and editing. RP: Methodology, Visualization, Writing–original draft. QJ: Software, Visualization, Writing–review and editing. YiN: Conceptualization, Formal Analysis, Funding acquisition,

Investigation, Methodology, Project administration, Resources, Supervision, Writing–review and editing.

Funding

The authors declare financial support was received for the research, authorship, and/or publication of this article. This work was supported by the National Natural Science Foundation of China (82060308), National Key Laboratory of Respiratory Diseases (SKLRD-OP-202208), Guizhou Provincial Science and Technology Projects (GPPH-NSFC-2020-6; GPPH-NSFC-2020-7; GCC [2022]037-1), Guizhou Immunotherapy Research Talent Base (RCJD 2018-11), Non-profit Central Research Institute Fund of Chinese Academy of Medical Sciences (2019PT320003) and funding from Ministry of Human Resources and Social Security of the People's Republic of China.

Acknowledgments

The authors want to thank the Central Laboratory of Guizhou Provincial People's Hospital for its help in the research.

Conflict of interest

The authors declare that the research was conducted in the absence of any commercial or financial relationships that could be construed as a potential conflict of interest.

Publisher's note

Supplementary material

The Supplementary Material for this article can be found online at: https://www.frontiersin.org/articles/10.3389/fphar.2023.1286061/full#supplementary-material

References

Arreola, R., Alvarez-Herrera, S., Pérez-Sánchez, G., Becerril-Villanueva, E., Cruz-Fuentes, C., Flores-Gutierrez, E. O., et al. (2016). Immunomodulatory effects mediated by dopamine. *J. Immunol. Res.* 2016, 3160486–3160531. doi:10.1155/2016/3160486

Arreola, R., Becerril-Villanueva, E., Cruz-Fuentes, C., Velasco-Velázquez, M. A., Garcés-Alvarez, M. E., Hurtado-Alvarado, G., et al. (2015). Immunomodulatory effects mediated by serotonin. *J. Immunol. Res.* 2015, 1–21. doi:10.1155/2015/354957

Chen, X., Bäumel, M., Männel, D. N., Howard, O. M. Z., and Oppenheim, J. J. (2007). Interaction of TNF with TNF receptor type 2 promotes expansion and function of mouse CD4+CD25+ T regulatory cells. *J. Immunol.* 179 (1), 154–161. doi:10.4049/jimmunol.179.1.154

Chen, Y., Yan, S.-M., Pu, Z., Feng, J., Tan, L., Li, Y., et al. (2022). Dopamine signaling promotes tissue-resident memory differentiation of CD8+ T cells and antitumor immunity. *Cancer Res.* 82 (17), 3130–3142. doi:10.1158/0008-5472.CAN-21-4084

Di Rosso, M. E., Palumbo, M. L., and Genaro, A. M. (2016). Immunomodulatory effects of fluoxetine: a new potential pharmacological action for a classic antidepressant drug? *Pharmacol. Res.* 109, 101–107. doi:10.1016/j.phrs.2015.11.021

Di Rosso, M. E., Sterle, H. A., Cremaschi, G. A., and Genaro, A. M. (2018). Beneficial effect of fluoxetine and sertraline on chronic stress-induced tumor growth and cell dissemination in a mouse model of lymphoma: crucial role of antitumor immunity. *Front. Immunol.* 9, 1341. doi:10.3389/fimmu.2018.01341

Dolina, J. S., Van Braeckel-Budimir, N., Thomas, G. D., and Salek-Ardakani, S. (2021). CD8+ T cell exhaustion in cancer. *Front. Immunol.* 12, 715234. doi:10.3389/fimmu.2021.715234

Eduardo, C.-R. C., Alejandra, T.-I. G., Guadalupe, D.-R. K. J., Herminia, V.-R. G., Lenin, P., Enrique, B.-V., et al. (2019). Modulation of the extraneuronal cholinergic system on main innate response leukocytes. *J. Neuroimmunol.* 327, 22–35. doi:10.1016/j.jneuroim.2019.01.008

Endo, M., Matsui, K., Akaho, R., Mitsui, K., Yan, Y., Imai, Y., et al. (2022). Depressive and anxiety symptoms among Japanese cancer survivors: Japan cancer survivorship research project. *BMC Cancer* 22 (1), 134. doi:10.1186/s12885-022-09215-x

Fritz, J. M., and Lenardo, M. J. (2019). Development of immune checkpoint therapy for cancer. *J. Exp. Med.* 216 (6), 1244–1254. doi:10.1084/jem.20182395

Govindaraj, C., Scalzo-Inguanti, K., Madondo, M., Hallo, J., Flanagan, K., Quinn, M., et al. (2013). Impaired Th1 immunity in ovarian cancer patients is mediated by TNFR2+ Tregs within the tumor microenvironment. *Clin. Immunol.* 149 (1), 97–110. doi:10.1016/j.clim.2013.07.003

Govindaraj, C., Tan, P., Walker, P., Wei, A., Spencer, A., and Plebanski, M. (2014). Reducing TNF receptor 2+ regulatory T cells via the combined action of azacitidine and the HDAC inhibitor, panobinostat for clinical benefit in acute myeloid leukemia patients. *Clin. Cancer Res.* 20 (3), 724–735. doi:10.1158/1078-0432.CCR-13-1576

He, T., Chen, Y., Yang, D., Islam, M. S., Chou, C.-K., Liu, J., et al. (2023). TNFR2 antagonistic antibody induces the death of tumor infiltrating CD4+Foxp3+ regulatory T cells. *Cell Oncol. (Dordr).* 46 (1), 167–177. doi:10.1007/s13402-022-00742-0

Kawano, S., Mitoma, H., Inokuchi, S., Yamauchi, Y., Yokoyama, K., Nogami, J., et al. (2022). TNFR2 signaling enhances suppressive abilities of human circulating T follicular regulatory cells. *J. Immunol.* 208 (5), 1057–1065. doi:10.4049/jimmunol.2100323

Lee, H.-C., Chiu, W.-C., Wang, T.-N., Liao, Y.-T., Chien, I. C., Lee, Y., et al. (2017). Antidepressants and colorectal cancer: a population-based nested case-control study. *J. Affect. Disord.* 207, 353–358. doi:10.1016/j.jad.2016.09.057

Li, P., Yang, Y., Yang, X., Wang, Y., Chou, C.-K., Jiang, M., et al. (2023). TNFR2 deficiency impairs the growth of mouse colon cancer. *Int. J. Biol. Sci.* 19 (4), 1024–1035. doi:10.7150/ijbs.72606

Liao, P., Jiang, M., Islam, M. S., Wang, Y., and Chen, X. (2023). TNFR2 expression predicts the responses to immune checkpoint inhibitor treatments. *Front. Immunol.* 14, 1097090. doi:10.3389/fimmu.2023.1097090

Liu, J., Deng, G.-H., Zhang, J., Wang, Y., Xia, X.-Y., Luo, X.-M., et al. (2015). The effect of chronic stress on anti-angiogenesis of sunitinib in colorectal cancer models. *Psychoneuroendocrinology* 52, 130–142. doi:10.1016/j.psyneuen.2014.11.008

Marcinkute, M., Afshinjavid, S., Fatokun, A. A., and Javid, F. A. (2019). Fluoxetine selectively induces p53-independent apoptosis in human colorectal cancer cells. *Eur. J. Pharmacol.* 857, 172441. doi:10.1016/j.ejphar.2019.172441

Mi, W., Yang, F., Li, H., Xu, X., Li, L., Tan, Q., et al. (2022). Efficacy, safety, and tolerability of ansofaxine (LY03005) extended-release tablet for major depressive disorder: a randomized, double-blind, placebo-controlled, dose-finding, phase 2 clinical trial. *Int. J. Neuropsychopharmacol.* 25 (3), 252–260. doi:10.1093/ijnp/pyab074

Moatti, A., Debesset, A., Pilon, C., Beldi-Ferchiou, A., Leclerc, M., Redjoul, R., et al. (2022). TNFR2 blockade of regulatory T cells unleashes an antitumor immune response after hematopoietic stem-cell transplantation. *J. Immunother. Cancer* 10 (4), e003508. doi:10.1136/jitc-2021-003508

Schneider, M. A., Heeb, L., Beffinger, M. M., Pantelyushin, S., Linecker, M., Roth, L., et al. (2021). Attenuation of peripheral serotonin inhibits tumor growth and enhances immune checkpoint blockade therapy in murine tumor models. *Sci. Transl. Med.* 13 (611), eabc8188. doi:10.1126/scitranslmed.abc8188

Shao, L., Li, W., Xie, Q., and Yin, H. (2014). Triple reuptake inhibitors: a patent review (2006 - 2012). *Expert Opin. Ther. Pat.* 24 (2), 131–154. doi:10.1517/13543776.2014.859676

Sharma, H., Santra, S., and Dutta, A. (2015). Triple reuptake inhibitors as potential next-generation antidepressants: a new hope? *Future Med. Chem.* 7 (17), 2385–2406. doi:10.4155/fmc.15.134

Sommershof, A., Scheuermann, L., Koerner, J., and Groettrup, M. (2017). Chronic stress suppresses anti-tumor TCD8+ responses and tumor regression following cancer immunotherapy in a mouse model of melanoma. *Brain Behav. Immun.* 65, 140–149. doi:10.1016/j.bbi.2017.04.021

Sung, H., Ferlay, J., Siegel, R. L., Laversanne, M., Soerjomataram, I., Jemal, A., et al. (2021). Global cancer statistics 2020: GLOBOCAN estimates of incidence and mortality worldwide for 36 cancers in 185 countries. *CA Cancer J. Clin.* 71 (3), 209–249. doi:10.3322/caac.21660

Takeuchi, Y., and Nishikawa, H. (2016). Roles of regulatory T cells in cancer immunity. *Int. Immunol.* 28 (8), 401–409. doi:10.1093/intimm/dxw025

Tam, E. M., Fulton, R. B., Sampson, J. F., Muda, M., Camblin, A., Richards, J., et al. (2019). Antibody-mediated targeting of TNFR2 activates CD8+ T cells in mice and promotes antitumor immunity. *Sci. Transl. Med.* 11 (512), eaax0720. doi:10.1126/scitranslmed.aax0720

Torrey, H., Khodadoust, M., Tran, L., Baum, D., Defusco, A., Kim, Y. H., et al. (2019). Targeted killing of TNFR2-expressing tumor cells and Tregs by TNFR2 antagonistic antibodies in advanced Sézary syndrome. *Leukemia* 33 (5), 1206–1218. doi:10.1038/s41375-018-0292-9

Tran, P., Skolnick, P., Czobor, P., Huang, N. Y., Bradshaw, M., McKinney, A., et al. (2012). Efficacy and tolerability of the novel triple reuptake inhibitor amitifadine in the treatment of patients with major depressive disorder: a randomized, double-blind, placebo-controlled trial. *J. Psychiatr. Res.* 46 (1), 64–71. doi:10.1016/j.jpsychires.2011.09.003

Vanamee, É. S., and Faustman, D. L. (2017). TNFR2: a novel target for cancer immunotherapy. *Trends Mol. Med.* 23 (11), 1037–1046. doi:10.1016/j.molmed.2017.09.007

Wang, X., Li, B., Kim, Y. J., Wang, Y.-C., Li, Z., Yu, J., et al. (2021a). Targeting monoamine oxidase A for T cell-based cancer immunotherapy. *Sci. Immunol.* 6 (59), eabh2383. doi:10.1126/sciimmunol.abh2383

Wang, Y.-C., Wang, X., Yu, J., Ma, F., Li, Z., Zhou, Y., et al. (2021b). Targeting monoamine oxidase A-regulated tumor-associated macrophage polarization for cancer immunotherapy. *Nat. Commun.* 12 (1), 3530. doi:10.1038/s41467-021-23164-2

Wherry, E. J., and Kurachi, M. (2015). Molecular and cellular insights into T cell exhaustion. *Nat. Rev. Immunol.* 15 (8), 486–499. doi:10.1038/nri3862

Whiteside, T. L. (2018). FOXP3+ Treg as a therapeutic target for promoting anti-tumor immunity. *Expert Opin. Ther. Targets* 22 (4), 353–363. doi:10.1080/14728222.2018.1451514

Wu, T. D., Madireddi, S., de Almeida, P. E., Banchereau, R., Chen, Y.-J. J., Chitre, A. S., et al. (2020). Peripheral T cell expansion predicts tumour infiltration and clinical response. *Nature* 579 (7798), 274–278. doi:10.1038/s41586-020-2056-8

Yan, R., Xia, J., Yang, R., Lv, B., Wu, P., Chen, W., et al. (2019). Association between anxiety, depression, and comorbid chronic diseases among cancer survivors. *Psycho-oncology* 28 (6), 1269–1277. doi:10.1002/pon.5078

Yang, W., Xiao, L., Yuan, Z., Huang, H., Xiang, Y., Liu, Z., et al. (2021a). Anxiety and depression in patients with physical diseases and associated factors: a large-scale field survey in general hospitals in China. *Front. Psychiatry* 12, 689787. doi:10.3389/fpsyt.2021.689787

Yang, Z., Li, Z., Guo, Z., Ren, Y., Zhou, T., Xiao, Z., et al. (2021b). Antitumor effect of fluoxetine on chronic stress-promoted lung cancer growth via suppressing kynurenine pathway and enhancing cellular immunity. *Front. Pharmacol.* 12, 685898. doi:10.3389/fphar.2021.685898

Zhang, L., Pan, J., Chen, W., Jiang, J., and Huang, J. (2020). Chronic stress-induced immune dysregulation in cancer: implications for initiation, progression, metastasis, and treatment. *Am. J. Cancer Res.* 10 (5), 1294–1307.

Zhang, Y., Guo, J., and Jia, R. (2021). Treg: a promising immunotherapeutic target in oral diseases. *Front. Immunol.* 12, 667862. doi:10.3389/fimmu.2021.667862

Zhu, L., Zhang, X., Chen, X., Yang, D., Nie, Y., Pan, R., et al. (2023). Anti-TNFR2 enhanced the antitumor activity of a new HMGN1/3M-052 stimulated dendritic cell vaccine in a mouse model of colon cancer. *Biochem. Biophys. Res. Commun.* 653, 106–114. doi:10.1016/j.bbrc.2023.02.039

frontiers | Frontiers in Pharmacology

TYPE Case Report
PUBLISHED 01 February 2024
DOI 10.3389/fphar.2024.1295134

OPEN ACCESS

EDITED BY
Nur Akmarina Mohd Said,
University of Malaya, Malaysia

REVIEWED BY
Haizhou Lou,
Zhejiang University, China
Ming Yi,
Zhejiang University, China

*CORRESPONDENCE
Ji Ma,
majimrn@163.com

†These authors have contributed equally to this work

RECEIVED 15 September 2023
ACCEPTED 15 January 2024
PUBLISHED 01 February 2024

CITATION
Zheng L, Sun L and Ma J (2024), Favorable response to PD-1 inhibitor plus chemotherapy as first-line treatment for metastatic gastric mixed neuroendocrine-non-neuroendocrine tumor: a case report.
Front. Pharmacol. 15:1295134.
doi: 10.3389/fphar.2024.1295134

Favorable response to PD-1 inhibitor plus chemotherapy as first-line treatment for metastatic gastric mixed neuroendocrine-non-neuroendocrine tumor: a case report

Lingnan Zheng[1†], Lingqi Sun[2†] and Ji Ma[1*]

[1]Abdominal Oncology Ward, Division of Medical Oncology, Cancer Center, West China Hospital, Sichuan University, Chengdu, China, [2]Department of Neurology, The Air Force Hospital of Western Theater Command, Chengdu, Sichuan, China

Gastric mixed neuroendocrine-non-neuroendocrine tumor (MiNEN), a rare malignancy, currently has no standard treatment. Here, we report a patient with pathologically confirmed gastric MiNEN following radical surgery with rapid postoperative distant tumor recurrence. Immunofluorescence results suggested intensive lymphocyte infiltration in the tumor. The programmed death receptor ligand 1 (PD-L1) immunohistochemistry 22C3 pharmDx assay showed tumor proportion score was 5% and combined positive score was 10. After 6 cycles of treatment with etoposide and cisplatin in combination with toripalimab, efficacy was assessed as a complete response. Our report shows that for gastric MiNEN patients with high expression of PD-L1, chemotherapy combined with immune checkpoint inhibitors may achieve more significant efficacy.

KEYWORDS

gastric MiNEN, immunotherapy, immune checkpoint inhibitors, PD-L1, chemotherapy

Introduction

Mixed neuroendocrine-non-neuroendocrine tumor (MiNEN) is a rare malignancy and has been found in a variety of organs. Gastric MiNEN accounts for less than 1% of all gastric cancers and is characterized by aggressive tumor behavior, high invasiveness, extensive lymph node dissemination and a poor prognosis (Ramos et al., 2021). However, due to the rarity of the disease, there is currently no standard treatment. Here, we report for the first time a gastric MiNEN patient with high expression of programmed death receptor ligand 1 (PD-L1) who rapidly developed disease recurrence and metastasis after radical surgery. The patient received first-line treatment with chemotherapy combined with toripalimab, a monoclonal antibody against human programmed death-1 (PD-1), and the lesions completely disappeared after 6 cycles of treatment without any obvious side effects.

Case report

In March 2022, a 64-year-old man presented to our hospital with abdominal pain. Gastroscopy revealed a neophyte in the cardia, followed by a biopsy indicating poorly

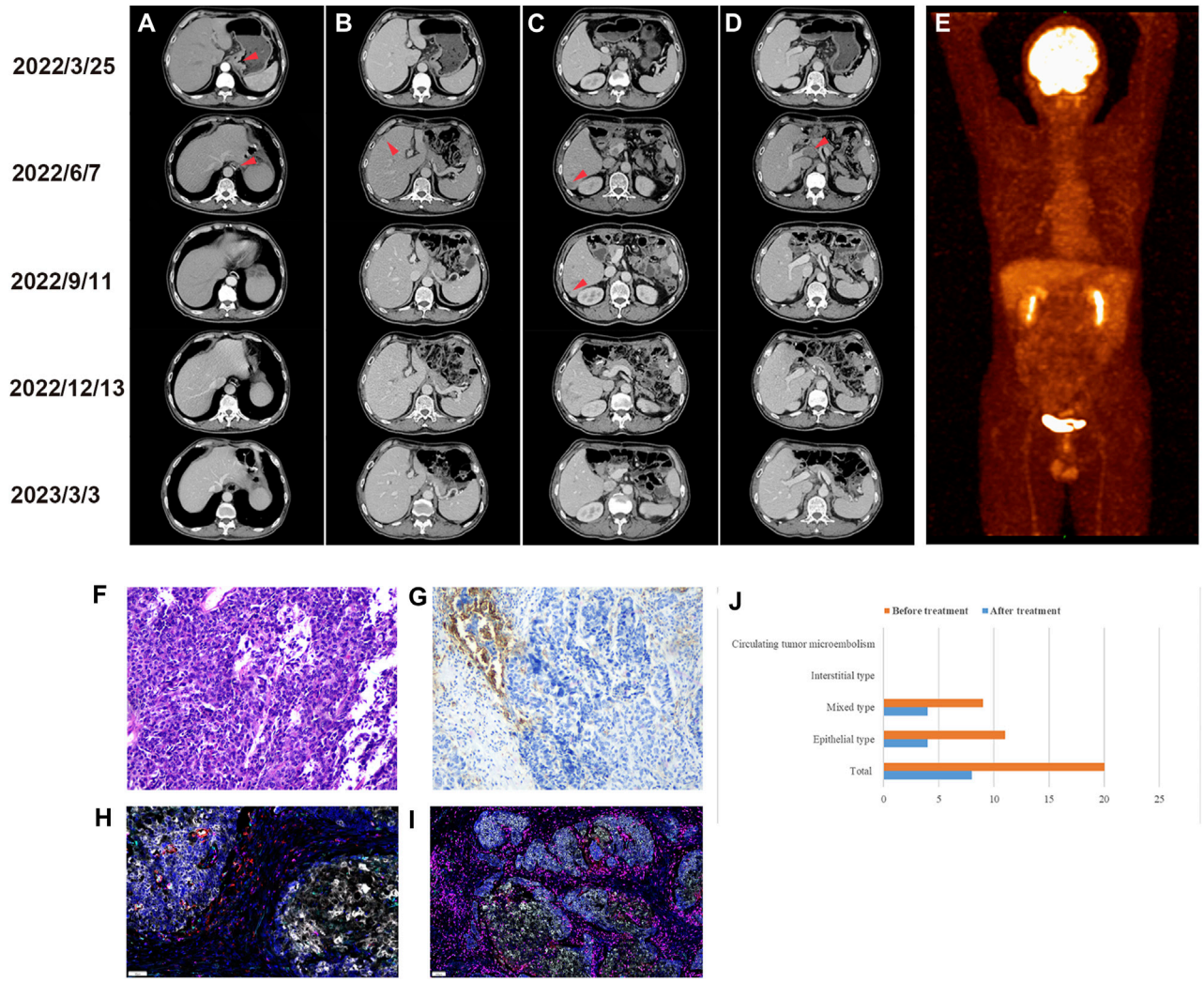

FIGURE 1
Imaging examination before and after treatment. **(A)** Preoperative CT images of cardiac lesions and postoperative anastomosis. **(B)** Preoperative and postoperative CT images of the left liver lobe **(C)** right liver lobe and **(D)** portal vein. **(E)** Positron emission tomography/computed tomography scan after six cycles of treatment. Preoperative examination (2022/3/25), postoperative examination (2022/6/7), after 3 cycles of treatment (2022/9/11), after 6 cycles of treatment (2022/12/13), last follow-up (2023/3/3). Immunohistochemical staining of gastric MiNEN. **(F)** Hematoxylin and eosin staining. **(G)** Immunohistochemistry of PD-L1. Multiple immunofluorescences of gastric MiNEN. Analysis of the tumor microenvironment including PD-1, PD-L1, T cells, tumor-associated macrophages, and natural killer cells was performed. The merging of fluorescence signals is shown. **(H)** Representative immunofluorescence staining for PD-1 (green), PD-L1 (yellow), CD8 (pink), CD68 (cyan) and CD163 (red). **(I)** Representative immunofluorescence staining for CD3 (pink), CD4 (red), CD20 (green), CD56 (cyan) and FoxP3 (yellow). **(J)** Changes in circulating tumor cells before and after treatment.

differentiated adenocarcinoma. An abdominal computed tomography (CT) scan showed uneven thickening of the cardia (Figure 1A). The patient subsequently underwent a radical total gastrectomy. Postoperative pathology suggested that the macroscopic type was Borrmann III. The tumor invaded the subserous connective tissue, without involving the visceral peritoneum. The histological diagnosis was MiNEN (Figure 1F), of which approximately 50% were large cell neuroendocrine carcinomas, 45% were poorly differentiated adenocarcinomas, and approximately 5% were squamous cell carcinomas. Moreover, nineteen lymph nodes were examined, with one node showing lymphatic metastasis and another node showing a gastrointestinal stromal tumor (very low risk). Immunohistochemical analysis revealed pMMR, and positive markers including CDX2, CK20, CD56, synaptophysin (Syn) and chromogranin A (CgA). The average Ki-67 labeling index was 80%. The stage was pT3N1M0. Postoperative detection of human peripheral blood circulating tumor cells (CTC) by multiple mRNA fluorescence *in situ* hybridization indicated that a total of 20 circulating tumor cells were detected, including 11 epithelial types, and 9 mixed types. We recommended postoperative adjuvant therapy for the patient. However, the patient's postoperative condition was not good, so the time for postoperative adjuvant therapy was delayed.

Approximately 2 months after surgery, a CT scan revealed liver metastasis (Figure 1B&C) with portal vein thrombosis (Figure 1D). Subsequently, the PD-L1 immunohistochemistry (IHC) 22C3 pharmDx assay and immunofluorescence (IF) were used to characterize the tumor

TABLE 1 Somatic mutation (driver mutation) identified in this patient.

Gene	Chr	Position	Ref	Alt	Variant classification	Gene_Description
TP53	Chr17	7,577,018	C	A	Splice_Site_mutation	Tumor protein p53
SETX	Chr9	135,156,882	T	A	Missense_mutation	Senataxin
RB1	Chr13	48,951,052	A	T	Splice_Site_mutation	Retinoblastoma 1
CFH	Chr1	196,645,183	C	T	Missense_mutation	Complement factor H
ZNF638	Chr2	71,582,901	T	C	Missense_mutation	Zinc finger protein 638
LRP1B	Chr2	141,114,006	CA	C	Frameshift_deletion	Low-density lipoprotein receptor-related protein 1B
SETX	Chr9	135,156,881	C	CA	Frameshift_insertion	Senataxin
LRP1B	Chr2	141,114,004	C	CT	Frameshift_insertion	Low-density lipoprotein receptor-related protein 1B

Chr: Chromosome, Ref: Reference base, Alt: Alternate base.

microenvironment (TME). The results of the PD-L1 IHC 22C3 assay showed that the tumor proportion score (TPS) was 5% and the combined positive score (CPS) was 10 (Figure 1G). However, the IF PD-L1 (E1L3N) assay showed TPS <1% and CPS <1. In addition, the composition of immune cells in the TME was determined by IF analysis, and the results (Figure 1H&I) showed $CD3^+$, $CD4^+$, and $CD8^+$ T cell infiltration in the tumor parenchyma and stroma (5.09% vs 14.94%, 0.35% vs 0.52%, 0.66% vs 0.30%, respectively). Moreover, the antitumor M1-like tumor-associated macrophages (TAMs) were more dominant than the pro-tumor M2-like phenotype in the tumor parenchyma (0.8% vs 0.06%), reflecting a favorable anti-tumor immune response. In addition, we analyzed the genetic characteristics by whole exon sequencing (WES). A total of 8 tumor driver genes were detected (Table 1), the tumor mutational burden (TMB) was 1.09363, and the frequency of microsatellite instability (MSI) occurrence in somatic cells (total number of MSI sites present in somatic variation/total number of MSI sites present in the sample) was 3.09%.

Subsequently, the patient received etoposide (150mg, ivgtt, d1-3, q3w) and cisplatin (50mg, ivgtt, d1-3, q3w) combined with toripalimab (240mg, ivgtt, d1, q3w) treatment. According to the Response Evaluation Criteria in Solid Tumors version 1.1, efficacy was assessed as partial remission after three cycles of treatment. After six cycles, both CT and positron emission tomography/computed tomography (PET/CT) scans showed complete regression of tumor lesions (Figure 1E). In addition, the number of CTCs was significantly reduced compared with the pre-treatment level (Figure 1J). Subsequently, the patient was treated with a maintenance regimen of S1 combined with toripalimab in December 2022. The patient underwent a CT scan in March 2023, and no signs of a tumor were found. Additionally, no significant immune-related side effects (irAEs) were observed during treatment.

Discussion

Gastrointestinal tumors with both exocrine and neuroendocrine components were first described by Cordier in 1924 (Jiang et al., 2023) and officially renamed MiNEN in the 2019 WHO classification system (Jiang et al., 2023). MiNEN consists of non-neuroendocrine components and neuroendocrine components, one of which must comprise at least 30% of the tumor. At present, the diagnosis of MiNEN is mainly based on immunohistochemical techniques and morphological characteristics. However, the differential diagnosis is difficult when both components are poorly differentiated, so the diagnosis of MiNEN remains challenging (Zhang et al., 2021). Due to its rarity, there is currently no standard treatment. Surgery remains by far the most important treatment option, and studies have shown that even patients with advanced disease may benefit from palliative primary tumor resection (Li et al., 2022). However, the recurrence rate after radical surgery is as high as 45.7% (Lin et al., 2021). In addition, stage T3-4 and lymph node metastasis are independent risk factors for distant recurrence, and the liver is the most common site for distant recurrence. For patients with advanced tumors that progress rapidly, chemotherapy is the preferred treatment.

In this work, the patient was diagnosed with poorly differentiated adenocarcinoma by preoperative biopsy, while the postoperative pathological diagnosis was MiNEN, suggesting that it is difficult to diagnose MiNEN by biopsy alone, and that it is recommended to evaluate pathological specimens after surgical removal of the entire tumor. Moreover, the TME characteristics of tumor-infiltrating lymphocytes (TILs) and PD-L1 positive expression suggest that this patient may benefit from immune checkpoint inhibitors (ICIs). The patient subsequently received treatment with chemotherapy in combination with toripalimab. Efficacy was assessed as CR after 6 cycles of treatment. To date, patients have a progression-free survival time of more than 10 months.

Notably, in this case, both IHC and IF were used to detect the expression of PD-L1, but the results were contradictory. In addition to considering the consistency of PD-L1 antibody clones, the discordant results may also be related to observer variability and tumor expression heterogeneity. The discordance between PD-L1 test results has been reported in previous studies, and such discrepancies may cause patients to miss opportunities to receive appropriate anti-PD-1/PD-L1 therapy (Yeong et al., 2020). Therefore, the analysis of multiple indicators is conducive to the more accurate identification of patients who may benefit from immunotherapy. In addition, the results of IF indicated intensive TILs in the tumor. As is well known, the main function of ICIs is to relieve immune suppression and normalize the function of immune cells, and the therapeutic effect is better for tumors with more infiltrated immune cells. Therefore, it is of great significance to analyze the composition of immune cells in tumors for screening potential beneficiaries of ICIs.

WES is a technique that is widely used clinically. With this technology, we can identify MSI, TMB and some gene mutations, which can help select patients suitable for ICIs. However, the results of WES in this patient did not provide definitive evidence for immunotherapy. In the future, in addition to optimizing sequencing technology, we will need more research to find valuable genes or mutations to guide clinical treatment.

In conclusion, this study is the first to report a patient with PD-L1 high expression gastric MiNEN, and the characteristics of the TME were consistent with adaptive immune resistance. The patient responded favorably to chemotherapy combined with toripalimab, achieving complete regression of the tumor lesion after six cycles of treatment, and no irAEs occurred during treatment. Therefore, this treatment strategy should be considered when treating these rare gastric MiNEN patients with high PD-L1 expression.

Data availability statement

The raw data supporting the conclusions of this article will be made available by the authors, without undue reservation.

Ethics statement

Written informed consent was obtained from the participant/patient(s) for the publication of this case report.

Author contributions

JM: Conceptualization, Data curation, Methodology, Writing–original draft, Writing–review and editing. LZ: Data curation, Investigation, Methodology, Project administration, Resources, Writing–original draft. LS: Conceptualization, Writing–review and editing.

Funding

The author(s) declare financial support was received for the research, authorship, and/or publication of this article. This research was supported by the Key Research and Development Project of Sichuan Province (2023YFS0171 to JM).

Acknowledgments

The authors would like to thank all the clinical staff of the Abdominal Oncology Ward, West China Hospital, Sichuan University, who provided great help to this study.

Conflict of interest

The authors declare that the research was conducted in the absence of any commercial or financial relationships that could be construed as a potential conflict of interest.

Publisher's note

References

Jiang, C., Yao, H., Zhang, Q., Shi, H., and Lin, R. (2023). Clinicopathological characteristics of mixed neuroendocrine-non-neuroendocrine neoplasms in gastrointestinal tract. *Pathol. Res. Pract.* 243, 154373. doi:10.1016/j.prp.2023.154373

Li, Z., Ren, H., Wang, T., Zhang, X., Zhao, L., Sun, C., et al. (2022). Resection of the primary tumor improves the survival of patients with stage IV gastric neuroendocrine carcinoma. *Front. Oncol.* 12, 930491. doi:10.3389/fonc.2022.930491

Lin, J., Zhao, Y., Zhou, Y., Tian, Y., He, Q., Lin, J., et al. (2021). Comparison of survival and patterns of recurrence in gastric neuroendocrine carcinoma, mixed adenoneuroendocrine carcinoma, and adenocarcinoma. *JAMA Netw. Open* 4 (7), e2114180. doi:10.1001/jamanetworkopen.2021.14180

Ramos, M., Pereira, M. A., Arabi, A. Y. M., Mazepa, M. M., Dias, A. R., Ribeiro, U., Jr., et al. (2021). Gastric mixed neuroendocrine non-neuroendocrine neoplasms: a western center case series. *Med. Sci. (Basel)* 9 (3), 47. doi:10.3390/medsci9030047

Yeong, J., Tan, T., Chow, Z. L., Cheng, Q., Lee, B., Seet, A., et al. (2020). Multiplex immunohistochemistry/immunofluorescence (mIHC/IF) for PD-L1 testing in triple-negative breast cancer: a translational assay compared with conventional IHC. *J. Clin. Pathol.* 73 (9), 557–562. doi:10.1136/jclinpath-2019-206252

Zhang, P., Li, Z., Li, J., Li, J., Zhang, X., Lu, Z., et al. (2021). Clinicopathological features and lymph node and distant metastasis patterns in patients with gastroenteropancreatic mixed neuroendocrine-non-neuroendocrine neoplasm. *Cancer Med.* 10 (14), 4855–4863. doi:10.1002/cam4.4031

frontiers | Frontiers in Pharmacology

TYPE Review
PUBLISHED 12 February 2024
DOI 10.3389/fphar.2024.1274209

OPEN ACCESS

EDITED BY
Nur Akmarina Mohd Said,
University of Malaya, Malaysia

REVIEWED BY
Marta Canel,
University of Edinburgh, United Kingdom
Bruno Tasso,
University of Genoa, Italy
Lingling Liu,
Medical University of South Carolina, United States

*CORRESPONDENCE
She-Gan Gao,
gsg112258@163.com
Xiao-Bing Chen,
zlyychenxb0807@zzu.edu.cn

†These authors have contributed equally to this work

RECEIVED 08 August 2023
ACCEPTED 30 January 2024
PUBLISHED 12 February 2024

CITATION
Hu H-H, Wang S-Q, Shang H-L, Lv H-F, Chen B-B, Gao S-G and Chen X-B (2024), Roles and inhibitors of FAK in cancer: current advances and future directions. *Front. Pharmacol.* 15:1274209. doi: 10.3389/fphar.2024.1274209

Roles and inhibitors of FAK in cancer: current advances and future directions

Hui-Hui Hu[1†], Sai-Qi Wang[1,2†], Hai-Li Shang[1], Hui-Fang Lv[1], Bei-Bei Chen[1,2], She-Gan Gao[3]* and Xiao-Bing Chen[1,2]*

[1]Department of Oncology, The Affiliated Cancer Hospital of Zhengzhou University and Henan Cancer Hospital, Henan Engineering Research Center of Precision Therapy of Gastrointestinal Cancer and Zhengzhou Key Laboratory for Precision Therapy of Gastrointestinal Cancer, Zhengzhou, China, [2]State Key Laboratory of Esophageal Cancer Prevention & Treatment, Zhengzhou University, Zhengzhou, China, [3]Henan Key Laboratory of Microbiome and Esophageal Cancer Prevention and Treatment, Henan Key Laboratory of Cancer Epigenetics, Cancer Hospital, The First Affiliated Hospital of Henan University of Science and Technology, Luoyang, China

Focal adhesion kinase (FAK) is a non-receptor tyrosine kinase that exhibits high expression in various tumors and is associated with a poor prognosis. FAK activation promotes tumor growth, invasion, metastasis, and angiogenesis via both kinase-dependent and kinase-independent pathways. Moreover, FAK is crucial for sustaining the tumor microenvironment. The inhibition of FAK impedes tumorigenesis, metastasis, and drug resistance in cancer. Therefore, developing targeted inhibitors against FAK presents a promising therapeutic strategy. To date, numerous FAK inhibitors, including IN10018, defactinib, GSK2256098, conteltinib, and APG-2449, have been developed, which have demonstrated positive anti-tumor effects in preclinical studies and are undergoing clinical trials for several types of tumors. Moreover, many novel FAK inhibitors are currently in preclinical studies to advance targeted therapy for tumors with aberrantly activated FAK. The benefits of FAK degraders, especially in terms of their scaffold function, are increasingly evident, holding promising potential for future clinical exploration and breakthroughs. This review aims to clarify FAK's role in cancer, offering a comprehensive overview of the current status and future prospects of FAK-targeted therapy and combination approaches. The goal is to provide valuable insights for advancing anti-cancer treatment strategies.

KEYWORDS

focal adhesion kinase, signal pathway, drug resistance, immune microenvironment, inhibitor, IN10018, defactinib

1 Introduction

Focal adhesion kinase (FAK), also known as PTK2, is a non-receptor tyrosine kinase encoded by the PTK2 gene. It plays a critical role in signal transduction mediated by both growth factor receptors and integrins (Kornberg et al., 1992). Upon activation by various extracellular signals received through transmembrane receptors on the cell surface, FAK aggregates in a focal adhesion manner in the cytoplasmic membrane. Autophosphorylation at tyrosine residue 397 (Tyr397), leading to FAK's activation and initiation of downstream signaling cascades. This process involves a conformational change exposing the phosphorylation site through lipid binding (Acebron et al., 2020; Le Coq et al., 2022). The FAK protein consists of three distinct

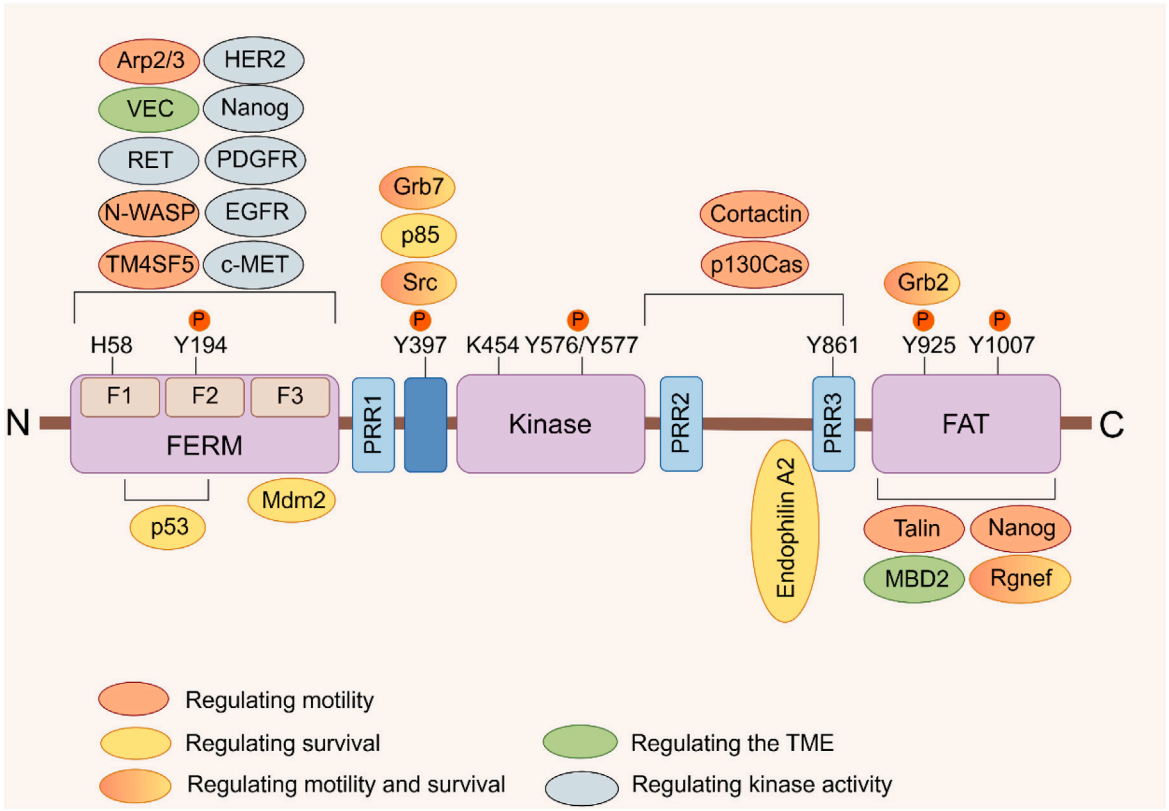

FIGURE 1
FAK domain structure. FAK consists of a central kinase domain flanked by a FERM homology domain on the N-terminal side and a C-terminal FAT domain. Both the terminal domains are separated from the kinase domain by a linker region containing proline-rich regions (PRR). Important tyrosine (Y) phosphorylation (P) sites are indicated; Y397, K454, and H58 play crucial roles in FAK activation. FAK binding partners are displayed at their interaction sites within FAK. The color signifies the function of FAK interacting proteins, which facilitate diverse activities of cancer cells by interacting with FAK (Sulzmaier et al., 2014).

domains: an N-terminal 4.1 ezrin-radixin-moesin domain (FERM), a central kinase domain, and a C-terminal focal adhesion targeting (FAT) domain (Figure 1) (Lim et al., 2008). Through its FERM domain, FAK acts as an intracellular scaffold facilitating the interconnection of multiple oncogenic signaling pathways via diverse protein-protein interactions. FAK positively regulates tumor progression by promoting cell proliferation, survival, intracellular signaling, and angiogenesis. It also contributes to maintaining the stability of the tumor microenvironment (TME) (Sulzmaier et al., 2014; Dawson et al., 2021). At the adhesion sites of cells with the extracellular matrix (ECM), FAK enhances cellular dynamics, migration, and invasion capabilities by participating in the formation of molecular complexes within the actin and adhesion regulation network (Sulzmaier et al., 2014; Schoenherr et al., 2017; Tapial et al., 2020).

FAK stands out as a key player in cancer pathogenesis, being abnormally activated across various cancer types. Its expression level not only is inversely linked to patient survival but also positions FAK as a pivotal target for thwarting tumor progression and curbing recurrence (Zeng et al., 2016; Kanteti et al., 2018; Aboubakar et al., 2019a; Aboubakar et al., 2019b; Qiao et al., 2020; Wei et al., 2021; Roy-Luzarraga et al., 2022). Rigorous meta-analyses underscore the significance of heightened FAK expression in predicting unfavorable overall survival (OS) outcomes in a spectrum of solid tumors. These include gastric cancer, ovarian cancer, endometrial cancer, glioma, breast cancer, and squamous cell carcinoma (Zeng et al., 2016; Qiao et al., 2020). Compared to non-small cell lung cancer (NSCLC), small-cell lung cancer exhibits a higher degree of malignancy and is more prone to early-stage metastasis. It is worth noting that the expression of FAK in small-cell lung cancer is significantly elevated compared to other types of lung cancer, which implying its potential association with the degree of malignancy as well as invasion and metastatic capabilities (Aboubakar et al., 2019b).

As a paralogous homolog of FAK, proline-rich tyrosine kinase 2 (PYK2) displays a similar multi-domain organization and protein binding sites to FAK, forming a subfamily of adhesion kinases together with FAK that is crucial in regulating signaling networks involved in tumor growth and metastasis (Sulzmaier et al., 2014; Naser et al., 2018). Unlike FAK, PYK2 does not localize to focal adhesions, relying instead on intracellular calcium mobilization for activation (Avraham et al., 2000). Moreover, inhibiting FAK can induce an increase in the expression or phosphorylation of PYK2 in cancer cells (Fan and Guan, 2011). The concurrent targeting of both FAK and PYK2 is believed to confer a more advantageous anti-cancer effect. FAK kinase inhibitors are typically classified as either FAK specific inhibitors or dual FAK/PYK2 inhibitors (Berger et al., 2021).

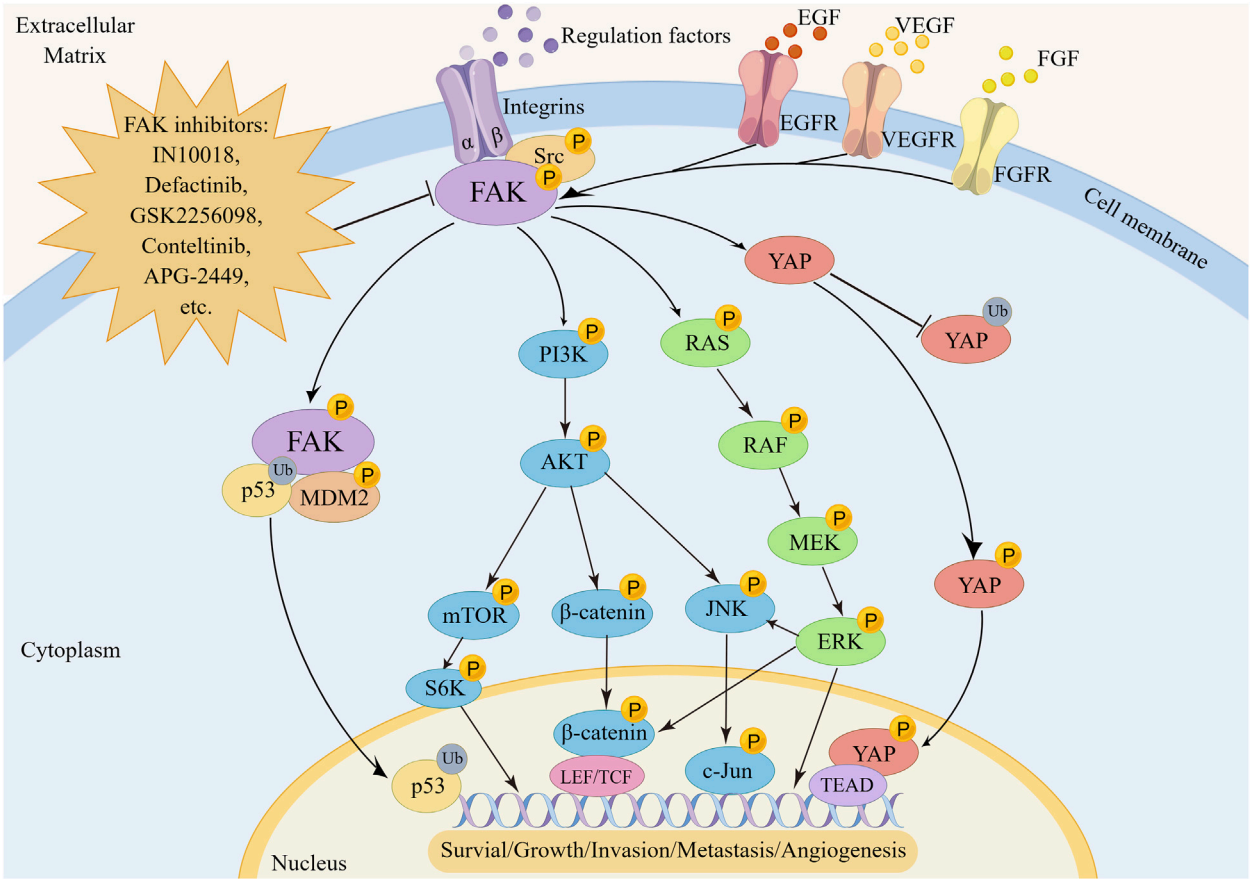

FIGURE 2
The regulatory mechanism of FAK in tumorigenesis, metastasis and angiogenesis. FAK promotes oncogenesis by activating transcription factors via the p53, YAP, RAS/RAF/MEK/ERK, PI3K/AKT, and downstream pathways including mTOR, β-catenin, or JNK.

However, there is currently no clinical evidence demonstrating specific differences in therapeutic efficacy between the use of FAK or dual FAK/PYK2 kinase inhibitors (Dawson et al., 2021). Multikinase inhibitors containing FAK, such as Conteltinib and APG-244, have exhibited significant efficacy in specific tumor types and are currently undergoing clinical investigation (Xing et al., 2022; Zhao et al., 2022). Despite the promising anti-tumor activity demonstrated in preclinical studies, the clinical efficacy of FAK inhibitors as a monotherapy for anticancer treatment remains limited. This limitation stems from the dual role of FAK, acting both as a kinase and a protein scaffold, which mediates drug resistance through crosstalk with specific signaling pathways in the network (Gerber et al., 2020). As adjuvant therapy, the combination of FAK inhibitors with conventional chemotherapy agents as shown enhanced anti-tumor potential (Dawson et al., 2021). Consequently, the exploration of combining FAK inhibitors with chemotherapy, radiotherapy or immunotherapy has become as a focal point of research in recent years.

This review critically delves into the role of FAK in regulating tumor cell signal transduction, diverse cellular activities, the immune microenvironment, and drug resistance. Additionally, it explores the current research progress on FAK inhibitors in anticancer therapy, aiming to provide new insights for the future development and application of FAK inhibitors in the field.

2 Role of FAK in different signaling pathways

2.1 PI3K/AKT signaling pathway

FAK plays a pivotal role in regulating the survival and development of tumor cells through mediating multiple signaling pathways (Figure 2). One key regulatory pathway for FAK is the PI3K/AKT signaling pathway, which mediates various cellular functions, such as proliferation, survival, migration, invasion, and metastasis (Fresno et al., 2004). When activated, FAK forms complexes with PI3K, boosting PI3K activation and generating more PIP3, initiating downstream pathway signaling. In uveal melanoma (UM), characterized by activating mutations in GNAQ/GNA11, encoding the Gαq protein, FAK has been identified as a central mediator of Gαq-driven signaling (Feng et al., 2019; Paradis et al., 2021). Additionally, a whole-genome CRISPR screen has revealed that activation of the PI3K/AKT pathway is not only essential for the survival of human UM cells but also contributes to drug resistance. Specifically, Gαq can upregulate FAK expression and subsequently activate PI3K by binding to its p85 regulatory subunit and inducing tyrosine phosphorylation, thereby initiating downstream signaling cascades associated with cancer promotion (Arang et al., 2023).

Targeting FAK effectively blocks this process. As a crucial upstream regulator of the PI3K/AKT pathway, FAK activates PI3K/AKT and its related downstream effectors, including mTOR, β-catenin and p53, promoting cancer progression (Claesson-Welsh and Welsh, 2013; Sulzmaier et al., 2014; Guo et al., 2020). The PI3K/AKT/mTORC1 pathway is a widely targeted therapeutic pathway for various cancer types (Popova and Jucker, 2021; Tewari et al., 2022). Despite the promising clinical activity of mTORC1 inhibitors, their effectiveness in treating breast cancer is limited, with certain patients developing rapid drug resistance. Inhibiting FAK has been shown to enhance the sensitivity of rapamycin resistant tumors to mTORC1 inhibition, revealing an inherent reliance of mTORC1-resistant tumors on FAK (Cuellar-Vite et al., 2022). Combining FAK inhibitors with mTORC1 inhibitors to improve efficacy against drug-resistant cancers appears feasible (Shi et al., 2016; Liao et al., 2022; Qiao et al., 2022; Wang Z et al., 2022; Yang F et al., 2022), although further validation through clinical studies is necessary. In addition, activation of the PI3K/AKT/β-catenin pathway by FAK is crucial for promoting β-catenin nuclear translocation, influencing the transcriptional regulation of tumor cell genesis (Xing et al., 2021; Lee et al., 2023).

2.2 P53 signaling pathway

P53, a prominent tumor suppressor gene, plays a crucial role in regulating tumor growth and maintaining the anti-cancer effect properties associated with cell cycle regulation (Hu et al., 2021). The relationship between FAK and p53 is intricate. Studies have demonstrated that p53 directly binds to the PTK2 promoter, inhibiting the transcription of PTK2 (Golubovskaya and Cance, 2010). Various drugs achieve FAK targeting effect by modulating this interaction (Lin et al., 2019; Klungsaeng et al., 2020; Miao et al., 2020; Shen et al., 2022). Furthermore, p53 can indirectly downregulate FAK expression. Wild-type p53 transactivates the transcription of immunoglobulin superfamily 9 (IGSF9), and the resulting IGSF9 interacts with FAK, inhibiting FAK/AKT signal transduction in breast cancer (Li H et al., 2022). Recent research has unveiled that the extracellular domain (ECD) of IGSF9 binds to T cells, inhibiting their proliferation and activation, thereby creating a microenvironment conducive to tumor growth (Liu X et al., 2023a). Consequently, upregulating IGSF9 expression to inhibit FAK function may not be an ideal strategy. Additionally, the impact of FAK as a scaffold protein on p53 can be critical. Studies indicate that nuclear FAK promotes the ubiquitination of p53 in a kinase-independent manner by enhancing MDM2 activity. The inactivation of p53 by FAK requires the binding of FAK FERM F1 leaf and p53 FERM F2 leaf, facilitating the nuclear localization of FAK, while FERM F3 leaf connects with MDM2, mediating proteasomal degradation (Lim et al., 2008; Steinberg et al., 2023). Targeting specifically the FAK FERM domain of FAK using its scaffold function may offer novel therapeutic avenues to counteract this pro-cancer effect (Pomella et al., 2022). However, clinical and preclinical studies have revealed that higher FAK copy number and gene overexpression are associated with worse disease-free survival in patients with mutant-type p53, but not in patients with wild-type p53 (Lakshmanan et al., 2021; Yu et al., 2021; Pifer et al., 2023). This could be attributed to the fact that mutated p53 loses its inhibitory effect on FAK transcription, restoring the positive influence of FAK on the biological behavior of tumor cells. Lakshmanan et al. developed two genetically engineered lung cancer mouse models $Kras^{G12D/+}$; $Trp53^{R172H/+}$; Ad-Cre (KPA) and $Kras^{G12D/+}$; Ad-Cre (KA), revealing the ST6GalNAc-1/MUC5AC axis as a mediator of mutant p53's regulation of FAK signal transduction. The p53 R175H mutation leads to increased expression of ST6GalNAc-I, promoting glycosylation of MUC5AC and enhancing its interaction with integrin β4. This, in turn, increases phosphorylation of FAK at Y397, ultimately promoting lung cancer invasion and liver metastasis (Lakshmanan et al., 2021).

2.3 RAS/RAF/MEK/ERK signaling pathway

Abnormal activation or gene mutation of the RAS/RAF/MEK signaling pathway is a crucial factor in sustaining tumor survival and invasion (Imperial et al., 2019). In recent years, targeting RAS, RAF, or MEK to disrupt pathway transduction has emerged as a promising breakthrough in cancer treatment (Song et al., 2023). Intriguingly, there is a close relationship between FAK expression and the transduction of the RAS/RAF/MEK pathway. FAK promotes the invasion and metastasis of tumor cells by regulating the activation of the RAS/RAF/MEK/ERK signaling pathway (Shao et al., 2022; Yoon et al., 2022). A study has identified a significant correlation between ERK5 activity and FAK expression, as well as Ser910 site phosphorylation in lung cancer and malignant melanoma. ERK5 increases the expression of the transcription factor USF1, which, in turn, upregulates the expression of FAK and activates the FAK signal to promote cell migration (Jiang W et al., 2020). Furthermore, TCGA cancer survival data indicates that lower RNA expression of PTK2 is associated with better survival outcomes in KRAS mutated tumors (Zhang L et al., 2021). This suggests that FAK could potentially serve as an effective biomarker for cancer development induced by abnormal KRAS signaling. Inhibiting the expression of KRAS G12C induces sustained activation of FAK, subsequently restoring the vitality of KRAS G12C mutant tumor cells, including a human CRC cell line (SW837), a human Pancreatic cancer cell line (Mia PaCa-2), and 3 human NSCLC cell lines (NCI-H23, NCI-H1792, and NCI-H2122), through the FAK/YAP pathway (Zhang L et al., 2021). High-throughput transcriptome sequencing of three cell lines from malignant peripheral nerve sheath tumors resistant to MEK inhibitors, revealed that the upregulation of FAK/SRC, leading to the reactivation of the ERK signaling pathway, is a crucial factor in cell resistance. Therefore, the compensatory activation of FAK-related pathways, such as FAK/SRC and FAK/YAP, is a crucial pathway contributing to the ineffectiveness of single targeted therapies for RAS, RAF, or MEK in KRAS mutant tumors. Combining FAK inhibition therapy can potentially restore the sensitivity of drug-resistant cells to MEK or KRAS inhibitors, improving their anti-tumor effect (Gu et al., 2022; Tarin et al., 2023). Based on these preclinical research findings, a phase II clinical trial (NCT04620330) is currently underway (Capelletto et al., 2022) to investigate the true efficacy of the combination therapy of FAK inhibitor defactinib and the RAF/MEK inhibitor VS-6766 for KRAS-mutant NSCLC. FAK holds the potential to serve as a promising

therapeutic target for future combination therapy in KRAS mutant tumors.

2.4 YAP signaling pathway

The Yes-associated protein (YAP), a primary downstream effector of the Hippo pathway, exhibits dynamic cellular localization, influencing its role as a transcriptional activator. While YAP in the cytoplasm undergoes ubiquitination and degradation, nuclear YAP acts on TEA domain DNA-binding proteins to induce gene transcription (Heng et al., 2021). Phosphorylation intricacies govern YAP's cytoplasmic-nuclear translocation. Phosphorylation at S127 and S397 suppresses nuclear localization, while Y357 phosphorylation enhances YAP stability and facilitates nuclear translocation, with FAK playing a crucial role in this phosphorylation process (Lachowski et al., 2018; Fard et al., 2023). In cholangiocarcinoma, FAK and activated AKT synergize to induce the YAP oncogene, promoting AKT/Jag1-driven biliary tract cancer occurrence (Song et al., 2021). Interestingly, YAP reciprocally activates FAK, contributing to tumor cell migration (Goto et al., 2020). The YAP-TEAD axis, highlighted by Jie Shen et al., plays a crucial role in inducing FAK activation by targeting platelet-derived growth factor 1 (THBS1) in breast cancer (Shen et al., 2018). The FAK-YAP signaling pathway emerges as a key player in chemotherapy resistance and cancer relapse. Activation of the FAK-YAP cascade, disrupts COL17A1, enabling LGR5+p27+ cancer stem cells (CSCs), to exit dormancy, re-enter the cell cycle, and restore proliferative capacity. Targeting YAP through TEAD inhibitors provides an effective strategy to impede tumor organoid regeneration, offering a novel approach for overcoming cancer recurrence following chemotherapy (Ohta et al., 2022). Furthermore, YAP-FAK contributes significantly to radiotherapy resistance. The focal adhesion component, p130Cas, regulates the YAP-FAK signaling pathway, mediating radiotherapy resistance in NSCLC. p130Cas directly interacts with FAK to regulate YAP activation and nuclear translocation (Li J et al., 2022). Targeting the p130Cas-FAK interaction merges as a potentially cost-effective strategy for overcoming YAP activation-mediated radioresistance in NSCLC.

3 Role of FAK in the occurrence and development of tumors

3.1 FAK promotes tumor cell survival and proliferation

FAK plays a pivotal role in promoting the survival and proliferation of tumor cells through both kinase-dependent and kinase-independent mechanisms, orchestrating downstream signal transduction. Recent insights highlight FAK's dual role in phenotype transition, with distinct functions in the cytoplasmic and nuclear compartments. In the cytoplasm, activated FAK initiates survival pathways in a PI3K and MAPK-dependent manner. Simultaneously, within the nucleus, the FERM domain of FAK hinders the activation of p53, thereby preventing inherent cell apoptosis (Del et al., 2022; Ke et al., 2022). Previous studies have delineated various mechanisms through which FAK promotes tumor cell survival and proliferation. These include activating NF-κB to mediate the expression of inhibitor of apoptosis proteins (IAPs), inducing upregulation of cyclin D1 through the ERK pathway activation, and interacting with receptor-interacting protein (RIP) via the death domain kinase to neutralize the pro-apoptotic function of RIP (Chuang et al., 2022). Moreover, FAK contributes to maintaining tumor cell survival by countering anoikis, a form of cell death induced by cell detachment from the ECM. FAK reduces the sensitivity of cancer cells to receptor ligands inducing death by stabilizing the TPL2 protein (Del et al., 2022). Additionally, FAK inhibits cellular senescence, a process crucial for maintaining cell survival (Fard et al., 2023; Steinberg et al., 2023; Tien et al., 2023). Notably, the Sema6C protein, initially recognized as Semaphorin Y, not only forms a complex with tyrosine kinases c-Abl, activating FAK, and leading to the nuclear localization of the YAP transcriptional co-activator. This interaction enables YAP-dependent cancer cells to survive under nutrient deprivation conditions. Inhibition of Sema6C expression reverses these effects, inducing cellular senescence (Fard et al., 2023).

The dysregulation of CDK4/6 in tumor cells is a critical factor in sustaining tumor cell proliferation, making CDK4/6 inhibitors a focal point in inhibiting tumor growth. However, utilizing CDK4/6 inhibitors as a standalone treatment often leads to the development of drug resistance. This resistance is thought to be linked to FAK signaling, which mediates CDK4/6-independent activation of CDK2, driving cell cycle progression and fostering cell survival even in the presence of CDK4/6 inhibitors (Jiang H et al., 2020). Furthermore, research suggests a correlation between CDK4/6 activity and the subcellular localization of FAK in B16F10 melanoma cells. Inhibiting FAK kinase activity promotes nuclear the localization of FAK. In its inactive state, nuclear FAK, leveraging its scaffold function, recruits CDH1 and CDK4/6 to its N-terminal FERM domain. This recruitment facilitates the ubiquitination and proteasomal degradation of CDK4/6, suppressing melanoma cell proliferation. Importantly, this process occurs exclusively when FAK is localized within the nucleus (Murphy et al., 2022). The scaffold structure of nuclear FAK has been observed in multiple studies to possess the ability to facilitate the degradation of various nuclear factors in multiple studies (Jeong et al., 2019; Zhou et al., 2019; Jeong et al., 2021; Jeong et al., 2022). Therefore, concurrent inhibition of FAK and CDK4/6 expression holds the potential to overcome drug resistance. Currently, preclinical studies in intrahepatic cholangiocarcinoma and diffuse gastric cancer (DGC) have demonstrated the synergistic anti-cancer effects of combining FAK and CDK4/6 inhibitors (Song et al., 2021; Peng et al., 2023) These findings provide a solid theoretical foundation for future clinical studies in this area.

3.2 FAK promotes tumor cell migration and invasion

The heightened expression of FAK is intricately linked with unfavorable outcomes for cancer patients due to its pivotal role in promoting tumor metastasis. FAK's influence on cell migration involves its participation in the integration and resolution of components within the focal adhesion complex, coupled with

dynamic interactions with intracellular Actin and the ECM. In migrating cells, the contraction of myosin stress fibers attached to the focal adhesion complex exerts force to regulate cell migration (Tapial et al., 2020; Le Coq et al., 2022). Additionally, various intracellular protein molecules have been identified that activate FAK, thereby promoting tumor cell invasion and migration (Hu et al., 2019; Jiang W et al., 2020; Dong et al., 2021; Kim et al., 2021). For example, PPFIA binding protein 1 induces the movement of glioblastoma U87 MG and U251 MG cell lines by interacting with FAK to activate Src and JNK (Dong et al., 2021). Similarly, Rho-associated protein kinase 1 (ROCK1) enhances the migratory ability of NSCLC cells through the PTEN/PI3K/FAK signaling pathway (Hu et al., 2019). Sialylation, a terminal glycosylation modification of glycoproteins, plays a crucial regulatory role in facilitating tumor cell adhesion and immune evasion (Jarahian et al., 2021; Pietrobono and Stecca, 2021). Sun et al. employed the CRISPR/Cas9 system to establish a stable FAK knockout (KO) cell line in HeLa cells, revealing that sialylation levels were significantly reduced in KO cells, leading to inhibited cell migration. Specifically, FAK primarily regulates N-glycan sialylation via the FAK/PI4KIIα/GolPH3/ST axis, reaffirming FAK's unique position in multiple pathways regulating cell migration (Sun et al., 2023).

Epithelial-mesenchymal transition (EMT) plays a crucial role in the infiltration and spread of cancer cells, and FAK expression is positively correlated with EMT. Epidermal growth factor induces EMT in colorectal cancer cells by activating FAK (Huang et al., 2020). Tspan9 stimulates osteosarcoma migration by inducing EMT via activation of the FAK/Ras/ERK1/2 signaling cascade (Shao et al., 2022). The activated ERK further promotes cell contraction and stimulates tumor cell movement by driving actin polymerization and edge protrusion adhesion turnover (Samson et al., 2022). FAK has been identified as a significant regulatory factor for interleukin-6 induced EMT in colorectal cancer (Huang et al., 2023). In DGC, the loss of CDH1 (encoding E-cadherin, a key regulator of the EMT) and RHOA Y42C mutation in gastric organs of engineered mice co-activate the FAK/AKT/β-catenin and YAP-TAZ pathways, promoting the transformation of normal gastric epithelial cells into highly invasive DGC cells (Zhang et al., 2020). Despite the single drug resistance observed with FAK inhibitors, studies have shown that combining FAK inhibitors with MAPK inhibitors can effectively eliminate compensatory ERK activation, synergistically inhibiting the migration and invasion of malignant tumors such as DGC and UM (Paradis et al., 2021; Peng et al., 2023). Further investigation is warranted to uncover the specific molecular mechanisms underlying this phenomenon.

3.3 FAK regulates tumor angiogenesis

Angiogenesis is essential for the malignant development of tumors, and key regulatory molecules such as vascular endothelial growth factor (VEGF), VEGFA, and vascular endothelial growth factor receptor 2 (VEGFR2) play crucial roles in this process (Wang et al., 2020; Shiau et al., 2021; Patel et al., 2023). VEGFA, with a strong affinity for VEGFR2, promotes angiogenesis by activating downstream pathways, including the FAK-paxillin pathway. This activation facilitates the proliferation, survival, and migration of vascular endothelial cells (Simons et al., 2016; Wang et al., 2020). The VEGFR2-FAK signaling pathway induces VEGFA secretion, promoting angiogenesis and vascular permeability (Li L et al., 2022). In triple-negative breast cancer (TNBC), The results showed a positive correlation between FAK and VEGFR2 expression was observed, and knockout of FAK inhibited endodermal tube formation and angiogenesis in zebrafish, suppressing suppressed VEGF and VEGFR2 expression at the molecular level (Shiau et al., 2021).

Temporal quantitative phosphoproteomic analysis of human umbilical vein endothelial cells revealed that FAK phosphorylation activation is an early phosphorylation-dependent signaling event in the VEGFA/VEGFR2 pathway, emphasizing the crucial role of FAK in initiating angiogenesis (Abhinand et al., 2023). Notably, distinct phosphorylation sites on EC-FAK have divergent effects on tumor angiogenesis *in vivo*. EC Cre+; FAK $Y397F^{/Y397F}$ small mutant mice exhibited constitutive reduction in tumor growth and angiogenesis, while EC Cre+; FAK $Y861F^{/Y861F}$ mice showed normal tumor growth without significant inhibition of angiogenesis. These effects were attributed to decreased VEGFR2 expression, attenuated integrin β1 activation, and disruption of downstream FAK/Src/PI3K/AKT signaling induced by EC FAK-Y397F (Pedrosa et al., 2019). However, studies by Marina Roy-Luzarraga et al. found that inducing endothelial FAK deficiency in both orthotopic and spontaneous mouse model of pancreatic ductal adenocarcinoma (PDA) did not hinder angiogenesis but reduced the incidence of tumor metastasis and improved mouse survival (Roy-Luzarraga et al., 2022). However, Combining EC-FAK inhibition with other tumor therapies, such as Doxorubicin for melanoma (Tavora et al., 2014), demonstrated potential effectiveness in suppressing tumor angiogenesis, suggesting distinct effects of FAK inhibition when combined with different cancer types. The impact of EC-FAK on tumor angiogenesis may be intricately linked to the regulation of EC barrier function (Jean et al., 2014; Roy-Luzarraga et al., 2022).

Contrary to FAK expression in ECs, FAK expressed in pericytes (perivascular cells) may exert an opposing regulatory effect on tumor angiogenesis (Lechertier et al., 2020). The loss of FAK in pericytes enhances GAS6-stimulated receptor tyrosine kinase Axl phosphorylation and upregulates Cyr61, promoting tumor growth (Lechertier et al., 2020; Zhang et al., 2023b). Notably, FAK-Y861 in pericytes plays a pivotal regulatory role in tumor vascular regression and control of tumor growth (Lees et al., 2021). Targeting FAK specifically in ECs rather than pericytes remains an urgent challenge for future anti-FAK therapy.

4 Role of FAK in TME

TME comprises a diverse array of cell types, including cancer cells, immune cells, dendritic cells, tumor-associated macrophages (TAMs), cancer-associated fibroblasts (CAFs), tumor blood vessels, lymphatics, adipocytes, and an ECM with collagen and elastin fibrous networks, along with numerous cytokines. This complex and dynamic ecosystem plays a pivotal role in evading immune responses and promoting tumor progression (Xiao and Yu, 2021). FAK influences various TME cell populations, ECM architecture, and associated signaling pathways involved in immunosuppression and matrix regulation, orchestrating the development of the immunosuppressive TME (Figure 3) (Osipov et al., 2019).

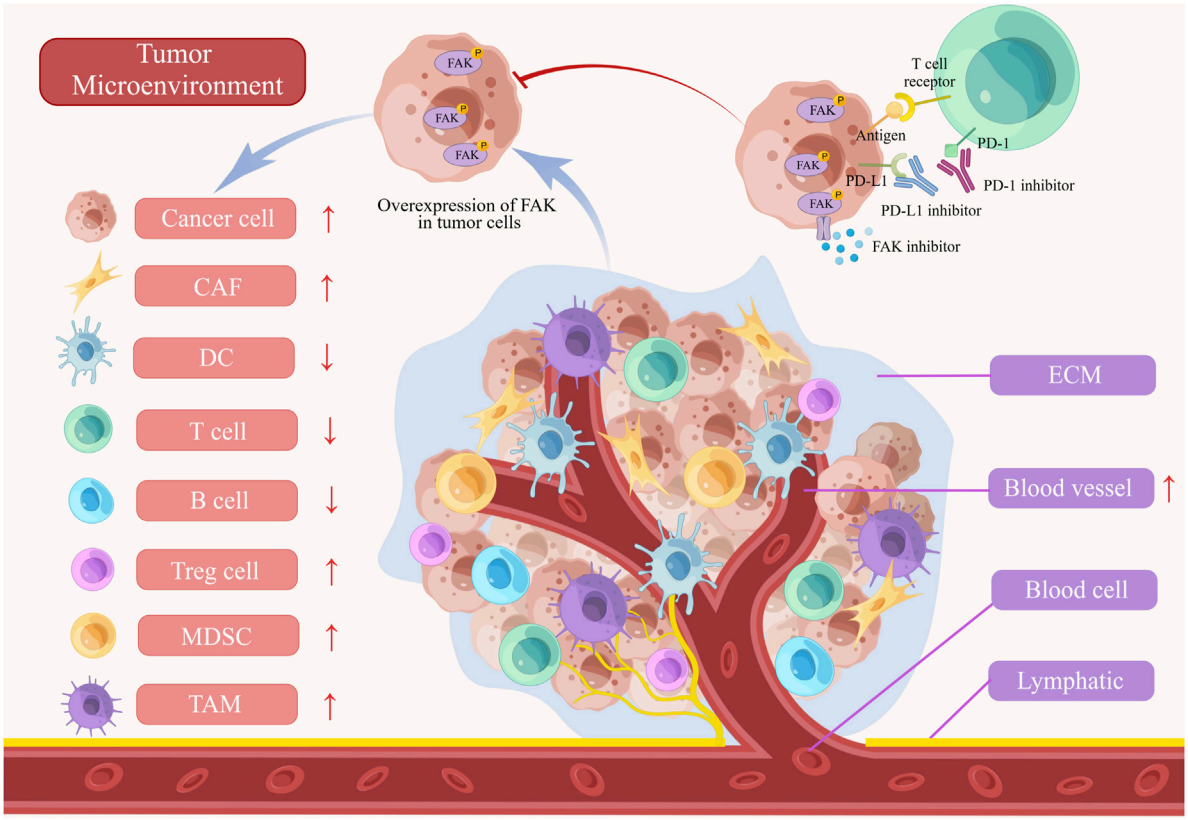

FIGURE 3
The role of FAK in tumor microenvironment (TME). The abnormal activation of FAK inhibits T cells, B cells, and dendritic cells (DCs) in the immune microenvironment. Furthermore, the activation of FAK leads to the promotion of myeloid-derived suppressor cells (MDSCs), tumor-associated macrophages (TAMs), cancer-associated fibroblasts (CAFs), and angiogenesis, all of which contribute to the progression of the tumors. FAK inhibitors, when combined with PD-1/PD-L1 inhibitors, demonstrate a more powerful anti-tumor effect by blocking tumor growth and enhancing immune cell functionality. ECM, extracellular matrix.

ECM is a crucial component in mediating FAK's regulation of the TME. CAFs are key regulators of tumor occurrence and progression, residing in the tumor matrix surrounding tumor cells. CAFs promote tumor fibrosis, resisting various therapies by synthesizing collagen and other ECM molecules. Lumican, overexpressed in CAFs, activates the integrin β1/FAK pathway, promoting the growth and migration of gastric cancer cells (Wang et al., 2017). In PDA, CAFs play a pivotal role in promoting clonal growth, self-renewal, and migration, associated with enhanced differentiation activity of CSCs. Inhibiting FAK kinase activity in PDA cells eliminates the influence of CAFs on clonal growth (Begum et al., 2019). Lysyl oxidase-rich extracellular vesicles from CAFs promote tumor EMT through the activation of the p-FAK/p-axis/YAP pathway, identified as a pivotal step in collagen cross-linking. Targeting FAK disrupts this process (Liu X et al., 2023b). However, FAK-targeted therapy can lead to stroma depletion in the TME and decreased resident fibroblasts, resulting in reduced TGF-β secretion and weakened inhibition of the STAT3 signaling pathway. Combining FAK and STAT3 targeting alleviates this impact (Jiang H et al., 2020). Discoidin domain containing receptor 1 (DDR1), crucial for ECM stability through collagen interaction, has FAK as an important downstream regulatory molecule. Targeting DDR1 reshapes the TME, inhibiting chemotherapy resistance induced by the ECM in pancreatic cancer through the DDR1/PYK2/FAK pathway (Ko et al., 2022). Matrix stiffness induces lipid metabolic crosstalk between tumor and stromal cells, leading to bevacizumab resistance in colorectal cancer liver metastases. FAK, in the FAK/YAP pathway, plays a crucial role in this process. Inhibiting FAK enhances anti-VEGF therapy efficacy by suppressing hepatic stellate cell lipolysis (Zheng et al., 2023).

Despite the promise of immune checkpoint inhibitors, only a fraction of cancer patients benefits from them due to the immunosuppressive effects within the TME, involving regulatory T cells (Tregs), myeloid-derived suppressor cells (MDSCs), and TAMs. Inhibiting FAK expression reduces the presence of these immunosuppressive cells, affecting CSCs differentiation, and creating a more favorable TME for anti-tumor immune responses (Osipov et al., 2019). Furthermore, FAK has been found to inhibit the expression of PD-L1 on tumor cells, enhancing the recognition efficiency of cytotoxic T cells (Li et al., 2019; Zhang D et al., 2022). Positive correlations between PD-L1 and FAK was discovered in PD-L1-positive triple-negative breast cancer (TNBC) tissue samples (Mohan et al., 2019). The infiltration of various immune cells ($CD8^+$ T cells, CAFs, and MDSCs) correlates with FAK expression. Blair et al. suggest that a promising strategy to modulate the immune microenvironment and enhance immunotherapy efficacy involves targeting stromal components in combination. Their study

showcased the effectiveness of co-inhibition strategies targeting hyaluronic acid degradation and FAK, in combination with PD-1 blockade. This combined approach specifically reduced the number of granulocytes and bone marrow-derived cells expressing C-X-C chemokine receptor type 4 (CXCR4). Simultaneously, it facilitated T cell infiltration leading to an enhancement in the therapeutic outcomes of immune-based interventions for pancreatic cancer (Blair et al., 2022). Combining the FAK inhibitors with anti-PD-1antibodies demonstrated enhanced anti-cancer effects in C57BL/6 J primary hepatocellular carcinoma model with complete immune function, reducing Tregs and TAMs while increasing $CD8^+$ T cell population (Wei et al., 2021). FAK also impedes antigen the processing and presentation in pancreatic cancer, contributing to immune evasion of pancreatic cancer. Depletion of FAK enhances anti-tumor activity by upregulating immune proteasome, MHC-I, and increasing $CD8^+$ T cell infiltration (Blanco-Gomez and Jorgensen, 2023; Canel et al., 2023). CD11b, a protein in myeloid cells, enhances T cell-mediated immunity through downregulation of interferon gene expression, leading to suppression of tumor progression by decreasing infiltrating myeloid cells. Inhibiting FAK-mediated mitochondrial dysfunction activates the STING/STAT1 pathway, contributing to this process (Schmid et al., 2018; Panni et al., 2019; Liu Y et al., 2023a).

FAK serves as a potential target for radiotherapy, modulating tumor immune responses. A study demonstrated that radiation alone or in combination with checkpoint immunotherapy failed to elicit antigen-specific T-cell responses in PDA. In contrast, In the p48-Cre/LSL-KrasG12D/p53Flox/Flox (KPC) genetically engineered mouse models, combined administration of FAK inhibitors with checkpoint immunotherapy and radiation led to complete tumor regression and long-term survival in spontaneous PDA mice. This highlights FAK inhibition's role in facilitating radiotherapy-induced tumor immunity and enhancing responsiveness to checkpoint immunotherapy (Lander et al., 2022). Additionally, combining low-dose radiotherapy with FAK inhibitors mitigated fibrosis and hypoxia in pancreatic cancer, promoting CD8+T cell infiltration and enhancing sensitivity to cancer radiotherapy (Chen H et al., 2022). Therefore, Clinical research is needed to assess the safety and efficacy of this combination therapy.

5 FAK mediates drug resistance

The pivotal role of FAK in regulating chemoradiotherapy resistance across various cancers underscores its potential as a therapeutic target. Targeting FAK has demonstrated sensitizing effects on both radiotherapy and various chemotherapy treatments (Allert et al., 2022; Gu et al., 2022; Jang et al., 2022; Li Y et al., 2022; Ling et al., 2022; Wang C et al., 2022; Yu et al., 2022; Gao et al., 2023). Most chemotherapy drugs, including platinum-based agents and fluoropyrimidine chemotherapy, exert their anticancer effects by inducing DNA damage in cancer cells (Newport et al., 2022). FAK, as a crucial regulatory protein in DNA damage repairs, orchestrates its regulatory function by facilitating the nuclear translocation of β-catenin. This process regulates the transcription of DNA damage repair genes, promoting cell survival and ultimately contributing to drug resistance. Targeting FAK emerges as a promising strategy to restore sensitivity to DNA damage therapy (Tavora et al., 2014; Newport et al., 2022; Roy-Luzarraga et al., 2022; Gao et al., 2023). Notably, Pifer et al. reported that targeting FAK suppresses homologous recombination and nonhomologous end-joining repair in p53-mutant HPV-negative head and neck squamous cell carcinoma cell lines, thereby enhancing the DNA-damaging effects of radiotherapy (Pifer et al., 2023). Additionally, in human CDH1-deficient cell line (SNU-668 and NUGC-4)-derived xenograft models in mice, ROS1 inhibitors activate the FAK-YAP-TRX signaling pathway, mitigating oxidative stress-induced DNA damage, thereby attenuating their anticancer efficacy (Gao et al., 2023).

Furthermore, FAK frequently facilitates the emergence of drug resistance in specific tumor types undergoing targeted therapy for particular gene mutations:1. BRAF/KRAS: Tumors harboring BRAF or KRAS mutations can effectively suppress the RAS/RAF/MEK/ERK pathway with BRAF or MEK inhibitors. However, tumor cells rapidly develop adaptive or acquired resistance mechanisms often accompanied by exhibit heightened expression of FAK and activation of the downstream Wnt/β-catenin signaling pathway (Fallahi-Sichani et al., 2017; Chen et al., 2018). This phenomenon may be related to the negative regulation of FAK signal transduction by the RAS/RAF/MEK pathway (Zheng et al., 2009). Additionally, CRISPR/Cas9 genome screening revealed significant enrichment of the Grb7 gene in KRAS mutant colorectal cancer cells exhibiting resistance to MEK inhibitors. This gene facilitates the activation of the FAK pathway through RTK signaling, triggering the ERK/MAPK signaling pathways and conferring resistance to MEK inhibition in tumor cells (Yu et al., 2022). 2. CDH1: CDH1-deficient tumors, characterized by a poor response to chemotherapy and increased susceptibility to drug resistance, often show upregulated FAK expression as a prognostic marker (Yuen et al., 2021). Treatment with FAK inhibitors has demonstrated significant efficacy against CDH1-deficient gastric cancer, characterized by downregulated E-cadherin and damaged membrane E-cadherin/β-catenin protein complexes a, resulting in reduced sensitivity of tumor cells to chemotherapy. The dense collagen matrix in gastric cancer cells further increases the interaction between integrin-mediated ECM and activated FAK/ERK signaling, facilitating the nuclear translocation of β-catenin and promoting the invasion and metastasis of tumor cells (Jang et al., 2018). In addition to CDH1 deficiency, DGC, often accompanied by RHOA gene mutation and activation of the YAP downstream signaling pathway, promotes tumor survival. FAK, a classic upstream regulator of YAP, inhibits the activation of the YAP pathway, restores the E-cadherin/β-catenin complex, and remodels ECM. Combining FAK inhibitors with chemotherapy enhances the anticancer effect synergistically (Gao et al., 2023). 3. HER2: FAK mediates resistance to anti-HER2 targeted drugs. The N-terminal FERM domain structure of FAK interacts with HER2, and the Src-FAK signaling pathway activates key downstream signaling pathways involved in HER2 crosstalk (Nahta, 2012). Activated FAK can further activate the downstream AKT, ERK and STAT3 pathways promoting drug resistance. Therefore, targeting FAK emerges as a promising strategy to overcome anti-HER2 drug resistance (Lazaro et al., 2013; Jin et al., 2017; Cooper and Giancotti, 2019; Castro-Guijarro et al., 2023). However, not all HER2-positive cancers exhibit sensitivity to FAK inhibition. Recent studies have demonstrated that HER2-positive breast cancer

patients with elevated levels of circCDYL2 experience rapid recurrence after anti-HER2 therapy compared with those with lower levels of circCDYL2. Mechanistic investigations have revealed that circCDYL2 stabilizes Grb7 by preventing its ubiquitination and degradation, enhancing its interaction with FAK, and sustaining downstream AKT and ERK1/2 activity, mediating trastuzumab resistance. The application of FAK inhibitors has been shown potential in ameliorating trastuzumab resistance in cells exhibiting high levels of circCDYL2 (Ling et al., 2022). Future research should focus on screening specific tumor types highly sensitive to FAK inhibitors to explore their potential clinical application value.

The presence of CSCs plays a significant role in conferring drug resistance and promoting tumor recurrence. FAK, as a critical regulator of CSC activity, exerts a significant influence (Yin et al., 2021; Jang et al., 2022). CSCs rely on the highly expressed laminin to bind to integrin α6β1, promoting FAK-mediated self-renewal signaling of CSCs (Cooper and Giancotti, 2019). Yin et al. found that ATP-binding cassette subfamily G member 1 mediates the signaling of extracellular matrix protein-1-integrin αXβ2 interaction, leading to the activation of FAK/Rho/cytoskeleton molecules and conferring cisplatin resistance on cancer cells by upregulating CD326-mediated stemness (Yin et al., 2021). Moreover, the overexpression of KRT17 is correlated with unfavorable OS and reduced responsiveness to platinum-based therapy in patients diagnosed with oral squamous cell carcinoma The interaction between KRT17 and plectin (a macromolecular cytoskeletal protein) triggers the activation of the integrin β4/FAK/ERK pathway, thereby facilitating the stabilization and nuclear translocation of β-catenin while augmenting oral squamous cell carcinoma stemness and CD44 expression (Jang et al., 2022).

6 Development and clinical research progress of FAK inhibitors

Targeting FAK has demonstrated efficacy in cancer therapy, particularly when standard treatments prove ineffective or in combination with other drugs. The ongoing development of novel FAK inhibitor reflects the significance of this approach. However, despite the active pursuit, no FAK inhibitor has yet received clinical approval. Most of them are currently in preclinical or clinical development stages (Quispe et al., 2022). FAK inhibitors can be categorized into allosteric site inhibition, ATP-competitive inhibition of kinase inhibitors, as well as FERM domain and FAT domain inhibitors. Notably, only ATP-competitive inhibitors of FAK have advanced to the clinical research stage (Mustafa et al., 2021b; Spallarossa et al., 2022). Consequently, this article will focus on providing a detailed overview of representative drugs within this class, covering their progress in both preclinical and clinical studies (Table 1). Certain studies within this class have shown promising advancements, instilling new hope for patients who are responsive to FAK inhibition therapy (Figure 4). Additionally, recent developments in FAK degraders based on PROTAC technology have addressed the limitation of FAK scaffold function being untargetable by small molecule inhibitors (Huo et al., 2022). This breakthrough opens avenues for exploring novel mechanisms of FAK degradation, aiming to enhance anticancer efficacy and gain new insights into targeted FAK therapy. The evolving landscape of FAK inhibitors, coupled with innovative approaches like PROTAC technology, holds the potential to reshape cancer therapy. Ongoing research endeavors are critical for advancing our understanding and application of these promising treatments.

6.1 IN10018 (BI 853520; Ifebemtinib)

IN10018 stands out as a highly efficient and selective ATP-competitive FAK inhibitor. Biomarker analysis and gene set enrichment studies have unveiled a heightened sensitivity of IN10018, particularly associated with the mesenchymal tumor phenotype. This sensitivity is notably correlated with elevated E-cadherin expression. Impressively, IN10018 demonstrates rapid and persistent inhibition of FAK autophosphorylation in the tumor tissue of immunodeficient mice (Hirt et al., 2018; Tiede et al., 2018). IN10018 shows robust anti-cancer activity both in breast cancer cells *in vitro* and multiple preclinical mouse models. It also inhibits the *in vitro* growth of malignant pleural mesothelioma cell spheroids, significantly reduces tumor weight in mice, and show effective inhibitory effects on cell proliferation and microvascular growth in tumor tissue (Laszlo et al., 2019). IN10018 also inhibit EMT and tumor growth *in vivo* of ovarian cancer cells through the FAK/AKT/mTOR signaling pathway (Li et al., 2021). Moreover, in KPC orthotopic murine model, IN10018 enhances the sensitiveness of PDA to radiotherapy. Compared with single radiotherapy or FAK inhibition therapy, the combination of FAK inhibitor and radiotherapy significantly increases the infiltration of $CD8^+$ T cells and macrophages (Osipov et al., 2021).

The initial findings from the phase I study of IN10018 in human subjects demonstrate its safety and excellent tolerability among advanced non-hematologic malignancy patients. The maximum tolerated dose (MTD) was determined to be 200 mg daily. Out of the 63 patients enrolled, 49 were evaluable, and 17 (27%) achieved disease stabilization as the best response, with four cases exhibiting stability for over 150 days (de Jonge et al., 2019). Additionally, a phase I research conducted with patients having advanced or metastatic solid tumors in Japan and Taiwan revealed favorable pharmacokinetics and safety profiles for IN10018. The median disease control duration was recorded at 3.7 months, indicating promising anti-tumor activity (Doi et al., 2019). The prospect of combination therapy involving IN10018 appears to be a feasible approach for maximizing the anti-tumor effects of FAK inhibitors. A phase I study of IN10018 combined with pegylated liposomal doxorubicin for platinum-resistant ovarian cancer showed an ORR of 56.7% (95% CI: 37.4%–74.5%) and a DCR of 86.7% (95% CI: 69.3%–96.2%) in the 30 evaluable patients. The observed median progression-free survival (PFS) among all 42 enrolled patients was 6.2 months (95% CI: 6.2 months–NA), suggesting that the combination of IN10018 and pegylated liposomal doxorubicin has elucidated therapeutic effects and manageable safety in platinum-resistant ovarian cancer patients (Wu X et al., 2022).

6.2 Defactinib (VS-6063)

Defactinib is a highly efficient and reversible dual inhibitor of FAK and Proline-rich tyrosine kinase 2 (PYK2), belonging to the

TABLE 1 Summary of FAK inhibitors in clinical studies.

Drug	Target	Tumor type	Clinical stage	NCT Trial No.	References
IN10018	FAK	Metastatic non-hematologic malignancy	I	NCT01335269	de Jonge et al. (2019)
IN10018	FAK	Advanced or metastatic solid tumors	I	NCT01905111	Doi et al. (2019)
IN10018 +PLD	FAK	Platinum-resistant ovarian cancer	I/II	NCT05551507	Wu X et al. (2022)
Defactinib	FAK/PYK2	Merlin protein low expression epithelioid sarcoma	II	NCT01870609	Fennell et al. (2019)
Defactinib	FAK/PYK2	KRAS mutant NSCLC	II	NCT01951690	Gerber et al. (2020)
Defactinib+ Pembrolizumab + Gemcitabine	FAK/PYK2 PD-1	Intractable pancreatic cancer	I	NCT02546531	Wang-Gillam et al. (2022)
Defactinib+ VS-6766	FAK/ PYK2RAF/MEK	KRAS mutant NSCLC	II	NCT04620330	Capelletto et al. (2022)
GSK2256098	FAK	Advanced solid tumor	I	NCT01138033	Soria et al. (2016)
GSK2256098+ Trametinib	FAK MEK	Advanced solid tumor	Ib	NCT01938443	Mak et al. (2019)
GSK2256098	FAK	NF2 Mutant Meningioma	II	NCT02523014	Brastianos et al. (2023)
Conteltinib	FAK/PYK2/ALK	Advanced ALK-positive NSCLC	I	NCT02695550	Xing et al. (2022)
APG-2449	FAK/PYK2/ALK	Advanced solid tumor	Ib/II	NCT03917043	Zhao et al. (2022)

Note: FAK, focal adhesion kinase; PLD, polyethylene glycol-conjugated liposomal doxorubicin; NF2, neurofibromatosis type 2; PYK2, protein tyrosine kinase; NSCLC, non-small cell lung cancer.

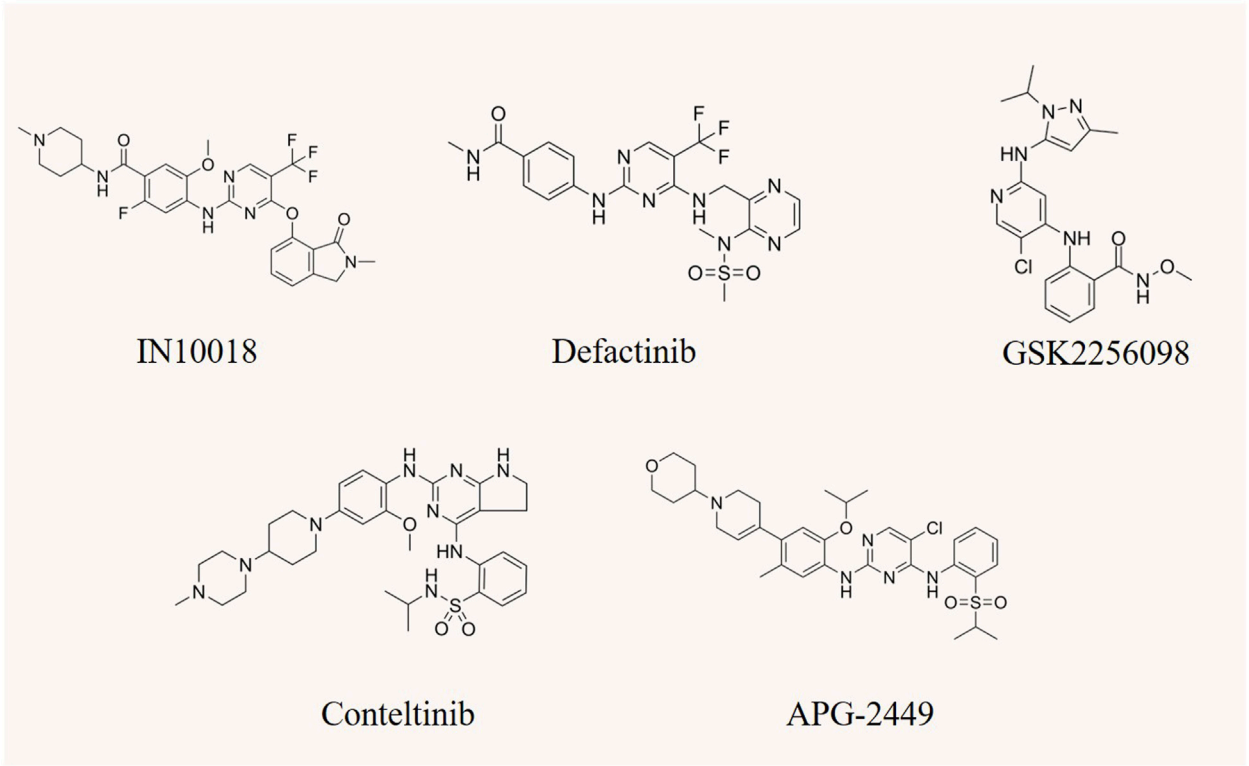

FIGURE 4
The chemical structure of FAK inhibitors IN10018, defactinib, GSK2256098, conteltinib, and APG-2449.

class of ATP-competitive inhibitors. Defactinib inhibits the phosphorylation of FAK Tyr397 in a time- and dose-dependent manner. Many studies have demonstrated that defactinib effectively inhibits in various types of FAK-overexpressing cancers by effectively blocking the PI3K/AKT and downstream signaling (Zhang B Y et al., 2021; Cuellar-Vite et al., 2022; Liu et al., 2024). Moreover, a negative correlation was found between FAK activation and the sensitivity of breast cancer cells to rapamycin. In preclinical models, the inhibition of FAK has shown the potential to increase the sensitivity of rapamycin-resistant tumors to mTORC1 inhibition, suggesting that targeting FAK signaling could be a feasible and effective strategy to enhance the efficacy of mTORC1 inhibitors in resistant cancers (Cuellar-Vite et al., 2022). Moreover, the combination of docetaxel and defactinib has demonstrated significant reductions in the survival rate of docetaxel-resistant prostate cancer cells *in vitro*. Additionally, it effectively inhibits the growth of PC3 xenograft tumors. Notably, FAK expression is positively correlated with advanced tumor stages in human primary prostate cancer (Lin et al., 2018). Defactinib, when combined with osimertinib (an EGFR inhibitor), synergistically inhibits the activation of AKT and induces apoptosis in NSCLC. This combined therapy exhibits a higher therapeutic effect *in vivo* compared to single-drug therapy, suggesting a feasible strategy to overcome drug resistance of NSCLC to EGFR-TKI (Tong et al., 2019). Le Large et al. (Le Large et al., 2021) confirmed that defactinib has anti-proliferative and anti-migratory effects in PDA with overexpressed FAK. When combined with albumin-bound paclitaxel, it synergistically inhibits cell proliferation both *in vitro* and *in vivo*. Uterine serous carcinoma (USC), a distinct subtype of endometrial cancer with higher malignant potential than endometrioid endometrial carcinoma, exhibits enhanced oxidative stress compared with endometrioid endometrial carcinoma tumors. This heightened oxidative stress leads to the phosphorylation of FAK, facilitating tumor invasion and metastasis through the ROS-FAK-PAX signaling pathway. Defactinib significantly inhibited the growth of the tumors of patient-derived orthotopic xenograft models in this context, emphasizing the potential of FAK inhibition in the treatment of USC (Lopez-Mejia et al., 2023).

A phase II trial of defactinib for low Merlin protein-expressing malignant pleural mesothelioma did not demonstrate improvement in PFS and OS compared with placebo after first-line chemotherapy (Fennell et al., 2019). Consequently, it is not recommended to use defactinib alone as maintenance therapy for advanced malignant pleural mesothelioma. However, a phase I study for previously treated advanced KRAS-mutant NSCLC showed that defactinib monotherapy had good overall tolerability, moderate clinical activity, and efficacy in heavily pretreated patients with KRAS-mutant NSCLC, irrespective of TP53 and CDKN2A status (Gerber et al., 2020). This suggests heterogeneity in the response to FAK inhibition across different cancers. In addition, a phase I study revealed that the combination of defactinib, pembrolizumab, and gemcitabine was well-tolerated and did not exhibit any dose-limiting toxicity in patients with refractory pancreatic cancer. The disease control rate (DCR) of 20 evaluable patients with refractory pancreatic cancer was 80%, with the median PFS of 3.6 months and OS of 7.8 months. The combination regimen showed good tolerability and safety, demonstrated preliminary efficacy, and increased the infiltration of T lymphocytes in tumors (Wang-Gillam et al., 2022). Currently, a phase II clinical study known as RAMP-202 aims to assess the effectiveness and safety of the combination treatment of VS-6766 (an RAF/MEK inhibitor) and defactinib in patients with advanced KRAS-mutant NSCLC who have experienced treatment failure with previous platinum chemotherapy and immunotherapy (Capelletto et al., 2022).

6.3 GSK2256098

GSK2256098 is an orally available small molecule compound that exhibits high selectivity in inhibiting FAK to block adhesion, proliferation, and migration of cancer cells (Auger et al., 2012). A preclinical study indicated that GSK2256098 effectively blocks the FAK signaling pathway mediated by CPNE8 in gastric cancer cell migration and metastasis (Zhang P et al., 2022). Additionally, it inhibits the proliferation of various PDA cells (Zhang et al., 2014). The efficacy of GSK2256098 is closely associated with the abnormal expression of certain genes or proteins. Research indicates that PTEN-mutant endometrial cancer patients exhibit markedly superior responses to GSK2256098 treatment compared with patients with PTEN-wild type endometrial cancer (Thanapprapasr et al., 2015). In a phase I trial involving late-stage solid tumor patients, GSK2256098 demonstrated a controllable safety profile, with most adverse reactions ranking grade 1–2, and the maximum tolerated dose (MTD) was determined to be 1000 mg twice daily. When targeting at or below MTD doses, GSK2256098 exhibits clinical activity in mesothelioma patients, especially those with Merlin protein deficiency (Soria et al., 2016). Another phase Ib trial showed that the combined use of trametinib (a MEK inhibitor) and GSK2256098 to treat solid tumors also demonstrated good safety, supporting the progress of further clinical research (Mak et al., 2019). As NF2 mutations serve as malignant markers of meningioma, FAK inhibition, and NF2 loss have been shown to have a synthetic lethality relationship. A phase II trial examined the effectiveness of GSK2256098 in the treatment of patients with NF2 mutant meningiomas. The results demonstrated that GSK2256098 improved 6-month PFS in patients with recurrent or progressive NF2 mutant meningioma compared with that in the control group (Brastianos et al., 2023). These findings suggest the need for further evaluation of GSK2256098 in this specific patient population.

6.4 Conteltinib (CT-707; SY-707)

Conteltinib is a multi-kinase inhibitor targeting FAK, PYK2, and anaplastic lymphoma kinase (ALK). Initially developed as an ALK inhibitor due to its strong inhibitory activity against ALK (IC_{50} = 2.4 nM), conteltinib demonstrated manageable safety, favorable pharmacokinetic properties, and anticancer effects in patients with advanced ALK-positive NSCLC in a phase I human clinical study (Xing et al., 2022). In a breast cancer mouse model, conteltinib was found to inhibit tumor growth and spontaneous metastasis to the lung (Liu P et al., 2022), with the inhibitory effect on tumor invasion and metastasis primarily attributed to FAK inhibition. Preclinical studies further support conteltinib's efficacy in inhibiting FAK kinase activity and blocking downstream

signaling in various tumors, including liver and lung cancer. In liver cancer, conteltinib inhibits the growth of cancer cells *in vitro* and xenografts derived from patients *in vivo* by blocking the IGF1R-YAP signaling axis activated by hypoxia (Zhu et al., 2018). Additionally, conteltinib overcomes sorafenib resistance in hypoxia-mediated liver cancer by inhibiting the YAP signaling pathway (Chen Y et al., 2022). Moreover, conteltinib synergizes with cabozantinib, a MET inhibitor, to inhibit the progression of liver cancer by blocking cabozantinib-induced FAK inactivation (Wang et al., 2016). This approach with FAK-containing kinase inhibitors offers a new therapeutic strategy for refractory metastatic cancers. Previous studies have highlighted the role of FAK inhibition in enhancing immune surveillance by overcoming fibrosis and improving immunosuppressive TME in KPC mouse models. This enhancement results in an improved response of PDA to T cell immunotherapy and PD-1 antagonists (Jiang et al., 2016; Blair et al., 2022). Building on this, a Phase Ib/II, open-label, dose-escalation, and dose-expansion study has been initiated to evaluate the safety, tolerability, pharmacokinetics, and antitumor activity of conteltinib in combination with toripalimab (anti- PD-1 monoclonal antibody) and gemcitabine in advanced pancreatic cancer (NCT05580445).

6.5 APG-2449

APG-2449 is a multi-kinase inhibitor targeting FAK, ALK, and ROS1 in various cancers. In esophageal squamous cell carcinoma, the combination of APG-2449 and ibrutinib effectively inhibits the survival and invasion of cancer cells, inducing cell cycle arrest in the G1/S phase and promoting apoptosis. Mechanistically, this combination therapy significantly reduces the phosphorylation of MEK/ERK and AKT (Luo et al., 2021). Furthermore, APG-2449 has demonstrated the ability to sensitize drug-resistant ovarian xenograft tumors to carboplatin and paclitaxel. The inhibitory effect of APG-2449 on FAK activity contributes to a reduction in CD44-positive and aldehyde dehydrogenase 1-positive CSCs within the TME, thereby improving drug resistance (Fang et al., 2022). Currently, a phase I clinical trial (NCT03917043) is underway to evaluate the safety and preliminary efficacy of APG-2449 in advanced solid tumors (Zhao et al., 2022).

6.6 Other FAK inhibitors

In addition to the aforementioned FAK inhibitors, several drugs entered clinical research based on promising anti-tumor activity in preclinical studies. Unfortunately, these candidates failed to demonstrate significant improvements in disease treatment during subsequent clinical trials. Examples include PF-00562271 (NCT00666926), VS-4718 (NCT01849744; NCT02651727), and CEP-37440 (NCT01922752). Additionally, numerous FAK-targeted drugs are still in preclinical research, such as BJG-03-025 (Groendyke et al., 2021), PF-573228 (Slack-Davis et al., 2007), and Y15 (Hochwald et al., 2009) (Table 2), demanding extensive preclinical research data to support their transition to clinical application.

Given the intricate crosstalk between FAK and multiple signaling proteins in tumor development, various dual or multiple inhibitors emerged to simultaneously target FAK and other pathways. Examples include HDAC2/FAK inhibitors (Compounds 6a (Mustafa et al., 2021a)), EGFR/FAK inhibitors (2-Arylquinolines (Elbadawi et al., 2022)), FAK/IGF-1R inhibitors (TAE-226 (Schultze et al., 2010) and INT2-31167 (Ucar et al., 2012)), and ALK/IGF-R1/FAK inhibitors (Certinib (Mehta et al., 2022)), FAK/ALK inhibitors (CEP-37440 (Ott et al., 2016)), and FAK/CDK4/6 inhibitors (Compounds 1–7 (Sun et al., 2021)). While most inhibitors have displayed promising anticancer activity in preclinical studies, certain drugs faced setbacks in further clinical investigation due to adverse effects (Wu L Y et al., 2022). Notably, TAE-226 remains in the preclinical research stage due to side effects causing severe dysregulation of glucose metabolism and blood glucose in animal models (Kurio et al., 2011). Recent preclinical studies have highlighted novel FAK inhibitors based on the lead compound TAE-226, such as 4-arylamino-pyrimidine derivatives (Long et al., 2023) and 2,4-diaminopyrimidine cinnamyl derivatives (Liu Y et al., 2023b). These compounds exhibit remarkable drug stability and potent anticancer activity, emphasizing the imperative need for further optimization of molecular structures to enhance drug safety, and stability, and reduce off-target effects for clinical application.

6.7 FAK degraders based on PROTAC

The successful development of FAK degraders through Proteolysis Targeting Chimera (PROTAC) technology has also opened up a new pathway for FAK targeted therapy (Pang et al., 2021). A PROTAC comprises three components: a warhead designed for specific binding to target proteins, an E3 ubiquitin ligand to recruit E3 ubiquitin ligases, and a linker to connect them. Specifically, PROTAC facilitates the proximity of the target protein with the E3 ubiquitin ligase, leading to ubiquitination and subsequent degradation through the proteasome system (Bekes et al., 2022). The primary distinction in FAK-PROTAC design lies in the variation of their ligands. The activity of PROTACs is closely associated with the expression of ligase RNA, DNA copy number, and protein levels (Luo et al., 2022). Currently, cereblon (CRBN) and Von Hippel-Lindau (VHL)-based PROTACs are extensively utilized due to their low molecular weight, favorable drug formation, and facile synthesis (Luo et al., 2022; Jiang et al., 2023). Utilizing PROTAC technology, a diverse range of degraders targeting androgen receptor (AR), estrogen receptor (ER), Bruton's tyrosine kinase (BTK), STAT3, BRD4, and other protein molecules have been developed. While certain drugs like ARV-110 (targeting AR) and ARV-471 (targeting ER) have exhibited remarkable efficacy in clinical trials, the degraders targeting FAK are yet to progress into the clinical stage (Chen Z et al., 2022; Liu Z et al., 2022; Zhao et al., 2023). Compared with the conventional small molecule inhibitors that solely inhibit kinase activity, PROTAC technology effectively eliminates both kinase-dependent enzymatic activity and scaffold function by inducing degradation of FAK (Figure 5). This approach circumvents drug resistance arising from the restoration of FAK functionality (Huo et al., 2022).

Cromm et alprepared PROTAC 3, a compound that efficiently degrades FAK at low concentrations, inhibiting 95% of Fak at 50 nM. This compound is created by conjugating a modified defactinib warhead to a VHL ligand via a linker. Their study findings demonstrate the superiority of PROTAC 3 over the FAK

TABLE 2 Summary of FAK inhibitors in preclinical studies.

Drug	Target	CAS number	IC_{50} to FAK	Start time	References
BJG-03-025	FAK	2553213-90-2	20.2 nM	2020	Groendyke et al. (2021)
PF-573228	FAK	869288-64-2	4 nM	2007	Slack-Davis et al. (2007)
Y15	FAK	4506-66-5	-	2009	Hochwald et al. (2009)
PF-562271	FAK/PYK2	717907-75-0	1.5 nM	2008	Roberts et al. (2008)
FAK-IN-9	FAK	2911655-93-9	27.44 nM	2023	Zhang et al. (2023a)
PROTAC FAK degrader 1	FAK	2301916-69-6	6.5 nM	2018	Cromm et al. (2018)
NVP-TAE 226	FAK/IGF-1R	761437-28-9	5.5 nM	2007	Liu et al. (2007)
GSK215	FAK	2743427-26-9	-	2021	Law et al. (2021)
BI-3663	FAK/PYK2	2341740-84-7	18 nM	2019	Popow et al. (2019)
BI-4464	FAK	1227948-02-8	17 nM	2019	Popow et al. (2019)
FAK inhibitor 2	FAK	2354405-14-2	0.07 nM	2019	Su et al. (2019)
FAK-IN-7	FAK	19948-85-7	11.72 μM	2012	Yang et al. (2012)
FAK-IN-8	FAK	1374959-91-7	5.32 μM	2012	Yang et al. (2012)
FAK-IN-5	FAK	2408317-70-2	-	2020	Jorda et al. (2020)
FAK inhibitor 5	FAK	2237234-47-6	0.6 nM	2013	Iwatani et al. (2013)
FAK-IN-3	FAK	2882094-29-1	-	2022	Wei et al. (2022)
FAK-IN-4	FAK	-	-	2022	Yang L et al. (2022)
EGFR-IN-46	EGFR/FAK	2764772-88-3	14.25 nM	2022	Elbadawi et al. (2022)
FAK-IN-2	FAK	2872588-02-6	35 nM	2021	Chen et al. (2021)

Note: CAS, chemical abstracts service; FAK, focal adhesion kinase; PYK2, proline-rich tyrosine kinase 2; IGF-1R, insulin-like growth factor 1 receptor; EGFR, epidermal growth factor receptor.

inhibitors defactinib in terms of activating FAK and inhibiting downstream proteins paxillin and AKT signaling (Cromm et al., 2018). Notably, both FAK encoding genes PTK2 and ASAP1 are located in the oncogenomic locus 8q24 and are associated with tumor metastasis and recurrence. By blocking FAK kinase activity and the interaction between FAK and ASAP1, PROTAC 3 exhibits high efficacy in inhibiting invasion and metastasis of ovarian cancer cells (Huo et al., 2022). GSK215 is a FAK highly selective PROTAC based on VHL E3 ligase adhesive and FAK inhibitor VS-4718. In mice, a single dose of GSK215 induced rapid and long-term degradation of FAK, having a lasting effect on FAK levels lasting approximately 96 h (Law et al., 2021). Additionally, another team developed and compared the consequences and advantages of the FAK degrader BSJ-04146 and the FAK inhibitor BSJ-04-175 in eliminating all FAK activities in cancer models. The results showed that, compared with kinase inhibition, the targeted degradation of FAK performed better in downstream signal transduction and cancer cell viability and migration (Koide et al., 2023). Based on the above findings, FAK-targeted PROTAC may emerge as a more promising research and development strategy, as well as a treatment modality, compared with FAK small molecular inhibitors in the foreseeable future.

In preclinical studies of lung cancer, two novel FAK-PROTACs (PROTAC-A13 and PROTAC B5) demonstrated superior FAK degradation compared with the FAK inhibitor PF-562271 (PROTAC-A13: 85% degradation at 10 nM; PROTAC-B5: 86.4% degradation at 10 nM), as well as potent anti-cancer activity (PROTAC-A13: IC50 value of 26.4 nM; PROTAC-B5: IC50 = 0.14 μM). At the same time, they exhibit excellent plasma stability and appropriate membrane permeability (Qin et al., 2022; Sun et al., 2022). Additionally, Professor Rao Yu's team developed a FAK PROTAC (FC-11) based on the CRBN ligand, which exhibiting remarkable degradation activity with a DC50 value of 310 pM (Gao et al., 2020b). Furthermore, the team investigated the practical application potential and side effects of this compound and discovered that after treatment with FC-11, there was a significant decrease in both sperm count and vitality in the mouse epididymis. However, no impact on the reproductive system was observed when using the FAK inhibitor PF562271. Importantly, discontinuing the administration of PF562271 restored sperm vitality (Gao et al., 2020a). These findings offer promising prospects for the future development of reversible male contraceptives.

7 Summary and prospect

FAK is frequently overexpressed in various cancer types and is associated with poor prognoses for cancer patients. FAK plays a crucial role in mediating signaling pathways such as p53, RAS/RAF/MEK, and YAP/TAZ, promoting tumor cell survival and progression. Additionally, FAK influences the tumor immune

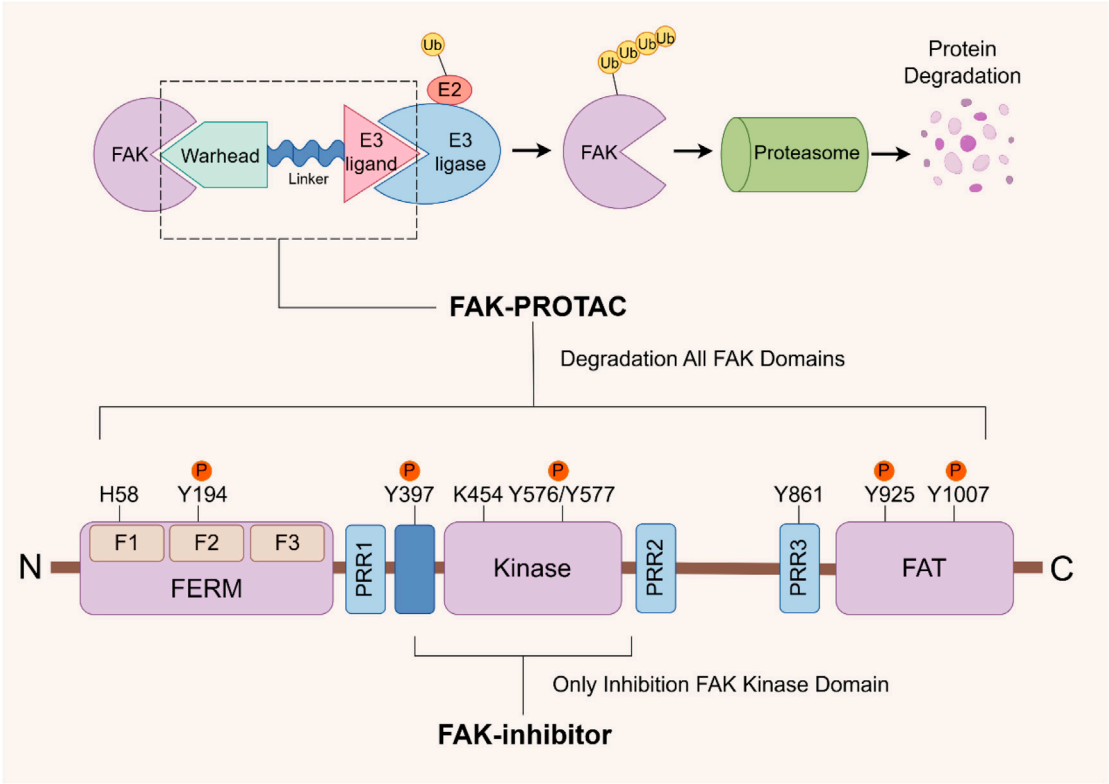

FIGURE 5
FAK- PROTAC domain structure and working principle. The FAK-PROTAC system comprises three essential components: a specifically designed warhead to bind to FAK, an E3 ubiquitin ligand responsible for recruiting E3 ubiquitin ligase, and a linker connecting the two. PROTAC functions by facilitating the proximity between FAK and E3 ubiquitin ligase, which subsequently leads to ubiquitination, followed by proteasome degradation. PROTAC: Proteolysis Targeting Chimera.

microenvironment, affecting the expression and chemotaxis of immune cells and modulating ECM density to promote metastasis and drug resistance. As a result, FAK has become an attractive therapeutic target. Numerous small molecular inhibitors of FAK have been developed, some progressing to the clinical research stage. While FAK kinase function inhibitors have demonstrated safety and efficacy, there are currently no clinically approved FAK inhibitors. Recently, the focus has shifted to the development of FAK degradation agents based on PROTAC technology (Qin et al., 2022; Sun et al., 2022; Koide et al., 2023). This approach aims to induce the complete loss of FAK function through ubiquitination, reducing the occurrence of drug resistance. Nevertheless, the improvement of both high selectivity and specificity of FAK degraders remains a primary focus for future research and development endeavors. Additionally, the CRISPR/Cas9 system, comprising a small guide RNA and a functional Cas9 endonuclease protein, serves as a potent gene editing tool capable of precisely disrupting or modifying FAK at the DNA level. Simultaneously, other genes such as MEK can be targeted for knockout to investigate potential synergistic effects between related genes, offering promisingly exploration and application prospects (Paradis et al., 2021; Sun et al., 2023).

Current research indicates that FAK inhibitors show limited efficacy as monotherapy in cancer treatment, but promising results emerge when combined with other drugs. Additionally, while explaining the role of FAK in signaling pathways and tumor development, we found promising therapeutic targets that can be synergistically combined with FAK. Specifically, significant synergies were noted when FAK inhibitors were combined with mTOR inhibitors (Shi et al., 2016; Cuellar-Vite et al., 2022), RAF/MEK inhibitors (Capelletto et al., 2022; Gu et al., 2022; Tarin et al., 2023), CDK4/6 inhibitors (Murphy et al., 2022; Peng et al., 2023), MAPK inhibitors (Peng et al., 2023), and VEGF inhibitors such as bevacizumab (Zheng et al., 2023). Furthermore, we observed an upregulation of FAK in specific tumor types with gene mutations or aberrant protein expression, such as BRAF/KRAS mutations, CDH1 deletions, EGFR or HER2 overexpression, and mediated drug resistance processes (Tong et al., 2019; Yuen et al., 2021; Yu et al., 2022; Castro-Guijarro et al., 2023). Therefore, identifying tumor types that exhibit increased sensitivity to FAK is important for enhancing targeted efficacy and screening specific populations responsive to FAK inhibition. Inhibition of FAK enhances the sensitivity to chemotherapy drugs or radiotherapy by modulating DNA damage repair genes (Tang et al., 2016), making it a potential ally for immunotherapy by reshaping the TME. Combination therapy with FAK inhibitors is considered a promising treatment strategy with broad research prospects. Ongoing clinical studies on FAK inhibitors are awaited to provide further guidance for current research strategies targeting FAK.

Author contributions

H-HH: Writing–original draft, Writing–review and editing, Data curation, Formal Analysis. S-QW: Funding acquisition, Writing–review and editing, Writing–original draft. H-LS: Validation, Writing–review and editing. H-FL: Investigation, Methodology, Writing–review and editing. B-BC: Data curation, Funding acquisition, Investigation, Writing–review and editing. S-GG: Conceptualization, Methodology, Supervision, Writing–review and editing. X-BC: Conceptualization, Supervision, Writing–review and editing.

Funding

The author(s) declare financial support was received for the research, authorship, and/or publication of this article. This work was funded by the National Natural Science Foundation of China (No. 82103560), Henan Medical Science and Technique Foundation of Henan Province (Nos. SBGJ202302029 and SBGJ202301004), Young and middle-aged health science and technology innovation talent training Project of Henan Province (Nos. YXKC2022048 and YXKC2020008), Science and Technique Foundation of Henan Province (No. 202102310413), and Natural Science Foundation of Henan Province (Nos. 232300421119 and 212300410270).

Acknowledgments

We would like to thank all the reviewers for their participation in the review, as well as Figraw for providing a drawing platform for the figures in this article.

Conflict of interest

The authors declare that the research was conducted in the absence of any commercial or financial relationships that could be construed as a potential conflict of interest.

Publisher's note

All claims expressed in this article are solely those of the authors and do not necessarily represent those of their affiliated organizations, or those of the publisher, the editors and the reviewers. Any product that may be evaluated in this article, or claim that may be made by its manufacturer, is not guaranteed or endorsed by the publisher.

References

Abhinand, C. S., Galipon, J., Mori, M., Ramesh, P., Prasad, T., Raju, R., et al. (2023). Temporal phosphoproteomic analysis of VEGF-A signaling in HUVECs: an insight into early signaling events associated with angiogenesis. *J. Cell Commun. Signal.* 17 (3), 1067–1079. doi:10.1007/s12079-023-00736-z

Aboubakar, N. F., Hoton, D., Ambroise, J., Lecocq, M., Vanderputten, M., Sibille, Y., et al. (2019a). Increased expression and activation of FAK in small-cell lung cancer compared to non-small-cell lung cancer. *Cancers* 11 (10), 1526. doi:10.3390/cancers11101526

Aboubakar, N. F., Vanderputten, M., and Ocak, S. (2019b). Role of focal adhesion kinase in small-cell lung cancer and its potential as a therapeutic target. *Cancers* 11 (11), 1683. doi:10.3390/cancers11111683

Acebron, I., Righetto, R. D., Schoenherr, C., de Buhr, S., Redondo, P., Culley, J., et al. (2020). Structural basis of Focal Adhesion Kinase activation on lipid membranes. *Embo J.* 39 (19), e104743. doi:10.15252/embj.2020104743

Allert, C., Waclawiczek, A., Zimmermann, S., Gollner, S., Heid, D., Janssen, M., et al. (2022). Protein tyrosine kinase 2b inhibition reverts niche-associated resistance to tyrosine kinase inhibitors in AML. *Leukemia* 36 (10), 2418–2429. doi:10.1038/s41375-022-01687-x

Arang, N., Lubrano, S., Rigiracciolo, D. C., Nachmanson, D., Lippman, S. M., Mali, P., et al. (2023). Whole-genome CRISPR screening identifies PI3K/AKT as a downstream component of the oncogenic GNAQ-focal adhesion kinase signaling circuitry. *J. Biol. Chem.* 299 (2), 102866. doi:10.1016/j.jbc.2022.102866

Auger, K. R., Smitheman, K. N., Korenchuk, S., Mchugh, C., Kruger, R., Aller, G. V., et al. (2012). 387 the focal adhesion kinase inhibitor GSK2256098: a potent and selective inhibitor for the treatment of cancer. *Eur. J. Cancer.* 48 (6), 118. doi:10.1016/s0959-8049(12)72185-8

Avraham, H., Park, S. Y., Schinkmann, K., and Avraham, S. (2000). RAFTK/Pyk2-mediated cellular signalling. *Cell. Signal.* 12 (3), 123–133. doi:10.1016/s0898-6568(99)00076-5

Begum, A., Mcmillan, R. H., Chang, Y. T., Penchev, V. R., Rajeshkumar, N. V., Maitra, A., et al. (2019). Direct interactions with cancer-associated fibroblasts lead to enhanced pancreatic cancer stem cell function. *Pancreas* 48 (3), 329–334. doi:10.1097/MPA.0000000000001249

Bekes, M., Langley, D. R., and Crews, C. M. (2022). PROTAC targeted protein degraders: the past is prologue. *Nat. Rev. Drug Discov.* 21 (3), 181–200. doi:10.1038/s41573-021-00371-6

Berger, B. T., Amaral, M., Kokh, D. B., Nunes-Alves, A., Musil, D., Heinrich, T., et al. (2021). Structure-kinetic relationship reveals the mechanism of selectivity of FAK inhibitors over PYK2. *Cell Chem. Biol.* 28 (5), 686–698.e7. doi:10.1016/j.chembiol.2021.01.003

Blair, A. B., Wang, J., Davelaar, J., Baker, A., Li, K., Niu, N., et al. (2022). Dual stromal targeting sensitizes pancreatic adenocarcinoma for anti-programmed cell death protein 1 therapy. *Gastroenterology* 163 (5), 1267–1280.e7. doi:10.1053/j.gastro.2022.06.027

Blanco-Gomez, A., and Jorgensen, C. (2023). FAK scaffolds immune escape in pancreatic cancer. *Gut* 73, 6–8. doi:10.1136/gutjnl-2023-330049

Brastianos, P. K., Twohy, E. L., Gerstner, E. R., Kaufmann, T. J., Iafrate, A. J., Lennerz, J., et al. (2023). Alliance A071401: phase II trial of focal adhesion kinase inhibition in meningiomas with somatic NF2 mutations. *J. Clin. Oncol.* 41 (3), 618–628. doi:10.1200/JCO.21.02371

Canel, M., Slawinska, A. D., Lonergan, D. W., Kallor, A. A., Upstill-Goddard, R., Davidson, C., et al. (2023). FAK suppresses antigen processing and presentation to promote immune evasion in pancreatic cancer. *Gut* 73, 131–155. doi:10.1136/gutjnl-2022-327927

Capelletto, E., Bironzo, P., Denis, L., Koustenis, A., Bungaro, M., and Novello, S. (2022). Single agent VS-6766 or VS-6766 plus defactinib in KRAS-mutant non-small-cell lung cancer: the RAMP-202 phase II trial. *Future Oncol.* 18 (16), 1907–1915. doi:10.2217/fon-2021-1582

Castro-Guijarro, A. C., Sanchez, A. M., and Flamini, M. I. (2023). Potential biomarkers associated with prognosis and trastuzumab response in HER2+ breast cancer. *Cancers* 15 (17), 4374. doi:10.3390/cancers15174374

Chen, G., Gao, C., Gao, X., Zhang, D. H., Kuan, S. F., Burns, T. F., et al. (2018). Wnt/β-Catenin pathway activation mediates adaptive resistance to BRAF inhibition in colorectal cancer. *Mol. Cancer Ther.* 17 (4), 806–813. doi:10.1158/1535-7163.MCT-17-0561

Chen, H., Tu, W., Lu, Y., Zhang, Y., Xu, Y., Chen, X., et al. (2022). Low-dose X-ray irradiation combined with FAK inhibitors improves the immune microenvironment and confers sensitivity to radiotherapy in pancreatic cancer. *Biomed. Pharmacother.* 151, 113114. doi:10.1016/j.biopha.2022.113114

Chen, T., Liu, Y., Shi, M., Tang, M., Si, W., Yuan, X., et al. (2021). Design, synthesis, and biological evaluation of novel covalent inhibitors targeting focal adhesion kinase. *Bioorg. Med. Chem. Lett.* 54, 128433. doi:10.1016/j.bmcl.2021.128433

Chen, Y., Yang, Q., Xu, J., Tang, L., Zhang, Y., Du, F., et al. (2022). PROTACs in gastrointestinal cancers. *Mol. Ther.-Oncolytics.* 27, 204–223. doi:10.1016/j.omto.2022.10.012

Chen, Z., Yuan, T., Yan, F., Ye, S., Xie, Q., Zhang, B., et al. (2022). CT-707 overcomes hypoxia-mediated sorafenib resistance in Hepatocellular carcinoma by inhibiting YAP signaling. *BMC Cancer* 22 (1), 425. doi:10.1186/s12885-022-09520-5

Chuang, H. H., Zhen, Y. Y., Tsai, Y. C., Chuang, C. H., Hsiao, M., Huang, M. S., et al. (2022). FAK in cancer: from mechanisms to therapeutic strategies. *Int. J. Mol. Sci.* 23 (3), 1726. doi:10.3390/ijms23031726

Claesson-Welsh, L., and Welsh, M. (2013). VEGFA and tumour angiogenesis. *J. Intern. Med.* 273 (2), 114–127. doi:10.1111/joim.12019

Cooper, J., and Giancotti, F. G. (2019). Integrin signaling in cancer: mechanotransduction, stemness, epithelial plasticity, and therapeutic resistance. *Cancer Cell* 35 (3), 347–367. doi:10.1016/j.ccell.2019.01.007

Cromm, P. M., Samarasinghe, K., Hines, J., and Crews, C. M. (2018). Addressing kinase-independent functions of Fak via PROTAC-mediated degradation. *J. Am. Chem. Soc.* 140 (49), 17019–17026. doi:10.1021/jacs.8b08008

Cuellar-Vite, L., Weber-Bonk, K. L., Abdul-Karim, F. W., Booth, C. N., and Keri, R. A. (2022). Focal adhesion kinase provides a collateral vulnerability that can Be leveraged to improve mTORC1 inhibitor efficacy. *Cancers* 14 (14), 3374. doi:10.3390/cancers14143374

Dawson, J. C., Serrels, A., Stupack, D. G., Schlaepfer, D. D., and Frame, M. C. (2021). Targeting FAK in anticancer combination therapies. *Nat. Rev. Cancer.* 21 (5), 313–324. doi:10.1038/s41568-021-00340-6

de Jonge, M., Steeghs, N., Lolkema, M. P., Hotte, S. J., Hirte, H. W., van der Biessen, D., et al. (2019). Phase I study of BI 853520, an inhibitor of focal adhesion kinase, in patients with advanced or metastatic nonhematologic malignancies. *Target. Oncol.* 14 (1), 43–55. doi:10.1007/s11523-018-00617-1

Del, M. G., Riemann, S., Schindler, S., Beissert, S., Kontermann, R. E., Ginolhac, A., et al. (2022). Focal adhesion kinase plays a dual role in TRAIL resistance and metastatic outgrowth of malignant melanoma. *Cell Death Dis.* 13 (1), 54. doi:10.1038/s41419-022-04502-8

Doi, T., Yang, J. C., Shitara, K., Naito, Y., Cheng, A. L., Sarashina, A., et al. (2019). Phase I study of the focal adhesion kinase inhibitor BI 853520 in Japanese and Taiwanese patients with advanced or metastatic solid tumors. *Target. Oncol.* 14 (1), 57–65. doi:10.1007/s11523-019-00620-0

Dong, C., Li, X., Yang, J., Yuan, D., Zhou, Y., Zhang, Y., et al. (2021). PPFIBP1 induces glioma cell migration and invasion through FAK/Src/JNK signaling pathway. *Cell Death Dis.* 12 (9), 827. doi:10.1038/s41419-021-04107-7

Elbadawi, M. M., Eldehna, W. M., Abd, E. A., Somaa, W. R., Albohy, A., Al-Rashood, S. T., et al. (2022). 2-Arylquinolines as novel anticancer agents with dual EGFR/FAK kinase inhibitory activity: synthesis, biological evaluation, and molecular modelling insights. *J. Enzym. Inhib. Med. Chem.* 37 (1), 349–372. doi:10.1080/14756366.2021.2015344

Fallahi-Sichani, M., Becker, V., Izar, B., Baker, G. J., Lin, J. R., Boswell, S. A., et al. (2017). Adaptive resistance of melanoma cells to RAF inhibition via reversible induction of a slowly dividing de-differentiated state. *Mol. Syst. Biol.* 13 (1), 905. doi:10.15252/msb.20166796

Fan, H., and Guan, J. L. (2011). Compensatory function of Pyk2 protein in the promotion of focal adhesion kinase (FAK)-null mammary cancer stem cell tumorigenicity and metastatic activity. *J. Biol. Chem.* 286 (21), 18573–18582. doi:10.1074/jbc.M110.200717

Fang, D. D., Tao, R., Wang, G., Li, Y., Zhang, K., Xu, C., et al. (2022). Discovery of a novel ALK/ROS1/FAK inhibitor, APG-2449, in preclinical non-small cell lung cancer and ovarian cancer models. *BMC Cancer* 22 (1), 752. doi:10.1186/s12885-022-09799-4

Fard, D., Testa, E., Panzeri, V., Rizzolio, S., Bianchetti, G., Napolitano, V., et al. (2023). SEMA6C: a novel adhesion-independent FAK and YAP activator, required for cancer cell viability and growth. *Cell. Mol. Life Sci.* 80 (4), 111. doi:10.1007/s00018-023-04756-1

Feng, X., Arang, N., Rigiracciolo, D. C., Lee, J. S., Yeerna, H., Wang, Z., et al. (2019). A platform of synthetic lethal gene interaction networks reveals that the GNAQ uveal melanoma oncogene controls the Hippo pathway through FAK. *Cancer Cell* 35 (3), 457–472. doi:10.1016/j.ccell.2019.01.009

Fennell, D. A., Baas, P., Taylor, P., Nowak, A. K., Gilligan, D., Nakano, T., et al. (2019). Maintenance defactinib versus placebo after first-line chemotherapy in patients with merlin-stratified pleural mesothelioma: COMMAND-A double-blind, randomized, phase II study. *J. Clin. Oncol.* 37 (10), 790–798. doi:10.1200/JCO.2018.79.0543

Fresno, V. J., Casado, E., de Castro, J., Cejas, P., Belda-Iniesta, C., and Gonzalez-Baron, M. (2004). PI3K/Akt signalling pathway and cancer. *Cancer Treat. Rev.* 30 (2), 193–204. doi:10.1016/j.ctrv.2003.07.007

Gao, H., Wu, Y., Sun, Y., Yang, Y., Zhou, G., and Rao, Y. (2020a). Design, synthesis, and evaluation of highly potent FAK-targeting PROTACs. *ACS Med. Chem. Lett.* 11 (10), 1855–1862. doi:10.1021/acsmedchemlett.9b00372

Gao, H., Zheng, C., Du, J., Wu, Y., Sun, Y., Han, C., et al. (2020b). FAK-targeting PROTAC as a chemical tool for the investigation of non-enzymatic FAK function in mice. *Protein Cell* 11 (7), 534–539. doi:10.1007/s13238-020-00732-8

Gao, J., Yao, Y., Liu, C., Xie, X., Li, D., Liu, P., et al. (2023). Synergism of FAK and ROS1 inhibitors in the treatment of CDH1-deficient cancers mediated by FAK-YAP signaling. *Int. J. Biol. Sci.* 19 (9), 2711–2724. doi:10.7150/ijbs.81918

Gerber, D. E., Camidge, D. R., Morgensztern, D., Cetnar, J., Kelly, R. J., Ramalingam, S. S., et al. (2020). Phase 2 study of the focal adhesion kinase inhibitor defactinib (VS-6063) in previously treated advanced KRAS mutant non-small cell lung cancer. *Lung Cancer* 139, 60–67. doi:10.1016/j.lungcan.2019.10.033

Golubovskaya, V. M., and Cance, W. (2010). Focal adhesion kinase and p53 signal transduction pathways in cancer. *Front. Biosci.* 15 (3), 901–912. doi:10.2741/3653

Goto, Y., Ando, T., Izumi, H., Feng, X., Arang, N., Gilardi, M., et al. (2020). Muscarinic receptors promote castration-resistant growth of prostate cancer through a FAK-YAP signaling axis. *Oncogene* 39 (20), 4014–4027. doi:10.1038/s41388-020-1272-x

Groendyke, B. J., Nabet, B., Mohardt, M. L., Zhang, H. S., Peng, K., Koide, E., et al. (2021). Discovery of a pyrimidothiazolodiazepinone as a potent and selective focal adhesion kinase (FAK) inhibitor. *ACS Med. Chem. Lett.* 12 (1), 30–38. doi:10.1021/acsmedchemlett.0c00338

Gu, Y., Wei, C., Chung, M., Li, H., Guo, Z., Long, M., et al. (2022). Concurrent inhibition of FAK/SRC and MEK overcomes MEK inhibitor resistance in Neurofibromatosis Type I related malignant peripheral nerve sheath tumors. *Front. Oncol.* 12, 910505. doi:10.3389/fonc.2022.910505

Guo, D., Zhang, D., Ren, M., Lu, G., Zhang, X., He, S., et al. (2020). THBS4 promotes HCC progression by regulating ITGB1 via FAK/PI3K/AKT pathway. *Faseb J.* 34 (8), 10668–10681. doi:10.1096/fj.202000043R

Heng, B. C., Zhang, X., Aubel, D., Bai, Y., Li, X., Wei, Y., et al. (2021). An overview of signaling pathways regulating YAP/TAZ activity. *Cell. Mol. Life Sci.* 78 (2), 497–512. doi:10.1007/s00018-020-03579-8

Hirt, U. A., Waizenegger, I. C., Schweifer, N., Haslinger, C., Gerlach, D., Braunger, J., et al. (2018). Efficacy of the highly selective focal adhesion kinase inhibitor BI 853520 in adenocarcinoma xenograft models is linked to a mesenchymal tumor phenotype. *Oncogenesis* 7 (2), 21. doi:10.1038/s41389-018-0032-z

Hochwald, S. N., Nyberg, C., Zheng, M., Zheng, D., Wood, C., Massoll, N. A., et al. (2009). A novel small molecule inhibitor of FAK decreases growth of human pancreatic cancer. *Cell Cycle* 8 (15), 2435–2443. doi:10.4161/cc.8.15.9145

Hu, C., Zhou, H., Liu, Y., Huang, J., Liu, W., Zhang, Q., et al. (2019). ROCK1 promotes migration and invasion of non-small-cell lung cancer cells through the PTEN/PI3K/FAK pathway. *Int. J. Oncol.* 55 (4), 833–844. doi:10.3892/ijo.2019.4864

Hu, J., Cao, J., Topatana, W., Juengpanich, S., Li, S., Zhang, B., et al. (2021). Targeting mutant p53 for cancer therapy: direct and indirect strategies. *J. Hematol. Oncol.* 14 (1), 157. doi:10.1186/s13045-021-01169-0

Huang, K., Gao, N., Bian, D., Zhai, Q., Yang, P., Li, M., et al. (2020). Correlation between FAK and EGF-induced EMT in colorectal cancer cells. *J. Oncol.* 2020, 5428920. doi:10.1155/2020/5428920

Huang, Y. H., Chen, H. K., Hsu, Y. F., Chen, H. C., Chuang, C. H., Huang, S. W., et al. (2023). Src-FAK signaling mediates interleukin 6-induced HCT116 colorectal cancer epithelial-mesenchymal transition. *Int. J. Mol. Sci.* 24 (7), 6650. doi:10.3390/ijms24076650

Huo, X., Zhang, W., Zhao, G., Chen, Z., Dong, P., Watari, H., et al. (2022). FAK PROTAC inhibits ovarian tumor growth and metastasis by disrupting kinase dependent and independent pathways. *Front. Oncol.* 12, 851065. doi:10.3389/fonc.2022.851065

Imperial, R., Toor, O. M., Hussain, A., Subramanian, J., and Masood, A. (2019). Comprehensive pancancer genomic analysis reveals (RTK)-RAS-RAF-MEK as a key dysregulated pathway in cancer: its clinical implications. *Semin. Cancer Biol.* 54, 14–28. doi:10.1016/j.semcancer.2017.11.016

Iwatani, M., Iwata, H., Okabe, A., Skene, R. J., Tomita, N., Hayashi, Y., et al. (2013). Discovery and characterization of novel allosteric FAK inhibitors. *Eur. J. Med. Chem.* 61, 49–60. doi:10.1016/j.ejmech.2012.06.035

Jang, M., Koh, I., Lee, J. E., Lim, J. Y., Cheong, J. H., and Kim, P. (2018). Increased extracellular matrix density disrupts E-cadherin/β-catenin complex in gastric cancer cells. *Biomater. Sci.* 6 (10), 2704–2713. doi:10.1039/c8bm00843d

Jang, T. H., Huang, W. C., Tung, S. L., Lin, S. C., Chen, P. M., Cho, C. Y., et al. (2022). MicroRNA-485-5p targets keratin 17 to regulate oral cancer stemness and chemoresistance via the integrin/FAK/Src/ERK/β-catenin pathway. *J. Biomed. Sci.* 29 (1), 42. doi:10.1186/s12929-022-00824-z

Jarahian, M., Marofi, F., Maashi, M. S., Ghaebi, M., Khezri, A., and Berger, M. R. (2021). Re-expression of poly/oligo-sialylated adhesion molecules on the surface of tumor cells disrupts their interaction with immune-effector cells and contributes to pathophysiological immune escape. *Cancers* 13 (20), 5203. doi:10.3390/cancers13205203

Jean, C., Chen, X. L., Nam, J. O., Tancioni, I., Uryu, S., Lawson, C., et al. (2014). Inhibition of endothelial FAK activity prevents tumor metastasis by enhancing barrier function. *J. Cell Biol.* 204 (2), 247–263. doi:10.1083/jcb.201307067

Jeong, K., Kim, J. H., Murphy, J. M., Park, H., Kim, S. J., Rodriguez, Y., et al. (2019). Nuclear focal adhesion kinase controls vascular smooth muscle cell proliferation and neointimal hyperplasia through GATA4-mediated cyclin D1 transcription. *Circ. Res.* 125 (2), 152–166. doi:10.1161/CIRCRESAHA.118.314344

Jeong, K., Murphy, J. M., Ahn, E. E., and Lim, S. S. (2022). FAK in the nucleus prevents VSMC proliferation by promoting p27 and p21 expression via Skp2 degradation. *Cardiovasc. Res.* 118 (4), 1150–1163. doi:10.1093/cvr/cvab132

Jeong, K., Murphy, J. M., Kim, J. H., Campbell, P. M., Park, H., Rodriguez, Y., et al. (2021). FAK activation promotes SMC dedifferentiation via increased DNA methylation in contractile genes. *Circ. Res.* 129 (12), e215–e233. doi:10.1161/CIRCRESAHA.121.319066

Jiang, H., Hegde, S., Knolhoff, B. L., Zhu, Y., Herndon, J. M., Meyer, M. A., et al. (2016). Targeting focal adhesion kinase renders pancreatic cancers responsive to checkpoint immunotherapy. *Nat. Med.* 22 (8), 851–860. doi:10.1038/nm.4123

Jiang, H., Liu, X., Knolhoff, B. L., Hegde, S., Lee, K. B., Jiang, H., et al. (2020). Development of resistance to FAK inhibition in pancreatic cancer is linked to stromal depletion. *Gut* 69 (1), 122–132. doi:10.1136/gutjnl-2018-317424

Jiang, H., Xiong, H., Gu, S. X., and Wang, M. (2023). E3 ligase ligand optimization of Clinical PROTACs. *Front. Chem.* 11, 1098331. doi:10.3389/fchem.2023.1098331

Jiang, W., Cai, F., Xu, H., Lu, Y., Chen, J., Liu, J., et al. (2020). Extracellular signal regulated kinase 5 promotes cell migration, invasion and lung metastasis in a FAK-dependent manner. *Protein Cell* 11 (11), 825–845. doi:10.1007/s13238-020-00701-1

Jin, M. H., Nam, A. R., Park, J. E., Bang, J. H., Bang, Y. J., and Oh, D. Y. (2017). Resistance mechanism against trastuzumab in HER2-positive cancer cells and its negation by Src inhibition. *Mol. Cancer Ther.* 16 (6), 1145–1154. doi:10.1158/1535-7163.MCT-16-0669

Jorda, R., Magar, P., Hendrychova, D., Pauk, K., Dibus, M., Pilarova, E., et al. (2020). Novel modified leucine and phenylalanine dipeptides modulate viability and attachment of cancer cells. *Eur. J. Med. Chem.* 188, 112036. doi:10.1016/j.ejmech.2020.112036

Kanteti, R., Mirzapoiazova, T., Riehm, J. J., Dhanasingh, I., Mambetsariev, B., Wang, J., et al. (2018). Focal adhesion kinase a potential therapeutic target for pancreatic cancer and malignant pleural mesothelioma. *Cancer Biol. Ther.* 19 (4), 316–327. doi:10.1080/15384047.2017.1416937

Ke, S., Liu, Z., Wang, Q., Zhai, G., Shao, H., Yu, X., et al. (2022). FAM107A inactivation associated with promoter methylation affects prostate cancer progression through the FAK/PI3K/AKT pathway. *Cancers* 14 (16), 3915. doi:10.3390/cancers14163915

Kim, H., Son, S., Ko, Y., and Shin, I. (2021). CTGF regulates cell proliferation, migration, and glucose metabolism through activation of FAK signaling in triple-negative breast cancer. *Oncogene* 40 (15), 2667–2681. doi:10.1038/s41388-021-01731-7

Klungsaeng, S., Kukongviriyapan, V., Prawan, A., Kongpetch, S., and Senggunprai, L. (2020). Targeted modulation of FAK/PI3K/PDK1/AKT and FAK/p53 pathways by cucurbitacin B for the antiproliferation effect against human cholangiocarcinoma cells. *Am. J. Chin. Med.* 48 (6), 1475–1489. doi:10.1142/S0192415X2050072X

Ko, S., Jung, K. H., Yoon, Y. C., Han, B. S., Park, M. S., Lee, Y. J., et al. (2022). A novel DDR1 inhibitor enhances the anticancer activity of gemcitabine in pancreatic cancer. *Am. J. Cancer Res.* 12 (9), 4326–4342.

Koide, E., Mohardt, M. L., Doctor, Z. M., Yang, A., Hao, M., Donovan, K. A., et al. (2023). Development and characterization of selective FAK inhibitors and PROTACs with *in vivo* activity. *ChemBioChem* 24 (19), e202300141. doi:10.1002/cbic.202300141

Kornberg, L., Earp, H. S., Parsons, J. T., Schaller, M., and Juliano, R. L. (1992). Cell adhesion or integrin clustering increases phosphorylation of a focal adhesion-associated tyrosine kinase. *J. Biol. Chem.* 267 (33), 23439–23442. doi:10.1016/s0021-9258(18)35853-8

Kurio, N., Shimo, T., Fukazawa, T., Takaoka, M., Okui, T., Hassan, N. M., et al. (2011). Anti-tumor effect in human breast cancer by TAE226, a dual inhibitor for FAK and IGF-IR *in vitro* and *in vivo*. *Exp. Cell Res.* 317 (8), 1134–1146. doi:10.1016/j.yexcr.2011.02.008

Lachowski, D., Cortes, E., Robinson, B., Rice, A., Rombouts, K., and Del, R. H. A. (2018). FAK controls the mechanical activation of YAP, a transcriptional regulator required for durotaxis. *Faseb J.* 32 (2), 1099–1107. doi:10.1096/fj.201700721R

Lakshmanan, I., Chaudhary, S., Vengoji, R., Seshacharyulu, P., Rachagani, S., Carmicheal, J., et al. (2021). ST6GalNAc-I promotes lung cancer metastasis by altering MUC5AC sialylation. *Mol. Oncol.* 15 (7), 1866–1881. doi:10.1002/1878-0261.12956

Lander, V. E., Belle, J. I., Kingston, N. L., Herndon, J. M., Hogg, G. D., Liu, X., et al. (2022). Stromal reprogramming by FAK inhibition overcomes radiation resistance to allow for immune priming and response to checkpoint blockade. *Cancer Discov.* 12 (12), 2774–2799. doi:10.1158/2159-8290.CD-22-0192

Laszlo, V., Valko, Z., Ozsvar, J., Kovacs, I., Garay, T., Hoda, M. A., et al. (2019). The FAK inhibitor BI 853520 inhibits spheroid formation and orthotopic tumor growth in malignant pleural mesothelioma. *J. Mol. Med.* 97 (2), 231–242. doi:10.1007/s00109-018-1725-7

Law, R. P., Nunes, J., Chung, C. W., Bantscheff, M., Buda, K., Dai, H., et al. (2021). Discovery and characterisation of highly cooperative FAK-degrading PROTACs. *Angew. Chem.-Int. Ed.* 60 (43), 23327–23334. doi:10.1002/anie.202109237

Lazaro, G., Smith, C., Goddard, L., Jordan, N., Mcclelland, R., Barrett-Lee, P., et al. (2013). Targeting focal adhesion kinase in ER+/HER2+ breast cancer improves trastuzumab response. *Endocr.-Relat. Cancer.* 20 (5), 691–704. doi:10.1530/ERC-13-0019

Lechertier, T., Reynolds, L. E., Kim, H., Pedrosa, A. R., Gomez-Escudero, J., Munoz-Felix, J. M., et al. (2020). Pericyte FAK negatively regulates Gas6/Axl signalling to suppress tumour angiogenesis and tumour growth. *Nat. Commun.* 11 (1), 2810. doi:10.1038/s41467-020-16618-6

Le Coq, J., Acebron, I., Rodrigo, M. B., Lopez, N. P., and Lietha, D. (2022). New insights into FAK structure and function in focal adhesions. *J. Cell Sci.* 135 (20), jcs259089. doi:10.1242/jcs.259089

Lee, C. C., Yu, C. J., Panda, S. S., Chen, K. C., Liang, K. H., Huang, W. C., et al. (2023). Epithelial cell adhesion molecule (EpCAM) regulates HGFR signaling to promote colon cancer progression and metastasis. *J. Transl. Med.* 21 (1), 530. doi:10.1186/s12967-023-04390-2

Lees, D. M., Reynolds, L. E., Pedrosa, A. R., Roy-Luzarraga, M., and Hodivala-Dilke, K. M. (2021). Phosphorylation of pericyte FAK-Y861 affects tumour cell apoptosis and tumour blood vessel regression. *Angiogenesis* 24 (3), 471–482. doi:10.1007/s10456-021-09776-8

Le Large, T., Bijlsma, M. F., El, H. B., Mantini, G., Lagerweij, T., Henneman, A. A., et al. (2021). Focal adhesion kinase inhibition synergizes with nab-paclitaxel to target pancreatic ductal adenocarcinoma. *J. Exp. Clin. Cancer Res.* 40 (1), 91. doi:10.1186/s13046-021-01892-z

Li, H., Cai, E., Cheng, H., Ye, X., Ma, R., Zhu, H., et al. (2022). FGA controls VEGFA secretion to promote angiogenesis by activating the VEGFR2-FAK signalling pathway. *Front. Endocrinol.* 13, 791860. doi:10.3389/fendo.2022.791860

Li, H., Gao, Y., and Ren, C. (2021). Focal adhesion kinase inhibitor BI 853520 inhibits cell proliferation, migration and EMT process through PI3K/AKT/mTOR signaling pathway in ovarian cancer. *Discov. Oncol.* 12 (1), 29. doi:10.1007/s12672-021-00425-6

Li, J., Yu, T., Yan, M., Zhang, X., Liao, L., Zhu, M., et al. (2019). DCUN1D1 facilitates tumor metastasis by activating FAK signaling and up-regulates PD-L1 in non-small-cell lung cancer. *Exp. Cell Res.* 374 (2), 304–314. doi:10.1016/j.yexcr.2018.12.001

Li, J., Zhang, X., Hou, Z., Cai, S., Guo, Y., Sun, L., et al. (2022). P130cas-FAK interaction is essential for YAP-mediated radioresistance of non-small cell lung cancer. *Cell Death Dis.* 13 (9), 783. doi:10.1038/s41419-022-05224-7

Li, L., Li, Z., Lu, C., Li, J., Zhang, K., Lin, C., et al. (2022). Ibrutinib reverses IL-6-induced osimertinib resistance through inhibition of Laminin α5/FAK signaling. *Commun. Biol.* 5 (1), 155. doi:10.1038/s42003-022-03111-7

Li, Y., Deng, Y., Zhao, Y., Zhang, W., Zhang, S., Zhang, L., et al. (2022). Immunoglobulin superfamily 9 (IGSF9) is trans-activated by p53, inhibits breast cancer metastasis via FAK. *Oncogene* 41 (41), 4658–4672. doi:10.1038/s41388-022-02459-8

Liao, W. L., Liu, Y. F., Ying, T. H., Shieh, J. C., Hung, Y. T., Lee, H. J., et al. (2022). Inhibitory effects of ursolic acid on the stemness and progression of human breast cancer cells by modulating argonaute-2. *Int. J. Mol. Sci.* 24 (1), 366. doi:10.3390/ijms24010366

Lim, S. T., Chen, X. L., Lim, Y., Hanson, D. A., Vo, T. T., Howerton, K., et al. (2008). Nuclear FAK promotes cell proliferation and survival through FERM-enhanced p53 degradation. *Mol. Cell.* 29 (1), 9–22. doi:10.1016/j.molcel.2007.11.031

Lin, H. M., Lee, B. Y., Castillo, L., Spielman, C., Grogan, J., Yeung, N. K., et al. (2018). Effect of FAK inhibitor VS-6063 (defactinib) on docetaxel efficacy in prostate cancer. *Prostate* 78 (4), 308–317. doi:10.1002/pros.23476

Lin, Y. T., Liang, S. M., Wu, Y. J., Wu, Y. J., Lu, Y. J., Jan, Y. J., et al. (2019). Cordycepin suppresses endothelial cell proliferation, migration, angiogenesis, and tumor growth by regulating focal adhesion kinase and p53. *Cancers* 11 (2), 168. doi:10.3390/cancers11020168

Ling, Y., Liang, G., Lin, Q., Fang, X., Luo, Q., Cen, Y., et al. (2022). circCDYL2 promotes trastuzumab resistance via sustaining HER2 downstream signaling in breast cancer. *Mol. Cancer.* 21 (1), 8. doi:10.1186/s12943-021-01476-7

Liu, P., Sun, Y., Liu, S., Niu, J., Liu, X., and Chu, Q. (2022). SY-707, an ALK/FAK/IGF1R inhibitor, suppresses growth and metastasis of breast cancer cells. *Acta Biochim. Biophys. Sin.* 54 (2), 252–260. doi:10.3724/abbs.2022008

Liu, T. J., Lafortune, T., Honda, T., Ohmori, O., Hatakeyama, S., Meyer, T., et al. (2007). Inhibition of both focal adhesion kinase and insulin-like growth factor-I receptor kinase suppresses glioma proliferation *in vitro* and *in vivo*. *Mol. Cancer Ther.* 6 (4), 1357–1367. doi:10.1158/1535-7163.MCT-06-0476

Liu, X., Hogg, G. D., Zuo, C., Borcherding, N. C., Baer, J. M., Lander, V. E., et al. (2023a). Context-dependent activation of STING-interferon signaling by CD11b agonists enhances anti-tumor immunity. *Cancer Cell* 41 (6), 1073–1090. doi:10.1016/j.ccell.2023.04.018

Liu, X., Li, J., Yang, X., Li, X., Kong, J., Qi, D., et al. (2023b). Carcinoma-associated fibroblast-derived lysyl oxidase-rich extracellular vesicles mediate collagen crosslinking and promote epithelial-mesenchymal transition via p-FAK/p-paxillin/YAP signaling. *Int. J. Oral Sci.* 15 (1), 32. doi:10.1038/s41368-023-00236-1

Liu, X., Wang, Y., Shao, P., Chen, Y., Yang, C., Wang, J., et al. (2024). Sargentodoxa cuneata and Patrinia villosa extract inhibits LPS-induced inflammation by shifting macrophages polarization through FAK/PI3K/Akt pathway regulation and glucose metabolism reprogramming. *J. Ethnopharmacol.* 318, 116855. doi:10.1016/j.jep.2023.116855

Liu, Y., Kong, L. J., Li, N., Liu, Y. H., Jia, M. Q., Liu, Q. G., et al. (2023a). Design, synthesis and biological evaluation of novel 2,4-diaminopyrimidine cinnamyl derivatives as inhibitors of FAK with potent anti-gastric cancer activities. *Bioorg. Chem.* 141, 106895. doi:10.1016/j.bioorg.2023.106895

Liu, Y., Wang, H., Zhao, X., Zhang, J., Zhao, Z., Lian, X., et al. (2023b). Targeting the immunoglobulin IGSF9 enhances antitumor T-cell activity and sensitivity to anti-PD-1 immunotherapy. *Cancer Res.* 83 (20), 3385–3399. doi:10.1158/0008-5472.CAN-22-3115

Liu, Z., Hu, M., Yang, Y., Du, C., Zhou, H., Liu, C., et al. (2022). An overview of PROTACs: a promising drug discovery paradigm. *Mol. Biomed.* 3 (1), 46. doi:10.1186/s43556-022-00112-0

Long, Z., Zuo, Y., Li, R., Le, Y., Dong, Y., and Yan, L. (2023). Design, synthesis and biological evaluation of 4-arylamino-pyrimidine derivatives as focal adhesion kinase inhibitors. *Bioorg. Chem.* 140, 106792. doi:10.1016/j.bioorg.2023.106792

Lopez-Mejia, I. C., Pijuan, J., Navaridas, R., Santacana, M., Gatius, S., Velasco, A., et al. (2023). Oxidative stress-induced FAK activation contributes to uterine serous carcinoma aggressiveness. *Mol. Oncol.* 17 (1), 98–118. doi:10.1002/1878-0261.13346

Luo, Q. Y., Zhou, S. N., Pan, W. T., Sun, J., Yang, L. Q., Zhang, L., et al. (2021). A multi-kinase inhibitor APG-2449 enhances the antitumor effect of ibrutinib in esophageal squamous cell carcinoma via EGFR/FAK pathway inhibition. *Biochem. Pharmacol.* 183, 114318. doi:10.1016/j.bcp.2020.114318

Luo, X., Archibeque, I., Dellamaggiore, K., Smither, K., Homann, O., Lipford, J. R., et al. (2022). Profiling of diverse tumor types establishes the broad utility of VHL-based ProTaCs and triages candidate ubiquitin ligases. *iScience* 25 (3), 103985. doi:10.1016/j.isci.2022.103985

Mak, G., Soria, J. C., Blagden, S. P., Plummer, R., Fleming, R. A., Nebot, N., et al. (2019). A phase Ib dose-finding, pharmacokinetic study of the focal adhesion kinase inhibitor GSK2256098 and trametinib in patients with advanced solid tumours. *Br. J. Cancer.* 120 (10), 975–981. doi:10.1038/s41416-019-0452-3

Mehta, S., Fiorelli, R., Bao, X., Pennington-Krygier, C., Derogatis, A., Kim, S., et al. (2022). A phase 0 trial of ceritinib in patients with brain metastases and recurrent glioblastoma. *Clin. Cancer Res.* 28 (2), 289–297. doi:10.1158/1078-0432.CCR-21-1096

Miao, J., Ye, P., Lan, J., Ye, S., Zhong, J., Gresham, A., et al. (2020). Paeonol promotes the phagocytic ability of macrophages through confining HMGB1 to the nucleus. *Int. Immunopharmacol.* 89, 107068. doi:10.1016/j.intimp.2020.107068

Mohan, N., Hosain, S., Zhao, J., Shen, Y., Luo, X., Jiang, J., et al. (2019). Atezolizumab potentiates Tcell-mediated cytotoxicity and coordinates with FAK to suppress cell invasion and motility in PD-L1(+) triple negative breast cancer cells. *OncoImmunology* 8 (9), e1624128. doi:10.1080/2162402X.2019.1624128

Murphy, J. M., Jeong, K., Ahn, E. E., and Lim, S. S. (2022). Nuclear focal adhesion kinase induces APC/C activator protein CDH1-mediated cyclin-dependent kinase 4/6 degradation and inhibits melanoma proliferation. *J. Biol. Chem.* 298 (6), 102013. doi:10.1016/j.jbc.2022.102013

Mustafa, M., Abd, E. A., Abdelhafeez, D. A., Abdelhamid, D., Mostafa, Y. A., Ghosh, P., et al. (2021a). FAK inhibitors as promising anticancer targets: present and future directions. *Future Med. Chem.* 13 (18), 1559–1590. doi:10.4155/fmc-2021-0015

Mustafa, M., Abd, E. A., Abdelhamid, D., Katkar, G. D., Mostafa, Y. A., Ghosh, P., et al. (2021b). A first-in-class anticancer dual HDAC2/FAK inhibitors bearing hydroxamates/benzamides capped by pyridinyl-1,2,4-triazoles. *Eur. J. Med. Chem.* 222, 113569. doi:10.1016/j.ejmech.2021.113569

Nahta, R. (2012). Pharmacological strategies to overcome HER2 cross-talk and Trastuzumab resistance. *Curr. Med. Chem.* 19 (7), 1065–1075. doi:10.2174/092986712799320691

Naser, R., Aldehaiman, A., Diaz-Galicia, E., and Arold, S. T. (2018). Endogenous control mechanisms of FAK and PYK2 and their relevance to cancer development. *Cancers* 10 (6), 196. doi:10.3390/cancers10060196

Newport, E., Pedrosa, A. R., Lees, D., Dukinfield, M., Carter, E., Gomez-Escudero, J., et al. (2022). Elucidating the role of the kinase activity of endothelial cell focal adhesion kinase in angiocrine signalling and tumour growth. *J. Pathol.* 256 (2), 235–247. doi:10.1002/path.5833

Ohta, Y., Fujii, M., Takahashi, S., Takano, A., Nanki, K., Matano, M., et al. (2022). Cell-matrix interface regulates dormancy in human colon cancer stem cells. *Nature* 608 (7924), 784–794. doi:10.1038/s41586-022-05043-y

Osipov, A., Blair, A. B., Liberto, J., Wang, J., Li, K., Herbst, B., et al. (2021). Inhibition of focal adhesion kinase enhances antitumor response of radiation therapy in pancreatic cancer through CD8+ T cells. *Cancer Biol. Med.* 18 (1), 206–214. doi:10.20892/j.issn.2095-3941.2020.0273

Osipov, A., Saung, M. T., Zheng, L., and Murphy, A. G. (2019). Small molecule immunomodulation: the tumor microenvironment and overcoming immune escape. *J. Immunother. Cancer.* 7 (1), 224. doi:10.1186/s40425-019-0667-0

Ott, G. R., Cheng, M., Learn, K. S., Wagner, J., Gingrich, D. E., Lisko, J. G., et al. (2016). Discovery of clinical candidate CEP-37440, a selective inhibitor of focal adhesion kinase (FAK) and anaplastic lymphoma kinase (ALK). *J. Med. Chem.* 59 (16), 7478–7496. doi:10.1021/acs.jmedchem.6b00487

Pang, X. J., Liu, X. J., Liu, Y., Liu, W. B., Li, Y. R., Yu, G. X., et al. (2021). Drug discovery targeting focal adhesion kinase (FAK) as a promising cancer therapy. *Molecules* 26 (14), 4250. doi:10.3390/molecules26144250

Panni, R. Z., Herndon, J. M., Zuo, C., Hegde, S., Hogg, G. D., Knolhoff, B. L., et al. (2019). Agonism of CD11b reprograms innate immunity to sensitize pancreatic cancer to immunotherapies. *Sci. Transl. Med.* 11 (499), eaau9240. doi:10.1126/scitranslmed.aau9240

Paradis, J. S., Acosta, M., Saddawi-Konefka, R., Kishore, A., Gomes, F., Arang, N., et al. (2021). Synthetic lethal screens reveal cotargeting FAK and MEK as a multimodal precision therapy for GNAQ-driven uveal melanoma. *Clin. Cancer Res.* 27 (11), 3190–3200. doi:10.1158/1078-0432.CCR-20-3363

Patel, S. A., Nilsson, M. B., Le, X., Cascone, T., Jain, R. K., and Heymach, J. V. (2023). Molecular mechanisms and future implications of VEGF/VEGFR in cancer therapy. *Clin. Cancer Res.* 29 (1), 30–39. doi:10.1158/1078-0432.CCR-22-1366

Pedrosa, A. R., Bodrug, N., Gomez-Escudero, J., Carter, E. P., Reynolds, L. E., Georgiou, P. N., et al. (2019). Tumor angiogenesis is differentially regulated by phosphorylation of endothelial cell focal adhesion kinase tyrosines-397 and -861. *Cancer Res.* 79 (17), 4371–4386. doi:10.1158/0008-5472.CAN-18-3934

Peng, K., Zhang, F., Wang, Y., Sahgal, P., Li, T., Zhou, J., et al. (2023). Development of combination strategies for focal adhesion kinase inhibition in diffuse gastric cancer. *Clin. Cancer Res.* 29 (1), 197–208. doi:10.1158/1078-0432.CCR-22-1609

Pietrobono, S., and Stecca, B. (2021). Aberrant sialylation in cancer: biomarker and potential target for therapeutic intervention? *Cancers* 13 (9), 2014. doi:10.3390/cancers13092014

Pifer, P. M., Yang, L., Kumar, M., Xie, T., Frederick, M., Hefner, A., et al. (2023). FAK drives resistance to therapy in HPV-negative head and neck cancer in a p53-dependent manner. *Clin. Cancer Res.* 30, 187–197. doi:10.1158/1078-0432.CCR-23-0964

Pomella, S., Cassandri, M., Braghini, M. R., Marampon, F., Alisi, A., and Rota, R. (2022). New insights on the nuclear functions and targeting of FAK in cancer. *Int. J. Mol. Sci.* 23 (4), 1998. doi:10.3390/ijms23041998

Popova, N. V., and Jucker, M. (2021). The role of mTOR signaling as a therapeutic target in cancer. *Int. J. Mol. Sci.* 22 (4), 1743. doi:10.3390/ijms22041743

Popow, J., Arnhof, H., Bader, G., Berger, H., Ciulli, A., Covini, D., et al. (2019). Highly selective PTK2 proteolysis targeting chimeras to probe focal adhesion kinase scaffolding functions. *J. Med. Chem.* 62 (5), 2508–2520. doi:10.1021/acs.jmedchem.8b01826

Qiao, D., Xing, J., Duan, Y., Wang, S., Yao, G., Zhang, S., et al. (2022). The molecular mechanism of baicalein repressing progression of gastric cancer mediating miR-7/FAK/AKT signaling pathway. *Phytomedicine* 100, 154046. doi:10.1016/j.phymed.2022.154046

Qiao, W., Wang, W., Liu, H., Guo, W., Li, P., and Deng, M. (2020). Prognostic and clinical significance of focal adhesion kinase expression in breast cancer: a systematic review and meta-analysis. *Transl. Oncol.* 13 (11), 100835. doi:10.1016/j.tranon.2020.100835

Qin, Q., Wang, R., Fu, Q., Zhang, G., Wu, T., Liu, N., et al. (2022). Design, synthesis, and biological evaluation of potent FAK-degrading PROTACs. *J. Enzym. Inhib. Med. Chem.* 37 (1), 2241–2255. doi:10.1080/14756366.2022.2100886

Quispe, P. A., Lavecchia, M. J., and Leon, I. E. (2022). Focal adhesion kinase inhibitors in the treatment of solid tumors: preclinical and clinical evidence. *Drug Discov. Today.* 27 (2), 664–674. doi:10.1016/j.drudis.2021.11.025

Roberts, W. G., Ung, E., Whalen, P., Cooper, B., Hulford, C., Autry, C., et al. (2008). Antitumor activity and pharmacology of a selective focal adhesion kinase inhibitor, PF-562,271. *Cancer Res.* 68 (6), 1935–1944. doi:10.1158/0008-5472.CAN-07-5155

Roy-Luzarraga, M., Reynolds, L. E., de Luxan-Delgado, B., Maiques, O., Wisniewski, L., Newport, E., et al. (2022). Suppression of endothelial cell FAK expression reduces pancreatic ductal adenocarcinoma metastasis after gemcitabine treatment. *Cancer Res.* 82 (10), 1909–1925. doi:10.1158/0008-5472.CAN-20-3807

Samson, S. C., Khan, A. M., and Mendoza, M. C. (2022). ERK signaling for cell migration and invasion. *Front. Mol. Biosci.* 9, 998475. doi:10.3389/fmolb.2022.998475

Schmid, M. C., Khan, S. Q., Kaneda, M. M., Pathria, P., Shepard, R., Louis, T. L., et al. (2018). Integrin CD11b activation drives anti-tumor innate immunity. *Nat. Commun.* 9 (1), 5379. doi:10.1038/s41467-018-07387-4

Schoenherr, C., Byron, A., Sandilands, E., Paliashvili, K., Baillie, G. S., Garcia-Munoz, A., et al. (2017). Ambra1 spatially regulates Src activity and Src/FAK-mediated cancer cell invasion via trafficking networks. *eLife* 6, e23172. doi:10.7554/eLife.23172

Schultze, A., Decker, S., Otten, J., Horst, A. K., Vohwinkel, G., Schuch, G., et al. (2010). TAE226-mediated inhibition of focal adhesion kinase interferes with tumor angiogenesis and vasculogenesis. *Invest. New Drugs.* 28 (6), 825–833. doi:10.1007/s10637-009-9326-5

Shao, S., Piao, L., Wang, J., Guo, L., Wang, J., Wang, L., et al. (2022). Tspan9 induces EMT and promotes osteosarcoma metastasis via activating FAK-ras-ERK1/2 pathway. *Front. Oncol.* 12, 774988. doi:10.3389/fonc.2022.774988

Shen, D., Zeng, Y., Zhang, W., Li, Y., Zhu, J., Liu, Z., et al. (2022). Chenodeoxycholic acid inhibits lung adenocarcinoma progression via the integrin α5β1/FAK/p53 signaling pathway. *Eur. J. Pharmacol.* 923, 174925. doi:10.1016/j.ejphar.2022.174925

Shen, J., Cao, B., Wang, Y., Ma, C., Zeng, Z., Liu, L., et al. (2018). Hippo component YAP promotes focal adhesion and tumour aggressiveness via transcriptionally activating THBS1/FAK signalling in breast cancer. *J. Exp. Clin. Cancer Res.* 37 (1), 175. doi:10.1186/s13046-018-0850-z

Shi, P. J., Xu, L. H., Lin, K. Y., Weng, W. J., and Fang, J. P. (2016). Synergism between the mTOR inhibitor rapamycin and FAK down-regulation in the treatment of acute lymphoblastic leukemia. *J. Hematol. Oncol.* 9, 12. doi:10.1186/s13045-016-0241-x

Shiau, J. P., Wu, C. C., Chang, S. J., Pan, M. R., Liu, W., Ou-Yang, F., et al. (2021). FAK regulates VEGFR2 expression and promotes angiogenesis in triple-negative breast cancer. *Biomedicines* 9 (12), 1789. doi:10.3390/biomedicines9121789

Simons, M., Gordon, E., and Claesson-Welsh, L. (2016). Mechanisms and regulation of endothelial VEGF receptor signalling. *Nat. Rev. Mol. Cell Biol.* 17 (10), 611–625. doi:10.1038/nrm.2016.87

Slack-Davis, J. K., Martin, K. H., Tilghman, R. W., Iwanicki, M., Ung, E. J., Autry, C., et al. (2007). Cellular characterization of a novel focal adhesion kinase inhibitor. *J. Biol. Chem.* 282 (20), 14845–14852. doi:10.1074/jbc.M606695200

Song, X., Xu, H., Wang, P., Wang, J., Affo, S., Wang, H., et al. (2021). Focal adhesion kinase (FAK) promotes cholangiocarcinoma development and progression via YAP activation. *J. Hepatol.* 75 (4), 888–899. doi:10.1016/j.jhep.2021.05.018

Song, Y., Bi, Z., Liu, Y., Qin, F., Wei, Y., and Wei, X. (2023). Targeting RAS-RAF-MEK-ERK signaling pathway in human cancer: current status in clinical trials. *Genes Dis.* 10 (1), 76–88. doi:10.1016/j.gendis.2022.05.006

Soria, J. C., Gan, H. K., Blagden, S. P., Plummer, R., Arkenau, H. T., Ranson, M., et al. (2016). A phase I, pharmacokinetic and pharmacodynamic study of GSK2256098, a focal adhesion kinase inhibitor, in patients with advanced solid tumors. *Ann. Oncol.* 27 (12), 2268–2274. doi:10.1093/annonc/mdw427

Spallarossa, A., Tasso, B., Russo, E., Villa, C., and Brullo, C. (2022). The development of FAK inhibitors: a five-year update. *Int. J. Mol. Sci.* 23 (12), 6381. doi:10.3390/ijms23126381

Steinberg, T., Dieterle, M. P., Ramminger, I., Klein, C., Brossette, J., Husari, A., et al. (2023). On the value of *in vitro* cell systems for mechanobiology from the perspective of yes-associated protein/transcriptional Co-activator with a PDZ-binding motif and focal adhesion kinase and their involvement in wound healing, cancer, aging, and senescence. *Int. J. Mol. Sci.* 24 (16), 12677. doi:10.3390/ijms241612677

Su, Y., Li, R., Ning, X., Lin, Z., Zhao, X., Zhou, J., et al. (2019). Discovery of 2,4-diarylaminopyrimidine derivatives bearing dithiocarbamate moiety as novel FAK inhibitors with antitumor and anti-angiogenesis activities. *Eur. J. Med. Chem.* 177, 32–46. doi:10.1016/j.ejmech.2019.05.048

Sulzmaier, F. J., Jean, C., and Schlaepfer, D. D. (2014). FAK in cancer: mechanistic findings and clinical applications. *Nat. Rev. Cancer.* 14 (9), 598–610. doi:10.1038/nrc3792

Sun, C., Feng, L., Sun, X., Yu, R., and Kang, C. (2021). Design and screening of FAK, CDK 4/6 dual inhibitors by pharmacophore model, molecular docking, and molecular dynamics simulation. *J. Biomol. Struct. Dyn.* 39 (15), 5358–5367. doi:10.1080/07391102.2020.1786458

Sun, Y., Isaji, T., Oyama, Y., Xu, X., Liu, J., Hanamatsu, H., et al. (2023). Focal-adhesion kinase regulates the sialylation of N-glycans via the PI4KIIα-PI4P pathway. *J. Biol. Chem.* 299 (8), 105051. doi:10.1016/j.jbc.2023.105051

Sun, Y., Wang, R., Sun, Y., Wang, L., Xue, Y., Wang, J., et al. (2022). Identification of novel and potent PROTACs targeting FAK for non-small cell lung cancer: design, synthesis, and biological study. *Eur. J. Med. Chem.* 237, 114373. doi:10.1016/j.ejmech.2022.114373

Tang, K. J., Constanzo, J. D., Venkateswaran, N., Melegari, M., Ilcheva, M., Morales, J. C., et al. (2016). Focal adhesion kinase regulates the DNA damage response and its inhibition radiosensitizes mutant KRAS lung cancer. *Clin. Cancer Res.* 22 (23), 5851–5863. doi:10.1158/1078-0432.CCR-15-2603

Tapial, M. P., Lopez, N. P., and Lietha, D. (2020). FAK structure and regulation by membrane interactions and force in focal adhesions. *Biomolecules* 10 (2), 179. doi:10.3390/biom10020179

Tarin, M., Nemati, F., Decaudin, D., Canbezdi, C., Marande, B., Silva, L., et al. (2023). FAK inhibitor-based combinations with MEK or PKC inhibitors trigger synergistic antitumor effects in uveal melanoma. *Cancers* 15 (8), 2280. doi:10.3390/cancers15082280

Tavora, B., Reynolds, L. E., Batista, S., Demircioglu, F., Fernandez, I., Lechertier, T., et al. (2014). Endothelial-cell FAK targeting sensitizes tumours to DNA-damaging therapy. *Nature* 514 (7520), 112–116. doi:10.1038/nature13541

Tewari, D., Patni, P., Bishayee, A., Sah, A. N., and Bishayee, A. (2022). Natural products targeting the PI3K-Akt-mTOR signaling pathway in cancer: a novel therapeutic strategy. *Semin. Cancer Biol.* 80, 1–17. doi:10.1016/j.semcancer.2019.12.008

Thanapprapasr, D., Previs, R. A., Hu, W., Ivan, C., Armaiz-Pena, G. N., Dorniak, P. L., et al. (2015). PTEN expression as a predictor of response to focal adhesion kinase inhibition in uterine cancer. *Mol. Cancer Ther.* 14 (6), 1466–1475. doi:10.1158/1535-7163.MCT-14-1077

Tiede, S., Meyer-Schaller, N., Kalathur, R., Ivanek, R., Fagiani, E., Schmassmann, P., et al. (2018). The FAK inhibitor BI 853520 exerts anti-tumor effects in breast cancer. *Oncogenesis* 7 (9), 73. doi:10.1038/s41389-018-0083-1

Tien, T. Y., Wu, Y. J., Su, C. H., Hsieh, C. L., Wang, B. J., Lee, Y. N., et al. (2023). Pannexin 1 modulates angiogenic activities of human endothelial colony-forming cells through IGF-1 mechanism and is a marker of senescence. *Arterioscler. Thromb. Vasc. Biol.* 43 (10), 1935–1951. doi:10.1161/ATVBAHA.123.319529

Tong, X., Tanino, R., Sun, R., Tsubata, Y., Okimoto, T., Takechi, M., et al. (2019). Protein tyrosine kinase 2: a novel therapeutic target to overcome acquired EGFR-TKI resistance in non-small cell lung cancer. *Respir. Res.* 20 (1), 270. doi:10.1186/s12931-019-1244-2

Ucar, D. A., Kurenova, E., Garrett, T. J., Cance, W. G., Nyberg, C., Cox, A., et al. (2012). Disruption of the protein interaction between FAK and IGF-1R inhibits melanoma tumor growth. *Cell Cycle* 11 (17), 3250–3259. doi:10.4161/cc.21611

Wang, C., Chen, J., Kuang, Y., Cheng, X., Deng, M., Jiang, Z., et al. (2022). A novel methylated cation channel TRPM4 inhibited colorectal cancer metastasis through Ca(2+)/Calpain-mediated proteolysis of FAK and suppression of PI3K/Akt/mTOR signaling pathway. *Int. J. Biol. Sci.* 18 (14), 5575–5590. doi:10.7150/ijbs.70504

Wang, D. D., Chen, Y., Chen, Z. B., Yan, F. J., Dai, X. Y., Ying, M. D., et al. (2016). CT-707, a novel FAK inhibitor, synergizes with cabozantinib to suppress hepatocellular carcinoma by blocking cabozantinib-induced FAK activation. *Mol. Cancer Ther.* 15 (12), 2916–2925. doi:10.1158/1535-7163.MCT-16-0282

Wang, X., Bove, A. M., Simone, G., and Ma, B. (2020). Molecular bases of VEGFR-2-mediated physiological function and pathological role. *Front. Cell. Dev. Biol.* 8, 599281. doi:10.3389/fcell.2020.599281

Wang, X., Zhou, Q., Yu, Z., Wu, X., Chen, X., Li, J., et al. (2017). Cancer-associated fibroblast-derived Lumican promotes gastric cancer progression via the integrin β1-FAK signaling pathway. *Int. J. Cancer.* 141 (5), 998–1010. doi:10.1002/ijc.30801

Wang, Z., Chen, W., Zuo, L., Xu, M., Wu, Y., Huang, J., et al. (2022). The Fibrillin-1/VEGFR2/STAT2 signaling axis promotes chemoresistance via modulating glycolysis and angiogenesis in ovarian cancer organoids and cells. *Cancer Commun.* 42 (3), 245–265. doi:10.1002/cac2.12274

Wang-Gillam, A., Lim, K. H., Mcwilliams, R., Suresh, R., Lockhart, A. C., Brown, A., et al. (2022). Defactinib, pembrolizumab, and gemcitabine in patients with advanced treatment refractory pancreatic cancer: a phase I dose escalation and expansion study. *Clin. Cancer Res.* 28 (24), 5254–5262. doi:10.1158/1078-0432.CCR-22-0308

Wei, W., Feng, Z., Liu, Z., Li, X., He, H., Ran, K., et al. (2022). Design, synthesis and biological evaluation of 7-((7H-pyrrolo[2,3-d]pyrimidin-4-yl)oxy)-2,3-dihydro-1H-inden-1-one derivatives as potent FAK inhibitors for the treatment of ovarian cancer. *Eur. J. Med. Chem.* 228, 113978. doi:10.1016/j.ejmech.2021.113978

Wei, Y., Wang, Y., Liu, N., Qi, R., Xu, Y., Li, K., et al. (2021). A FAK inhibitor boosts anti-PD1 immunotherapy in a hepatocellular carcinoma mouse model. *Front. Pharmacol.* 12, 820446. doi:10.3389/fphar.2021.820446

Wu, L. Y., Wang, J., Wang, L., Lu, W. G., Wang, K., Lin, A., et al. (2022). A phase Ib study of IN10018 in combination with pegylated liposomal doxorubicin (PLD) in patients with platinum-resistant ovarian cancer. *J. Clin. Oncol.* 40 (16), 5567. doi:10.1200/jco.2022.40.16_suppl.5567

Wu, X., Wang, J., Liang, Q., Tong, R., Huang, J., Yang, X., et al. (2022). Recent progress on FAK inhibitors with dual targeting capabilities for cancer treatment. *Biomed. Pharmacother.* 151, 113116. doi:10.1016/j.biopha.2022.113116

Xiao, Y., and Yu, D. (2021). Tumor microenvironment as a therapeutic target in cancer. *Pharmacol. Ther.* 221, 107753. doi:10.1016/j.pharmthera.2020.107753

Xing, P., Wang, Y., Zhang, L., Ma, C., and Lu, J. (2021). Knockdown of lncRNA MIR4435-2HG and ST8SIA1 expression inhibits the proliferation, invasion and migration of prostate cancer cells *in vitro* and *in vivo* by blocking the activation of the FAK/AKT/β-catenin signaling pathway. *Int. J. Mol. Med.* 47 (6), 93. doi:10.3892/ijmm.2021.4926

Xing, P., Zhao, Q., Zhang, L., Wang, H., Huang, D., Hu, P., et al. (2022). Conteltinib (CT-707) in patients with advanced ALK-positive non-small cell lung cancer: a multicenter, open-label, first-in-human phase 1 study. *BMC Med.* 20 (1), 453. doi:10.1186/s12916-022-02646-0

Yang, F., Xu, K., Zhang, S., Zhang, J., Qiu, Y., Luo, J., et al. (2022). Discovery of novel chloropyramine-cinnamic acid hybrids as potential FAK inhibitors for intervention of metastatic triple-negative breast cancer. *Bioorg. Med. Chem.* 66, 116809. doi:10.1016/j.bmc.2022.116809

Yang, L., Li, X., Huang, W., Rao, X., and Lai, Y. (2022). Pharmacological properties of indirubin and its derivatives. *Biomed. Pharmacother.* 151, 113112. doi:10.1016/j.biopha.2022.113112

Yang, X. H., Xiang, L., Li, X., Zhao, T. T., Zhang, H., Zhou, W. P., et al. (2012). Synthesis, biological evaluation, and molecular docking studies of 1,3,4-thiadiazol-2-amide derivatives as novel anticancer agents. *Bioorg. Med. Chem.* 20 (9), 2789–2795. doi:10.1016/j.bmc.2012.03.040

Yin, H., Wang, J., Li, H., Yu, Y., Wang, X., Lu, L., et al. (2021). Extracellular matrix protein-1 secretory isoform promotes ovarian cancer through increasing alternative mRNA splicing and stemness. *Nat. Commun.* 12 (1), 4230. doi:10.1038/s41467-021-24315-1

Yoon, H. Y., Maron, B. Y., Girald-Berlingeri, S., Gasilina, A., Gollin, J. C., Jian, X., et al. (2022). ERK phosphorylation is dependent on cell adhesion in a subset of pediatric sarcoma cell lines. *Biochim. Biophys. Acta-Mol. Cell Res.* 1869 (8), 119264. doi:10.1016/j.bbamcr.2022.119264

Yu, C., Luo, D., Yu, J., Zhang, M., Zheng, X., Xu, G., et al. (2022). Genome-wide CRISPR-cas9 knockout screening identifies GRB7 as a driver for MEK inhibitor resistance in KRAS mutant colon cancer. *Oncogene* 41 (2), 191–203. doi:10.1038/s41388-021-02077-w

Yu, V. Z., So, S. S., and Lung, M. L. (2021). Gain-of-function hot spot mutant p53(R248Q) regulation of integrin/FAK/ERK signaling in esophageal squamous cell carcinoma. *Transl. Oncol.* 14 (1), 100982. doi:10.1016/j.tranon.2020.100982

Yuen, M. L., Zhuang, L., Rath, E. M., Yu, T., Johnson, B., Sarun, K. H., et al. (2021). The role of E-cadherin and microRNA on FAK inhibitor response in malignant pleural mesothelioma (MPM). *Int. J. Mol. Sci.* 22 (19), 10225. doi:10.3390/ijms221910225

Zeng, X. Q., Li, N., Ma, L. L., Tseng, Y. J., Zhao, N. Q., and Chen, S. Y. (2016). Prognostic value of focal adhesion kinase (FAK) in human solid carcinomas: a meta-analysis. *PLoS One* 11 (9), e0162666. doi:10.1371/journal.pone.0162666

Zhang, B. Y., Zhang, Y., Zhang, J. W., Liu, P., Jiao, B., Wang, Z. Q., et al. (2021). Focal adhesion kinase (FAK) inhibition synergizes with KRAS G12C inhibitors in treating cancer through the regulation of the FAK-YAP signaling. *Adv. Sci.* 8 (16), e2100250. doi:10.1002/advs.202100250

Zhang, D., Wang, G., Yu, X., Wei, T., Farbiak, L., Johnson, L. T., et al. (2022). Enhancing CRISPR/Cas gene editing through modulating cellular mechanical properties for cancer therapy. *Nat. Nanotechnol.* 17 (7), 777–787. doi:10.1038/s41565-022-01122-3

Zhang, H., Schaefer, A., Wang, Y., Hodge, R. G., Blake, D. R., Diehl, J. N., et al. (2020). Gain-of-Function RHOA mutations promote focal adhesion kinase activation and dependency in diffuse gastric cancer. *Cancer Discov.* 10 (2), 288–305. doi:10.1158/2159-8290.CD-19-0811

Zhang, J., He, D. H., Zajac-Kaye, M., and Hochwald, S. N. (2014). A small molecule FAK kinase inhibitor, GSK2256098, inhibits growth and survival of pancreatic ductal adenocarcinoma cells. *Cell Cycle* 13 (19), 3143–3149. doi:10.4161/15384101.2014.949550

Zhang, J., Li, W., Wang, W., Chen, Q., Xu, Z., Deng, M., et al. (2023a). Dual roles of FAK in tumor angiogenesis: a review focused on pericyte FAK. *Eur. J. Pharmacol.* 947, 175694. doi:10.1016/j.ejphar.2023.175694

Zhang, J., Xu, K., Yang, F., Qiu, Y., Li, J., Li, J., et al. (2023b). Design, synthesis and evaluation of nitric oxide releasing derivatives of 2,4-diaminopyrimidine as novel FAK inhibitors for intervention of metastatic triple-negative breast cancer. *Eur. J. Med. Chem.* 250, 115192. doi:10.1016/j.ejmech.2023.115192

Zhang, L., Zhao, D., Wang, Y., Zhang, W., Zhang, J., Fan, J., et al. (2021). Focal adhesion kinase (FAK) inhibitor-defactinib suppresses the malignant progression of human esophageal squamous cell carcinoma (ESCC) cells via effective blockade of PI3K/AKT axis and downstream molecular network. *Mol. Carcinog.* 60 (2), 113–124. doi:10.1002/mc.23273

Zhang, P., Cao, X., Guan, M., Li, D., Xiang, H., Peng, Q., et al. (2022). CPNE8 promotes gastric cancer metastasis by modulating focal adhesion pathway and tumor microenvironment. *Int. J. Biol. Sci.* 18 (13), 4932–4949. doi:10.7150/ijbs.76425

Zhao, H. Y., Chen, J. H., Song, Z. B., Zhao, Y. Q., Guo, Y. B., Wu, G., et al. (2022). First-in-human phase I results of APG-2449, a novel FAK and third-generation ALK/ROS1 tyrosine kinase inhibitor (TKI), in patients (pts) with second-generation TKI-resistant ALK/ROS1(+) non-small cell lung cancer (NSCLC) or mesothelioma. *J. Clin. Oncol.* 40 (16), 9071. doi:10.1200/jco.2022.40.16_suppl.9071

Zhao, H. Y., Xin, M., and Zhang, S. Q. (2023). Progress of small molecules for targeted protein degradation: PROTACs and other technologies. *Drug Dev. Res.* 84 (2), 337–394. doi:10.1002/ddr.22026

Zheng, Y., Xia, Y., Hawke, D., Halle, M., Tremblay, M. L., Gao, X., et al. (2009). FAK phosphorylation by ERK primes ras-induced tyrosine dephosphorylation of FAK mediated by PIN1 and PTP-PEST. *Mol. Cell.* 35 (1), 11–25. doi:10.1016/j.molcel.2009.06.013

Zheng, Y., Zhou, R., Cai, J., Yang, N., Wen, Z., Zhang, Z., et al. (2023). Matrix stiffness triggers lipid metabolic cross-talk between tumor and stromal cells to mediate bevacizumab resistance in colorectal cancer liver metastases. *Cancer Res.* 83 (21), 3577–3592. doi:10.1158/0008-5472.CAN-23-0025

Zhou, J., Yi, Q., and Tang, L. (2019). The roles of nuclear focal adhesion kinase (FAK) on Cancer: a focused review. *J. Exp. Clin. Cancer Res.* 38 (1), 250. doi:10.1186/s13046-019-1265-1

Zhu, H., Wang, D. D., Yuan, T., Yan, F. J., Zeng, C. M., Dai, X. Y., et al. (2018). Multikinase inhibitor CT-707 targets liver cancer by interrupting the hypoxia-activated IGF-1R-YAP Axis. *Cancer Res.* 78 (14), 3995–4006. doi:10.1158/0008-5472.CAN-17-1548

Frontiers in Pharmacology

Explores the interactions between chemicals and living beings

The most cited journal in its field, which advances access to pharmacological discoveries to prevent and treat human disease.

Discover the latest Research Topics

See more →

Frontiers

Avenue du Tribunal-Fédéral 34
1005 Lausanne, Switzerland
frontiersin.org

Contact us

+41 (0)21 510 17 00
frontiersin.org/about/contact